School of Engineering
Department of Civil Engineering

Distinguished Ground Improvement Projects by Dynamic Compaction or Dynamic Replacement

Babak Hamidi

This thesis is presented for the Degree of
Doctor of Philosophy
of
Curtin University

October 2014

Declaration

To the best of my knowledge and belief this thesis contains no material previously published by any other person except where due acknowledgment has been made. This thesis contains no material which has been accepted for the award of any other degree or diploma in any university.

Babak Hamidi

Signature:

Date:

Abstract

Dynamic Compaction is a ground improvement technique that was invented by the late French engineer, Louis Menard, in the mid-1970s. In this technique deep layers of granular soil are compacted by dropping a significantly heavy pounder from a considerable height. The pounder impacts vibrate the ground, rearrange the soil grains in a denser configuration, and densify a thick layer of soil that otherwise could have been subject to failure or unacceptable deformations under loads.

In approximately the 40 years that has gone by since the invention of dynamic compaction this technique has been become a well-established and popular ground improvement method, and has been the subject of research by various academic institutions. However, consolidated and comprehensive information is outdated, and publications remain scattered.

This thesis attempts to collect and compile a thorough and comprehensive documentation of previous research that has been published on dynamic compaction and dynamic replacement or related matters on these technologies to assist in the development and progress of this branch of ground improvement technologies, with incorporation of views that are closely related to the state-of-the-art of the industry.

The author has had the opportunity to participate in numerous distinguished dynamic compaction and dynamic replacement projects under the mentorship and guidance of the world's leading expert on the subject, and has had the unique opportunity to be exposed to the views of the engineers who have developed and led the advancements of this ground improvement technology. For documentary purpose and for enabling others to use the knowledge and experience that has been acquired, a number of these projects have been described, reviewed and analysed in this thesis. Discussions include construction methods, quality control and verification processes, comparison of results with previously published research, and development of new formulations.

Acknowledgements

It is with the most sincere gratitude that I acknowledge the attention and guidance that my supervisor, Professor Hamid Nikraz, has given to this work. His brilliance, patience, and good nature have provided inspiration and motivation that shall guide me for many years. His friendship and support will be always cherished.

I am also grateful to Menard for providing the data and information that has been used in Chapter 3, without which this thesis would have been impossible.

Finally, I wish to acknowledge my parents, Amir and Narsin, for their encouragement throughout my academic endeavors, my wife, Azin, for her support, and my mentor, Mr Serge Varaksin, for reshaping my views on applied geotechnical engineering.

List of Publications during the Course of this Thesis

Published Peer Reviewed Journal Papers

1. Hamidi, B., Nikraz, H. & Varaksin, S. (2009) A Review on Impact Oriented Ground Improvement Techniques. *Australian Geomechanics Journal,* 44, 2, 17-24.

2. Hamidi, B., Nikraz, H. & Varaksin, S. (2009) Arching in Ground Improvement. *Australian Geomechanics Journal,* 44, 4 (December), 99-108.

3. Hamidi, B., Nikraz, H. & Varaksin, S. (2011) The Treatment of a Loose Submerged Subgrade Fill Using Dynamic Compaction. *International Journal of Pavement Research and Technology,* 4, 2 (March), 124-130.

4. Hamidi, B., Varaksin, S. & Nikraz, H. (2013) Relative Density Concept is not a Reliable Criterion. *Ground Improvement,* 166, GI2, 78-85.

5. Hamidi, B., Varaksin, S. & Nikraz, H. (2013) Relative Density Correlations are not Reliable Criteria. *Ground Improvement,* 166, GI4, 96–208.

6. Hamidi, B., Debats, J. M., Nikraz, H. & Varaksin, S. (2013) Offshore Ground Improvement Records. *Australian Geomechanics Journal,* 48, 4, 111-122.

Published Peer Reviewed Conference Papers

7. Hamidi, B., Nikraz, H. & Varaksin, S. (2010) Treatment of Thick Saturated Loose Subgrades Using Dynamic Compaction. *3rd International Conference on Problematic Soils (PS10)*, Adelaide, 7-9 April, 121-128.

8. Hamidi, B., Nikraz, H. & Varaksin, S. (2010) Soil Improvement of a Very Thick and Large Fill by Dynamic Compaction. *3rd International Conference on Problematic Soils (PS10)*, Adelaide, 7-9 April, 129-138.

9. Hamidi, B., Nikraz, H. & Varaksin, S. (2010) Application of Dynamic Compaction in Port of Ras Laffan Expansion Project. *6th Australasian Congress on Applied Mechanics (ACAM6)*, Perth, Australia, 12-15 December, Paper 1148.

10. Hamidi, B., Varaksin, S. & Nikraz, H. (2010) Dynamic Replacement for Constructing Embankments and Walls on Soft Soil. *3rd International Conference on Problematic Soils (PS10)*, Adelaide, 7-9 April, 105-112.

11. Hamidi, B., Varaksin, S. & Nikraz, H. (2010) Treatment of a Hydraulically Reclaimed Port Project by Dynamic Compaction. *3rd International Conference on Problematic Soils (PS10)*, Adelaide, 7-9 April, 113-120.

12. Hamidi, B., Varaksin, S. & Nikraz, H. (2010) Correlations between CPT and PMT at a Dynamic Compaction Project. *2nd International Symposium on Cone Penetration Testing (CPT10)*, Huntington Beach, California, 9-11 May, paper 2-04.

13. Hamidi, B., Varaksin, S. & Nikraz, H. (2010) Implementation of Optimized Ground Improvement Techniques for a Giga Project. *GeoShanghai 2010 Conference, ASCE Geotechnical Special Publication No 207: Ground Improvement and Geosynthetics*, Shanghai, 3-5 June, 87-92.

14. Hamidi, B., Varaksin, S. & Nikraz, H. (2010) Predicting Soil Parameters by Modelling Dynamic Compaction Induced Subsidence. *6th Australasian Congress on Applied Mechanics (ACAM6)*, Perth, Australia, 12-15 December, Paper 1150.

15. Hamidi, B., Yee, K., Varaksin, S., Nikraz, H. & Wong, L. T. (2010) Ground Improvement in Deep Waters Using Dynamic Replacement. *20th International Offshore and Polar Engineering Conference*, Beijing, 20-26 June, 848-853.

16. Hamidi, B., Nikraz, H. & Varaksin, S. (2011) A Case Study of Vibration Monitoring in a Dynamic Compaction Project. *14th Asian Regional Conference on Soil Mechanics and Geotechnical Engineering* Hong Kong, 23-27 May, Paper No. 405.

17. Hamidi, B., Nikraz, H. & Varaksin, S. (2011) Ground Improvement Acceptance Criteria. *14th Asian Regional Conference on Soil Mechanics and Geotechnical Engineering* Hong Kong, 23-27 May, Paper No. 404.

18. Hamidi, B., Nikraz, H. & Varaksin, S. (2011) Dynamic Compaction Vibration Monitoring in a Saturated Site. *International Conference on Advances in Geotechnical Engineering (ICAGE)*, Perth, 7-9 November, 267-272.

19. Hamidi, B., Varaksin, S. & Nikraz, H. (2011) The Application of Dynamic Compaction to HFO Tanks. *International Conference on Advances in Geotechnical Engineering (ICAGE)*, Perth, 7-9 November, 627-632.

20. Hamidi, B., Nikraz, H. & Varaksin, S. (2011) Application of Dynamic Replacement in a Steel Pipe Factory. *International Conference on Advances in Geotechnical Engineering (ICAGE)*, Perth, 7-9 November, 867-872.

21. Hamidi, B., Nikraz, H. & Varaksin, S. (2011) Advances in Dynamic Compaction. *Indian Geotechnical Conference IGC2011*, Kochi, India, 15-17 December, Paper No. H-146.

22. Hamidi, B., Varaksin, S. & Nikraz, H. (2011) Predicting Menard Modulus using Dynamic Compaction Induced Subsidence. *International Conference on Advances in Geotechnical Engineering (ICAGE)*, Perth, 7-11 November, 221-226.

23. Hamidi, B., Varaksin, S. & Nikraz, H. (2011) Dynamic Compaction for Treating Millions of Square Meters of Sand. *International Conference on Advances in Geotechnical Engineering (ICAGE)*, Perth, 7-9 November, 475-480.

24. Hamidi, B., Varaksin, S. & Nikraz, H. (2011) A Case of Vibro Compaction Vibration Monitoring in a Reclaimed Site. *International Conference on Advances in Geotechnical Engineering (ICAGE)*, Perth, 7-9 November, 861-866.

25. Hamidi, B., Varaksin, S. & Nikraz, H. (2011) Application of Dynamic Surcharging for Construction of Tanks on Reclaimed Ground. *International Conference on Advances in Geotechnical Engineering (ICAGE)*, Perth, 7-9 November, 873-878.

26. Hamidi, B., Nikraz, H. & Varaksin, S. (2012) The Application of Dynamic Compaction on Marjan Island. *11th Australia New Zealand Conference on Geomechanics - Ground Engineering in a Changing World: ANZ 2012*, Melbourne, 15-18 July, 1202-1207.

27. Hamidi, B., Nikraz, H. & Varaksin, S. (2012) Application of Dynamic Compaction in Reclaimed Roads. *2012 AGS Symposium: Advances in Geotechnics of Roads and Railways*, Sydney, 10 October, 115-124.

28. Hamidi, B., Varaksin, S. & Nikraz, H. (2012) The Effectiveness of Vibration Reduction Trenches in a Dynamic Replacement Project. *11th Australia New Zealand Conference on Geomechanics - Ground Engineering in a Changing World: ANZ 2012*, Melbourne, 15-18 July, 253-258.

29. Hamidi, B., Varaksin, S. & Nikraz, H. (2012) Construction of Raw Sugar Silos Using Dynamic Replacement. *International Conference on Ground Improvement and Ground Control - Transport Infrastructure Development and Natural Hazards Mitigation (ICGI2012),* 2, Wollongong, NSW, Australia, 30 October - 2 November, 1069-1074.

30. Hamidi, B., Varaksin, S. & Nikraz, H. (2012) Application of Dynamic Compaction in a Project with Smart Acceptance Criteria. *International Conference on Ground Improvement and Ground Control - Transport Infrastructure Development and Natural Hazards Mitigation (ICGI2012),* 2, Wollongong, NSW, Australia, 30 October - 2 November, 1075-1081.

31. Varaksin, S. & Hamidi, B. (2012) Ground Improvement Case Histories and Advances in Practice. *International Conference on Ground Improvement and Ground Control - Transport Infrastructure Development and Natural Hazards Mitigation (ICGI2012),* 1, Wollongong, NSW, Australia, 30 October - 2 November, 209-222.

32. Varaksin, S. & Hamidi, B. (2013) Pressuremeter for Design and Acceptance of Challenging Ground Improvement Works. *18th International Conference on Soil Mechanics and Geotechnical Engineering (18th ICSMGE), Parallel session: ISP6 - Pressio 2013*, Paris, 2-6 September.

33. Hamidi, B., Nikraz, H. & Varaksin, S. (2015) Correlation between PMT & CPT after Dynamic Compaction in Reclaimed Calcareous Sand. 1*2th Australia New Zealand Conference on Geomechanics (ANZ 2015)*, Wellington, 22-25 February

Published Non Peer Reviewed Conference Papers

34. Hamidi, B. & Varaksin, S. (2012) Lessons Learned from Millions of Square Metres of Ground Improvement. *International Symposium on Ground Improvement (IS-GI) Brussels 2012,* 2, Brussels, 29 May - 1 June, 29-39.

35. Varaksin, S. & Hamidi, B. (2014) Contributions of the Pressuremeter to Ground Improvement and Perspectives for the Future. *The International Scientific and Technical Conference Devoted to the 80th Anniversary of the Geotechnical Department of St Petersburg State University,* 1, St Petersburg, Russia, 4-6 February, 550-555.

Accepted Conference Papers

36. Hamidi, B., Varaksin, S. & Nikraz, H. (2105) A Study on the Variation of PMT Parameters Ratio after Dynamic Compaction of Saturated Sands. *16 African Region Conference on Soil Mechanics and Geotechnical Engineering, Parallel session: ISP7 Pressio 2015, 60 Years of Pressuremeter*, Tunisia, 1-2 May.

Accepted Book Chapters

37. Hamidi, B. & Varaksin, S. (Accepted) Dynamic Compaction and Dynamic Surcharging at Dubai's Palm Jumeira STP. *In*: Buddhima, I., eds. *Ground Improvement: Case Histories and New Directions.* Oxford, Elsevier.

Table of Contents

Notations

Notation	Definition
$(P_{LM})_i$	limit pressure before soil improvement
$(P_{LM})_j$	limit pressure after soil improvement
$(Q''_1)_\delta$	Ultimate footing inclined load
$(Q'_1)_\delta$	Ultimate footing inclined load
A	Pounder base area
a	Radius of contact Horizontal radius of semi-prolate spheriod Acceleration size (or diameter) of pile caps Slope of the volume versus pressure calibration plot in PMT percentage of strain induced for doubling P_{LM}
A'	Effective footing area
a_c	Area replacement ratio
A_c	Pile cap or DR column area
AE	Applied energy
A_E	Area of cell unit
a_{max}	Peak ground acceleration (PGA)
A_{ry}	Vibration reduction ratio
A_s	Area of soil in cell unit
A_w	Equivalent wall area
B	Bulk modulus of elasticity of the mixture Footing (loading) width
b	Vertical radius of semi-prolate spheroid Pile cap width Percentage of strain induced for doubling E_M
B'	Effective footing width
B''	Effective footing width
B_0	Reference footing width of 0.6 m
B_a	Bulk modulus of elasticity of air
B_s	Bulk modulus of solid particles

Notation	Definition
B_w	Bulk modulus of elasticity of water
c	Coefficient of depth of improvement Cohesion of soil
$C_{\gamma d}$	Error propogation factor
$C_{\gamma dmax}$	Error propogation factor
$C_{\gamma dmin}$	Error propogation factor
C_0	Experimental coefficient for correlation of relative density to CPT cone resistance
c_1	Speed damping factor for depth of improvement
C_1	Experimental coefficient for correlation of relative density to CPT cone resistance
c_2	Stratigraphic coefficient for depth of improvement
C_2	Experimental coefficient for correlation of relative density to CPT cone resistance
C_a	Arching coefficient
c_c	Cohesionof DR column
C_c	Compression index beyond the critical pressure
C_D	A parameter that reflects any densification by such disturbance mechanisms as vibration and blasting, which are not related to the ideally static increase in effective vertical stress.
c_d	Depth constant for depth of improvement
c_e	Energy constant for depth of improvement
c_i	Cohesion of segment *i*
C_{oc}	Over consolidation coefficient
CPT	Cone penetration test
c_R	Proportion coefficient
CRR_{Mw}	Cyclic resistance ratio for earthquake with magnitude M_w
c_s	Subsoil (soft soil) cohesion
CSR	Cyclic shear ratio
CSR_i	Reduced cyclic shear ratio
c_t	Cohesion of trench
c_u	Undrained shear strength

Notation	Definition
C_α	Secondary compression index
D	Depth of improvement or influence
d	Pounder or column diameter Distance between pounder and monitoring point
D_{50}	Mean particle diameter
D_B	Diameter of base of crater
d_c	Column diameter
D_c	Crater depth Constrained modulus of the DR column
DC	Dynamic compaction
D_d	Relative density
D_f	Depth of footing
d_i	Inside diameter of the heavy duty steel casing or pipe in the pressuremeter test
D_i	Interim depth of improvement
DR	Dynamic replacement
D_s	Constrained modulus of the soil
D_T	Diameter of top of crater
E	Elastic (Young) modulus Impact energy= WH Arching efficacy or the portion of load that is supported by the piles
e	Void ratio Load eccentricity
E^+	Spherical or compression modulus
E_c	Elastic (Young) modulus of column Weighted value of E_M immediately below the footing
E_d	Harmonic mean of E_M in all layers down to the depth of 8B
E_i	Harmonic mean of moduli of layer *i*
E_M	Menard modulus
E_{M^+}	Menard reload modulus
e_{max}	Maximum index void ratio or the reference void ratio of a soil at the minimum index density/unit weight

Notation	Definition
e_{min}	Minimum index void ratio or the reference void ratio of a soil at the maximum index density/unit weight
E_{oed}	Oedometric modulus
E_s	Elastic (Young) modulus of in-situ soil
E_y	Young modulus
F	Safety factor for bearing capacity
f	Frequency Predominant frequency
$f(z)$	Improvement factor at elevation z
f_1	Maximum improvement factor observed at ground level
f_2	Improvement factor obtained at the depth of influence of dynamic compaction
f_B	Bottom factor
F_c	Fines content
f_C	Cushion (crushed stone platform) factor
f_M	Material (soil) factor
f_{shell}	Factor for correlating relative density of calcareous sand to silica sand
g	Gravity acceleration
G	Shear modulus
G_c	Shear modulus of the column
G_{ceq}	Equivalent shear modulus
G_r	Ratio of column's to soil's shear moduli
G_s	Specific gravity of the solid particles Shear modulus of the soil
H	Pounder drop height Height of embankment
h	test spacing in borehole
H_c	Thickness of compressible layer
h_c	Critical depth of embedment
HDR	High energy dynamic replacement
h_e	Equivalent foundation depth
h_g	Arching height

Notation	Definition
h_k	Pressuremeter test spacing in a borehole
H_p	Depth of probe below the control unit
H_T	Isolation trench depth
I	Energy intensity= applied energy per unit area Improvement factor
i_e	Bearing capacity reduction factor for eccentric loading
i_δ	Bearing capacity reduction factor for inclined loading
$i_{\delta e}$	Bearing capacity reduction factor for inclined and eccentric loading
$i_{\delta\beta'}$	Bearing capacity reduction factor for inclined loading near a slope
k	A bearing factor varying from 0.8 to 9 according to the embedment, the shape of the foundation level after construction
K	Peak particle velocity intercept Compression or volume change (bulk) modulus
K_0	Earth pressure coefficient Ratio of effective horizontal to vertical stresses when the soil is over consolidated
K_a	Active earth pressure coefficient
K_G	Shear reduction factor
K_M	Compression modulus
K_o	Coefficient of horizontal earth pressure at rest
K_{ONC}	Ratio of effective horizontal to vertical stresses when the soil is normally consolidated
K_P	Passive earth pressure coefficient
K_s	Ratio of vertical to horizontal stresses in the soil prior to loading
L	Distance from edge of crater to where heave reduces to zero Foundation length
l	Length of PMT measuring cell
l_i	Length of segment *i*
L_R	Wave length
L_T	Isolation trench length
m	Pounder mass Load distribution ratio

Notation	Definition
	Number of measurements
	Number of pressuremeter tests in the borehole within the improvement zone
M	Ratio of net limit pressure at depths of h and depth of h+B
MHHW	Mean High High Water
MLLW	Mean Low Low Water
MPM	Menard pressuremeter
N	Number of blows
	Number of blows required to reach maximum depth of improvement
	SPT blows per 0.3 m
	Resistance of the foundation against normal loads
n	Porosity
	Vibration attenuation rate
	Stress distribution ratio
	Number of times PMT limit pressure has doubled
N_{60}	SPT blow counts corrected to 60% efficiency
N_{78}	SPT blow count corresponding to an energy rod ratio of about 78% from the theoretical free-fall energy
N_c	Bearing capacity coefficient
NGL	Natural ground level
N_i	Interim number of blows
N_q	Bearing capacity coefficient
N_γ	Bearing capacity coefficient
OCR	Over consolidation ratio
P	Normal load
	Number of passes
	Pressure exerted by the PMT probe on the soil
	Power
p	Surface load stress on the soil
P^*_{LM}	Net PMT limit pressure
p'	Effective normal stress
P_c	Pressure loss correction in pressuremeter test

Notation	Definition
P_f	Creep or end of pseudo elastic phase pressure in the pressuremeter test
PGA	Peak ground acceleration (PGA)
P_i	Pressure in pressuremeter test for reaching probe contacting borehole wall
P_{LM}	PMT limit pressure
P_{LM_k}	Pre-improvement PMT limit pressure
P_{LM_min}	Minimum pre-improvement PMT limit pressure
PMT	Pressuremeter test
P_o	Total at rest horizontal earth pressure at the test level (at the time of the test)
PPV	Peak particle velocity
p_r	Pressure at which changes of volume change to pressure change; i.e., d(Δ*V*)/d(Δ*p*), is a minimum in PMT
P_R	Pressure reading on the PMT control unit
P_u	Pressure reading in PMT corresponding to a volume increase equal to the initial volume of the borehole
PVS	Pseudo vector sum
P_δ	Hydrostatic pressure between the PMT control unit and probe
Q	Footing load
q	Shear Stress Design normal pressure applied on the footing
Q'	Footing load
Q''	Footing load
Q''_1	Ultimate footing vertical load
q^*	Net ultimate bearing capacity
q^*_a	Net allowable bearing capacity
q^*_c	Net CPT cone resistance
Q'_1	Ultimate footing vertical load
q_a	Allowable bearing capacity
q_c	CPT cone resistance
q_{cNC}	CPT cone resistance of normally consolidated sand
q_{cOC}	CPT cone resistance of over consolidated sand
q_{cR}	CPT cone resistance at reference time

Notation	Definition
q_o	Total overburden pressure at the periphery of the foundation level after construction Total vertical stress
q_u	Ultimate bearing capacity
q_{ult}	Ultimate external pressure on footing width
r	Distance of the wave front from the source Distance of any point on the contact surface of two spheres Pounder radius $(P_{LM})_j/(P_{LM})_i$
R	Sphere radius Half width of foundation
R^2	Coefficient of determination
R_B	Radius of base of crater
r_d	Depth factor in liquefaction evaluation
ρ_{dmax}	The reference dry density/unit weight of a soil in the densest state of compactness that can be attained using a standard laboratory compaction procedure that minimizes particle segregation and breakdown
ρ_{dmin}	The reference dry density/unit weight of a soil in a standard state of compactness at which it can be placed using a standard laboratory procedure which prevents bulking and minimizes particle segregation
RIC	Rapid Impact Compactor
RL	Reduced level
R_T	Distance from the source of excitation to the isolation trench
R_T	Radius of top of crater
r_u	excess pore water pressure to initial effective vertical stress ratio
S	Degree of saturation Shearing force
s	Spacing between adjacent piles or columns Displacement, settlement
$S_{\gamma d}$	Standard deviation for γ_d
$S_{\gamma dmax}$	Standard deviation for γ_{dmax}
$S_{\gamma dmin}$	Standard deviation for γ_{dmin}

Notation	Definition
s_d	Diagonal spacing between the piles or columns
S_{Dd}	Standard deviation for D_d
S_i	Average heave (or settlement) for markers located at the same radius from the centre of the print
S_{max}	Assumed maximum heave at edge of crater
s_n	Creep or self-weight settlement after n years Settlement at measurement number n
SPT	Standard Penetration Test
t	Time
T	wave period
ton	Metric tonne
t_R	Reference time
TVS	True vector sum
u	Displacement of an element in the x direction Pore pressure
$\mathring{u}$	Particle velocity
V	Total volume Corrected increase in volume of the measuring portion of the PMT probe
v	Wave propagation velocity Particle velocity Pounder velocity
V_a	Air volume
v_c	Phase or longitudinal wave propagation velocity
V_C	Volume loss correction in pressuremeter test
V_{crater}	Volume of crater
V_{heave}	Volume of heave
V_i	Intercept of volume calibration line in PMT Corrected volume reading at the pressure where the PMT probe makes contact with the borehole
V_m	Corrected volume reading in the centre portion of the ΔV volume increase in the pressuremeter test
v_{mix}	Compression wave propagation velocity in the solid-air-water mixture

Notation	Definition
V_o	Zero volume reading
v_p	Primary wave, P-wave, or compression wave velocity
v_R	Rayleigh wave velocity
V_r	Injected volume at the end of each pressure increment in PMT Volume at which changes of volume change to pressure change; i.e., d(ΔV)/d(Δp), is a minimum in PMT
V_R	Volume of reading on PMT's readout device
v_s	Secondary wave, S-wave or shear wave velocity
V_s	Solid volume
V_v	Void volume
V_W	Water volume
w	Amplitude of the vertical component of the R-wave at distance r from the source
W	Pounder weight
w_s	Uniformly distributed surcharge loading
W_T	Isolation trench width
y	Stress distribution factor such as Boussinesq or Westergaard
z	Level of point Depth from ground surface
Z_n	Wave amplitude in the n^{th} cycle
α	Coefficient of attenuation (in terms of distance^{-1}) Rheological factor for calculating settlement
α_B	Number of blows ratio
α_z	Depth of improvement ratio
β	Angle between the footing and excavation level Coefficient relating net limit pressure to undrained shear strength
$\beta(F)$	A coefficient that is a function of the safety factor for bearing capacity
γ	Unit weight
γ_a	Unit weight of air
γ_c	DR column density Shear strain in the column
γ_d	Dry density/unit weight of a soil deposit or fill at the given void ratio

Notation	Definition
γ_{dmax}	The reference dry density/unit weight of a soil in a standard state of compactness at which it can be placed using a standard laboratory procedure which prevents bulking and minimizes particle segregation
γ_{dmin}	The reference dry density/unit weight of a soil in the densest state of compactness that can be attained using a standard laboratory compaction procedure that minimizes particle segregation and breakdown
γ_{eq}	Equivalent density
γ_s	Subsoil (soft soil) density Shear strain in the soil
γ_t	Trench unit weight
γ_w	Unit weight of water
δ	Load inclination angle from the vertical
δ	Logarithmic wave damping coefficient
$\Delta D_d/D_d$	Relative deviation in relative density
Δe	Change of void ratio
ΔN_f	Fines content correction
ΔP	Corrected pressure increase in the centre part of the straight line portion of the pressure-volume curve of the pressuremeter test
Δq_c	Vertical stress increase at the compressible layer
δ_t	Unit weight of test liquid in PMT
ΔV	Corrected volume increase in the centre part of the straight line portion of the pressure-volume curve, corresponding to Δ*P* pressure increase
$\Delta\varphi$	Change of internal friction angle
$\Delta\varphi_b$	Change of internal friction angle beneath the pounder
$\Delta\varphi_c$	Change of internal friction angle at the grid centre
$\Delta\varphi_m$	Change of internal friction angleat the middle of the grid side
ε	Strain
$\varepsilon(z)$	Strain at depth z
ε_{DC_k}	Dynamic compaction induced strain in layer (test spacing in borehole) k
ε_{o_k}	The pre-strain for each layer that demonstrates the strain difference of that layer compared to the lowest P_{LM} value
ε_R	Rayleigh distribution strain

Notation	Definition
ζ	Reduction between the centres of the two spheres
ζ	Lehr's damping coefficient
η	Shear displacement
κ	Deformation modulus reduction factor
λ	Lamé's constant Wave length
λ_c	Shape factor for calculation of compressive component of settlement
λ_d	Shape factor for calculation of deviatoric component of settlement
μ	Coefficient of friction
ν	Poisson ratio
ν_s	Soil Poisson ratio
ϖ	Average water content of soil
ρ	Mass density
ρ_d	Dry density of soil
ρ_d	Dry density/unit weight of a soil deposit or fill at the given void ratio
ρ_{tot}	Total mass density
σ	Normal stress Total normal stress on the failure plane Scale parameter of the Rayleigh distribution
σ_c	Stress in DR column
σ'_c	Vertical stress on the pile caps
$\sigma'_{c\text{-}H}$	Horizontal stress in DR column
$\sigma'_{c\text{-}V}$	Vertical stress in DR column
σ_h	Lateral confining stress on the cylindrical surface of the DR column
σ_{rL}	Limiting (lateral) stress
σ_{ro}	Total (initial) in-situ lateral stress
σ_s	Stress in soil
σ_u	Upper yield value of the soil
σ_v	Total vertical stress
σ'_v	Effective vertical stress
σ_{v_max}	Maximum vertical stress below footing
σ_{v_min}	Minimum vertical stress below footing

Notation	Definition
σ_{vo}	Total (initial) vertical stress at the level of the footing base
σ'_{vo}	Effective initial overburden pressure
σ_x	Axial stress Average normal stress
σ'_{zo}	Uniform stress at subsoil level
τ	Shear strength
τ_{ave}	Input (equivalent average) shear stress
τ_c	Shear stress in the column
τ_s	Shear stress in the soil
φ	Internal friction angle
φ'	Effective internal friction angle
φ_c	DR column internal friction angle
φ_s	Subsoil (soft soil) internal friction angle
φ_t	Trench friction angle
ω	Undamped natural frequency
ω_d	Damped natural frequency

List of Tables

List of Figures

Foreword

Mr Babak Hamidi has gone through an exceptional itinerary. Following the completion of his civil engineering studies he commenced by working for a number of years in his country of origin. He proceeded on to joining a ground improvement contractor in the Middle East specialized in dynamic compaction techniques their design execution on turnkey basis; his dream was to follow and advance the developments and ideas of Louis Menard, an objective that was not only totally realized but even complemented.

During this period he was exposed to a number of the mega projects in the region and his knowledge of soils under dynamic impacts became extensive. Even the questionable theoretical concept of “dynamic surcharge” was first brought to reality and success on the Dubai Palm project through his dedicated involvement. In summary, practice came before the theoretical basis.

After his immigration to Australia, the idea to work on a document to assemble his and others accumulated knowledge became more appealing. The aim of this work was to analyze limited available theories on soil behavior under dynamic impacts, quality control and development of technologies in terms of practical execution.

This “encyclopedia” can be considered as the first available complete document on the “dynamic compaction or consolidation” process available for academics and practitioners for the next decade. I would like to highlight within this document, the years of hard work and persistence, as without these attributes this thesis would not have been written, this combined with a full time activity.

Only experience is a lantern that is worn on the back and never illuminates the past path (Confucius).

This work combined with further research and intuition will greatly contribute to the future and to the state of the art.

Serge Varaksin
I.S.C. Chairman
TC211 – Ground Improvement Technical Committee
International Society of Soil Mechanics and Geotechnical Engineering
26 February 2014

1 Introduction

1.1 Introduction

As construction and development progresses, available land in locations of interest becomes scarcer and scarcer, and developers are forced to consider construction on sites with soils whose in-situ properties are not able to satisfy design requirements. Classically, structures on such sites would have been built on piles, but construction of piles is expensive, and time consuming. Hence, geotechnical engineers have been seeking other alternatives for providing safe foundations, and have developed *ground improvement*.

Ground improvement can be categorised as (Chu et al., 2009):

- Ground improvement without admixtures in non-cohesive soils or fills
- Ground improvement without admixtures in cohesive soils
- Ground improvement with admixtures or inclusions
- Ground improvement with grouting type admixtures
- Earth reinforcement

Louis Menard, who had invented the *pressuremeter test* in 1954 (Communication Department of Menard, 2007), developed *dynamic compaction* (*DC*) in 1969 (Menard Soltraitement) and *dynamic replacement* (*DR*) in 1975 (Communication Department of Menard, 2007).

In dynamic compaction the mechanical properties of soil is improved by applying high energy blows to the ground by dropping a heavy pounder a multiple number of times from significant heights. The impact creates waves that propagate in the soil, and re-arrange the particles in a denser configuration. The decrease of voids and increase in inner granular contact will directly lead to improved soil properties. Dynamic compaction is classified as ground improvement without admixtures in non-cohesive soils or fills.

The efficiency of dynamic compaction decreases with the increase of fines content in saturated soils due to the built-up of pore water pressure and realisation of plastic displacement in lieu of void reduction; hence, in such ground conditions the process of dynamic replacement, which is classified as ground improvement with admixtures or inclusions, can be adopted. In this latter technique the impact crater is backfilled with coarse granular material and the column is further pushed into the ground and enlarged by applying additional blows.

In the pressuremeter test a cylindrical probe is inflated in the ground. The measurements of applied pressure and volume changes of the probe during the test realises the pressuremeter *limit pressure* and *Menard modulus*. Foundation bearing capacity can be calculated using the limit pressure (Centre D'Etudes Menard, 1975) without correlating the test results to the parameters that are used in the classical Mohr-Coulomb failure criterion based solutions and bearing capacity factors (Bolton and Lau, 1993, Prandtl, 1920, Terzaghi, 1943). Foundation settlements can also be calculated by using the Menard modulus and breaking down the settlement to its volumetric and deviatoric components. The reliability of the pressuremeter test and its calculation procedures (Centre D'Etudes Menard, 1975, Menard and Rousseau, 1962) has made this test the ideal verification method in ground improvement projects in general and Menard invented techniques in particular.

Louis Menard died in 1978, but his legacy remained with his first generation of engineers who turned the company that bore Menard's name to one of the world's leading ground improvement specialist contracting firms. Serge Varaksin who joined Menard as a young engineer was one of those first generation engineers who before his retirement became overseas manager and deputy managing director of the company, and was appointed as the chairman of ISSMGE (International Society of Soil Mechanics and Foundation Engineering) Ground Improvement Technical Committee TC211 by ISSMGE's President.

The author has had the honour of working for numerous years in industry under the mentorship of Mr Varaksin. Combined with the more than 10,000,000 m^2 of dynamic compaction and dynamic replacement projects that the author was involved with has given him the unique opportunity to participate in DC and DR state-of-the-art projects with the world's leading expert.

Although information on dynamic compaction and dynamic replacement has been published, the information appears to be scattered, and years has gone by since Lukas (1986, 1995) last undertook the gathering of information on the subject. It is the author's feeling that since then significant advances have developed and evolved in the understanding of DC and DR, in the equipment, and construction methods, which justifies a comprehensive review of these technologies and their processes. Also, the author has been involved in a number of world record projects, and first time projects that require documentation and preservation in order not lost in history. Furthermore, the retirement of first generation of DC and DR engineers carries the risk of knowledge loss, and it is imperative that their experience and skills be maintained for future generations. Thus, this project is an attempt to gather and consolidate

information on DC and DR, and to document a number of distinguished projects based on the author's years of personal experience on the subject, and topics that, in his view, appear to be frequently confused and misunderstood in practice.

1.2 Objectives

The objective of this thesis is to:

- Collect the scattered information on dynamic compaction and dynamic replacement
- Retrieve information on DR and DC that may have been lost or forgotten
- Review and discuss state-of-the-art research and publications on DC and DR
- Collect, document and analyse distinguished state-of-the-art DC and DR projects
- Identify geotechnical problems and optimised treatment solutions
- Identify optimised construction procedures in DC and DR projects
- Document verification and testing procedures in DC and DR projects
- Compare results of projects introduced and studied in this thesis with previous works and data, with concentration on Menard Pressuremeter Tests
- Develop new formulations and calculation procedures
- Make recommendations and develop guidelines for future projects

1.3 Scope

This thesis will be presented in four chapters.

The current chapter, i.e., Chapter 1, is the introductory section of the thesis, and provides a brief introduction on DC and DR for ground improvement and the pressuremeter test for verification of results. The objectives of this endeavour, the thesis' scope of works, and its significance will also be presented in this chapter.

A comprehensive and thorough literature review and discussion will be presented in Chapter 2. This review will commence with a brief introduction of Louis Menard's contributions and achievements before presenting the basics of the theory of waves and vibrations in various cases. Next, the mechanisms of dynamic compaction and dynamic replacement in different ground conditions will be reviewed. This will be followed by reviewing the suitability of dynamic compaction in different ground conditions, and studying

DC parameters, which comprise of depth of improvement, crater depth, grid spacing, number of compaction phases, number of pounder drops per phases, and extents of improvement. Ground response to dynamic compaction, such as the improvement profile and ageing of improved ground, will also be discussed. Similarly, design parameters of dynamic replacement, which includes soil arching, column load capacity and liquefaction mitigation analysis methods will be reviewed. As by this stage the reader will have sufficient understanding of DC and DR mechanisms and parameters, the discussion will move forward towards construction with the review of advances in equipment that is then followed by assessing compaction vibrations and introducing methods for estimating DC induced vibrations. A section in this chapter has also been allocated to quality control, verification and testing, interpreting pressuremeter test results and calculating foundation bearing capacity and settlement using the pressuremeter parameters. Chapter 2 in concluded with a discussion of special topics that appear to be frequently confused and misunderstood in practice.

A number of distinguished state-of-the-art projects are documented, reviewed, and analysed in Chapter 3, and the results will be compared with previous studies. This chapter will also include new formulas for estimating DC induced vibration, estimating crushed rock internal friction angle from the pressuremter test, and an innovative method to estimate pressuremeter parameters based on DC induced ground settlements.

The conclusions of this thesis and recommendations will be presented in Chapter 4.

1.4 Significance

In general, ground improvement is an efficient and economical alternative to piling for providing safe foundations, and in particular, dynamic compaction is one the most suitable techniques for treating granular soils. This technology has been used for more than 40 years to treat millions of square metres of soil. Although numerous researches have been carried out to expand our understanding of this technique, most of the publications are scattered, and some are no longer available to the public. This thesis will be an attempt to gather and consolidate these publications as literature review.

As the author has had the unique chance to participate in a number of state-of-the-art and world record projects, this thesis is also an opportunity to document, review, analyse and preserve these projects in an academic form that could be of practical use for future projects.

Review of previous work combined with presentation of the distinguished projects that will be presented also provides an opportunity to compare results, update formulations, develop new concepts, and make recommendations for future projects.

2 Literature Review

2.1 Chapter Organisation

This chapter has been allocated to the review of literature related to dynamic compaction, dynamic replacement, and the pressuremeter test. The sections of this chapter include information that is required to understand the processes of dynamic compaction and dynamic replacement, performing and interpreting the pressuremeter test, and a number of issues that the author has identified as subjects of general confusion among engineers who do not have a thorough understanding of these ground improvement technologies.

Section 2.2 pays tribute to Louis Ménard, the inventor of the pressuremeter test, dynamic compaction and dynamic replacement. Among other contributions, Ménard also formulated the equations to interpret the results of the pressuremeter tests, and developed new concepts for calculating bearing capacity and foundation settlements. This section also briefly introduces dynamic compaction and dynamic replacement.

A basic knowledge of the theory of waves will be of great assistance to understand the mechanism of dynamic compaction; hence, Section 2.3 will review waves in a number of mediums, and in a homogeneous, isotropic, elastic half space medium. The review is then further advanced by considering waves generated by a vertical oscillation, followed by the introduction of damping. As in reality ground can be composed of layers of soil or rock with various properties, elastic waves in layered system and mixed media will also be discussed.

The theory and mechanism of dynamic compaction and dynamic replacement will be reviewed in Section 2.4. The discussion will be commenced in the micro level with the simplified behaviour of elastic spheres subjected to shear, normal, a combination of the two loads, and crushing of particles. Liquefaction is also discussed as it is a key process of dynamic compaction in saturated soils. Further to the discussed basics, it will then be possible to advance the discussion to the mechanism of dynamic compaction and dynamic replacement in various ground conditions. At the end of Section 2.4 the reader will have an understanding of the theory of wave propagation in the ground, and the mechanism of dynamic compaction.

Practical and design issues of dynamic compaction will commence at Section 2.5, and the first discussion of the section will focus on ground conditions in which dynamic compaction can be deemed as a suitable ground improvement technique. Then fundamental design aspects including depth of improvement, crater depth, grid spacing, number of phases and number of drops will be discussed. This section will also include a review of the improvement profile,

and the phenomenon of improvement continuation with time. The discussion in this section will be concluded by determining the required extents of ground improvement and reviewing several dynamic compaction design methods.

Similar to its preceding section, Section 2.6 will review dynamic replacement's design issues, and includes a comprehensive discussion on soil arching and calculation methods to determine load distribution in the ground, load capacity of dynamic replacement columns, and liquefaction assessment of composite ground.

Advances in dynamic compaction equipment will be reviewed in Section 2.7, and includes discussions on compaction rigs, pounders and alternative impact oriented ground improvement techniques that are sometimes erroneously referred to as dynamic compaction or a derivative of dynamic compaction.

Noting that the basis of dynamic compaction and dynamic replacement is the propagation of waves in the ground, the ability to assess the vibrations generated by dynamic compaction, and their effects on nearby structures is of great importance. Hence, this subject will be reviewed in depth in Section 2.8. Vibration assessment will commence with the review of the vibration studies that eventually led to the current better known standards. Air vibrations and human response to vibrations will also be reviewed. Estimation of vibrations based on empirical formulas and mitigation of vibrations by application of vibration barrier or isolation trenches will conclude this section.

Quality control and testing of dynamic compaction works will be reviewed in Section 2.9. This important section of Chapter 2 includes the heave and penetration test and a complete discussion on the pressuremeter test. The pressuremeter components and test procedure will be explained, and the commonly used testing frequencies used in industry will be defined. Also, a detailed review of calculation methods for determining bearing capacity and foundation settlements will be presented. This section also includes correlations of pressuremeter parameters with other testing methods.

Although Chapter 2 could have been concluded with Section 2.9, it is the author's belief that literature review of ground improvement methods would be incomplete if no discussion is made on ground improvement acceptance criteria. Section 2.10 includes a brief discussion of acceptance criteria specifications, and an in depth review of research that demonstrates the unreliability of relative density concept and correlations as acceptance criteria. Other

special topics that will be discussed in this section are ground condition after sand reclamations and the application of dynamic compaction in offshore projects.

A summary of the sections of Chapter 2 are shown in Figure 2-1.

Figure 2-1: Summary of literature review topics presented in the thesis

2.2 Tribute to Louis Ménard

Louis Ménard, shown Figure 2-2, was born on 4 May 1931 in the Bay of Mont-Saint-Michel, France (Communication Department of Menard, 2007). He attended the civil engineering school of the prestigious *École des Ponts et Chaussées* in 1952. During the summer that he was employed to carry out compaction tests on a new runway in Paris, Ménard realised that while strength-deformation properties were important, field tests and measurements were not able to measure them. Consequently, he developed the first prototype of the *Ménard pressuremter* as his dissertation and filed for a patent for it in 1954 at the age of 23.

Figure 2-2: Louis Ménard (1931-1978)

Ménard later improved his invention and carried out the first tests with the new probe while studying for a Master's degree (Menard, 1957) under the supervision of Professor Peck at the University of Illinois and filed for a second pressuremeter patent in 1959.

The year 1962 was a big year for Ménard. By then, the Pressuremeter Test, commonly abbreviated to *PMT* had become an internationally recognised in-situ soil testing method, and Ménard was revolving the accepted theories of soil mechanics. In the same year he set up a bilingual technical journal, *Sols-Soils* and split his company in two, *Techniques Louis*

Ménard (Louis Ménard Technologies) and *Études Pressiométriques Louis Ménard* (Louis Ménard Pressuremeter Measuring).

There was still more to come for Ménard in 1969. Although others may have tried to compact the soil by dropping weights onto the ground surface, it was Ménard who made a major breakthrough by lifting a substantially heavy weight, or *pounder*, and dropping from a considerable height, the technique he called *compactage dynamique*, translating to *dynamic compaction* and commonly abbreviated to *DC*. Ménard first implemented dynamic compaction at Bormes-Les-Mimosas in the French Riviera by renting a crane. This project never became famous because there are no photographs available of that endeavour; however, there is a photograph of Ménard's third project (Figure 2-3) at the marina in Mandelieu-la-Napoule, also in the Riviera, that has made that project better known. This latter project was 110,000 m^2 of reclamation, and was to be become a development with five storey buildings. Ménard used an 8 ton pounder with a drop height of 10 m. The energy applied in that project was 10 times what is typically used in more recent times (Communication Department of Menard, 2007).

Figure 2-3: Dynamic compaction was used for the first time ever in 1969 for the ground improvement works of a building construction site in Mandelieu-la-Napoule, France (Communication Department of Menard, 2007)

Louis Ménard invented and promoted Dynamic Compaction (DC) as early as 1969, but it was not until 29 May 1970 that he officially patented his invention in France. Ménard obtained two patents, firstly *compactage dynamique* or dynamic compaction for damped fills, then

consolidation dynamique or dynamic consolidation for liquefaction mitigation (Varaksin, 2014). These techniques were later also patented in many other countries, including Argentina, Australia, Austria, Bahrain, Bangladesh, Belgium, Canada, Egypt, France, Germany, Great Britain, Greece, Hong Kong, Italy, Japan, Lebanon, Malaysia, Mexico, the Netherlands, New Zealand, Norway, the Philippines, Saudi Arabia, Singapore, Spain, Sweden and the United States.

It was in 1973 and during the Compagnie Française de l'Azote project in Le Havre, France that Ménard became a true contractor. He soon signed overseas contracts for carrying out projects in Sweden and Switzerland.

Ménard invented *dynamic replacement* (*DR*) in 1975 (Menard Soltraitement), but still had more new ideas and innovations to offer until his death on 15 January 1978. Ménard also had a mind set for developing equipment that were capable of lifting very heavy and extremely heavy pounders, including the mega machine that was capable of lifting 40 ton pounders 40 m (Mayne et al., 1984) and the Giga machine, shown in Figure 2-4, that still holds the world record for lifting a 172 ton pounder during the ground improvement works of Nice International Airport in France (Gambin, 1983).

Figure 2-4: The Giga Machine holds the world record for lifting a 172 ton pounder at Nice International Airport dynamic compaction project (Communication Department of Menard, 2007)

Ménard's contribution to ground improvement has not gone unnoticed and based on the proposal of TC211, the Technical Committee of Ground Improvement, the International Society of Soil Mechanics and Geotechnical Engineering (ISSMGE) board voted unanimously (12 in favour, none abstaining, none opposing) to create a ISSMGE TC211 lecture called "Louis Ménard Lecture" (Briaud, 2011).

2.3 Review of the Theory of Waves

The concepts of dynamic compaction and dynamic replacement are based on the propagation of energy waves in the soil medium, and it is not possible to properly comprehend these techniques without an introduction and understanding of the theory of waves.

2.3.1 Waves in a Bounded Elastic Medium

The equation of motion in a bounded elastic medium, such as a rod, can be expressed by the partial differential equation:

$$\frac{\partial^2 u}{\partial t^2} = v^2 \frac{\partial^2 u}{\partial x^2} \qquad 2\text{-}1$$

u = the displacement of an element in the x direction

t = time

v = the wave propagation velocity

The *phase velocity* or *longitudinal wave propagation velocity* for a longitudinal wave, v_c, can be determined to be:

$$v_c{}^2 = \frac{E}{\rho} \qquad 2\text{-}2$$

E = Young's modulus

ρ = mass density; i.e., $\rho = \gamma/g$

γ = unit weight

g = gravity acceleration

If σ_x is the axial (compressive or tensile) stress induced by the longitudinal wave, then *particle velocity,* $\mathring{u}$ *,* will be:

$$\dot{u} = \frac{\sigma_x v_c}{E} \qquad 2\text{-}3$$

Although many people confuse longitudinal velocity, v_c, with the particle velocity, $\mathring{u}$, comparison of Equations 2-2 and 2-3 clearly demonstrates that these parameters are two different entities that are only proportional to one another. It can also be understood from the same equations that v_c and $\mathring{u}$ are in the same direction when the stress is compressive, but are in opposite directions when the stress is tensile. Another important observation that can be made from Equations 2-2 and 2-3 is that while v_c is only a function of material properties, $\mathring{u}$ is additionally a function of the applied stress.

It can also be proven that for a torsional wave the *shear wave velocity* is:

$$v_s{}^2 = \frac{G}{\rho} \qquad 2\text{-}4$$

G = shear modulus; i.e.:

$$G = \frac{E}{2(1+\nu)} \qquad 2\text{-}5$$

ν = Poisson's ratio

2.3.2 Waves in an Infinite, Homogeneous, Isotropic, Elastic Medium

The equations of motion and wave propagation have also been solved (Richart et al., 1970) for an infinite, homogeneous, isotropic, elastic medium. It can be determined that the velocity of the *dilatational wave* v_p, also known as the *primary wave*, *P-wave*, *compression wave* or *irrotational wave*, is equal to:

$$v_p = \sqrt{\frac{\lambda + 2G}{\rho}} \qquad 2\text{-}6$$

λ = Lamé's constant.

Similarly, the velocity of the *distortional wave*, v_s, also known as the *secondary wave*, *S-wave*, *shear wave* or *equivoluminal wave*, can be determined to be equal to:

$$v_s = \sqrt{\frac{G}{\rho}} \qquad 2\text{-}7$$

It can be noted that while the particle motion associated with the compression wave in the bounded elastic medium and the dilatational wave in the infinite medium are the same, the wave propagation velocities are different. The comparison of Equation 2-2 and Equation 2-6 indicates that compression waves travel faster in an infinite medium than in a rod because while there can be lateral displacements in a rod, the same is not true in the infinite medium.

The comparison of Equation 2-4 and Equation 2-7 demonstrates that the shear waves propagate in the rod and the infinite medium with the same velocity.

Particle motion associated with the compression wave is a push-pull motion parallel to the direction of the wave front; however, the particle motion associated with the shear wave is a transverse displacement normal to the direction of the wave front.

2.3.3 Waves in a Homogeneous, Isotropic, Elastic, Half Space Medium

In addition to the compression and shear waves that propagate in an infinite medium, there is also a third wave in a homogenous, isotropic, elastic half space medium. This wave, which is called the *Rayleigh* or *R-wave* in recognition of the first person who studied it, (Rayleigh, 1885) is confined to a zone near the boundary of the half space, and has later been described in detail (Lamb, 1904).

If $K = {}^{v_R}/_{v_S}$ and $\alpha = {}^{v_s}/_{v_p}$ then it can be shown that:

$$K^6 - 8K^4 + 24(-16\alpha^2)K^2 + 16(\alpha^2 - 1) = 0 \qquad 2\text{-}8$$

where

$$\alpha^2 = \frac{G}{\lambda + 2G} = \frac{1 - 2\nu}{2 - 2\nu} \qquad 2\text{-}9$$

From Equation 2-8, it is evident that K^2 and consequently v_R is independent of the frequency of the wave.

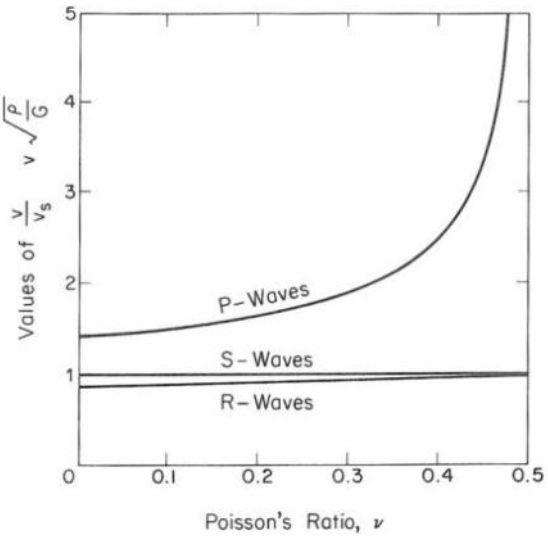

Figure 2-5: Relations between Poisson's ratio and P, S and R-wave velocities in an elastic half space medium (Richart, 1962)

Ratios of v_R/v_S and v_s/v_p can be obtained for values of Poisson's ratio ranging from 0 to 0.5 (Richart, 1962). These ratios are graphically shown in Figure 2-5.

As shown in Figure 2-6, the horizontal and vertical displacement components of the R-waves, respectively denoted by $U(z)$ and $W(z)$, can be determined for different Poisson ratios and depths. It can also be observed in this figure that the largest displacements and consequently most of the vibration energy are within a depth that is about one third to one half of the wave length.

Under the conditions considered by Lamb, the waves spread out from the point source in the form of a symmetrical annular wave system. The characteristic wave system shown in Figure 2-7 will develop if input is of short duration. This wave system has three main features corresponding to the arrivals of the P, S and R-waves. A particle at the surface first undergoes a displacement in the form of an oscillation due to the arrival of the P-wave. After a relatively quiet period the particle experiences another oscillation due to the arrival of the S-wave. Lamb refers to these events as the *minor tremor*. The *major tremor,* which has oscillations with much larger magnitudes occur when the R-waves arrive. Obviously, the time interval between the wave arrivals becomes greater with increasing distances from the source.

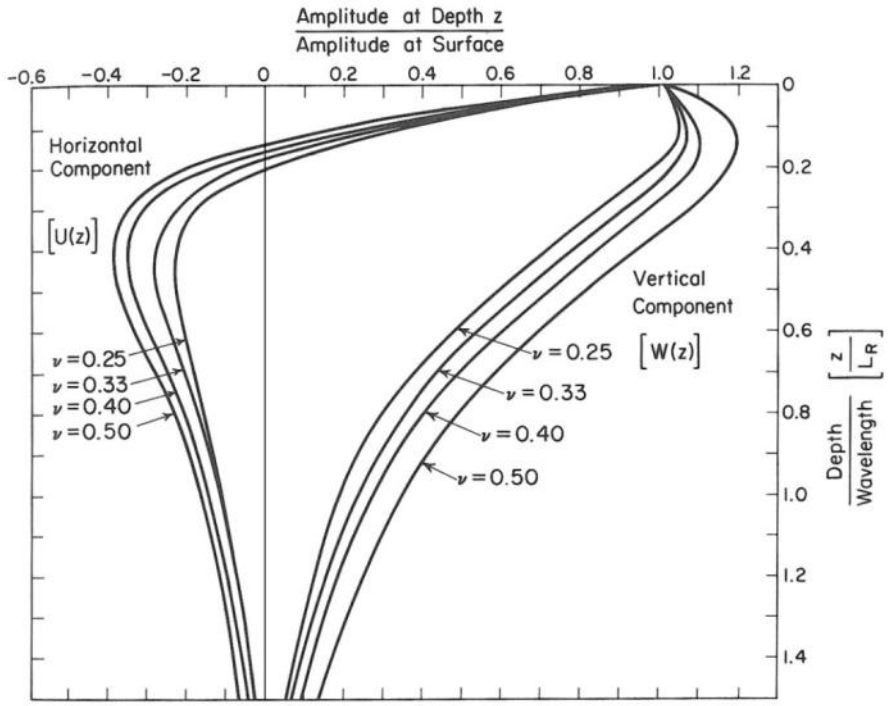

Figure 2-6: Amplitude ratio versus dimensionless depth for R-waves (Richart et al., 1970)

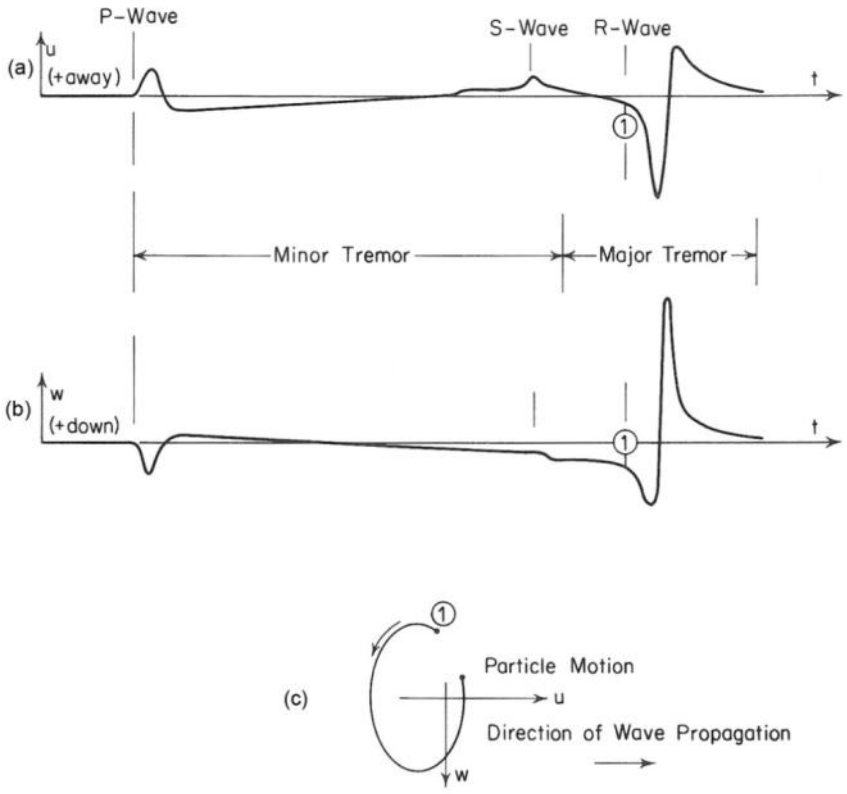

Figure 2-7: Wave system from surface point source in ideal medium (Lamb, 1904)

2.3.4 The Wave Field Generated by a Vertical Oscillation

(Richart et al., 1970)also discuss the wave field generated by a circular footing undergoing vertical oscillations at the surface of the half space. The basic features of this wave field at a relatively large distance from the source, i.e., a distance of 2.5 times the wave length (Lysmer, 1966), is shown in Figure 2-8. In this figure, the distances from the source of waves to the wave front are drawn in proportion to the velocity of each wave for a medium with a Poisson ratio of 0.25 (also refer to Figure 2-7 for the comparison of the wave velocities).

The body waves, i.e., the P and S-waves, propagate radially outward from the source along a hemispherical wave front that is shown by the heavy black lines of Figure 2-8. The R-waves propagate radially outward along a cylindrical wave front.

The volume of material that is encompassed by each of the waves increases as the wave travels away from the source. Hence, the energy density, i.e., the energy per unit volume, in each wave front decreases with distance from the source. This decrease in energy density and consequently the decrease in displacement amplitude is called *geometrical damping,* which should not be confused with *material damping* that is a result of energy loss due to hysteresis damping and internal sliding of soil particles (Thevanayagam et al., 2006).

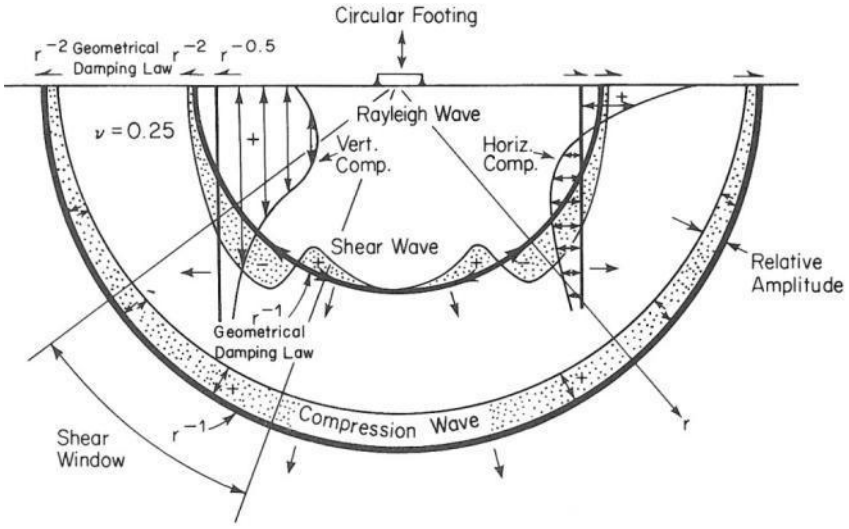

Figure 2-8: Distribution of displacement waves from a circular footing on a homogeneous, isotropic, elastic half space (Woods, 1968)

Material damping is the decrease in amplitude of vibration with distance from a source due to energy losses in the soil (designated as *attenuation*). Attenuation should be distinguished from geometrical damping which occurs in elastic systems because of the spreading out of the wave energy from a source.

If *r*= the distance of the wave front from the source, then it can be shown (Ewing et al., 1957)that the amplitudes decrease proportionally to:

$1/r^2$ for P and S-waves along the surface of the half space

$1/r$ for P and S-waves at other places

$1/r^{½}$ for R-waves

This means that the *body waves'* geometrical damping is highest along the surface of the medium.

The shaded zones along the wave fronts for the body waves indicate the relative amplitude of particle displacement as a function of the dip angle or the angle measured downwards from the surface at the centre of the source (Hirona, 1948, Miller and Pursey, 1954). The region of shear wave front in which the larger amplitudes occur is referred to as the *shear window*.

It has been determined (Miller and Pursey, 1955) that for a vertically oscillating, uniformly distributed, circular energy source on the surface of a homogeneous, isotropic, elastic half space the distribution of the total energy among the three elastic waves is:

P-wave: 7%

S-wave: 26%

R-wave: 67%

2.3.5 Internal Damping and Attenuation

In the previous section of this chapter it was stated that the amplitude of the R-wave decreases proportionally with $1/r^{½}$; i.e.:

$$w = w_1\sqrt{\frac{r_1}{r}} \qquad 2\text{-}10$$

r_1 = distance from source to point of known amplitude

r = distance from source to point in question

w_1 = amplitude of the vertical component of the R-wave at distance r_1

w =amplitude of the vertical component of the R-wave at distance r from the source

However, the wave amplitude decreases faster in soils because soil is not an ideal elastic medium and there is an internal or material damping. Both geometrical damping and material damping can be taken into account for R-wave attenuation (Bornitz, 1931):

$$w = w_1\sqrt{\frac{r_1}{r}}e^{-\alpha(r-r_1)} \qquad 2\text{-}11$$

α= coefficient of attenuation (in terms of 1/distance)

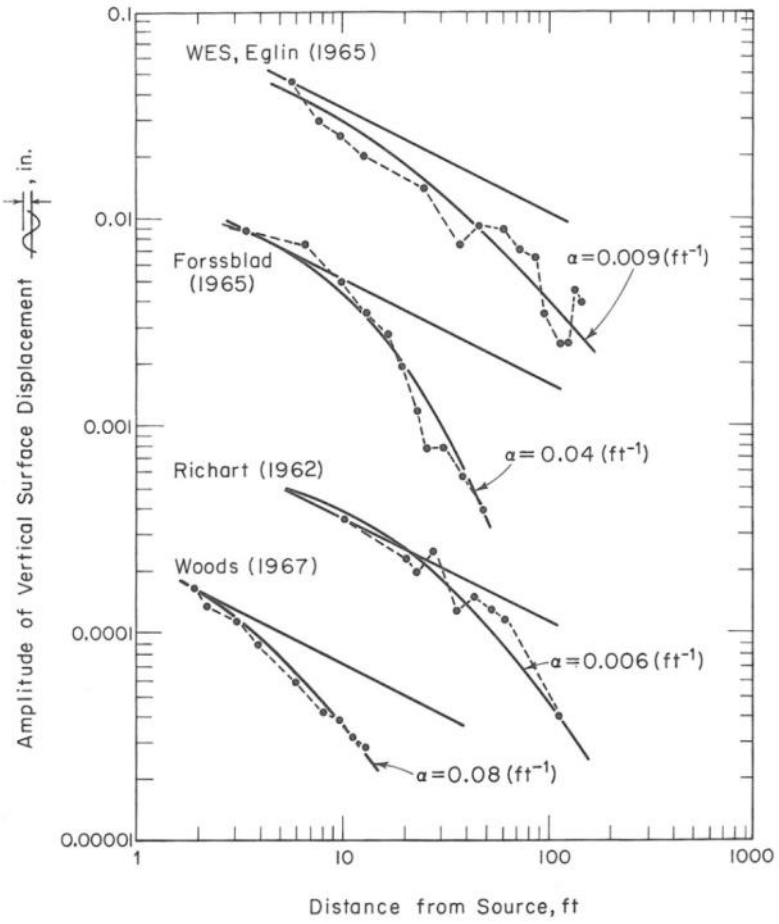

Figure 2-9: Attenuation of surface wave with distance from source of steady-state excitation (Richart et al., 1970)

Values for α have been suggested to be from 0.03 to 0.13 m^{-1} (Barkan, 1962). Figure 2-9 suggests a wider range from 0.02 to 0.26 m^{-1} (Richart et al., 1970). Based on results measurements of ground vibration due to dynamic loads such as dynamic compaction,

vibrocompaction and ball dropping, Woods and Jedele (1985) proposed α values for different soil descriptions, vibration frequencies and SPT N values aas shown in (Table 2-1).

α (m^{-1})		Soil Description and SPT blow counts
5 Hz	50 Hz	
0.01 – 0.03	0.1 – 0.3	Weak or soft soils: lossy soils, dry or partially saturated peat and muck, mud, loose beach sand, recently plowed ground, etc. N<5
0.003 – 0.01	0.03 0.1	Competent soils: most sands, sandy clays, silty clays, gravels, silts and weathered rock 5<N<15
0.0003 – 0.003	0.003 – 0.03	Hard soils: dense compacted sand, dry consolidated clay, consolidated glacial till and some exposed rock 15<N<50
<0.0003	<0.003	Hard, competent rock: bedrock and freshly exposed hard rock N>50

Table 2-1: Attenuation coefficient α for different soil descriptions and vibration frequencies (Woods and Jedele, 1985)

The coefficient α increases with dominant frequency, as a higher frequency wave will pass through more motion cycles than will low frequency waves when travelling the same distance. For material damping, decay is a function of energy loss per cycle of deformation, not distance per second. This frequency dependency explains why in a general sense dominant frequency declines with distance for the same wave type. The lower frequency components have travelled fewer deformational cycles and have lost proportionally less energy (Dowding, 2000).

Although material damping occurs in soil, it can be understood from Equation 2-11 and Equation 2-12 that it is geometrical damping that produces most of the attenuation of the R-wave. Prange (1977) has also concluded that material damping is generally small for granular media. Energy attenuation is related to the square of the amplitude of vibration (Wolf, 1994).

2.3.6 Elastic Waves in Layered Systems

When a body wave that is propagating in an elastic medium reaches and interface with another elastic medium, some of the incident wave energy will reflect into the first medium and some of the energy wave will be transmitted into the second medium.

The nature of the reflected and refracted waves have been determined (Zoeppritz and Kosten, 1919) using the theory of elasticity. In the study, shear wave was separated into two components before consideration of energy partition at the interface. The two components considered were the SV and SH-waves, respectively designating the motion in a plane perpendicular to the plane of the interface and a plane parallel to the interface. Upon encountering an interface, an incident P-wave, shown in Figure 2-10a will have four resultants:

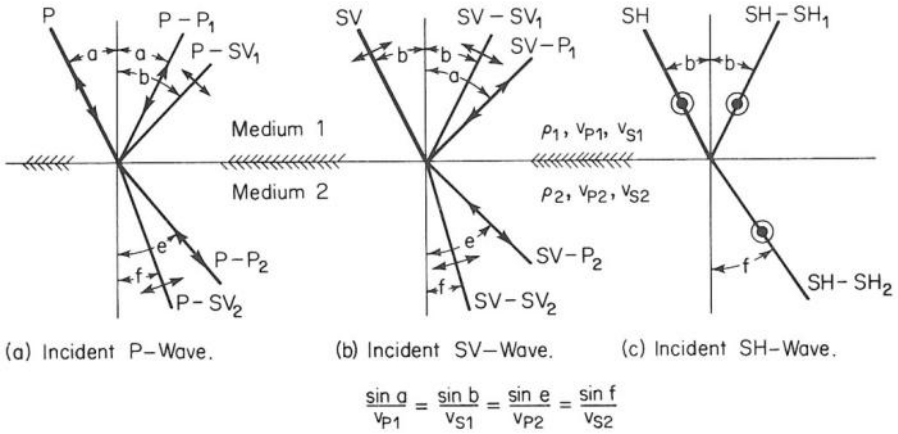

Figure 2-10: Partition of elastic wave at interface between two elastic media (Richart et al., 1970)

1. A reflected P-wave (P-P1)
2. A reflected SV-wave (P-SV_1)
3. A refracted P-wave (P-P_2)
4. A refracted SV-wave (P-SV_2)

Similarly, the resultant waves from an incident SV-wave will be (see Figure 2-10b):

1. A reflected SV-wave (SV-SV_1)
2. A reflected P-wave (SV-P_1)
3. A refracted SV-wave (SV-SV_2)
4. A refracted P-wave (SV-P_2)

However, an incident SH-wave only produces SH-waves. P-waves are not produced because the SH-wave does not have a component normal to the plane of the interface. The resultant waves from an incident SH-wave, shown in Figure 2-10, are:

1. A reflected SH-wave (SH-SH_1)

2. A refracted SH-wave (SH-SH_2)

The angle at which a resultant wave leaves the interface depends on the angle at which the incident wave approaches the interface and the ratio of the wave velocities of the two media. From Snell's law:

$$\frac{\sin a}{v_{S1}} = \frac{\sin b}{v_{S1}} = \frac{\sin e}{v_{P2}} = \frac{\sin f}{v_{S2}} \qquad 2\text{-}12$$

Where the angles *a, b*, *e* and *f* are measured from the normal to the interface (see Figure 2-10) and:

v_{p1} = velocity of the P-wave in medium 1

v_{s1} =velocity of the S-wave in medium 1

v_{p2} =velocity of the P-wave in medium 2

v_{s2} =velocity of the S-wave in medium 2

Noting that *the energy transmitted by an elastic wave is proportional to the square root of the displacement amplitude*, the equations for the distribution of energy among the resultant waves can be written with consideration of the below parameters:

A= amplitude of incident P-wave

B= amplitude of incident S-wave

C= amplitude of reflected P-wave

D= amplitude of reflected S-wave

E= amplitude of refracted P-wave

F= amplitude of refracted S-wave

ρ_1= density of medium 1

ρ_2= density of medium 2

For incident P-wave:

$$(A - C)\sin a + D\cos b - E\sin e + F\cos f = 0 \quad \text{2-13}$$

$$(A + C)\cos a + D\sin b - E\cos e - F\sin f = 0 \quad \text{2-14}$$

$$-(A + C)\sin 2a + D\frac{v_{P1}}{v_{S1}}\cos 2b + E\frac{\rho_2}{\rho_1}\left(\frac{v_{S2}}{v_{S1}}\right)^2\frac{v_{P1}}{v_{P2}}\sin 2e - F\frac{\rho_2}{\rho_1}\left(\frac{v_{S2}}{v_{S1}}\right)^2\frac{v_{P1}}{v_{S2}}\cos 2f = 0 \quad \text{2-15}$$

$$-(A - C)\cos 2b + D\frac{v_{S1}}{v_{P1}}\sin 2b + E\frac{\rho_2}{\rho_1}\frac{v_{P2}}{v_{P1}}\cos 2f + F\frac{\rho_2}{\rho_1}\frac{v_{S2}}{v_{P1}}\sin 2f = 0 \quad \text{2-16}$$

For incident SV-wave:

$$(B + D)\sin b + C\cos a - E\cos e - F\sin f = 0 \quad \text{2-17}$$

$$(B - D)\cos b + C\sin a + E\sin e - F\cos f = 0 \quad \text{2-18}$$

$$(B + D)\cos 2b - C\frac{v_{S1}}{v_{P1}}\sin 2a + E\frac{\rho_2}{\rho_1}\frac{{v_{S2}}^2}{v_{S1}v_{P2}}\sin 2e - F\frac{\rho_2}{\rho_1}\frac{v_{S2}}{v_{S1}}\cos 2f = 0 \quad \text{2-19}$$

$$-(A - D)\sin 2b + C\frac{v_{P1}}{v_{S1}}\cos 2b + E\frac{\rho_2}{\rho_1}\frac{v_{P2}}{v_{S1}}\cos 2f + F\frac{\rho_2}{\rho_1}\frac{v_{S2}}{v_{P1}}\sin 2f = 0 \quad \text{2-20}$$

For incident SH-wave:

$$B + D - F = 0 \quad \text{2-21}$$

$$B - D - \frac{\rho_2}{\rho_1}\frac{v_{S2}}{v_{P1}}\frac{\cos f}{\cos b}F = 0 \qquad 2\text{-}22$$

The above equations demonstrate that the amplitude of each resultant wave is a function of:

1. The angle of incidence of the incident wave
2. The ratio of the wave velocities in the two media
3. The ratio of densities of the two media.

In the event that the media and consequently the media's densities and wave velocities are known, the amplitude of each resultant wave can be calculated. As an example and for a situation where wave velocity and density in medium 1 are greater than medium 2, e.g. when waves travelling in a very dense soil reach a very loose soil, Figure 2-11 and Figure 2-12 show the amplitude ratios of reflected and refracted waves over a range of incident angles.

If there is more than one interface and as shown in Figure 2-13, waves may be reflected back to the surface from each interface. When reflected waves return to the surface of the half space they encounter the interface between the solid medium and void where they will be totally reflected. Multiple total reflections within the upper layer can generate another type of surface wave called *Love* or *L-wave* in recognition of the first person who described this wave type. (Ewing et al., 1957) describe the L-wave as a horizontally polarized shear wave trapped in a superficial layer and propagated by multiple total reflections. L-waves propagate with a velocity that is between the S-wave velocity of the superficial layer and the S-wave velocity of the next lower layer.

It is necessary for the phase velocity of the L-wave to be less than the shear wave velocity in the next lower layer for the L-waves to be confined to the superficial layer. L-wave will not occur if the superficial layer is the higher velocity layer.

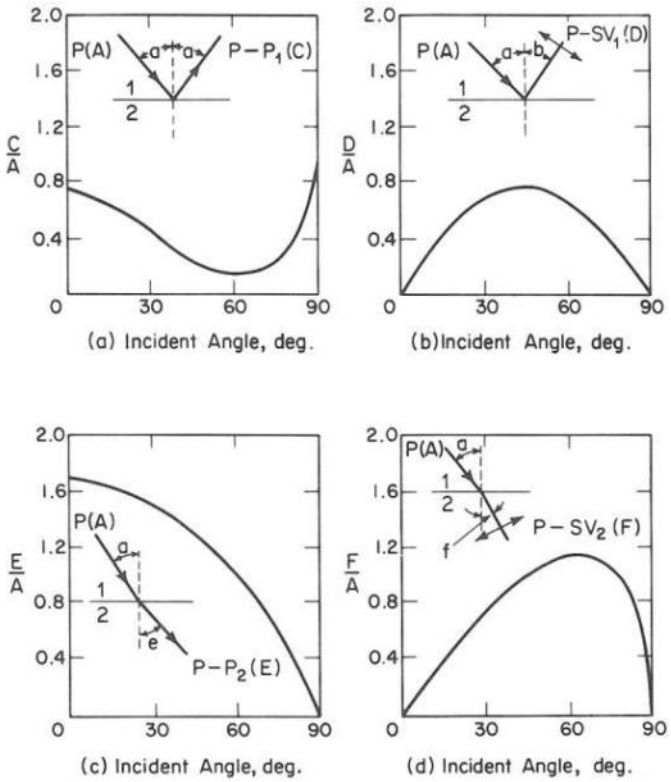

Figure 2-11: Example of amplitude ratio versus incident angle for P-wave (McCamy et al., 1962)

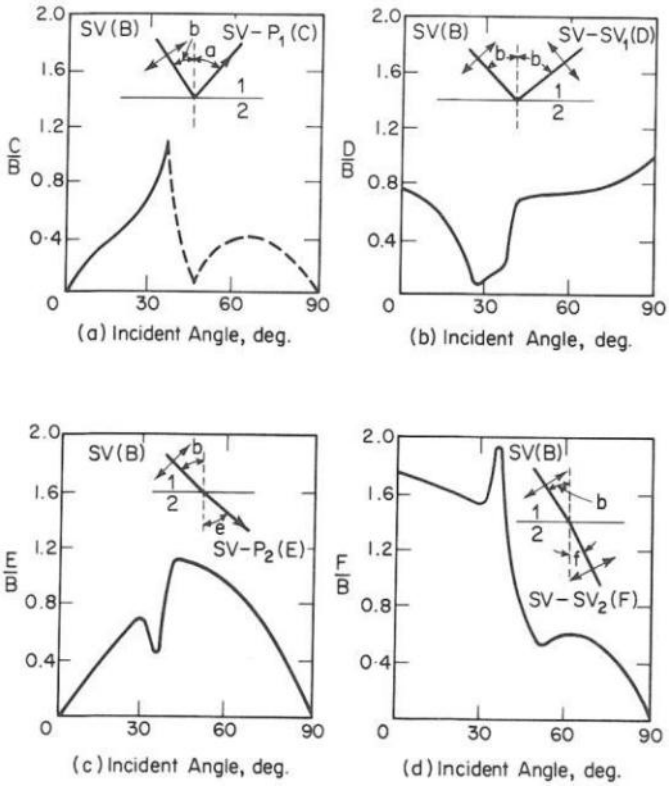

Figure 2-12: Example of amplitude ratio versus. incident angle for S-wave (McCamy et al., 1962)

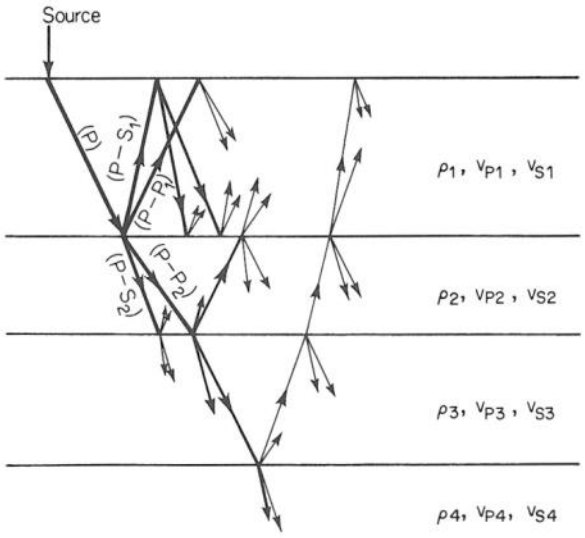

Figure 2-13: Multiple wave reflections and refractions in a layered half-space (Richart et al., 1970)

2.3.7 Propagation of Waves in Mixed Media

Up to this point, this section has been about ideal solids, but soil is not such an ideal medium, and is composed of solids and voids, which may be filled with air or water and described either by *porosity*, n, or *void ratio*, e. By definition porosity is the ratio of void volume, V_v, to total volume, V. Likewise void ratio is the ratio of void volume to the solid volume, V_s.

$$n = \frac{V_v}{V} \qquad 2\text{-}23$$

$$e = \frac{V_v}{V_s} = \frac{n}{1-n} \qquad 2\text{-}24$$

In a completely saturated soil, the voids are totally filled with water, and the degree of saturation, S, is 100 per cent. The theory of propagation of waves in fluids is relatively simpler than in elastic solids because *ideal fluids do not have shear stiffness, cannot develop shearing resistance, shear waves do not occur*, and only compression waves need to be considered.

Depending on the water temperature and salinity, the bulk modulus of elasticity of water, B_w, it can be calculated to be in the order of 2,200 MPa which suggests that, in comparison to soil, water is quite incompressible. Solids suspended in liquids may produce an influence on the propagation of the compression wave because their presence influences both the mass density and the compressibility of the mixture. The effect of *small amount of air in the*

water portion of the mixture is to reduce the compression wave velocity significantly. For any given saturation, *S*, the volumes of air, V_a, water, V_w, and solid , V_s, per unit volume V of the soil are:

$$V_a = \frac{(1-S)}{1+e}V \tag{2-25}$$

$$V_w = \frac{Se}{1+e}V \tag{2-26}$$

$$V_s = \frac{1}{1+e}V \tag{2-27}$$

The total mass density of the solid -air-water mixture, ρ_{tot}, is:

$$\rho_{tot} = \frac{\gamma_w}{g}\left(\frac{Se}{1+e} + \frac{(1-S)e\gamma_a}{(1+e)\gamma_w} + \frac{G_s}{1+e}\right) \tag{2-28}$$

G_S= specific gravity of the solid particles

γ_w = unit weight of water

γ_a =unit weight of air

The bulk modulus of elasticity of the mixture, B, is:

$$\frac{1}{B} = \frac{e}{1+e}\frac{1}{B_{aw}} + \frac{1}{1+e}\frac{1}{B_s} \tag{2-29}$$

where:

$$B_{aw} = \frac{B_w}{1 + \frac{V_a}{V}\left(\frac{B_w}{B_a} - 1\right)} \tag{2-30}$$

B_s=bulk modulus of solid particles

B_a=bulk modulus of elasticity of air

The compression wave propagation velocity in the solid-air-water mixture, v_{mix}, is:

$$v_{mix} = \sqrt{\frac{B}{\rho_{tot}}} \qquad 2\text{-}31$$

It has been calculated (Richart et al., 1970) that only a small percentage (0.1%) of air in a saturated mixture can reduce the bulk modulus of elasticity of water by 16 times.

Theory and research on wave propagation in porous saturated solids (Biot, 1956) shows the strong influence of the structural coupling involved in the compression waves and the lack of structural coupling for the shear waves. Hence, it can be confidently stated that field measurements of shear waves in saturated soils determine the shear wave velocity in the soil structure.

2.4 Theory & Mechanism of Dynamic Compaction & Dynamic Replacement

The concept of this dynamic compaction is improving the mechanical properties of the soil by transmitting high energy impacts to loose soils that initially have low bearing capacity and high compressibility potentials. The impact creates body and surface waves that propagate in the soil, and as shown in Figure 2-14, re-arrange the particles in a denser configuration. The decrease of voids and increase in inner granular contact will directly lead to improved soil properties.

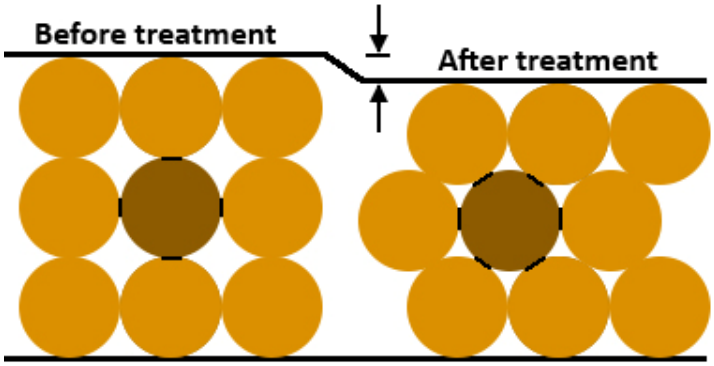

Figure 2-14: Displacement and rearrangement of the soil grains in a denser configuration

Impact energy is delivered by dropping a heavy weight or pounder from a significant height. The pounder weight is most often in the range of 8 to 25 tons although lighter or heavier weights are occasionally used. Drop heights are usually in the range of 10 to 20 m although 40 ton pounders have been dropped from 40 m by Menard's Mega machine.

The behaviour of soil under the impact of the dynamic compaction or dynamic replacement pounder is very complex and a function of a long list of parameters such as soil grading and fines content, water content, soil layers, loading history, liquefaction and dissipation of pore pressures, pounder drop height, pounder weight, pounder shape, pounder size, etc.

The deformation of granular materials upon loading involves particle rearrangement and particle deformation (Cascante and Santamarina, 1996). Particle rearrangement and consequent fabric changes occur at middle and large shear strains (in general greater than 10^{-4}). Fabric changes are affected by surface roughness, degree of frustration of particle rotation, particle size distribution and inter-particle forces. On the other hand, particle deformation is the prevailing deformation mechanism at low strains and depends mainly on

the inter-particle contact response and material properties including elastic, visco-plastic and brittle behaviours.

2.4.1 Behaviour of Elastic Spheres Subject to Shear Loads

As a first approximation to a mass of cohesionless soil, an array of identical spheres with radius, R, shall be assumed (Richart et al., 1970). The spheres are packed in a simple cubic packing pattern in which each sphere is in contact with six neighbouring spheres, and there are no large voids due to the absence of any missing spheres (Figure 2-15a). This is the loosest possible arrangement for equal sized spheres (Figure 2-15c), and produces a void ratio equal to 0.91.

$$e = \frac{V_v}{V_s} = \frac{V - V_s}{V_s} = \frac{8R^3 - \frac{4}{3}\pi R^3}{\frac{4}{3}\pi R^3} = 0.91$$

If the layer on top of the first layer of spheres is translated by a shear load along a path indicated by A-A' in Figure 2-15a, then each sphere of the second layer will fit in a pocket formed by the depression between four spheres of the first layer. If such a translation is applied to all layers, then the pyramidal or face-centred cubic packing of Figure 2-15b will be realised. The void ratio of the new packing can be calculated to be 0.35.

$$e = \frac{V_v}{V_s} = \frac{V - V_s}{V_s} = \frac{\frac{32}{\sqrt{2}}R^3 - 4\left(\frac{4}{3}\pi R^3\right)}{4\left(\frac{4}{3}\pi R^3\right)} = 0.35$$

The void ratio for the tetrahedral or close-packed hexagonal packing (Figure 2-15e) is also 0.35. This reduction in void ratio will decrease the volume or thickness of the packing system by 29.3%.

$$\Delta V = \frac{\Delta e}{1 + e} = 0.293$$

Even further reduction of void ratio is possible if all the spheres are not the same size, and smaller spheres (or in soils, the grains) can be re-arranged to fill in the remaining voids.

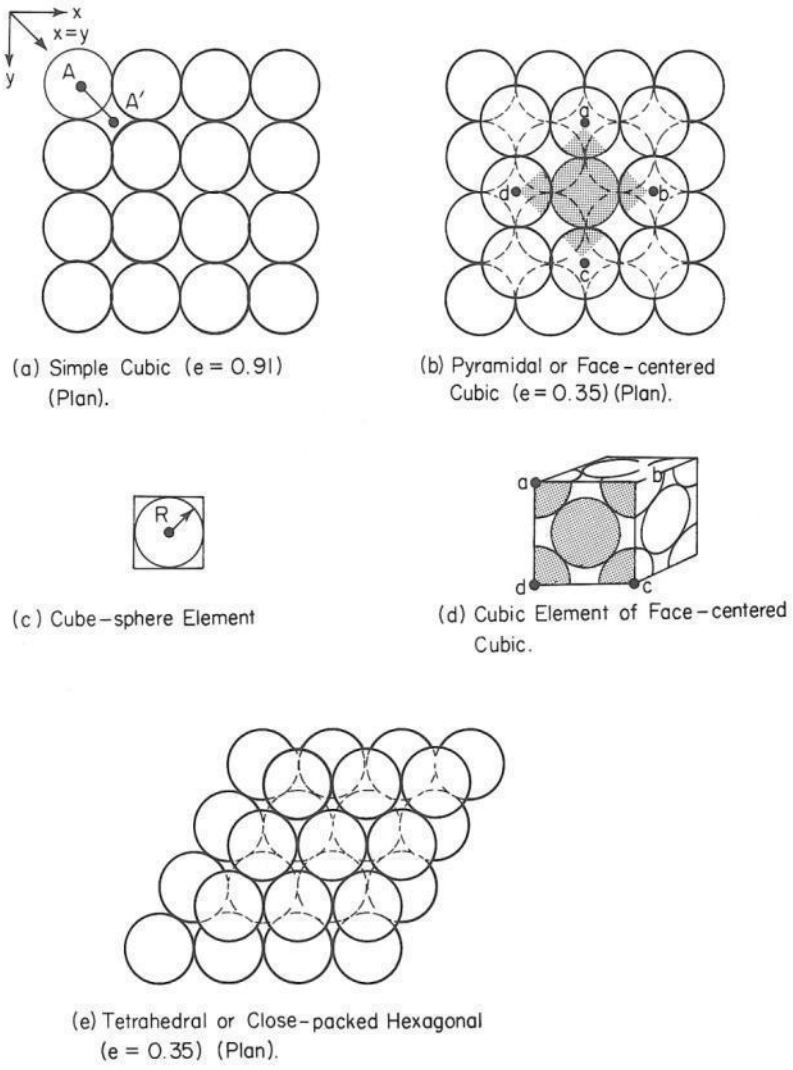

(a) Simple Cubic (e = 0.91) (Plan).

(b) Pyramidal or Face-centered Cubic (e = 0.35) (Plan).

(c) Cube-sphere Element

(d) Cubic Element of Face-centered Cubic.

(e) Tetrahedral or Close-packed Hexagonal (e = 0.35) (Plan).

Figure 2-15: Modes of regular packing of equal spheres (Richart et al., 1970)

2.4.2 Behaviour of Elastic Spheres Subject to Normal Loads

The behaviour of elastic spheres subject to a normal load has also been studied (Hertz, 1881, Timoshenko and Goodier, 1951). Figure 2-16a and Figure 2-16b show respectively two spheres of equal radius *R* just touching and the deformation that occurs when a normal force presses them together.

Upon application of the normal load, *P*, the radius of contact, *a*, will be:

$$a = \sqrt[3]{\frac{3(1-\nu)}{8G}PR} \qquad 2\text{-}32$$

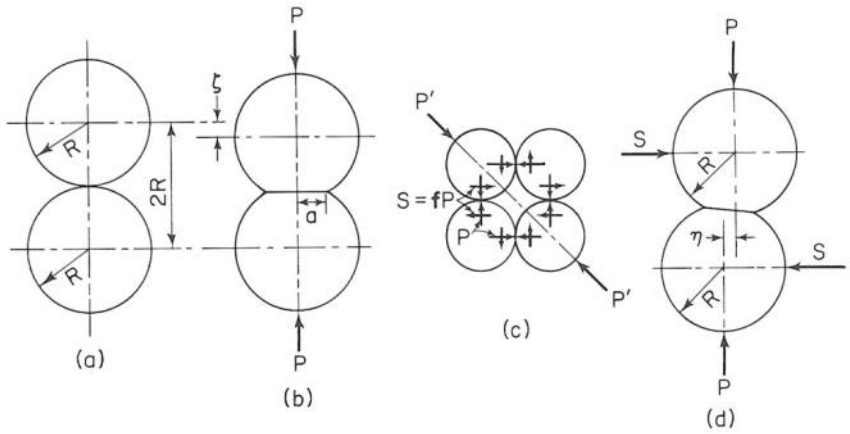

Figure 2-16: Behaviour of equal spheres in contact. (a) Spheres just touching, (b) deformation by normal force, (c) shearing forces between particles in cubic packing, (d) lateral deformation by shearing forces (Richart et al., 1970).

The reduction between the centres of the two spheres, ζ, will be:

$$\zeta = \frac{2a^2}{R} \qquad 2\text{-}33$$

The normal stress, σ, at any point on the contact surface that is at a distance r from the contact surface can be calculated to be:

$$\sigma = \frac{3P}{2\pi a^2}\sqrt{1-\left(\frac{r}{a}\right)^2} \qquad 2\text{-}34$$

The maximum stress (in the centre of the contact surface) is 1.5 times the average stress value, and can be calculated to be:

$$\sigma = \frac{3P}{2\pi a^2} = \frac{4Ga}{(1-\nu)\pi R} \qquad 2\text{-}35$$

The average stress equals to the force transmitted through a row of spheres divided by the effective square cross section of the row (see Figure 2-15c).

$$\sigma_x = \frac{P}{4R^2} \qquad 2\text{-}36$$

2.4.3 Behaviour of Elastic Spheres Subject to Normal and Shear Loads

A more complicated situation may arise when, as shown in Figure 2-16c, the force is applied along a diagonal direction, creating normal and shear forces. This problem has been studied theoretically (Cattaneo, 1938, Deresiewicz, 1974, Mindlin, 1949, Mindlin and Deresiewicz, 1953).

The equations for normal loading were explained in Section 2.4.2. If, as shown in Figure 2-16d, the two spheres of Figure 2-16b are subjected to a normal load and a shearing force, S, then:

$$\sigma_x = \frac{S}{4R^2} \qquad 2\text{-}37$$

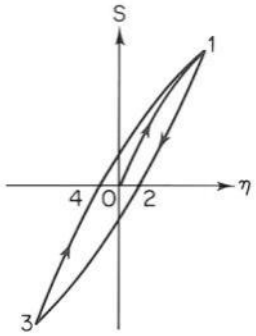

Figure 2-17: Hysteresis loop formed by shearing force-displacement relations for two equal spheres pressed together and subjected to shearing forces (Richart et al., 1970).

The shear force produces a shear displacement, η, between the centres of the spheres. If η is plotted against S for loading and unloading cycles (without exceeding the limit of μP, where μ= the coefficient of friction between the spheres), the hysteresis loop of Figure 2-17 will be produced.

These studied show that a concave stress-strain will be recognised when lateral expansion of the mass of spheres is permitted, and that the stress-strain behaviour depends on the amount of lateral strain developed during axial loading. This discussion also demonstrates that energy is dissipated through friction before sliding.

2.4.4 Crushing of Soil Particles

In addition to the strain-strain behaviour that was modelled and described by elastic spheres that are subjected to normal and shear loads, soil particles can be crushed or broken during loading. The latter will increase volume reduction. For the type of deformation where soil grains move past or around each other, crushing at sliding contacts or breakage of particles decreases the rate of dilation corresponding to a given principal stress ratio (Hardin, 1985).

Hardin (1985) assesses that the amount of particle crushing that occurs in an element of soil under stress depends on the particle size distribution, particle shape, state of effective stress, effective stress path, void ratio, particle hardness (hardness of cementing material or weakest constituent of a particle and weakest particles of an element) and the presence or absence of water. Based on the equations that Hardin has developed, he demonstrates that the crushing hardness of angular shaped particles is more than round shaped grains.

The potential for breakage of a soil particle increases with its size. The normal contact forces in a soil element increase with particle size. Also, the probability of a defect in a given particle increases with size. The breakage of soil particles in a rock fill under moderate stresses may be quite evident, whereas very high stresses are required to crush silt size particles.

In principle, it would be possible to crush all soil particles under extremely high stresses to an extent that no particles remain larger than 0.074 mm. Thus, it may be expected that crushing and breakage of soil particles will increase with the magnitude of the state of effective stress.

The amount of crushing produced by a hypothetical stress may be expected to decrease with increasing particle concentration because the particle contact forces will be reduced by increased concentration. Hence, it can be visualised that loose soils with higher void ratios are subject to more breakage than dense soils.

2.4.5 Liquefaction

Liquefaction is the phenomenon in which the soil loses its strength due to increase in pore water pressure. In cohesionless soils the shear strength, τ, of the soil is due to internal friction only. In a saturated state it may be expressed as:

$$\tau = (\sigma - u)\tan\varphi' \qquad 2\text{-}38$$

σ= total normal stress on the failure plane

u = pore pressure

φ'= effective angle of internal friction

It can be well observed that an increase in u will result in a decrease in τ to the point where the soil's strength becomes zero and the soil liquefies.

Saturated soils can liquefy due to repetitive pounder impacts. The dynamic forces disturb the (granular) soil skeleton, and tend to force the particles to compact into a denser arrangement, which consequently will mitigate liquefaction potential.

In granular DR columns, conceptually, even if high excess pore water pressure build-up occurs within the remediated soil, the imposed shear stresses during seismic loading will be shared between the dense granular columns and the in-situ soil in proportion to the relative stiffness of the two materials; thus increasing overall stability (Adalier and Elgamal, 2004, Baez and Martin, 1993).

As is the case for dynamic replacement columns, according to Murali Krishna and Madhav (2009) granular inclusions mitigate liquefaction because:

- Granular columns function as drains and permit rapid dissipation of induced pore pressures by virtue of their high permeability with the additional advantage that they tend to dilate as they get sheared during an earthquake event.

- Excess pore water pressures generated by cyclic loading are dissipated almost as fast as they are generated due to significant reduction in the drainage path.

- Granular columns compact, reinforce, and improve the deformation properties of the in-situ soil.

- Granular columns are installed in to a very dense state, and are thus not prone to liquefaction. The columns also replace a percentage of in-situ liquefiable soil.

- Granular columns modify the nature of earthquake experienced by the in situ soil.

Furthermore, Adalier and Elgamal (2004) report a number of advantages for maintaining low excess pore water pressure to initial effective vertical stress ratio (r_u):

1. A large portion of the overall soil strength and stiffness is preserved. This will enable the stratum to continue providing the necessary vertical and lateral support to the overlying structure. Maintaining strength may substantially decrease the extent of lateral ground deformation due to dynamic excitation.

2. Preventing large total and differential settlements, which are often associated with r_u values above 0.5 to 0.6 (Ishihara and Yamazaki, 1980, Lee and Albeisa, 1974, Nagase and Ishihara, 1988, Seed et al., 1976, Tokimatsu, 1979). Large settlements at high r_u values are caused by the high volume compressibility of liquefied soil at low confining stresses.

3. Reducing high hydraulic gradients that may cause migration of fine soil particles into the gravel drain; thus reducing the drainage capability.

Seed and Booker (1977) have proposed that the permeability of gravel columns should be at least two orders of magnitude larger than the surrounding soil to avoid significant generation of excess pore water pressure within the columns.

2.4.6 The Mechanism of Dynamic Compaction in non-Saturated Granular Soils

In non-saturated soils, wave energy produces a stress that overcomes the inter-granular friction resistance of the soil grains, and displaces the soil. The grains are consequently arranged in a denser configuration, and the soil undergoes a settlement (see Figure 2-14). The re-arranged soil matrix will have more inter-granular connections; i.e., more friction and thus better mechanical properties.

Similarly, Lukas (1986) describes the process of dynamic compaction densification in moist (partially saturated) soils above the water table primarily due to compaction. Without entering any theories, he states that the energy imparted into the ground causes the particles to move closer together, and consequently results in an increase in the unit weight and strength, and a reduction in the compressibility of the soil.

Nashed (2005) notes that impact energy loss is responsible for the improvements experienced by the deposits due to densification techniques.

Airey et al. (2012) have performed small scale laboratory dynamic compaction tests using high speed photography and digital image correlation techniques to investigate the deformation patterns, calculate soil strains and observe strain localisation. In the experiment a 2 to 1 dry mixture of Sydney sand and non-plastic feldspar silt was used. The test results for drop heights that were 150 to 300 mm suggest that densification occurs due to a series of shock or compaction bands that propagate through the soil, starting from just below the tamper base. Likewise, the sequence of the photographs suggest the compaction bands move through the soil, gradually slow down and ultimately come to a stop at some distance away from the pounder. The conclusion is that as expected, in this process the displacements do not diminish steadily with depth below the pounder. Also the bands were still detectable in the cumulative displacement vectors at the end of the series of drops, and most of the volumetric compression beneath the pounder was concentrated in these bands. Airey et al. reason that shear and volume strain are negligible in between the bands because the positive strains in front of the band are counteracted by negative strains behind it, so that the net effect on the soil after the compaction band has passed is negligible. With further impacts additional compacted bands that lead to the numerous shear strain bands are formed. This experiment was carried out to six blows, and the expectation of Airey et al. was that with more flows, there will be more shear bands filling in much of the space between the pounder and the furthest shear band.

The findings of Airey et al. are very interesting, but do not agree with the personal experience of the author and conclusions of other dynamic compaction physical modellings. The author has performed dynamic compaction with limited number of blows in loose dry sands, but the verification tests, including *Cone Penetration Tests* (CPT) and Pressuremeter Tests, have not shown any signs of banded improvement patterns.

Hajialilue-Bonab and Rezaei (2009) and Hajialilue-Bonab and Zare (2014) have also carried out particle image velocimetry of dynamic compaction to detect soils displacements at high speed. In their experiment Hajialilue-Bonab and Rezaei used fine dry sand from Ana Khatoun, east of Tabriz, and applied up to 15 blows per test. In order to model an axisymmetrical half space, in this experiment pounders in the shape of half discs and weighing 6.5 to 20.04 N were dropped tangentially to the transparent Perspex facing from heights of 567.5 mm to 912.5 mm. Hajialilue-Bonab and Rezaei have not reported strain bands as reported by Airey

et al. (2012). The initial relative density of the test shown in Figure 2-18 was 25%. Depth and radius in Figure 2-18 were normalised by dividing them by the pounder diameter. Figure 2-18(a) shows the variation in relative density after 15 blows. Figure 2-18(b) shows the variation of normalised depth of improvement for different number of pounder drops. The results of this experiment is compatible with what has been reported by Lukas (1986), and it appears that the depth of improvement changes little after the first several pounder blows. Hajialilue-Bonab and Zare (2014) who have advanced the research of Hajialilue and Rezaei (2009) by performing similar particle image velocimetry of dynamic compaction physical modelling have also arrived at similar results to Hajialilue and Rezaei for single and double point poundings.

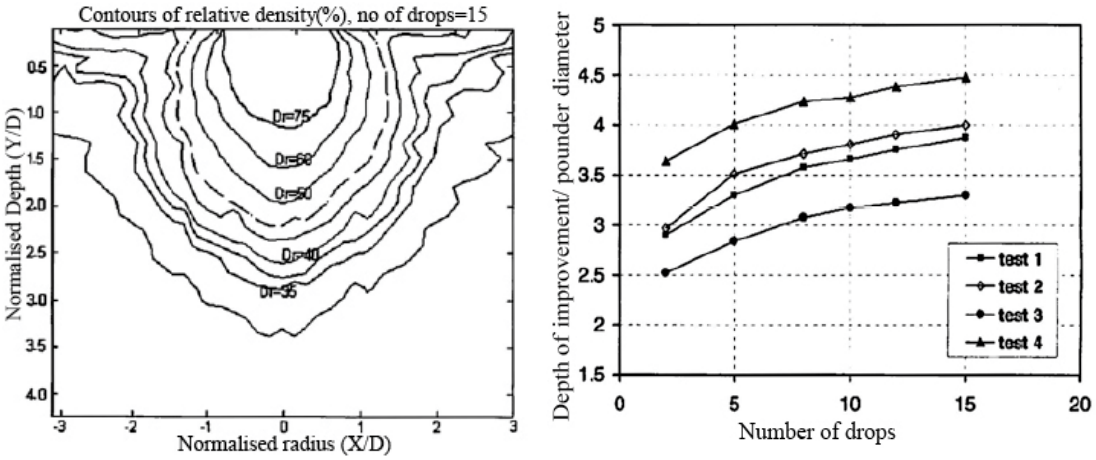

Figure 2-18: (a) Distribution of relative density variations and (b) variation of relative density versus depth under the pounder centre for different number of impacts (Hajialilue-Bonab and Rezaei, 2009)

The author has understood from his personal experience that many people are under the incorrect impression that dynamic compaction is caused by compression. This may be due to a simple misunderstanding that compaction is a result of compression. However, this is not the case; it has already been explained in the previous section that (shear) displacement can cause substantial amounts of settlement simply by rearranging the soil matrix. The contact stress and deformation of soil grains under normal loading was also explained and formulated. The amount of plastic compression that a soil grain will undergo is negligible. Some grains may crush due to the high impact stresses, but that also results in additional settlements originating from shear displacement of the grains and smaller grains fitting into the smaller voids of the soil matrix.

Gu and Lee (2002) have studied the mechanics of dynamic compaction in dry sand using two-dimensional finite element analyses with a large-strain dynamic formulation and a cap model for soil behaviour. Included in the study was the mechanism of ground improvement for a case in which the pounder weight and drop height were respectively 20 tons and 20 m, and the changes at four points, marked as A to D in Figure 2-19, were examined. Points A and B were 0.1 m away from the centreline, and points C and D were 4 m away from the centreline. Point A and C were at the depth of 2 m, and point B and D were 6 m deep.

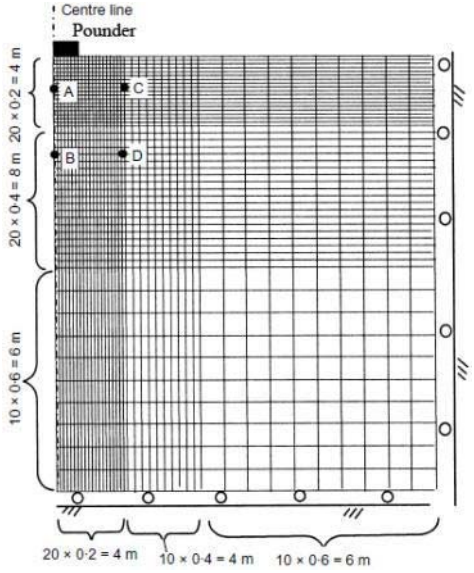

Figure 2-19: Two-dimensional axisymmetric mesh (Gu and Lee, 2002)

The stress path of point *A* during the first three blows is shown in Figure 2-20 . On the first impact, the stress path initially follows the elastic K_0 compression line closely until the first cap is reached. From this point onwards, plastic strains become more and more dominant. As plastic strains are governed by the associated flow rule rather than Hooke's law for elastic strains, the earth pressure coefficient and stress path are different in the two conditions. Therefore, as plastic strains begin to dominate soil deformation, the stress path stirs towards the plastic K_0 compression line, and follows the latter line closely for much of the loading phase, and as the cap expands. Towards the end of the loading phase, the stress path moves towards the shear yield surface, and this path continues for the initial unloading phase.

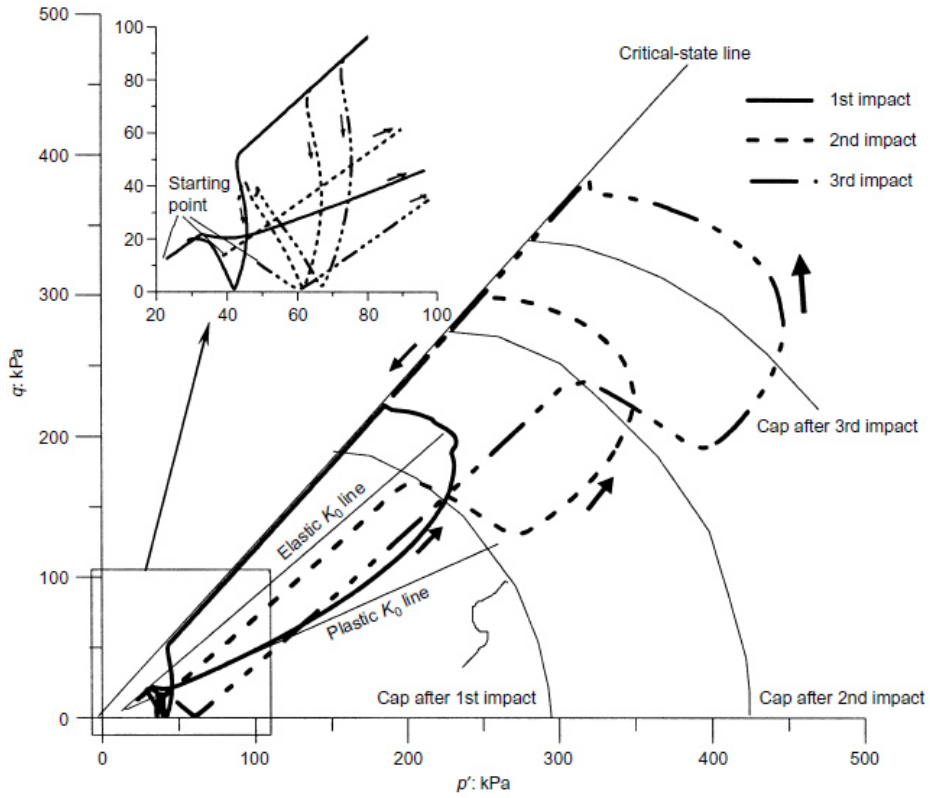

Figure 2-20: Computed p'-q (mean effective normal versus shear) stress path at point A located 2 m below ground surface and 0·1 m from centreline (Gu and Lee, 2002)

Gu and Lee explain the stress path by the effects of lateral inertia as explained by Goh et al. (1998) who have noted that lateral inertia causes lateral strains to lag behind vertical strains in a sand column. Prior to the onset of lateral strains, the sand column compresses in nearly K_0 condition. For the soil beneath the tamper, the onset and rate of increase of lateral strains are also much slower than those of vertical strains, so that the nearly K_0 condition will persist until a sufficiently large lateral strain has occurred. In the first impact a significant proportion of the void ratio reduction occurs at less than 0·2% lateral strain magnitude. As lateral strain accumulates, the stress path diverges from the K_0 line towards the shear failure line under triaxial compression. This effect continues into early unloading, even when the mean effective normal stress, p', is decreasing, being sustained by the lateral outward momentum of the soil beneath the pounder. As the soil dilates, the cap shrinks to the point where lateral outward momentum is dissipated. Towards the end of unloading, the high K_0 induces a passive (or extension) stress state. Since q, the shear stress is always positive, as shown in the inset of Figure 2-20, the transition from a compression to an extension state is demonstrated by kinks in the stress paths at the hydrostatic axis.

Further blows produce larger peak compressive stresses at the same location. Also, the computed zone of improvement deepens with successive blows because, by then, the overlying soil responds elastically more during the loading phase, which results in less energy dissipation. Therefore, additional blows create a deepening compacted soil plug, which enhances propagation of the impulsive stress further downwards. However, the incremental improvement at a given point reduces with successive blows. The net decrease in void ratio attenuates significantly by the third impact, but the crater depth continues to increase. The rapid attenuation of void ratio decrease occurs because progressively higher stresses are needed to enforce further plastic volumetric compression. Furthermore, with successive blows, progressively larger portions of the stress path remain in the elastic zone during loading. By the time plastic volumetric strain commences, significant lateral strains have already occurred, and the stress path starts veering towards the shear yield surface. Thus, with successive blows, the state of the soil along or near the centreline moves from K_0 compression to active shear upon loading. Hence, for regions directly below and near to the crater surface, limiting improvement is reached when plastic volumetric compression is entirely offset by shear-induced dilatancy.

As shown in Figure 2-21, the compaction process is similar at point *B*; however, more blows will be required to achieve a yield surface of equal size, which indicates that the rate of improvement will be slower. Gu and Lee reason that this is due to the lower impulsive stress and the smaller rate of increase in peak dynamic stress, which arises from the dissipative and dispersive effects of the overlying soil. Thus the number of blows needed is determined largely by the soil near the outer fringe of the zone of improvement. Furthermore, there will be little or no dilatancy after the peak stress is reached because the dynamic stress level is lower, and the geostatic stress level at greater depths is higher.

The stress path at point *C* is shown in Figure 2-22. Here, the early loading stress path of each impact is much steeper than those directly beneath the tamper. Furthermore, the peak lateral stress is higher than the peak vertical stress, indicating that the soil is in a passive state. Therefore, the soil outside the tamper footprint is compacted largely by passive compression arising from the lateral outward momentum of the soil beneath the tamper. Also, there is a delay in the onset of improvement in point *C* compared with point A, which, according to Gu and Lee, can be explained by the time needed to overcome the lateral inertia and build up the lateral compressive wave. On the other hand, there is also a smaller delay

between points *B* and *D*, which is consistent with the change in the shape of wavefront from planar to spherical.

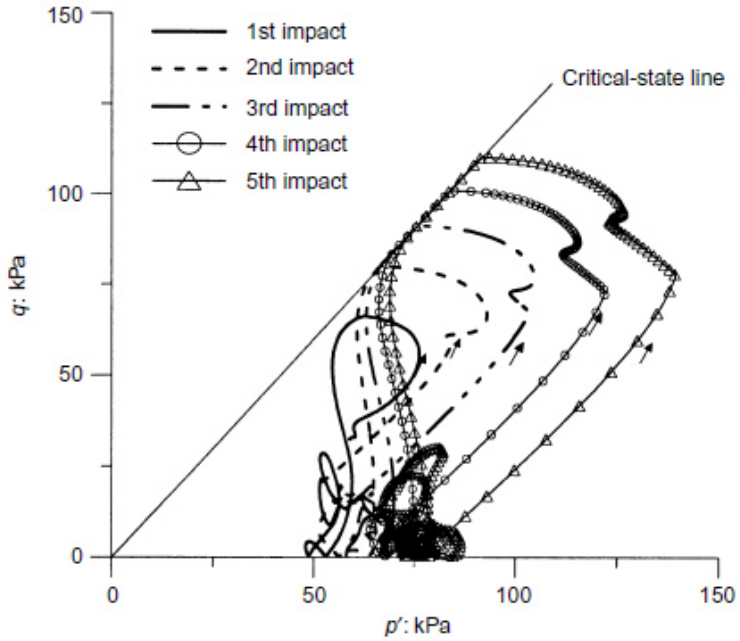

Figure 2-21: Computed *p'-q* stress paths at point B located 6 m below ground surface and 0·1 m from centreline (Gu and Lee, 2002)

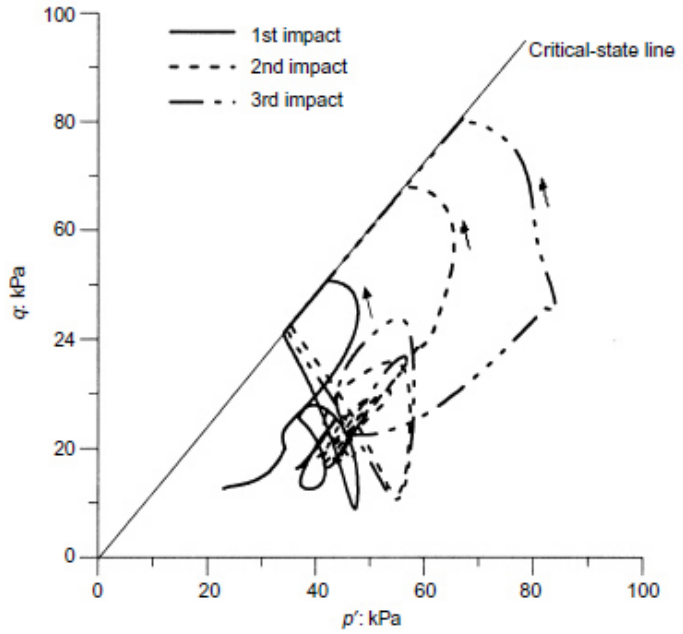

Figure 2-22: Computed p'-q stress paths at point C located 2 m below ground surface and 4 m from centreline (Gu and Lee, 2002)

2.4.7 The Mechanism of Dynamic Compaction in Saturated Granular Soils

In saturated granular soils the pounder impact creates a wave that increases the pore pressure until the soil liquefies, and the soil grains rearrange in a denser configuration. According to Lukas (1986), in saturated soils the energy applied to the soil causes an immediate increase in pore pressure and a reduction in effective stress. As the pore pressure dissipates the soil particles move into a denser state of packing under the confining pressures of the overburden.

As shown in Figure 2-23, Gambin (1997) notes that due to the cycles of compression and depression in the liquid phase, compression waves tend to dislocate the arrangement of the sand grains. If the initial arrangement is loose, the shear waves can then re-arrange the grains into a denser state due to the weight of the soil.

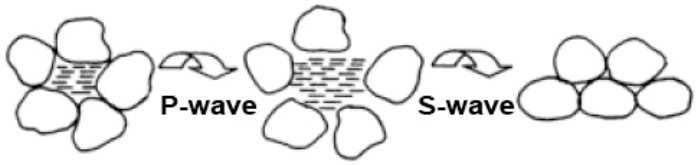

Figure 2-23: Effects of waves in the densification of loose sands (Gambin, 1997)

Liquefaction of saturated granular soils is a process involving energy dissipation due to frictional loss along grain contacts during cyclic loading, leading to contact slips and instability of the soil structure and an increase in excess pore pressures (Thevanayagam et al., 2006). Studies have shown that the magnitude of induced excess pore pressure due to undrained cyclic undrained loading in a saturated energy soil is related to cumulative energy dissipated per unit volume of soil. If the energy dissipated in the saturated loose soil due to dynamic compaction exceeds the energy required to cause liquefaction on a per volume soil basis, then the soil liquefies. Thervanayagem et al. (2006) add that the objective of a vibratory densification scheme is to impart sufficient energy to the soil to be improved by repeated applications of vibratory energy to repeatedly liquefy and densify the soil until its density increases sufficiently.

Without reference, Slocombe (2004) states that laboratory and in-situ tests have consistently shown that in order to achieve maximum density, the lowest number of stress impulses to attain the required energy input will provide the optimum result and further adds that saturated granular soils normally require higher treatment overall energy, in a larger number of tamping passes, than if the soils were essentially dry.

2.4.8 The Mechanism of Dynamic Compaction in Saturated Cohesive Soils

Irrespective of the published case studies (Menard and Broise, 1975, Perucho and Olalla, 2006) that have demonstrated the effectiveness of dynamic compaction for the treatment of saturated cohesive soils, the application of this technique to such soils has always been controversial, and it is the personal experience of the author that the improvement obtained by dynamic compaction in soils classified as Zone 2 and Zone 3 in Lukas' diagram (Figure 2-35), if any, is only a fraction of what could have been achieved in a granular soil of Zone 1.

It is a fact that the classical consolidation theory (Terzaghi and Frohlich, 1936) that was anticipated for explaining the behaviour of saturated cohesive soils does not describe how dynamic compaction could treat saturated soils. However, the reason may be understood once the theory's assumptions are reviewed and compared to the process that takes place during dynamic compaction.

Louis Menard, himself, explains how dynamic compaction is able to treat saturated cohesive soils in the famous paper that he wrote with Broise (1975). This historic paper was the first publication about dynamic compaction in English and many people mistakenly believe that it is the first paper to have ever been published about dynamic compaction (in fact papers were previously published in French e.g. Menard (Menard, 1972). Menard explains his consolidation theory based on compressibility, liquefaction, permeability and thixotropic recovery.

Terzaghi assumes that fine saturated soils are incompressible when subject to rapid loadings because their low permeability does not allow the rapid drainage of pore water and the settlement due to volume changes, however Menard's early observations indicated that performing dynamic compaction did cause the saturated impermeable soils to settle immediately. According to Menard and Broise, subsequent research showed that most quaternary soils contained between 1 to 4% of gas in the form of micro-bubbles. As a first approximation, Menard and Broise assumed that the variations in volume of the micro-bubbles may be essentially governed by the laws of Marriotte and Henry, but went on to state that in fact other less known phenomena also play a fundamental role.

The gas volume in the soil gradually reduces as the soil undergoes repeated impacts. As the percentage of gas approaches zero the soil begins to react as an incompressible material and

liquefies. Menard and Broise define the energy level to reach this stage as the *saturation energy*.

Menard and Broise note that liquefaction in natural soils will often occur gradually. Most natural deposits are layered and structured, and the silty or sandy components will liquefy before the clayey material. It is important that liquefaction of these layers occur while liquefaction of the main clay body must be avoided in order to prevent remoulding of the soil mass. It is therefore imperative to know the exact level of energy corresponding to this threshold condition which is essential to develop high pore-water pressures as to reach high permeability. Once the saturation energy has been reached, further introduction of energy would be totally wasted.

A particular feature that Menard and Broise observed on dynamic compaction sites was the initial very rapid dissipation of pore water pressure, which could not be explained by the coefficient of permeability measured before dynamic compaction. Menard and Broise consider this phenomenon as general and apparent in all soils when conditions tend towards liquefaction, regardless of the grain size. They state that a very slight local increase of pore water pressure is sufficient to commence tearing of the solid tissues by splitting, and the flow of liquid quite naturally concentrates in these newly created fissures.

Figure 2-24: Appearance of water fountains from the fissures due to dynamic compaction

By concentrating the pounding energy at regular grid locations, vertical fissures that are regularly distributed around the impact points are created. These preferential drainage areas are generally perpendicular to the direction of the lowest stress. As shown in Figure 2-24, fountains of water that appear near the craters sometime after pounding under certain geological conditions are initiated and fed by this flow network.

It is the opinion of Varaksin (2014) that rapid dissipation of pore water pressure could be expected and is not unusual when loading is removed. Also, regardless of the air bubbles compression, the experience of the author suggests that improvement in clay is small and in the order of a few per cent.

Menard and Broise have noted that irregular and disorderly pounding can disrupt the continuity of the fissures and render reconstitution more difficult for later and better planned dynamic compaction passes. They also hypothesise that the impact waves transform the absorbed (solid) water into free water. This would encourage an increase in the sectional area of the fissures. The reverse of this phenomenon occurs when the soil resets due to *thixotropy*.

A considerable reduction in shear strength can be initially observed during dynamic compaction. The minimum value will occur when the soil is liquefied or approaching liquefaction. At that time the soil is completely torn, and the absorbed water that plays an important part in stiffening of the soil structure is partially transformed to free water. As pore water pressure dissipates, a substantial increase in shear strength and deformation modulus can be noted. This phenomenon that may continue for several months, and in the opinion of Menard and Broise is due to the closer contact between the particles as well as the gradual fixation of new layers of absorbed water is called thixotropy.

The mentioned above discussion can be presented as shown in Figure 2-25 by using a modified presentation of Terzaghi's hydraulic system of a cylinder filled with incompressible fluid and supported by a spring. Unlike the classical consolidation model, in the dynamic consolidation model the pore water filling the cylinder is considered to be partially compressible due to the presence of micro-bubbles. In the classical model there is no friction in between the piston and the cylinder. In Menard and Broise's model there is friction, which results in hysteresis in the interaction between the hydraulic pressure increase and the intensity of piston surcharge. Hence, a reduction in the pressure of the liquid does not automatically result in a piston movement or a change in the spring. This illustrates a fact that is often observed in foundation soils; i.e., the reduction of pore water pressure without a corresponding settlement of the construction being investigated. In the classical model the spring stiffness (the soil's modulus of deformation) is assumed to be constant. However, considerable modifications of the modulus can be observed under the influence of alternating loading. The absorbed water plays an important part in the process as it becomes partially free. This results in a weakening of the mechanical bond between the solid particles.

Consequently, there will be a reduction in the overall strength of the material. In the classical model, permeability is assumed to be constant, but in Menard and Broise's model, permeability is represented by a variable nozzle section.

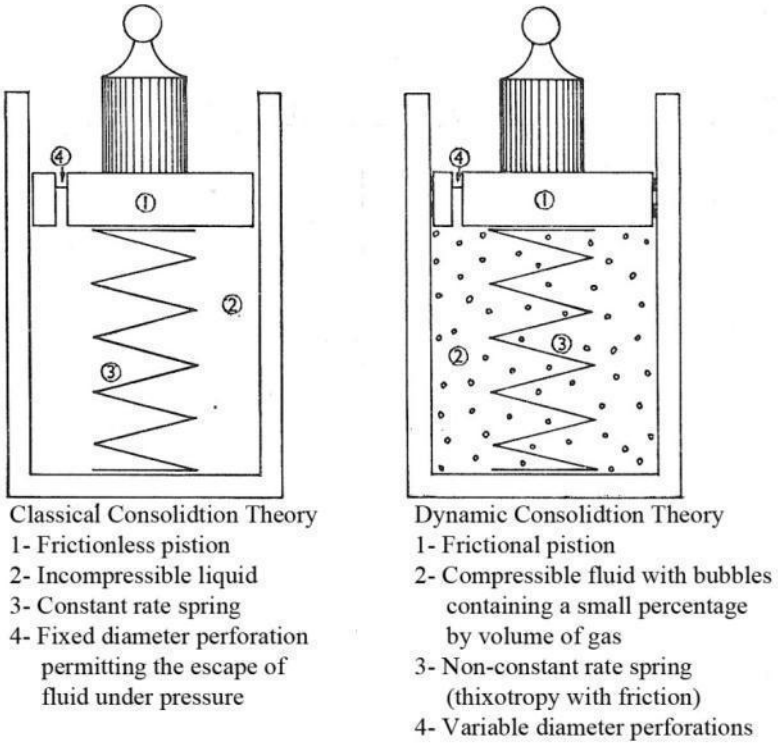

Figure 2-25: Comparison of the classical and dynamic theories of consolidation (Menard and Broise, 1975)

Figure 2-26(a) illustrates the changes in the soil after one pass. The topmost diagram shows the energy applied to the soil by a series of impact at the same print location. The diagram below it presents the soil's volumetric changes, which is then followed by the diagram showing the changes in the pore water pressure. The bottommost diagram refers to the changes of the bearing capacity as a function of time.

Figure 2-26(b) presents diagrams similar to what is shown in Figure 2-26(a) but for multiple numbers of passes. Menard and Broise note that although energy follows an arithmetic progression, the volume changes and bearing capacity do not follow the same law.

While in highly permeable soils, such as sands and gravels, the excess pore water pressure usually dissipates within minutes after the impact, in semi-pervious soils such as silty soils, the time required for excess pore pressure dissipation can range from a few days to a few weeks. In saturated fine soils, it may take weeks for the pore water pressure to dissipate.

Consequently, this has discouraged some researchers such as Lukas (1986) to use dynamic compaction in (pseudo) impervious soils.

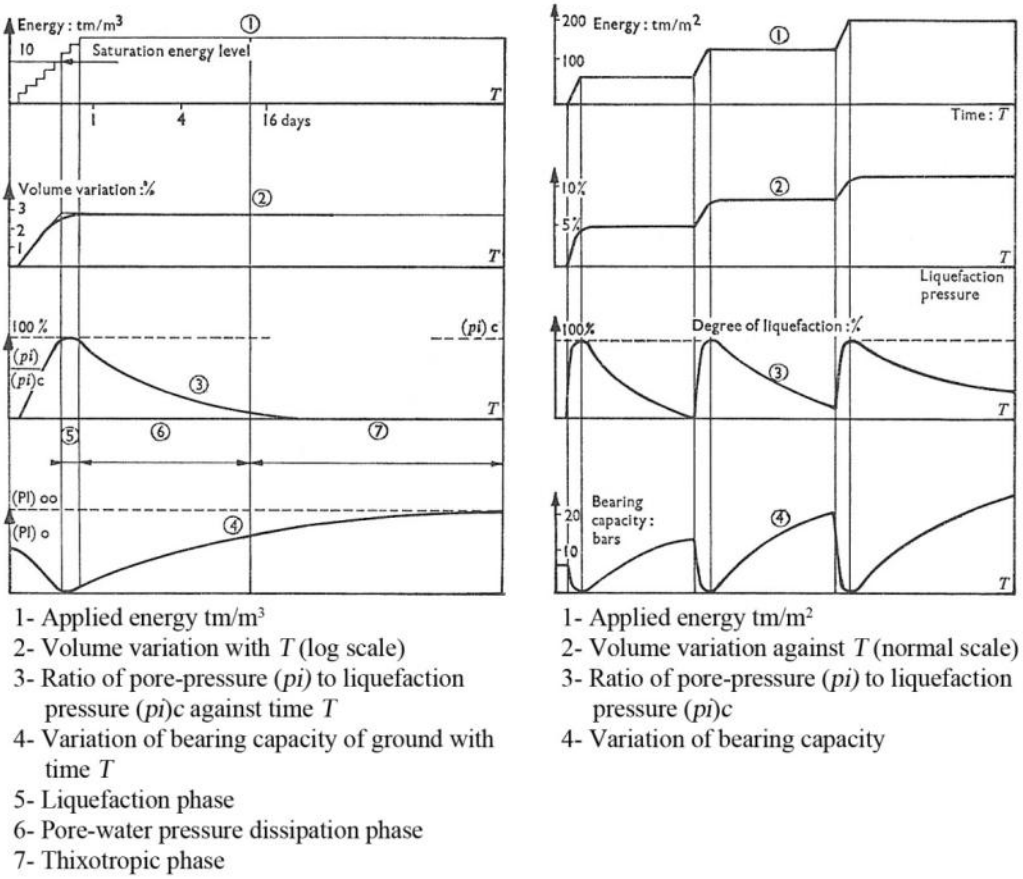

Figure 2-26: (a) Changes in the soil conditions after one dynamic compaction pass, and (b) changes in the soil conditions after a multiple number of DC pass (Menard and Broise, 1975)

2.4.9 The Mechanism of Dynamic Replacement in Saturated Cohesive Soils

There is almost no publication describing the process of dynamic replacement in saturated cohesive soils. What is known by the author is that if sufficient time is not given for the pore water pressure to dissipate, the pounder impacts will cause mostly plastic displacement rather than volumetric change in the soil. In other words, the soil will deform plastically with minimal, if any, volumetric changes, which will result mostly in soil displacement rather than reduction of voids and consolidation. If the overburden pressure of the soil is high, then the displacement will be more laterally oriented. Otherwise the soil will also be pushed towards the ground, and the working platform will heave and perhaps even crack.

If the soil does not displace or only somewhat displaces due to the impact, then the pounder impact must have compacted it. This means that the in-situ soil is behaving more granular (or pervious) than anticipated, and the result of pounding is a mixture of dynamic compaction and dynamic replacement.

When dynamic replacement is implemented, the foundation system usually includes a well compacted granular blanket on top of the DR columns. As illustrated in Figure 2-27, in such a case the loads will be transferred to the soft soil – DR column system by *arching* in the transitional granular layer that is called the *load transfer plataform*. The arching effect and the load distribution by arching will be further discussed in Section 2.6.1.

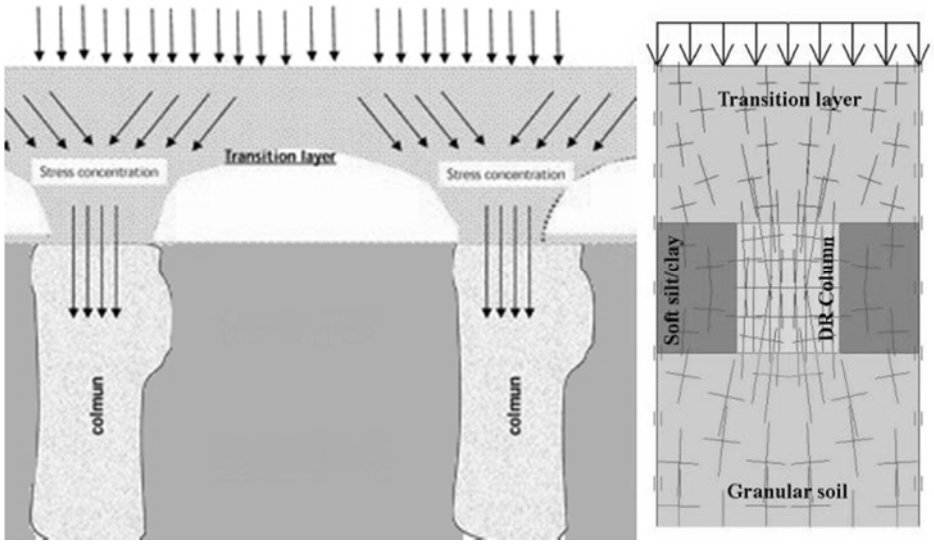

Figure 2-27: The mechanism of load transfer to the improved DR – in-situ soil system

The dynamic replacement crater is backfilled with crushed stone that is dynamically compacted, and pushed into the ground. Additional blows will further drive the material down, with penetration decreasing per blow, to a point where further blows will negligibly compact or drive the crushed stone down any further.

2.4.9.1 Failure Mechanisms in Dynamic Replacement

Hughes and Withers (1974) have performed experiments on model sand columns that were 150 mm long. Column diameters were from 12.5 to 38 mm and as shown in Figure 2-28, loads were only applied to the top of the columns. It can also be noted that the columns were terminated within the soft clay layer with the same cohesion throughout the layer. As shown in Figure 2-29, Hughes and Withers noticed that irrespective of the column length, the pattern of vertical and radial deformation of the columns were basically the same, and

considerable vertical and lateral distortion that occurred at the top of the column rapidly diminished with depth. At failure a length of about four column diameters were significantly strained.

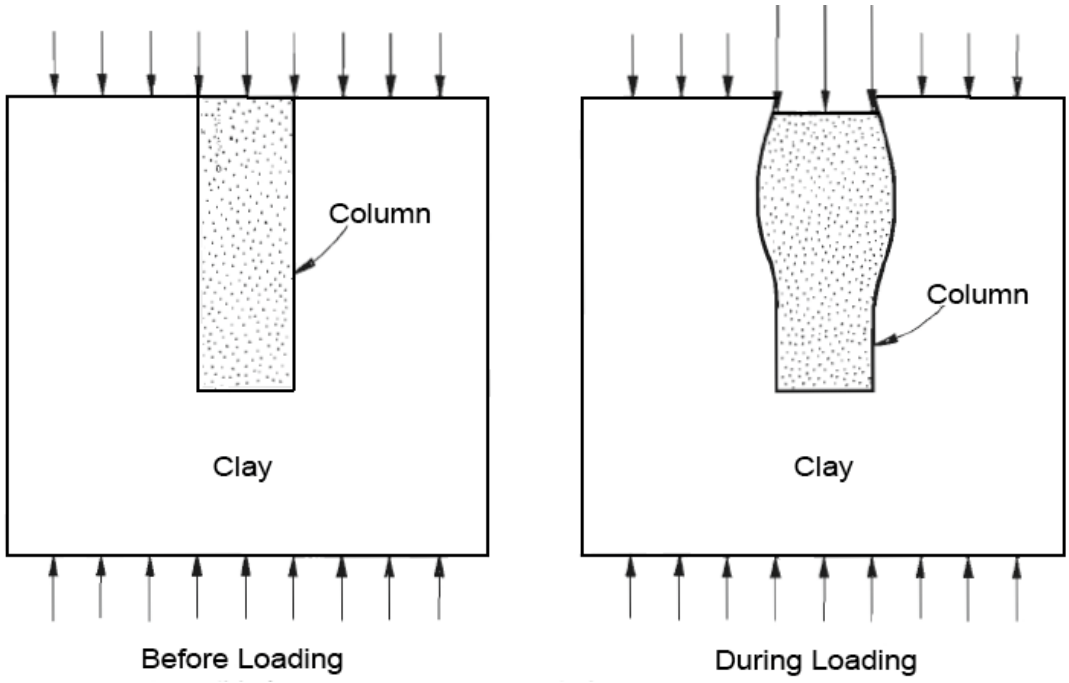

Figure 2-28: Consolidation stresses on the clay before the test, and consolidation stresses on the clay and the loading stresses on the column during the test (Hughes and Withers, 1974)

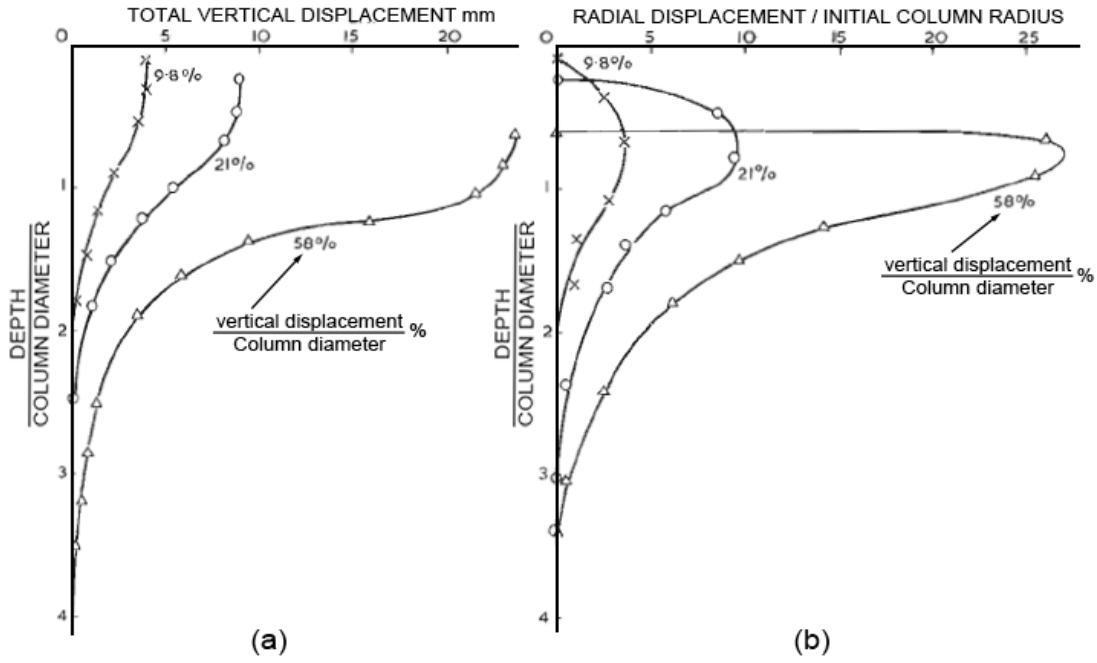

Figure 2-29: (a) Vertical displacement within the column versus depth (b) Radial displacement at the edge of the column / initial column radius versus depth (Hughes and Withers, 1974)

The results showed that the ultimate strength of an isolated column loaded at its top only was governed primarily by the maximum lateral reaction of the soil around the bulging zone, and that the extent of vertical movement within the column was limited. In this particular experiment the vertical movement did not go below four column diameters, and Hughes and Withers concluded that it appeared that if the column length to diameter ratio was less than 4, then the column would fail by end bearing before bulging.

It is interesting to note that although the clay properties at the top and at depth were both the same, column bulging happened only at the top. By equating the forces on a horizontal element of the column and with the assumption that the undrained cohesion was constant over the depth of the column, Hughes and Withers calculated that the vertical stress at depth reduces to zero at a critical depth (4.1 column diameters when the undrained cohesion is constant throughout the treatment depth). As the column length is reduced some of the applied vertical stress will be taken by the soil at the base, and the columns will utilise end bearing resistance. If the columns are made so short that the stress at the base exceeds the bearing capacity of the soil (about 9 times the undrained cohesion), then end bearing failure mode will occur before the bulging. When the length of the column is equal to the critical depth end bearing and bulging failure occur simultaneously, and beyond the critical depth, the stresses in the column reduce to below the ultimate bearing of the cohesive soil and the column will fail by bulging.

Another conclusion of this experiment was that when the undrained cohesion was constant in the soft soil, once the column exceeded about four times its diameter, then any additional length did not increase the column's load capacity because the column failed by bulging, and not in end bearing. However, the author notes that although the ultimate load capacity of the column will not increase beyond about four times its diameter, it may still be necessary to construct longer columns to solve other problems such as settlements and liquefaction.

The failure mechanism as discussed by Hughes and Withers is an idealised condition with the assumption that soil properties are constant throughout the treatment depth. However, this hypothetical ground condition may not be case in many instances. As shown in Figure 2-30, isolated zones of very soft cohesive soils can result in significant bulging at both shallow and deep depths.

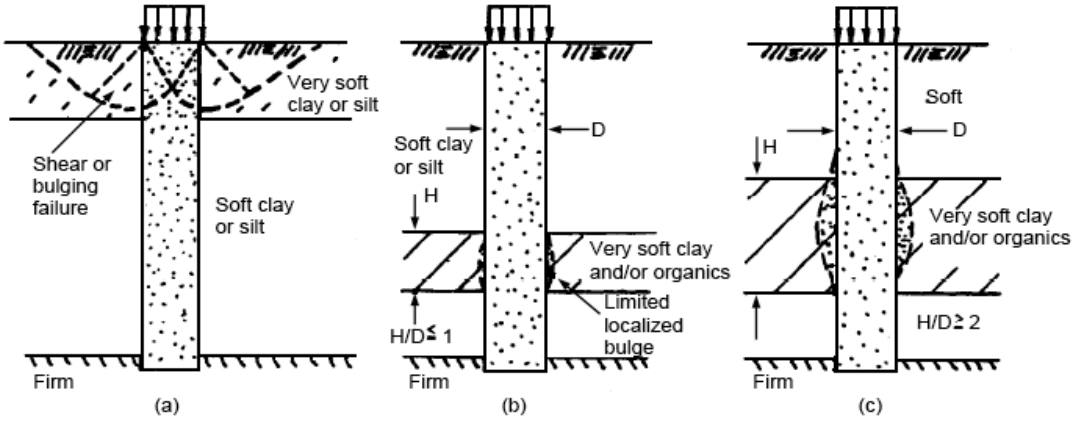

Figure 2-30: Column failure mechanism in non-homogeneous cohesive soil: (a) Soft layer at surface – bulging or shear failure, (b) Thin very soft layer – contained local bulge, (c) Thick very soft layer – bulging failure (Barksdale and Bachus, 1983)

Hughes and Withers also noticed that, as shown in Figure 2-31, only the clay within a cylinder with a diameter of about 2.5 times the column diameter is significantly affected by the loading. This suggests that the columns could act independently if placed more than 2.5 diameters apart.

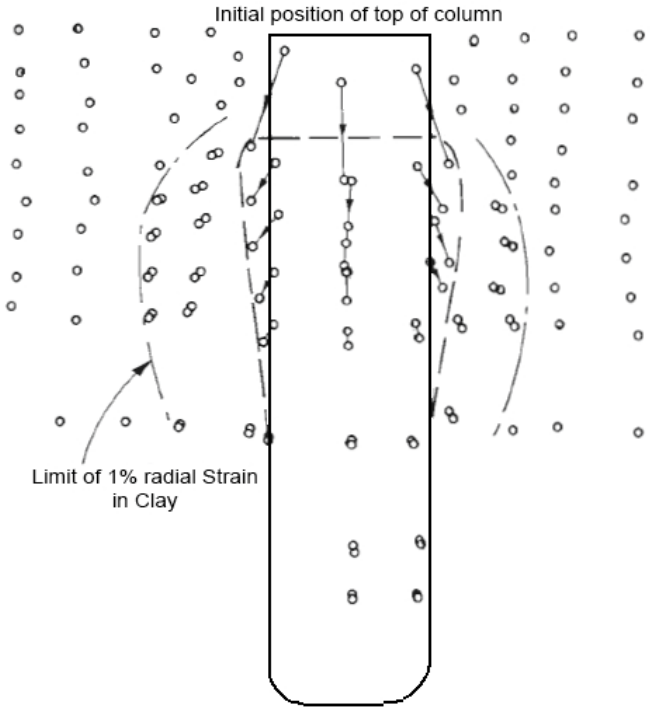

Figure 2-31: Tracing of the superposition of markers due to after loading. A selection of the markers are joined by arrows (Hughes and Withers, 1974)

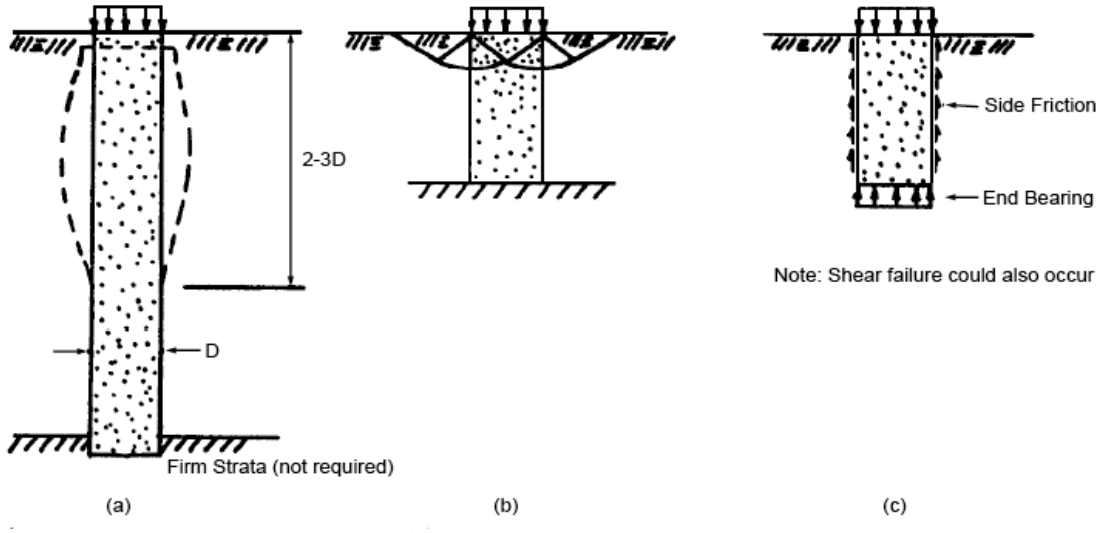

Figure 2-32: Failure Mechanisms of a single (DR) column in a homogeneous soft layer: (a) Long columns with firm or floating support – bulging failure, (b) Short column with rigid base – shear failure, (c) Short floating column - punching failure (Barksdale and Bachus, 1983)

Based on the works of Hughes and Withers (1974), and as shown in Figure 2-32, Barksdale and Bachus (1983) have considered the case where a column is loaded just over the area of the column. Without explaining the reason for the difference between what they understand is the critical length where either bulging or end bearing will govern, they report that when the column length is greater than three (but show a variable length of two to three in their illustrations) diameters, the column will fail by bulging (Figure 2-32a). This may be because they have envisaged a more general case where the undrained cohesion increases and not constant with depth.

The column length to diameter ratio in dynamic replacement is usually from about 1 to 3.5, which is less than 4, and columns are generally pushed down onto a supportive layer. Hence, it could be expected that DR columns in soft soils will usually fail in end bearing mode.

Barksdale and Bachus suggest that the granular working platform serves a dual purpose by not only spreading the load in arching to the column, but also by improving the performance of the columns. The granular blanket forces the bulge to a lower depth where the overburden pressure is greater, and hence will probably result in a larger ultimate load capacity of the column. This is shown in Figure 2-33.

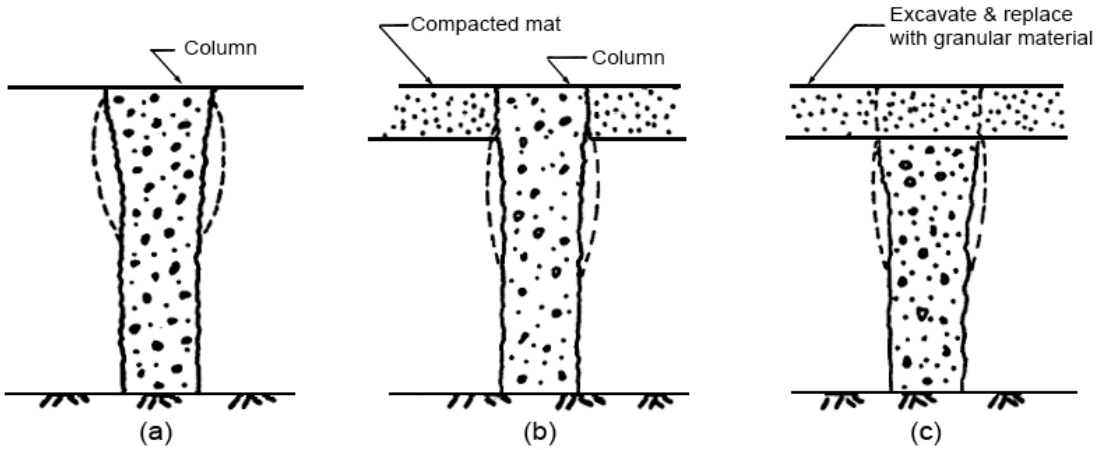

Figure 2-33: Effect of compacted granular working platform on the behaviour of the column: (a) Construction of column without compacted mat, (b) Construction of compacted granular mat prior to the construction of the column, (c) Construction of the column prior to the construction of the compacted granular mat (Barksdale and Bachus, 1983)

Apparently referring to the experiments of Hughes and Withers (1974), Barksdale and Bachus comment that small scale models studies show that the bearing capacity and settlement behaviour of a single column is significantly influenced by the method of applying the load. As shown in Figure 2-34, applying the load through a rigid foundation over an area greater than the column increases the vertical and lateral stress in the surrounding soft soil. The larger bearing area and the additional support of the column result in less bulging and greater ultimate load capacity.

Other possible failure modes of dynamic compaction columns are shown in Figure 2-32(a) and Figure 2-32(b). Shear failure can occur in short columns or columns that are founded on dense soil. Madhav and Vitkar (1978) assess that if the width of a trench (that is a plane strain equivalent of a axisymmetrical DR column) is more than three times the width of the loaded area, then a general shear failure mechanism can be considered, but for larger loaded areas they propose an alternative analysis. Alternatively, short columns on soft ground can fail in punching shear.

Hughes and Withers assess that the behaviour of a typical column within the group is the same as that of an isolated column, and justify that this approach produces an upper bound to an estimate of the settlements and hence can be considered to be conservative.

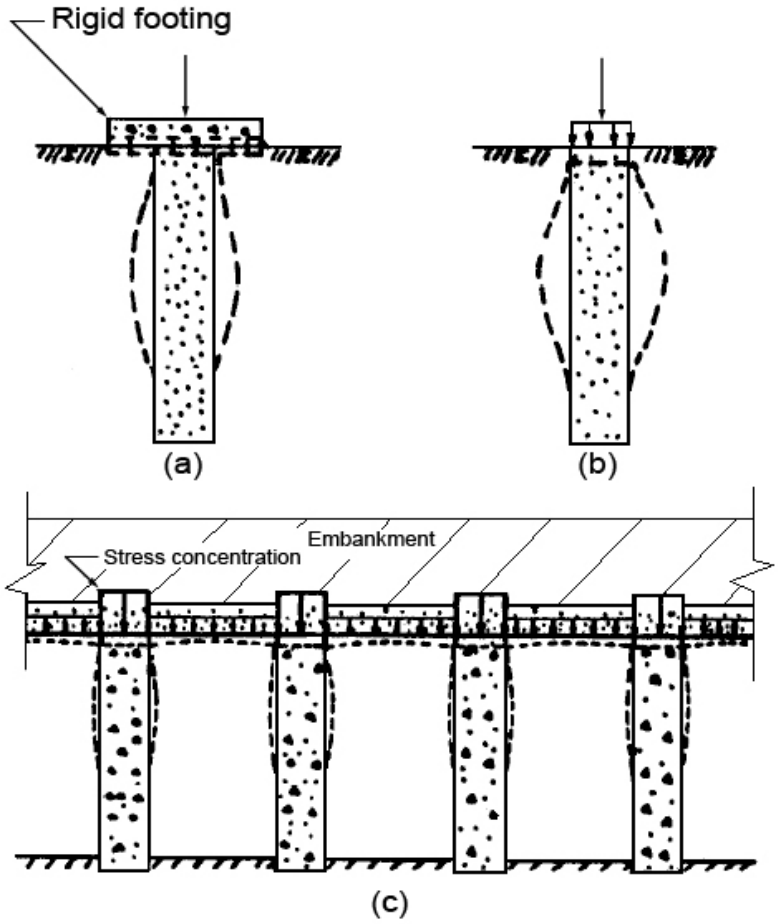

Figure 2-34: Different loading types applied to columns: (a) Rigid footing loading, (b) Plate load test, (c) Embankment loading (Barksdale and Bachus, 1983)

Barksdale and Bachus further remark that the ultimate load capacity of an isolated single column is slightly less than a column group. As surrounding columns are added to form the group, the interior columns are confined and hence somewhat stiffened by the surrounding columns which results in a slight increase in the ultimate load capacity per column. Barksdale and Bachus speculate that a group of columns in a soft soil probably undergo a combined bulging and local bearing type failure. A *local bearing failure* is the punching of a relatively rigid column (or column group) into the surrounding soft soil.

2.5 Design Guidelines for Dynamic Compaction

2.5.1 Suitability of Dynamic Compaction

Varaksin (1981) identifies the main limits of dynamic compaction to be low soil permeability, depth of low permeability soils, thickness of compressible soils, organic content and very soft initial state of soil. He further clarifies that dynamic compaction becomes less and less effective as the soil permeability reduces to less than 10^{-7} m/s when the impermeable layer is too thick. If the soft layer is not located well within the depth of influence, then the degree of densification may become negligible. The depth of influence is limited by the impact energy (and thus the lifting capacity of the equipment). When soil to be compacted includes layers of high organic content, then dynamic compaction can only be applied if the allowable settlement of the structure is less than the long term settlements. Also, if natural soils have a very low resistance and high water content, it is often not possible to obtain sufficient practical improvement.

As shown in Figure 2-35, Lukas (1986) has categorised the applicability of dynamic compaction to soils into three zones of improvement based on soil's grading; i.e., pervious soils, semi pervious soils and impervious soils. Figure 2-35 supplements Table 2-2.

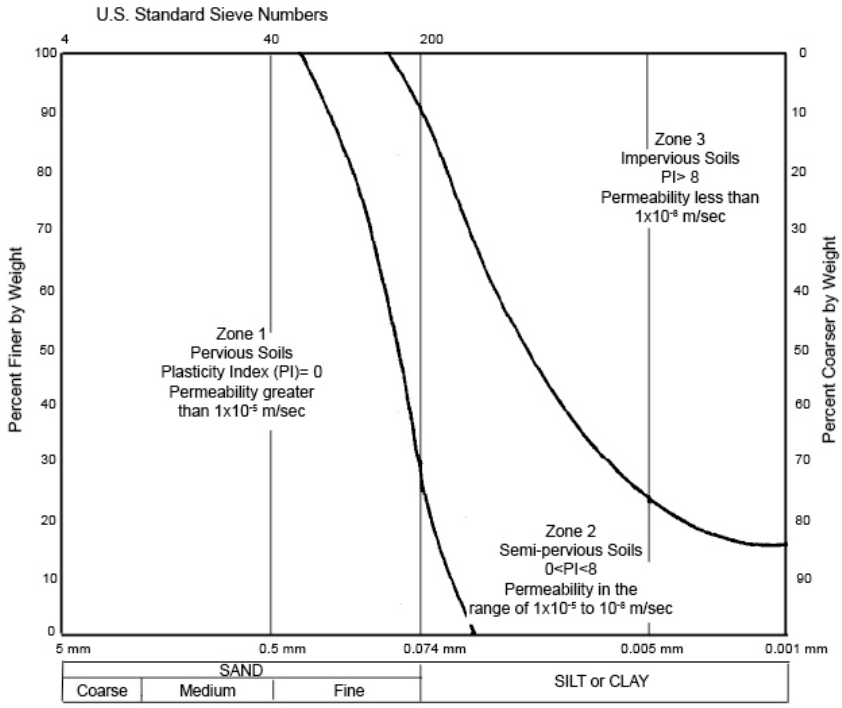

Figure 2-35: Categorising of soil for dynamic compaction suitability (Lukas, 1986)

General Soil Type	Most likely fill class	Most likely AASHTO soil type	Degree of saturation	Suitability for DC
Pervious deposits in the grain size range of boulders to sand with 0% passing the 0.075 mm sieve *Coarse portion of Zone 1**	Building rubble	A-1-a	High or low	Excellent
	Boulders	A-1-b		
	Broken concrete	A-3		
Pervious deposits containing not more than 35% silt *Fine portion of Zone 1**	Decomposed landfills	A-1-6 A-2-4 A-2-5	High	Good
			Low	Excellent
Semi-pervious soil deposits, generally silty soils containing some sand but less than 25% clay with plasticity index is less than 8 *Zone 2**	Fly ash Mine spoil	A-5	High	Fair
			Low	Good
Impervious soil deposits, generally where plasticity index is greater than 8 *Zone 3**	Clay Fill Mine spoil	A-6 A-7-5 A-7-6 A-2-6	High	Not recommended
			Low	Fair – minor improvement- water content should be less than plastic limit
Miscellaneous fill including organic deposits, metal and wood	Recent municipal landfill	None	Low	Fair – long term settlement anticipated due to decomposition. Limit use to embankments.
Highly organic deposits Peat-organic silts		None	High	Not recommended unless sufficient granular fill added and energy applied to mix granular with organic

* These zones are identified on Figure 2-35.

Table 2-2: Suitability of Deposits for Dynamic Compaction (Lukas, 1986)

Among factors influencing the depth of improvement, Luongo (1992) notes that groundwater level and fines content generally influence the effectiveness of dynamic compaction. He further adds that experience indicates that dynamic compaction is generally less effective when the percentage of clay content is greater than 15%, which is a much larger percentage than the personal experience of the auhtor.

Inefficiency of dynamic compaction in soils with high fines content has led to the development of dynamic replacement. As shown schematically in Figure 2-36, in DR the pounder is dropped several times until a crater, which is more plastic displacement than compaction, is formed in the ground. Then the crater is backfilled with crushed stone, and the stone is compacted by dropping the pounder onto it several times. Backfilling of the crater may be done once or several times depending on the ground conditions.

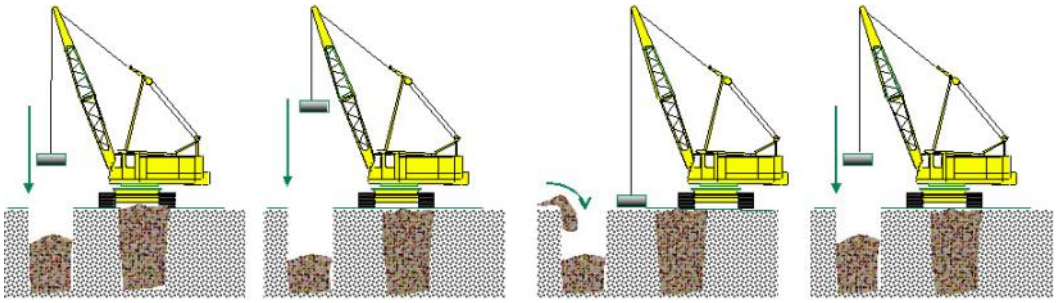

Figure 2-36: The process of dynamic replacement

2.5.2 Depth of Improvement

2.5.2.1 Effect of Impact Energy

The *depth of influence* or *depth of improvement* is a loosely defined term that signifies the depth where there is no more significant improvement in the soil. Menard and Broise (1975) developed an empirical relationship in which as a first approximation the energy per blow, being the product of the pounder weight, *W* (in tons) and drop height, H (in m), was greater than the square of the depth of influence, D:

$$WH > D^2 \qquad 2\text{-}39$$

Varaksin (1981) later proposed that depth of improvement can be predicted by using Equation 2-40:

$$D = c_1 c_2 \sqrt{WH} \qquad 2\text{-}40$$

c_1= speed damping factor

c_2= stratigraphic coefficient, which in the studied case was 0.7

Others such as Leonards et al. (1980), Lukas (1980), Mayne et al. (1984), and Luongo (1992) also reported lower depth of improvement values than the square root of impact energy and Equations 2-39 and 2-40 gradually became better known as Equation 2-41 with a single depth of improvement coefficient, *c*:

$$D = c\sqrt{WH} \qquad 2\text{-}41$$

Although the effect of pounder weight and drop height are of the same order in Equation 2-41, and thus it would appear that the depth of improvement would be equally sensitive to either of them, Menard and Broise (1975) noted that a marked increase in energy efficiency was observed when the impact velocity became greater than the velocity of the wave transmission in the liquefying soil, and thus the tendency to increase the drop height to optimise energy efficiency. Menard and Broise also stated that the maximum depths that correspond to a good efficiency for dynamic compaction are distinctly greater for partially immersed soils than for soils completely out of the water, and added that efficiency is a function of the shape and dimensions of the pounder, the drop height, and the periods of delay observed between phases.

Varaksin (1981) proposed that in Equation 2-40, c_1 should be taken as 1 if the pounder is dropped in free fall, and in the special case of his paper c_2 was taken as 0.7. Later Varaksin and Racinais (2009) further clarified the coefficients by proposing that c_1 should be taken respectively as 0.9 or 1 when the pounder is dropped with a cable or dropped in free fall, and that c_2 should be taken respectively as 0.5 or 0.7 when the soil is heterogeneous or granular.

Lukas (1986) assesses that as the impact energy is proportional to the square of the impact velocity, since the measured velocity of a cable dropped pounder was 90% of the theoretical impact velocity, then the energy delivered to the ground would be approximately 80% of the theoretical potential energy. However, the velocity of free fall pounders appeared to be 97% of the theoretical velocity, and thus free fall impact would deliver 94% of the theoretical impact energy. Therefore, the impact energy of a free falling pounder would be 18% more than a cable dropped pounder. Lukas notes that this has been taken into account in Equation 2-41. Similarly, Yee (1999) suggests that c_1 should be taken as 0.9 for cable drops or 1.2 for free falls, and c_2 should be assumed to be from 0.3 to 0.7 depending on the soil type.

Lukas (1980) observed from post dynamic compaction pressuremeter or Standard Penetration Tests (SPT) that the measured depth of improvement was about 65 to 80% of the maximum value predicted in Equation 2-39. Lukas also reports that the number of passes applied to the treated areas did not appear to affect the depth of improvement.

Leonards et al. (1980) proposed that an increase of more than 3 to 5 SPT blows could be a suitable criterion for determination of depth of influence, and reported that Equation 2-39 expressed as an equality appeared to overestimate the depth of improvement (this is of no surprise because Equation 2-39, was an inequality in the first place that gave an upper bound value, but had turned into the form of an equality in American publications), and that applying a coefficient of 0.5 in Equation 2-41 was able to relate to field measurements more accurately.

The presence of fine soil reduces the efficiency of dynamic compaction. Leonards et al. (1980) observed that clay layers or seams greatly attenuated the effective depth of compaction. They also noted that a suitable criterion for the depth of improvement would depend on the soil type and its initial state of compaction.

Chen and Lin (2002) carried out laboratory scale dynamic compaction on Mai-Liao sand with various fines content to understand the effect of fine soil layers. In their experiment they inserted a manometer under the centre of the pounder's impact point at the bottom of the testing tank. As part of the experiment they varied the fines content of the soil. Without being clear on the soil's water content, Chen and Lin present Figure 2-37 that shows that the relationship of the dynamic compaction induced stress measured by the manometer and fines content. It can be observed that the measured vertical stress reduces as fines content increases. Beyond a certain point, increase of impact energy or momentum does not appear to have any effect. Chen and Lin also experimented by placing thin dry fine soil layers with various thicknesses on the ground surface and above dry sand. The result of this series of trials also showed that increasing the thickness of the fine soil layer reduced the measured vertical stress. Similarly, when the water content of the fine soil layer on ground surface was increased, it was observed that the measured vertical stress reduced. The reduction of vertical stress was more when the fine soil layer was clay rather than silt. Chen and Lin then varied the location of the thin fine layer of soil and experimented with different water contents in the fine soil. This series of experiments indicated that the measured vertical stress reduces as the fine soil layer becomes more superficial.

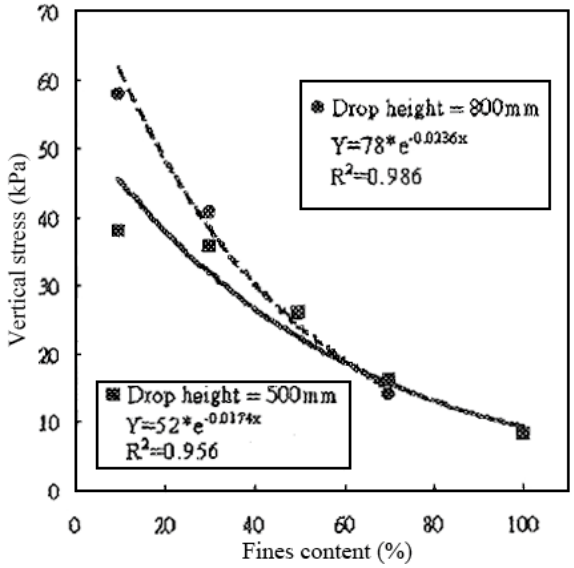

Figure 2-37: The effect of fines content on measured vertical stress(Chen and Lin, 2002)

Mitchell (1981) states that the definition of depth of influence is itself subjective and depends both on the method of measurement and the engineer's definition of what constitutes a measurable ground improvement. He also notes that depth of influence should depend on factors other than just the impact energy; soil type being the most important. Other factors that have been mentioned by him include type of drop (frictionless free drop or dropped with a cable, which is frictional due to the drum and sheaves), and the presence of soft layers that have a damping influence on the dynamic forces. Figure 2-38 shows the depth of influence as a function of impact energy.

Mayne et al. (1984) compiled data from several sites, and as shown Figure 2-39, concluded that the coefficient for depth of improvement is in between 0.3 and 0.8.

Lukas (1986) assessed that other than the pounder weight and drop height other parameters such as soil type, energy applied, base pressure, cable drag, and layer hardness also influence the depth of improvement. Soil type indeed has an important influence on the depth of improvement, and Lukas categorises soils based on their grading into three zones of pervious, semi pervious and impervious (see Figure 2-35). Based on data review, he proposes that the coefficient of depth of improvement should be in the order of 0.35 to 0.4 for partially saturated cohesive fills situated above groundwater level. Lukas notes that optimum water content of fill for dynamic compaction is not known, but speculates that it is probably near the optimum water content as determined by the modified Proctor compaction, which can be estimated as being equal to the soil's plastic limit minus 7 percent (NAVDOCS, 1962).

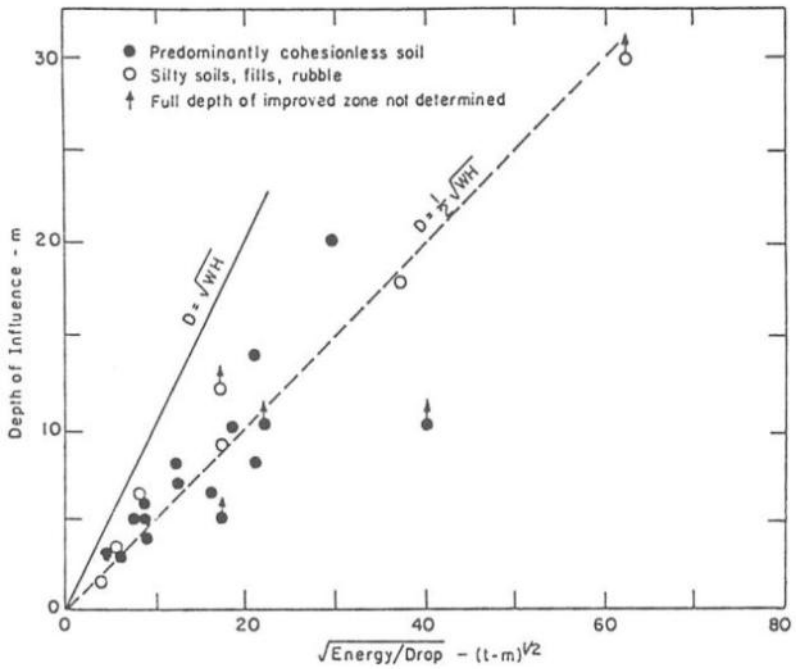

Figure 2-38: Depth of influence as a function of impact energy (Mitchell, 1981)

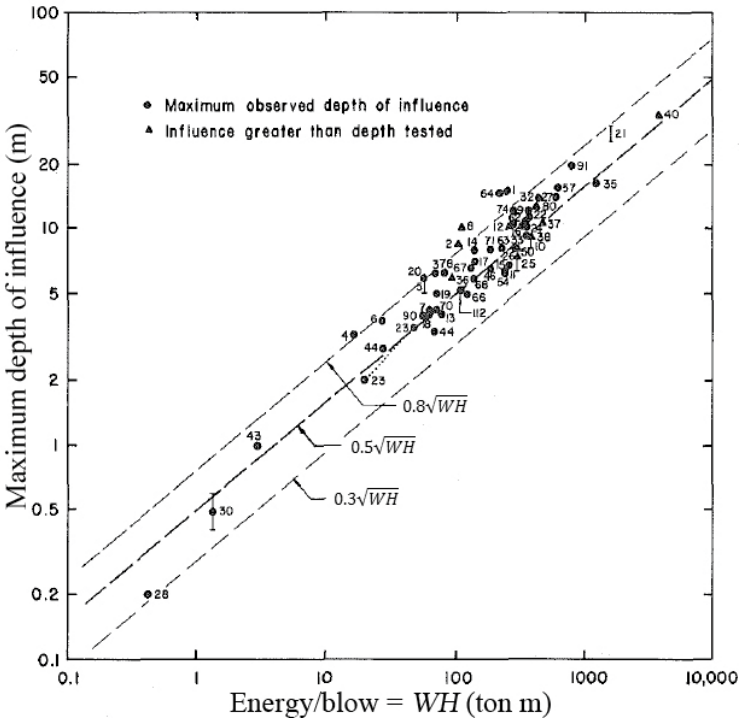

Figure 2-39: Trend between apparent maximum depth of influence and energy/blow (Mayne et al., 1984)

Lukas (1986) considers that the pounder's static pressure; i.e., the weight of the pounder divided by the pounder's base area, also has an effect on energy efficiency. He notes that commonly used pounders have static pressures of 40 to 75 kPa, and further adds that from one end low base pressures could develop a crust of soil and prohibit any soil improvement

below the crust, and from the other end base pressures higher than those mentioned above could result in the pounder punching into the ground upon impact, which reduces energy efficiency. It is the author's experience that nowadays the commonly used pounder static pressure is more than what was envisaged by Lukas as an upper bound, and pressures in the magnitude of 90 kPa are used in most projects. However, the author agrees with Lukas that heavy pounders with smaller base areas punch through the soil, and are thus used in dynamic replacement to create displacement cavities.

When hard or cemented layers occur within the upper portions of the deposits being compacted, these layers will distribute the impact stresses; therefore, the impact energy will not propagate as deep as in a loose deposit. On the other hand, if the hard layer is located near the bottom of the improvement zone, then the presence of the hard layer can improve the densification as a portion of the compression and shear waves reflect and cause additional compaction (Lukas, 1986).

Soil Type	Degree of saturation	Recommended *c* values
Pervious soil deposits	High	0.5
Granular soils	Low	0.5 to 0.6
Semi-previous soil deposits	High	0.35 to 0.4
Primarily silts with plastic index less than 8	Low	0.4 to 0.5
Impervious deposits	High	Not recommended
Primarily clayey soils with plastic index greater than 8	Low	0.35 to 0.4 Soils should be at a water content less than the plastic limit

Table 2-3: Coefficient of depth of improvement for different soil types (Lukas, 1986)

Lukas (1986) proposes that Table 2-3 can be used for conditions when pounders are dropped using single cable lines, with total impact energy ranging from 100 to 300 tm/m^2, and static base pressure varying from 39 to 82 kN/m^2.

As compaction mechanism is similar to Proctor compaction test, depth of influence is greater in partially saturated cohesionless soils. The depth of improvement in saturated soils is less because the sudden large energy release gives rise to immediate build-up of pore pressure, which greatly attenuates dynamic loading with depth (Luongo, 1992).

Based on data obtained from 30 sites, Luongo also proposed Equation 2-42 as a modification for prediction of depth of improvement. It can be noted that Luongo's equation is of the first order of energy and not a function of the square root of the impact energy.

Category		Deposit		
		Pervious	Semi-pervious	Partially saturated impervious fill
General	LB[1]	*D*= 5.6 + 0.009*WH*	*D*= 1.4 + 0.016*WH*	*D*= 2.0 + 0.012*WH*
	Avg[1]	*D*= 7.9 + 0.009WH	*D*= 3.4 + 0.016*WH*	*D*= 2.6 + 0.012*WH*
	UB[1]	*D*= 10.1 + 0.009*WH*	*D*= 5.3 + 0.016*WH*	*D*= 3.3 + 0.012*WH*
sample range		125<*WH*<400 tm	150<*WH*<400 tm	250<*WH*<400 tm
High Groundwater Level	LB[1]	*D*= 4.6 + 0.012*HW*	insufficient data	dynamic compaction not recommended
	Avg[1]	*D*= 7.4 + 0.012*HW*		
	UB[1]	*D*= 10.1 + 0.012*HW*		
sample range		125<*WH*<400 tm		
Low Groundwater Level	LB[1]	insufficient data	*D*= 1.7 + 0.016*WH*	*D*= 2.0 + 0.012*WH*
	Avg[1]		*D*= 3.3 + 0.016*WH*	*D*= 2.6 + 0.012*WH*
	UB[1]		*D*= 4.9 + 0.016*WH*	*D*= 3.3 + 0.012*WH*
sample range			200<*WH*<400 tm	
Pounder base area 4-5 m^2	LB[1]	[2]*D*= -0.2 + 0.024*WH*	*D*=-0.4 + 0.024*WH*	[2]*D*= 4.9 + 0.004*WH*
	Avg[1]	[2]*D*= 1.5 + 0.024*WH*	*D*= 1.3+ 0.024*WH*	[2]*D*= 5.1 + 0.004*WH*
	UB[1]	[2]*D*= 3.2 + 0.024*WH*	*D*= 3.0+ 0.024*WH*	[2]*D*= 5.4 + 0.004*WH*
sample range		200<*WH*<325 tm	150<*WH*<400 tm	250<*WH*<350 tm

[1]LB= lower bound values, AVG= average values, UB= upper bound values

[2]Because of the small number of samples these equations should be interpreted with caution.

Table 2-4: Predicted depth of improvement for different soil deposits (Luongo, 1992)

$$D = c_d + c_e WH \qquad 2\text{-}42$$

In Equation 2-42, D, H and W are the same variables with the same units as Equation 2-41, and

c_d= depth constant

c_e= energy constant

The mean depth of improvements which have been derived from Luongo's (1992) analysis is shown in Table 2-4. Luongo warns that the equations of Table 2-4 should be used with great caution, and only as a guideline since depth of improvement observed will not only depend on the variables discussed, but also on specific site characteristics, the definition of depth of improvement, and the method of measurements used to quantify depth of improvement. In Table 2-4 rock fill deposits are not considered, impact energy is from 100 tm to 400 tm, the reduction of impact energy due to cable drag and absorbing layers is considered, high groundwater level is equal to or less than half of the depth of improvement, low groundwater level is greater than half of the depth of improvement, and data used for depth of improvement for pounder area category includes both high and low groundwater levels.

Rollins and Kim (1994) studied 6 mostly semi impervious, primarily silt, collapsible deposits and found the coefficient of depth of improvement, *c*, to be 0.4; however, the coefficient of determination, R^2 was a low 0.4. They also tried a second order polynomial, which turned out to give a much better prediction with R^2 of 0.9. This relationship is shown in Equation 2-43. In comparison with the best fit line, the best fit curve predicted somewhat greater depths of improvement at lower energies but somewhat lower depths at the very highest energies. 16 years later Rollins and Kim (2010) published an updated study which included an additional 9 case studies. While this study remained in line with their earlier publication, R^2 for the polynomial regression reduced to 0.75.

$$D = 0.586\sqrt{WH} - 0.009WH \qquad 2\text{-}43$$

Van Impe and Bouazza (1996) reviewed data of dynamic compaction in solid waste materials, and concluded that the coefficient in Equation 2-41 was from 0.35 to 0.65. The lower limit corresponded to old landfills; i.e., fills older than 15 to 20 years, and the upper limit was for young landfills; i.e., fills that were less than 15 years old.

Vuola and Hartikainen (1999) somewhat modified Equation 2-41, and proposed the depth of improvement equation for layered ground to be as given in Equation 2-44.

$$D = f_C f_M f_B \sqrt{WH} \qquad 2\text{-}44$$

f_C = cushion (crushed stone platform) factor

f_M = material (soil) factor

f_B = bottom factor

According to Vuola and Hartikainen f_c can be taken as 1 if the cushion is proper. An unproper cushion reduces maximum depth of improvement. In their specific research they report f_c to be approximately 0.8 to 0.9 in one of the investigated sites. Vuola and Hartikainen propose from literature sources that f_M is in the range of 0.65 to 0.75 for saturated sand, and derive a value of 1.5 to 2 for f_B when they encountered rock on one of the sites. They state that rock at a finite depth increases the maximum compaction depth, and contribute the reason to impact waves reflecting from the bottom. Wave interference increases dynamic stresses and strains in soil, and increases compaction depth.

Hajialilue-Bonab and Rezaei (2009) have proposed one of the most rational criterion for depth of influence by relating this depth to volumetric strain rather than in-situ field tests or relative density values. In their study, they assume that depth of influence is the depth at which volumetric strain reduces to 1.5%. In order to predict this depth, Hajialilue-Bonab and Rezaei developed a laboratory scale physical model of dynamic compaction, and used particle image velocimetry to plot soil (fine poorly graded dry sand) deformations, and based on energy intensities (pounder impact energy divided by pounder base area) of 0.837 to 5.566 kN.m/m^2 they developed a relationship between the depth of improvement, D (in m), pounder weight, W (in tons), pounder drop height, H (in m), diameter, d (in m), number of drops per print, N, and pounder base area, A (in m^2) which is presented in Equation 2-45; however, the author notes that there is an inconsistency in their paper as D appears in two forms in the publication, sometimes in the numerator and sometimes in the denominator of the right hand side of the proposed equation.

$$\frac{D}{d} = 0.7669\mathrm{Ln}\left(\frac{NWH}{AD}\right) - 3.004 \qquad 2\text{-}45$$

With D appearing in the denominator, the form of parameters presented in Equation 2-45 is similar to Equation 2-70 that will be presented later, but the author has inserted values for the parameters, and the equation yields unrealistic results.

Inserting D in the numerator, as shown in Equation 2-46, yields more acceptable results. The author has corresponded with Hajialilue-Bonab and Rezaei and awaits their feedback at the time of compilation of this thesis.

$$\frac{D}{d} = 0.7669\text{Ln}\left(\frac{NWH}{A}D\right) - 3.004 \qquad \text{2-46}$$

Hajialilue-Bonab and Rezaei noticed that, as shown in Figure 2-40, normalised depth of influence and normalised crater depth appear to have a linear relationship, and thus also proposed alternative formulas, to predict the depth of influence based on crater depth, D_c. These formulas are presented in Equations 2-47 and 2-48.

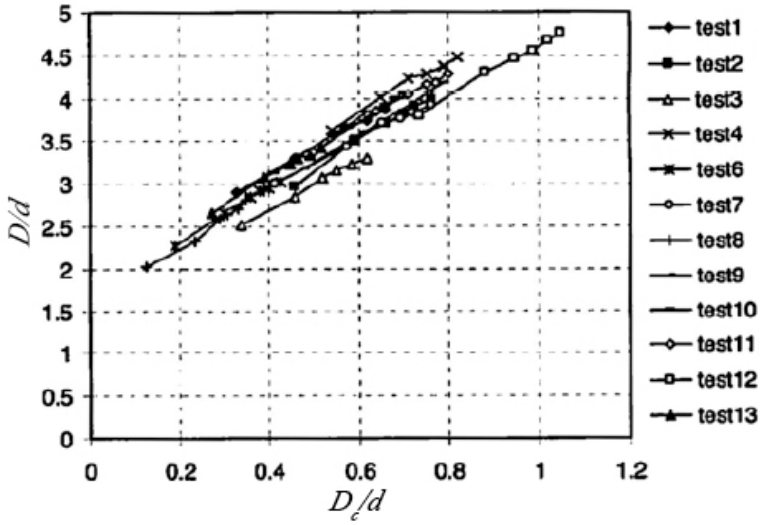

Figure 2-40: Correlation between depth of influence and crater depth (Hajialilue-Bonab and Rezaei, 2009)

$$\frac{D}{d} = 3.1\frac{D_c}{d} + 1.75 \qquad \text{2-47}$$

Or:

$$D = 3.1D_c + 1.75d \qquad \text{2-48}$$

d = pounder diameter

It is the author's experience that the estimated depth of influence from Equations 2-47 or 2-48 is an underestimation of what should be expected in the field, and what is predicted by other methods. For example, with a conservative value of c= 0.63 for granular soil, Equation 2-41 predicts that the depth of improvement for a 15 ton pounder, with a diameter of 1.6 m, that is dropped from 20 m would be 10.9 m. Equations 2-47 or 2-48 predict the

crater depth to reach such a depth of improvement would have to be about 2.6 m, which is much more than what is measured on site.

2.5.2.2 Effect of Pounder size on Depth of Improvement

Ghasessemi et al. (2009b) performed a numerical stimulation of dry and moist sands using a finite element programme to determine depth of improvement. In the studied conditions, pore flow did not exist, and a cap model was assumed to define the soil behaviour. Ghassemi et al. conducted a series of numerical models using different combinations of pounder weights ranging from 15 to 25 tons, drop heights varying from 10 to 20 m and pounder radii of 0.8 to 1.8 m. In all analyses 15 drops were modelled, and the depth of improvement was determined based on the increase in relative density.

The obtained results suggested that the influence of sand type and initial relative density was small when the results were presented in terms of change in relative density; hence, they focused their study on cases in which initial relative density was 40%. The study also showed that the soil did not undergo any significant compaction after 15 blows. Assuming that SPT blow counts (with 60% efficiency) increase by 3 at depth of improvement, and by considering a relationship between SPT blow counts and relative density (Skempton, 1986), they calculated that after 15 blows, relative density would increase by 4% at depth of improvement.

As shown in Figure 2-41, Ghassemi et al. observed that the coefficient of depth of improvement in Equation 2-41 reduces as impact energy increases. Ghassemi et al. have not proposed an equation for the relationship between *c* and *WH* (impact energy per drop), but it can be approximated from Figure 2-41 that:

$$c = 0.65 - \frac{WH}{2500} \qquad 2\text{-}49$$

By replacing the Equation 2-49 into Equation 2-41, it can be derived that:

$$D = \left(0.65 - \frac{WH}{2500}\right)\sqrt{WH} \qquad 2\text{-}50$$

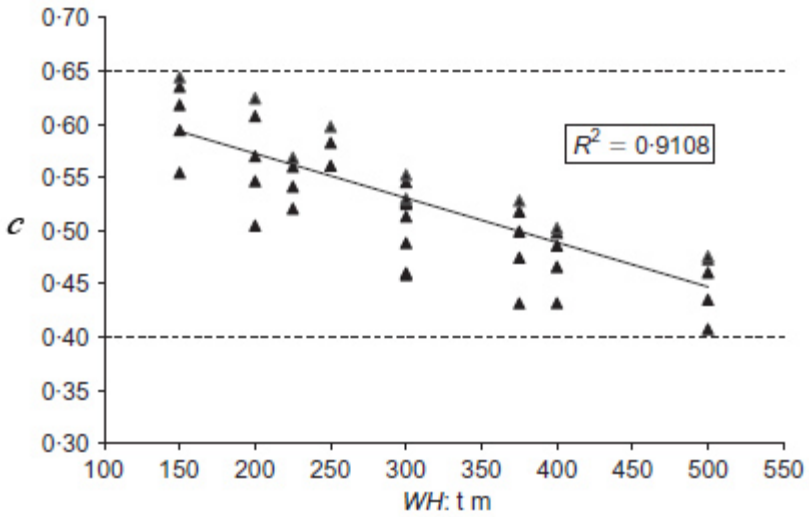

Figure 2-41: Variation of c with impact energy per drop (Ghassemi et al., 2009b)

By reviewing the results of the analyses, Ghassemi et al. proposed a relationship in which, as formulated in Equation 2-51, the depth of improvement is a function of pounder weight, pounder drop height and pounder radius, r (in m).

$$D = 2\sqrt[4]{WHr} \qquad 2\text{-}51$$

Ghassemi et al. have not attempted to relate Equation 2-51 to Equation 2-41, but the author has done so. If the 4th root of *WH* is multiplied in the numerator and denominator of the right hand side of Equation 2-51, the same equation can be presented in the form of Equation 2-522-54.

$$D = 2\sqrt[4]{\frac{r}{WH}}\sqrt{WH} \qquad 2\text{-}52$$

In other words, the coefficient of depth of improvement is as per Equation 2-53

$$c = 2\sqrt[4]{\frac{r}{WH}} \qquad 2\text{-}53$$

Although it could be expected that depth of improvement would increase with the pounder radius and stress bulb size, it is rather unexpected that the efficiency of penetration has an

inverse relationship with the impact energy itself. The same trend could be observed from Equation 2-49.

Zou et al. (2005) has cited that Fei et al. (2002) has performed a series of model tests of dynamic compaction on loess, and have developed Equation 2-54 for depth of influence.

$$D = \sqrt{\frac{W^{\frac{2}{3}}HN}{d\rho_d(1-\bar{\omega})}} \qquad 2\text{-}54$$

In addition to the parameters that have previously been defined

ρ_d = dry density of soil (in kg/m^3)
$\bar{\omega}$= average water content of soil.

Input of real figures into Equation 2-54 yields unrealistically low values of depth of improvement. For example if W= 16.5 m, H= 20 m, d= 1.54 m, N= 15 blows, ρ_d = 1650 kg/m^3 and $\bar{\omega}$= 10%, then depth of improvement will be a mere 0.92 m. At the same time, depth of improvement can be predicted to be approximately 8 m using the same values for the parameters that are used in Equation 2-51. The author has tried to communicate unsuccessfully with Zou et al. for a clarification.

2.5.2.3 Effect of Momentum

Even though most research has been concentrated on impact energy (WH), and Menard and Broise had observed a marked increase in energy efficiency when the impact velocity became greater than the velocity of the wave transmission in the liquefying soil, and thus the tendency to increase the drop height to optimise energy efficiency, it is of interest to study the influence of impact momentum on the volume and depth of improvement.

Oshima and Takada (1994, 1997, 1998) have studied the influence of momentum in dynamic compaction. They reason that if the ground is plastic and the pounder does not rebound after impact; i.e., the impact is perfectly inelastic, then pounder penetration into the ground could be considered to be governed by the law of conservation of momentum rather than by the law of conservation of energy. They further add that this is because of the large loss of energy due to plastic deformation of the ground and the emission of heat and sound. Based on results of measurements of actual field work and centrifuge model tests and laboratory

compaction tests, Oshima and Takada conclude that the period of pounder impact is proportional to the quotient of the pounder weight divided by the pounder base area, and is not influenced by the drop height. They also conclude that maximum acceleration of the pounder during penetration into the ground is proportional to the square root of the drop height.

Oshima and Takada performed a number of centrifuge dynamic compaction tests using various pounder weights under constant pounder drop heights, different pounder drop heights under constant pounder weights, and combined pounder weight sand drop heights with constant kinetic energy per blow. Oshima and Takada did not observe any substantial differences among the tests when pounder drop height, pounder base area, total kinetic energy ($mgHN$, where m is pounder weight) and total pounder momentum (mvN, where v is given in Equation 2-57) were kept constant, but the pounder weight was made variable. However, they did notice deeper and enlarged improvement volume when the pounder weight, pounder base area and total kinetic energy were kept constant, but total momentum was increased by varying the drop height and number of blows. When the pounder weight, drop height, and base area were combined in such a way that the kinetic energy per blow and pounder weight per unit area of pounder base remained constant, it was also observed that the depth and volume of improvement increased with the increase of momentum. From these results Oshima and Takada concluded that it was clear that pounder weight had a predominant effect on compaction of sandy soils, followed by the ram drop height and number of blows, and that the compacted volume size was more influenced by pounder momentum rather than pounder kinetic energy. They also concluded that the depth and radius of improvement was proportional to the logarithm of total pounder momentum, and that the volume of compaction could be estimated by the total pounder momentum. Oshima and Takada proposed that it is possible to estimate the maximum depth and radius of the bulb shown in Figure 2-42 for any increase of relative density by using Equations 2-55 and 2-56.

$$Z = a_z + b_z \log mvN \qquad 2\text{-}55$$

$$R = a_R + b_R \log mvN \qquad 2\text{-}56$$

$$v = \sqrt{2gH} \qquad 2\text{-}57$$

a_z, b_z, a_R and b_R are constants.

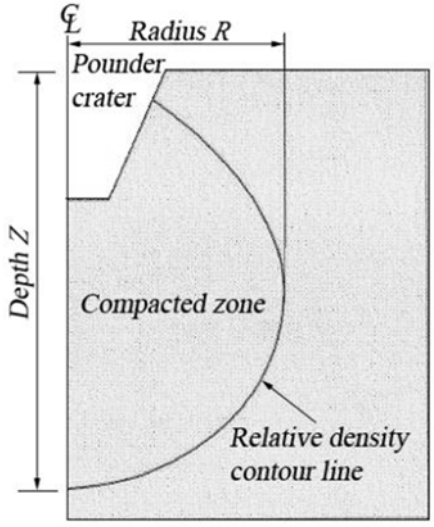

Figure 2-42: Definition of depth and radius of compacted zone for any relative density contour line (Oshima and Takada, 1997)

Gu and Lee (2002) studied the mechanics of dynamic compaction using two-dimensional finite element analyses, and similar to Oshima & Takada (1998), assumed that depth of improvement was the depth at which the increase in relative density reduced to 5%. The computed results indicated that the soil under study did not undergo any significant further compaction after about 15 blows. The coefficient of depth of improvement in the numerical study was in the range of 0.55 to 0.625, and comparison of results with the findings of Oshima & Takada (1998) showed that the error between the numerical and experimental depth of improvement was less than 10%. The analyses also showed that in the initial blows stress wave propagation induces transient elasto-plastic K_o compression due to lateral inertia, which preserves the plane wavefront, and reduces the attenuation rate of the dynamic stresses with depth. With multiple blows, the effect changes to one of triaxial compression, which sets a limit on the degree of improvement that can be achieved in the near field. At greater depths, the wavefront adopts a bullet shape, and the attenuation rate rises, which sets a limit on the depth of improvement. Both of these phenomena are consistent with the existence of a threshold.

Similar to the conclusions of Oshima and Takada (1994, 1997), the numerical analyses of Gu and Lee also showed that, in addition to energy per blow, depth of improvement is also

dependant on momentum per blow. As can be seen in Figure 2-43, even if energy per blow is kept constant, an increase in momentum will enlarge the zone of improvement, and deepen the depth of influence.

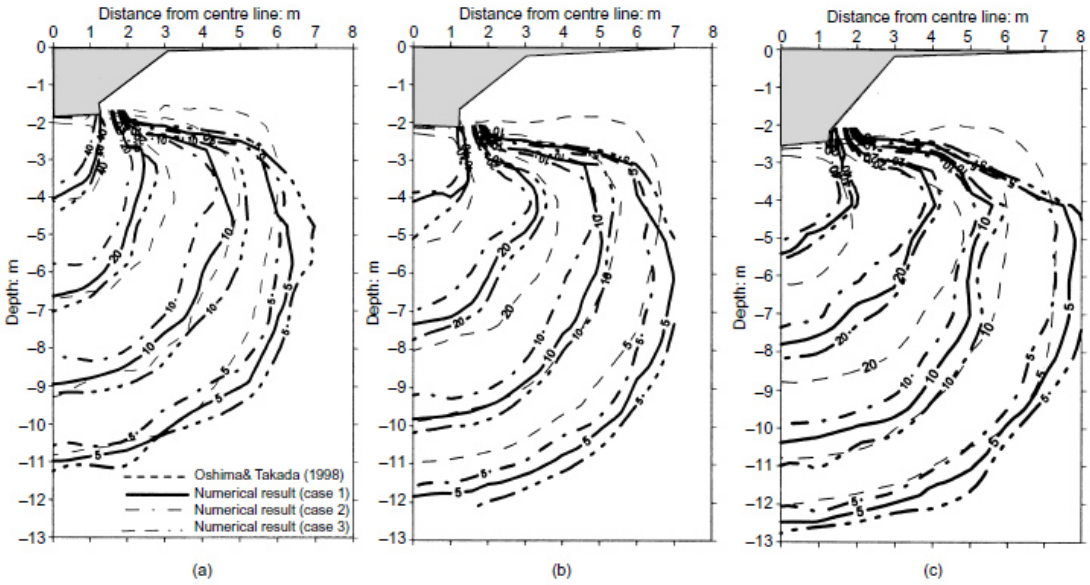

Figure 2-43: Contours of increase in relative density (%) for (a) W= 20 t, H= 20 m, (b) W=40 t, H= 10 m, and (c) W= 80 t, H= 5 m (Gu and Lee, 2002)

Hajialilue-Bonab and Rezaei (2009) who have performed low energy laboratory scale dynamic compaction physical modelling have also assessed the importance of impact energy and impact momentum by performing three tests on dry sand. In these tests, impact energy per blow (WH) and pounder base area were kept constant; however, pounder momentum was made variable. Figure 2-44 shows the variation of depth of influence with the number of blows. It can be observed that with constant energy, a greater improvement and influence depth can be achieved with greater impact pressure (WH/A) in comparison with low pressure impact, and it was concluded that the influence of pounder weight was more significant than the drop height. In other words, the influence of momentum was greater than the influence of applied energy.

2.5.2.4 Effect of Number of Blows and Energy Intensity

Research funded by the Federal Highway Administration (Lukas, 1986) has shown that depth of improvement does not significantly increase in sandy and silty sand formations after 2 to 7 blows. Therefore, dropping the weight up to 30 or 40 times will improve the degree of treatment within the depth of influence, but not the improvement depth itself. The greater

the total energy used, the greater the level of improvement will be, but only within the zone of maximum influence.

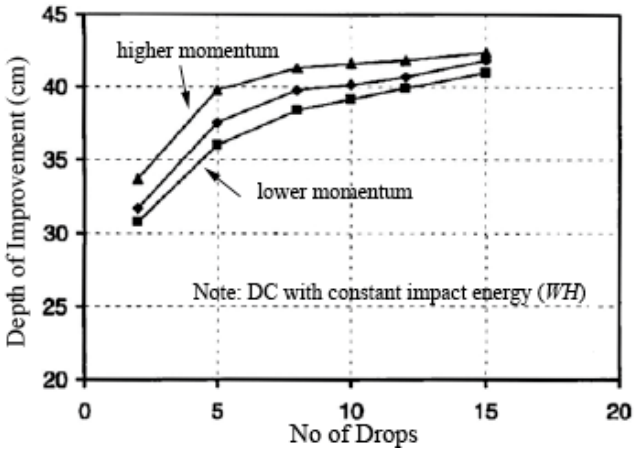

Figure 2-44: Depth of improvement with constant impact energy and varying momentum (Hajialilue-Bonab and Rezaei, 2009)

Hajialilue-Bonab and Rezaei (2009) who carried out low energy laboratory scale dynamic compaction physical modelling on dry sand, have also studied the relationship of normalised depth (ratio of depth of improvement to pounder diameter) with the number of blows. In the series of tests the impact energy and momentum of the print were kept constant, but the impact energy intensity or energy per unit area of impact (not the average energy intensity over the treatment area) was made variable. Figure 2-45 shows the relationship between the normalised depth of influence depth and the number of drops for one of these series of tests. What can be observed is for all curves, depth of improvement initially increases rapidly with the number of blows, but the rate of improvement then reduces until the increase in depth of influences appears to be levelling off after the 12th to 15th blow. The same can also be concluded from the test results presented in Figure 2-44.

It can also be seen that with the same impact energy and momentum, depth of improvement is greater when the impact energy intensity is more (in other words, when the pounder diameter is less). Hajialilue-Bonab and Rezaei observed that for larger impact energy intensities, larger displacements occur at shallow depth beneath the pounder compared to when impact energy intensity is lower, but displacements decrease significantly at greater depths. Thus, they concluded that most of the applied energy is consumed to create large deformations in the soil mass beneath the pounder. As the pounder base area decreases and the stress bulb become smaller, the influence radius consequently decreases.

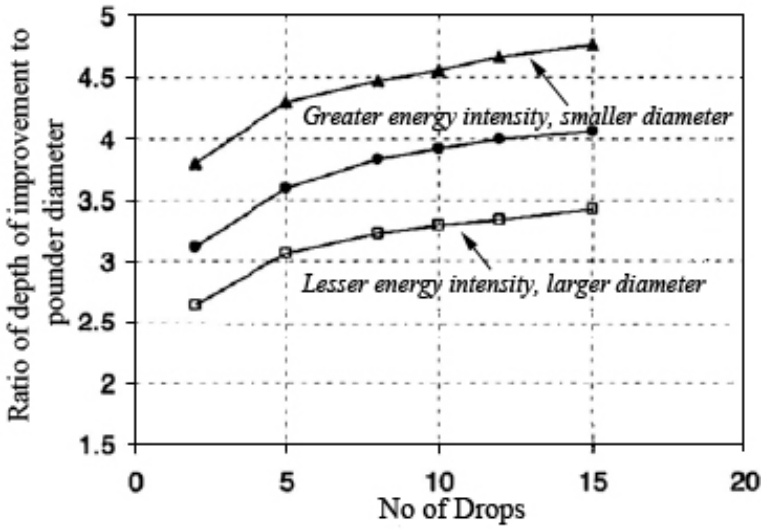

Figure 2-45: Relationship between normalised depth of improvement and number of drops for different energy intensities

As part of their numerical study of dynamic compaction application to dry sands, Lee and Gu (2004) note that maximum depth of improvement will be achieved if sufficient number of blows are applied. If the actual (interim) number of blows is insufficient to reach the maximum achievable depth of improvement, then the interim depth of improvement will be less than the maximum achievable depth of improvement. The interim depth of improvement (strictly for dry sand) can be calculated as

$$D_i = \alpha_z D \qquad 2\text{-}58$$

D_i = interim depth of improvement

α_Z = depth of improvement ratio (dimensionless)

$$\alpha_z = \sqrt{2\alpha_B - {\alpha_B}^2} \qquad 2\text{-}59$$

$$\alpha_B = \frac{N_i}{N} \qquad 2\text{-}60$$

α_B = number of blows ratio (dimensionless)

N= number of blows required to reach maximum depth of improvement

N_i= interim number of blows

Ghassemi et al. (2009a) suggest that Equation 2-61 is able to fit numerical and experimental results better than Equation 2-59, and compare the two equations in Figure 2-46.

$$\alpha_z = \sqrt{\frac{2\alpha_B - {\alpha_B}^2}{1.2}} \qquad 2\text{-}61$$

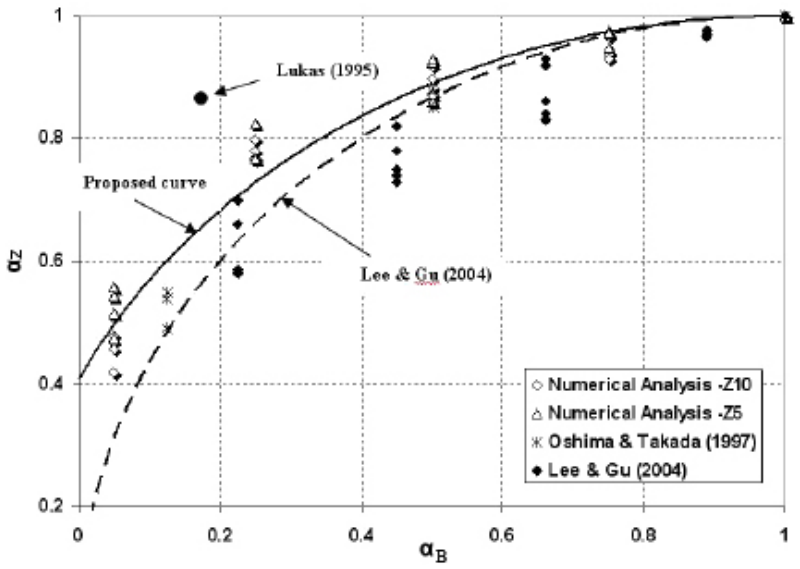

Figure 2-46: Interim depth of improvement ratio (Ghassemi et al., 2009a)

2.5.2.5 Effect of Pounder Size and Shape

Gu and Lee (2002) have carried out a numerical study on dynamic compaction of dry sands have noted that, as shown in Figure 2-47, as the radius increases, the depth of improvement initially increases, but then decreases. In other words, the maximum depth of improvement is achieved with neither the smallest nor the largest radius, but rather with an intermediate radius. Gu and Lee reason that if the pounder radius is too small, then the lateral confinement on the soil directly beneath the footing will be maintained only for a relatively short duration, thereby limiting the depth at which one dimensional wave propagation occurs. On the other hand, if the pounder radius is too large, then the impact force will be distributed over too large an area, thereby reducing the impact stress, and thus limiting the depth of improvement.

Ghassemi et al. (2009b) who have carried out a numerical study on dynamic compaction have proposed Equation 2-51, also repeated hereunder, which relates the depth of improvement to pounder radius.

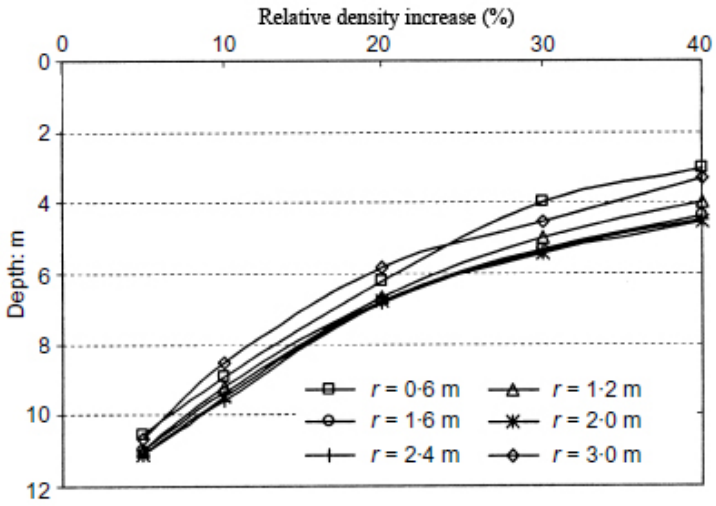

Figure 2-47: Increase in relative density along centreline for various tamper radii (Gu and Lee, 2002)

$$D = 2\sqrt[4]{WHr}$$

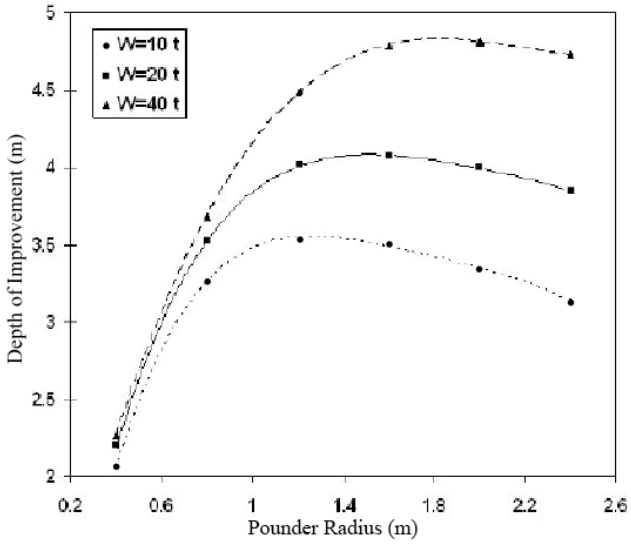

Figure 2-48: Relation between tamper radius and depth of improvement (Ghassemi et al., 2009a)

Ghassemi et al. (2009a) speculate that there should be an optimum pounder radius whose value depends on the pounder weight because most pounder's static pressure are in a certain range (the author believes that impact energy could have been a better basis than pounder weight). Figure 2-48 shows the relationship between depth of improvement and pounder for a series of numerical cases in which one drop has been applied from 20 m height. It can be observed that the variation of depth of improvement depth with pounder radius for each pounder weight appears to have a peak at which the maximum depth of improvement has been achieved.

Laboratory scale dynamic compaction physical modelling using circular flat bottom and conical bottom pounders have been carried out to determine the effect of pounder bottom shape on the efficiency of dynamic compaction (Arslan et al., 2007, Feng et al., 2000, Feng and Ke, 2005, Feng and Yuan, 2009). Feng et al. (2000) performed their study on fine poorly graded Mai-Liao sand with 8% fines content and commercial grade Ottawa sand, with no fines, poorly graded and coarser than Mai-Liao sand that had relative densities of 30 to 40% in dry states and 60% in wet states. Feng and Ke (2005) report that Mai-Liao sand particles are platy shaped rather than the more common bulky shaped grains. In addition to the flat bottom pounder, conical pounders with apex angles of 60, 90 and 120^{o} (Feng and Yuan, 2009) were also used in the study; however, Feng et al. (2000) have only published the results for the flat bottom and conical bottom pounder with an apex angle of 90^{o} (see Figure 2-49). Feng and Yuan (2009) explain in their discussion about Arslan et al.'s (2007) paper that that the 90^{o} conical bottom pounder worked the best, regardless of the type of sands used in the model test programme. The 60^{o} conical bottom pounder penetrated excessively into the specimen, and the 120^{o} conical bottom pounder created craters smaller than that created by the 90^{o} conical bottom pounder. The flat bottom and conical pounders reported by Feng et al. both weighed the same.

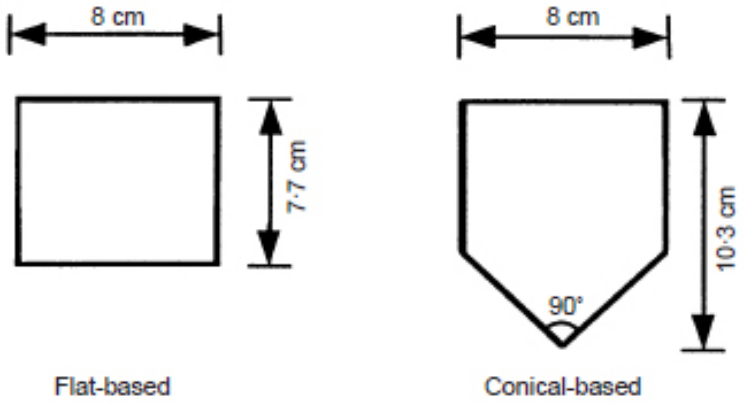

Figure 2-49: Side view of cylindrical pounders (Feng et al., 2000)

While the craters in the dry Mai-Liao sand specimens all had bowl shapes, the craters in the wet Mai-Liao sand specimens were nearly cylindrical in shape, and heave was absent around the craters in these tests. The craters in the dry Ottawa sand specimens also had bowl shapes; however, unlike the Mai-Liao sand specimens, heave was clearly appearing around those craters. Feng et al. observe that the ratio of net crater volume, being the difference between crater and peripheral heave volumes, was 1.29 to 1.95 times larger when using a conical bottom pounder compared to when a flat bottom pounder was used in dry Mai-Liao sand. The same ratio varied from 1.33 to 1.73 when the sand was wet. However, when dry Ottawa

sand was used, it was observed that net crater volume was 3 to 4% larger for the flat bottom pounder rather than the conical bottom pounder.

Feng and Ke (2005) also performed laboratory scale dynamic compaction on dry Mai-Liao sand with relative density of 50% and fines content of 3.4%, 8% and 14% using flat bottom and conical bottom pounders shown in Figure 2-49. Although the net crater volume in this series of tests was also consistently larger in conical bottom pounders compared to flat bottom pounders; however, the ratio was not as pronounced as what Feng et al. (2000) have reported. Here the net crater volume ratio of conical to flat bottom pounders was 1.08 to 1.21 for 3.4% fines content, 1.09 to 1.18 for 8% fines content and 1.05 to 1.12% for 14% fines.

Figure 2-50 shows the mini cone resistance profiles under the pounder centre for tests with fines content of 3.4%, 8%, and 14%. It can be seen that the cone penetration resistance increases sharply at depths about 10 to 20 cm, which is right below the bottom of the crater. Feng and Ke note that the depth of the crater was at about 10 cm, and that the sharp increase was due to a direct compaction from the impact of the flat bottom pounder. The lesser amount of cone resistance increase at depths greater than 20 cm was attributed to the transmission of body waves downwards through the test specimen. Figure 2-50 indicates that the conical bottom pounder induces somewhat lower maximum cone resistances than the flat bottom pounder in all tests. Feng and Ke suggest that this may be due to the conical bottom pounder inducing lesser amounts of downwards compaction. The differences in the post dynamic compaction cone resistances are even less at greater depths between the conical and flat bottom pounders, and the depth of improvement between the two cases appears to be the same.

Figure 2-51 shows mini cone resistances measured at distances of 1, 2 and 3 pounder diameters from the pounder centres for tests carried out on Mia-Laio sand with 14% fines content. It can be observed that at the distance of one pounder diameter from the pounder centre the maximum cone resistance induced by the flat bottom tamper is about the same as that of the conical bottom tamper; however, as the distance from the pounder centre increases the maximum cone resistance induced by the conical bottom pounder becomes greater than the flat bottom pounder. Feng and Ke suggest that this is because the conical bottom pounder moves more sand particles laterally as it penetrates into the sand than what is achieved by the flat bottom pounder. Feng and Ke note that they have also observed the same behaviour for Mia-Laio sand with 3.4% and 8% fines content.

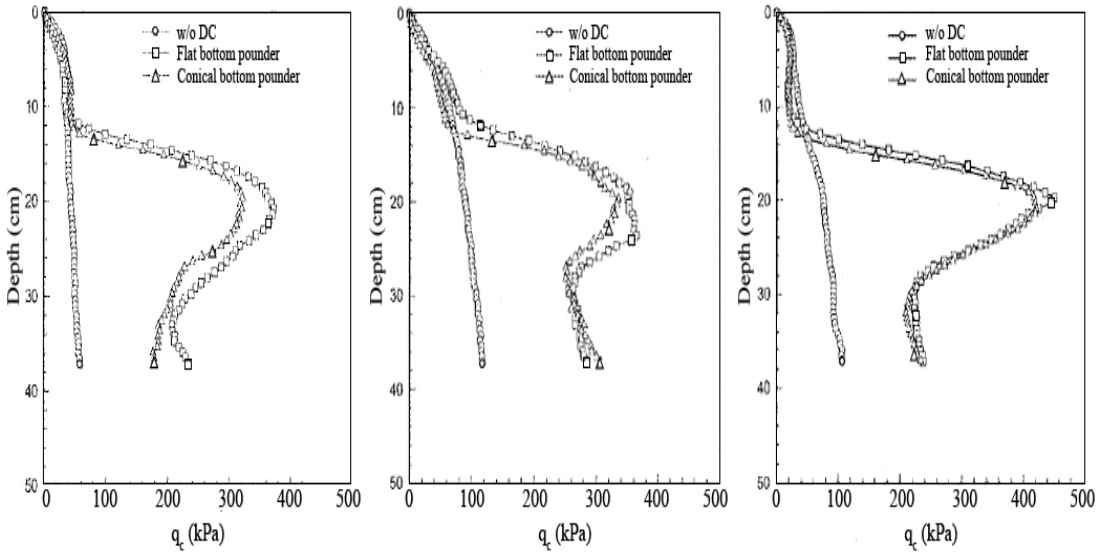

Figure 2-50: Mini cone penetration resistance at below centre of pounder with fines content (a) 3.4%, (b) 8% and (c) 14% (Feng and Ke, 2005)

Arslan et al. (2007) have also compared the efficiency of conical bottom pounders with flat bottom pounders by performing laboratory scale dynamic compaction on loose, medium dense and dense Sakarya River sandy gravel. There is a discrepancy in the reported soil grading as one of the figures in Arslan et al.'s paper shows coarse gravel size material on the testing surface, but the maximum grain size of the soil is reported to be less than 2 mm, and material has been classified by the paper's authors as well graded sand. The internal friction angles of the loose, medium dense and dense soil used in the tests were respectively 30^o, 35^o and 40^o.

The pounders used in Arslan et al.'s experiment all weighed about the same. The conical bottom pounders used for each density of soil had the same side angle with the horizon as the internal friction angles; i.e., 30^o, 35^o and 40^o, which would be equivalent to apex angles of 120^o, 110^o and 100^o. It is the author's opinion that this will make efficiency comparison of any one apex angle in looser or denser soils somewhat difficult.

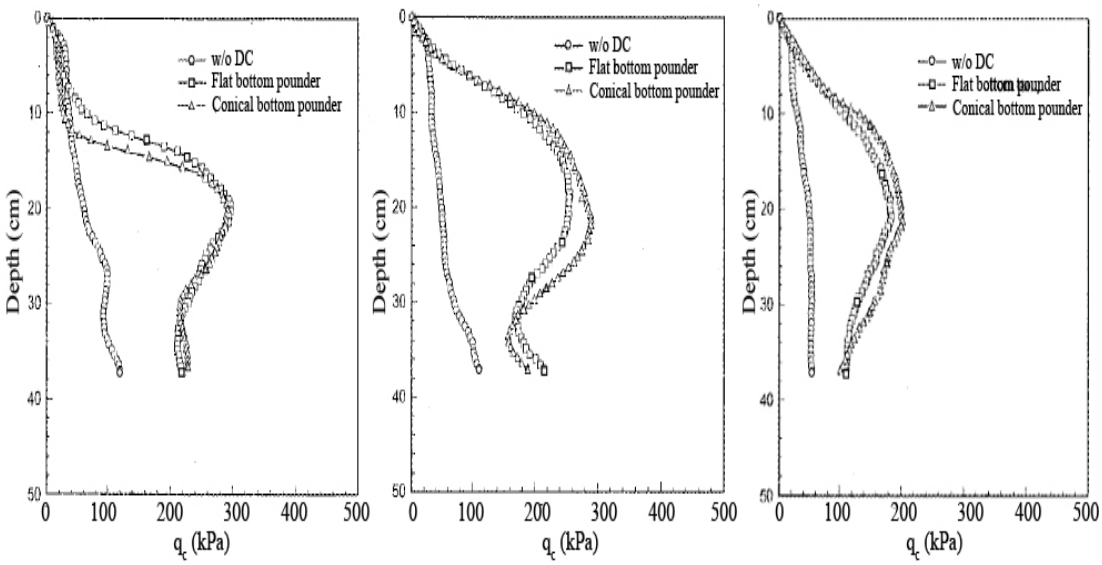

Figure 2-51: Mini cone penetration resistance for test series with 14% fines content. Distances of impact points from the centre of pounder were (a) 1 pounder diameter, (b) 2 pounder diameters, and (c) 3 pounder diameters (Feng and Ke, 2005)

Arslan et al. measured the crater depths and crater top diameters in two orthogonal directions, and assumed that the compaction volume is equal to the volume of a cylinder with the crater diameter at its base and the crater height. The author believes this is an oversimplification because even in the figures provided in Arslan et al.'s paper the crater sides are clearly not vertical, and the is no reference to potential surface subsidence or heave around the crater. The results of this study suggest that crater depth and ground area are from -5% up to about 38% larger for conical bottom pounders compared to flat bottom pounders.

2.5.3 Crater Depth

Crater depth may also be an indication of the dynamic compaction performance. Mayne et al. (1984) observed that, as shown in Figure 2-52, when crater depth measurements are normalised with respect to the square root of energy per blow, the results fall within a narrow band.

Hajialilue-Bonab and Rezaei also noticed that, as shown in Figure 2-40, in laboratory scale dynamic compaction tests, normalised depth of influence and normalised crater depth appeared to have a linear relationship, which led to the formulation of Equations 2-47 and 2-48.

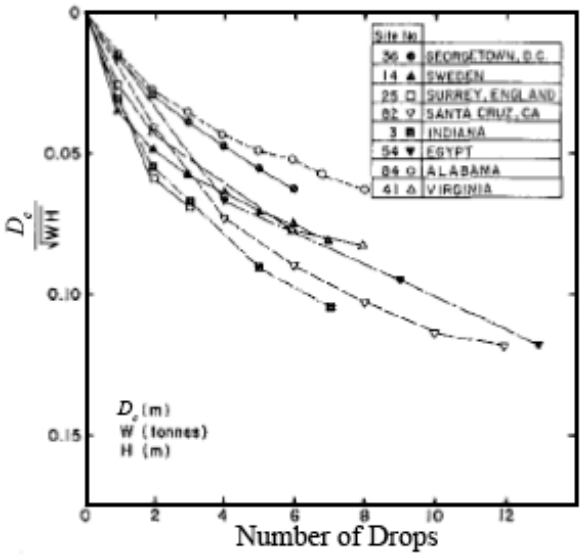

Figure 2-52: Normalised crater measurements (Mayne et al., 1984)

2.5.4 Grid Spacing, Number of Phases and Number of Drops

Applying dynamic compaction in spaced out grids is a more efficient treatment method than dropping the pounder contiguously because in the latter pattern a very dense intermediate layer will be formed, which will attenuate energy propagation into the soil mass. Menard & Broise (1975) note that efficiency depends quite closely on progressive consolidation of the layers, commencing with the deepest and finishing with the surface, by means of an adequate distribution of impacts.

Figure 2-53: Application of Dynamic Compaction in a grid

As shown in Figure 2-53, the initial phase of treatment is carried out on a wide grid with the maximum amount of impact energy or drops per impact point (more commonly called *print*).

The objective of this phase is to treat the deepest soil layers. The second phase, which is also a deep treatment, and is intended to treat the intermediate soil layer, may be carried out with less energy or drops. If necessary, the final phase, called *ironing* will comprise of closely spaced grid points with one or two low energy blows per print for improving the superficial loose soil layer above the crater depth.

Mayne (1984) comments that grid spacing is usually at least equal to the thickness of the compressible layer (the author interprets that it was probably meant to be as first phase spacing). Lukas (1986) states that in semi-pervious soils with high groundwater level, spacing between prints should be wide enough and in the order of 10 to 15 m to allow for pore water pressure dissipation. He further adds that, as a rule of the thumb, print spacing is taken equal to the treatment thickness in some projects. Mayne suggests that in granular deposits where groundwater level is not close to the ground surface, print spacing can be reduced, and energy can be applied in one or two passes. For shallow depth treatment, print spacing as close as 2 m have been used effectively. Later, Lukas (1995) noted that a spacing of 1.5 to 2.5 times the diameter or width of the pounder is common (the author interprets that is was probably meant as inclusive of all deep phases of compaction), and adds that in fine grain soils where there is a concern with pore water pressures developing in the soil, compaction should be done in two or more phases. The first phase would involve dropping the pounder at every second or third drop point location. After a period of time to allow for dissipation of pore pressures, the intermediate drop point locations could be compacted as part of the second or third phase.

Although 7 to 15 drops of high level energy are applied normally at each print (Lukas, 1995), the author notes that the number of blows is a parameter that should be determined or defined as a part of the design process, and has personally been involved in projects with the number of blows per print ranging from 3 to 30 blows.

Chow et al. (1994) have proposed a method for predicting the change in the soil's internal friction angle based on a trial case study (Harada and Suzuki, 1984) in which a 12 ton pounder was dropped from 20 m onto a single print to treat 7 to 8 m of mainly loose sand with pockets of silty clay. CPTs were carried out before and after dynamic compaction at 0, 3, 6, and 9 m away from the print location as part of the trial DC.

Chow et al. used a correlation (Meyerhof, 1976) to estimate the soil's internal friction angle from the CPT values, and assessed the increase of internal friction angles ($\Delta\varphi$) of the soil at

various distances. Denoting $\Delta\varphi_b$ as the increase of internal friction angle beneath the pounder, $\Delta\varphi/\Delta\varphi_b$ versus normalised distance is plotted in Figure 2-54. The distance has been normalised using the pounder diameter or its equivalent diameter. $\Delta\varphi/\Delta\varphi_b$ is shown for depths of $0d$, $1d$, $2d$ and $3d$ beneath the pounder. It can be observed that the ratio is insignificant for depths below $3d$. Chow et al. also used data from tips of driven piles and caissons (Meyerhof, 1959) to show the similarity of trends.

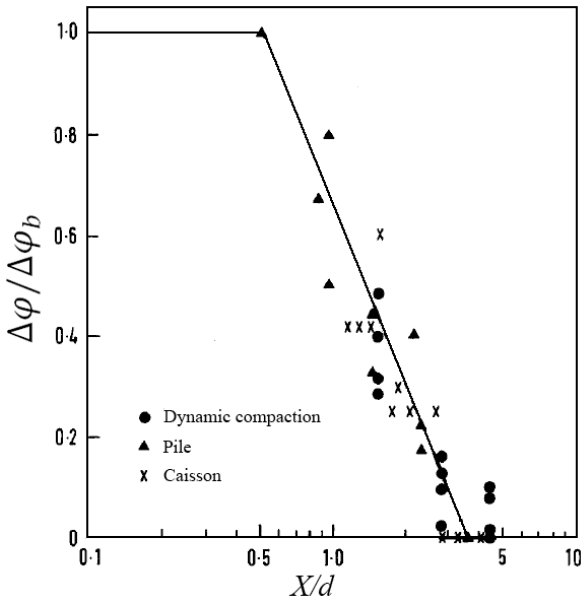

Figure 2-54: Relationship between ratio of increase of internal friction angles and normalised depths (Chow et al., 1994)

$\Delta\varphi/\Delta\varphi_b$ obtained at equal lateral distance but at different depths showed some variations, but they did not appear to be significant; hence, Chow et al. assumed that $\Delta\varphi/\Delta\varphi_b$ was a function of distance and independent of depth. Consequently they proposed that:

$$\frac{\Delta\varphi}{\Delta\varphi_b} = 1.0 \quad \text{for } \frac{X}{d} \leq 0.5 \qquad \text{2-62}$$

$$\frac{\Delta\varphi}{\Delta\varphi_b} = 0.642 - 1.180 \log\left(\frac{X}{d}\right) \quad \text{for } 0.5 < \frac{X}{d} \leq 3.5 \qquad \text{2-63}$$

$$\frac{\Delta\varphi}{\Delta\varphi_b} = 0 \quad \text{for } \frac{X}{d} \geq 3.5 \qquad \text{2-64}$$

Chow et al. note that although Equations 2-62 to 2-64 are basically meant for the prediction of the lateral extent of soil improvement around the pounder at a single drop point, modification of $\Delta\varphi_b$ by considering the densification of soil within the grid brought about by the pounder impact on the surrounding prints can allow the extension of the equations for evaluating the effect of multiple points.

For design purposes, the two most critical locations to achieve a uniform level of improvement are at the centre of the grid and at the middle of the side of the grid. Chow et al. have provided the relationship between $\Delta\varphi/\Delta\varphi_b$ and the ratio of distance to grid spacing for these two points in Figure 2-55. As before, in the analysis $\Delta\varphi/\Delta\varphi_b$ is assumed to be independent of depth. When spacing is close, the influence of impacts at neighbouring prints will be significant, and should be included in the analysis following the sequence of pounding. Chow et al. note that they have carried out the analyses for $s/d > 1$, since when $s/d \leq 1$ the centre of the grid and the middle of the side of the grid are located directly beneath the pounder and $\Delta\varphi/\Delta\varphi_b$ is assumed to have values of 1.

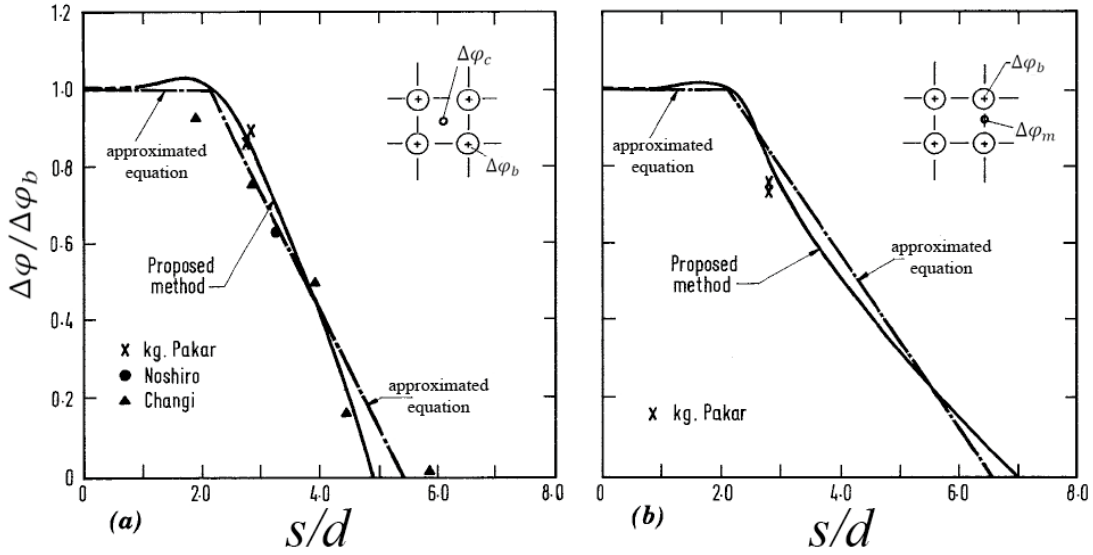

Figure 2-55: Increase in internal friction angles ratio for (a) grid centre point and (b) midpoint of grid side (Chow et al., 1994)

According to Chow et al., for design purposes the effect of print spacing on the increase of internal friction angle at the grid centre, $\Delta\varphi_c$, can be approximated by two linear equations:

$$\frac{\Delta\varphi_c}{\Delta\varphi_b} = 1.0 \quad \text{for } \frac{s}{d} \leq 2.1 \qquad 2\text{-}65$$

$$\frac{\Delta\varphi_c}{\Delta\varphi_b} = 1.60 - 0.29\left(\frac{s}{d}\right) \quad \text{for } 2.1 < \frac{X}{d} \leq 5.5 \qquad \text{2-66}$$

Similarly, for design purposes the effect of print spacing on the increase of internal friction angle at the midpoint of the grid side, $\Delta\varphi_m$, can be approximated by two other linear equations:

$$\frac{\Delta\varphi_m}{\Delta\varphi_b} = 1.0 \quad \text{for } \frac{s}{d} \leq 2.1 \qquad \text{2-67}$$

$$\frac{\Delta\varphi_m}{\Delta\varphi_b} = 1.49 - 0.23\left(\frac{s}{d}\right) \quad \text{for } 2.1 < \frac{X}{d} \leq 6.5 \qquad \text{2-68}$$

Hajialilue-Bonab and Zare (2014) have also studied the effect of grid spacing by advancing the physical modelling scheme and particle image velocimetry method (Hajialilue-Bonab and Rezaei, 2009) to detect soils displacements. In their experiment Hajialilue-Bonab and Zare used poorly graded fine dry Sofian sand, and dropped pounders in the shape of half discs, with 100 mm diameter and weighing 12.5 N, tangentially to a transparent Perspex facing from 750 mm height. As a base, displacements were recorded for a single print that was subjected to 12 consecutive blows, and for comparative purposes two prints with varying spacing of $6d$, $5d$, $4d$ and $3d$ were subjected to 12 blows.

Figure 2-56 shows the displacement vectors after 12 blows when pounder spacing was $5d$, and Figure 2-57 shows the angle of displacement vectors at various normalised depth for the same case. It can be observed that ground beneath the pounder centrelines and the spacing midpoint line displaced vertically. The displacement angle decreases as distance from the pounding centreline increases, and then begins to increase. It can also be seen that deeper points appear to displace more vertically than horizontally.

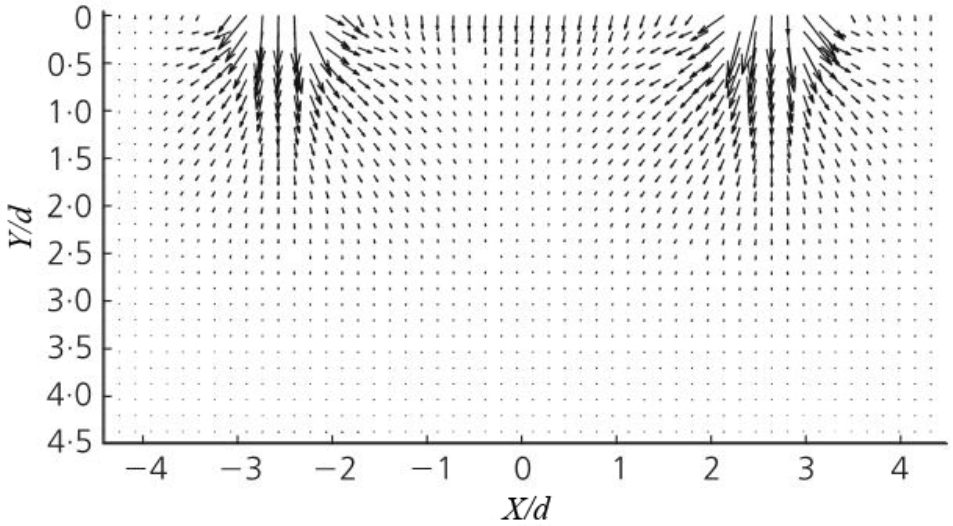

Figure 2-56: Displacement vectors after 12 blows when spacing= 5d (Hajialilue-Bonab and Zare, 2014)

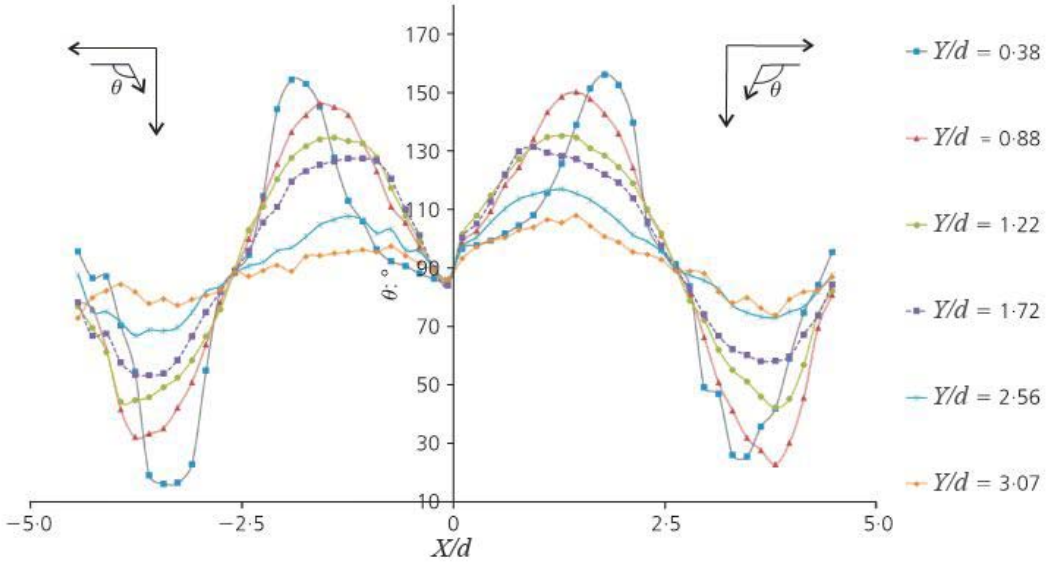

Figure 2-57: Displacement angle at different normalised depths and distances (Hajialilue-Bonab and Zare, 2014)

Figure 2-58 shows the displacement contour of 0.05d after applying 12 blows to the left print (n_1 series) followed by 12 blows to the right print (n_2 series) when pounder spacing was 3d. It can be observed that, as expected, progression of pounding at the first print increases the displacement bulb volume under the first print and at its periphery, but displacement at the location of the second print is much less and appears more parallel than bulb shaped.

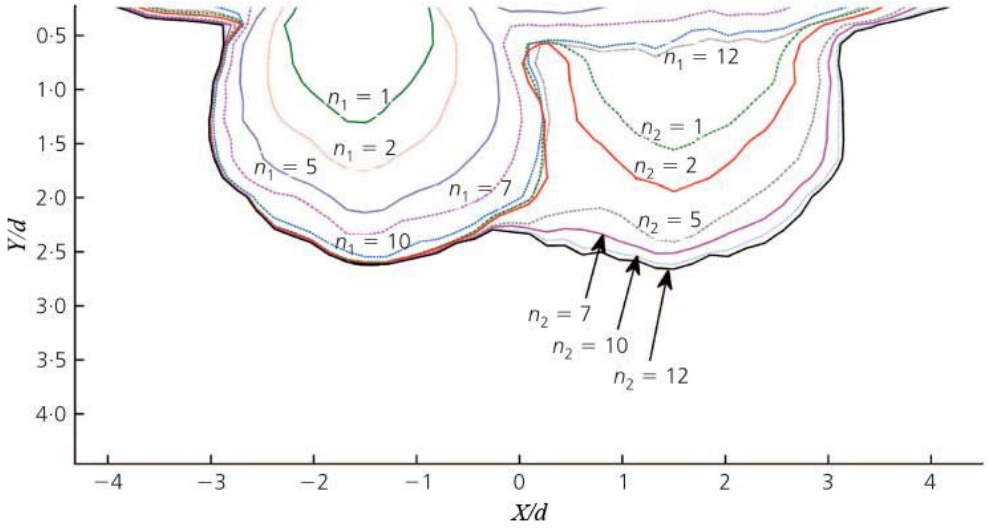

Figure 2-58: Displacement contours of 0.05d for different number of drops when pounder spacing= 3d (Hajialilue-Bonab and Zare, 2014)

Pounding of the second (right) print does not induce any observable or significant displacement under the first print, but increases the displacements between the two prints. Progression of pounding generates further displacement under the second print and in between the prints, and at higher blows the displacement contour appears to move towards a uniform horizontal distribution.

What is also noticeable is that, generally, displacement contours under the second print were deeper than the contours beneath the first print. Hajialilue and Zare reason that this is because the soil in the zone of the second print has been compacted slightly by the first print's pounding, and compaction of the second print would commence on the compacted soil. Thus, it could be understood that in practical dynamic compaction works pounding of the second phase prints will not improve the soil under the first phase prints, but pounding of the first phase prints will (assuming the grid spacing is close enough) effect treatment of the second phase, and lesser blows could be required for reaching the same depth of improvement. This conclusion of Hajialilue and Zare is in compliance with the author's field experience.

Figure 2-59 shows the displacement contours for tests in which pounder spacing were 6d and 3d. It can be observed that in both tests displacement of superficial layers under the pounder is greater than the displacement in between the prints; however, displacement tends to become uniform as depth increases. Reducing pounder spacing increases displacement uniformity of the upper layers, and suggests that it will be possible to realise reasonably uniform ground layers by selecting an appropriate dynamic compaction grid size. Hajialilue

and Zare's experiment does not include an ironing phase; however, it can be expected that after filling the craters, levelling the site, and performing an ironing phase with a close grid spacing the superficial layers will also become reasonably uniform.

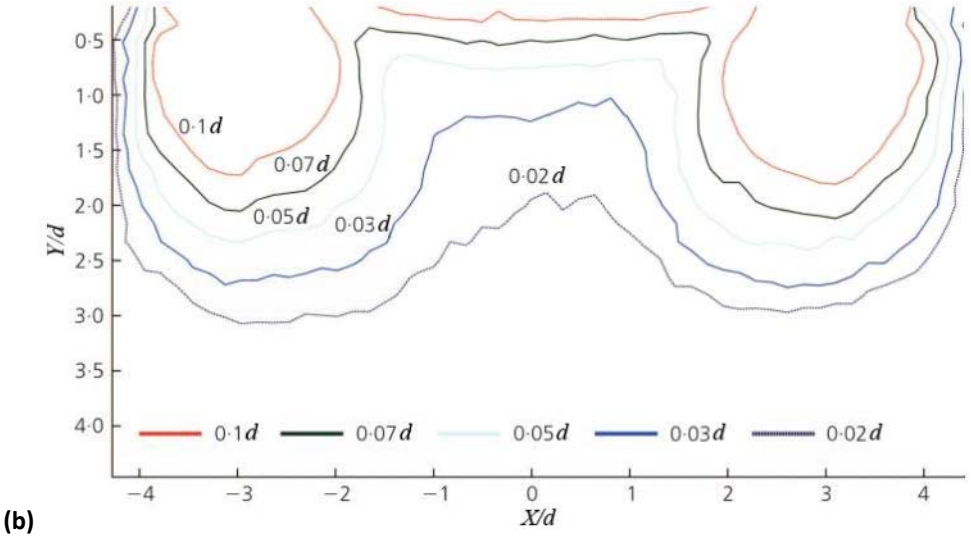

(b)

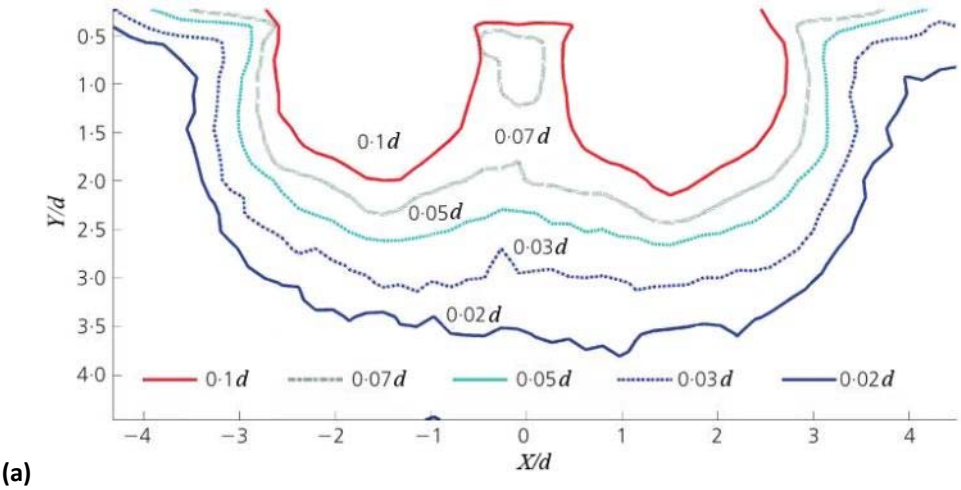

(a)

Figure 2-59: Displacement contours for (a) pounder spacing= 6d and (b) pounder spacing= 3d (Hajialilue-Bonab and Zare, 2014)

Figure 2-60 shows the strain diagrams for tests in which pounder spacing were 6d, 5d, 4d, and 3d. Once again it can be observed that reduction of pounder spacing increases the trend of uniformity, and points at the same depth will tend to have the same compaction.

Hajialilue and Zare also studied change in relative density at the spacing midpoint line for various pounder spacing. The result of this part of the study is shown in Figure 2-61. As expected, increase of relative density reduces as (normalised) depth increases; however, the rate of reduction decreases as print spacing is reduced. Figure 2-61 also suggests that increase of relative density curves for print spacing of 4d, and 3d are almost the same

Considering that the magnitude of energy intensity in this physical model is much less than field dynamic compaction, noting that this experiment does not extend to the midpoint between 4 prints on a grid (that is further away from the prints that the midpoint between two prints), and with recognition that print spacing (inclusive of phases 1 and 2 of deep dynamic compaction) of field work is usually less than $4d$, it is the author's opinion that this experiment should not necessarily lead to a conclusion that additional improvement will always be negligible when grid spacing is reduced to less than. However, the experiment results are an indication that additional improvement could be negligible when spacing is reduced to less than a certain figure.

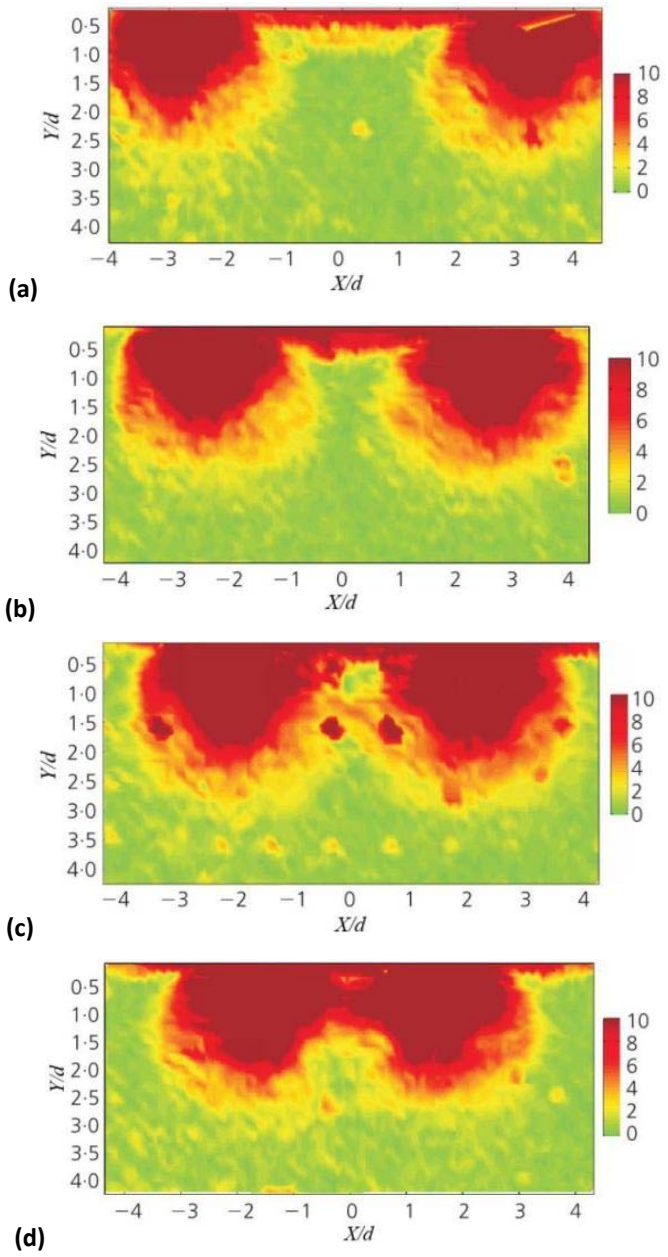

Figure 2-60: Strain diagrams after 12 blows with pounder spacing being equal to (a) $6d$, (b) $5d$, (c) $4d$ and (d) $3d$ (Hajialilue-Bonab and Zare, 2014)

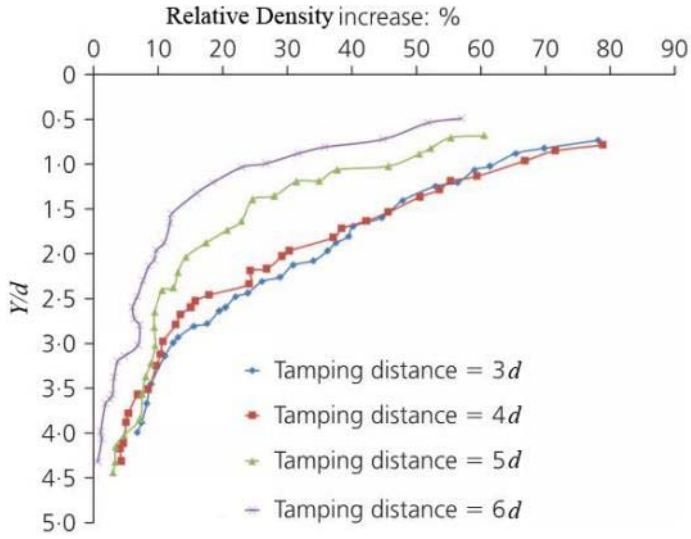

Figure 2-61: Increase of relative density at the between prints centreline (Hajialilue-Bonab and Zare, 2014)

To understand the significance of pounding sequence, Hajialilue and Zare extended their experiment by carrying out pounding with spacing of $3d$ in two ways; i.e., in the first test the first print was initially subjected to 12 consecutive blows followed by 12 consecutive blows to the second print, and in the second test prints were alternatively subjected to blows until they both received 12 non-consecutive blows. The result of this phase of the experiment showed that alternating the blows between the first and second prints was able to create larger displacements than compacting each print by consecutive pounding. The author notes that common practice in industry is consecutive pounding of each print and then moving on to the next print. Although common practice may result in lesser treatment, and alternating pounding is certainly worth further investigation, it may however, not be practical to alternate the blows between the prints as this will greatly reduce production due to increase of setting up time.

2.5.5 Improvement Profile

The magnitude of soil improvement by dynamic compaction is dependant, among a number of parameters, on the amount of applied impact energy and initial density of the soil. For commonly used energy ranges; i.e., 100 to 300 tm/m^2, improvement in the properties of soils is in the order of 100 to 400% increase in strength as measured by tests such as SPT, CPT or PMT (Lukas, 1986). Table 2-5 presents the magnitude of soil improvement for representative soil types. The higher values are for soils that are initially loose and the lower values are for soils that are initially denser.

Soil Type	Anticipated amount of improvement*
Pervious coarse grained soils – sands and gravels	300 to 400%
Semi pervious soils • Silty sands • Silts and partially saturated clayey silts	 100 to 400% 100 to 250%
Partially saturated impervious soils – clay fills and mine spoils	200 to 400%
Landfills	200 to 400%
Building rubble	200 to 300%

* For applied energies of 100 to 300 tm/m^2

Table 2-5: Anticipated relative improvement for different types of soils (Lukas, 1986)

Based on the data that he had studied, Leonards (1980) speculates that it appears there may be an upper bound to the densification that can be achieved, which corresponds approximately to CPT cone resistance, q_c, of 15 MPa. Lukas (1986) proposes that typical upper bound values for SPT, CPT and PMT would be as summarised in Table 2-6. The highest values occur in coarse pervious soils and the lowest values can be envisaged for landfills.

Soil Type	SPT *N* (blows)	CPT q_c (MPa)[1]	PMT P_{LM}[2] (kPa)[1]
Pervious coarse grained soils: Sands and gravels	40 to 50	19 to 28	1900 to 2400
Semi pervious • Sandy silts • Silts and clayey silts	 34 to 50 25 to 35	 13 to 17 9 to 13	 1400 to 1900 1000 to 1400
Partially saturated impervious deposits, clay fill, mine spoil	30 to 40[3]	N/A	1400 to 1900
Landfill	20 to 40[3]	N/A	500 to 1000

1. Rounded
2. Limit pressure
3. Higher test values will occur when sampling on large particles present in the soil mass.

Table 2-6: Post dynamic compaction upper bound test values (Lukas, 1986)

Figure 2-62 schematically shows a soil profile for any test before and after dynamic compaction (Lukas, 1986). Figure 2-62(a) shows improvement after the deep phases of compaction. It can be seen that while the soil parameters have increased beyond a certain

depth, the superficial layer of soil above the crater depth has loosened. Maximum improvement as suggested in Table 2-6 usually occurs at depths of about $D/2$ to $D/3$. Implementation of light pounding or ironing after the deep compaction phases is able to increase the superficial layer's compaction, and as shown in Figure 2-62(b), the soil parameters increase consequently. The depth of influence and depth of maximum improvement does not change at this phase, and remains at where they were.

Varaksin and Racinais (2009) propose that the ground improvement profile after dynamic compaction can be formulated in the form of a parabola, which can be written as shown in Equation 2-69.

$$f(z) = \frac{f_2 - f_1}{D^2}(z - \mathrm{NGL})^2 + f_1 \qquad 2\text{-}69$$

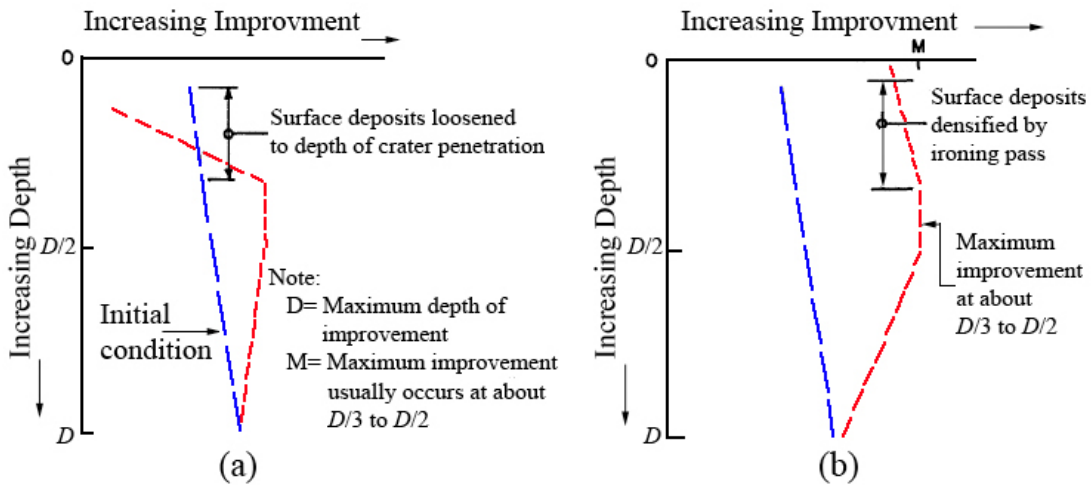

Figure 2-62: (a) Initial stages of pounding, and (b) after densification, including the ironing pass (Lukas, 1986)

z= point level

NGL= natural ground level

$f_1 = f_{max}$= maximum improvement factor observed at ground level, which is a unit dependant parameter that was equal 0.008 times total compaction energy (in tm/m^2) in the case studied by Varaksin and Racinais.

f_2= 1= improvement factor obtained at the depth of influence.

f(z)= improvement factor at elevation z

As illustrated in Figure 2-63, Lukas (1986) has studied the lateral ground movement in dynamic compaction, and has measured lateral movement in three types of soils at distances of 3 m and 6 m from the pounder's drop point. From his records, it appears that the ground movement initially increases to a point, but then drops off until at some point soil particle movements become negligible.

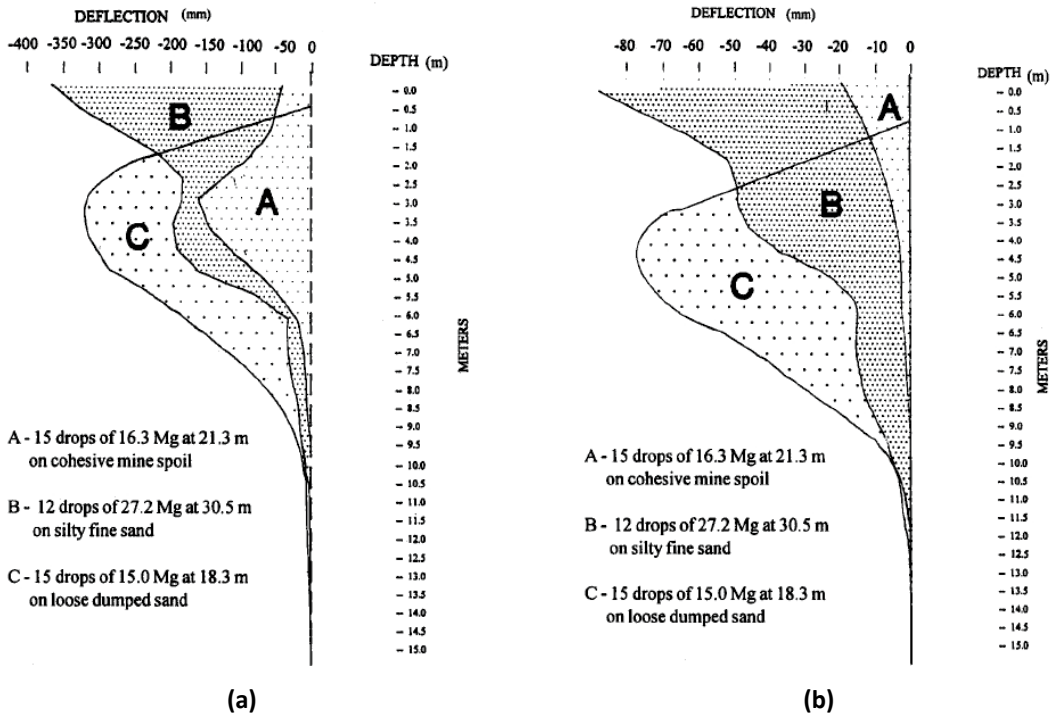

Figure 2-63: Lateral movement (a) 3 m and (b) 6 m away from pounder drop point (Lukas, 1986)

Similar results have also been achieved in laboratory scale dynamic compaction by Bonab and Rezaei (2009). As shown in Figure 2-64, a sickle shape curve characterises the soil displacement profile along vertical lines of soil. The curves become flatter as they go farther away from the impact centre. It was observed that the displacement of soil in any given horizontal plane has a bell shaped curve.

Poran and Rodriguez (1992) cite Heh (1990) and Poran et al. (1991) for a laboratory model dynamic compaciton test programme on dry sand. As shown in Figure 2-65, Heh computed, and plotted the density contours for the final state of the sand for each test. Based on these results it appeared that density contours could be approximated as upside-down semi-prolate spheriods with dimensions of a and b respectively for the horizontal and vertical radii, as shown in Figure 2-66. The parameters a and b were measured from the centre of the original ground surface, above the centre of the base of the crater.

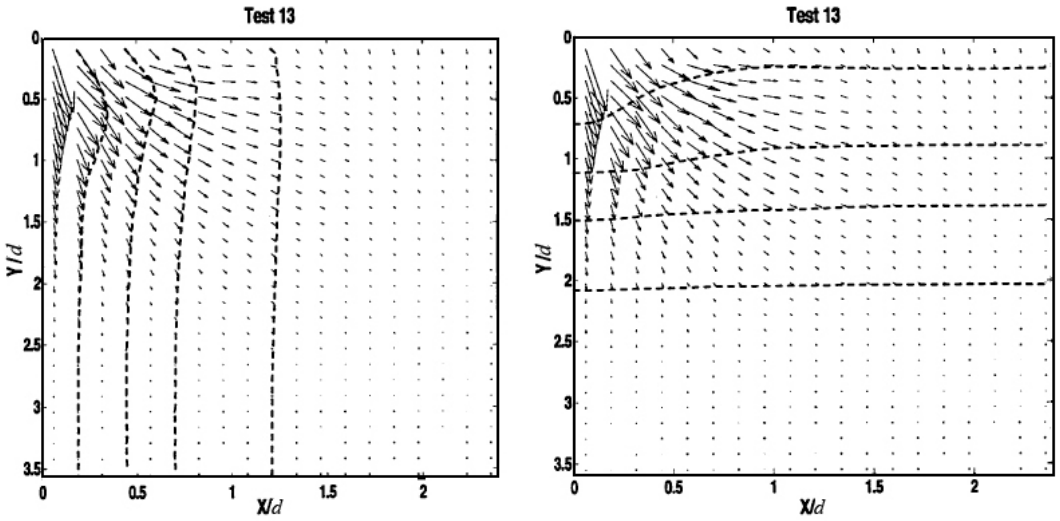

(a) (b)

Figure 2-64: Normalised (to pounder diameter) displacement vectors after 10th impact for (a) vertical lines and (b) horizontal lines of soil (Hajialilue-Bonab and Rezaei, 2009)

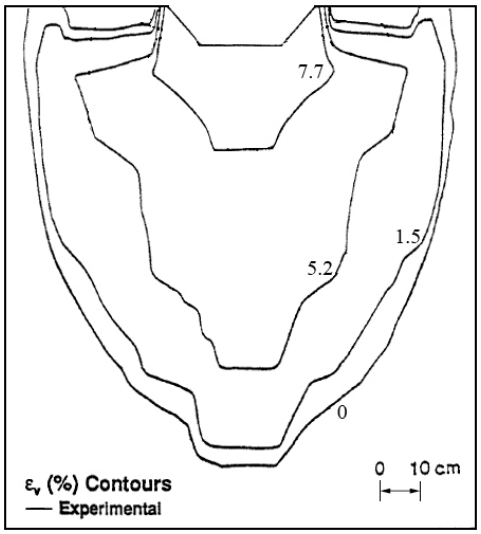

Figure 2-65: Experimental contour of plastic volumetric strains, modified from Poran and Rodriguez (1992)

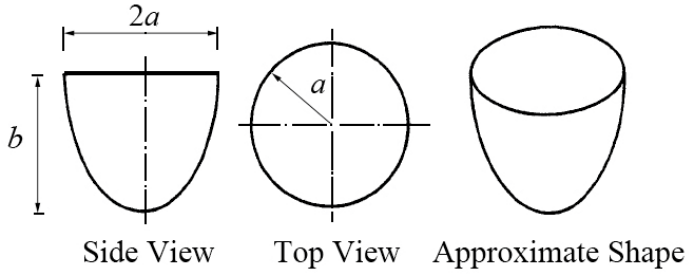

Figure 2-66: A semi-prolate spheroid can be used to approximate the volume of density contours (Poran and Rodriguez, 1992)

Total specific energy and semi-prolate spheroid dimensions were respectively normalised to $NWH/(A.b)$, a/d and b/d to minimise the effects of model size, and a study was conducted to determine a relationship between normalised total specific energy and the normalised dimensions for different relative density (volumetric strain) contours.

d = pounder diameter

N= number of drops per print

A= pounder base area

The best linear fits for these semi-log relationships are:

$$\frac{b}{d} = j + k \log\left(\frac{NWH}{Ab}\right) \quad \text{2-70}$$

$$\frac{a}{d} = l + m \log\left(\frac{NWH}{Ab}\right) \quad \text{2-71}$$

j, k, l and m are regression curve fitting parameters that are presented in Table 2-7 along with their coefficient of determination, R^2. $NWH/(Ab)$ is in kPa. For non-circular pounders, d is the width of the pounder.

State of improvement				
	Unaffected	Slight	Moderate	Strong
Volumetric strain (%)	0	1.5	5.2	7.7
Relative density (%)	25	35	65	85
j	-12.59	-13.22	-15.27	-15.27
k	8.08	7.91	7.79	6.25
R^2	8.84	8.84	0.90	0.53
l	-2.49	-2.39	-4.25	-4.43
m	1.97	1.90	2.32	1.99
R^2	0.79	0.71	0.81	0.65

Table 2-7: Curve fitting coefficients for Equations (Poran and Rodriguez, 1992)

For simplicity, Berry et al. (2004) have proposed to model the void reduction of the soil profile using the Rayleigh distribution in the form of a Rayleigh distribution, which can be mathematically written in the form of Equation 2-72:

$$\varepsilon(z) = \frac{z}{\sigma^2} e^{-z^2/2\sigma^2} \qquad 2\text{-}72$$

z= depth from surface

σ= depth of maximum strain

$\varepsilon(z)$= strain at depth z

it is noted that Hajialilue-Bonab and Zare (2014) who have also carried out physical modelling of dynamic compaction have not observed the same improvement pattern as Heh (1990) that has been used as the basis of Poran and Rodriguez's method (see Section 2.5.8.2). A comparison of results obtained by Heh and Hajialilue-Bonab and Zare is shown in Figure 2-67. Hajialilue-Bonab and Zare explain that the results of the two studies were not similar because the characteristics such as applied energy and momentum of the two experiments were very different. Noting that Poran and Rodriguez (1992) propose their research as a design method (see Section 2.5.8.2), the author is in the opinion that further research should be carried out.

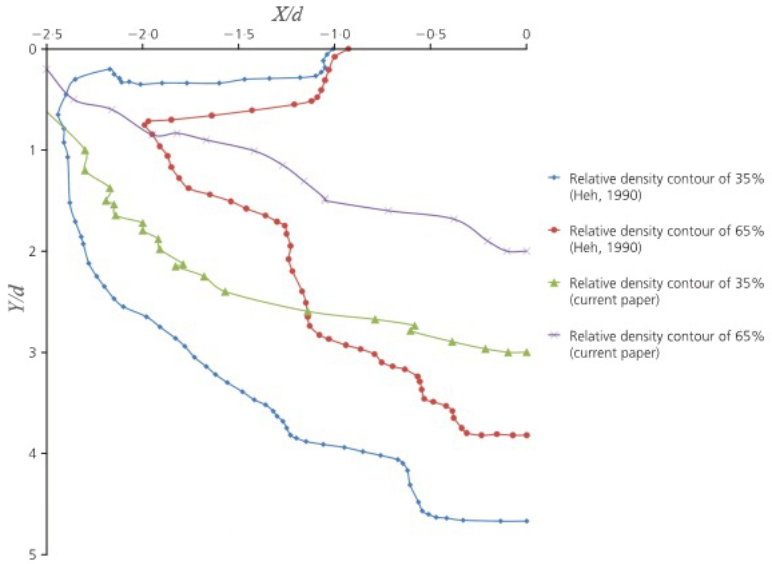

Figure 2-67: Comparison of relative density contours presented by Heh (1990) and Hajialilue-Bonab and Zare (2014)

2.5.6 Ageing and the Effect of Time

Varaksin (1981) has reported a dynamic compaction case history at an industrial site in Ashuganj, Bangladesh. In that project a Menard Tripod was used to lift a 40 ton pounder 23 metres. During the post ground improvement verification testing excess pore water pressure with low dissipation rates was observed at depth in the lower silt and sand (8 to 18 m deep).

The phenomenon was monitored in the upper silt layer where the drainage conditions were more favourable. Testing was performed 25, 40 and 60 days after dynamic compaction. It was observed that the PMT limit pressure, Menard modulus of deformation and ratio of Menard modulus to limit pressure had increased as time had gone by. Varaksin notes that this phenomenon is often observed without noticeable volume change after dissipation of total pore water pressure, and notes that it is analogous to thixotropic recovery.

Mitchell (1981) notes evidence indicated that in many sands time-dependant increases in strength and decreases in compressibility develop after any of the deep compaction methods. He adds that since these changes continue over long periods of many weeks or even months, they cannot be explained in terms of pore water pressure dissipation, which in the case of clean sand, continues at most for only several minutes. Mitchell is not able to explain this phenomenon, but concludes that the evaluation of ground shortly after completion of deep densification will yield conservative results.

Varaksin (2014) recalls that Mitchell reports a vibro compaction project in Nigeria in which CPT results improved after 6 months by approximately 20%, but there could be doubts to whether the re-tests were carried out at the exact locations of the original tests or by an offset that was closer to the vibroflot. In Varaksin's opinion clean sand will probably not improve at all just 1 week after ground improvement, but silty soils may experience a continuance of improvement.

Mitchell and Solymar (1984) reiterate that the specific mechanisms leading to an improvement in the soil parameters was not well understood, but speculate that the observed behaviour is, in some respects, similar to thixotropic strength gain in fine-grained soils. They note that in the case of sands, the extent of strength loss on disturbance followed by strength gain at rest was not known, nor was it evident that the process occurred without chemical changes, and add that the most probable cause of the observed phenomena seemed to involve the formation of silica acid gel films on particle surfaces and the precipitation of silica or other material from solution or suspension as a cement at particle contacts.

Mitchell and Solymar cite Denisov and Reltov (1961) who had suggested that hydrolysis can cause disruption of the silicate particle surface accompanied by formation of soluble compounds and silica gel. The gel adheres to the surface in a thin layer and has cementing properties. Denisov and Reltov had performed experiments to study the force required to

dislodge a quartz sand particle from a quartz plate on which the particle rested. The investigation showed that the adhesion force increased with the time of contact between particle and plate. For a test in air the force approximately doubled during the first 20 hours after the particle was placed on the plate. If after this period the particle and plate were placed in water for 14 days, then the force increased by a factor of more than three.

Mitchell and Solymar note that pressure and sand particle surface characteristics may also be important in this phenomenon. They cite Pettijohn et al. (1972) who had noted that pressure solution may be important due to high stress at grain contacts, and that due to the high pressure, higher solubility leads to a preferential solution. They also cite Bely et al. (1975) who had noted that sands with polished grains have fewer opportunities for structural connections, chemical and biological processes are not so active, and the content of physically linked moisture is less than for particles with scaly surfaces.

As a discussion to Mitchell and Solymar's (1984) paper Schmertmann (1987) appears to doubt that dissolution and precipitation of silica, leading to cementation at inter particle contacts, is the likely major factor in explaining the strengthening behaviour of sand, but briefly proposes two alternative explanations. Analogous to thixotropic behaviour in fine soils, Schmertmann considers time dependant particle re-orientations in sands important enough to be included as a secondary ageing contribution to the computation of settlements. Schmetmann notes that a dispersive particle re-orientation takes place in all soils with time, and that this results in a seemingly purely frictional gain in modulus and strength with time. He also gives increases in horizontal stresses due to time dependant recovery as a second explanation.

Similar to Schmertmann (1987), in Mesri et al.'s opinion (1990) a possible mechanism for the time dependant increase of clean sand strength is the continued rearrangement of sand particles during secondary compression. They note that improved frictional resistance to deformation develops with time with a gradual increase in interlocking of particle surface roughness and increased geometrical particle interference through more efficient packing.

Mesri et al. propose that in the absence of continued cone penetration testing subsequent to compaction, the empirical equation that is presented in Equation 2-73 can be used for predicting and extrapolating post soil densification CPT cone resistance from measurements that are carried out immediately after ground modification.

$$\frac{q_c}{q_{c_R}} = \left(\frac{t}{t_R}\right)^{C_D C_\alpha / C_c} \quad \text{2-73}$$

q_c = cone resistance at any time greater than reference time, t_R

q_{cR} = cone resistance at reference time

t_R = reference time, which must be greater than end of primary consolidation time

t = any time greater than the reference time

C_D = a parameter that reflects any densification by such disturbance mechanisms as vibration and blasting, which are not related to the ideally static increase in effective vertical stress.

C_α = secondary compression index

C_D = compression index beyond the critical pressure.

These two indices can be calculated from Equations 2-74 and 2-75:

$$C_\alpha = \frac{\Delta e}{\Delta \log t} \quad \text{2-74}$$

$$C_c = \frac{\Delta e}{\Delta \log \sigma'_v} \quad \text{2-75}$$

Δe = change in void ratio

σ'_v = effective vertical stress

Michalowski and Nadukuru (2011a, 2011b, 2012) comment that rearrangement of particles and restructuring are the results of an underlying process, and cannot be considered to be themselves the cause of time dependant strength gain. To explain particle rearrangement and strength gain they propose the hypothesis of *static fatigue* also known as *stress corrosion cracking* (as the process is dependent on the presence of moisture).

When two soil grains come into contact, the micro-morphologic features undergo compression, shear and bending, which will cause fracturing in the microscopic asperities and crystalline debris fragments. This fracturing, which is referred to as static fatigue by Michalowski and Nadukuru is a time delayed process, and does not occur immediately after the contact is loaded. Micro cracking causes the grains to move microns closer together by a distance comparable with a fraction of the size of the asperities on the grain surface. Grain convergence leads to firmer contacts, and consequently an increase in the contact stiffness,

which propagates through the spatial scales to be manifested at the macroscopic scale as an increase in macroscopic shear modulus; i.e., the elastic property in macro-scale. This process is time-delayed, as stress corrosion cracking does not occur at all contacts simultaneously.

As a consequence of the change in elastic moduli, the horizontal stress in a sand bed (under one-dimensional deformation conditions) will increase; however, the vertical stress will remain unchanged because it is governed by gravitational forces. Consequently, the deviatoric stress will reduce, and the stress state will move further away from the yield line, which will lead to an increase in the cone penetration resistance.

2.5.7 Extents of Improvement

2.5.7.1 Conventional Applications

USACE (US Army Corps of Engineers, 1999) defines conventional ground improvement as applications of soil treatment for intents such as improving bearing capacity, slope stabilisation, increasing the rate of consolidation settlement and improving seepage barriers.

When a site is compacted uniformly over the entire area, a peripheral band appears with characteristics that are intermediate between the non-compacted surrounding zone and the compacted interior zone. This band follows the line of the perimeter and has a width equal to approximately two times the thickness of the layer that is being improved (Menard and Broise, 1975). Thus, the uniformly improved zone will have dimensions that are reduced by two times the treatment thickness, and an offset width from net treatment area has to be included in the treatment program to obtain effective treatment throughout the target area. Menard and Broise comment that the offset width may be reduced by implementation of specific measures such as increasing the energy applied at the periphery, which involves complementary inspections to avoid the appearance of frontiers in the densification of the soil with consequent differential settlements beneath the construction.

Lukas (1995) lightly touches the issue of extent of ground improvement, and suffices to note that the offset width should be equal to the depth of the loose deposit.

USACE (1999) states that for conventional ground improvement, increasing the rate of consolidation settlement and improving seepage barriers, the depth of treatment should extend either to the depth of influence of the structure or to the bottom of the layer requiring improvement. Based on an approximate load spread of 2 to 1, USACE also specifies that the

areal extent of treatment for conventional applications should extend outside the perimeter by at least a distance equal to half the thickness of the treated layer.

2.5.7.2 Application for Liquefaction

Mitchell et al. (1995) note that loss of strength in improved ground can result during earthquakes due to inward migration of pore pressure plumes from adjacent liquefied soil, and add that common design is to extend the treatment a distance equal to the depth of the layer being compacted.

Liu and Dobry (1997) performed a series of centrifuge tests to study the effect of improved depth on foundation settlement induced by liquefaction. For their experiment they constructed model sand deposits with relative densities of approximately 52%. They then used a vibrating tube to vibrate the soil in 19 points per test to compact areas equal to 1.6 times the diameter of test footing to a relative density of approximately 90%. The testing model is shown in Figure 2-68.

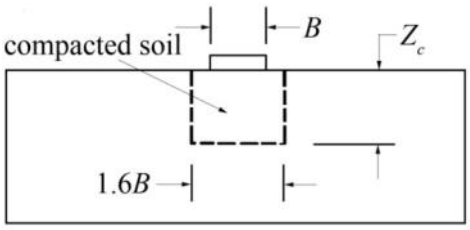

Figure 2-68: Test model for studying seismic response of shallow foundations in liquefiable sand (Liu and Dorby, 1997)

The improvement depth was made variable, and its ratio to the footing diameter was made variable from as low as 0 to as high as 2.76. As shown in Figure 2-69, it was observed that footing settlement decreased as ratio of improvement depth to footing diameter increased. The rate of settlement reduction was initially high to about when ratio of improvement depth to footing diameter reached a value of approximately 1.5, beyond which the footing settlement increased only marginally. As shown in Figure 2-70, the experiment also demonstrated that the ratio of footing settlement to free surface (non-footing) soil decreased at a higher rate up to about when ratio of improvement depth to footing diameter reached 2 (the thickness of treated ground at that ratio was about 70% of the liquefiable layer) beyond which the settlement ratio remained at unity. Liu and Dobry noted that they were not able to confirm that what they have observed in their specific experiment would also be applicable when conditions are different, but their experiment has been able to

provide enough evidence to demonstrate that liquefiable soil foundations will settle less when the ratio of treatment depth to footing width increases.

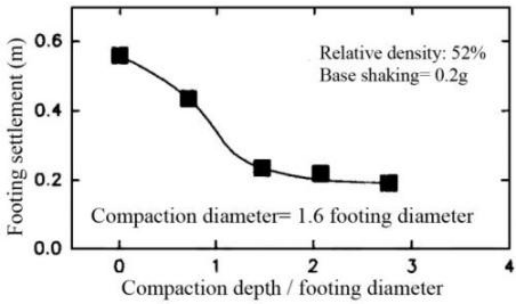

Figure 2-69: Foundation settlement versus normalised compaction depth (Liu and Dorby, 1997)

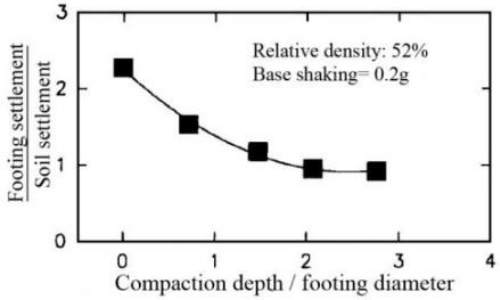

Figure 2-70: Footing settlement normalised by free field soil settlement versus normalised compaction depth (Liu and Dorby, 1997)

Liu and Dobry plotted the ratio of average foundation settlement to thickness of thickness of liquefaction, compared it with the ratio of building width to thickness of liquefaction for the 1964 Niigata and Luzon earthquakes. Their conclusion was that as the centrifuge data points without soil compaction fell within the earthquake field band, then using building width to normalise field data and footing width to normalise centrifuge data could be linked, and that it seemed reasonable to assume that the entire width of the building rather than the sizes of the individual footings determined the overall pore pressure response under the buildings.

Akiyoshi et al. (1993) have also conducted a series of tests using a shaking table and by performing numerical analyses to assess the effect of ground improvement with sand compaction piles for mitigation of liquefaction. In their experiment the saturated sand models initially had relative densities of about 22%. Then each model was compacted in 16 locations with mini sand piles that were 70 mm in diameter and 500 mm long. Depending on the compaction energy that was applied, the average relative density of the compacted areas were 40 to 50%.

It was observed that depending on the amount and extent of compaction the ground still liquefied gradually. However, the numerical analyses showed slow accumulation of excess pore water pressure in the compacted area and rapid accumulation in the uncompacted peripheral areas. After the excess pore water pressures reached a peak in the uncompacted areas, they began to dissipate. Akiyoshi et al. note that the results indicated that the compacted area gradually liquefied due to seepage flow from the adjacent liquefied area.

Figure 2-71 shows the distribution of excess pore water pressure ratios at four transient times for a ground model with width to depth ratio of compacted area being 1.6 and depth of compacted area to total ground thickness equalling unity. It can be understood from Figure 2-71(d) that the angle between the boundary of compacted and non-compacted areas and the line corresponding to the excess pore water pressure ratio curve of 0.5 is approximately 30 to 35%, in the case when most of the compacted area does not liquefy. Akiyoshi et al. comment that the compacted triangular zone between these two lines can be considered to liquefy readily as a result of the influence of the adjacent liquefied uncompacted area. The results of this study appeared to be consistent with the experimental results that were performed by Japan's Port and Harbour Research Institute, PHRI (Iai et al., 1987).

Figure 2-72 shows the relationship between the maximum excess pore water pressure ratio at two depths of the centre point of the treated area and the width to depth ratio of the compacted area. It can be observed that the excess pore water pressure ratio decreases as the width to depth ratio of the compacted area increases. It appears that in Akiyoshi et al.'s experiment the maximum excess pore water pressure ratio of the centre point of improved soil was less than 0.5 when the width to depth ratio of the compacted area was greater than 1.5. Akiyoshi et al. note that although the amount of data was limited, there may be an optimum compaction width for design purposes.

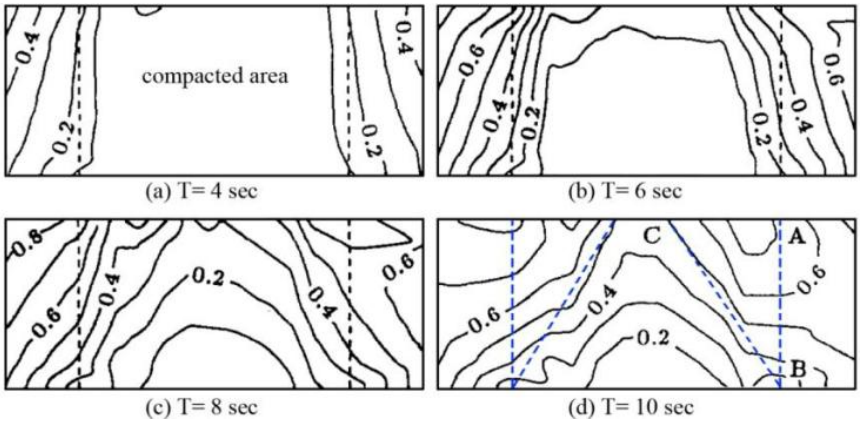

Figure 2-71: Distribution of excess pore water pressure ratio at different transient times for a ground model with width to depth ratio of compacted area being 1.6 and depth of compacted area to total ground thickness equalling unity; modified from Akiyoshi et al. (1993)

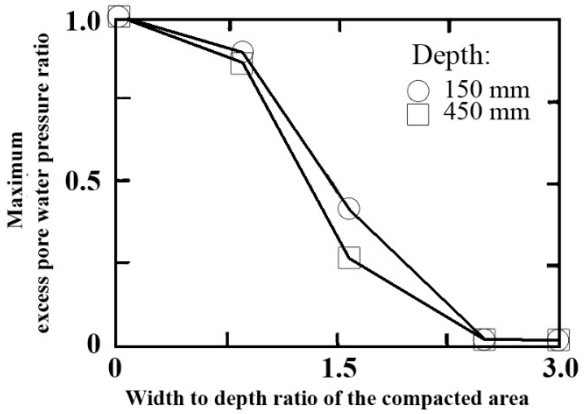

Figure 2-72: Relationship between maximum excess pore water pressure ratio and width to depth ratio of compacted area when treatment depth equals liquefaction thickness (Akiyoshi et al., 1993)

USACE (1999) states that for liquefaction mitigation, the depth of treatment should generally extend to the bottom of the layer that requires improvement, particularly for large or heavily loaded structures. USACE seems less stringent for lightly loaded structures, and notes that it may not be necessary to treat the entire liquefiable layer for such structures. Yet, USACE further adds that design procedures for an improved crust over liquefiable soils are not well established, and refers to Ishihara (1985) who presents correlations between minimum thickness of a non-liquefiable surface layer, the maximum thickness of an underlying liquefiable soil layer and surface manifestations of liquefaction for free field conditions or lightly loaded structures. USACE also specifies that areal extent of treatment for liquefaction protection should extend generally outside the perimeter of the structure at least by a distance equal to the thickness of the treated layer.

Hausler (2002) cites Cooke and Mitchell (1999) for also commenting that standard practice for improvement of liquefiable soil beneath most structures is to extend ground improvement to the bottom of the liquefiable material. Hausler (2002) also cites PHRI, (1997) for recommending ground improvement to be carried out through the full thickness of the potentially liquefiable soil, but at the same time cites Japanese Geotechnical Society, JGS, (1998) that ground improvement contractors in Japan are not required to extend treatment to below the depth of 20 m for most buildings, bridges and railway structures, and to below the depth of 15 m for oil storage tanks and LNG storage tanks. According to Hausler, JGS (1998) recommends that lateral extent of ground improvement be equal to ½ of the improved depth. Hausler also cites PHRI for reporting that as shown in Figure 2-73, the Japan Fire Defence Agency, which regulates hazardous facilities such as oil tanks, has regulations in place since 1974 that specifies that the lateral extent of the ground improvement area should be equal to or greater than 2/3 of the compaction depth.

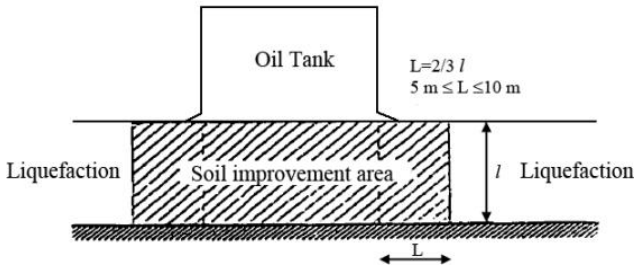

Figure 2-73: Ground improvement zone as specified by Japan Fire Defence (Port and Harbour Research Institute, 1997), as cited by Hausler (2002).

Hausler (2002) notes that shaking table tests and seepage analyses performed by PHRI shows that, as shown in Figure 2-74, an area of softening or instability exists above a failure plane at 30^{o} with the vertical plane between the improved and unimproved zones, and adds that according to the simplified design procedure set forth by PHRI, the strength of this area should not be expected to contribute to bearing capacity, and the treated area should be designed wide enough to obtain sufficient bearing capacity from shear resistance along the Terzaghi failure surface.

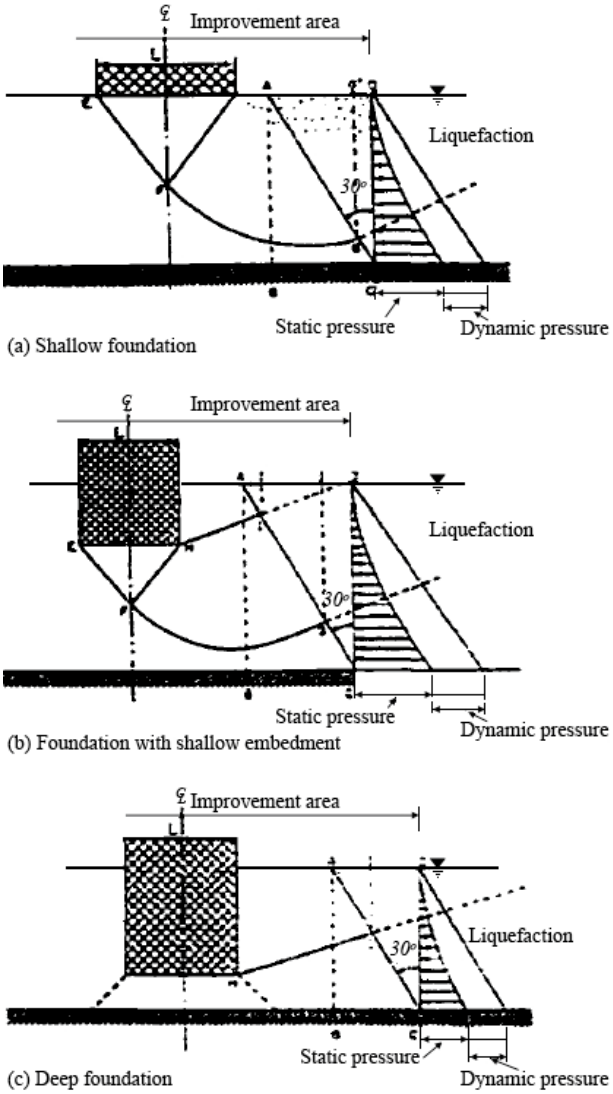

Figure 2-74: Stability of treated zone without contribution of a 30o wedge (Port and Harbour Research Institute, 1997), as cited by Hausler (2002).

2.5.8 Design Methods

2.5.8.1 Lukas (1995)

Although the oldest and most relied on rules of thumb, the design guidelines proposed by Lukas (1995) are the closest to industry practices. He proposes six steps:

1. Selection of pounder weight and drop height based on the required depth of improvement (refer to Section 2.5.2).

2. Determination of applied energy to achieve the required depth of improvement:

For this purpose he proposes the utilisation of Table 2-8 for the selection of the unit energy for the proper deposit classification. Volumetric compaction energy can be converted to planar energy intensity by multiplying the volumetric energy by the treatment thickness.

Type of deposit	Unit applied energy		Per cent standard Proctor Energy
	KJ/m^3	tm/m^3	
Pervious coarse grained - Zone 1	200-250	20-25	33-41
Semi pervious fine grained soils – Zone 2 and clay fills above water table – Zone 3	250-350	25-35	41-61
Land fills	600-1100	60-110	100-180

Note: Standard Proctor energy= 600 kJ/m^3

Table 2-8: Applied energy guidelines (Lukas, 1995)

3. Determination of the treatment area:

   3.1. For level sites, use a grid spacing throughout the area in need of improvement and an offset area beyond the project boundaries equal to the depth of improvement (refer to Section 2.5.7 for a more comprehensive discussion and alternative offset widths).

   3.2. If slope stability is a concern, improvement over a wider plan area may be required.

   3.3. At load concentration areas, apply additional energy as needed.

4. Determination of grid spacing and number of drops

   For this purpose Lukas proposes the implementation of Equation 2-76:

$$AE = IP = \frac{NWHP}{s^2} \qquad 2\text{-}76$$

AE= Applied energy

I= energy intensity= applied energy per unit area

N= number of blows

P= number of passes

W= weight of pounder

H= drop height

s= grid spacing

In Equation 2-76, grid spacing is the final distance inclusive of phase 1 and phase 2 prints. The number of passes is not the number of phases; it refers to applying (equal amount of) blows to the same prints of the grid.

4.1. Select a grid spacing ranging from 1.5 to 2.5 times the diameter of the pounder

4.2. Enter W and H from Step 1 and applied energy intensity from Step 2 into Equation 2-76.

4.3. Use Equation 2-76 to calculate the product of N and P. Lukas suggests that generally 7 to 15 drops are made at each print, and adds that if the calculations indicate significantly more than 15 or less than 7 blows, then grid spacing should be adjusted.

5. Multiple passes

Lukas speculates that prediction of crater depths or ground heave in advance of dynamic compaction is difficult, and assesses that multiple passes should be applied when very loose deposits like landfills are present or where silty deposits are nearly saturated.

He suggests that:

5.1. Crater depths should be limited to the height of the pounder plus 0.3 m to allow for non-complicated extraction of the pounder from the ground.

5.2. Energy application should stop if ground heave occurs. Although heaving is a sign of non-volumetric plastic displacement, the author does not believe that any amount of heaving necessitates the termination of compaction efforts. Indeed, it is preferable to observe net volumetric change, being the difference between volume of compaction and volume of heave, and to terminate pounding when impact energy does not lead to any significant net compaction.

5.3. If 5.1 and 5.2 occur before the required number of blows has been applied, then multiple passes should be used to allow for dissipation of pore water pressures.

6. Surface stabilising layer:

Not needed for Zone 1 soils (refer to Section 2.5.1), but may be possibly required for nearly saturated Zone 2 soils. The surface stabilising layer is usually required for landfills.

6.1. When a surface stabilising layer is used, the thickness ranges generally from 0.3 to 0.9 m.

6.2. Lukas (1995) does not mention the ironing phase in his guideline, but does mention it elsewhere in his publication.

2.5.8.2 Poran and Rodriguez (1992)

Poran and Rodriguez (1992) have proposed a design method for dry sands based on test models reported by Heh (1990) and Poran et al. (1991), which has already been explained in Section 2.5.4. In this method, Poran and Rodriguez estimate the soil mass that has been compacted to a certain strain or relative density using semi-prolate spheriods, with side, top and approximate shape shown in Figure 2-66. Based on Equations 2-70 and 2-71, and Table 2-7, Poran and Rodriguez developed the charts shown in Figure 2-75 to demonstrate the relationship between the normalised semi-prolate spheriod's horizontal and vertical radii (respectively a and b, as shown in Figure 2-66) and normalised total specific energy, $NWH/(Ab)$ (in kPa). The definitions for the variables in the chart are given in Section 2.5.4. The least and most improvement lines refer to DC induced plastic volumetric strains of respectively 1.5% and 7.7%. Poran and Rodriguez contemplate that the parameter range obtained from the model test results in the laboratory is also adequate for actual dynamic compaction works, and as more field data is investigated, it will be possible to further calibrate these relationships for different soil conditions.

Poran and Rodriguez (1992) recommend that the numerical average improvement lines shown in Figure 2-75 and redrawn in Figure 2-76 be used for the purpose of dyanmic compaction design. In this process, the vertical radius of the semi-prolate spheriod should be taken as equal to the depth of improvement. Poran and Rodriguez do not explain why they make such a recommendation, and the significance and consequences of this decision. These lines that correspond to strain values are indeed a fundemental component of the design, and all other steps of the design will be impacted greatly and directly by this choice. In the end, it is not clear what criteria are to be satisfied by these choices of lines.

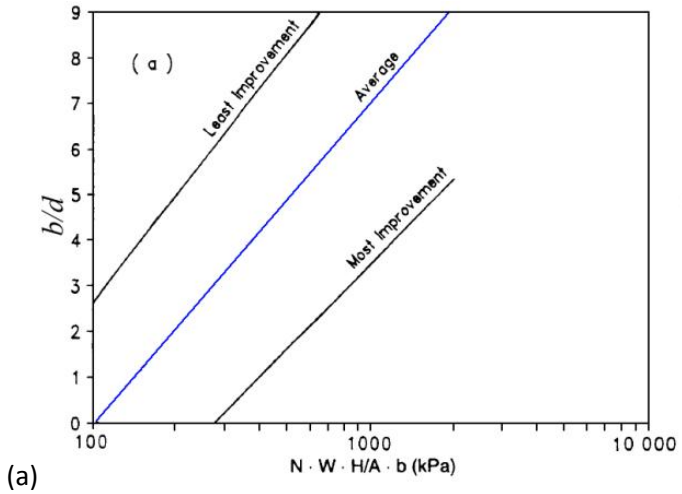

(a)

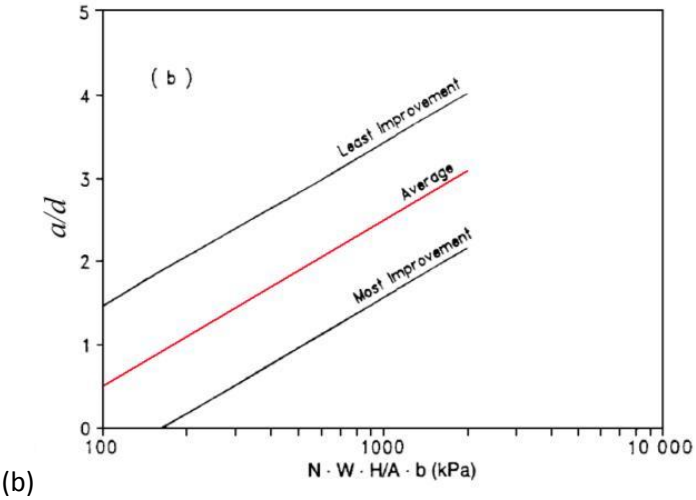

(b)

Figure 2-75: Range of improvement in soil mass for (a) b/d and (b) a/d versus total normalised specific energy (Poran and Rodriguez, 1992)

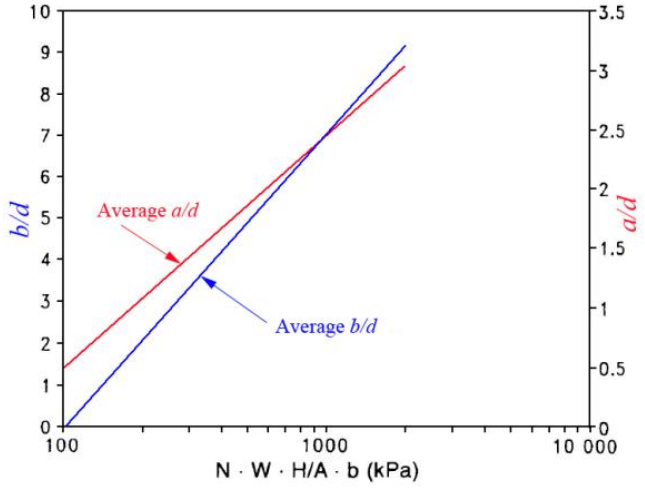

Figure 2-76: Proposed design chart for dynamic compaction in sandy soils (Poran and Rodriguez, 1992)

Poran and Rodriguez propose that the following steps should be used for the preliminary design of dynamic compaction in dry sandy soils:

1. Examination of soil data and defining the required depth of improvement.

2. Determination of W, H and d, and calculation of WH and A. The equivalent diameter for non-circular pounders is to be taken as the pounder's width.

3. The value of $NWH/(Ab)$ is found from the b/d line of Figure 2-76 using the calculated b/d value, and the required number of blows is calculated from the value of $NWH/(Ab)$ that was extracted from Figure 2-76, and rounded up to the nearest whole number.

4. The value of a/d is determined by using the a/d line in Figure 2-76 for the appropriate $NWH/(Ab)$ that was found in step 3, and then the value of a is obtained from the ratio of a/d for grid spacing design.

5. With the value of a, the grid pattern for the first and subsequent passes may be designed (based on the semi-prolate spheroid shape) to obtain the most complete overlap of improved soil mass to the desired depth.

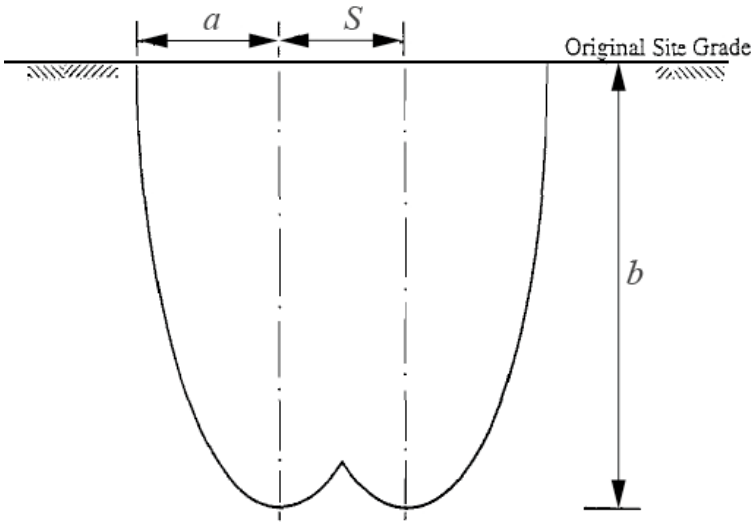

Figure 2-77: Overlapping of semi-prolate spheroids, modified from Poran and Rodriguez (1992)

Poran and Rodriguez do not explain why they are targeting the most complete overlap; as there is no discussion about the amount of improvement in the overlapping zone, the author speculates that it is their intention to minimise the volume of soil outside of the semi-prolate spheriods in between the prints, shown in Figure 2-77, which does not receive the same amount of treatment as in the semi-prolate spheriods themselves. They are also not clear on

the procedure for determining the most complete overlap of improved soil mass to the desired depth, and suffice by presenting an example in which they deem that considering a grid spacing equal to $0.9a$ is appropriate.

2.5.8.3 Jahangiri et al. (2011)

Based on two dimensional finite element analyses using a cap model, Jahangiri et al. (2011) have developed a design method for dynamic compaction. In their approach, it is assumed that the soil beneath the pounder centre reaches its maximum achievable compaction, and subsequent pounder blows at adjacent points does not induce further improvement at that location. Therefore, it is also assumed that the degree and depth of improvement along the vertical axis of prints is unlikely to be significantly affected by the compaction of adjacent prints. However, there is significant overlapping of lesser improved zones that are further away from the print location.

Jahangiri et al. use the notion of relative degree of improvement, I_r (Lee and Gu, 2004), as defined in Equation 2-77, rather than relative density to take into account the effects of initial relative density and soil properties.

$$I_r = \frac{D_d - D_{do}}{100 - D_{do}} \cdot 100(\%) \qquad 2\text{-}77$$

D_d = relative density

D_{do} = initial relative density

As can be seen in Figure 2-78, for a single DC print (left point), relative degree of improvement, I_r, is achieved at depth *z*. The second print (right point) is assumed to be at a distance away from the first print in such a way that two improved bulbs with ½ of the relative degree of improvement, $I_r/2$, intersect one another also at depth Z. Jahangiri et al. assume that by using the relative degree of improvement in the overlapping area will also become I_r using the law of superposition. Noting that the left and right prints have equal bulbs, it is concluded that grid spacing should be double the distance between the centre of each print and the intersection point.

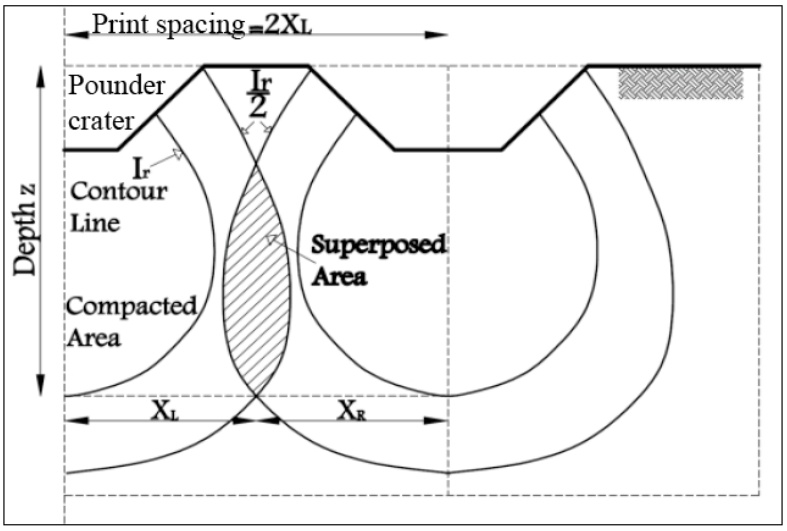

Figure 2-78: Schematic scheme for evaluation of print spacing (Jahangiri et al., 2011)

Jahangiri et al. have performed a number of analyses with various drop heights, pounder weights, pounder radii and number of drops to develop charts for grid spacing when I_r is 8, 15, 30, 46 or 62%. Review of the analyses suggested that trends of variation of grid spacing were tightly bounded when I_r was 8, 15 and 30%. These were considerably different from when I_r was 46 or 62%, but the average difference for cases with I_r values of 46 and 62% was minor and only 5.7%. Thus, two charts were developed for determination of grid spacing based on NWH/A, pounder radii, r, and I_r. Figure 2-79 and Figure 2-80 show the relationships when I_r is respectively equal to 8, 15 and 30%, and 46% and 62%. Jahangiri et al. note that for pounder radii other than what has been indicated in the figures; i.e., 0.5, 1 and 1.5 m, interpolation may be used, but do not clarify how to proceed for other I_r values.

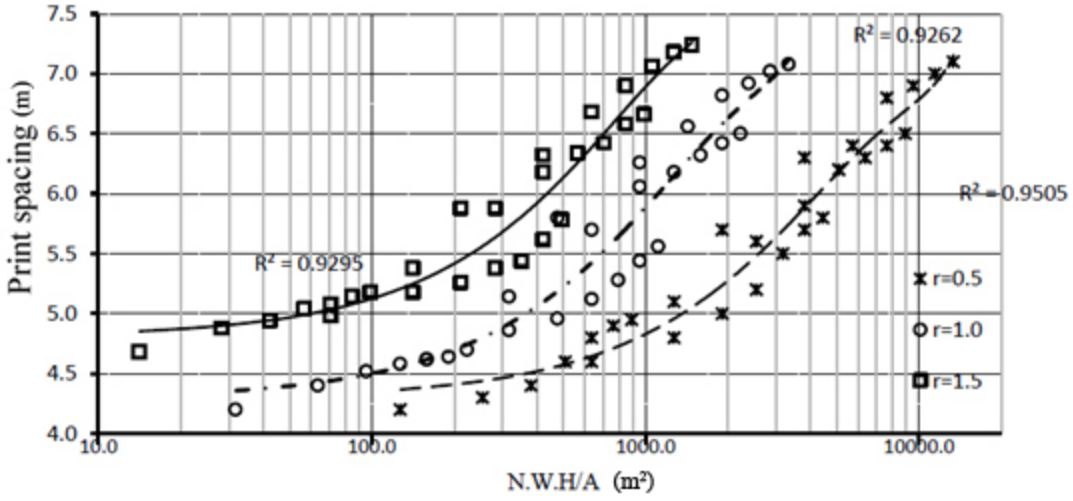

Figure 2-79: Print spacing curves for I_r= 8%, 15% and 30% (Jahangiri et al., 2011)

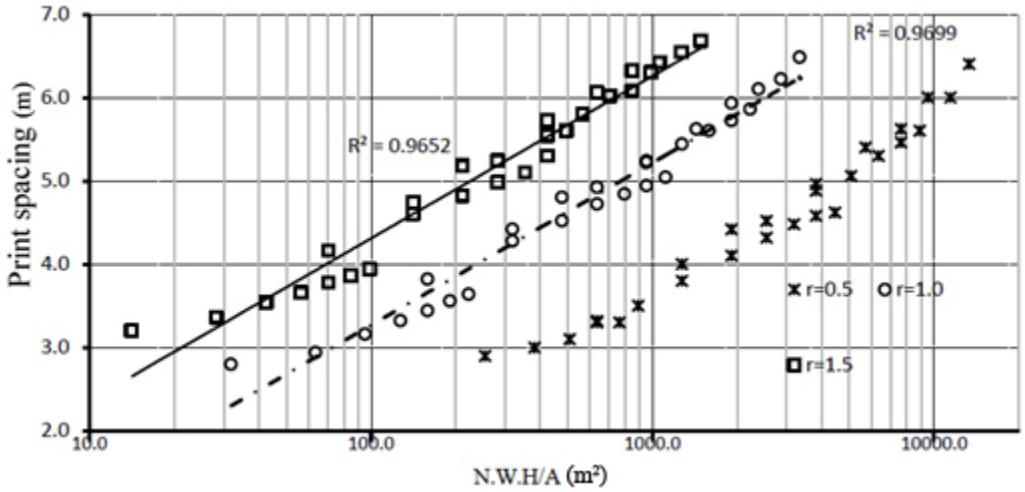

Figure 2-80: Print spacing curves for I_r = 46% and 62% (Jahangiri et al., 2011)

In the opinion of the author the method proposed by Janhangiri et al. is very promising, but application of the law of super position to soil that has undergone potentially nonlinear very large plastic strains is very questionable, and without further study, it is doubtful that a simple summation of I_r halves will yield true and accurate results in the overlapping zones.

2.6 Design Guidelines for Dynamic Replacement

2.6.1 Soil Arching

It was mentioned in Section 2.4.9 that loads are distributed between the in-situ soil and DR columns by arching through the load transfer platform. A number of different methods are available for estimating the amount of load that is transferred to the DR columns. The most relevant methods are discussed in this section.

Punching of the column into the upper granular fill may be improved by using geotextiles or higher grade compacted fill in the lower layers of the embankment that will act as the load transfer platform.

2.6.1.1 British Standard

One of the first researchers who studied soil arching were Marston and Anderson (1913) who evaluated soil loadings on buried pipelines. Their formula was later adopted and modified in BS 8006:1995 (British Standards Institution, 1995) for the two dimensional calculation of average pressure acting on a pile cap.

Although BS 8006 assumes plane strain behaviour and does not consider the actual three dimensional arching that occurs in reality when there are no beams, this method is nevertheless used by engineers to determine the ratio of load that the piles (or columns) support. Van Eekelen & Bezuijen (2008) have reviewed BS 8006, and have proposed an adaptation of the equations so that the method becomes three dimensional and vertical equilibrium is satisfied. Van Eelelen and Bezuijen's modifications are especially of interest for calculating the tensile stresses in geotextiles that could be used for basal reinforcement in conjunction with the rigid inclusions.

To ensure localised differential deformations cannot occur at the surface of embankments (which can be a problem with shallow embankments) BS 8006 recommends that the relationship between embankment height and pile cap spacing be maintained to

$$H \geq 0.7(s - a) \qquad \text{2-78}$$

Where

a= size (or diameter) of pile caps (assuming full support can be generated at the edges of the caps),

s = spacing between adjacent piles, and

H = height of the embankment.

According to BS 8006 the ratio of vertical stress exerted on top of the pile caps to the average vertical stress at the base of the embankment can be estimated by

$$\frac{\sigma'_c}{\sigma'_v} = \left(\frac{C_a a}{H}\right)^2 \qquad 2\text{-}79$$

Where

σ'_c = vertical stress on the pile caps,

σ'_v = equal to $\gamma H + w_s$ and is the average vertical stress at the base of the embankment,

γ = unit weight of the embankment fill,

w_s = uniformly distributed surcharge loading, and

C_a= the arching coefficient and is as shown in Table 2-9

Pile Arrangement	Arching coefficient
End-bearing piles (unyielding)	$C_a = \frac{1.95H}{a} - 0.18$
Friction and other piles (normal)	$C_a = \frac{1.5H}{a} - 0.07$

Table 2-9: Arching coefficient

2.6.1.2 Hewlett and Randolph

Hewlett and Randolph (1988) studied two and three dimensional soil arching of piled embankments in granular fills. Analogous to dynamic replacement, Hewlett and Randolph assume in their analysis that no slab is used and the piles (columns in the case of DR) are placed at a relatively wide spacing.

According to Hewlett and Randolph field evidence suggests that pile caps (columns in the case of DR) covering as little as 10% of the area beneath the embankment may carry more than 60% of the weight of an embankment due to arching action in the fill.

Hewlett and Randolph also note that in the model test that they used, with a constant ratio of column spacing to column width, the settlement of the surface of the sand fill was less for the smaller width columns. The observed deformities of the sand indicated that arching occurred across adjacent columns. Between the columns, sand close to the subsoil (foam rubber in the test model) underwent significant settlement (as compared to the settlement of the fill's surface). Shear distortion was concentrated in fans originating from the corners of the columns. Sand was observed to settle uniformly well above the pile caps; however, the bottom layer of sand remained straight between the piles, which showed uniform settlement, and suggested that the pressure on the subsoil was uniform.

Based on pile cap (column in the case of DR) size and spacing, height of embankment fill and friction angle of the granular fill that formed the embankment, Hewlett and Randolph developed two dimensional (plane strain) and three dimensional expressions for determining the proportion of weight of the embankment that is carried directly by the pile cap. Having estimated the proportion of load carried by the columns, the overall performance of the embankment may be deducted from a separate analysis of the subsoil and membrane.

In the plane strain case, where long arches are supported by continuous ledges, as shown in Figure 2-81, it is assumed that the horizontal band of soil that contains the arch is weightless, and the sand in the infilling regions beneath the arches and the cusps between the arches does not mobilise any strength (isotropic stress state). Within each arch, the tangential direction is the direction of major principal stress, and the radial direction is the direction of minor principal stress. Static equilibrium requires that the arches are semi-circular, of uniform thickness, and span adjacent ledges with no overlap of arches.

For an embankment of height, H, spanning pile caps of width, b, at centreline spacing, s, the efficacy, E, or the portion of load that is supported by the piles can be calculated to be expressed by

$$E = 1 - \frac{b}{s}\left(1 - \frac{s}{2H}\right)\left(1 - \frac{b}{s}\right)^{K_p - 1} \qquad 2\text{-}80$$

K_p is the Rankine passive earth pressure coefficient, and is equal to

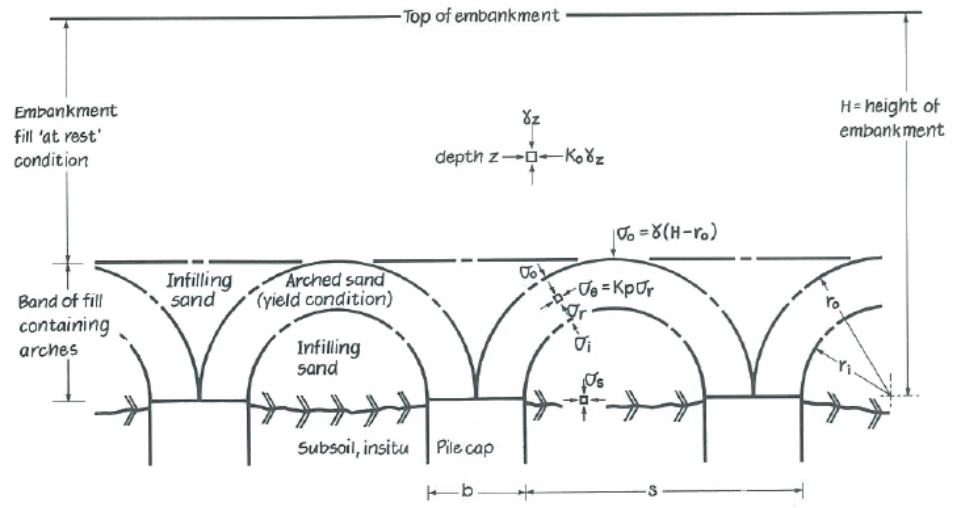

Figure 2-81: Plane strain (2 dimensional) arching of soil (Hewlett and Randolph, 1988)

$$K_p = \frac{1 + sin\varphi}{1 - sin\,\varphi} = tan^2\left(45^\circ + \frac{\varphi}{2}\right) \qquad 2\text{-}81$$

φ is the internal friction angle of the sand fill. The remainder of the fill weight can be assumed to be uniformly distributed on the subsoil.

As shown in Figure 2-82, the case of most relevance for embankment piling (or DR installation) is for three dimensional spatial arching above a grid of piles where sand vaults form. The vaults are comprised of a series of domes. The crown of each dome is approximately hemispherical, and its radius is equal to half of the diagonal spacing ($s/\sqrt{2}$) of the piles.

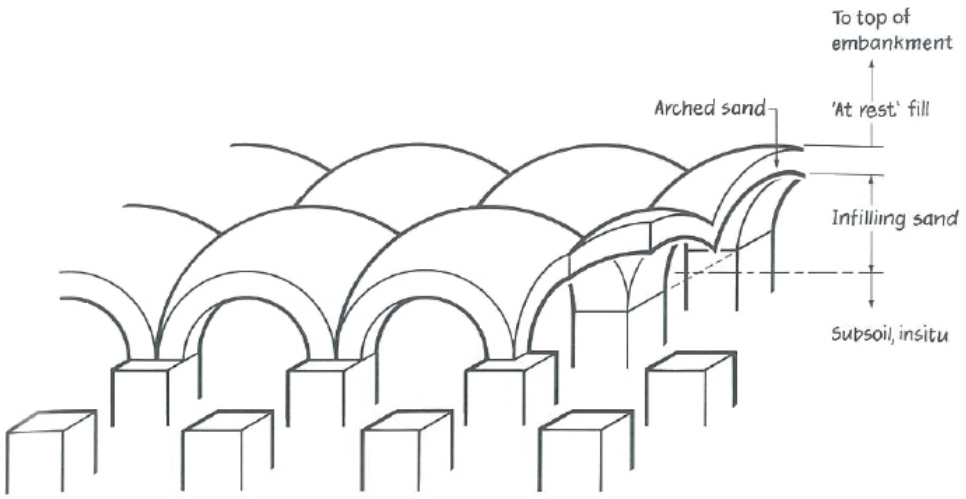

Figure 2-82: Isometric view of a grid of pile caps (DR columns) and a series of domes forming vaults spanning between them (Hewlett and Randolph, 1988)

In this case, the crown of the dome is not necessarily the weakest region of the system of vaulting. The limited area of support at the pile caps may lead to a bearing failure at that point. The approach adopted by Hewlett and Randolph follows the analysis used for consideration of equilibrium at the crown of the arches. Integration of the tangential stress in the arch at pile cap level allows an estimate to be made of the overall force that may be taken by the pile cap.

Analysis of the two regions; i.e., the crown and base of the arches (bearing capacity of the pile cap punching into the granular fill) leads to two separate estimates of the efficacy of the pile support of which, the lower estimate should be used for design.

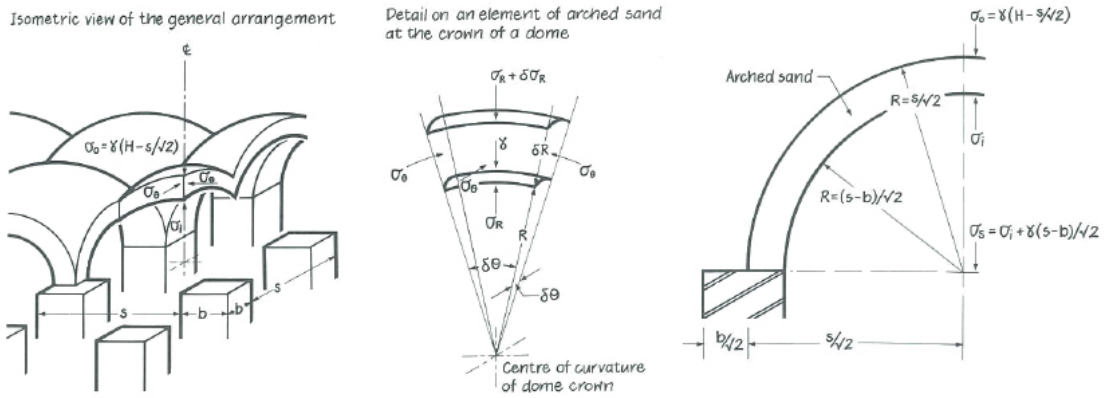

Figure 2-83: Analysis of arching at the crown of a dome. The diagram on the right represents a diagonal section through a pile cap and dome crown. (Hewlett and Randolph, 1988)

At the crown of the arch (Figure 2-83), the form of analysis is similar to that for the plane strain case, except for the spherical geometry and the inclusion of self-weight. It can be demonstrated that based on the analysis of the crown, the efficacy of the piles will be

$$E = 1 - \left[1 - \left(\frac{b}{s}\right)^2\right][A - AB + C] \qquad 2\text{-}82$$

$$A = \left[1 - \left(\frac{b}{s}\right)^2\right]^{2(K_p - 1)} \qquad 2\text{-}83$$

$$B = \frac{s}{\sqrt{2H}}\left(\frac{2K_p - 2}{2K_p - 3}\right) \qquad 2\text{-}84$$

$$C = \frac{s-b}{\sqrt{2H}}\left(\frac{2K_p - 2}{2K_p - 3}\right) \qquad 2\text{-}85$$

As shown in Figure 2-84, the vault comprises of four plane strain arches at the pile cap, with each occupying a quadrant of the cap. It can be analytically demonstrated that efficacy will be:

$$E = \frac{\beta}{1+\beta} \qquad 2\text{-}86$$

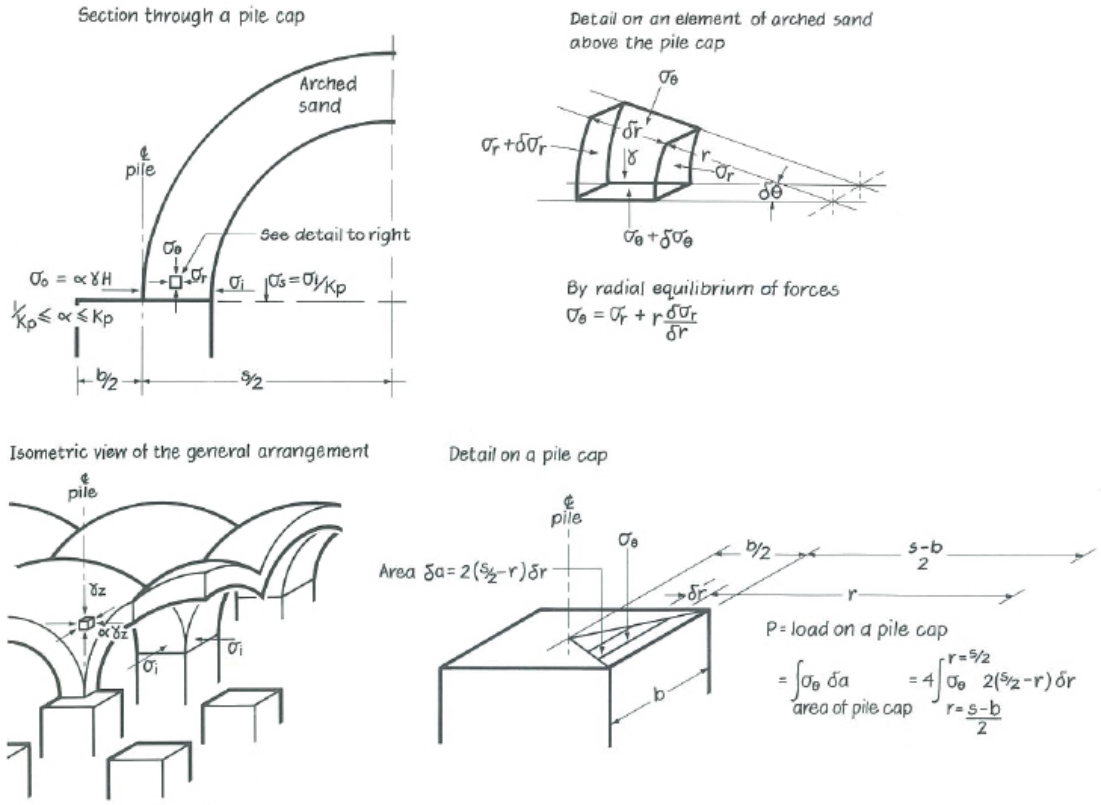

Figure 2-84: Arching in the sand fill immediately over a pile cap (Hewlett and Randolph, 1988)

Where:

$$\beta = \frac{2K_p}{K_p+1} \times \frac{1}{1+\frac{b}{s}} \times \left[\left(1-\frac{b}{s}\right)^{-K_p} - \left(1+\frac{b}{s}K_p\right)\right] \qquad 2\text{-}87$$

Efficacy will be the minimum of the values calculated from Equations 2-82 and 2-86. As in the case of plane strain, the remainder of the fill weight can be assumed to be uniformly distributed on the subsoil.

As might have been expected, at low embankment heights relative to the spacing of columns (b/s), the performance of the columns is governed by the condition at the crown of each arch. However, as the height of the embankment increases, the critical region transfers to the columns.

As noted by Hewlett and Randolph themselves, this analysis approach has a lower bound nature, and field studies indicate that the columns' efficacy is actually more than calculated. For example, while calculations indicated an efficacy of 0.61, field measurements indicated that in fact 82% of the embankment load was taken by the piles.

2.6.1.3 German Code EBGEO (2004)

EBGEO 2004 Section 6.9 is a recommendation for piled embankments design procedure issued by *Deutsche Gesellschaft für Geotechnik* or the German Geotechnical Society (DGGT, 2004) in July 2004. The method adopts the so-called multi-shell arching theory based on Zaeske's (2001) research. Satibi (2009), Kempfert et al. (2004), and Rainthel et al. (2008) have reviewed the German Code recommendations. Their papers have been used as references for this section.

The German method EBGEO 2004 is recommended for the design of embankment on rigid end-bearing piles. For the design of embankment on floating piles, further elaboration of the design procedure is required (Satibi, 2009).

As shown in Figure 2-85, in EBGEO 2004 it is assumed that the piles are spaced at diagonal distances. Denoting the pile (or DR column) diameter and diagonal spacing between the piles respectively with d and s_d, in rectangular grids:

$$s_d = \sqrt{{s_x}^2 + {s_y}^2} \qquad 2\text{-}88$$

In triangular grids:

$$s_d = \max\{s_x, s_y\} \qquad 2\text{-}89$$

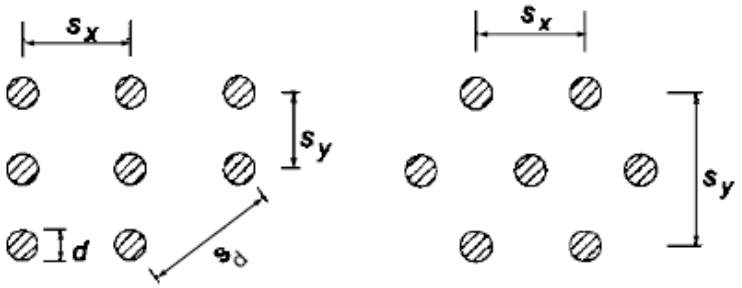

Figure 2-85: Point support definitions (rectangular-triangular) (Kempfert et al., 2004) after Zaeske (2001)

Similar to Hewlett and Randolph (1988), EBGEO 2004 assumes that the arches have the shape of hemispherical domes spanning between the pile caps. However, as shown in Figure 2-86, EBGEO 2004 considers that the arches consist of multi-shell domes. The topmost arching shells take the shape of hemispherical domes with the radius being equal to $0.5 s_d$. Inside the topmost shells, there are multi-spherical shaped arching shells with radii larger than $0.5 s_d$ to infinity for the lowest arching shell. The lowest arching shell is tangential to the surface of the soft subsoil.

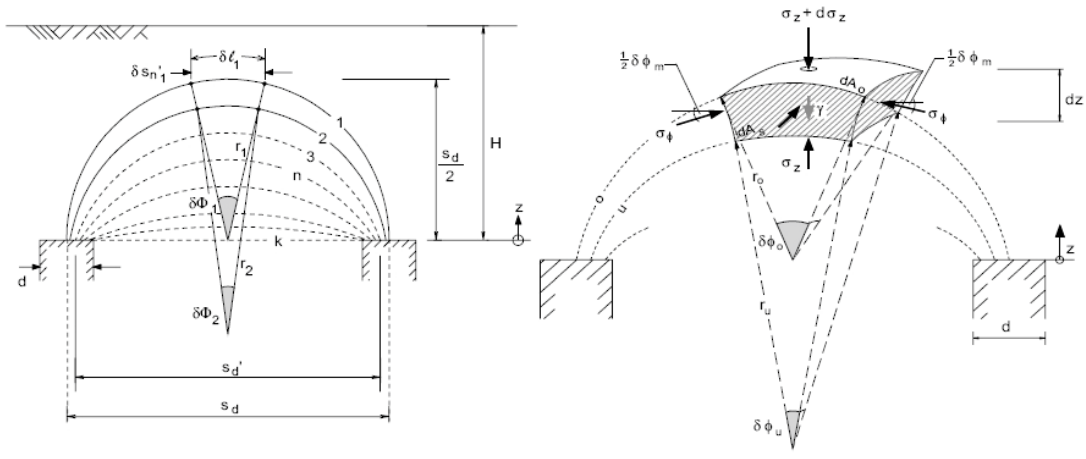

Figure 2-86: Theoretical arching model (Kempfert et al., 2004) after Zaeske (2001)

By evaluation of forces equilibrium of an element, and solving the differential equation it can be derived that the vertical stress at the lowest arching shell (at the soft subsoil) will be:

$$\sigma'_{z0} = \lambda_1{}^{\chi}\left(\gamma + \frac{w_s}{H}\right)\Bigg[H\left(\lambda_1 + h_g{}^2\lambda_2\right)^{-\chi} + h_g\left(\left(\lambda_1 + \frac{h_g{}^2\lambda_2}{4}\right)^{-\chi} - \left(\lambda_1 + h_g{}^2\lambda_2\right)^{-\chi}\right)\Bigg] \quad \text{2-90}$$

$$\lambda_1 = \frac{1}{8}(s_d - d)^2 \quad \text{2-91}$$

$$\lambda_2 = \frac{s_d + 2ds_d - d^2}{2s_d{}^2} \quad \text{2-92}$$

$$\chi = \frac{d\left(K_p - 1\right)}{\lambda_2 s_d} \quad \text{2-93}$$

σ'_{zo}= uniform stress at subsoil level,

γ = unit weight of the embankment fill,

w_s = uniformly distributed surcharge loading, and

K_p = passive earth pressure coefficient, and

h_g = arching height and can be calculated from

$$h_g = \frac{s_d}{2} \quad for\ H \geq \frac{s_d}{2} \quad ; \quad h_g = H \quad for\ H < \frac{s_d}{2} \quad \text{2-94}$$

When the pile cap is not circular, the diameter may be taken as the equivalent diameter based on pile cap area, A_c:

$$d = \sqrt{\frac{4A_c}{\pi}} \quad \text{2-95}$$

The effective pressure acting on top of pile cap can be calculated to be:

$$\sigma'_c = [(\gamma H + w_s) - \sigma'_{z0}] + \frac{A_E}{A_c} + \sigma'_{z0} \quad \text{2-96}$$

A_E = area of one unit cell, see Figure 2-87 (Balaam and Booker, 1981, Goughnour and Bayuk, 1979).

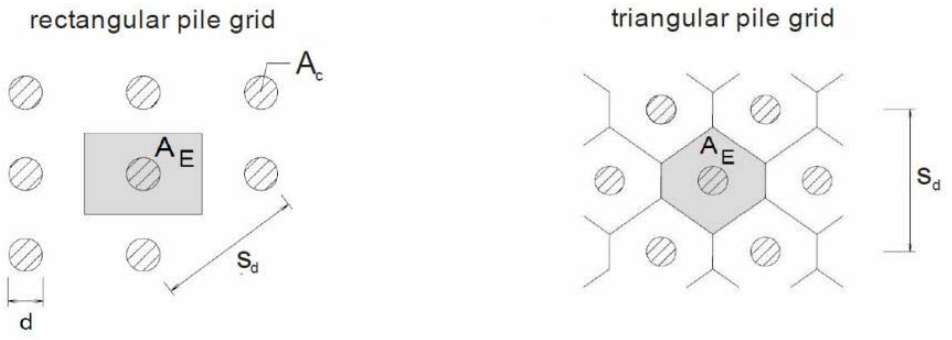

Figure 2-87: Area of one pile cell (Satibi, 2009) after DGGT (2004)

Similar to Hewlett and Randolph (1988), this analytical model is also based on the lower bound theorem of plasticity (Satibi, 2009).

ABGEO 2004 requires that the embankment height be at least $0.7s_d$ to ensure that soil arching fully develops.

2.6.1.4 Vertical Equilibrium Load Distribution

Aboshi et al. (1979, 1991) cite Murayama (1962) for establishing equations, which demonstrate that vertical stresses on a (DR) column and the surrounding soil can be calculated through the equilibrium of vertical stresses acting on the composite ground. Defining the area *replacement ratio*, a_c, as the area of one DR column (sand column in the original research) to the total area of the DR unit cell, and *stress distribution ratio* (*also referred to as the stress concentration ratio*), n, as the ratio of the stress in the soil to the stress in the DR column:

$$a_c = \frac{A_c}{A_c + A_s} \qquad 2\text{-}97$$

$$n = \frac{\sigma_c}{\sigma_s} \qquad 2\text{-}98$$

σ = average stress on unit cell

σ_c = stress in DR column

σ_s = stress in soil

A_c = area of DR column

A_s = area of soil in unit cell

Then, if:

σ_h = lateral confining stress on the cylindrical surface of the DR column, and

σ_u = upper yield value of the soil

c = soil cohesion

The parameters defined above are shown schematically in Figure 2-88. It can be calculated that:

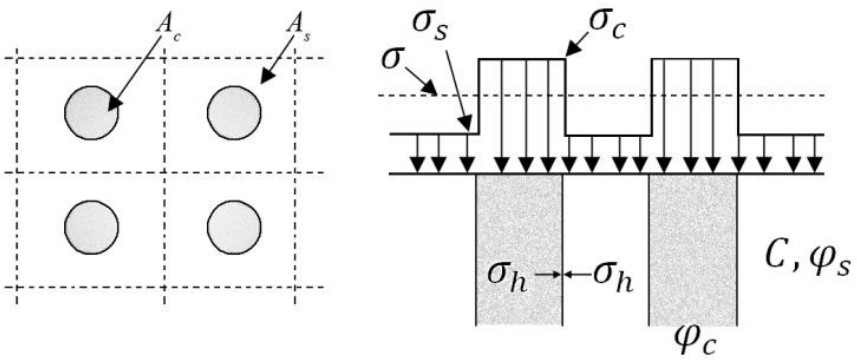

Figure 2-88: Stress distribution between soil and columnar inclusions (Aboshi et al., 1979, 1991)

$$\sigma(A_c + A_s) = \sigma_s A_s + \sigma_c A_c \quad \text{2-99}$$

$$\sigma_h \geq \frac{1 + \sin\varphi_c}{1 - \sin\varphi_c}\sigma_c \quad \text{2-100}$$

$$\sigma_h \leq \sigma_s + \sigma_u \quad \text{2-101}$$

$$\sigma_u = 2c \quad \text{2-102}$$

From Equations 2-100 to 2-102:

$$\frac{\sigma_c}{\sigma_s} = \frac{1 + \sin\varphi_c}{1 - \sin\varphi_c}\left(1 + \frac{\sigma_u}{\sigma_s}\right) \quad \text{2-103}$$

$$\sigma_s = \frac{\sigma}{1 + (n-1)a_c} \qquad 2\text{-}104$$

$$\sigma_c = \frac{n\sigma}{1 + (n-1)a_c} \qquad 2\text{-}105$$

At the beginning of loading the composite ground under k_o consolidation process, n equals unity; i.e., the stresses in the soil and the DR column are the same; however, in the course of consolidation n reaches a yielding value (Aboshi et al., 1979).

While the area replacement ratio and average stress on the unit cell are known, it is also necessary to determine the value of n to calculate σ_s and σ_c. However, n itself is the ratio between σ_s and σ_c, and an additional assumption is required before the stresses in the soil and DR column can be determined. Varaksin (1981) assumes that the settlement of the in-situ soil and column are the same, which is a reasonable assumption for large dimension foundations, but does not explain his calculation method. If the DR column and the in-situ soil deform one dimensionally (i.e., the DR column is fully confined with no lateral deformation), then at the end of consolidation n should be equal to the ratio of the column modulus to the soil modulus; i.e.:

$$n = \frac{E_c}{E_s} \qquad 2\text{-}106$$

E_c = elastic (Young) modulus of the DR column

E_s = elastic (Young) modulus of the soil

This assumption is still used, and can be found in commercial software; however, even the software producers caution that while n can theoretically reach high values, experience shows that it is smaller. In reality, n is not the ratio of the elastic modulus although it has been suggested that the elastic modulus could be used as an upper bound (Barksdale and Bachus, 1983). Barksdale and Bachus note that using elastic theory it can be demonstrated that:

$$n = \frac{D_c}{D_s} \qquad 2\text{-}107$$

D_c = constrained modulus of the DR column

D_s = constrained modulus of the soil, which is the elastic modulus in one dimensional deformation, and for three dimensional deformation will be (Lambe and Whitman, 1979):

$$D_s = \frac{(1-\nu_s)E_s}{(1+\nu_s)(1-2\nu_s)} \qquad 2\text{-}108$$

ν_s = soil Poisson ratio

Although no value for n has been proposed in literature for DR columns, Barksdale and Bachus note that while application of Equation 2-108 will yield n values in the range of 25 to 500 (Castro and Sagaseta (2009) put the range of constrained modului ratio for stone columns at 10 to 50), field measurements suggest that n is between 2 to 5 for stone columns. Enoki et al. (1991) proposes n to be from 1 to 3 for sand columns. Hence, Barksdale and Bachus do not recommend the use of the compatibility method and Equation 2-108 in soft clays.

By comparing equations that are based on total column confinement and when columns are able to deform laterally, Castro and Sagaseta (2009) demonstrate that lateral deformations always reduce the stress concentration ratio by subtracting a term from the oedometric modulus of the column and adding another term to that of the soil.

Based on numerical studies, the influence of the horizontal deformation and plastic behaviour of a (stone) column on the distribution of stresses between the soil and the column is shown in Figure 2-89. With lateral confinement, n starts from zero and reaches a final value equal to the ratio of constrained moduli (40); however, as already discussed, this does not agree with reality. The consideration of elastic radial deformations reduces the final value n of to 25, with a non-zero initial value due to the presence of immediate settlement. Plastic strains in the column further reduce the final value of n to realistic values (around 5), with a small influence of the dilation angle of the column material (Castro and Sagaseta, 2009).

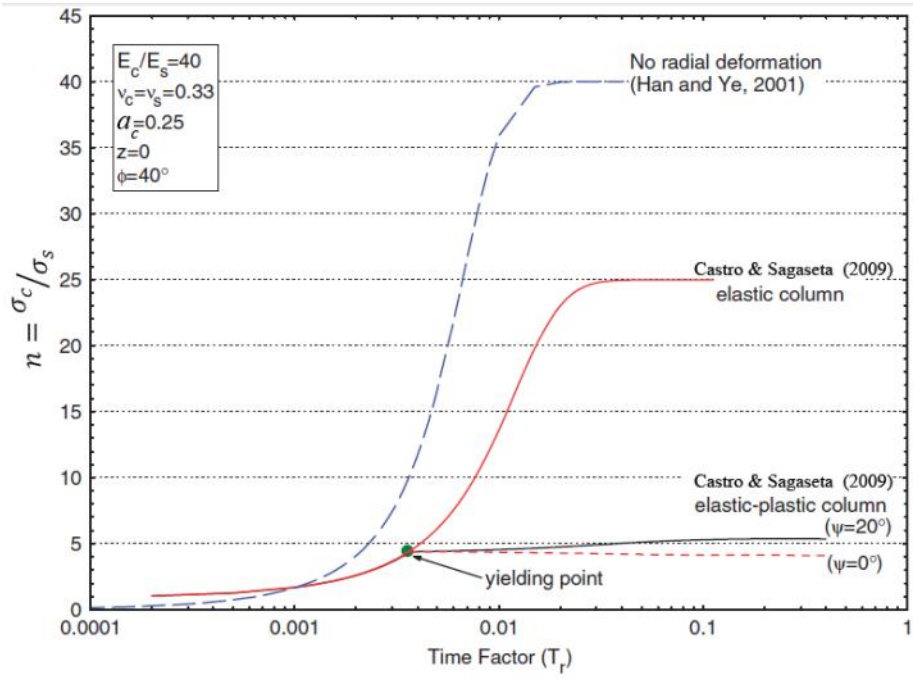

Figure 2-89: Influence of radial deformation and plastic strains on n (Castro and Sagaseta, 2009)

2.6.1.5 Numerical Methods

In addition to the analytically derived methods that can predict the distribution of loads between the columnar inclusions and the soft soil, it is also possible to make similar evaluations based on finite element software. This type of calculation is becoming more and more preferable as commercially available software are becoming more and more capable of calculating settlements, stresses, pore pressures and weak planes in various complicated scenarios. Needless to say, the accuracy of such analyses is based on the constitutive laws, geometrical model and assigned properties of material.

According to Satibi (2009), Zaeske (2001) shows that three dimensional behaviour can be well approached using plane strain analysis with the geometrical idealisation as suggested by Bergado and Long (1994). Axisymmetrical or plane strain analysis of soil arching requires less computer capacity, is faster to compute and is much easier to perform compared to three dimensional analysis. Hence, a practical but at the same time well modelled axisymmetrical or plane strain analysis may have significant advantages.

Several methods can be used for modelling the geometry for the purpose of soil arching analysis in DR columns. The geometrical idealisation models include axisymmetrical, plane strain and three dimensional.

2.6.1.5.1 Axisymmetrical Geometry Models

In axisymmetrical geometry modelling one three dimensional DR cell (see Figure 2-87) is transformed into a circular cell with the area of DR column and soil remaining the same. The transformation of a squared cell into a circular cell is shown in Figure 2-90. Figure 2-91 shows the equivalent unit cell diameters when the column arrangements are square, triangular or hexagonal (Balaam and Booker, 1981). The axisymmetrical finite element analysis uses one radian of the circular DR column cell in its calculation.

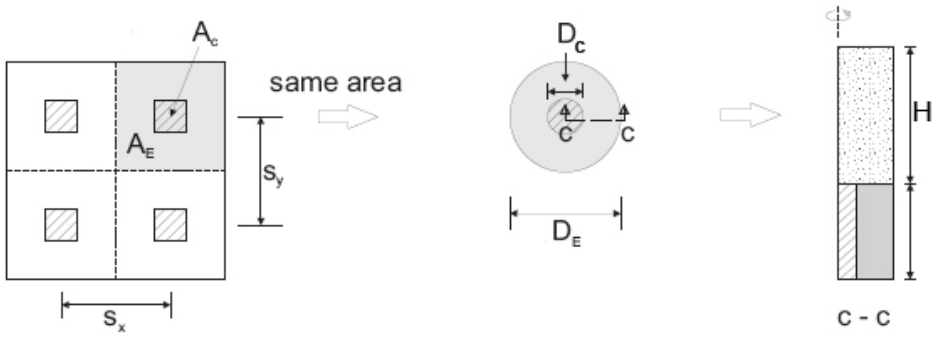

Figure 2-90: Axisymmetrical geometrical idealisation of one DR cell (Satibi, 2009)

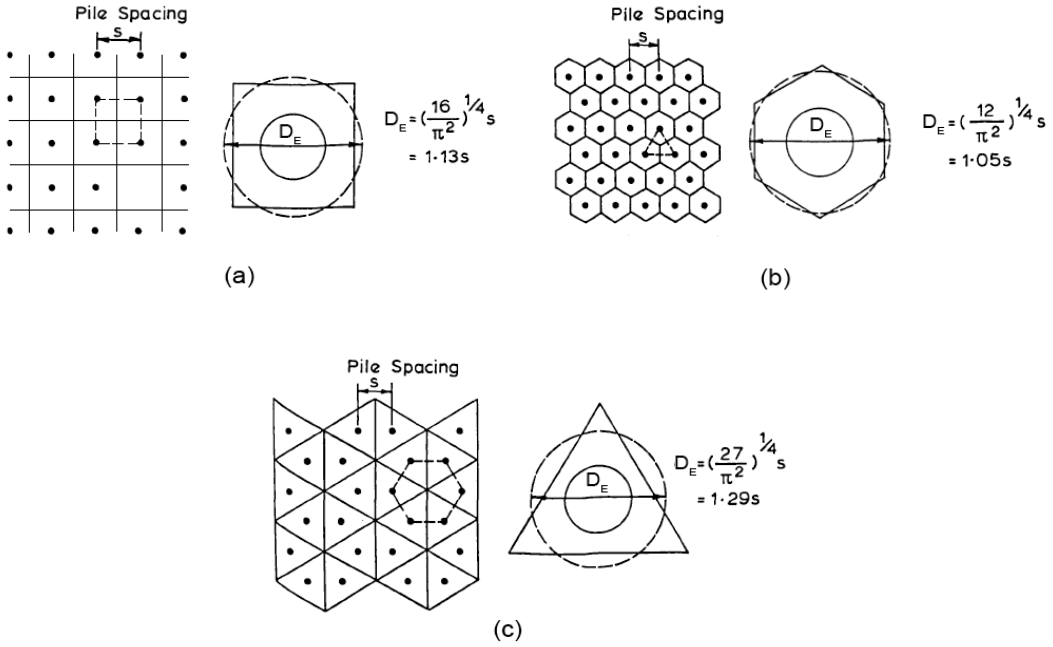

Figure 2-91: Equivalent unit cell diameters (a) Square arrangement of columns, (b) Triangular arrangement of columns, (c) Hexagonal arrangement of columns (Balaam and Booker, 1981)

In this model, it is assumed that each unit cell works independently and with only vertical strain. Thus, this assumption is valid when a very large area is loaded, such as tanks, storage

areas, etc. This model may also is used for modelling a single footing on one DR as the problem can be envisaged to be a large area with a central load and zero load elsewhere.

Mitchell and Huber (1985) have tried to include the effects of the surrounding inclusions on the central unit cell in an axisymmetrical model in an innovative way. In their method, it can is assumed that in addition to the central DR column, there are also concentric DR rings with radii that increase according to the DR column spacing. The thicknesses of the DR rings are calculated based on the area replacement ratio.

As shown in Figure 2-92, the limit of study for the first ring is assumed to be a concentric circle in the middle of the first and second DR rings. Once the area replacement ratio is known, the total DR column area can be determined. Consequently, the area of the first DR ring will be the difference between the total DR area in the limit of ring study and the central DR column. It can be assumed that the area of the first DR ring is equal to the product of the thickness multiplied by the ring circumference. Michel and Huber have performed an example calculation, but the thickness of the first ring can be calculated to be as per Equation 2-109. The same concept can be applied for determining the thickness of the other rings.

$$t_1 = \frac{\pi(1.5s)^2 a_c - A_c}{2\pi s} \qquad 2\text{-}109$$

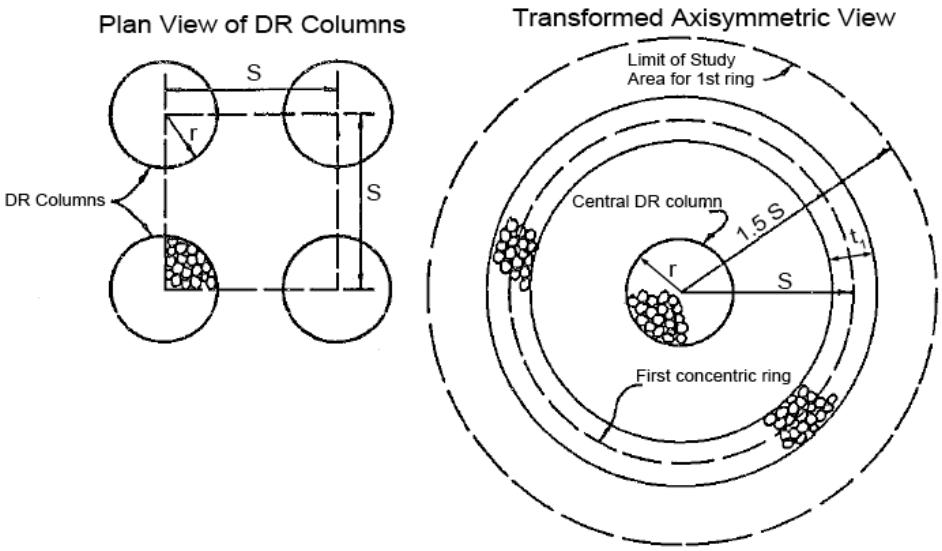

Figure 2-92: Axisymmetrical model with concentric rings modified from Mitchell and Huber (1985)

2.6.1.5.2 Plane Strain Geometry

The assumption that the unit cells work independently with only vertical strain and without any lateral displacement is not always correct. In some problems, such as construction of embankments on soft ground, as shown in Figure 2-93, lateral deformation and spreading can occur, and its value can be an indication of the ground stability condition. In such cases, plane strain models are more meaningful, and will represent the actual conditions more realistically.

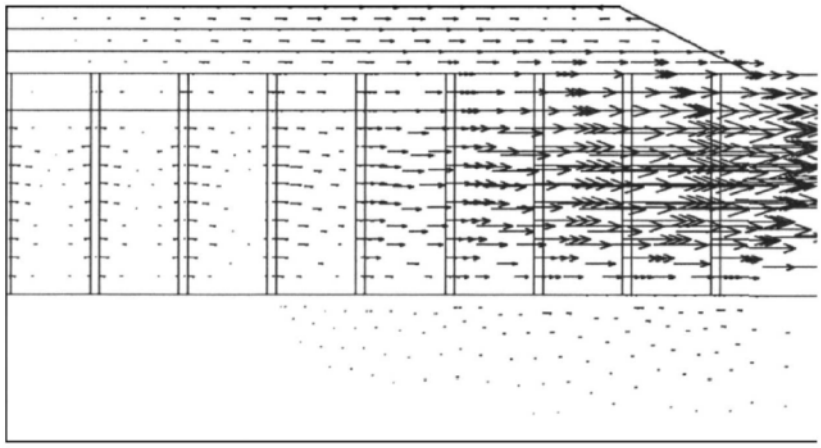

Figure 2-93: Horizontal displacements in plane strain models (Tan et al., 2008)

2.6.1.5.2.1 Plane Strain Geometry with Equivalent Column Stiffness

One of the methods that can be found in literature for transforming three dimensional grids of columns into a continuous wall in plane strain condition is by assuming an equivalent wall stiffness (Kempfert and Gebreselassie, 2006, Satibi, 2009). As shown in Figure 2-94, in this method the thickness of the wall is the same as the width (equivalent width for circular DR columns) of the original inclusion. However, the equivalent wall stiffness (modulus) E_{eq} is taken as the weighted average of column and soil stiffness based on an elastic approach.

$$E_{eq} = \frac{E_c A_c + E_s (A_w - A_c)}{A_w} \qquad 2\text{-}110$$

E_c = DR column Young modulus

E_s = soft subsoil Young modulus

A_w = equivalent wall area

Satibi (2009) notes that when this method is used, the improved area ratio (in other words the area of the DR column) becomes larger. As a consequence, the volume of fill below the arch becomes less as compared to the actual three dimensional conditions.

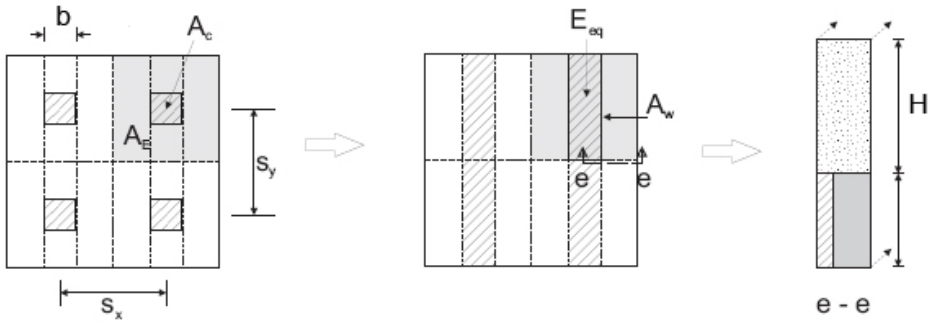

Figure 2-94: Plane strain geometrical idealisation with equivalent stiffness (Satibi, 2009)

2.6.1.5.2.2 Plane Strain Geometry (Bergado and Long)

According to Bergado and Long (1994), and as shown in Figure 2-95, the three dimensional grid of DR columns can be transformed into rows of continuous walls with equivalent thicknesses, t_{eq}, in plane strain geometry. The thickness of the continuous wall is calculated based on the assumption that the ratio of improved area; i.e., the ratio of DR column area to one unit cell area, A_c/A_E, is constant. In a rectangular grid:

$$\frac{A_c}{A_E} = \frac{t_{eq} s_y}{s_x s_y} \qquad 2\text{-}111$$

or more simply:

$$t_{eq} = s_x \frac{A_c}{A_E} = s_x a_c \qquad 2\text{-}112$$

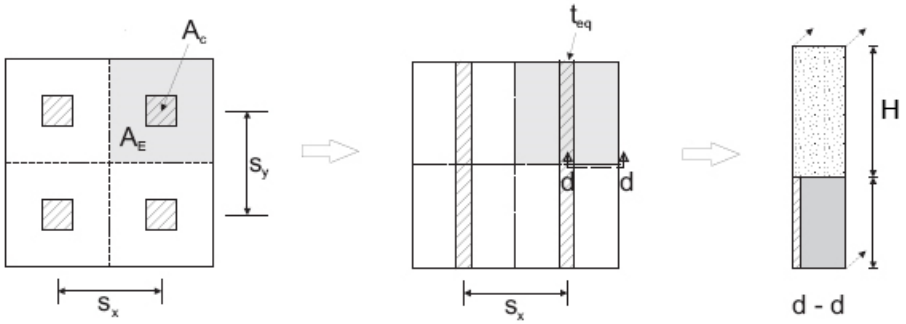

Figure 2-95: Plane strain geometrical idealisation after Bergado (Satibi, 2009)

2.6.1.5.2.3 Plane Strain with Equivalent Homogenised Continuum

As shown in Figure 2-96, in this model the DR columns and in-situ soil are assumed to have equivalent properties:

$$c_{eq} = a_c c_c + (1 - a_c) c_s \quad \text{2-113}$$

$$tan\, \varphi_{eq} = m\, tan\, \varphi_c + (1 - m)\, tan\, \varphi_s \quad \text{2-114}$$

$$\gamma_{eq} = a_c \gamma_c + (1 - a_c) \gamma_s \quad \text{2-115}$$

c_{eq} = equivalent cohesion

φ_{eq} = equivalent internal friction angle

γ_{eq} = equivalent density

c_c = DR column cohesion

c_s = subsoil (soft soil) cohesion

φ_c = DR column internal friction angle

φ_s = subsoil (soft soil) internal friction angle

γ_c = DR column density

γ_s = subsoil (soft soil) density

a_c = area replacement ratio

m = load distribution ratio, and is equal to

$$m = \frac{n a_c}{1 + (n - 1) a_c} \quad \text{2-116}$$

Dimaggio (1987) has expressed Equation 2-114 slightly differently and in the form of:

$$tan\, \varphi_{eq} = a_c\, tan\, \varphi_c + (1 - a_c)\, tan\, \varphi_s \quad \text{2-117}$$

Equation 2-117 is based on the original understandings of the composite column-soil behaviour, and with the thought that that for shear loading undrained conditions were appropriate. However, as additional projects and knowledge progressed the understanding of importance of load distribution ratio greatly increased, and a move toward a drained

strength approach was developed; i.e., Equation 2-114 (DiMaggio, 2009). Thus it is generally Equation 2-114 that is used in calculations.

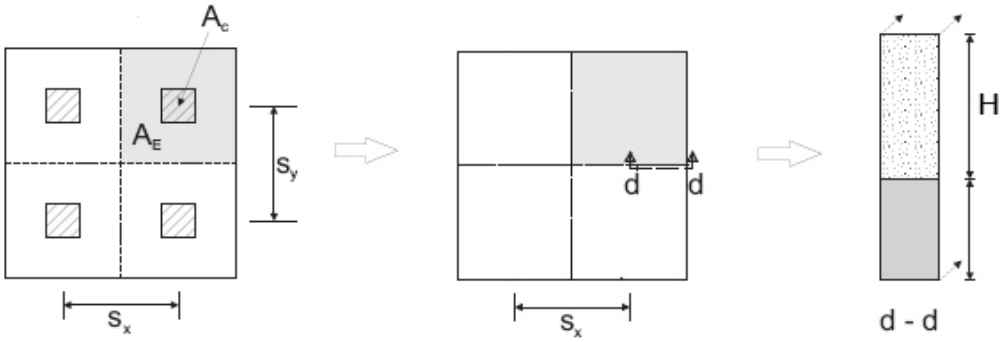

Figure 2-96: Plane strain geometrical idealisation with equivalent homogenized continuum

2.6.1.5.2.4 Three Dimensional Geometry

As shown in Figure 2-97, in three dimensional analyses, a 3D geometry is used. As in previous cases, a material constitutive model is still an important constituent part of the analysis, and will govern the material stress-strain behaviour in the analysis.

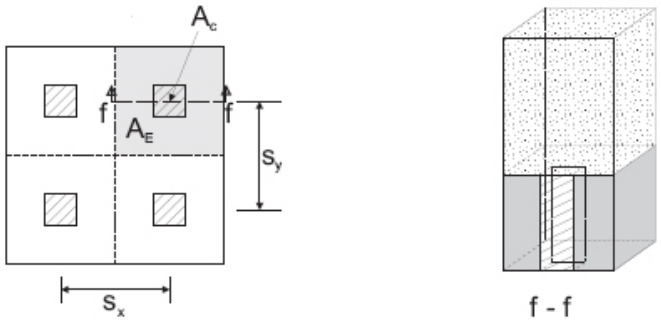

Figure 2-97: three dimensional geometrical idealisation (Satibi, 2009)

2.6.2 Ultimate Load Capacity

After determining the DR column load and stress, it is also possible to determine its stability by comparing the load (stress) with the ultimate load (stress) capacity.

Hughes and Withers (1974) assume that in a floating column the vertical stress (load) that is transferred to the column (through arching) reduces as the depth increases. With the assumption that the cohesion in the soft layer is constant, and by equating forces on a horizontal level within the column (Figure 2-98), they calculated the vertical stress at any level of the column to be:

$$\sigma_{vz} = \sigma_v + \frac{z}{d}(\rho d - 4c) \qquad 2\text{-}118$$

σ_{vz} = vertical stress in the column at level z

σ_v = vertical stress at the column

z = distance of horizontal level from the top of the column

d = column diameter

ρ = density of the column

c = soft soil cohesion

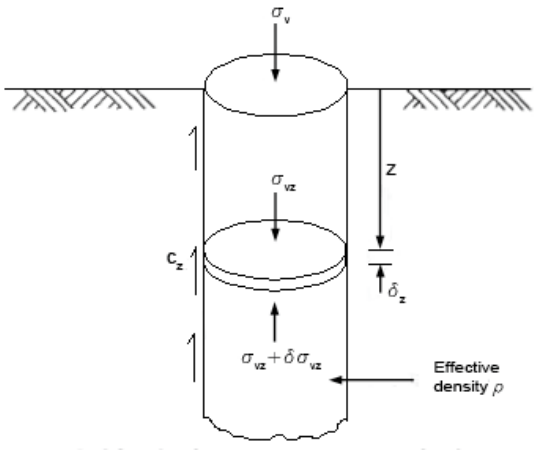

Figure 2-98: Vertical stresses on a typical horizontal level in the column (Hughes and Withers, 1974)

Equation 2-118 can be readily modified for the condition in which the cohesion is not constant throughout the column length, but is rather equal to c_i throughout a length segment l_i, and consequently:

$$\sigma_{vz} = \sigma_v + \frac{z}{d}\left(\rho D - \frac{4\sum c_i l_i}{z}\right) \qquad 2\text{-}119$$

Equations 2-118 and 2-119 suggest that if the column is long enough, then the stress in the column would become zero at a point.

As reported by Greenwood (1991) although the form of the results of Hughes and Withers is valid, full scale tests carried out on single stone column going down to firm ground at the depth of 11 m in Uskmouth indicated that while in the early stages of loading little stress was transferred deep into the column (because skin friction against the strong soil crust sustained stress distributed from the plate load), at higher loadings the stone column sustained higher

stress levels at the depth of 1.8 m (where the stress gauge was installed) than those applied at the surface. A possible explanation was given as stress being redistributed due to deformation of the soft clay below the crust and hence causing the crust to transfer its weight to the column by skin friction. Greenwood (1991) also reports a loading test on a group of columns constructed under an embankment load in East Brent (Somerset) where the effect of containment on soil between columns enhanced their bulging resistance. Consequently, the columns transmitted stress to full depth.

If the column is long or resting on a dense layer, then failure can be expected to be by bulging in the top of the column (or a lower softer layer). On the other hand, if the column is short and not resting on a dense layer, then it may fail in end bearing (punching).

2.6.2.1 Ultimate Load Capacity due to Bulging

According to Barksdale and Bachus (1983) the lateral confining stress that constrains a column is usually taken as the ultimate passive resistance that the soft surrounding soil can mobilise as the column bulges outward against the soil. Since the column is assumed to be in a state of failure, the ultimate vertical stress that the column can support will be the product of the reciprocal of the active pressure (which is the passive pressure) of the column and the lateral confining stress.

The passive resistance developed by the surrounding soil can be better modelled as an infinitely long cylinder that expands about the axis of symmetry. The expanding cylindrical cavity simulates approximately the lateral bulging of the column into the surrounding soil. Even if the column bulges outward within a length of 2 to 4 column diameters (Barksdale and Bachus, 1983, Hughes and Withers, 1974), the model of an infinitely long expanding cylinder appears to give reasonably good results.

Hughes and Withers (1974) idealised the bulge as a cylindrical expansion into the clay, and concluded that it resembles a pressuremeter test in which a cylinder is expanded against the side of a borehole. They then assumed the soil to be an elasto-plastic material, and used the limiting stress theory of Gibson and Anderson (1961) to calculate the limiting stress:

$$\sigma_{rL} = \sigma_{ro} + c\left[1 + ln\frac{E}{2c(1+\nu)}\right] \qquad 2\text{-}120$$

σ_{rL} = limiting (lateral) stress

σ_{ro} = total (initial) in-situ lateral stress

E = elastic modulus

v = Poission's ratio

σ_{ro} can be taken as (Greenwood, 1991):

$$\sigma_{ro} = K_s(\gamma z + yp) \quad \text{2-121}$$

K_s = the ratio of vertical to horizontal stresses in the soil prior to loading and is from 0.6 to 1 in soft clays.

γ = effective unit weight at depth z

p = surface load stress on the soil

y = stress distribution factor such as Boussinesq or Westergaard.

Hughes and Withers assess that based on detailed examination of many field records of quick expansion pressuremeter tests it is possible to approximate Equation 2-120 to:

$$\sigma_{rL} = \sigma_{ro} + 4c + u \quad \text{2-122}$$

u is the pore pressure.

At the same time if the granular material in the bulged region near the top of the column is in a critical state of stress then the relationship between the vertical stress, $\sigma'_{c\text{-}V}$, and horizontal stress, $\sigma'_{c\text{-}H}$, in the column could be expressed by:

$$\sigma'_{c-H} = K_a \sigma'_{c-V} \quad \text{2-123}$$

K_a is the active earth pressure, and equal to:

$$K_a = \frac{1 - sin\varphi}{1 + sin\,\varphi} = tan^2\left(45^\circ - \frac{\varphi}{2}\right) \quad \text{2-124}$$

Hence, Hughes and Withers conclude that:

$$\sigma'_{c-V} = \frac{1+sin\varphi}{1-sin\,\varphi}(\sigma_{ro} + 4c + u) \qquad 2\text{-}125$$

As shown in Figure 2-99, stability can be assessed directly by comparing the horizontal stresses in the DR column with the restraining strength of the soft soil using the Menard pressuremeter. The horizontal stress in the DR column must be less than the soil's strength for the column not to fail (Varaksin, 1981). In other words the pressuremeter limit pressure, P_{LM}, must be more than the horizontal stress that is exerted by the DR column; i.e.:

$$P_{LM} \geq K_a \sigma'_{c-V} \qquad 2\text{-}126$$

or

$$\sigma'_{c-V} \leq \frac{1+sin\varphi}{1-sin\,\varphi} P_{LM} \qquad 2\text{-}127$$

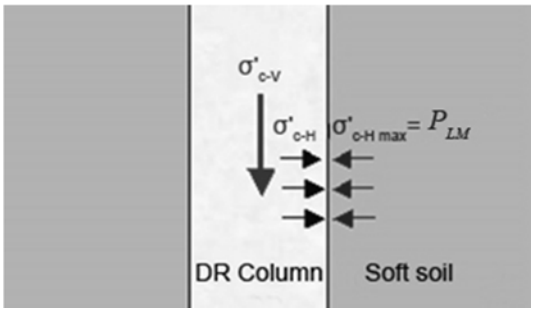

Figure 2-99: Stability condition of a DR column against bulging

It is the author's experience and internal practice to use a safety factor of 2. As an example for φ= 37°, K_a= 4, and consequently $\sigma'_{c\text{-}V} \leq 2\ P_{LM}$.

2.6.2.2 Ultimate Load Capacity due to Bearing Capacity Failure

As shown in Figure 2-32b, if the column is short and on firm strata, failure may be by shear (general bearing). Madhav and Vitkar (1978) have developed a solution for the ultimate bearing capacity of a footing on a granular trench (plane strain case) based on the general shear failure mechanism using the upper bound theorem based on kinematic considerations, shown in Figure 2-100. Expressions for internal energy were based on Chen (1969) due to cohesion mobilised along various boundaries of failure surfaces, and the work done by the

weight of soil, the surcharge, and the external load. Equating the work done by the external load, q_{ult}, to the energies dissipated by cohesion and the work done on account of soil weight and surcharge, the final equation can be written as:

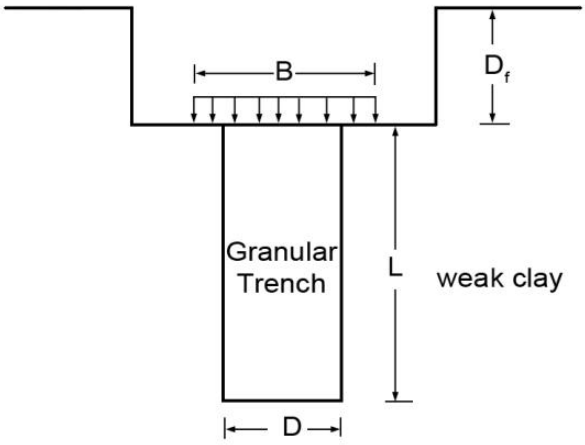

Figure 2-100: Granular trench in weak clay (Madhav and Vitkar, 1978)

$$q_{ult} = c_s N_c + \frac{1}{2}\gamma_s B N_\gamma + D_f \gamma_s N_q \qquad 2\text{-}128$$

where

$$N_c = \frac{c_t}{c_s} N_{ct} + N_{cs} \qquad 2\text{-}129$$

$$N_\gamma = \frac{\gamma_t}{\gamma_s} N_{\gamma t} + N_{\gamma s} \qquad 2\text{-}130$$

and

q_{ult} = ultimate external pressure on footing width

c_s = soil cohesion

γ_s = soil unit weight

B = footing (loading) width (see Figure 2-100)

D_f = depth of footing (see Figure 2-100)

c_t = trench cohesion

γ_t = trench unit weight

Parameter	Range
D/B	0-2
φ_t	20-50°
φ_s	0°
c_t/c_s	0-1
γ_t/γ_s	1

Table 2-10: Ranges of parameters

N_c, N_γ and N_q are dimensionless factors that can calculated for the best upper bound value; i.e., the minimum value of the ultimate bearing capacity of the strip footing. The bearing factors have been evaluated for the ranges listed in Table 2-10, and are presented in Figure 2-101 to Figure 2-103. In Table 2-10, φ_t and φ_s are respectively the trench and soil internal friction angles.

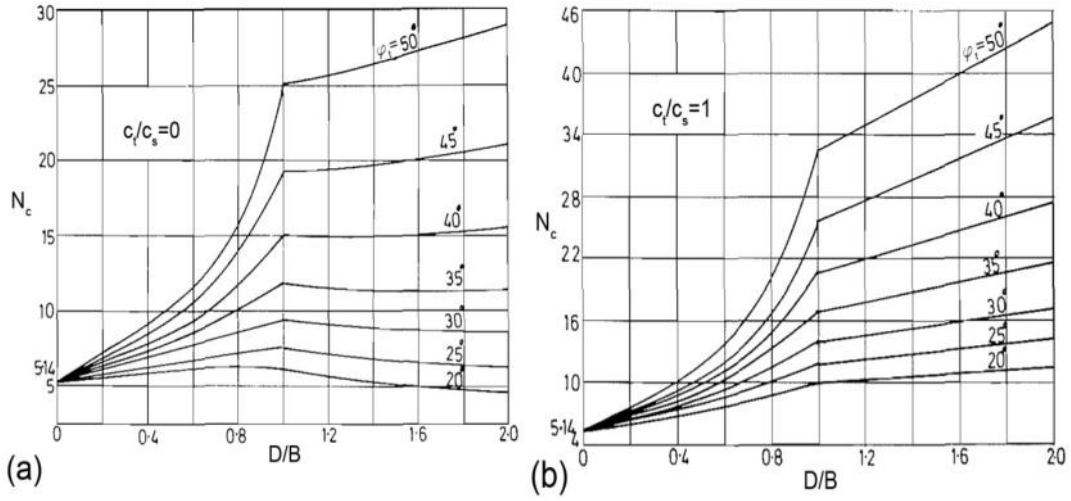

Figure 2-101: Bearing capacity factor N_c (Madhav and Vitkar, 1978)

When the soil and the trench cohesions and internal friction angles are the same the soil-trench system reduces to a homogeneous medium, and the values of the bearing capacity factors become the same as those of Chen (1975). for an axisymmetrical case, equation 2-128 must be modified by incorporating shape factors for the three bearing capacity factors as suggested by Vesic (1975).

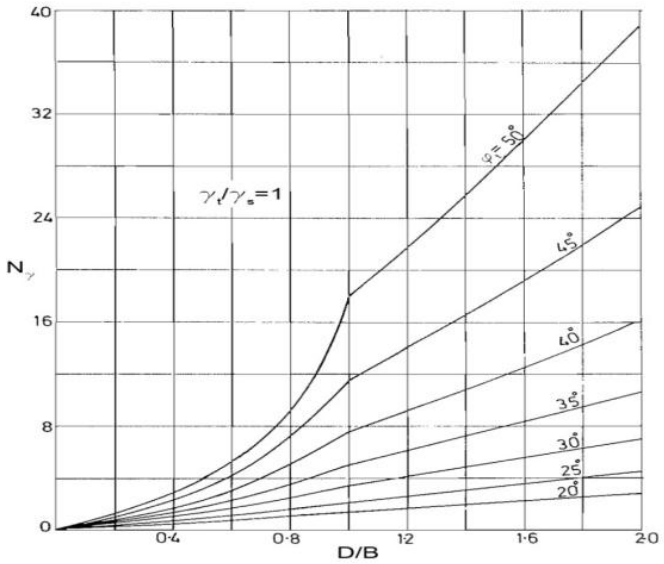

Figure 2-102: Bearing capacity factor N_Υ (Madhav and Vitkar, 1978)

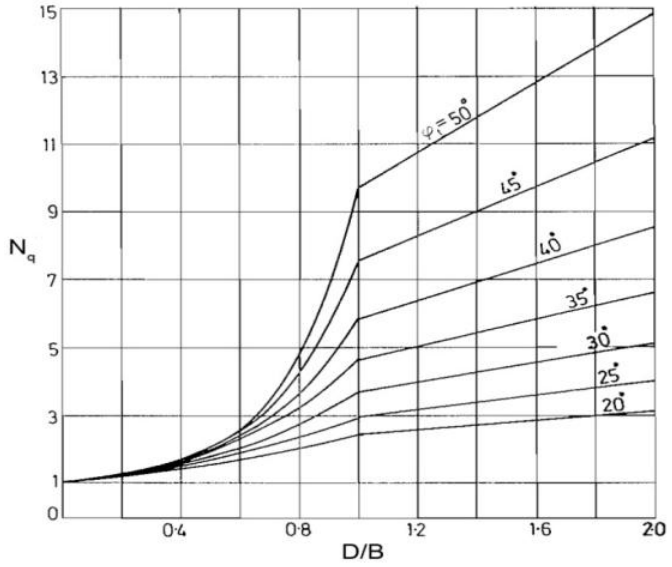

Figure 2-103: Bearing capacity factor N_q (Madhav and Vitkar, 1978)

The values of N_c vary significantly with D/B, φ_t and c_t/c_s. When D/B= 0, the problem reduces to the homogeneous case with soft soil having zero internal friction angle, and the value of N_c coincides with Prandtl's value of 5.14. For D/B= ∞, N_c should coincide with Prandtl's values corresponding to φ_t. For an intermediate ratio of c_t/c_s, N_c values can be interpolated.

The ultimate capacity of a punching (local bearing capacity) failure can be determined by calculating the end bearing capacity of the column using conventional bearing capacity theories and adding the skin friction load developed along the side of the column (Barksdale and Bachus, 1983). Barksdale and Bachus suggest that the bearing capacity of an isolated

stone column or column located within a group can be expressed in terms of the ultimate stress applied to the column:

$$q_{ult} = c_u N_c \qquad 2\text{-}131$$

q_{ult} = ultimate stress that the column can carry

c_u = undrained shear strength of the surrounding cohesive soil

N_c = bearing capacity factor for the stone column

Barskdale and Bachus propose N_c is within the range of 18 to 22, but report that others have suggested higher values. For example, Mitchell (1981) recommends a value of 25 and Dayte (1982) proposes 40 for uncased rammed stone columns.

2.6.3 Liquefaction

Research (Hausler, 2002, Mitchell et al., 1995) shows that ground improvement techniques are indeed able to mitigate liquefaction potential; however, commonly used methods for evaluation of liquefaction potential such as Youd et al (2001) cannot be used immediately when treatment is by columnar inclusions, such as dynamic replacement, because the ground is non-homogeneous, and the properties of the columns and the soil are different.

Baez and Martin (1993) have proposed a method for the assessment of liquefaction potential based on shear reduction. Baez and Martin do not take the column's drainage ability into account because the time for a positive effect of the drainage is limited to the duration of the earthquake.

The basic assumption in evaluating the distribution of stresses according to the stiffness of the individual elements is that shear strains for both loose and stiff material are compatible. Baez and Martin deem that this assumption is valid because there is no inertial loading from the superstructure directed to the columns that cause displacements in directions other than that of the ground motion. Therefore, they assume that:

$$\gamma_s = \gamma_c \qquad 2\text{-}132$$

or

$$\frac{\tau_s}{G_s} = \frac{\tau_c}{G_c} \quad \text{2-133}$$

γ_s = shear strain in the soil

γ_c = shear strain in the column

τ_s = shear stress in the soil

τ_c = shear stress in the column

G_s = shear modulus of the soil

G_c = shear modulus of the column

The shear modulus can be calculated from:

$$G = \frac{E}{2(1+\nu)} \quad \text{2-134}$$

To satisfy equilibrium, the input force from the soil's inertial loading at the given depth must be equal to the sum of the forces distributed to each of the elements. As per Seed and Idriss (1971):

$$\tau_{ave} A \approx \tau_s A_s + \tau_c A_c \quad \text{2-135}$$

τ_{ave} = input (equivalent average) shear stress and is equal to

$$\tau_{ave} = 0.65 \frac{a_{max}}{g} \sigma r_d \quad \text{2-136}$$

Also

a_{max} = peak ground acceleration (PGA)

σ = total stress at depth in question

r_d = depth factor

Similar to the area replacement ratio (a_c) that was defined in Equation 2-97, the ratio of the column to soil shear can be defined as:

$$G_r = \frac{G_c}{G_s} \quad \text{2-137}$$

The above equations that were used by Baez and Martin can be combined to find the average shear stress in the column and in the soil:

$$\tau_c = \frac{\tau}{a_c + \frac{1}{G_r}(1 - a_c)} \quad \text{2-138}$$

$$\tau_s = \frac{\tau_c}{G_r} \quad \text{2-139}$$

Equation 2-139 shows that the stresses will be concentrated in the column proportionally to G_r. Hence, the shear stress in the soil will be less than when there are no columnar inclusions. The influence of the columns can be taken into account in the commonly used liquefaction assessment methods by the introduction of the shear stress reduction factor K_G:

$$K_G = \frac{\tau_s}{\tau_{ave}} = \frac{CSR_i}{CSR} \quad \text{2-140}$$

CSR= cyclic shear ratio

CSR$_i$ = reduced cyclic shear ratio

$$CSR = \frac{\tau_{ave}}{\sigma'_{vo}} \quad \text{2-141}$$

σ'_{vo}= effective initial overburden pressure

K_G can be applied to *CSR* to calculate the reduced cyclic shear ratio.

$$CSR_i = \frac{CSR}{1 + a_c(G_r - 1)} \quad \text{2-142}$$

Figure 2-104 shows the relation between shear stress reduction factor and area replacement ratio for different values of G_r.

The stone columns are considered to be able to resist liquefaction if cyclic resistance ratio exceeds cyclic stress ratio; i.e., $CRR_{Mw} \geq CSR_i$ (Youd et al., 2001).

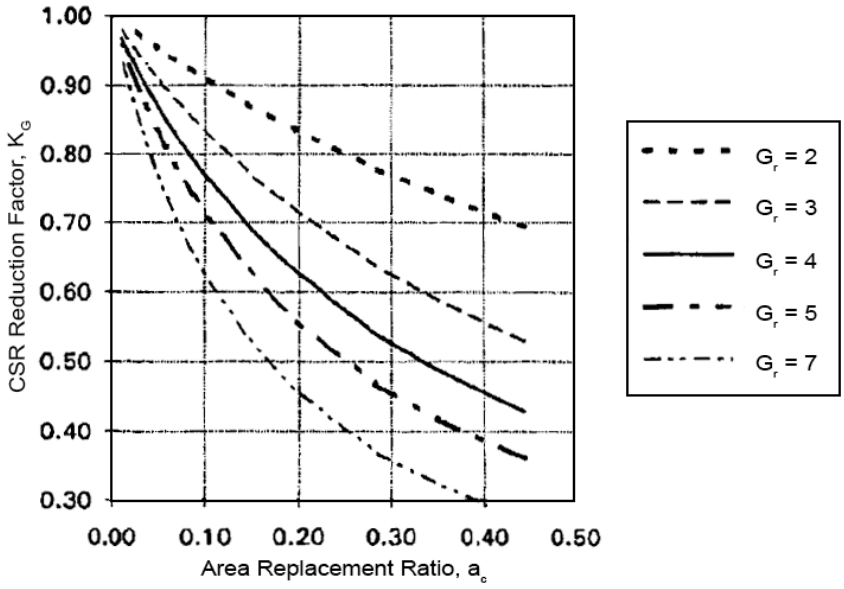

Figure 2-104: Effect of concentrated shear stresses on the CSR (Baez and Martin, 1993)

Goughnour and Pestana (1998) argue that in general, the shear modulus of the column (stone) is much greater than that of the soil, and the difference between the two increases with increasing pore pressure generated as a result of seismic loading. They note that if unconstrained, wave propagation would be much faster in the stone than in the soil, and since the cyclic excitation is the same, then the frequencies must also be the same. Therefore, the wave length has to be much shorter for the waves traveling through the soil. In reality, the columns are physically constrained by the soil, and unless gaps open up between the columns and the soil, the two must move more or less together. The velocity of the wave would result from the compatible movement of the soil and the stone column, and a very complicated stress state would exist, with heavy stress concentrations at the interface of the columns and soil.

Therefore, Goughnour and Pestana question the compatibility of shear strains between the column and soil after these conditions, and develop an equivalent shear modulus, G_{ceq}, for the column in the form of Equation 2-143, which accounts for the flexural bending.

$$G_{ceq} = \left(\frac{\pi d}{2\lambda}\right)^2 E_c \qquad 2\text{-}143$$

d= column diameter

λ= wave length in column

Assuming that v= 0.3, Equation 2-143, can be written in terms of G_s:

$$G_{ceq} = 6.4\left(\frac{d}{\lambda}\right)^2 G_c \qquad 2\text{-}144$$

Goughnour and Pestana assess that $G_{ceq} > G_c$ for values of $d/\lambda < 0.4$. In such cases the columns will act as shear beams, and will accommodate the imposed deformations predominately through shear strains. Without giving specific reasoning, they also conclude that for a case where the columns are very short compared to their diameters, i.e., when height to diameter ratio is in the order of 3 to 5 or less, they would act as shear beams.

Dynamic replacement columns are at least 1.5 m and typically 2 to 2.5 m in diameter and at most 6 m long. It can be observed that the maximum height to diameter ratio will be 4, and thus based on Goughnour and Pestana's assessment it is possible to use the method of Baez and Martin (1993) for this ground improvement technique.

2.7 Advances in Equipment

2.7.1 Dynamic Compaction Rigs

Once it was established that there is a direct relationship between depth of improvement and pounder weight and drop height (Menard and Broise, 1975), the notion of increasing these two parameters to achieve greater depths of improvement seemed inevitable.

Early on, when Louis Menard performed dynamic compaction at Mandelieu-la-Napoule, he used an 8 ton pounder that was dropped from 10 m (Communication Department of Menard, 2007). Assuming a coefficient of depth of improvement as low as 0.5 would yield a treatment depth of about 4.5 m, which at that time was quite an accomplishment compared to what was achievable using vibratory roller compactors. Soon after, Menard was able to identify heavy duty cranes that were capable of efficiently lifting pounders weighing up to about 15 tons using single cable lines, and dropping the pounder in pseudo free fall. Implementation of multiple cable lines was not of interest as such lifting processes would proportionally reduce impact velocity, increase friction, and consequently reduce impact energy, efficiency and depth of improvement.

Although true free fall without cable connections provided more impact energy, it introduced practical difficulties. The release of the pounder caused the crane boom to spring back; thereby ramming the hook block forcefully into the boom, and potentially damaging it. Shock absorbers such as truck tyres were frequently used to reduce collision forces. Also, it was observed that pounder lifting point was slightly offset from pounder impact point; therefore, crane operators had to compensate the offset based on their experience. Furthermore, reconnecting the pounder to the hook is a costly activity as it is a slow and time consuming process that also requires manual labour.

Although dropping the pounder in pseudo free fall with a single cable line proved to be more efficient and practical than dropping the pounder in true free fall, lift capacity of even heavy duty cranes was limited to about 15 tons. Hence, depth of improvement remained limited to about 8 to 10 m. Even though this was a great accomplishment in itself, and satisfied the needs of numerous projects, there were still other sites that required greater treatment depths.

In order to overcome crane lifting limitations, Louis Menard developed, and manufactured his own rigs. The 700 tm rig, shown in Figure 2-105, was able to lift 25 ton pounders. The ability to assemble and disassemble this rig facilitated its transportation, and made it an attractive choice for overseas projects. The mega-machine was capable of delivering 1,600 tm of energy per impact. This machine, shown in Figure 2-106 was used for the ground improvement works of Bern to Biel Highway in Switzerland (Communication Department of Menard, 2007).

Figure 2-105: Dynamic compaction using the 700 tm rig

Figure 2-106: Dynamic compaction using 1,600 tm mega machine (Communication Department of Menard, 2007)

The tripod, shown in Figure 2-107, was an extremely light weight structure that was capable of delivering 1,600 tm of energy per impact by dropping a 40 ton pounder from 40 m. Similar to the 700 tm machine, this rig could also be reassembled, and was successfully used in several countries including the United States, Japan, Dominican Republic, Bangladesh and Mexico.

Figure 2-107: Dynamic compaction using the Menard tripod

Figure 2-108: Dynamic compaction using the giga-machine

Undoubtedly, the giga-machine, shown in Figure 2-108, is the most spectacular rig that has ever been built. This rig had 168 wheels, 7 km of hydraulic hoses, and was specifically built to treat 20,000,000 m^3 of rip rap fill in Nice Airport (Communication Department of Menard, 2007). Impact was provided by dropping pounders weighing 130 to 170 tons from 22 m (Gambin, 1983). The giga-machine was decommissioned after the project.

As much as the 700 tm rig, the tripod, the mega-machine and giga-machine had their special applications, they were specifically produced, their numbers were limited and they could not be manufactured commercially or in great numbers. However, the introduction of a new generation of high production heavy duty cranes that were able to lift pounders using two single cable lines that were connected to two hoist drums increased lift capacity from 15 to 25 tons. One of such rigs is shown in Figure 2-109.

Figure 2-109: Dynamic compaction using 25 ton pounder

Other than Menard rigs, Lampson also modified a crane that was rented for performing dynamic compaction using a 30 ton pounder that was dropped from 30 m for the Thermal Public School project in Palm Spring, USA. This rig is shown in Figure 2-110. In China, dynamic compaction has been performed using cranes that have been modified by adding two additional legs to the boom and turning it into a tripod (Varaksin, 2014).

2.7.2 Pounders

Pounders can be made of any material, but they are usually made of reinforced concrete (Figure 2-112) encased in a steel box or steel plates bound together by large steel bolts

(Figure 2-113); however, it is the personal experience of the author that concrete pounders are short lived and steel plate pounders can be used over and over again with minimum maintenance. Dynamic replacement pounders have smaller bases to increase shearing and punching into the ground.

Figure 2-110: Lampson crane modified by dynamic compaction

Figure 2-111: Dynamic compaction in China using cranes that have been modified into tripods

Figure 2-112: Reinforced concrete pounder encased in a steel box

Figure 2-113: steel pounders composed of steel plates

While studies have recently been conducted on the efficiency of conical bottom pounders (Arslan et al., 2007, Feng et al., 2000, Feng and Ke, 2005) almost all pounders that are used in the industry have flat bottoms. As shown in Figure 2-114, marine dynamic compaction pounders appear as large graters to decrease water resistance.

More recently, an innovative and patented pounder release and automatic grab system called *MARS* has been developed, and will be further described in the case studies presented in this thesis.

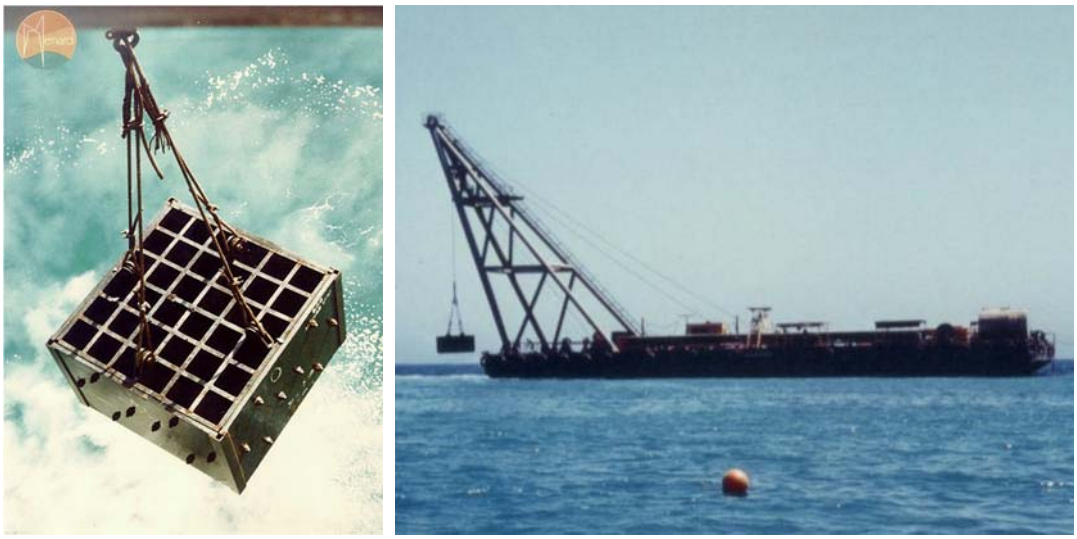

Figure 2-114: Marine dynamic compaction pounder used for seabed improvement at Kuwait Naval Base (Communication Department of Menard, 2007)

2.7.3 Alternative Impact Oriented Ground Improvement Techniques

Dynamic compaction is neither the only ground improvement technique that utilises impact energy to compact the soil nor is it a generic name for soil improvement methods that are based on impact energy. Dynamic compaction is a term that was chosen by Louis Menard to specifically define the technology that he had invented. The author notes that in recent years, as a marketing tool, there is a trend by some contractors to utilise the term dynamic compaction on its own or with a prefix or suffix to express an alternative impact oriented ground improvement method. Although this may win those contractors some projects, in the opinion of the author it will and has brought confusion; thus the author strongly recommends that terminology be used properly. Rapid impact compaction and impact roller compaction are two impact oriented techniques that will be considered hereunder.

2.7.3.1 Rapid Impact Compaction

According to BSP's website (British Steel Piling (BSP)), the *Rapid Impact Compactor* or *RIC* was developed in the early 1990s in conjunction with the British Military as a means of quickly repairing damaged aircraft runways. As shown in Figure 2-115, dynamic energy is imparted by a weight dropping from a controlled height onto a steel foot that has a diameter of about 1.5 m. Energy is transferred to the ground safely and efficiently as the RIC's foot remains in contact with the ground and no flying debris is ejected.

Compared to dynamic compaction, instead of dropping a *heavy* weight from a *great* height once or twice a minute, the RIC drops a lighter weight, typically weighing 5 to 9 tons, from a relatively lower height of up to 1.2 m at a rate of 40 to 60 impacts per minute.

Figure 2-115: Rapid Impact Compactor

The primary usage of RIC in the UK is for shallow compaction of floor slab and roadway subgrades (Terra Systems). However, the introduction of this technology to other countries such as the United States and Australia has been associated with a degree of confusion as the technique is sometimes incorrectly referred to by terms such as *dynamic compaction*, *light dynamic compaction, controlled dynamic compaction* or *rapid dynamic compaction*.

Disregarding the energy loss due to having to overcome the inertia of the plate resting on the ground and by applying Equation 2-41, it can be observed that depth of improvement for a 9 ton weight that is dropped from 1.2 m will be respectively 2.3 m and 3 m for coefficients of 0.7 and 0.9. Application of Equation 2-51 with a pounder radius of 0.75 will not make much of a difference and will result in the depth of improvement being 3.4 m. It can be observed that while larger depths of improvement have been reported, the magnitudes of improvement are considerably less than dynamic compaction, but still quite compatible with the original purpose of developing the RIC technology, and the improved depths should generally satisfy FAA (1995) requirements for the compaction of subgrade soil in airports.

2.7.3.2 Impact (Roller) Compaction

Classical circular roller compactors are capable of compacting approximately 0.2 to 0.3 m of graded soil, but treatment thickness may sometimes be substantially more and a

considerable amount of time, money and carbon emissions will be needed to treat the soil in multiple layers.

The idea of increasing the treatment thickness by implementing non-cylindrical multi-sided geometrical rollers was first recognised and patented in 1935 in Sweden, but it was only 20 years later and in South Africa when impact roller compaction was developed (Avalle, 2004). Today, impact roller compactors, shown in Figure 2-116, that are sometimes also called impact compactors weigh 8 to 16 tons, have 3 to 5 sides, and operate at practical speeds in the range of 8 to 11km/hr depending on the ground conditions. When travelling speed exceeds 11km/hr the drum begins to skip as the drum revolution increases (Geoquip). The drum tends to act with less impact and eventually will run as a circular wheel given sufficient revolutions per minute.

Figure 2-116: Impact roller compaction

Impact rollers do not have a motorised form of energy such as the vibratory roller, and derive their energy by turning on their corner and falling onto the flat side. The number of sides of an impact roller affects its energy rating. Since an impact roller turns on its corner and falls onto its flat side, the greater the difference of these radii the greater the lift height. Three sided rollers produce the maximum lift while five sided rollers produce the least lift. Lifts are from 0.15 to 0.23 m (Broons Hire, Geoquip).

Impact roller compaction is also sometimes incorrectly referred to as dynamic compaction, rolling dynamic compaction or even worse, *high impact energy dynamic compaction*. On its website, Landpac (Typical Myths About Impact Compaction) notes that:

"… Impact Compaction (IC) and Dynamic Compaction (DC) have some very different characteristics that make them distinct from one another. DC is performed through a very large parcel of energy being imparted over a very short time duration by means of a heavy

pounder dropped from a great height onto the soil. The repetition of such compaction cycles is performed at a very low frequency. IC on the other hand is performed through a far smaller parcel of energy being imparted to the soil over far greater time durations by means of an eccentrically shaped weight rolling over the soil. The repetition of these compaction cycles is performed at a far greater frequency that DC."

Even though impact roller compaction is not dynamic compaction, for comparative purposes it can be observed that by applying Equation 2-41 the depth of improvement for an 11 ton weight dropped from 0.23 m will be respectively 1.1 m and about 1.4 m with coefficients of 0.7 and 0.9. Based on the tests that they had performed, Berry et al. (2004) have proposed an alternative method for predicting the profile of improvement in unsaturated soils based on the measurement of ground settlements and a distribution of plastic strains similar to an adapted Schmertmann strain influence diagram. According to this study the improvement depth is 2 to 3 times the compactor's width (900 mm) and the maximum improvement is achieved at about 0.67 to 1 times the compactor's width. This will yield an improvement depth of 1.8 to 2.7 m. Kelly and Gil (2012) also note that ground improvement by impact roller compaction is typically measured to effective depths of 2 to 3 m (see Figure 2-117) . The schematic comparison of depth of treatment between impact roller compaction, rapid impact compaction and dynamic compaction is shown in Figure 2-118.

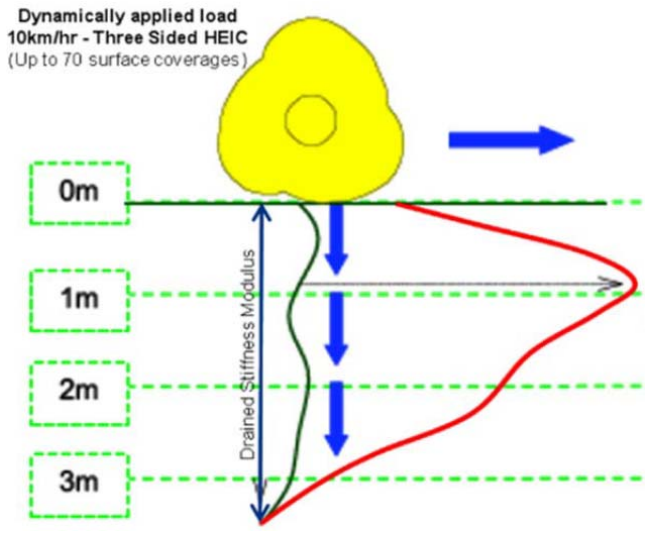

Figure 2-117: Impact roller compaction depth of improvement (Kelly and Gil, 2012)

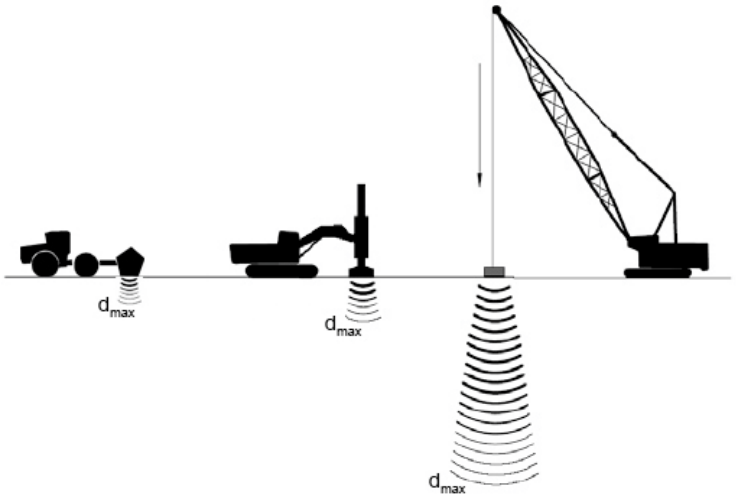

Figure 2-118: Schematic comparison of depth of improvement between impact roller compaction, RIC and DC

2.8 Assessment of Dynamic Vibrations

Dynamic compaction's concept is based on generation of waves with sufficiently large enough energy (and thus magnitude) to be able to re-arrange the soil in a denser state; hence, it is of utmost importance to be able to understand safe and acceptable vibration limits. It has come to the attention of the author that in practice many engineers are insufficiently familiar with how to properly measure and interpret vibrations. It is the objective of this section to clarify how safe vibration limits were developed, how to predict vibration magnitudes, how to properly measure the vibrations, how to compare the measurements with allowed tolerance, and how to potentially reduce vibration effect on nearby structures.

2.8.1 Development of Safe Vibration Limits

From 1930 to 1942 the US Bureaus of Mines (USBM) conducted an extensive research program to study the seismic effects of quarry blasting on buildings (Nicholls et al., 1971). Vibration amplitudes ranged from 25 microns to 12.7 mm, frequencies were from 4 to 40 Hz, and three classifications of damage were proposed based on the degree of plaster failure. The damage indices were:

- No damage
- Minor damage: fine plaster cracks, opening of old cracks
- Major damage: fall of plaster, serious cracking

There was no sharp distinction between the damage classes. Also, as a note, many other factors such as ageing, settling, shrinkage, etc. can result in similar damage; hence, it was and is important to perform a dilapidation survey to assess the structures' soundness prior to generating vibrations.

USBM's report (Thoenen and Windes, 1942) of the tests recommended an index of damage based on acceleration. If accelerations were less than 0.1g, no damage was expected. Minor damage was expected for accelerations ranging from 0.1g to 1 g, and major damage was expected for values greater than 1 g. Duvall and Fogelson (1962) statistically showed that these data gave contradictory results because while minor damage correlated with acceleration, major damage correlated with particle velocity. Hence, the concept of

implementing particle velocity in lieu of acceleration for prediction of (major) damage was formed.

Langefors, Kilhstrom and Westerberg (1958) also carried out extensive studies to relate between damage and ground vibrations from nearby blasting, and developed a four degree damage classification for plaster failure based on particle velocity as follows:

- No noticeable damage: 71 mm/s
- Fine cracking and fall of plaster: 109 mm/s
- Cracking: 160 mm/s
- Serious cracking: 231 mm/s

Statistical analyses of these data showed that the degree of both major and minor damage correlated with particle velocity.

Similarly, Edwards and Northwood (1960) carried out a number of tests and classified damage as follows:

- Threshold: opening of old cracks and formation of new plastic cracks
- Minor: Superficial, not affecting the strength of the structure
- Major: resulting in serious weakening of the structure

They also concluded that damage was more closely related to particle velocity than to displacement or acceleration, that damage was likely to occur with a particle velocity of 100 to 125 mm/s, and recommended a safe vibration limit of 50 mm/s.

Figure 2-119 shows the results of the three tests carried out by USBM, Duvall & Fogelson and Edwards and Northwood. It can be observed that the regression line with a slope of -1 on the log displacement versus log frequency diagram, which represents a constant particle velocity, provides a better damage correlation than the 0 and -2 slope lines that respectively represent constant displacement and constant acceleration. The best regression for particle velocity for predicting major damage, minor damage and safe limit are respectively 193 mm/s, 137 mm/s and 50 mm/s. As shown in Figure 2-120, the same data can be plotted for the logarithm of particle velocity versus logarithm of frequency.

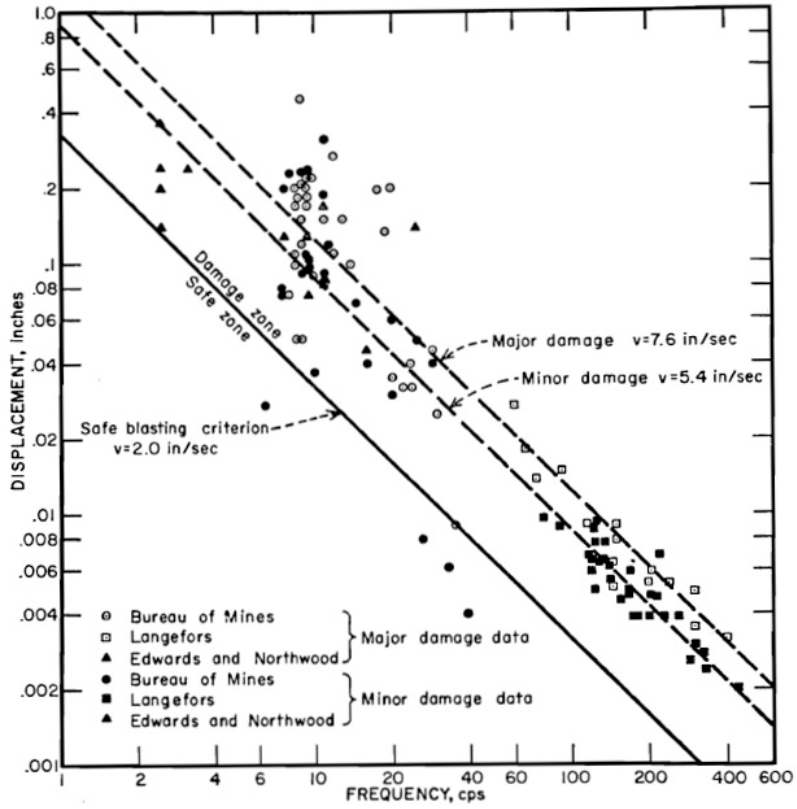

Figure 2-119: Displacement versus frequency, combined date with recommended vibration criterion (Nicholls et al., 1971)

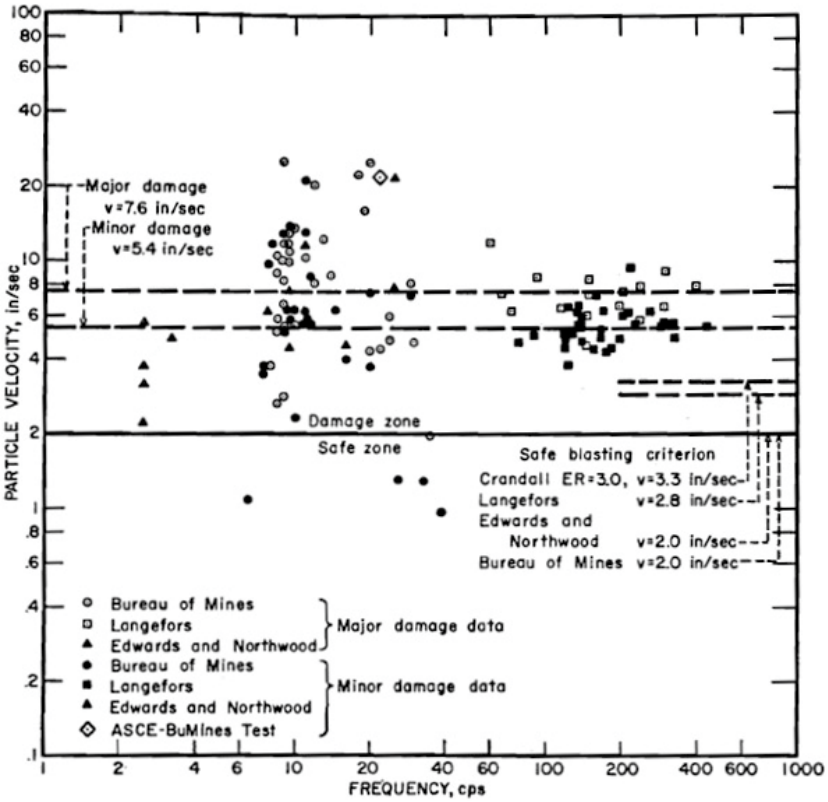

Figure 2-120: Particle velocity versus frequency with recommended safe limit criterion (Nicholls et al., 1971)

The recommended safe vibration criterion of 50 mm/s particle velocity was a probability type criterion, and if the observed particle velocity exceeded the safe limit in any of the three orthogonal components there was a reasonable chance that residential structures could be damaged. The safe vibration criterion was not a value below which damage would not occur, and above which it would occur. Many structures could experience vibration levels greatly in excess of 50 mm/s with no observable damage; however, the probability of damage to a residential structure would increase or decrease as the vibration level deviates from 50 mm/s.

USBM (Nicholls et al., 1971) recommended that velocity gages should be preferably mounted on or in the ground rather than the structure because most of the data used in establishing the damage criterion were obtained in that manner. Mounting the gages in the ground was understood to alleviate the necessity of considering the response of a large variety of structures. Also, particle velocity was (and is) be observed in three mutually perpendicular directions. A safe vibration criterion was based on the measurement of individual components, and if the peak particle velocity (PPV) of any component exceeded 50 mm/s, then damage was likely to occur.

Collection of large amounts of data will result in considerable amount of data about the mean PPV curve; thus most regulations require that without instrumentation maximum probable velocities be used rather than average values (Dowding, 2000).

According to Siskind et al. (1980), Pennsylvania was the first American state to adopt the 50 mm/s PPV criterion as a safe standard in 1957; however, in 1974 the State was forced to adopt stricter controls because of citizen pressure and lawsuits involving both annoyance and alleged damage to residences. Consequently in 1974, USBM began to reanalyse the blast damage problem, expand the study of Duvall and Fogelson (1962), and overcome its more serious shortcomings. Part of the new study included emphasis on the frequency dependency of structure response and damage, and recognising that the response characteristics and frequency content of the vibrations are critical to response levels and damage probabilities. Also, an analysis was made of various studies of human tolerance to vibrations, although most data were from steady state rather than impulsive sources (Siskind et al., 1980).

The measured response of residential structures was a critical indicator of troublesome or potentially damaging ground vibrations, and corner motion measurements were used to assess the racking (shearing) motions of the gross structure (see Figure 2-121). Cracking from

vibration can occur where excessive stresses and strains are produced within the planes of the walls or between walls at the corners. Consequently, the vibration in the corners is assumed to indicate cracking potential because it corresponds to whole structure response. Other types of response cause different but consequential results. Mid-wall motions normal to the wall surface that are primarily responsible for window sashes rattling, picture frames tilting and dishes giggling were also measured. Even though structures are designed to resist normal vertical loads, differential vertical motions can produce high strains in floors and ceilings.

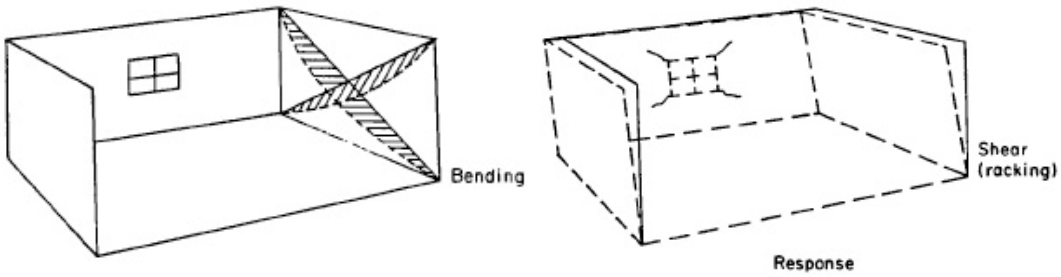

Figure 2-121: Types of motion that can cause damage to a building (Siskind et al., 1980)

Although the study recognised that a simple measurement of peak particle velocity was an oversimplification, it concluded and recommended the continuation of utilisation of peak particle velocity as the primary measure of ground motion to assess damage.

A simple amplification factor was determined directly from the vibration time histories, and maximum structure velocities and their times of occurrence were noted. Ground velocities and frequencies were then picked off the records at the corresponding moments of time or immediately preceding the time of peak structure vibrations. The ratios of the two velocities were plotted against the frequency of the corresponding ground motion, and as expected from the natural resonance frequencies, maximum amplifications were found to be associated with ground motions between 5 to 12 Hz. The highest amplification factors for corner motion were approximately 4, with 1.5 being a typical value. Ground motions above 45 Hz produced little or no amplification of the corner measured structure motion.

With many responses occurring at lower frequencies, particularly up to 25 Hz, the maximum mid-wall motion amplification factors were found to be greater than for the corners. As with corner motions, amplification factors for ground motions above 45 Hz were less than unity.

These results suggested that frequencies below 10 Hz are most serious for potential damage from structure racking. Vibrations with frequencies of less than about 25 Hz can excite high

levels of mid-wall motion, and generate most of the secondary noises, rattling and other annoyances.

It was understood that for structures not exceeding two stories, constructed on firm foundation, with dimensions of typical residences and with vibration durations not longer than a few seconds, the safe vibration level defined as levels unlikely to produce interior cracking or other damages in residences was determined as presented in Table 2-11 (Siskind et al., 1980).

Type of structure	Ground vibration – peak particle velocity mm/s	
	At low frequency (<40 Hz)	At high frequency (≥40 Hz)
Modern homes, dry wall interiors	19	50
Older homes, plaster on wood lath construction for interior walls	12.7	50

Table 2-11: Safe levels of blasting vibrations for residential type structures, from USBM RI 8507 (Siskind et al., 1980)

Dry walls defined as gypsum wallboards that consist of 10 mm to 15 mm gypsum plaster panels with paper laminates covering both sides of the wall appeared to be more capable of withstanding vibrations because the 0.4 mm thick paper contributed greatly to the strength of the board, and concealed cracking of the plaster core.

Older homes often had interior walls of thick plaster over wood lath support, which was more susceptible to damage. A minimum safe level of 12.7 mm/s was adopted based on probability analyses of low frequency shots and the overall study with an assumption of 5% probability for very superficial cracking. However, this vibration level was also lower than the lowest level in cases where damage was observed. The 12.7 mm/s level should provide protection from damage in more than 95% of the cases.

Safe vibration criteria were developed for residential structures, having two frequency ranges with a sharp discontinuity at 40 Hz, and an intermediate frequency case that was higher than the structures' resonances (4 to 12 Hz) and lower than 40 Hz. By using a combination of measured structure amplification and damage summaries, as shown in Figure 2-122, a smooth set of criteria were developed (Siskind et al., 1980).

Estimation of the predominant frequency was still a problem. Where the wave train is simple, the period corresponding to the peak level can be directly measured. Otherwise, spectral analysis will be required (According to Siskind et al. (1980), for frequencies less than 40 Hz, all spectral peaks within 6 dB (50%) amplitude of the predominant frequency must be analysed). Occasionally the peak level occurs early in the wave and at a high frequency, with a long duration wave train of somewhat lesser amplitude following. In the opinion of Siskind et al. the safest approach was to consider the low frequency part of the time history separately, and where it was below 40 Hz, to use the 19 mm/s or 12.7 mm/s criteria of Figure 2-122.

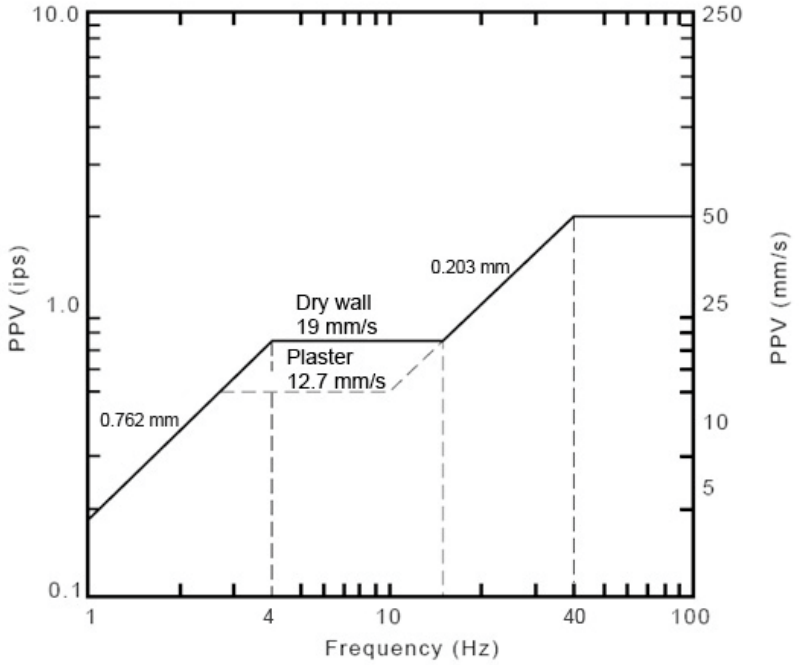

Figure 2-122: USBM RI 8507 safe vibration limit criteria (Siskind et al., 1980)

Three years after the publication of USBM RI 8507 (Siskind et al., 1980) the Office of Surface Mining Reclamation Enforcement (OSM) published its regulation regarding safe vibration levels (Office of Surface Mining Reclamation Enforcement, 1983). Disregarding the clause that refers to the scaled distance equation for determining the weight of the explosion charge, the regulation states that at the location of any dwelling, public building, school, church or community or institutional building the maximum peak particle velocity shall be less than the values stated in Table 2-12 and Figure 2-123. It can be observed that OSM's regulation is in fact a modification of USBM RI 8507's criteria.

Distance from vibration source (m)	Maximum allowable peak particle velocity for ground vibration (mm/s)*
0 to 90	31.75
91 to 1,500	25.4
1,501 and beyond	19

*: Ground vibration shall be measured as particle velocity. Particle velocity shall be recorded in three mutually perpendicular directions. The maximum allowable peak particle velocity shall apply to each of the three measurements.

Table 2-12: Maximum allowable peak particle velocity for ground vibration (OSM, 1983)

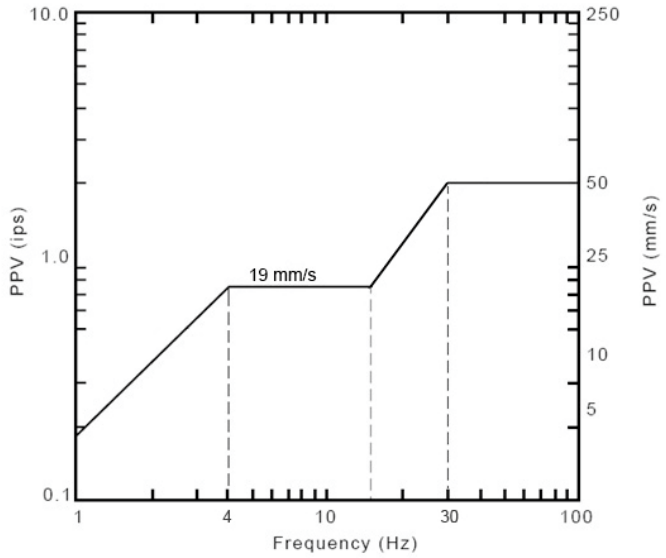

Figure 2-123: OSM Safe vibration level criteria (Office of Surface Mining Reclamation Enforcement, 1983)

The separate and independent study of vibration damage from blasting, pile driving, and machine sources by Studer and Suesstrunk (1981) resulted in similar criteria where limiting particle velocities depend upon frequency, and justified the use of USBM or OSM damage criteria for dynamic compaction operations.

2.8.2 Air Vibrations and Damage

Nicholls et al. (1971) cite that Windes (1942, 1943) has carried out an investigation for USBM, and has concluded that window glass failure occurs before any other type of structural failure due to air blast. In Windes' investigation some window panes broke by an overpressure of 7 kPa. The condition of the glass in the windows contributed directly to the damage

experience. Poorly mounted panes, which have been prestressed by improperly inserted glazier's points or other causes, may fail when subjected to overpressures as low as 0.7 kPa. Based on the research for USBM, Windes concluded that under normal blasting conditions the problem of damage from air blast was insignificant.

Edwards and Woods (1960) also measured the air blast pressure during their vibration studies. The measured overpressure ranged from 0.07 to 1.4 kPa at locations outside the structures that were being monitored. These pressures were considerably below the levels expected to cause damage, and none of the damage that occurred in any of the structures was attributed to air blast.

Air vibration, even in blasting operations, is not considered to be a significant factor in causing damage to residential structures in most operations; however, it can be a nuisance to humans.

2.8.3 Human Response to Vibration

Humans notice and react to vibration at levels that are lower than the damage threshold. Vibration levels that are completely safe for structures by all standards can be quite unpleasant when viewed subjectively by people.

Reiher and Meister (1931) studied the subjective human tolerance to 5 minute vertical and horizontal vibratory motions in a variety of positions. Responses to slightly perceptible vibrations occurred at 0.25 mm to 0.84 mm/s, and the threshold of strong perceptible vibrations was 2.55 mm/s. It was noted that over the range of 4 to 25 Hz, the results were essentially independent of frequency.

Nicholls et al. (1971) adapted Figure 2-124 from Goldman (1948) to show the subjective response of the human body to steady state vibratory motion in the frequency range of 2 to 50 Hz. These limits are based on the results for sinusoidal vibrations.

Although most studies of human tolerance to vibrations have been conducted on steady state sources or those of relatively longer duration than a transient vibration (as what would be the case for dynamic compaction), it can be expected that the vibration limits required for a reasonable comfort from a long term vibration source would be more restrictive than for sources of short duration at infrequent occurrence. Several researchers have recognised that the duration of the vibration was critical to its undesirability (Siskind et al., 1980). Most

evidently, a higher level could be tolerated if the event was short. Consequently, steady state vibration data cannot be comprehensively applied to vibrations originating from dynamic compaction.

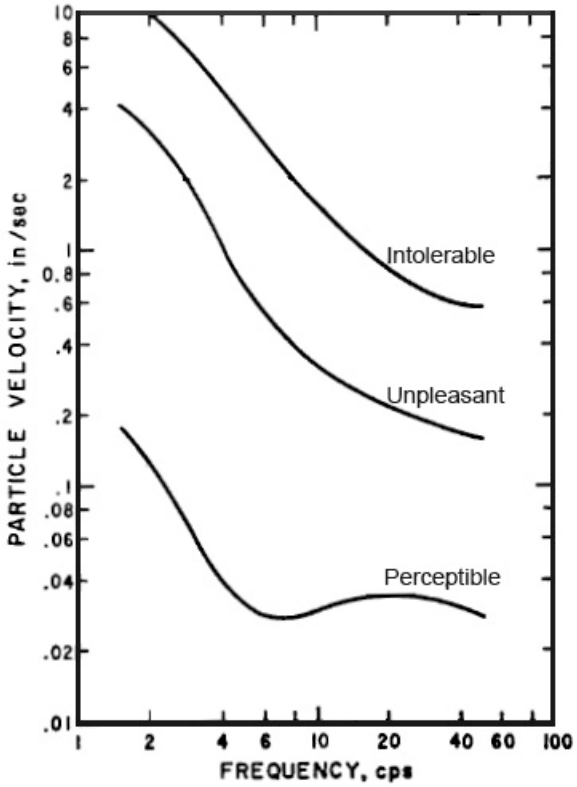

Figure 2-124: Subjective response of the human body to steady state vibratory motion (Nicholls et al., 1971)

As shown in Figure 2-125, Power (1966) plotted the percentage of complaints versus particle velocity for the Salmon underground nuclear detonation which was technically a transient vibration, but lasted 90 seconds. More than 35% of the families located in the zone where 50 mm/s was exceeded filed complaints. This particle velocity is in the intolerable subjective response zone, and complaints could have been anticipated. In the perceptible zone, less than 8% of the families complained. This data indicates that a vibration level of 10 mm/s should not be exceeded if complaints and claims are to be kept below 8%.

Chang (1973) analysed human vibration response literature with particular attention to event durations, and concluded that Reiher and Meister's responses could be multiplied by a factor of 10 for short events.

Athernon et al. (1976) studied impact and floor motions produced by walking. His impact tests consisted of 3 to 5 cycles of motion at 19 Hz (the floor resonance) or events of

approximately 200 msec duration. The disturbing level mean was 89 to 112 mm/s or over 5 times higher than Goldman's steady state intolerable level of 19.5 mm/s at 20 Hz.

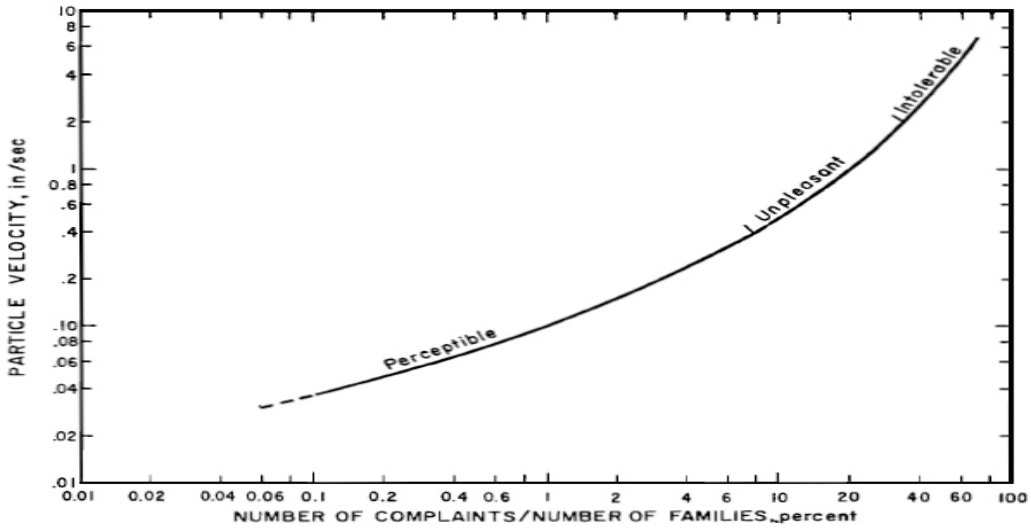

Figure 2-125: Complaint history of Salmon underground nuclear detonation with superposed subjective response (Power, 1966)

As shown in Figure 2-126, Wiss (1981) has also made a comparison of human response to transient vibration (Wiss and Parmelee, 1974) and steady state vibration (Reiher and Meister, 1931).

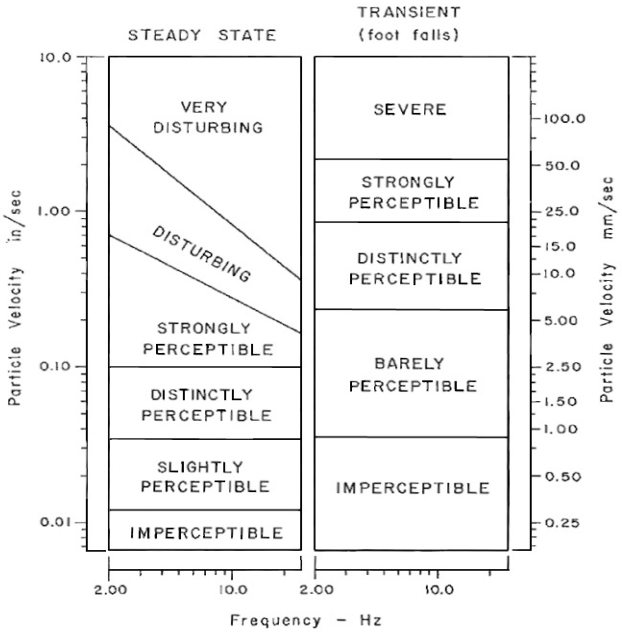

Figure 2-126: Comparison of Human Response to steady state (Reiher and Meister, 1931) and transient vibration (Wiss and Parmelee, 1974)

2.8.4 Standards

2.8.4.1 British Standards

BS 7385-2:1993 (British Standards Institution, 1993), which is still current, clearly defines peak particle velocity as the maximum value of any one of three orthogonal component particle velocities measured during a given time interval. This definition is very important as it will be seen that sometimes PPV is conservatively redefined using true vector sum (*TVS*), as formulated in Equation 2-146, or erroneously redefined using pseudo vector sum (*PVS*), presented in Equation 2-147.

BS 7385-2:1993 specifies that measurements should be taken at the base of the building on the side of the building facing the source of vibration, to define the vibration input to the building. Where this is not feasible, the measurement should be obtained on the ground, outside of the building. BS 5228-2:2009 (British Standards Institution, 2009) further explains the measuring positions, and specifies that when the purpose of vibration measurement is to assess the possibility of structural damage, the preferred primary position of monitoring is in the lowest storey of the building, either on the foundation of the outer wall, in the outer wall, or in recesses in the outer wall. For buildings having no basement, the point of measurement should be not more than 0.5 m above ground level. For buildings with more than one storey, vibration might be amplified within the building. In the case of horizontal vibration, such amplification might be in proportion to the height of the building, whereas vertical vibration tends to increase away from walls, towards the mid-point of suspended floors. Vibration measurements may also be taken on structures to provide information on the coupling between the soil and the foundations and amplification effects within a building. When the building is higher than four floors (approximately 12 m), additional measuring points should be added every four floors and at the top of the building. Measurements should be made on the side of the building facing the source. When the purpose of vibration measurement is to evaluate human exposure to vibration in the building, measurements should be taken on the structural surface supporting the human body.

BS 5228-2:2009 also recommends to measure in terms of PPV if the risk of damage to the building is the primary concern, and there is also an interest in human reaction; however, if the concern is purely for human tolerance, then weighted acceleration is the preferred parameter that should be measured. The PPV can be measured in three orthogonal axes at a point on the ground or inside a property.

BS 7385-1:1990 (British Standards Institution, 1990) and BS ISO 4866:2010 (British Standards Institution, 2010) that has now replaced BS 7385-1:1990 give guidance on the measurement and evaluation of vibration in buildings in the frequency range of 4 Hz to 250 Hz, and define three categories of vibration-induced damage (cosmetic, minor and major).

Referring to Siskind et al. (1980), BS 7385-2:1993 suggest that the probability of damage tends towards zero at 12.5 mm/s peak component particle velocity, and provides limits for transient vibration, above which cosmetic damage could occur as given numerically in Table 2-13 and graphically in Figure 2-127. In the lower frequency region where strains associated with a given vibration velocity magnitude are higher, the guide values for the building types corresponding to *Line 2* are reduced. Below a frequency of 4 Hz, where a high displacement is associated with a relatively low peak component particle velocity value a maximum displacement of 0.6 mm (zero to peak) should be used. Minor damage is possible at vibration magnitudes that are greater than twice those given in Table 2-13, and major damage to a building structure may occur at values greater than four times the tabulated values. This document suggests that where the dynamic loading caused by continuous vibration is such as to give rise to dynamic magnification due to resonance, especially at the lower frequencies where lower guide values apply, then the guide values in Table 2-13 may need to be reduced by up to 50 %.

BS 6472:1992 (British Standards Institution, 1992), now replaced by BS 6472-1:2008 (that was not available to the author at the time of compilation of this thesis), provides guidance on potential disturbance to persons exposed to vertical building vibration in the frequency range most applicable to excavation equipment; i.e., 8 to 80 Hz. The levels of vibration that may be expected to give rise to adverse comment from some people are shown in Table 2-14. These values should be regarded as conservative criteria for assessing loss of amenity, particularly for relatively short term exposure to emissions from construction or excavation projects.

In residences, adverse comment may arise during daytime as a result of continuous floor vibration levels in the order of 0.3 to 0.6 mm/s. At night time the residential criterion is equivalent to a vertical peak vibration level of only 0.2 mm/s. This latter level is barely above the threshold of human perception.

Line	Type of Building	Peak component particle velocity in frequency range of predominant pulse

		4 to 15 Hz	15 Hz and above
1	Reinforced or framed structures. Industrial and heavy commercial buildings	50 mm/s at 4 Hz and above	
2	Unreinforced or light framed commercial type buildings	15 mm/s at 4 Hz increasing to 20 mm/s at 15 Hz	20 mm/s at 15 Hz increasing to 50 mm/s at 40 Hz and above

Note 1: Values referred to are at the base of the building.

Note 2: For *Line 2*, at frequencies below 4 Hz, a maximum displacement of 0.6 mm (zero to peak) should not be exceeded.

Table 2-13: Transient vibration guide for cosmetic damage (British Standards Institution, 1993)

In offices, vertical vibration levels in the order of 0.6 mm/s are usually acceptable. The occupants of workshops are likely to be more tolerant, and would normally accept vertical vibration levels in the order of 1.2 mm/s without adverse comment.

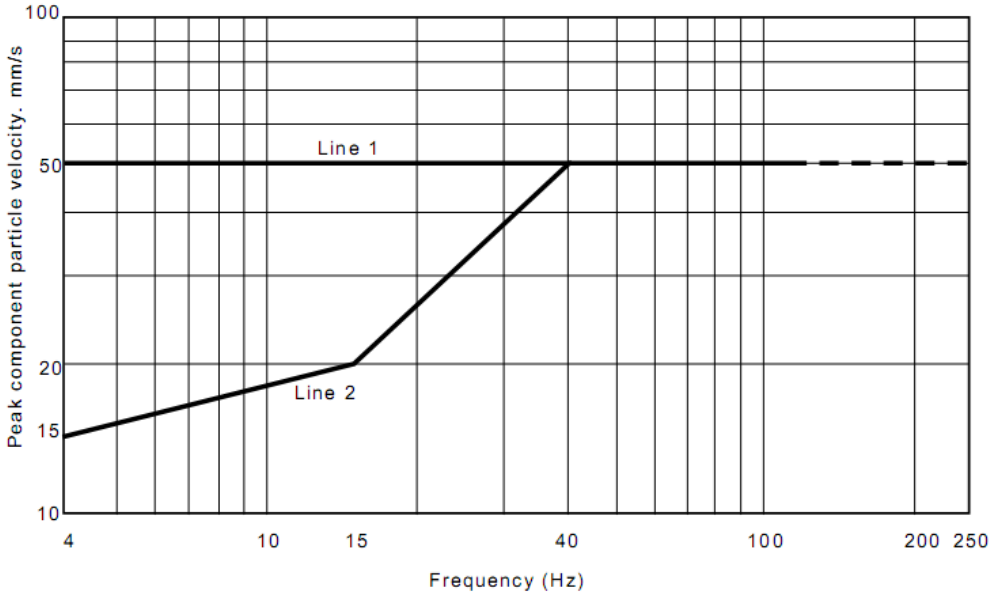

Figure 2-127: Transient vibration guide for cosmetic damage(British Standards Institution, 1993)

However, as Section 4.1 of BS 6472:1992 states, situations can exist where vibration magnitudes above those generally corresponding to minimal adverse comment level can be tolerated, particularly for temporary disturbances and infrequent and intermittent events, such as those associated with construction projects. While this document provides reasonable human comfort design goals for long term vibration, significantly higher levels of short term vibration can be tolerated by many people for construction projects.

Type of space occupancy	Time of Day	Vibration levels in mm/s over the frequency range 8 to 80 Hz likely to cause adverse comment			
		Continuous vibration		Intermittent vibration & impulsive vibration excitation with several occurrences per day	
		Vertical	Horizontal	Vertical	Horizontal
Critical working areas (e.g. some hospital operating theatres, some precision laboratories, etc.)	Day Night	0.14 0.14	0.4 0.4	0.14 0.14	0.4 0.4
Residential	Day Night	0.3 to 0.6 0.2	0.8 to 1.6 0.6	8.4 to 12.6 2.8	24 to 36 8
Offices	Day Night	0.6 0.6	1.6 1.6	18 18	51 51
Workshops	Day Night	1.2 1.2	3.2 3.2	18 18	51 51

Table 2-14: Maximum BS 6472 Curve Numbers - Human Comfort (8 to 80 Hz)

Hiller and Hope (1998) have compared the different sections of British Standards in Figure 2-128.

2.8.4.2 Australian Standards

While AS 2187.2 (Standards Australia, 2006) recognises both USBM RI8507 and BS 7385-2, which are frequency dependant. This Standard also anticipates regulations for users who do not have the facilities to use frequency dependant assessment method. In such conditions the Standard recommends ground vibration limits for control of damage to structures and human comfort to be as shown in Table 2-15 and Table 2-16.

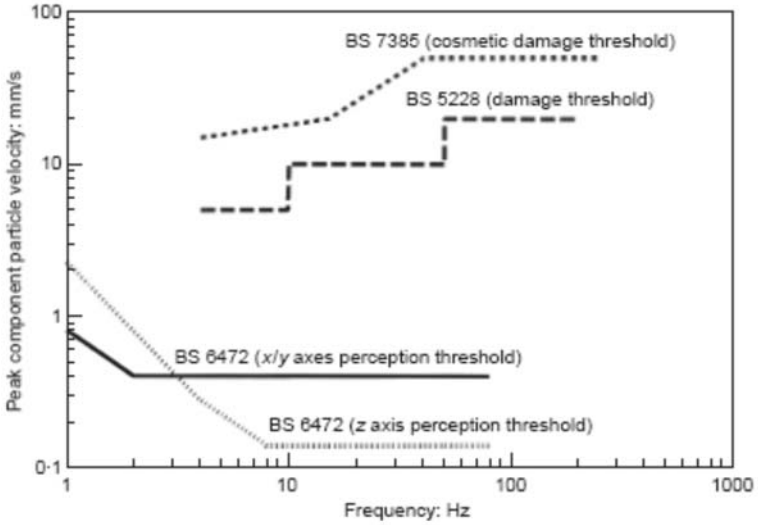

Figure 2-128: Summary guidance on vibration criteria given in British Standards. Damage thresholds are those for domestic buildings (x-axis is front-to-back, y-axis is side-to-side, z-axis is head-to-toe) (Hiller and Hope, 1998)

Table 2-15 and Table 2-16 do not cover high rise buildings, buildings with long span floors, specialist structures such as reservoirs, dams and hospitals, or buildings housing scientific equipment sensitive to vibration. These require special considerations, which may necessitate taking additional measurements on the structure itself, to detect any magnification of ground vibrations that might occur within the structure. Particular attention should be given to the response of suspended floors.

Category	Peak component particle velocity (mm/s)
Other structures or architectural elements that include masonry, plasterboard in their construction	Table 2 (BS) and referral to USBM RI 8507 and BS 7385-2
Unoccupied structures of reinforced concrete or steel construction	100 mm/s maximum unless agreement is reached with the owner that a higher limit may apply
Service structures, such as pipelines and cables	Limit to be determined by structural design methodology

Table 2-15: Recommended ground vibration limits for control of damage (AS 2187.2)

Category	Type of operation	Peak component particle velocity (mm/s)
Sensitive site*	Operations lasting longer than 12 months	5 mm/s for 95% blasts per year 10 mm/s maximum unless agreement is reached with the occupier that a higher limit may apply
Sensitive site*	Operations lasting for less than 12 months	10 mm/s maximum unless agreement is reached with occupier that a higher limit may apply
Occupied non-sensitive sites, such as factories and commercial premises	All	25 mm/s maximum unless agreement is reached with occupier that a higher limit may apply. For sites containing equipment sensitive to vibration, the vibration should be kept below manufacturer's specifications or levels that can be shown to adversely affect the equipment operation.

* A sensitive site includes houses and low rise residential buildings, theatres, schools and other similar buildings occupied by people.

Table 2-16: Ground vibration limits for human comfort chosen by some regulatory authorities (AS 2187.2)

2.8.4.3 Beyond Code Recommendations

It can be understood that the codes of practice and standard guidance and recommendations originate mostly from USBM research (Duvall and Fogelson, 1962, Nicholls et al., 1971, Siskind et al., 1980, Thoenen and Windes, 1942, Windes, 1942, Windes, 1943) that have targeted low rise buildings and limits of human annoyance, but that do not cover all structures and infrastructure. In the absence of guidelines engineering judgement and experience may become very helpful, and with knowledge that code limits are probabilistic, sometimes it may be acceptable to exceed code recommendations (that have been developed for low rise structures). For example, pipelines may be more tolerant to vibrations. Wiss (1981) indicates that particle velocities of 76 mm/s have not damaged pipes and mains. He also indicates that high pressure pipelines have withstood particle velocities in the range

of 254 to 508 mm/s without experiencing any distress as apparent from dynamic strain gage measurements.

At the same time it should be noted that at close distances, it may be the permanent physical movement or ground displacement that leads to damage rather than vibration and particle velocity. Both field studies (Lukas, 1986), see Figure 2-63, experimental studies (Hajialilue-Bonab and Rezaei, 2009), see Figure 2-64, and numerical analysis (Poran and Rodriguez, 1992), see Figure 2-66, have shown that the soil around the pounder impact point undergoes displacement, and even if a nearby structure or infrastructure is not sensitive to vibration, ground distortion may become a source of concern. Lukas (1986) notes that as the pounder strikes the ground a significant portion of the movement is downward, but lateral displacements occur, and have been reported in literature.

Based on the fact that dynamic compaction will generate high vibration amplitudes and low vibration frequencies, the US Naval Facilities Engineering Command, NAVFAC, (1997) has necessitated to maintain the minimum distances to adjacent facilities as follows:

- Piles and bridge abutment 4.5 to 6 m
- Liquid storage tanks 9 m
- Reinforced concrete building 15 m
- Dwellings 30 m
- Computers (not isolated) 90 m

The author would personally exert extreme caution for any dynamic compaction activity closer than 10 m, but has personal experience of implementing dynamic compaction at distances much closer than 90 m to computers, and suspects that NAVFAC may be referring to main frame computers used in the 1980s that were probably more sensitive to vibration that the typical computer that is used nowadays.

2.8.5 Evaluation of Dynamic Compaction Vibrations

2.8.5.1 Vibration Frequency

Field observations indicate that the ground vibration caused by dynamic compaction is in the range of 2 to 20 Hz (Mayne, 1985, Mitchell, 1981). Van Impe (1989) has mentioned 5 to 12 Hz, and Romana Ruiz and Jurado (1999) have measured vibration frequencies to be 4 to 18 Hz. Hwang and Tu (2003, 2006) have carried out vibration monitoring using a 25 ton pounder

that was dropped from 5, 10, 15 and 20 m. Figure 2-129 shows the vertical, radial and tangential particle velocity histories at different distances. It can be observed that while the vertical and radial particle velocity amplitudes are distinctively higher than the tangential amplitude, the tangential wave form is more complicated. The high frequency peaks in the front part of the wave trains attenuate quickly with distances in all three directions, but the low frequency peaks in the rear part of the wave trains attenuate slowly with distance.

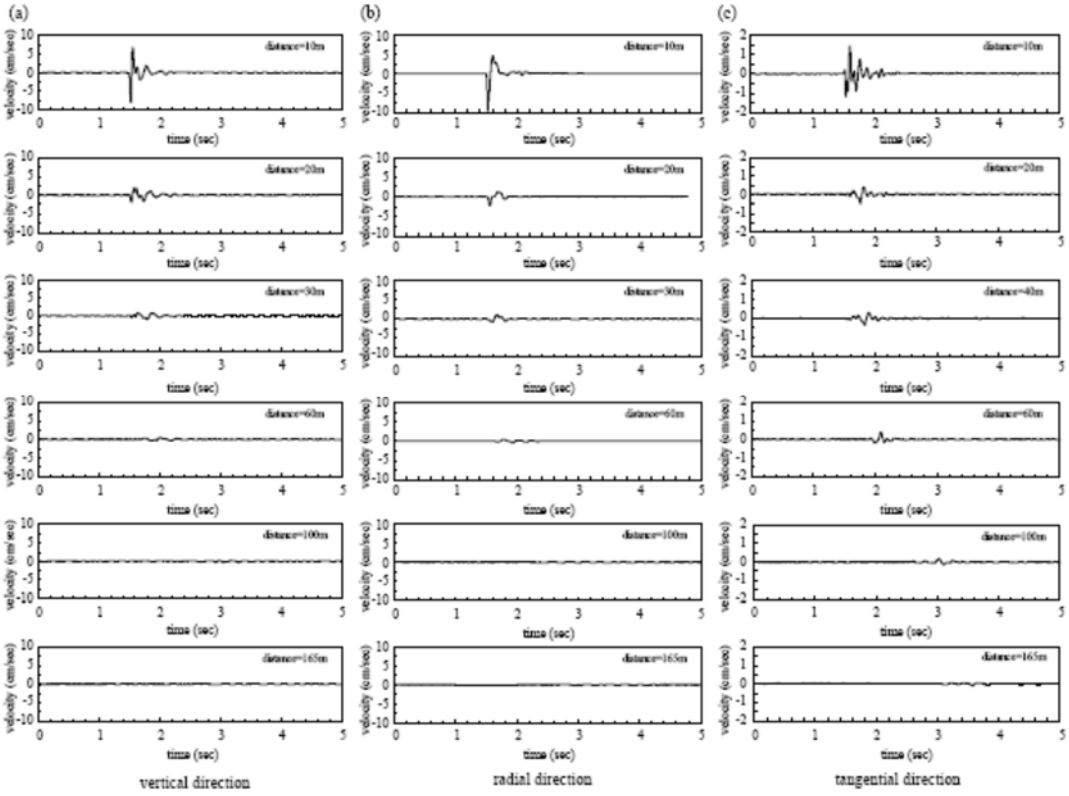

Figure 2-129: Vertical, radial and tangential particle velocities' histories at different distances (Hwang and Tu, 2003, 2006)

Figure 2-130 shows the Fourier amplitude spectra of the vertical, radial and tangential velocities at various distances from the pounder impact point. The spectra's shapes at different distances are similar in the same direction. The spectrum at the distance that is closer to the impact point has a more noticeable predominant frequency band and a corresponding peak than the farther distance. Hwang and Tu reason that this is due to energy focusing at near distance and multiple refractions and reflections of stress waves in between the soil layers. The primary frequency of vertical vibration was in the range of 10 to 20 Hz, and the radial vibration had two primary frequencies, from 3 to 4 Hz and from 12 to 13 Hz. The entire vibration frequency contents were primarily in the range of 0 to 40 Hz for all three directions.

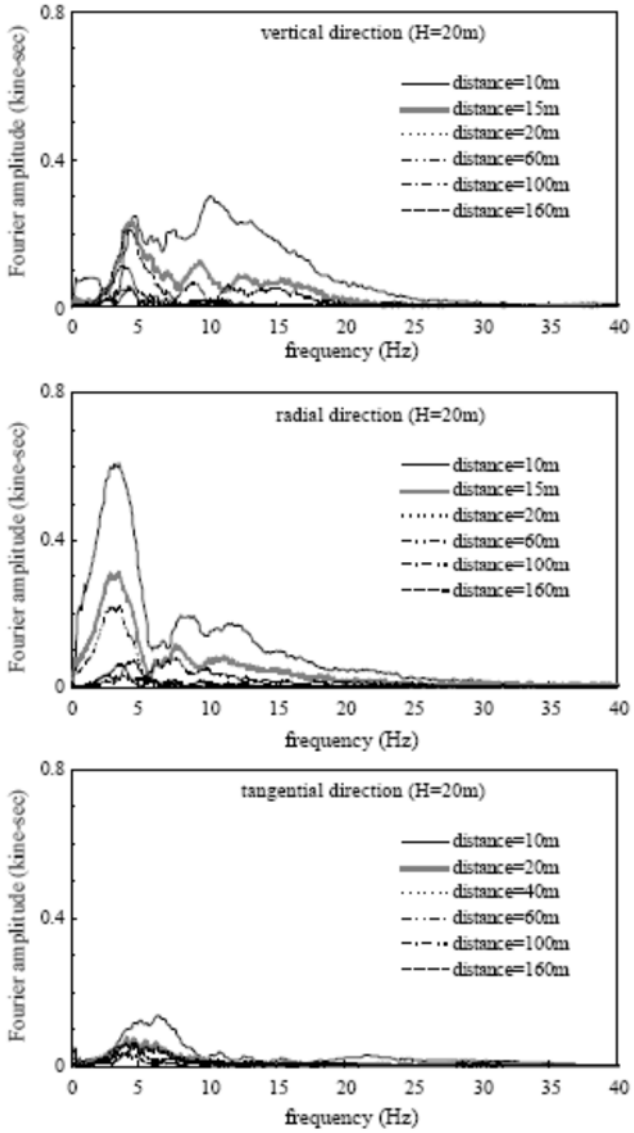

Figure 2-130: Fourier amplitude spectra of the vertical, radial and tangential velocities at various distances from the pounder impact point (Hwang and Tu, 2003, 2006)

2.8.5.2 Measurement and Prediction of Peak Particle Velocity

Hwang and Tu (2003, 2006) did not propose an equation to estimate PPV (referred to as peak ground velocity in their paper), but have studied the attenuation relationship of PPV with distance in all three directions for nine consecutive impacts. As shown in Figure 2-131, they observed that the attenuation relationships were very close and vibration characteristic of dynamic compaction seemed to be reliably reproducible.

It is interesting to note that unlike the measurements of Romana Ruiz and Jurado (1999), Hwang and Tu's measurements do not indicate that the number of blows on a location will significantly change PPV. The personal experience of the author suggests that PPV increases

as the ground becomes denser. Mayne (1985) has also observed that vibration levels increase as the treated area is compacted, and notes that a maximum level of particle velocity is achieved generally after one or two phases of heavy tamping or about 150 tm/m^2.

It can be seen in Figure 2-131 that the vertical and radial particle velocities are greater than the tangential particle velocity near the impact point. The attenuation rate is highest in the radial direction and lowest in the tangential direction. At far distances greater than 100 m the particle velocity in all three directions are almost the same.

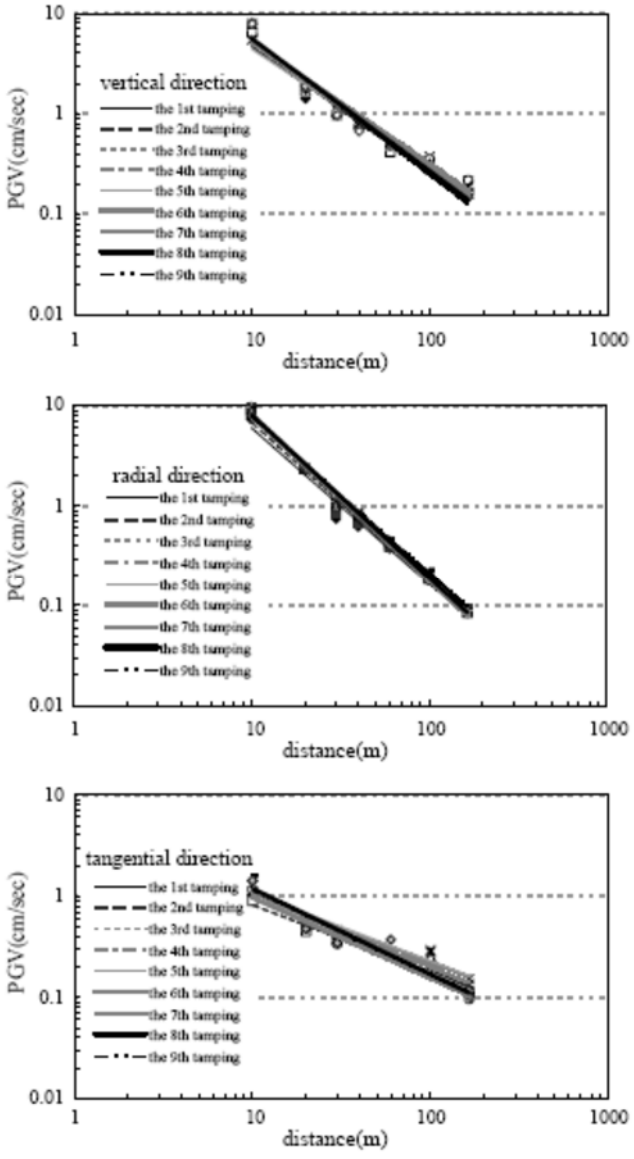

Figure 2-131: Attenuation relationship of PPV with distance in all three directions for nine consecutive impacts (Hwang and Tu, 2003, 2006)

Figure 2-132 shows the results of Hwang and Tu's study on PPV attenuation for different drop heights. As expected, higher drop heights (more energy and momentum) generate larger PPV. It can also be observed that the attenuation rate is more for the higher drops.

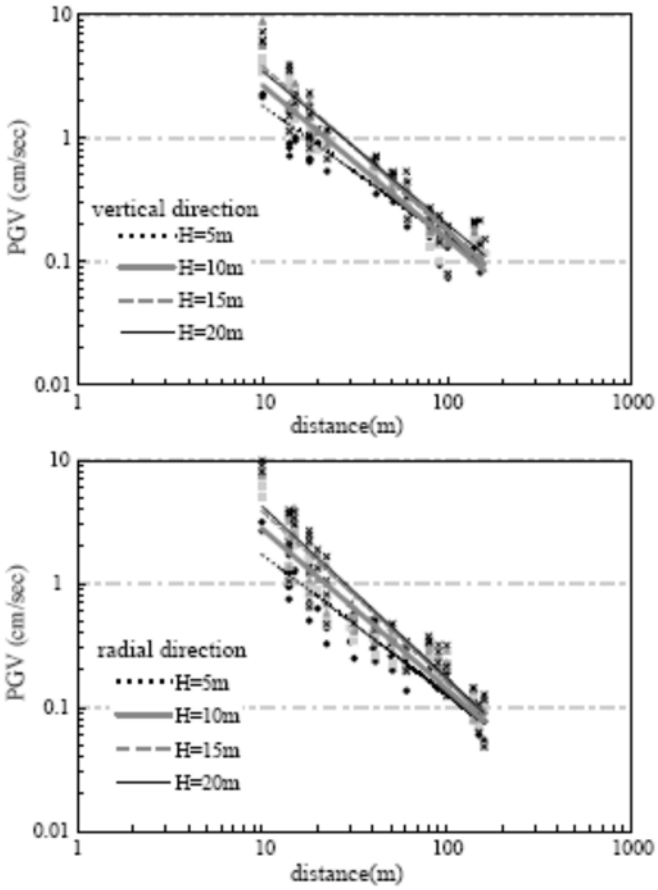

Figure 2-132: *PPV* attenuation for different drop heights (Hwang and Tu, 2003, Hwang and Tu, 2006)

An interesting observation in this study can be seen in Figure 2-133 in which the vertical and radial Fourier spectrum at 10 m is presented for different drop heights; the spectral shapes of different drop heights are the same. Higher drops have a more distinct peak spectral value and clearer predominant frequencies. It seems that the attenuation differences for 15 and 20 m drop heights are small. In the opinion of Hwang and Tu, this seems to indicate that the ground has a capacity limit for storing the vibration energy. When the drop height is greater than a certain value the induced vibrations have no significant difference, and Hwang and Tu understood that the redundant potential energy may have been consumed to create deeper impact craters.

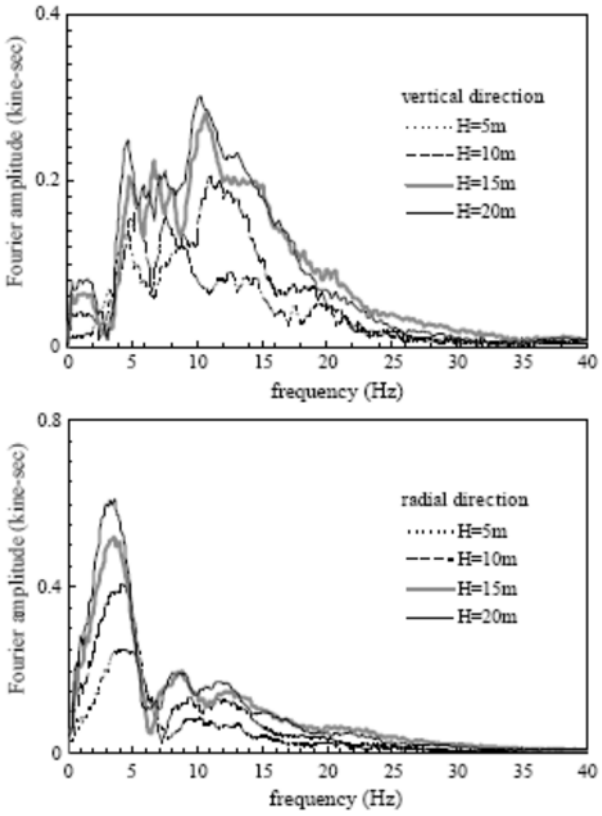

Figure 2-133: Vertical and radial Fourier spectra at 10 m distance for different falling heights (Hwang and Tu, 2003, Hwang and Tu, 2006)

Obviously, and as shown in Figure 2-134, the best way to ensure the accuracy of the estimated PPV value is to directly measure it on site by the vibration meter. This should be done definitely if the contract specifies it, or if there are reasons of concern for the parties involved in the project or the third parties.

Figure 2-134: Vibration metre for measuring peak particle velocity

The relationships among peak values of harmonic waves may be expressed by (Mayne, 1985) and can be used to estimate the other parameters:

$$a = 2\pi f v = (2\pi f)^2 s \qquad \text{2-145}$$

a = acceleration

f = frequency of vibrations

v = particle velocity

s = displacement

Vibration measurements should be taken in three mutually orthogonal directions simultaneously. Damage criteria developed by USBM, OSM and others have been based on the maximum single value of the three directional components. This is also in line with standards such as BS 7385-2:1993 (British Standards Institution, 1993). Since real waves are three dimensional and the transducer axes of the 1980s technology may not be exactly in line with the source of vibrations, Mayne (1985) notes that some engineers prefer to calculate the true vector sum (TVS) of the triaxial components:

$$TVS = \sqrt{(x_t)^2 + (y_t)^2 + (z_t)^2} \qquad \text{2-146}$$

where all values are obtained at the same time. Needless to say, TVS will yield a conservative figure that is always larger than PPV.

Mayne has also noted that several individuals (Dobson and Slocombe, 1982, Skipp and Buckley, 1977) have mistakenly expressed the vibration levels in terms of the pseudo vector sum (PVS), formulated in Equation 2-147. This error is still appearing in more recent works (Mostafa, 2010).

$$\mathrm{P}VS = \sqrt{(x_{max})^2 + (y_{max})^2 + (z_{max})^2} \qquad \text{2-147}$$

Implementation of *PVS* is unjustified as it is too conservative and not related to a maximum velocity at a particular time (that has been the basis of all codes of practice). The maximum

particle velocity values in the three orthogonal directions rarely, if ever, occur at the same time, and there does not seem to be any evidence to indicate that they will happen simultaneously. Mayne has assessed that at most *PVS* values could be 73% higher than the maximum single component velocity, and typically, *TVS* values are about 10 to 40% higher than the maximum single component velocity.

Wiss (1981) has proposed to express peak particle velocity (PPV) in terms of both distance, d, and impact energy, E, in a single expression:

$$PPV = K\left(\frac{d}{\sqrt{E}}\right)^{-n} \qquad 2\text{-}148$$

n= vibration attenuation rate. The value of n is generally from 1 to 2, with a relatively common value of 1.5

K= intercept

$d/\sqrt{E}$ = scaled distance

As shown in Figure 2-135, Mayne et al. (1984) compiled the results of 14 dynamic compaction sites. Soil types at these sites included silty sands, sandy clay, rubble, coal spoil and debris fill. For preliminary estimates of ground vibration levels, a conservative upper limit appeared to be:

$$PPV \leq 70\left(\frac{\sqrt{WH}}{d}\right)^{1.4} \qquad 2\text{-}149$$

PPV is in mm/s, d and H are in metres and W is in tons. The variable $\sqrt{WH}/_{d}$ is defined as *inverse scaled distance*.

Later and based on a mix of single maximum component and *TVS* measurements (that should lead to conservative figures) of 12 sites, Mayne (1985) proposed an upper limit conservative PPV in the form of:

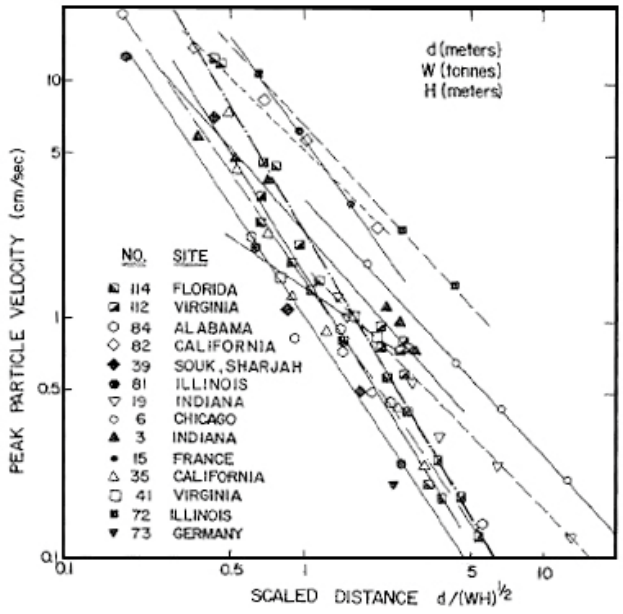

Figure 2-135: Attenuation of ground vibrations measured on different dynamic compaction projects (Mayne et al., 1984)

$$PPV \leq 92\left(\frac{\sqrt{WH}}{d}\right)^{1.7} \qquad 2\text{-}150$$

Annex E of BS 5228-2:2009 (British Standards Institution, 2009) that is for informative purposes has converted Equation 2-150 to SI units, and predicts dynamic compaction induced PPV using Equation 2-151.

$$PPV \leq 0.037\left(\frac{\sqrt{WH}}{d}\right)^{1.7} \qquad 2\text{-}151$$

d is between 5 to 100 m, and WH is between 1.0 to 12 MJ.

In another approach and as shown in Figure 2-136, in order to get a close trend and based on information accrued by monitoring vibrations produced by different drop heights from a site in Alexandria, Virginia, Mayne believes that while pounder weight may affect vibration frequency, the magnitude of vibration particle velocities is slightly more influenced by the drop height. Therefore, he has proposed to estimate PPV (in the same units as impact velocity) by normalisation (dividing by the theoretical impact velocity of the falling pounder

$\sqrt{2gH}$), and plotting it against the normalised distance to impact (by dividing d by the pounder radius r):

$$\frac{PPV}{\sqrt{2gH}} \leq 0.2\left(\frac{d}{r}\right)^{-1.7} \qquad 2\text{-}152$$

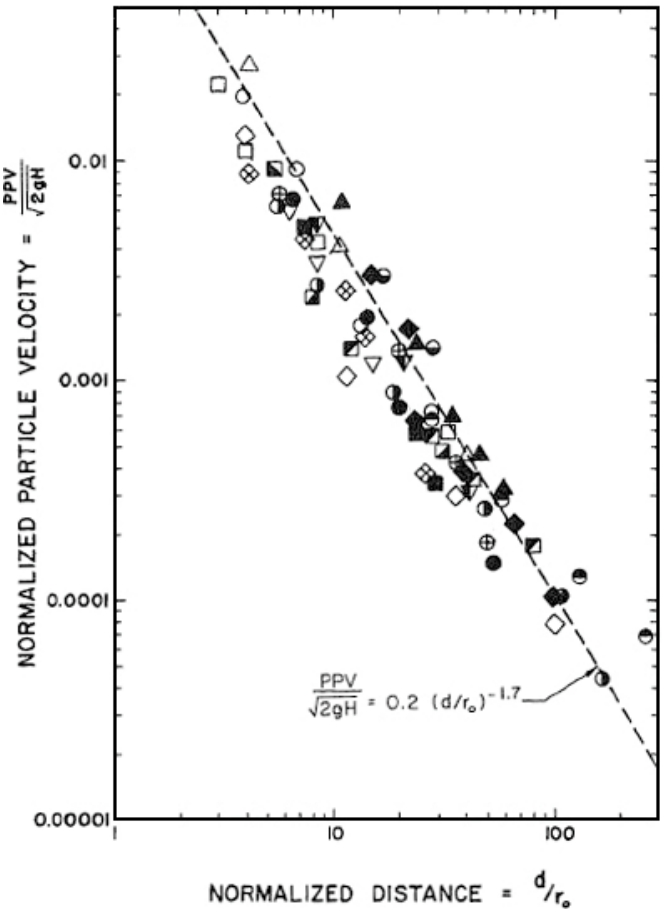

Figure 2-136: Observed attenuation of normalised PPV with normalised distance (Mayne, 1985)

For impact energies in the range of 250 to 300 tm, Varaksin (1981) and Chapot et al. (1981) estimated PPV to be (Figure 2-137) as presented in Equation 2-153.

$$PPV = 340d^{-1.1} \text{ mm/s} \qquad 2\text{-}153$$

The measurements of Romana Ruiz and Jurado (1999) for an impact energy of 252 tm were in agreement with Equation 2-153 only for the first impact and for distances greater than 10 m. The vibration levels increased rapidly with subsequent impacts; in some cases up to 2 or 3 times.

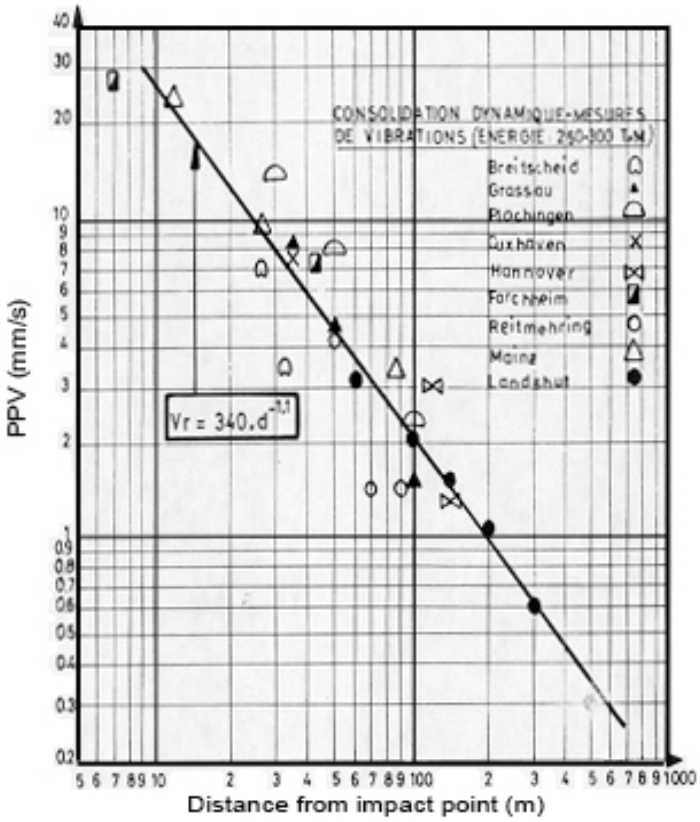

Figure 2-137: Peak Particle Velocity for impact energy in the range of 250-300 tm (Chapot and et al., 1981, Varaksin, 1981)

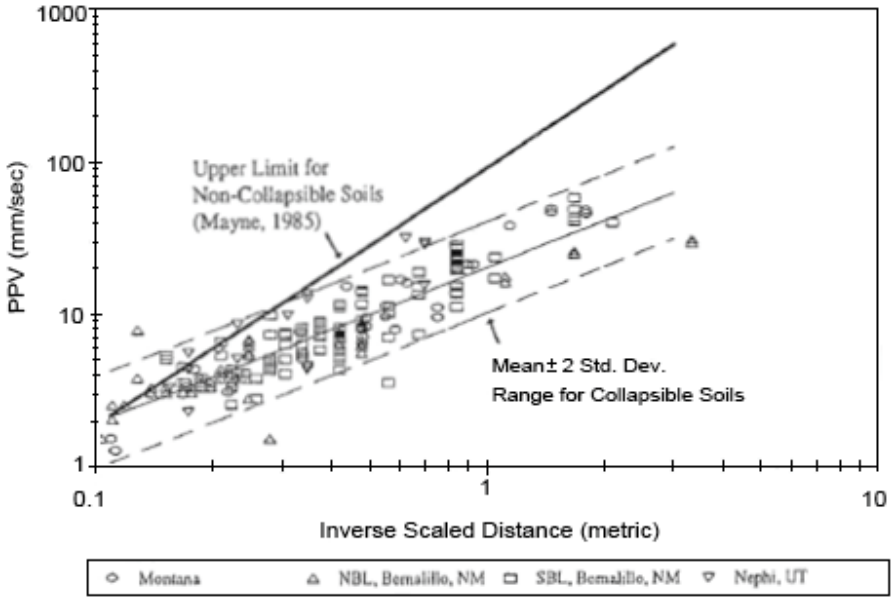

Figure 2-138: Plot of peak particle velocity versus inverse scaled distance for collapsible soils (Rollins and Kim, 1994)

Based on a number of projects and as shown in Figure 2-138, Rollins and Kim (1994) have estimated PPV in collapsible soils to be less than non-collapsible soils, and as presented in Equation 2-154.

$$PPV \leq 20\left(\frac{\sqrt{WH}}{D}\right)^{1.03} \qquad 2\text{-}154$$

2.8.6 Mitigation and Isolation of Vibrations

It was discussed in Section 2.3.5 that wave amplitudes attenuate with distance; however, this reduction is sometimes not sufficient to mitigate or eliminate the risk of dynamic compaction induced damages. In such situations, it may be necessary to reduce the vibrations by implementing special measures.

It can be understood from the equations of Section 2.8.5.2 that PPV is a function of impact energy; hence, the simplest way to reduce the vibration amplitude appears to be the reduction of impact energy itself. This can be merely achieved by reducing either the pounder weight or the pounder drop height. In such cases, energy deficiency may be compensated for by increasing the number of pounder drops per print.

This technique is applicable only when lesser impact energies are sufficient to satisfy the technical specifications and design criteria; otherwise alternative solutions such as construction of vibration reduction barriers or trenches should be considered.

As shown in Figure 2-139 the concept of isolation by wave barriers is based on reflection, scattering and diffraction of wave energy. Wave barriers could be solid, fluid or void zones in the ground. At a solid to solid interface both *P* and *S*-waves are transmitted, at a solid to fluid boundary only *P*-waves are transmitted, and finally at a solid to void interface no waves are transmitted. Thus, it appears obvious that the most effective wave barrier is a void trench.

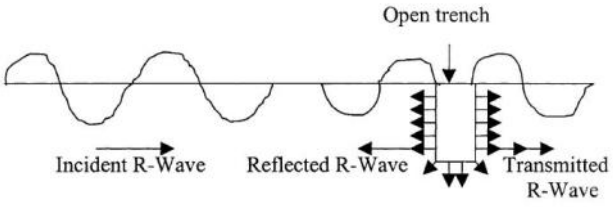

Figure 2-139: Vibration isolation using an open trench (Shrivastava and Kameswara Rao, 2002)

It has been shown (Thau and Pao, 1966) theoretically that in an elastic medium a thin crack is sufficient to screen vertically polarised *SH*-waves which are analogous to the vertical component of the *R*-wave at the surface of the half wave.

An *active barrier* reduces vibrations at the source. On the other hand, *passive barriers* screen vibrations at the location of the receiver. In dynamic compaction the print location is constantly changing, and it is not possible to construct an active barrier. Hence, only passive vibration reduction isolators are applicable.

Woods and Richart (1967) and Woods (1968) have carried out broad investigations to develop guidelines for the design of *active* and *passive* barriers. The variables in the tests that Woods and Richart carried out were the trench depth, H_T, the trench length, L_T, the trench width, W_T, and the distance from the source of excitation to the trench, R_T. The trench sizes ranged from 0.3 m deep by 0.3 m long by 0.1 m to 1.2 m deep by 2.4 m long by 0.3 m wide, the vibration excitation was at 1.5 and 3 m from the trench, and the vertical vibration frequencies were 200, 250, 300 and 350 Hz. The variables were made dimensionless by dividing them by the wave length L_R.

From practical considerations, the critical dimension for trench barriers was the scaled depth H_T/L_R; therefore, for each distance from the source, the shallowest trench that satisfied the criterion of reducing the vertical ground motion amplitude to 25% of its value without barriers was determined. The minimum scaled depth for the passive trenches was generally $1.2< H_T/L_R <1.5$. To evaluate the total trench area on the screened zone, a quantity $H_T L_T/L_R^2$ was computed for each trench. There was a general trend toward increasing $H_T L_T/L_R^2$ with increasing R_T/L_R. Figure 2-140 shows the amplitude ratio contour diagram for a trench that satisfied the criterion. It can be observed that the wave amplitude has magnified in front of and near the end of the trench.

Curves of vertical displacement amplitude versus distance along a line of symmetry from the vibrator through the trench are shown in Figure 2-141 for five tests. It can be seen that the larger trenches are more effective than the smaller ones. Once again, it can be observed that the amplitudes were magnified in front of the trench.

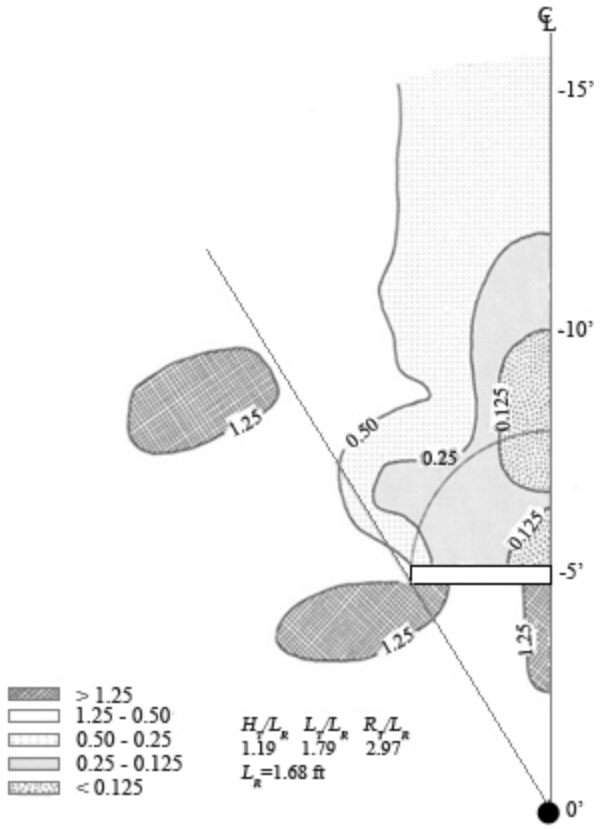

Figure 2-140: Schematic of test layout for active isolation in the field (Woods, 1968)

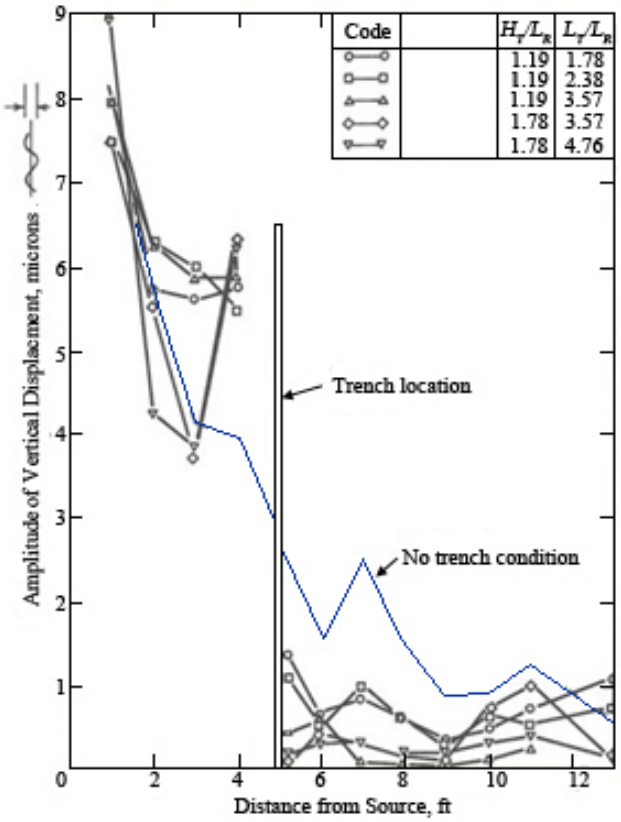

Figure 2-141: Amplitude of vertical displacement versus distance from source for five tests (Woods, 1968)

It can also be noticed from Figure 2-141 that the trenches are more effective at closer distances behind the trench than at further distances. In fact it appears that beyond a certain point the trench will become inefficient. This is in line with BS 5228-2:2009 that proposes that for maximum effects the trench should be as close to the source or to the receiver as possible.

Based on the study of Thau and Pao (1966) it was assumed that the width of an open trench would not be an important variable. Woods performed a few tests to evaluate this assumption, and it was found that an increase in width did not cause a significant change in either the magnitude of reduction or the shape of the screened zone.

Another hypothesis was that open trenches would be more effective than sheet walls as surface wave barriers. A number of sheet wall barrier tests were performed, and it was found that in general sheet-wall barriers are not as effective as open trench barriers for reducing vibration amplitudes.

Shrivastava and Kameswara Rao (2002) have performed numerical modelling of the same problem using vertical and horizontal impulse loads. Their study suggests that for vertical impulses, an increase in the length or depth of the trench reduces the amplitude ratio behind the trench, but this reduction becomes less as the distance to the trench increases (Figure 2-142 and Figure 2-143).

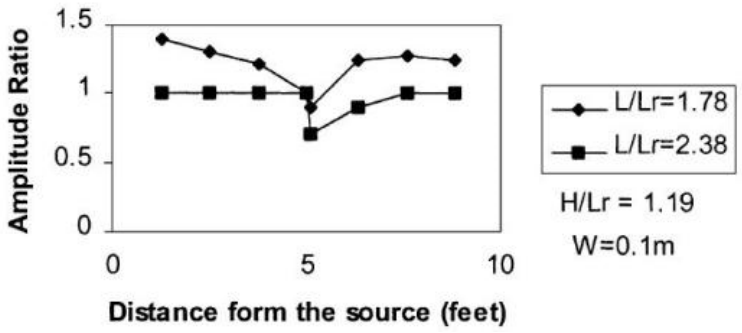

Figure 2-142: Effect of length of trench on vibration amplitude (Shrivastava and Kameswara Rao, 2002)

Tsai and Chang (2009) have also studied vibration isolation for trenches with walls by using the boundary element method. Their research shows that vibration reduction ratio (A_{ry}) is 2 to 10 times more for open trenches with sheet pile or diaphragm walls as compared to when the trench has no wall (Figure 2-144).

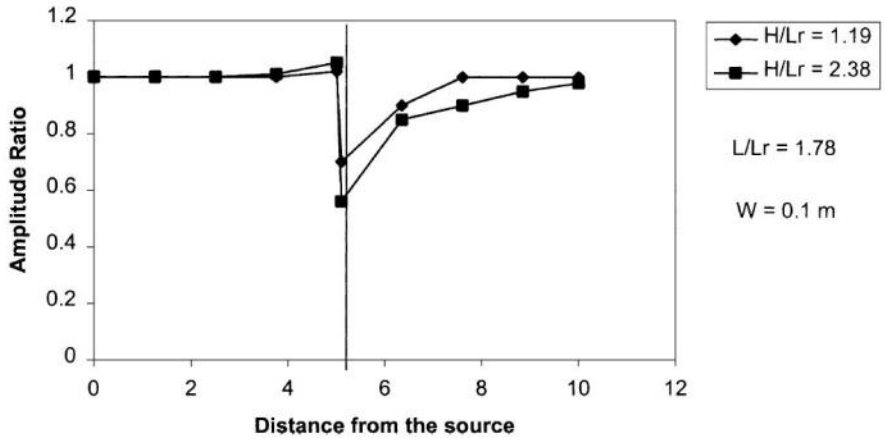

Figure 2-143: Effect of depth of trench on vibration amplitude (Shrivastava and Kameswara Rao, 2002)

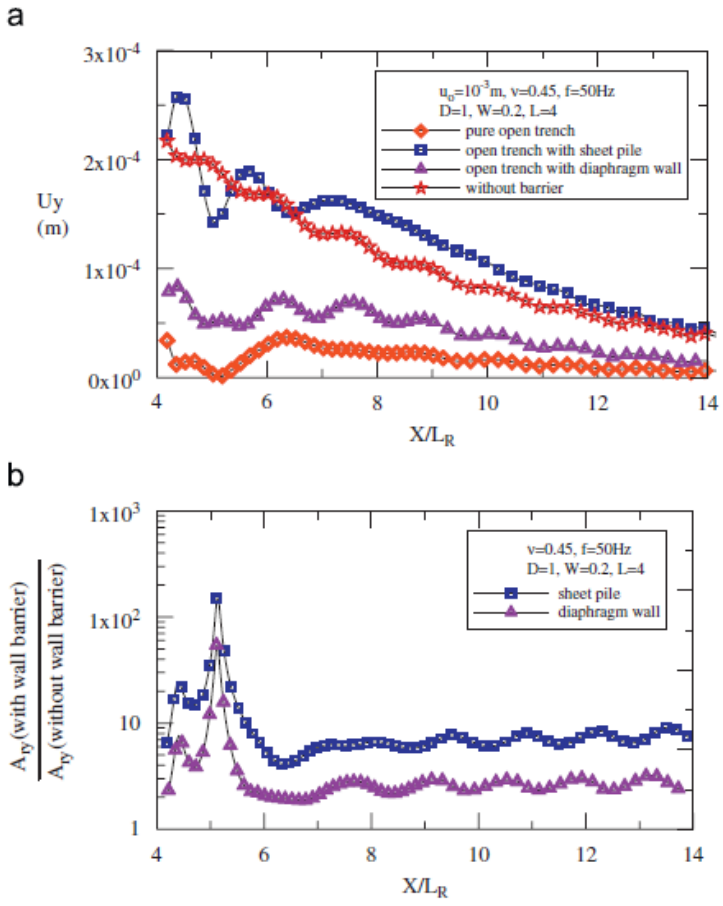

Figure 2-144: The comparison of screening effectiveness between the open trench barriers: (a) the amplitude of ground vibration behind the barriers and (b) the ratio of A_{ry} was based on the amplitude with and without the walls (Tsai and Chang, 2009).

Tsai and Chang also found that changes in either Poisson's ratio or trench width had insignificant influence of on vibration amplitude changes for both cases of sheet pile and

diaphragm wall trenches. According to Tsai and Chang, Poisson's ratio does not have a significant effect because the vibration isolation by a trench is primarily achieved by the screening of R-waves rather than P-waves (refer to Section 0; *P*-wave velocity varies greatly with Poisson' ratio).

Other research (Gazetas, 1982) indicates that most of the Rayleigh wave energy is contained in a near surface zone that is about one third to half of a wave length thick. Hence, it can be understood that the trench depth must be at least a third of the wave length to be rather efficient.

In their research, Hwang and Tu (2003, 2006) also tested the effectiveness of shallow isolation trenches, 3 m deep by 1 m wide, which were 10 to 20 m wide and 15 to 150 m away from the impact point. Their findings indicate that vertical, radial and tangential particle velocities were basically the same with and without the trenches.

Based on the work of others (Ahmad and Al Hussaini, 1991, Liao and Sangrey, 1978, Watts, 1990) and taking into consideration that most of the Rayleigh wave energy is contained in a near surface zone about one third to one half of a wavelength thick, Hiller and Hope (1998) proposed that the isolation barrier depth should be at least one third the wave length:

$$H_T = 0.3L_R = \frac{v_R}{f} \approx \frac{v_S}{f} \qquad \text{2-155}$$

f is the predominant frequency, and v_R is the speed of propagation of a Rayleigh wave in the ground or, approximately, the shear wave speed, v_S.

It can be concluded from the above that:

1. It is most effective is vibration reduction barriers are constructed in the form of open trenches without walls.
2. The width of an open trench causes small changes to the amount of vibration reduction. Hence, and from the practical point, it is sufficient to make the trench width equal to the width of the excavator shovel.
3. The maximum amplitude reduction can be expected to be closest to the back of the trench; hence, it is best to excavate the trench as close as possible to the zone that is to be protected. In any case, sufficient distance must be maintained in order not to endanger the stability of the structures behind the trench.

4. Deep trenches are able to reduce the vibration amplitude more than shallow trenches. The trench depth should be 0.3 times the wave length to be able to effectively reduce the amplitude of ground motion. In practice the trenches will be generally 3 to 4 m deep. Practically speaking and if there is a ground water table, the depth of excavation will have to be limited to the level of the ground water.
5. Trenches with larger areas (length and depth) are more effective. In any case and as is done in practice, it is best to extend the trench along the boundary where vibrations must be reduced in order to get the best results.

Although reducing vibrations by excavationof open trenches is common practice in dynamic compaction, not much has been published on isolation trenches application in DC. Varaksin (1981) notes that dynamic compaction can be performed very close to rigid structures that are less than 20 m away, and adds that for normal buildings in good condition a safe distance of 30 m is necessary. For sensitive buildings in good condition, he recommends safe distance of 50 m. In case the mentioned distances cannot be honoured, he suggests that vibrations can be reduced by digging a wave isolation trench that is 1.5 to 2.5 m deep. Varaksin makes a note that damping appears to be more important than what theory would predict because even though Rayleigh wave energy is mostly distributed over half the wave length, shallow trenches such as shown in Figure 2-145 (reduction of particle velocity of Rayleigh wave versus distance from pounder impact point) demonstrate effectiveness.

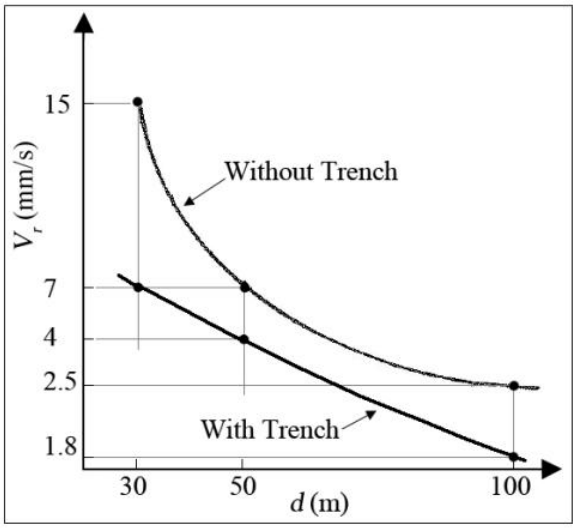

Figure 2-145: Effectiveness of shallow trenching for reduction of vibration (Varaksin, 1981)

It is the opinion of Varaksin (2014) that trenches are best effective when they are close (5-6 m) to the impact, and loose efficiency at greater distances (50 m) as the trench depth has to be one third of wave length, and R wave lengths are around 140 m.

2.9 Quality Control

2.9.1 Heave and Penetration Test

In the earlier sections of this chapter it was shown experimentally (Hajialilue-Bonab and Rezaei, 2009) and numerically (Gu and Lee, 2002) that the rate and amount of improvement reduces as further pounder blows are applied to the ground until improvement increase tends towards negligible amounts. This would suggest that monitoring the rate of compaction could be a good indication of the efficiency of dynamic compaction. This may be achieved by measurement of ground deformation during consecutive pounder blows.

Measurement of crater depth *per se* does not appear to be an acceptable means of measuring improvement efficiency because simple crater depth measurement could lead to erroneous conclusions. The crater depth is not only a function of the induced settlement under the pounder, but rather the resultant of induced settlement and crater sides collapse back into the crater floor. This suggests that measurement of the crater volume would be a more meaningful than the simple measurement of crater depth. Furthermore, measurement of crater volume on its own would still not be able to accurately predict the efficiency of compaction as it does not take the deformations of ground around the crater into consideration. Indeed the efficiency of compaction can be best determined if all volumetric changes within the crater dimensions and beyond the crater zone are included in the assessment.

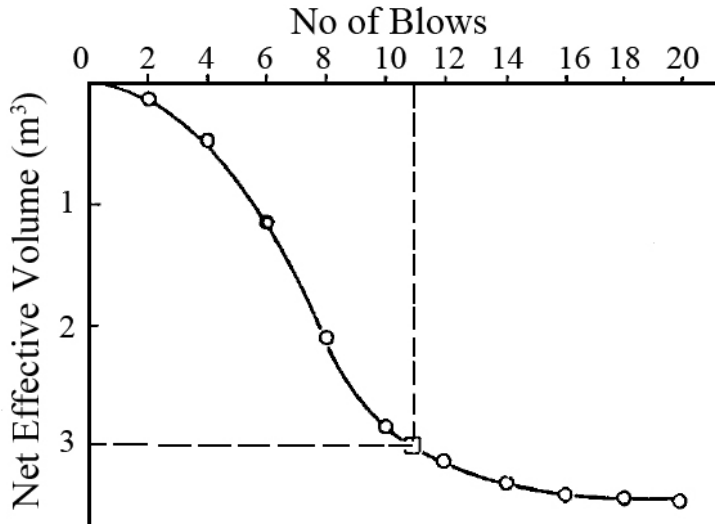

Figure 2-146: Net effective volume change, modified from Lukas (1986)

Figure 2-146 shows the relationship between the number of pounder blows and net effective volume change, which is the resultant of the summation of volume change of soil in the crater and around the crater, and can be used to determine the appropriate number of blows that achieves an optimum amount of compaction.

While the change in soil volume in the crater is always positive (penetration and reduction of volume), the peripheral soil can be positive or negative (heave and increase of volume caused by iso-volumetric plastic deformations). It is possible that while the pounder continues to penetrate the ground, and increase the crater depth, the soil is undergoing plastic deformation, the peripheral ground is heaving, and the net compaction volume is increasing with a low or negligible rate. In such cases, dynamic compaction is being performed with little or no efficiency. Figure 2-147 shows a case encountered during the ground improvement works for a saturated very silty sand/sandy silt section of Dubai Airport Runway where the heave and penetration volumes were almost the same (Serridge, 2002) from the very beginning. This means that application of dynamic compaction in areas with soil behaviour similar to Figure 2-147 would not have had any effect, and dynamic replacement should have been considered.

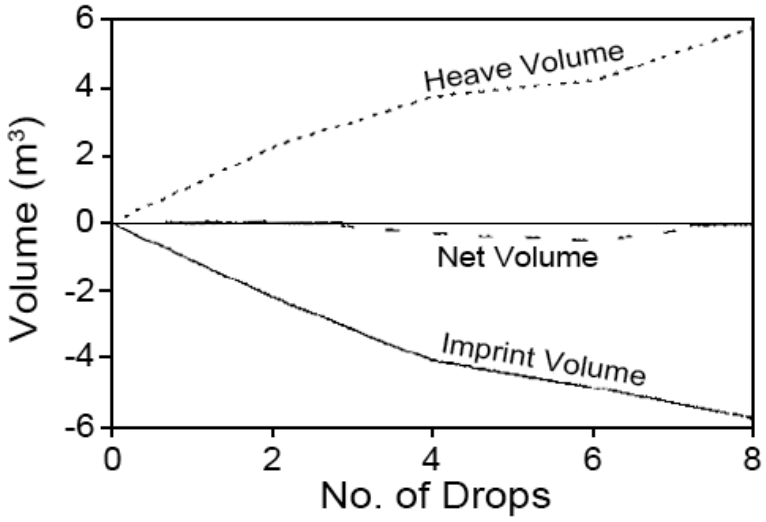

Figure 2-147: Inefficiency of pounder blows identifiable from measurement of net volume change (Serridge, 2002)

To calculate the crater volume, the ground level should be determined before the first blow. The base area of the crater will be the same as the pounder base area; however, as can be seen in Figure 2-148, the crater diameter at ground level is usually larger, and should be measured in at least 2 directions to obtain an average value. The depth of crater can be

measured by placing the staff on the pounder, and adding the pounder height to the readings.

Figure 2-148: heave and penetration test

Once the crater dimensions are known the volume can be estimated using any calculation method. If the top and base of the crater are assumed to be circular with radii R_T and R_B, then the volume of a crater with height, D_c, can be estimated by a truncated cone:

$$V_{crater} = \frac{1}{3}\pi D_c({R_T}^2 + {R_B}^2 + R_T R_B) \qquad 2\text{-}156$$

Lukas (1986) estimates this volume by taking an average value for the top and base diameters, and assuming a cylindrical shape. This would yield a volume equal to:

$$V_{crater} = \pi D_c \left(\frac{R_T + R_B}{2}\right)^2 \qquad 2\text{-}157$$

It can be calculated that estimation of the volume using a truncated cone will yield the same value as a cylinder when the top and base radii are equal, but will always be slightly greater when the top radius is larger than the base radius. The difference between the two volumes is approximately 4% when the top radius is double the base radius and approximately 8%

when the ratio of the radii is 3; hence, it is preferable to use a truncated cone volume to estimate the crater volume.

For estimation of heave volume (which could very well be settlement as well) Lukas (1986) proposes that within each quadrant, four markers should be set around the print, with the closest marker being about 0.5 m away from the edge of the print. The furthest marker is suggested to be about 5 m away from the centreline of the print. The remaining markers should be equally spaced out between the first and last markers. The elevation of the 16 markers should be determined before the first drop and at two drop intervals. The average heave (or settlement) for markers located at the same radius from the centre of the print, S_i, should be calculated using Equation 2-158.

$$S_i = \frac{S_{i\ \text{quadrant 1}} + S_{i\ \text{quadrant 2}} + S_{i\ \text{quadrant 3}} + S_{i\ \text{quadrant 4}}}{4} \qquad 2\text{-}158$$

The heave can then be calculated based on the average heave at various distances. Lukas notes that heave is generally greatest near the edge of the print, and reduces to small amounts further away from the print, and suggests that, as shown in Figure 2-149, heave calculation can be simplified by assuming a linear heave pattern instead of the actual average marker heaves. The volume of heave (or settlement) from the simplification will yield:

$$V_{heave} = \pi S_{max} L(^{L}/_{3} + R_T) \qquad 2\text{-}159$$

L= Distance from edge of crater to where heave reduces to zero

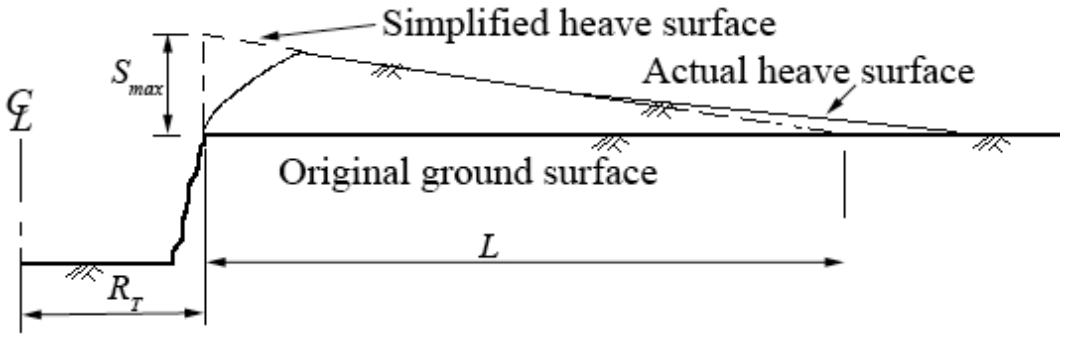

Figure 2-149: Heaved ground section (Lukas, 1986)

It is the author's experience that choosing the first set of markers at a distance of 0.5 m from the print may be too close when the soil is very loose and this ring of markers may fall within

the crater volume. Hence, it may be preferable to allow for an extra intermediate ring of markers or to set the first row of markers at a greater distance from the print. Also, dividing the ground into 3 parts may be less time consuming, but with sufficient accuracy as setting the markers at quadrants.

2.9.2 Menard Pressuremeter Test

Noting that the pressuremeter test, dynamic compaction and dynamic replacement have all been the inventions and developments of Louis Menard, it is not surprising that for the 20 years that Menard held the patents of DC and DR, PMT was carried out systematically as the verification test. Although nowadays Menard Pressuremeter, MPM, is not the only type of pressuremeter device, all references to PMT in this thesis is meant to refer to the Menard Pressuremeter Test. Review of literature shows that to date all major standards such as ASTM (2007) and ENV 1997-3 (European Standard, 2000) have derived from Menard's testing procedure, interpretation and calculation rules (Centre D'Etudes Menard, 1975).

The pressuremeter test is an in situ stress-strain test that is performed on the wall of a borehole using a laterally expanding cylindrical probe, and ultimately provides a failure value in shear mode. PMT is somewhat different from other in-situ tests, such as SPT or CPT, which are or were originally used in geotechnical design on the basis of correlations (Gambin and Frank, 2009). In this test a cylindrical cavity is subjected to pressure increments typically at 1 m intervals of depth, and the resulting expansion is measured in terms of a volume increase. The result of the test is a failure and a small strain (10^{-2}) deformation parameter, which make the test a very suitable device for predicting bearing capacity (shear failure) and deformations.

2.9.2.1 Description of the Pressuremeter

The Menard pressuremeter consists of three main elements; i.e., a radially expandable cylindrical probe that is placed inside the borehole at the desired test level, a control or monitoring unit that remains on the ground surface, and the tubing that allows the probe to be pressurised.

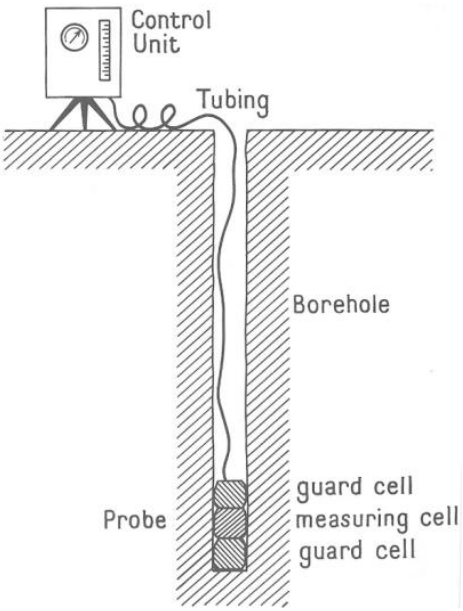

Figure 2-150: The main elements of the Menard pressuremeter (Baguelin et al., 1978)

Instead of a long chamber, the probe is made up of three independent cells stacked on top of each other. Each cell has a rubber membrane, top and bottom discs, and a rigid steel backbone. All cells are inflated to the same pressure simultaneously. The top and bottom cells are called guard cells because they protect the middle cell, which is the measuring cell, from the end effects caused by the finite length of the probe, and allow it to expand only in the radial direction, as if the probe had an infinite length. This results in plane strain deformation conditions (Baguelin et al., 1978). The combined height of the measuring and guard cells should be at least six times the cell diameters (ASTM, 2007).

To protect the probe membranes against the sharp surface of a borehole, the probe can be initially placed inside a *slotted casing*, which is a thick steel tube with a number of longitudinal slots that allow the tube to expand laterally. Commonly, the casing has six slots, each about 1 mm wide. There are a number of standard sizes of slotted casings, but the most widely used has an outside diameter of 63 mm, an inside diameter of 49 mm, and protects a 44 mm diameter probe.

The control unit is a container with a front panel on which all the measuring instruments are installed, and its function is to control and monitor the expansion of the probe. A coaxial tubing connects the probe to the instruments, and is used to pressurise the probe cells. The inner tube carries water to the measuring cell, and the annular space between the inner and outer tubes allows gas, usually nitrogen, to reach the guard cells. Placing the tube supplying

the measuring cell inside the outer tube does not allow the inner tube to expand, which would result in erroneous readings of the amount of injected water and volume change.

2.9.2.2 Calibration

Prior to inserting the probe in the borehole, the equipment should be calibrated to compensate for pressure losses, P_c, (due to probe rigidity) and volume losses, V_c, (due to expansion of tubing and compressibility of any part of the testing equipment) by recording the expansion of the probe for equal increments of pressure (or volume). Pressure and volume calibration curves are shown in Figure 2-151.

Pressure correction must be deducted from the pressure readings obtained during the test. Volume loss correction must also be deducted from the measured volumes during the test. The latter correction is relatively small in soils, and although ASTM (2007) allows it to be neglected if it is less than 0.1 % of the nominal volume of the measuring portion of the not inflated probe per 100 kPa of pressure, it notes that in very hard soils or rock, the correction is significant and must be applied. In agreement with ASTM, ISSMFE or the International Society of Soil Mechanics and Foundation Engineering, (Amar et al., 1991) notes that as long as Menard modulus, E_M, is less than 100 MPa volume losses are usually negligible.

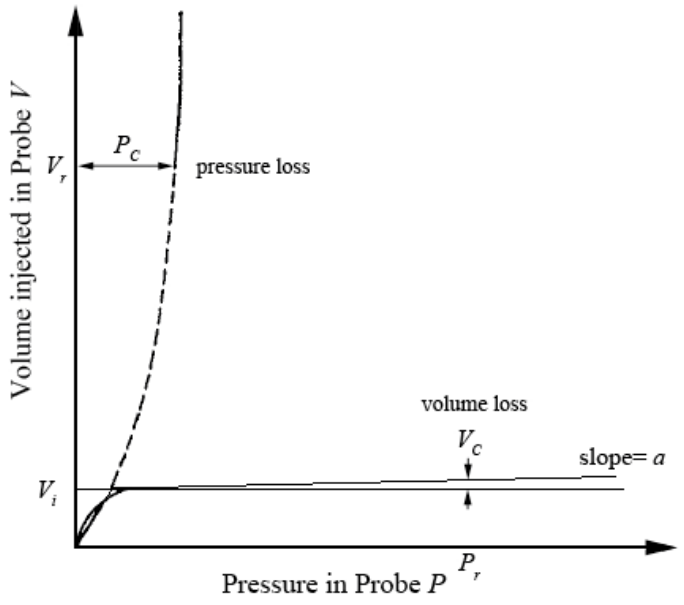

Figure 2-151: Pressure and volume calibration curves (ASTM, 2007)

2.9.2.3 Testing Procedure

ASTM (2007) allows pre-drilled pressuremter tests to be carried out by two procedures; i.e., either by equal pressure increments or by equal volume increments; however, as the more common procedure is the first method, only the first method will be considered here.

The pressuremeter cavity is prepared either by drilling a borehole, or by advancing a sampler. To ensure adequate volume change capability, the probe must be inserted in a borehole with a diameter close to that of the probe. If the borehole diameter is too large the probe's expansion limit may be reached before completion of the test, and if the hole is too tight then the probe will have to be forced into the hole, and the PMT pressure versus volume curve will not show a pseudo linear phase. ISSMFE (Amar et al., 1991) recommends that the hole diameter should not exceed the instrument diameter by more than 10%. Menard (Centre D'Etudes Menard, 1975) and later ASTM (2007) have specified probe diameters for typical probe diameters as shown in Table 2-17. ASTM further stipulates that the borehole diameter shall be from 1.03 times to 1.2 times the nominal probe diameter. If used, borehole diameters should also be adapted for slotted casings.

Hole diameter designation*	Diameter (mm)					Zero volume reading V_0 (cm^3)
	Probe	Borehole				
		Menard		ASTM		Menard
		Minimum	Maximum	nominal	Maximum	535
AX	44	46	52	45	53	535
BX	58	60	66	60	70	535
NX	74	76	80	76	89	790

* Probe diameters are based on the standards of the Diamond Core Drill Manufacturer's Association (DCMA)

Table 2-17: typical probe and borehole diameters (ASTM, 2007, Centre D'Etudes Menard, 1975)

Before the probe is positioned in the hole for testing an accurate determination should be made of the zero volume reading, V_0, which is the volume of the measuring portion of the uninflated probe at atmospheric pressure. Menard (Centre D'Etudes Menard, 1975) has already determined the values of V_0 for different probes; however, as shown in Figure 2-151, V_0 can be estimated by fitting a straight line extension of the volume correction curve to zero pressure (ASTM, 2007):

$$V_0 = \frac{\pi {d_i}^2 l}{4} - V_i \qquad 2\text{-}160$$

V_i= intercept of volume calibration line

d_i= inside diameter of the heavy duty steel casing or pipe

l= length of the measuring cell

The probe should then be lowered to the test depth, which is the midpoint depth of the probe. In the equal pressure increment method, pressure is applied in approximately equal increments. Too small steps will result in an excessively long test, and too large steps may yield results with inadequate accuracy.

Menard (Centre D'Etudes Menard, 1975) suggests testing increments to be preferably 10, but accepts from 5 to 14 increments as well. ASTM (2007) suggests that pressure steps should be determined in such a way that about 7 to 10 load increments are obtained. Menard requires that volume variations be recorded after 15 seconds, 30 seconds and 1 minute; however, ASTM does not require the 15 seconds reading.

The minimum centre to centre of probe spacing between consecutive tests in a borehole should not be less than 1.5 times the length of the inflatable part of the probe. Common spacing are from 1 to 3m (ASTM, 2007).

In soft, loose, and sensitive soils, the hole should be predrilled ahead of the testing depth only far enough so that the cuttings settling at the bottom of the hole will not interfere with the test; however, in stiff soils and weathered rocks where degradation due to exposure is not significant, the hole can be predrilled to several test depths When the probe is driven into the soil, testing can take place continuously (ASTM, 2007).

Menard (Centre D'Etudes Menard, 1975) advises that to obtain as complete a load deformation curve as possible, the measured volume should reach 700 cm^3 if the pressuremeter limit pressure, P_{LM}, is less than 800 kPa and 600 cm^3 if 800< P_{LM} < 1,500 kPa, but suggests that in other cases the test must be carried out up to pressures of approximately 2,000 to 2,500 kPa in soils and up to 5,000 to 7,000 kPa in rocks. According to ASTM (2007) when equal pressure increments are used, the test increments should be increased until the

expansion of the probe during one load increment exceeds about one fourth of V_0 that is typically about 200 cm^3 for a 800 cm^3 probe.

Prebored pressuremeter design rules were established historically based on testing without unload-reload loops (ASTM, 2007); however, ASTM encourages the performance of unload-reload cycle(s).

2.9.2.4 Testing Frequency

Lukas (1986) proposes the below guidelines for verification of ground improvement performance:

1) Regardless of the size of the improved area, there should be at least two borings with in-situ testing. A minimum of one boring with in-situ testing should be carried out for approximately every 1,000 m^2 of area that was compacted for a structure, or 4,000 m^2 of embankment.

2) The borings should extend through the thickness of the deposit that is compacted. Testing should be carried out at depth intervals not exceeding 1.5 m to determine the degree and depth of improvement.

3) Additional borings and tests should be carried out in areas where anomalies were observed during compaction. This would include areas where the crater depths were significantly greater than average, or where the ground settlement was greater than normal. The purpose of these tests would be to verify that the magnitude of improvement in these areas is similar to adjacent areas.

It is the author's personal experience that performing one boring per every 2,000 m^2 of improved ground in large scale projects with uniform ground conditions will be sufficient and satisfactory. Also, it is the author's experience that observation of the prints can assist in identifying soft or hard spots or zones that react differently to the pounder impact from what was observed during the heave and penetration test. These spots or zones can then be further investigated.

2.9.2.5 Calculation of PMT parameters

Once pressure and volume readings are corrected, the pressure versus volume curve can be drawn to produce a curve similar to what is shown in Figure 2-152. The pressure transmitted to the soil by the probe is as shown in Equation 2-161 (ASTM, 2007).

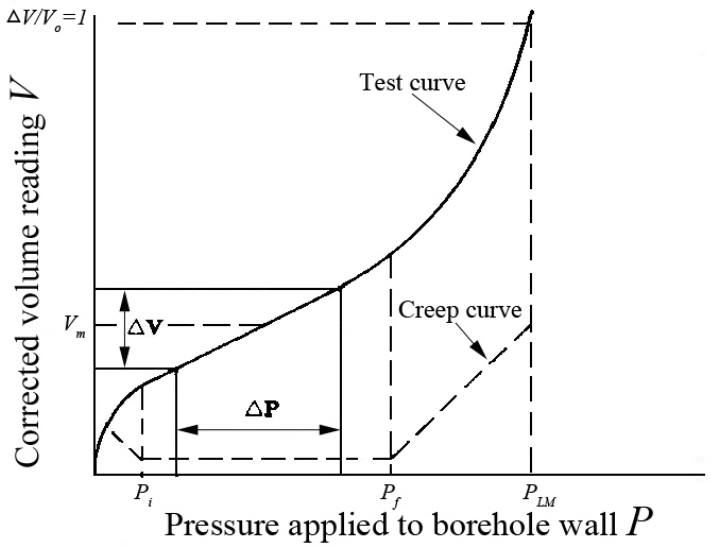

Figure 2-152: Typical pre-drilled PMT curve (Amar et al., 1991, ASTM, 2007)

$$P = P_R + P_\delta - P_C \qquad 2\text{-}161$$

P= pressure exerted by the probe on the soil

P_R= pressure reading on the control unit

P_δ= hydrostatic pressure between the control unit and the probe, which can be calculated using Equation 2-162.

P_C = pressure loss correction. The maximum value of P_C should be less than 50% of P_{LM} (ASTM, 2007).

$$P_\delta = H_p \delta_t \qquad 2\text{-}162$$

H_p = depth of probe below the control unit

δ_t = unit weight of test liquid in instrument

The corrected volume reading of the probe from the volume readings is (ASTM, 2007):

$$V = V_R - V_C \qquad 2\text{-}163$$

V= corrected increase in volume of the measuring portion of the probe

V_R = volume of reading on readout device

V_C = volume loss correction made at the test pressure readings corresponding to $P = P_R + P_\delta$, and can be calculated from Equation 2-164.

$$V_C = V_r - aP_r \qquad 2\text{-}164$$

V_r = injected volume at the end of each pressure increment, P_r

a = slope of the volume versus pressure calibration plot

As shown in Figure 2-152, *creep* or end of pseudo elastic phase pressure, P_f, is obtained by plotting the volume differences between the 30 seconds and 1 minute readings against the applied pressure. Figure 2-152 also shows that three distinct parts can be found on the test curve; i.e., the inflation of the probe until the membrane reaches the borehole walls ($P \leq P_i$), the pseudo elastic response of the soil to the probe pressure ($P_i \leq P \leq P_f$), and the plastic response of the soil ($P_f \leq P$) up to $\Delta V/V_o$=1 (volume of probe has doubled to twice the zero volume). In the pseudo elastic zone the creep curve appears to be a straight line, and a constant soil deformation modulus called Menard modulus, E_M, can be measured to be (Centre D'Etudes Menard, 1975):

$$E_M = 2(1+\nu)(V_0 + V_m)\frac{\Delta P}{\Delta V} \qquad 2\text{-}165$$

ν = Poisson ratio

V_0 = zero volume reading

V= corrected volume reading of the measuring portion of the probe

ΔP= corrected pressure increase in the centre part of the straight line portion of the pressure-volume curve (see Figure 2-152)

ΔV= corrected volume increase in the centre part of the straight line portion of the pressure-volume curve, corresponding to ΔP pressure increase (see Figure 2-152)

V_m = corrected volume reading in the centre portion of the ΔV volume increase.

Menard (Centre D'Etudes Menard, 1975) assigns an arbitrary value of 0.33 to the Poisson ratio. This assumed value has no impact on estimation of settlement as the same value is assigned in Section 2.9.2.7. ENV 1997-3 (European Standard, 2000) also accepts this assumption. Equation 2-165 can therefore be presented as:

$$E_M = 2.66(V_0 + V_m)\frac{\Delta P}{\Delta V} \qquad 2\text{-}166$$

For the popular AX probe, using V_0 as presented in Table 2-17 (535 cm^3), and for V_m approximately equalling 200 cm^3, Menard yields 2(1+ν)(V_0 + V_m)≈ 2,000 cm^3.

Menard (Centre D'Etudes Menard, 1975) defines limit pressure, P_{LM}, as the abscissa of the asymptote to the pressuremeter curve, and notes that this parameter can be determined directly from the curve, but is more conveniently taken as the pressure corresponding to a volume increase equal to the initial volume of the borehole. Since the initial volume of an AX or BX probe is in the order of 600 cm^3 (V_0= 535 cm^3 plus the volume injected to contact the borehole wall), the reading may be assumed for a reading of 700 cm^3 (see Figure 2-153). Thus:

$$P_{LM} = P_u - P_i + \text{water head} \qquad 2\text{-}167$$

P_u =pressure reading corresponding to a volume increase equal to the initial volume of the borehole

P_i = pressure at which the probe makes contact with the borehole.

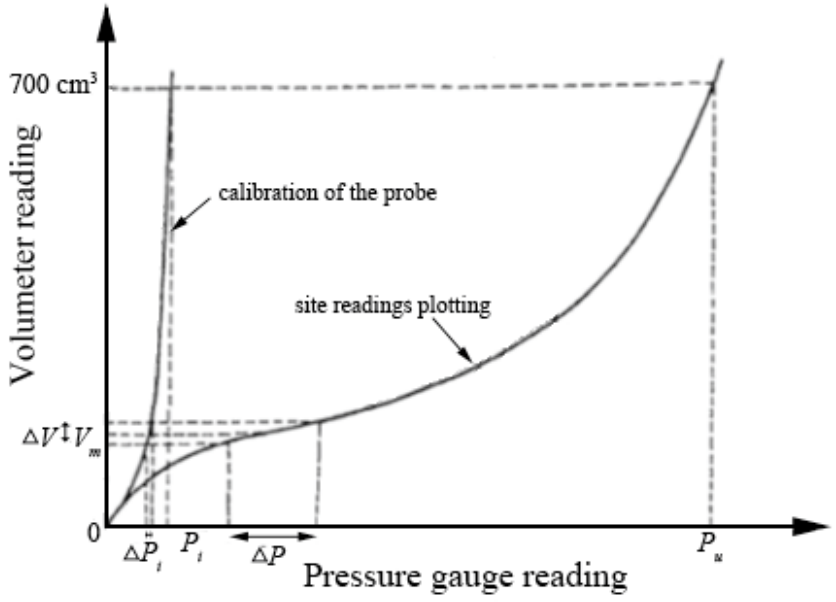

Figure 2-153: Pressuremeter pressure versus volume curve (Centre D'Etudes Menard, 1975)

If the volumetric increase attained during a test is less than what has been mentioned, it is still possible to extrapolate the value of P_{LM} with precision, provided that P_f has been exceeded during the test.

Extrapolating P_{LM} can be done based on the relative or reciprocal volume theories (Centre D'Etudes Menard, 1975). In the latter method, if the plot of pressure is drawn against the reciprocal of volume, a straight line can be passed through the last few readings corresponding to the plastic phase. Menard notes that the point at which the extension of the straight line intersects the 700 cm^3 ordinate corresponds to $P_{LM;\ however,}$ the borehole volume does not necessarily have to be 700 cm^3, and as shown in Figure 2-154, can vary from his rational figure.

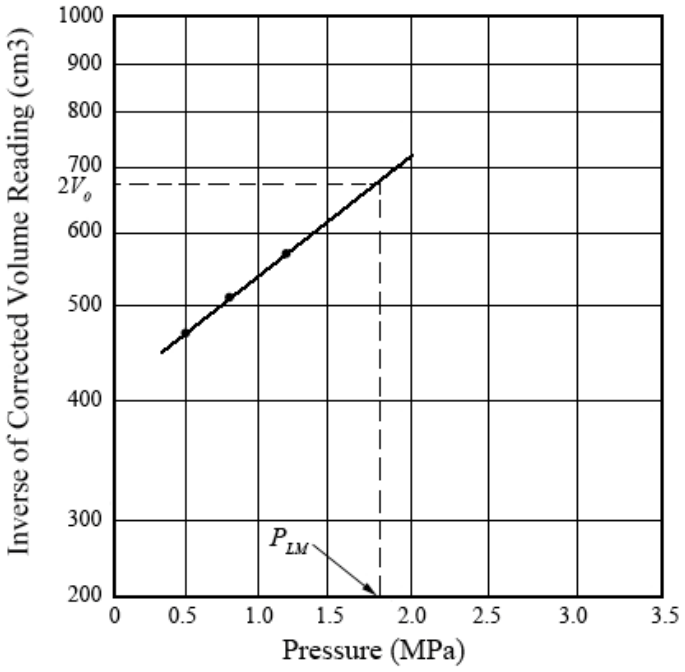

Figure 2-154: Extrapolation of P_{LM} (Amar et al., 1991)

In a similar approach Baguelin et al. (1978), ASTM (2007) note that while theoretical P_{LM} is defined as the pressure where infinite expansion of the probe occurs, for practical purposes P_{LM} is defined as the pressure where the probe volume reaches twice the original soil cavity volume, defined as $V_0 + V_i$ (see Figure 2-155), where V_i is the corrected volume reading at the pressure at which the probe makes contact with the borehole (corresponding to P_i in Figure 2-152).

As shown in Figure 2-156, ENV 1997-3 (European Standard, 2000) defines P_{LM} as the pressure required to double the total volume of the cavity from the point (p_r, V_r) at which changes of

volume change to pressure change; i.e., d(ΔV)/d(Δp), is a minimum. V_r is the injected volume corresponding to pressure p_r, and V_0 is the deflated volume of the probe.

Menard (Centre D'Etudes Menard, 1975) notes that an approximate value of P_{LM} can also be obtained considering the below statistical results:

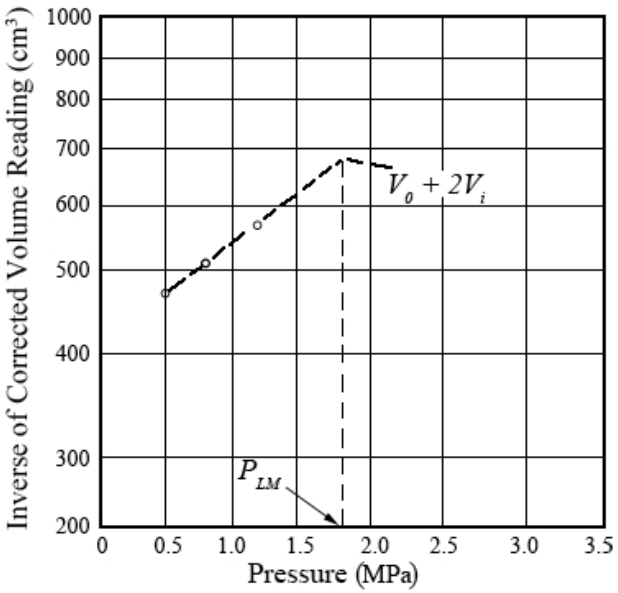

Figure 2-155: Determination P_{LM} from inverse of volume versus pressure (ASTM, 2007)

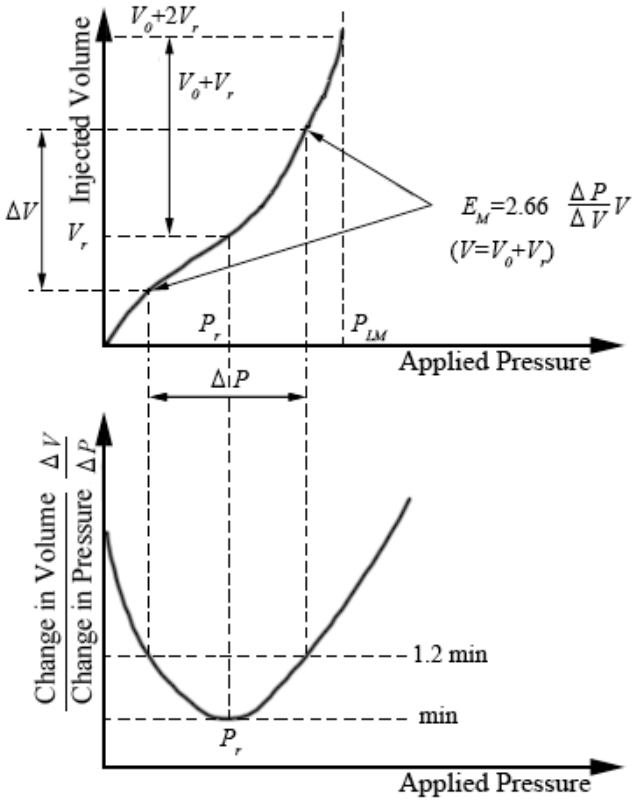

Figure 2-156: Interpretation of E_M and P_{LM} from PMT from ENV 1997-3 (European Standard, 2000)

- P_f is equal to approximately ½ to 2/3 P_{LM}.
- For every geological formation, there is a constant E_M/P_{LM} value that also depends on the ground type (see Table 2-22 and Table 2-23).

Table 2-17 presents typical ranges of E_M and P_{LM} (Centre D'Etudes Menard, 1975).

Soil or ground	E_M (MPa)	P_{LM} (kPa)
mud, peat	0.2 to 1.5	20 to 150
soft clay	0.5 to 3	50 to 300
medium clay	3 to 8	300 to 800
stiff clay	8 to 40	600 to 2,000
marl	5 to 60	600 to 4,000
loose silty sand	0.5 to 2	100 to 500
silt	2 to 10	200 to 1,500
sand and gravel	8 to 40	1,200 to 5,000
sedimentary sands	7.5 to 40	1,000 to 5,000
limestone	80 to 20,000	3,000 to 10,000$^+$
recent fill	0.5 to 5	50 to 300
old fill	4 to 15	400 to 1,000

Table 2-18: typical ranges of E_M and P_{LM} for some main types of soil and ground (Centre D'Etudes Menard, 1975).

2.9.2.6 Estimation of Bearing Capacity

Ultimate bearing capacity of a foundation can be calculated using Equation 2-168 (Centre D'Etudes Menard, 1975):

$$q_u = q_o + k(P_{LM} - P_o) \qquad 2\text{-}168$$

q_u= ultimate bearing capacity

q_o= total overburden pressure at the periphery of the foundation level after construction. This term is defined slightly different in ENV 1997-3's informative Annex C.1 as the total (initial) vertical stress at the level of the foundation base. This parameter is calculated from the unit weight of soil and depth of footing.

k= a bearing factor varying from 0.8 to 9 according to the embedment and the shape of the foundation level after construction

P_o= total at rest horizontal earth pressure at the test level (at the time of the test). ENV 1997-3 defines P_o according to Equation 2-169.

$$P_o = K_o(\sigma_v - u) + u \qquad 2\text{-}169$$

K_o= coefficient of horizontal earth pressure at rest. Menard (Centre D'Etudes Menard, 1975) notes that experience shows that in very loose soil or compact soil K_o is respectively approximately 1 or 0.5; however, Appendix C.1 of ENV 1997-3 assumes conveniently that K_o is equal to 0.5.

σ_v= total vertical stress

u= pore water pressure

Instead of q_u, Annex C.1 of ENV 1997-3 presents Equation 2-168 in the form of

$$\frac{N}{A'} = q_o + k(P_{LM} - P_o) \qquad 2\text{-}170$$

N= resistance of the foundation against normal loads

A'= effective base area as defined in ENV 1997-1 (European Standard, 2004)

The difference between P_{LM} and P_o is defined as *net limit pressure*, P^*_{LM} (Centre D'Etudes Menard, 1975):

$$P^*_{LM} = P_{LM} - P_o \qquad 2\text{-}171$$

Likewise, the net ultimate bearing capacity, q^*, is:

$$q* = q_u - q_o \qquad 2\text{-}172$$

k can be obtained from Figure 2-157 or Figure 2-158 (Centre D'Etudes Menard, 1975) respectively for isolated (square or circular) footings or strip footings. Soil categories referred to in these figures are defined in Table 2-19.

h_e is the equivalent foundation depth, and h_c is the critical depth of embedment or the depth below which an embedded foundation maintains a constant ultimate net bearing capacity. Amar et al (1991) cite Menard (1963a) for noting that the ratio of spherical to cylindrical limit

pressures remain constant below the critical depth, if the soil properties also remain constant. This depth is a function of soil category and half width of foundation (R=B/2). Relative values of h_c/R are shown in Table 2-20. As can be seen in these two Figures, the minimum value of k is 0.8 when the footing is on the ground surface.

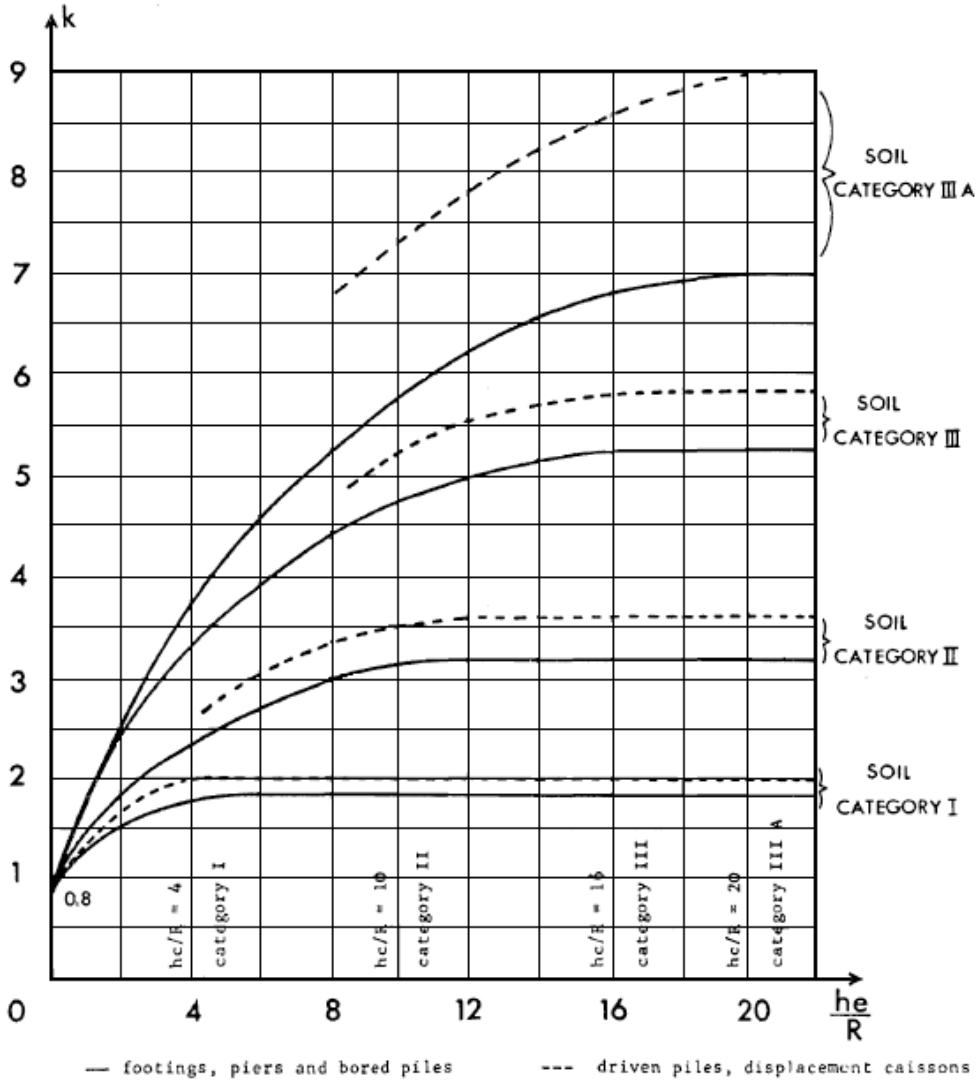

h_e= equivalent foundation depth, h_c= critical depth of embedment, R= half width of footing

Figure 2-157: Bearing factor for isolated square or circular footings, piers and piles (Centre D'Etudes Menard, 1975)

Baguelin et al. (1978) recommend that for rectangular footings, with widths and lengths respectively equal to B and L, that are neither square nor infinitely long, k can be assumed to vary linearly between the two extremes, and can be calculated using Equation 2-173.

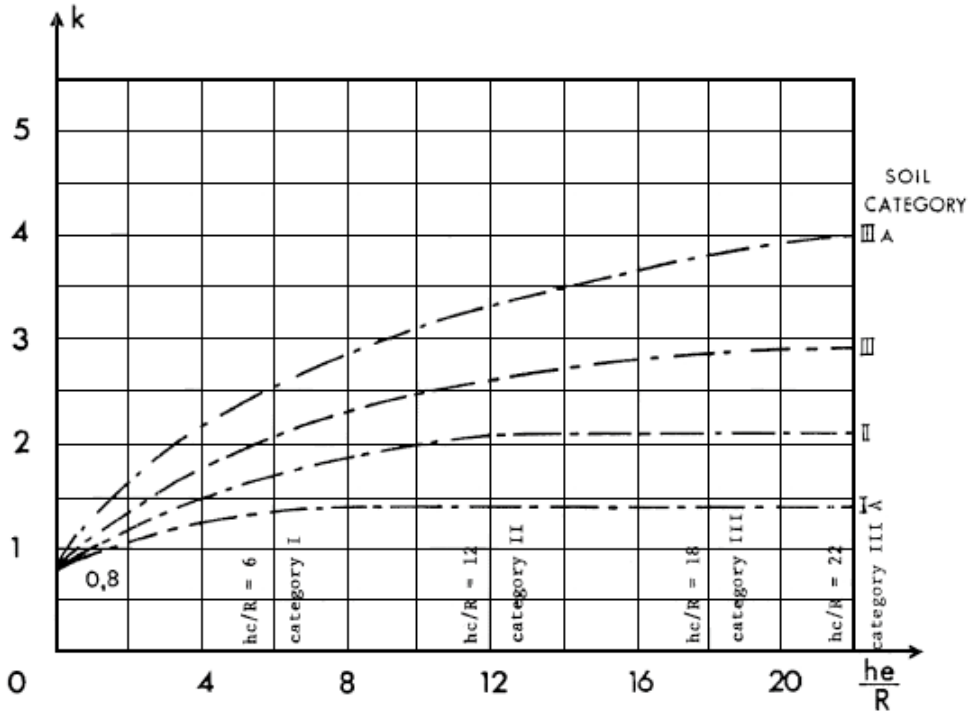

h_e= equivalent foundation depth, h_c= critical depth of embedment, R= half width of footing

Figure 2-158: Bearing factor for strip footings and diaphragm walls (Centre D'Etudes Menard, 1975)

Soil category	Nature of soil	P_{LM} (kPa)
I	Clay	0 to 1200
	Silt	0 to 700
II	Firm clay or marl	1,800 to 4,000
	Compact silt	1,200 to 3,000
	Compressible sand	400 to 800
	Soft or weathered rock	1,000 to 3,000
III	Sand and gravel	1,000 to 2,000
	Rock	4,000 to 10,000
IIIA	Very compact sand and gravel	3,000 to 6,000

Table 2-19: Soil categories for determination of bearing factor (Centre D'Etudes Menard, 1975)

Soil category	Foundation type	
	Circular or Square	Continuous
I	4	6
II	10	12
III	16	18
IIIA	20	22

Table 2-20: h_c/R for different soil categories and foundation types (Centre D'Etudes Menard, 1975)

$$k = k_{strip} + (k_{square} - k_{strip})\frac{B}{L} \qquad 2\text{-}173$$

Annex C.1 of ENV 1997-3 has summarised the bearing factor for spread foundations as shown in Table 2-21.

Soil category		P_{LM} (kPa)	k
Clay and silt	A	< 700	$0.8[1 + 0.25(0.6 + 0.4\,B/L)\,h_e/B]$
	B	1,200 to 2,000	$0.8[1 + 0.35(0.6 + 0.4\,B/L)\,h_e/B]$
	C	> 2,500	$0.8[1 + 0.50(0.6 + 0.4\,B/L)\,h_e/B]$
Sand and gravel	A	< 500	$1 + 0.35(0.6 + 0.4\,B/L)\,h_e/B$
	B	1,000 to 2,000	$1 + 0.50(0.6 + 0.4\,B/L)\,h_e/B$
	C	> 2,500	$1 + 0.80(0.6 + 0.4\,B/L)\,h_e/B$
Chalk			$1.3[1 + 0.27(0.6 + 0.4\,B/L)\,h/B]$
Marl and weathered rock			$1 + 0.27(0.6 + 0.4\,B/L)\,h_e/B$

B= foundation width, L= foundation length, h_e= equivalent foundation depth

Table 2-21: bearing factor for spread foundations, ENV 1997-3 (European Standard, 2000)

Menard (Centre D'Etudes Menard, 1975) notes that it has often been the custom in dealing with pressuremeter results to tabulate the value P_{LM} – *water head*. The calculation and presentation of results is greatly simplified by identifying P_{LM} with P_{LM} – *water head* as the error introduced is less than 2 % for most dry sites.

When the footing is on ground with variable strengths at different depths, the equivalent limit pressure, P^*_{LMe}, is defined as the geometric mean of P^*_{LM} values obtained near the level of the foundation:

$$P^*_{LMe} = \sqrt[3]{P^*_{LM1}P^*_{LM2}P^*_{LM3}} \qquad 2\text{-}174$$

P^*_{LM1}= geometric mean of values measured in levels +1.5B to +0.5B above the founding level

P^*_{LM2}= geometric mean of values measured in levels +0.5B to -0.5B

P^*_{LM3}= geometric mean of values measured in levels -0.5B to -1.5B

This is equivalent to taking the arithmetic mean of the logarithms (see Equation 2-175), and therefore gives less weight to the higher P^*_{LMe} values.

$$\ln(P^*_{LMe}) = \frac{1}{3}[\ln(P^*_{LM1}) + \ln(P^*_{LM2}) + \ln(P^*_{LM3})] \quad 2\text{-}175$$

For shallow foundations, P^*_{LM1} is not introduced, and the equivalent limit pressure becomes:

$$P^*_{LMe} = \sqrt[2]{P^*_{LM2} P^*_{LM3}} \quad 2\text{-}176$$

Menard (Centre D'Etudes Menard, 1975) assumes that the variation between the limit pressures of each elevation band does not exceed ±30% of P^*_{LMe}, and advises that should this limit be exceeded, then the problem should be considered in more detail. Menard recommends to plot P^*_{LMe} against depth, and to smooth out all the peaks in the graph. Baguelin et al. (1978) assume the variation between the limit pressures does not exceed ±40% of P^*_{LMe}.

When the ground properties vary with depth, it is necessary to define the equivalent depth of embedment h_e relative to the soil of the founding elevation. This depth can be calculated by using Equation 2-177 (Centre D'Etudes Menard, 1975) when limit pressure can be defined as a function of depth or Equation 2-178 when limit pressure values are variable in different ground layers.

$$h_e = \frac{1}{P^*_{LMe}} \int_0^h P^*_{LM}(z)\mathrm{d}z \quad 2\text{-}177$$

$$h_e = \frac{1}{P^*_{LMe}} \sum_{i=1}^{n} P^*_{LMi} \Delta z_i \quad 2\text{-}178$$

Menard (Centre D'Etudes Menard, 1975) proposes a safety factor of 3 for bearing capacity; therefore, the allowable bearing capacity, q_a, can be expressed as:

$$q_a = q_o + \frac{k}{3}(P_{LM} - P_o) \quad 2\text{-}179$$

In terms of net allowable bearing capacity, q_a, can be expressed as:

$$q^*_a = \frac{k}{3} P^*_{LM} \quad \text{2-180}$$

When loads are eccentric, Menard (Centre D'Etudes Menard, 1975) notes that failure may occur either by general punching of the footings or by localised failure in the zone of highest loading due to tilting. He states that general stability will be achieved if:

$$\frac{\sigma_{v\_max} + \sigma_{v\_min}}{2} < q_a \quad \text{2-181}$$

σ_{v_max}= maximum vertical stress below footing

σ_{v_min}= minimum vertical stress below footing

When relative embedment depth h/R > 1, with a simplification, stability against tilting can be achieved if:

$$\sigma_{v\_max} < 1.5 q_a \quad \text{2-182}$$

Baguelin et al. (1978) proposes that effects of eccentricity can be taken into account conservatively by reducing the footing width to an effective width, B', which will result in a concentric load on a fictitious footing with a smaller width. B' can be calculated from Equation 2-183 (Meyerhof, 1953):

$$B' < B - 2e \quad \text{2-183}$$

e= eccentricity of the load (see Figure 2-159)

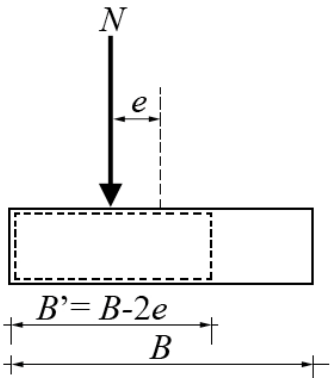

Figure 2-159: Eccentric loading on footing, Baguelin (1978) after Meyerhof (1953)

Once the footing's eccentric load has been transformed into a concentric load acting on a reduced width, then it will be possible to determine the bearing capacity using Equation 2-168.

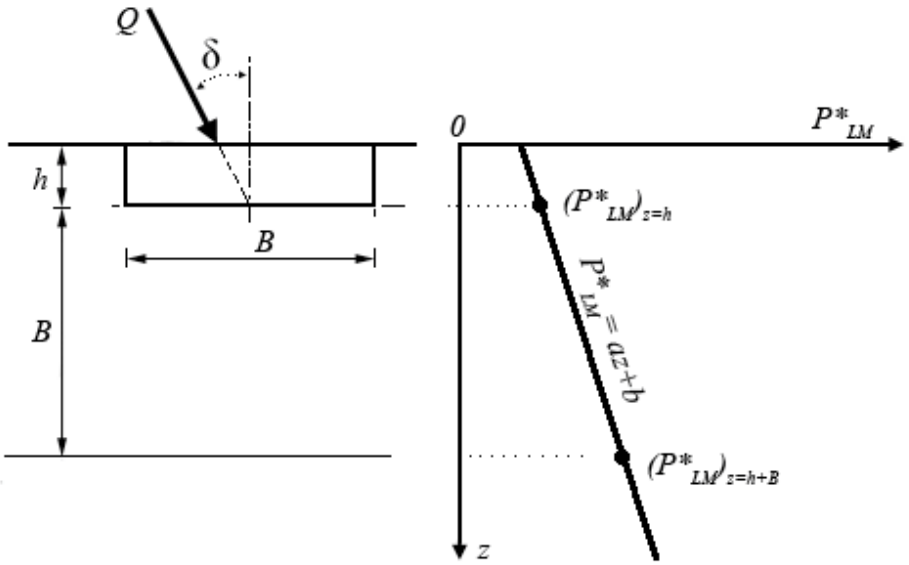

Figure 2-160: Inclined load on footing (Baguelin et al., 1978)

Baguelin et al. also propose a procedure for determination of bearing capacity for inclined concentric loads when variation of limit pressure is linear in depth. If the ratio of net limit pressure at depths of h and h+B (see Figure 2-160) is expressed by M (see Equation 2-184), then a reduction factor i_δ should be applied when the load is inclined from the vertical at an angle of δ degrees. When the inclination angle is between 0 and 30 or 35°, i_δ can be calculated from Equation 2-185:

$$M = \frac{(P^*_{LM})_{z=h}}{(P^*_{LM})_{z=h+B}} \qquad 2\text{-}184$$

$$i_\delta = \left(1 - \frac{\delta^o}{90}\right)^2 (1-\lambda) + \left(1 - \frac{\delta^o}{20}\right)\lambda \qquad 2\text{-}185$$

$$\lambda = \lambda_D \lambda_M \qquad 2\text{-}186$$

For $0 < \frac{h}{B} < 1$ $\qquad \lambda_D = 1 - \frac{h}{B}$ $\qquad 2\text{-}187$

For $\frac{h}{B} > 1$ $\lambda_D = 0$ 2-188

For $0 < M < 1$ $\lambda_M = 1 - M$ 2-189

For $M > 1$ $\lambda_M = 0$ 2-190

For special cases when net limit pressure is constant in depth, or when the footing embedment depth is at least equal to the footing width:

$$i_\delta = \left(1 - \frac{\delta^o}{90}\right)^2 \quad \text{2-191}$$

The bearing capacity of footings resting on sloping ground or near excavations must be reduced by a coefficient that is a function of β, the angle between the footing and excavation level. This reduction factor is shown in Figure 2-161 (Centre D'Etudes Menard, 1975).

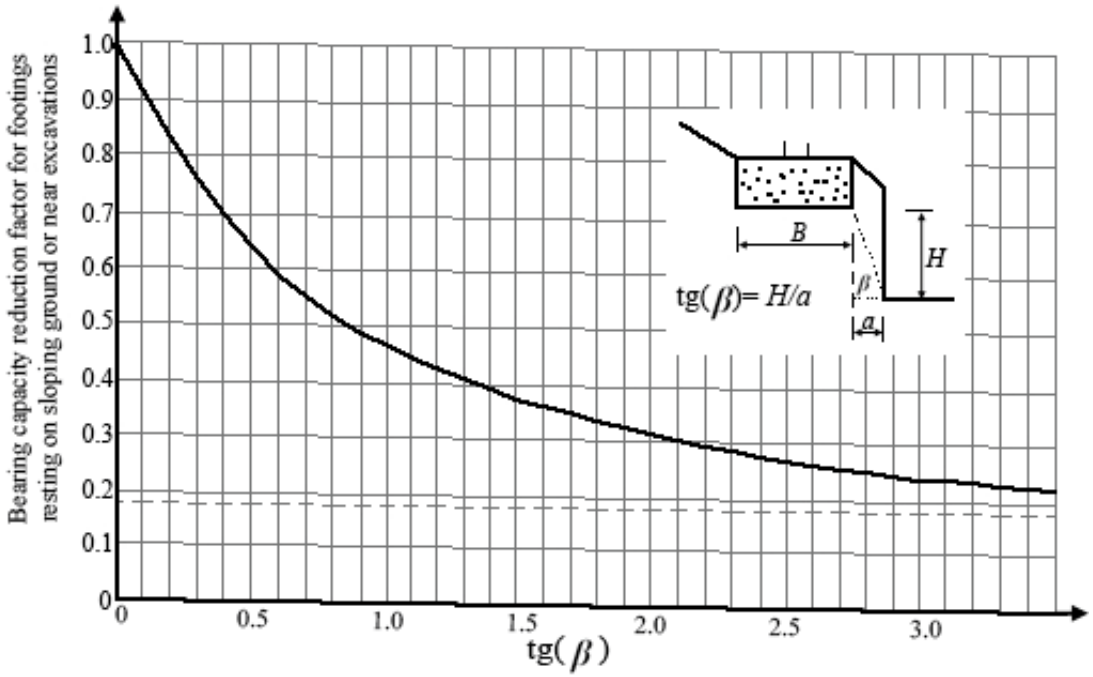

Figure 2-161: Bearing capacity reduction factor for footings resting on sloping ground or near excavations (Centre D'Etudes Menard, 1975)

Baguelin et al. (1978) propose the same reductive approach that was used for estimation of bearing capacity of foundations subject to inclined loading to determine the bearing capacity

reduction factor near slopes and hillsides. However, in the latter case, the inclination angle, δ, is replaced, β', which is shown in Figure 2-162. Thus Equation 2-185 becomes:

$$i_{\beta'} = \left(1 - \frac{\beta'}{90}\right)^2 (1 - \lambda) + \left(1 - \frac{\beta'}{20}\right)\lambda \qquad 2\text{-}192$$

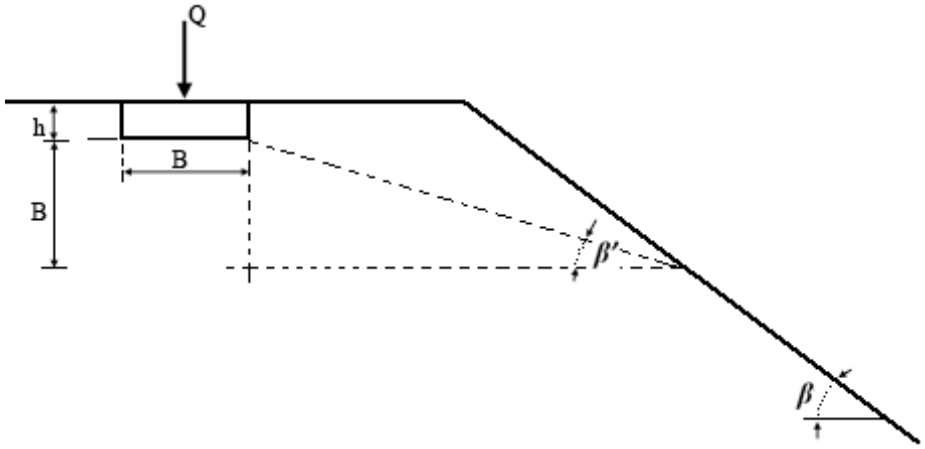

Figure 2-162: Footing near slope or hillside (Baguelin et al., 1978)

Baguelin et al. note that for steep slopes it is necessary to assess the stability of the slope itself, and further add that the pressuremeter can only be considered to give a rough estimate of the soil conditions for slope stability analyses.

When the load is inclined in such a way that the resultant force acts towards the hillside the combined bearing capacity reduction factor, $i_{\delta\beta}$, will be used with the same approach as described above (Baguelin et al., 1978). Hence, Equation 2-185 will becomes:

$$i_{\delta\beta'} = \left(1 - \frac{\delta + \beta'}{90}\right)^2 (1 - \lambda) + \left(1 - \frac{\delta + \beta'}{20}\right)\lambda \qquad 2\text{-}193$$

On the other hand, when the resultant force acts away from the hillside a bearing capacity reduction factor is calculated with a similar approach for the condition yielding the higher factor between the two below cases (Baguelin et al., 1978):

- When the rupture develops towards the level ground and away from the slope: In this case the bearing capacity reduction factor is based only on the load inclination angle, i_δ, and Equation 2-185 will be applicable.

- When the rupture develops away from the level ground and toward the slope: In this case the bearing capacity reduction factor, $i_{\delta\beta}$, will be based on the difference between β' and the inclination angle, δ, and Equation 2-185 will take the form of Equation 2-194.

$$i_{\delta\beta'} = \left(1 - \frac{\beta' - \delta}{90}\right)^2 (1 - \lambda) + \left(1 - \frac{\beta' - \delta'}{20}\right)\lambda \qquad 2\text{-}194$$

If the load is both inclined and eccentric, as shown in Figure 2-163, then Baguelin et al. envisage two possible cases:

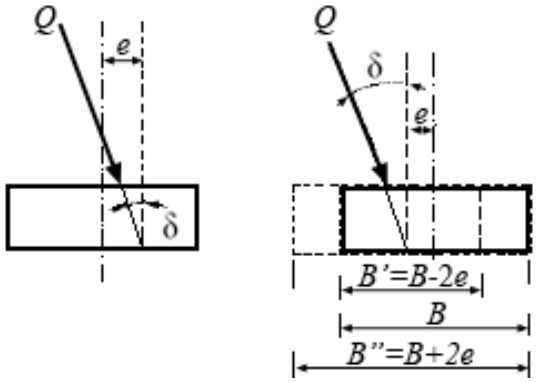

Figure 2-163: Footing subject to inclined and eccentric load (Baguelin et al., 1978)

- For the case shown in Figure 2-163(a) the effect of the combination of inclined and eccentric loading is to magnify the bearing capacity reduction factor, $i_{\delta e}$, which, as shown in Equation 2-195, is calculated as the product of the reduction factors i_δ and i_e. The latter factor, i_e, is calculated for footing width B.

$$i_{\delta e} = i_\delta \times i_e \qquad 2\text{-}195$$

- For the case shown in Figure 2-163 (b) the effects tend to cancel out one another, and it will be necessary to consider failure occurring possibly to the left or to the right.

  For failure to the left, i_e due to the eccentricity of the load is corrected by dividing it by i_δ because of the inclination of the load (using the actual footing width B for M and λ_D). If the resulting value of i_e/i_δ is less than 1, then the ultimate load, Q_1, that

the footing can carry if it was loaded vertically and concentrically, is multiplied by this ratio to give the first estimate of the ultimate inclined load, $(Q'_1)_\delta$:

$$\text{If} \quad \frac{i_e}{i_\delta} < 1 \qquad (Q'_1)_\delta = Q_1 \frac{i_e}{i_\delta} \qquad \text{2-196}$$

For failure to the right, the ultimate vertical load, Q''_1, that is concentric with a fictitious footing with width of $B''= B + 2e$ is computed. This ultimate load is then corrected for the load inclination using the actual width, B, for M and λ_D. Therefore, i_δ is the same as what is calculated for the footing failure towards the left. This will lead to Equation 2-197. The inclined, eccentric design load, $(Q'_1)_{e\delta,}$ to use for the footing is the lesser of $(Q'_1)_\delta$ and $(Q''_1)_\delta$.

$$(Q"_1)_\delta = Q"_1 \times i_\delta \qquad \text{2-197}$$

When the load is inclined and eccentric, and the ground is sloped, then the foregoing rules are combined as required to suit the particular condition (Baguelin et al., 1978).

2.9.2.7 Estimation of Settlement under External Loading

Menard and Rousseau (1962) have carried out full scale field tests on footings, and have observed that contrary to the formulas derived from the elastic theory for homogeneous, elastic medium, settlement does not increase in direct proportion to the width of the footing.

According to Menard and Rousseau (1962) and Menard (Centre D'Etudes Menard, 1975), foundation settlement due to external loads is the result of two completely different phenomena; i.e., volumetric compression and shear deformation. The first phenomenon is caused by the spherical component of the stress tensor. The increase of bulk pressure (volumetric compression) causes a reduction in volume of the material in relation to the modulus of volumetric compression. On the other hand, the latter phenomenon is caused by the deviatoric components of the stress tensor, and displacements occur without variation in volume of the material.

The spherical and deviatoric components of the stress tensor are very different at depth; the spherical component has a maximum value right under the base of the footing; however, the deviatoric component has a maximum value at a depth that is equal to half the width of the

footing. Shear deformation is dominant under footings, shafts and piles, but volumetric compression predominates under rafts or embankments. As compared to shear deformation, the relative importance of volumetric compression increases as the safety factor against failure increases (Centre D'Etudes Menard, 1975). Figure 2-164 shows the variation of vertical strain components with depth along the vertical axis below a rigid circular footing (Baguelin et al., 1978).

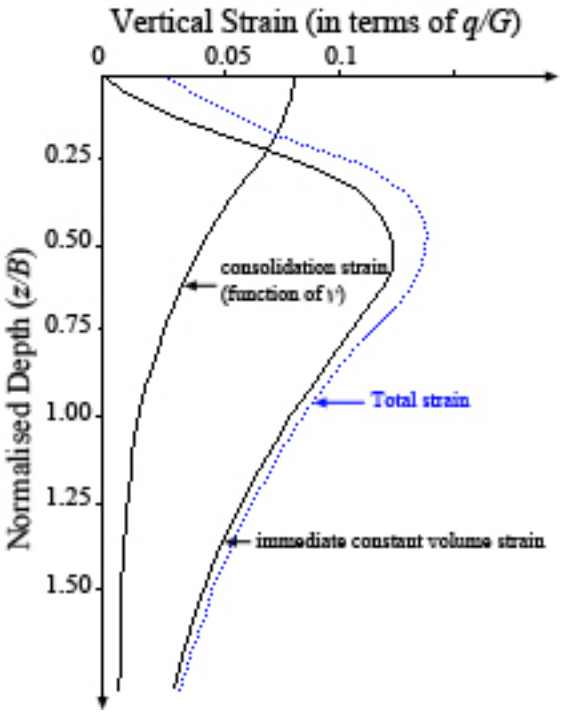

Figure 2-164: Variation of vertical strain components with depth along the vertical axis below a rigid circular footing (Baguelin et al., 1978)

Total (final) settlement, s, can be estimated for a footing with width and length respectively equal to B and L, that is embedded (strictly speaking, the equivalent embedment depth) by at least the footing width (Centre D'Etudes Menard, 1975, Menard and Rousseau, 1962). In Equations 2-198 and 2-199, the first and second terms that are multiplied by the mean contact added stress respectively represent the influence of the deviatoric and volumetric stress tensors. Menard (Centre D'Etudes Menard, 1975) notes that there is also a negligible term corresponding to a purely elastic settlement that has been omitted from the equation.

When B > 0.6 m: $$s = (q - \sigma_{vo})\left[\frac{2}{9}\frac{B_0}{E_d}\left(\lambda_d \frac{B}{B_o}\right)^{\alpha} + \frac{\alpha\lambda_c}{9E_c}B\right] \quad \text{2-198}$$

When B <0.6 m: $$s = (q - \sigma_{vo})\left[\frac{2}{9}\frac{B_0}{E_d}(\lambda_d B)^{\alpha} + \frac{\alpha\lambda_c}{9E_c}B\right] \quad \text{2-199}$$

q= design normal pressure applied on the footing

σ_{vo}= total (initial) vertical stress at the level of the footing base

B_o= reference footing width, equal to 0.6 m

B= footing width

α= rheological factor, given in Table 2-22 and Table 2-23. It can be noted that this factor can be different in the two terms of Equations 2-198 and 2-199 according to the prevalent material in each zone of influence.

λ_d and λ_c= shape factors, given in Table 2-24.

E_c= weighted value of E_M immediately below the footing; i.e., as shown in Figure 2-165, E_M from under the footing to a depth equal to half the footing width (Centre D'Etudes Menard, 1975):

$$E_c = E_1 \quad \text{2-200}$$

E_1= weighted value of E_M from under the footing to the depth of half the footing width

E_d= harmonic mean of E_M in all layers down to the depth of $8B$ (or 16 times half footing width, R) below the footing

Soil	Peat		Clay		Alluvium (silt)		Sand		Sand & gravel	
	$\frac{E_M}{P_{LM}}$	α	$\frac{E_M}{P_{LM}}$	α	$\frac{E_M}{P_{LM}}$	α	$\frac{E_M}{P_{LM}}$	α	$\frac{E_M}{P_{LM}}$	α
Over consolidated			>16	1	>14	2/3	>12	½	>10	1/3
Normally consolidated		1	9-16	2/3	8-14	½	7-12	1/3	6-10	¼
Weathered or disturbed			7-9	½		½		1/3		¼

Table 2-22: Rheological factor for different soils and ratios of E_M/P_{LM} (Centre D'Etudes Menard, 1975)

Rock	α
Extensively fractured	0.33
Unaltered	0.5
Weathered	0.67

Table 2-23: Rheological factor for rock (Centre D'Etudes Menard, 1975)

Menard and Rousseau (1962) note that α can be expressed as a function of the ratio of the standard modulus to the reload modulus:

$$\alpha = \left(\frac{E_M}{E_M{}^+}\right)^{1/2+\mu} \quad \text{2-201}$$

$E_M{}^+$= reload modulus

μ=a small value compared to ½ that depends on secondary factors

Without reference, Baguelin et al. note that Centre D'Etudes Menard sometimes uses the ratioimprov $E_M/\ E_M{}^+$ (without the power) for defining α; however, this this may be due to a typing mistake as Equation 2-201 appears to be in more agreement with reality.

L/B	1		2	3	5	20
	circle	square				
λ_d	1	1.12	1.53	1.78	2.14	2.65
λ_c	1	1.1	1.2	1.3	1.4	1.5

Table 2-24: Shape factors λ_d and λ_c for different footing length to width ratios (Centre D'Etudes Menard, 1975)

As shown in Figure 2-165, E_d is calculated by dividing the ground beneath the footing base into 16 layers, each with a thickness equal to half the footing width. The subscript of each modulus designates the layer number and location. The harmonic mean of the moduli is calculated for each layer or group of layers using Equation 2-202:

$$E_i = \frac{1}{n}\sum_{j=1}^{n}\frac{1}{E_j} \quad \text{2-202}$$

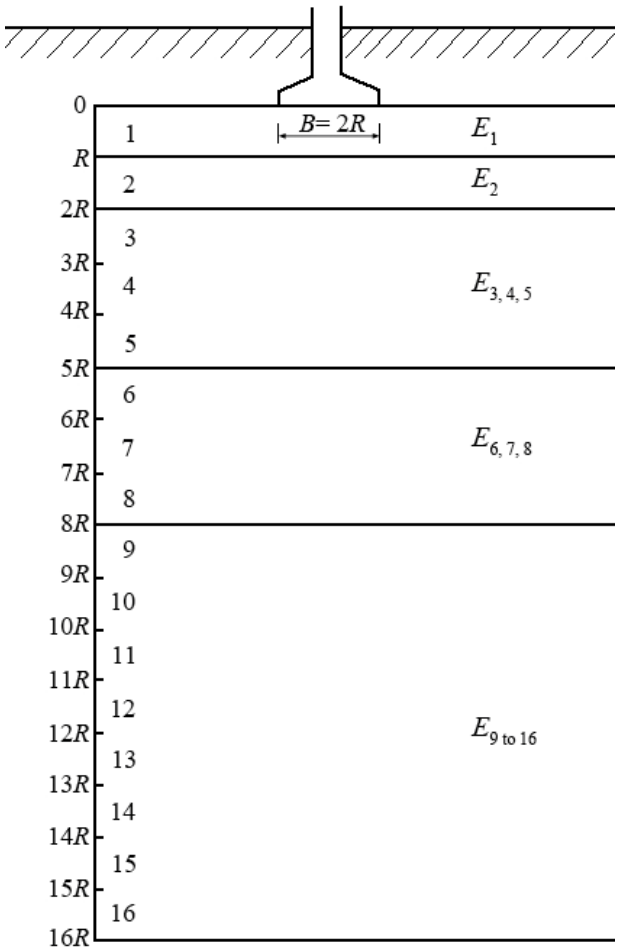

Figure 2-165: Layers of ground under the footing that are taken into consideration for the calculation of E_d (Centre D'Etudes Menard, 1975)

E_i= harmonic mean of moduli of layer *i*

n= number of moduli layer *i*

E_j= moduli values in layer *i*

E_d can be calculated from Equation 2-203 (Centre D'Etudes Menard, 1975):

$$E_d = \frac{4}{\frac{1}{E_1} + \frac{1}{0.85E_2} + \frac{1}{E_{3,4,5}} + \frac{1}{2.5E_{6,7,8}} + \frac{1}{2.5E_{9\ to\ 16}}} \qquad 2\text{-}203$$

$E_{(p\ to\ q)}$ is the harmonic mean of the moduli of layers *p* to *q*. If $E_{9\ to\ 16}$ is not known, but is assumed to be larger than the values of the upper layers then:

$$E_d = \frac{3.6}{\frac{1}{E_1} + \frac{1}{0.85E_2} + \frac{1}{E_{3,4,5}} + \frac{1}{2.5E_{6,7,8}}} \quad \text{2-204}$$

Similarly, if $E_{6,7,8}$ is also not known then:

$$E_d = \frac{3.2}{\frac{1}{E_1} + \frac{1}{0.85E_2} + \frac{1}{E_{3,4,5}}} \quad \text{2-205}$$

Equations 2-198 and 2-199 are applicable to foundations that are embedded at a depth that is at least equal to the width of the footing. If the depth of embedment is equal to half the footing width then the settlement should be increased by 10%. When the footing is found on ground level, the calculated settlement should be increased by 20%.

The above discussion is applicable when the variation of pressuremeter moduli is not very large with depth.

In the special case when the layer of soft soil is underlain by a layer of better properties at a depth that is less than one half of the width of the footing, the settlement can be calculated using Equation 2-206:

$$s = \int_0^h \frac{\alpha(z)\beta(F)q(z)}{E_M(z)} dz \quad \text{2-206}$$

α(z)= rheological factor of the soil layer at depth z

E_M(z)= Menard modulus at depth z

$q(z)$= increase of vertical pressure at depth z

$\beta(F)$= a coefficient that is a function of the safety factor for bearing capacity, F. This coefficient can be calculated from Equations 2-207 and 2-208 (Centre D'Etudes Menard, 1975):

$$\text{If} \quad F > 3 \qquad \beta(F) = 1 \quad \text{2-207}$$

If $F < 3$ $$\beta(F) = \frac{2}{3}\frac{F}{F-1}$$ 2-208

When a weak compressible layer of soil is interbedded between two layers, Menard (Centre D'Etudes Menard, 1975) proposes that the best procedure is to make a calculation for the settlement (using Equation 2-198 or Equation 2-199) of a soil that is assumed to be homogeneous, and then to add the settlement corresponding to the soft layer. The settlement corresponding to the soft layer can be estimated from:

$$s = \alpha_c \left(\frac{1}{E_{Mc}} - \frac{1}{E_M}\right) H_c \Delta q_c \quad \text{2-209}$$

As shown in Figure 2-166, parameters with subscript *c* in Equation 2-209 pertain to the compressible layer. H_c is the thickness of the compressible layer and Δq_c is the vertical stress increase at the compressible layer.

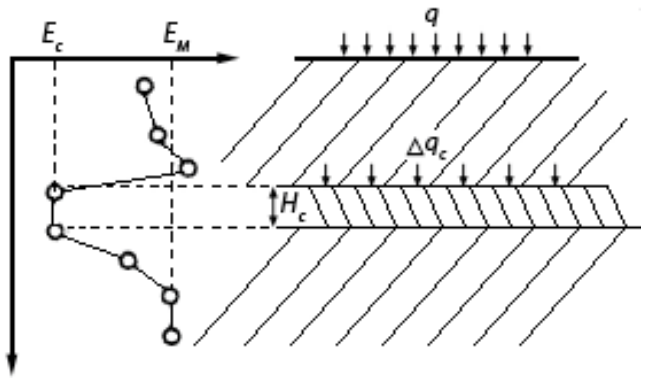

Figure 2-166: Compressible layer embedded between two layers (Centre D'Etudes Menard, 1975)

When footings are closely spaced, the stress bulbs overlap, and a more complex method of settlement calculation is required. As an example, Figure 2-167 shows a building that is supporting three basement walls. The shallow footing pressure is q_S, and the mean uniform pressure under the building foot print is q_R. The stress distribution due to the loads can be divided into four parts (Centre D'Etudes Menard, 1975), i.e.:

- A spherical component of intensity q_R in the zone A_R.
- A deviatoric component of intensity q_R external to the zone A_R.
- A spherical component of intensity q_S - q_R under each footing (A_S)
- A deviatoric component of intensity q_S - q_R external to zones A_S

The settlement of the building is then given by:

$$s = s_c(q_R) + s_d(q_R) + s_c(q_S - q_R) + s_d(q_S - q_R) \qquad 2\text{-}210$$

The first and last two terms of Equation 2-210 are respectively calculated for a bearing area equal to the building's foot print and t that of the footing.

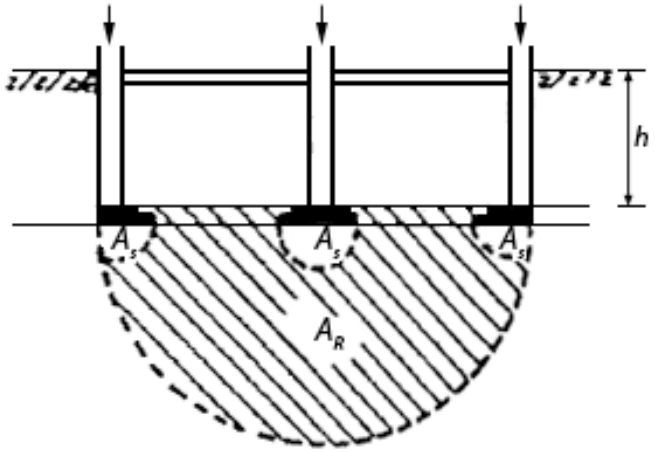

Figure 2-167: Settlement calculation for footings with overlapping stress bulbs (Centre D'Etudes Menard, 1975)

2.9.2.8 Self-Bearing

Natural unconsolidated soils and young fills will undergo large settlements with the passage of time under self-weight (Centre D'Etudes Menard, 1975). The rate of settlement can be accelerated by wetting, vibrations, or any phenomenon that tends to temporarily reduce the shearing resistance between grain contact points, thereby allowing the soil to settle into a more compact state.

The self-bearing condition of a soil; i.e., the level of soil parameters that a soil must have so as not to settle under its own weight, can be related either to physical or mechanical properties of the soil. Experience suggests that pressuremeter limit pressure is a suitable characteristic (Centre D'Etudes Menard, 1975). Table 2-25 presents the required limit pressure for soils with less than 10 m depth to achieve the condition of self-bearing. The influence of external random phenomena such as water table variation, seasonal moisture content change, road traffic vibrations, etc. have been considered in this table. For depths greater than 10 m, P^*_{LM} values given in Table 2-25 should be increased.

Soil type	P^*_{LM} (kPa) for self-bearing condition
Clay	250 to 300
Silt	400
Sand	600
Sand & gravel	800
Soils with organic content	20% increase in P^*_{LM} for 1% organic content

Table 2-25: P^*_{LM} (kPa) for self-bearing condition (Centre D'Etudes Menard, 1975)

According to Menard (Centre D'Etudes Menard, 1975) the self-weight settlement of a 10 m thick soft clay layer with , P^*_{LM}= 100 kPa will be 1 cm per year. As a first approximation the one year settlement of any soft layer can be estimated as a function of its limit pressure (in kPa units) by using Equation 2-211:

$$\text{For } P_{LM} < \frac{200}{\alpha}\ (\text{kPa}) \qquad s = \frac{h\ (\text{cm})}{1000}\frac{1-\alpha\frac{P_{LM}}{200}}{\alpha\frac{P_{LM}}{200}} \qquad \text{2-211}$$

Refer to Table 2-22 for the values of α. As previously noted, self-weight settlement rate will increase due to external causes.

2.9.2.9 Relationships and Correlations

2.9.2.9.1 Moduli

The settlement calculation method described in Section 2.9.2.7 is a valuable tool for estimating shallow footing settlement; however, there are certain conditions that may require alternative calculation methods; e.g. application of numerical methods or estimating settlement of footings with relatively large dimensions compared to the thickness of the compressible soil. In these two examples, the deformation parameters that are required are respectively the Young and oedometer moduli.

The relationship between Young and oedometer moduli is:

$$E_{oed} = \frac{1-\nu}{(1+\nu)(1-2\nu)}E_y \qquad \text{2-212}$$

All experts agree that Menard has determined a relationship as

$$E = \frac{E_M}{\alpha} \qquad 2\text{-}213$$

However, the ambiguity appears to be in what E is. In his most renowned publication, Menard (Centre D'Etudes Menard, 1975) himself notes that E_M is a distortion modulus of the soil measured in a deviatoric stress field, which characterises the pseudo-elastic phase of the pressuremeter test. This parameter must not be confused with the oedometer modulus, E_{oed}, which is measured in an isotropic or spherical stress condition. Menard further adds that precise experimental relationships exist between E_M and E_{oed}, and refers the relationship to later parts of his publication. This would suggest that the correct form of Equation 2-213 is:

$$E_{oed} = \frac{E_M}{\alpha} \qquad 2\text{-}214$$

Senior engineers, such as Mr Serge Varaksin, who have worked with Louis Menard for years agree with the form of Equation 2-214. While implying Menard and Rousseau (1962) as reference, Amar et al. (1991) have also used the same equation in their publication (The author notes that he has not been able to find such a relationship in Menard and Rousseau's paper, but this could be due to the limited knowledge of the author with the French language).

On the other hand, Baguelin et al. (1978), who cite Menard (Centre D'Etudes Menard, 1975), and Leblanc (1982) suggest that the correct form of Equation 2-213 is as presented in Equation 2-215.

$$E_y = \frac{E_M}{\alpha} \qquad 2\text{-}215$$

As mentioned above, the author has not found such a relationship in Menard's 1975 publication. Baguelin et al. also note that the compression modulus, K_M, can be used instead of E_M in Equation 2-206 by using Equation 2-216, and define the volume change or compression (also known as bulk) modulus, K, as indicated in Equation 2-217

$$K_M = \frac{E_M}{\alpha} \quad \text{2-216}$$

$$K = \frac{E}{3(1-2\nu)} \quad \text{2-217}$$

Gambin (1979), also suggest that α relates E_M to E_y.

A review of other less known Menard publications is able to clarify the more correct form of Equation 2-213 is Equation 2-214. In his earlier publications (Menard, 1963b), instead of E_d and E_c, Menard initially formulates settlement using a deviatoric modulus that is measured by the pressuremeter test and a spherical modulus that is measured by the oedometer or deducted from the PMT. Later (Menard et al., 1964) he clarifies the spherical modulus, E^+, as:

$$E^+ = \frac{E_M}{\alpha} \quad \text{2-218}$$

Dauvisis and Menard (1964) then define E^+ as the compression modulus, and use Equation 2-218 to calculate the second term of Equations 2-198 and 2-199. More clearly, Menard and Lambert (1966) defines α/E_c as the inverse of the oedometer modulus that can be calculated from the PMT modulus and α in the zone where the constraints tensor is predominantly spherical or isotropic.

2.9.2.9.2 Estimation of Shear Strength

Baguelin et al. (1978) note that theoretical solutions (Bishop et al., 1945, Hill, 1950, Salencon, 1966) based on ideal elastic-plastic assumptions reduce to Equation 2-219 for an undrained condition with Poisson ratio equaling 0.5, and add that Menard (Etude Pressiometrique Louis Menard, 1967) suggests that the undrained shear strength, c_u, can be estimated using Equation 2-220.

$$c_u = \frac{{P^*}_{LM}}{1 + \ln\left(\frac{E}{3c_u}\right)} \quad \text{2-219}$$

$$c_u = \frac{P^*_{LM}}{1 + \ln\left(\frac{E_M/\alpha}{3c_u}\right)} \quad \text{2-220}$$

Both Equation 2-219 and Equation 2-220 can be written in the form of:

$$c_u = \frac{P^*_{LM}}{\beta} \quad \text{2-221}$$

Baguelin et al. comment that typical values of E/c_u for clay might range from 200 to 2000 (D'Appolonia et al., 1971), which will result in values of 5.2 to 7.5 for β. Briaud (1992) comments that in fact β depends on the ratio of shear modulus to the undrained shear strength, and with this ratio being from about 100 to 600, β will be from 5.6 to 7.4 and 6.5 on average. Menard (Etude Pressiometrique Louis Menard, 1970, Menard, 1965) proposes that the ultimate or residual strength of a clay can be computed using Equation2-222:

$$c_u = \frac{P^*_{LM}}{5.5} \quad \text{2-222}$$

Amar et al. (1991) cite Amar and Jezequel (1972) for limiting the application of Equation2-222 to conditions in which net limit pressure, P^*_{LM}, is less than 300 kPa, and proposing Equation 2-223 when net limit pressure is greater than 300 kPa.

$$c_u = \frac{P^*_{LM}}{10} + 25 \text{ (kPa)} \quad \text{2-223}$$

2.9.2.9.3 Estimation of Drained Friction Angle

Baguelin et al. (1978) cite Menard (Etude Pressiometrique Louis Menard, 1970) for proposing Equation 2-224 and publishing Figure 2-168 for estimating the drained friction angle, φ', from the net limit pressure.

$$P^*_{LM} = 2.5 \times 2^{\frac{\varphi' - 24}{4}} \quad \text{2-224}$$

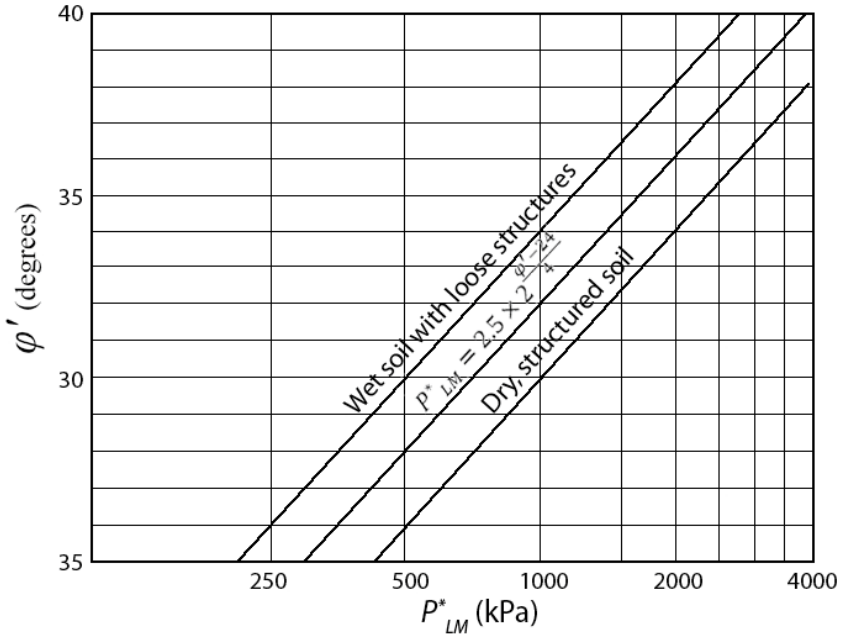

Figure 2-168: Graph for estimating drained friction angle from net limit pressure (Etude Pressiometrique Louis Menard, 1970)

Baguelin et al. also note that Muller (1970) quotes the same relationship in a slightly different form:

$$P^*_{LM} = b \times 2^{\frac{\varphi' - 24}{4}} \qquad 2\text{-}225$$

b= 1.8 for homogeneous, wet soil

b= 2.5 on average

b= 3.5 for dry, heterogeneous soil

2.9.2.9.4 Correlation with CPT

Baguelin et al. (1978) have reviewed, and interpreted a number of CPT-PMT correlations such as those published by Van Wambeke (1962), Cassan (1968, 1969), Jezequel et al. (1968) and Nazaret (Nazaret, 1972) that were originally printed in French publications. Baguelin et al. note that while most correlations in technical publications are based on the ratio of q_c/P_{LM}, in spite of introducing uncertainties, the ratio of net values q^*_c/P^*_{LM} would be more representative. q^*_c is the net CPT cone resistance, and can be calculated from:

$$q^*_c = q_c - q_o \qquad 2\text{-}226$$

q_o is the total vertical stress. In general q^*_c/P^*_{LM} and q_c/P_{LM} are close because q_o and P_o are small compared to q_c and P_{LM}, but can be quite different at depth in soft clays.

Jezequel et al (1968) studied the influence of depth on q^*_c/P^*_{LM} at the hydraulic fill dikes of a tidal power project in Rance, France. The fill used was composed of clean sand with dry density equal to 1.5 t/m^3. q^*_c/P^*_{LM} in the upper 1.5 m layer of fill was from 9.11 to 12.03. Even though q_c varied from 2 to 10 MPa, q^*_c/P^*_{LM} was about 6.7 throughout the remainder of the 20 m thick fill.

Nazaret (1972) did not observe the same independency of q^*_c/P^*_{LM} from q^*_c in his study on Loire sand, and reports a tendency of the ratio to increase with the increase of q^*_c.

Baguelin et al. interpret that the high values of q^*_c/P^*_{LM} near the ground surface are due to the differences between shallow and deep failure conditions. CPT has a small diameter, and rapidly reaches its critical depth. However, PMT has to reach an embedment depth of about 1.5 m (1 m in clays, 2 m in sands) before the test is no longer influenced by the surface of the ground.

According to Baguelin et al. soil type has the greatest effect on q^*_c/P^*_{LM}, and for depths of about 5 to 20 m there seems to be a narrow correlation between q^*_c and P^*_{LM}. Baguelin et al. consider that reasonable averages of q^*_c/P^*_{LM} can be considered to be as presented in Table 2-26.

Soil Description	q^*_c/P^*_{LM}
Very soft to soft clays	close to 1 or from 2.5 to 3.5
Firm to very stiff clay	from 2.5 to 3.5
Very stiff to hard clay	from 3 to 4
Very loose to loose sand and compressible silt	from 1 to 1.5 and from 3 to 4
Compact silt	from 3 to 5
Sand and gravel	from 5 to 12

Table 2-26: q^*_c/P^*_{LM} for different soil types according to Baguelin et al. (1978)

Baguelin et al. understand that it is very likely that dilatancy is a key factor in sands and gravels, and q^*_c/P^*_{LM} could prove to be a reliable indicator of the importance of dilatancy in the resistance of a particular soil. They conceive that a soil is probably non-dilatant or slightly dilatant if q^*_c/P^*_{LM} is about 5 to 6, and a ratio of 8 to 12 probably suggests a soil that is probably dilatant.

Campanella et al. (1979) also performed a study on the plastic silt and silty clay fluvial deposits of the Fraser River delta at Sea Island, Vancouver. Their study showed that q_c/P_{LM} is approximately 2.1 to 4 in the plastic silts, which is of the same magnitude as what Baguelin et al. had concluded.

Based on theoretical and experimental studies, Van Wieringen (1982) proposed that q_c can be correlated to P_{LM} using Equations 2-227 and 2-228.

For clays $$q_c = 3P_{LM} \quad \text{2-227}$$

For sands $$q_c = 15(\tan \varphi')^{1.75} P_{LM} \quad \text{2-228}$$

Briaud et al. (1985) collected 82 PMT borings data from various projects from 1978 to 1985, and proposed the correlations of Table 2-27 (Briaud, 1992).

Soil type	PMT parameter	Correlation to CPT
Clay	P_{LM}	0.2 q_c
	E_M	2.5 q_c
Sand	P_{LM}	0.11 q_c
	E_M	1.15 q_c

Table 2-27: Correlation between PMT and CPT (Briaud et al., 1985)

2.9.2.9.5 Correlation with SPT

Based on research (Cassan, 1968, Cassan, 1969, Hobbs and Dixon, 1969, Waschkowski, 1974, Waschkowski, 1976), carried out on Leucate and Dunkirk sands, Devonian marl of Monmouthshire, and silty sands of Blois region, Baguelin et al. (1978) observed a large scatter in the ratio of SPT blow counts, N, to P_{LM}, and described a major reason for this scatter being the fact that reaming was not used. They concluded that N/P_{LM}, with limit pressure in kPa, varies from 1/50 to 1/20, and as a provisional recommendation propose:

For sands $$\frac{N}{P_{LM}} = \frac{1}{50} \quad (P_{LM} \text{ in kPa}) \quad \text{2-229}$$

Using Meyerhoff's correlation q_c/N= 400, with cone resistance in kPa, Equation 2-229 will yield q_c/P_{LM}= 8, which is within the range proposed in Table 2-26. In view of the large scatter of N in clay, Baguelin et al. do not propose any correlation.

Briaud (1992) proposes that in sands:

$$\frac{N}{P_{LM}} = \frac{1}{47.9} \quad (P_{LM} \text{ in kPa}) \qquad 2\text{-}230$$

$$\frac{N}{E_M} = \frac{1}{383} \quad (P_{LM} \text{ in kPa}) \qquad 2\text{-}231$$

More recently, Bozbey and Togrul (2010) have proposed Equations to for correlating PMT parameters to SPT blow counts corrected to 60% efficiency, N_{60}, during a case study in Istanbul.

For sands $P_{LM} = 330{N_{60}}^{0.51} \quad (P_{LM} \text{ in kPa}),\ R^2 = 0.74$ 2-232

For sands $E_M = 1330{N_{60}}^{0.77} \quad (P_{LM} \text{ in kPa}),\ R^2 = 0.82$ 2-233

For clays $P_{LM} = 260{N_{60}}^{0.57} \quad (P_{LM} \text{ in kPa}),\ R^2 = 0.67$ 2-234

For clays $E_M = 1610{N_{60}}^{0.71} \quad (P_{LM} \text{ in kPa}),\ R^2 = 0.7$ 2-235

2.9.3 Dynamic Compaction Testing Methods of the Future

Currently, dynamic compaction quality control and verification is performed as spot checks at a certain frequency (refer to Section 2.9.2.4). Observation of ground behaviour during impact, and the crater sizes can also be of great assistance in identifying soft or hard spots or zones. It could be expected that quality control would greatly improve, if the observational procedure was to be integrated into the verification process using a continuous monitoring mechanism.

Based on roller integrated compaction metres that continuously measure the acceleration of the roller drum and calculate a roller measuring value from the acceleration signal,

Continuous Compaction Control (CCC) measuring technology was initiated in Europe in the 1970s for use on vibratory rollers compacting granular material (Briaud and Saez, 2012, Forssblad, 1980, Thurner and Sandström, 1980, White and Vennapusa, 2010). For vibratory rollers, an accelerometer that is mounted to the roller drum provides spatial records of compaction quality when linked to position measurements and a documentation system. An alternative to accelerometer-based vibratory measurements is the measurement of rolling resistance or machine drive power, and can be applied to both vibratory and non-vibratory roller operations. When the measurement system provides *Automatic Feedback Control* (AFC) for roller vibration amplitude or frequency, it is referred to as *Intelligent Compaction* (IC).

Roller measurement values calculated based on accelerometer measurements use one of two different approaches; i.e., calculation of a ratio of selected frequency harmonics for a set time interval, or calculation of ground stiffness or elastic modulus based on a drum-ground interaction model and some assumptions. Regardless of the technology, the basis of CCC and IC is that the measurement values are related to traditional compaction measurements, and will be useful as part of effective earthwork compaction operations and quality control and quality assurance practices (White and Vennapusa, 2010).

White and Vennapusa (2010) note that the below measurement technologies have been developed for roller compaction methods:

- Compaction Meter Value (CMV) (Sandström, 1994)
- Oscillometer Value (OMV) (Thurner and Sandström, 2000)
- *Compaction Control Value (*CCV*)* (Scherocman et al., 2007)
- Roller-Integrated Stiffness (ks) (Anderegg and Kaufmann, 2004)
- Omega Value (Kröber et al., 2001)
- Vibratory Modulus (EVIB) Value (Kröber et al., 2001)

Similar measurement systems and technologies are not available for dynamic compaction CCC, but research in this field is under way, and Kopf and Paulmichl (2004) have developed a concept (published in German) that has been cited in several publications (Adam and Brandl, 2009, Adam et al., 2007, Kopf et al., 2010).

Pounder acceleration during impact can be measured to determine the reaction forces of the ground; however, these reaction forces are influenced by soil compaction, replacement,

liquefaction, excessive pore water pressures, local ground failure, plastic and elastic deformations, etc. Consequently, Kopf and Paulmichl consider that the reaction force is not suitable as a clear characteristic value required for a reliable compaction control. However, in their opinion, the decay of free soil vibrations caused by the falling pounder after each impact is characteristic of the soil-pounder interaction, and enables a site-specific optimisation and quality control of dynamic compaction. The decaying pounder acceleration after impact can be seen in the measured example of Figure 2-169.

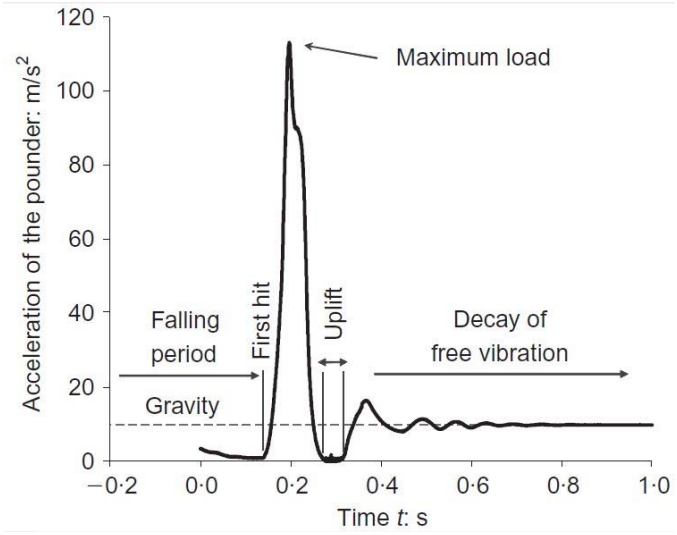

Figure 2-169: Acceleration of pounder after impact (Adam et al., 2007)

The idea of Kopf and Pualmichl's (2004) concept is to create a correlation between measured vibration parameters and soil parameters of an idealised linear-elastic half space with the assumption that an elastic decay of free soil vibrations under still (possibly meant as constant and without change) increased pore water pressures can be modelled and solved using a theoretical analysis similar to a viscously damped single degree of freedom system (SDOF). Consequently, measuring the acceleration of the falling pounder during the decay of free soil vibrations will provide the damped frequency, ω_d, and Lehr's damping coefficient, ζ, if a viscously damped SDOF system is assumed.

During dynamic compaction the pounder penetrates deeper and deeper into the ground (refer to Section 2.4.6 to 2.4.9). This changes the dynamic conditions of the system depending. In order to quantify the specific effects, extensive parameter studies were performed using the boundary element method, which only requires the discretisation of the boundary (Banerjee, 1994), and is particularly suitable for linear-elastic half space problems. Kopf and Pualmichl note that the assumption of linear-elastic soil behaviour is applicable and with sufficient accuracy because the decay of the vibration after impact behaves as an elastic

problem. The pounder-half space system was simulated in the frequency domain using a rotational-symmetric model. The penetration depth, D_c, is variable, and using the SDOF analogy, an analytic approximate solution exists for the case in which the pounder has not penetrated the ground. Approximations are also available for the spring and damping coefficient when the depth of penetration is greater than zero, but they are limited to geometrical properties and the penetration depth. Therefore, boundary element method numerical simulations that did not consider material damping were carried out to analyse the decay of free soil vibrations.

Numerical calculations suggested that Lehr's damping coefficient derived from the SDOF analogy depended only on Poisson's ratio, was practically independent of the deformation modulus of the half space, and varied with depth for all penetration depths. The influence of the pounder penetration depth, i.e., the crater depth, can be calculated by a reduction factor κ, which is a function of Poisson's ratio.

In summary, the steps for deriving the soil parameters from the measured vibration parameters are:

1. Determination of the damped natural frequency, $\omega_d/2\pi$, and the Lehr's damping coefficient, ζ, from the post impact decaying free vibration parameters (period, T, and consecutive maximum wave amplitudes Z_n and Z_{n+1}, refer to Figure 2-170). ω_d the logarithmic damping coefficient, δ, are respectively calculated from the decaying free wave using Equations 2-1 and 2-237. As can be seen be seen in Figure 2-171, in reality the ground is not a linear-elastic half space with negligible material damping, and the actual decaying acceleration wave period and logarithmic damping coefficient may vary in the cycles. ζ and the (undamped) natural frequency, ω, are respectively calculated from Equations 2-238 and 2-239.

$$\omega_d = 2\pi/T \qquad 2\text{-}236$$

$$\delta = \ln\left(\frac{Z_n}{Z_{n+1}}\right) \qquad 2\text{-}237$$

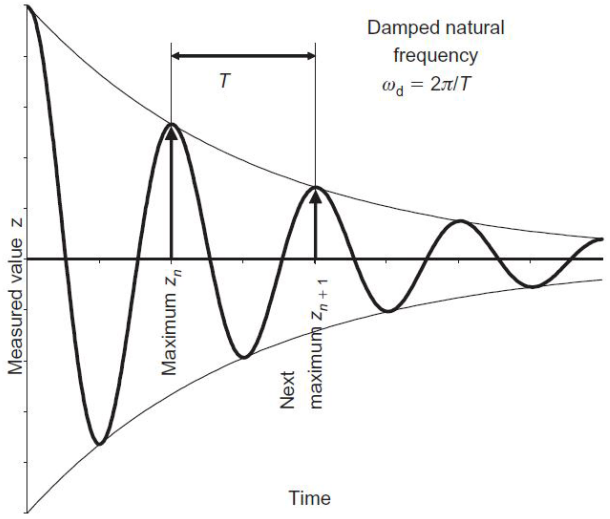

Figure 2-170: (Idealised) decaying wave (Adam et al., 2007)

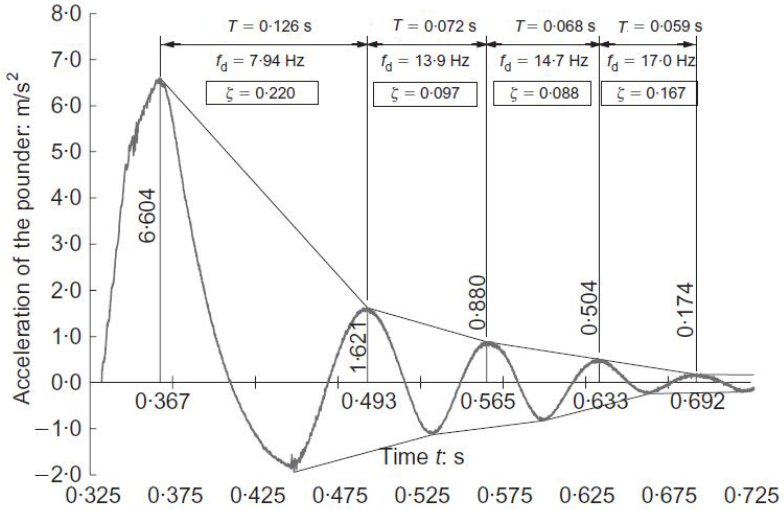

Figure 2-171: Decaying acceleration wave measured after pounder impact (Adam et al., 2007)

$$\zeta = \frac{\delta}{2\pi\sqrt{1+\left(\frac{\delta}{2\pi}\right)^2}} \qquad 2\text{-}238$$

$$\omega = \frac{\omega_d}{\sqrt{1-\zeta^2}} \qquad 2\text{-}239$$

2. Estimation of Poisson's ratio, ν, from the chart of Figure 2-172, and by using ζ and the actual pounder penetration depth. It is noted that this chart has been developed based on a pounder with diameter and weight being respectively 1.8 m and 16.5 t.

The Young modulus and soil density used were respectively 16 MPa and 2 t/m^3, and no damping was included in the calculations.

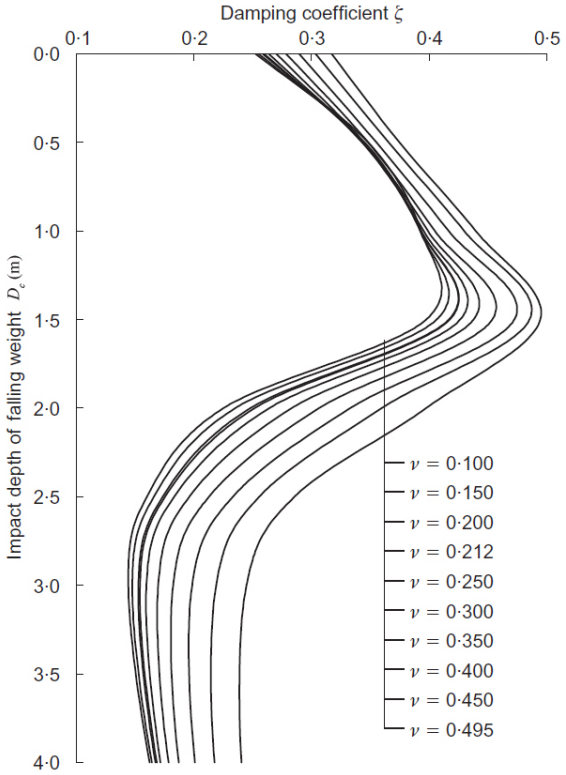

Figure 2-172: Chart for estimation of Poisson's ratio (Adam et al., 2007)

3. The (uncorrected) half space modulus is determined from the chart of Figure 2-173 based on the natural frequency (reciprocal of ω) and Poisson's ratio for the case of no pounder penetration into the ground (D_c= 0). It is noted that, as before, this chart has been developed based on a pounder with diameter and weight being respectively 1.8 m and 16.5 t, and no damping.

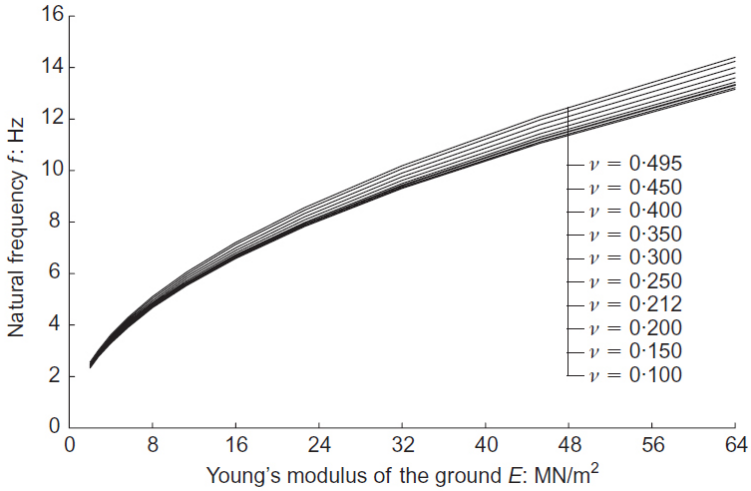

Figure 2-173: Chart for estimation of Young modulus for the case of D_c= 0 (Adam et al., 2007)

4. The corrected Young modulus is calculated by multiplying the uncorrected modulus derived from of the previous step by κ, which is estimated from the chart of Figure 2-174. This chart has been developed based on a pounder with diameter and weight being respectively 1.8 m and 16.5 t. The Young modulus and soil density used were respectively 16 MPa and 2 t/m^3, and no damping was included in the calculations.

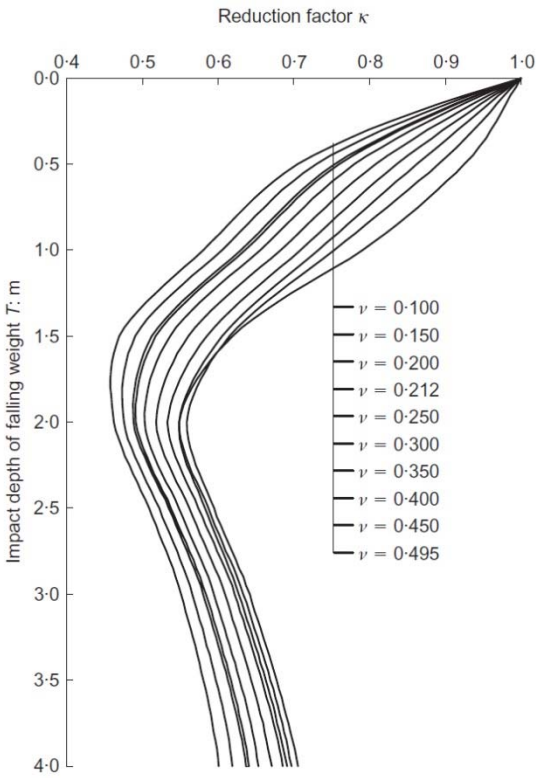

Figure 2-174: Chart for estimation of κ (Adam et al., 2007)

The method presented above appears to be very promising; however, the impact of some assumptions used in this analogy, such as assuming zero material damping, requires further consideration. Also, the ground is assumed to be a linear elastic half space, and the deformation modulus that is derived applies to the whole of the half space mass. This is obviously not compatible with reality, and it is well established that the effect of improvement diminishes with depth.

2.10 Special Topics

It is the experience of the author that a number of questions are frequently asked by clients, consultants, associates and engineers who are considering the application of ground improvement in general and dynamic compaction or dynamic replacement in particular. These topics are reviewed in this section.

2.10.1 Ground Improvement Specifications and Acceptance Criteria

Ground improvement is generally taken into consideration after it has been established by some means that the in-situ ground conditions are not able to satisfy the project requirements. It will then be necessary to develop the ground treatment specification and consequently the acceptance criteria, which can have numerous forms.

It is the objective of this section to review and to compare a number of possible and common methods of how soil improvement specifications are prepared and stipulated. Some specifications and acceptance criteria potentially inherit more risk and cost than others, and the outcome of a project may be determined by the quality of specifications and criteria rather than the success of the works.

2.10.1.1 Acceptance Criteria Based on Work Quality

Sometimes, prior to the tender and the award of the contract to a tenderer, ground improvement specifications are developed in full detail by the party who has prepared the tender documents. In such a case, based on the geotechnical advisor's design, which is usually not made available, a ground improvement technique is specified, the scope of work to be performed is described in detail, and the construction method is outlined.

The responsibility of the contractor will usually include the procurement of the working team, equipment, material and execution of the works according to the specification's instructions.

In this type of project acceptance criteria is generally non-technical and based on performing the works according to the specified dimensions, spacing, quality and quantity of materials that have been used.

Testing may be specified, but it will not be (or at least in a fair contract it should not be) the contractor's responsibility to meet any specific value as other parties have been engaged in

the development of the methodology and design of ground improvement. Should test results fail to meet expectations, then the contractor will be required to perform additional work using the same technology or an alternative ground improvement method, and would be fully paid for any extra work if the works were carried out properly in the first place,.

As an example, the ground improvement method in the specification may be stipulated to be dynamic replacement. The column spacing, number of phases, number of blows per print, pounder weight and drop height, and execution method will all be specified, and the contractor will have to provide the working team, DR rig, pounders, other equipment, and material, and perform the works according to what has been described in the specifications.

Even if tests carried out after the works demonstrate that the technical requirements of the project have not been satisfied; e.g. achieving the required DR column diameter or penetration depth, should the contractor have performed the works correctly, he will be exempted from all other responsibilities and consequences. Correction of the works to meet the project's requirements will be the responsibility of others.

At first glance this approach and development of acceptance criteria may appear to be favourable. Indeed this is the way that many projects are performed in most engineering fields, and under the influence of other disciplines, ground improvement is sometimes carried out in a similar manner.

Although it is acknowledgeable that developing a design by an experienced geotechnical engineer will provide certain amounts of confidence, especially in the absence of specialised ground improvement contractors, due to the history of development of ground improvement technologies and the heterogeneity of the soil, in the presence of specialist ground improvement contractors, this method possesses a number of major draw backs that inevitably deviate the project's path from an optimised approach.

It should not be forgotten that academia and consulting engineers have been the front runners of many engineering disciplines, and consequently it is not surprising that they drive the concepts of those fields. However, if we look back at the histories of ground improvement techniques, it can be observed that almost all have been developed, advanced or patented by contracting companies. For example, further to the invention of jet grouting by the Japanese in the early 1970s (Ichese et al., 1971), almost all major further developments and supplementary innovations that have been patented in the United States are by specialist contracting companies (Shibazaki and Yoshida, 1995, Tokoro et al., 1984, Yahiro and Yoshida,

1977). Later, research by academia has provided the theoretical background and understanding of the method; e.g. the theoretical modelling of jet grouting (Modoni et al., 2006). The same concept is true with other ground improvement techniques; i.e., dynamic compaction, dynamic replacement, Menard vacuum, controlled modulus columns (Communication Department of Menard, 2007), vibro compaction and stone columns (Better Ground), and many other techniques.

In most cases, eliminating the input of specialist contractors saves the project neither time nor money. As much as an academician or geotechnical consultant may be up to date with the latest ground improvement developments, it is always possible that specialist contractors have further advanced a technique or developed a new idea that can bring savings to the project.

While most tenders accept alternatives, it still appears to be a waste to allocate time and money to prepare a detailed design and specification of ground improvement, only to replace it with an alternative in the final stage. It is the author's belief, in the presence of specialist ground improvement contractors, that identifying the ground's problems, developing a concept based on budget, time, environmental and other constraints, and allowing the industry to propose an optimised solution will more readily meet the interests of the project.

Stipulating non-technical acceptance criteria results in success only if the anticipated methodology works perfectly and when there are no problems. However, serious problems may arise if things do not work out well. Remedial solutions may not be possible with on-site capacity, and the contractor may not have the technology or resources to execute an alternative solution. Furthermore, even if there are no latent conditions, any rectification of the ground improvement solution beyond the design will immediately become a cost to the owner and most probably a delay in the construction programme.

It is definitely better for acceptance criteria to be a technical requirement rather than tied to the quality and quantity of performed work. There is truly no justification to allocate the project's financial resources and time to developing a detailed solution that may be subject to major and fundamental changes and derivations during later stages. It seems best for the project's consultant to identify the need for ground improvement, to identify feasible solutions that would be able to satisfy the technical requirements, to provide a realistic budget for planning purposes, to prepare a specification for ground improvement works that

is open to solutions that are able to satisfy technical requirements and to supervise the works in a manner that will verify that technical acceptance criteria have been satisfied.

2.10.1.2 Acceptance Criteria Based on Minimum Test Results

A better approach for developing ground improvement specification and acceptance criteria would be when the criteria are based on technical performance rather than complying with a rigid methodology.

In such cases, acceptance criteria are sometimes stipulated to be a minimum test value (or envelope) or a correlation to the test value. Sometimes the specified testing method is impractical. For example, it may be stipulated to carry out in-situ density tests for the ground improvement works of a road that is to be constructed on a thick reclamation. Although this testing method may be appropriate for thin layers of roller compacted soil in a typical road construction project and it is not impossible to obtain undisturbed samples from deep depths, questions can and should be raised that is the envisaged test method the appropriate procedure for the specific project conditions, and will it be able to suitably, technically, practically and economically demonstrate that design requirements have been satisfied.

Possibly being aware of the above discussion, sometimes the specifications supposedly facilitate the application of an impractical testing method by correlating it to a practical and more suited testing procedure. For example the specifications may stipulate a minimum in-situ density for a thick reclamation project, but as it is impractical to perform such tests, the density acceptance criterion may be correlated to CPT cone resistance. One should wonder about the objective of going through all this trouble to develop a correlation that is simply a best fit curve with some values for the standard deviation and coefficient of determination while it would seem more rational to develop the acceptance criteria simply based on the cone resistance without correlating to density at all. This example demonstrates how the background and mentality of engineers who have gained expertise in other fields may deviate ground improvement acceptance criteria to what is more acceptable in the other field.

Although quite often referenced in many publications, relative density is also a very unsuitable acceptance criterion that has found its way into ground improvement projects, especially in reclaimed sites. Due to the importance of this topic, Section 2.10.2 “Unreliability and Unsuitability of Relative Density as a Ground Improvement Criterion” has been allocated to this subject.

Quite commonly, ground improvement acceptance criteria are based on minimum (or an envelope of minimum) passing values of practical, efficient and economical field tests such as SPT, CPT or PMT. This, itself, is an important step forward as it recognises that establishing acceptance criteria based on direct measurement of parameters is much more rational and beneficial than relying on redundant correlations. However, there is probably still another step that must be taken forward.

The question that should now be posed is on the mechanism of determining the minimum passing values. Those figures are most probably based on a calculation that has been carried out by the geotechnical engineer to ensure certain design requirements such as bearing capacity, total and differential settlements, liquefaction mitigation or long term consolidation have been satisfied. However, we must note that a condition in which the soil layers in the test just reach the minimum passing value that have been determined by the geotechnical engineer is only one possibility of the hundreds of results that can still satisfy the design criterion.

Certainly in ground improvement techniques such as dynamic replacement, stone columns, jet grouting, deep soil mixing and controlled modulus columns, in which inclusions are introduced into the soil and vertical loads are distributed between the in-situ soil and the inclusions by arching the concept of minimum passing value becomes meaningless. Indeed, the in-situ soil improves negligibly, and it is only the added elements that improve the soil mass.

It is evident that this type of acceptance criteria rules out the techniques that may be most applicable. Of course, the specification may be written to stipulate average minimum passing values, but that does not cover all aspects either. For example, an average minimum value will still not be able to address the issue of column bulging in very soft saturated clays. The cycle of adding clauses to the specification can go on and on.

Even if the ground improvement technique; e.g. dynamic compaction or vibro compaction, does not incorporate inclusions, most probably there will be test results that are well above the minimum passing value. A minimum passing criterion neglects the benefits of the additional improvement, and does not take it into consideration. However, a recalculation may very well be able to demonstrate that design requirements can still be satisfied what all layers actually passing the specified minimum acceptance value.

One may argue that in the minimum passing value criterion provides a higher safety factor and is on the conservative side, and ignores the benefits of layers with better than required properties. As true as this argument is, adding more and more safety factors well beyond what is considered as sound engineering practices is poor engineering practice that will inevitably lead to more effort, energy, construction time and costs. Highly conservative engineering is not an achievement. Today, we do have enough knowledge about ground improvement technologies to be able to design soil treatment without resorting to such out dated procedures.

Acceptance criteria based on minimum passing values may unjustifiably and unnecessarily lead to non-conformance while still meeting the foundation design requirements, and it is the opinion of the author that acceptance must be developed in a more appropriate manner.

2.10.1.3 Acceptance Criteria Based on Design Criteria

Having discussed acceptance criteria that are usually unable provide the best performance with minimum cost and time requirements, it can now be proposed that optimal acceptance criteria should be directly based on design criteria. Indeed, there is no better way of making sure that a certain aspect of design has been fulfilled than directly verifying that specific criterion itself.

Relevant tests should be carried out simply to verify that ground conditions after soil improvement are able to satisfy the design requirements. In reality there is no need to add proxies to the specifications by introducing minimum passing values or correlations. The foundation design requires certain conditions to be met; e.g. achieving a defined bearing capacity subject to a limit on the total and differential settlements.

Of course, tests and measurements must be made to demonstrate that design criteria have been satisfied, so the testing programme and interpretation method should be clearly defined.

With this information, the specialist contractor will know exactly what is expected, and will be able to offer his best proposal. If the contractor believes that alternatives to the specifications can benefit the project, he should clearly propose the alternative offer based on alternative design criteria or verification testing. The designer can then assess the proposals, and select the best proposal with minimal complications during construction.

2.10.2 Unreliability and Unsuitability of Relative Density as a Ground Improvement Criterion

2.10.2.1 History

The concept of relative density (D_d) was first introduced by Terzaghi (1925) to bring the behaviour characteristics of soils together on a common basis in consistent and practically useful relations and to provide a tool for communications between engineers (Burmister, 1948). It was suggested that this parameter would be an appropriate means to define the looseness and denseness of sand or sand-gravel soils in a meaningful way because important properties were assumed to correlate quite well by this means.

Relative density is a definition rather than an inherent property of the soil. *Per se*, it has no significance and influence on performance and compared it may be possible to satisfy design criteria with a higher safety factor without even complying with the relative density criterion.

In fact, confusion in the use of relative density began as soon as engineers started utilising it as a soil parameter because there was no common definition or set of standards to work from (Holtz, 1973b). Recognising that some kind of standard would be necessary, Section D, Subcommittee 3 of Committee D-18 of ASTM was established in 1954 for determining the minimum and maximum densities of sand and gravel soils. The work of the Subcommittee resulted in ASTM D2049-69 (ASTM, 1969), which was approved by Committee D-18 in 1964.

It was the opinion of the majority of Subcommittee members that the benefits of a reasonably good standard method far out weighted any disadvantages of the particular test that was then proposed (Holtz, 1973b). In addition, it was felt that by getting a tentative standard published, many persons and organisations would work with it, evaluate its suitability, and suggest beneficial modifications and improvements.

The introduction of relative density as a criterion for acceptance whereas it is compared with a critical value to give a yes or no type of answer has led to considerable amount of research, most of which point towards the insufficiency of its accuracy and reliability, and it is the opinion of the author that although still popular and systematically used by those engineers who have never looked deeply into this concept, the truth is that after years of having had its suitability evaluated, relative density has not fulfilled expectations and should be abandoned as a criterion altogether. That seems to be already under way. There was a time when liquefaction analysis was found on the concept of relative density (Seed and Idriss,

1967, Seed and Idriss, 1971); however, today while the same methodology has been retained, relative density has lost colour and is no longer part of liquefaction evaluation procedure (Youd et al., 2001), and in the process of re-evaluating the concept of relative density, as proposed by Selig and Ladd (1973), ASTM withdrew its D2049-69 standard for measuring relative density as early as 1984, and has replaced it with the more meaningful standards for measuring maximum and minimum index densities (ASTM, 2006a, ASTM, 2006b). In its new standards, ASTM (2006a) cautiously states that it is generally recognised that either relative density or per cent compaction is a good indicator of the state of compactness of a given soil mass. However, the engineering properties, such as strength, compressibility, and permeability of a given soil, compacted by various methods to a given state of compactness can vary considerably. Therefore, considerable engineering judgment must be used in relating the engineering properties of soil to the state of compactness. Mayne (2006) cautiously notes that in his opinion relative density is a rather weak parameter. Likewise, Bowles (1996) states that in his opinion the relative density test is not of much value since it is difficult to obtain maximum and minimum unit weight values within a range of about ±0.5 kN/m^3.

2.10.2.2 Relative Density and Points of Concern

2.10.2.2.1 The Definition of Relative Density and its Intended Range of Application

ASTM (2006a, 2006b) defines relative density a ratio, expressed as a percentage, of the difference between the maximum index void ratio and any given void ratio of a cohesionless, free-draining soil; to the difference between its maximum and minimum index void ratios, or:

$$D_d = \frac{e_{max} - e}{e_{max} - e_{min}} \times 100 \qquad \text{2-240}$$

e_{max}= maximum index void ratio or the reference void ratio of a soil at the minimum index density/unit weight.

e_{min}= minimum index void ratio or the reference void ratio of a soil at the maximum index density/unit weight.

e= the in situ or stated void ratio of a soil deposit or fill.

Equation 2-8 can also be expressed in terms of maximum and minimum indexes and dry densities or dry unit weights (ASTM, 2006a, ASTM, 2006b) as formulated in Equation 2-241 and Equation 2-242.

$$D_d = \frac{\rho_{dmax}(p_d - \rho_{dmin})}{\rho_d(p_{dmax} - \rho_{dmin})} \times 100 \qquad 2\text{-}241$$

$$D_d = \frac{\gamma_{dmax}(\gamma_d - \gamma_{dmin})}{\gamma_d(\gamma_{dmax} - \gamma_{dmin})} \times 100 \qquad 2\text{-}242$$

ρ_{dmax} or γ_{dmax} = the reference dry density/unit weight of a soil in the densest state of compactness that can be attained using a standard laboratory compaction procedure that minimizes particle segregation and breakdown.

ρ_{dmin} or γ_{dmin} = the reference dry density/unit weight of a soil in a standard state of compactness at which it can be placed using a standard laboratory procedure which prevents bulking and minimizes particle segregation.

ρ_d or γ_d = dry density/unit weight of a soil deposit or fill at the given void ratio.

ASTM makes a number of statements that deserve review and consideration. Firstly, the applications of ASTM testing methods are conditioned to a range of selected soils, or in other words, the concept of relative density is not applicable to all other soils. According to ASTM (2006a, 2006b), for its testing methods to be applicable, the soil can contain up to 15%, by dry mass, of soil particles passing a 75-µm sieve, provided they still have cohesionless, free-draining characteristics. Also, for determination of minimum index density and unit weight of soils, the three accepted methods are applicable to soil in which 100%, by dry mass, of soil particles pass respectively a 75 mm, 19 mm and 9.5 mm sieves. In the first method the soil may contain up to 30%, by dry mass, of soil particles retained on a 37.5 mm sieve, and the third method is applicable only to fine and medium sands which may contain up to 10%, by dry mass, of soil particles retained on a 2 mm sieve (ASTM, 2006b). To summarize, as shown in Figure 2-175, at best, relative density is applicable only to soils with less than 15% of the material being silt or clay and can have gravel up to a diameter of 75 mm provided that 70% of the grain size are less than 37.5 mm and the soil is still cohesionless and free draining.

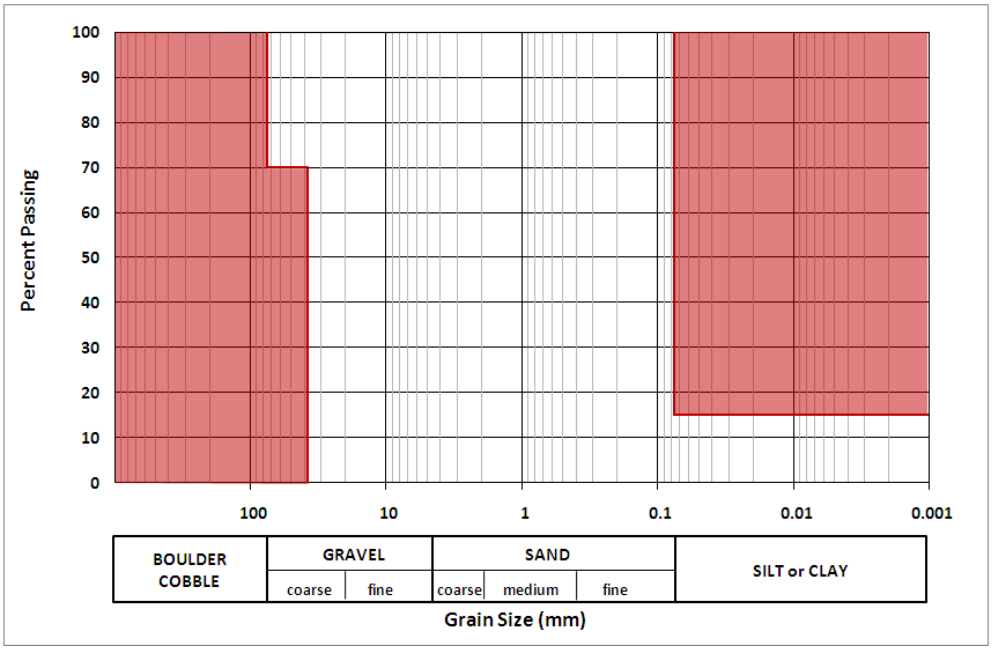

Figure 2-175: Applicable range of relative density (non-shaded areas) as defined by ASTM

ASTM has rightfully introduced the term free draining even though the applicable zone of relative density is for sands and gravels. As much as sands and gravels are assumed to be free draining, the author have come across non-free draining sands with less than 15% fines content, but containing high amounts of clay. For example in the dynamic compaction project of Salam Resort (unpublished), on the seashore of Bahrain, sieve analyses showed that fines content of the soil was less than 20% and the soil was identified as sand; however clay content was relatively higher than normally encountered and approximately 10%. When ground improvement was carried out on the site it was observed that the soil was not draining, as would be expected in sand, and reduction of pore water pressure to initial values required a period of more than one week.

Engineers who have been involved in reclamation projects know very well that even if specifications limit the soil's grain sizes to the limits defined by ASTM, there is still a good chance that due to segregation of material or change of material source, layers or bands of soil with higher fines content will be realised here and there. On the other end, there are many situations where the soil contains larger cobbles and boulders.

When developing a specification it would seem rational to stipulate acceptance criteria that will most likely not require reassessment and revision during the project. In the author's opinion relative density does not comply with this statement, as in the event that further supplementary investigations prove that the soil is non-free draining, then the specifications

will not apply to the soil any longer and alternative criteria must be sought. It may be simply a more reasonable approach to stipulate the alternative specification in the first place.

If the over and undersize percentage of materials are identified in advance, the oversize may be separated or crushed or the material may be mixed to reduce the fines content, but there are techniques, such as dynamic compaction, that can treat soils containing more fines and oversized cobbles than allowed by ASTM (for example, refer to the treatment of rock fill by dynamic compaction at Udevalla, Sweden in Section 2.10.4) and the extra activities and costs could have been avoided by stipulation of an appropriate acceptance criterion.

If over or undersize materials are detected after reclamation, one ill-advised solution may be to remove the soil and to replace it with soil that meets the required grading; however, this is more easily said than done. Alternatively, there are others who may re-define the grading range defined in relative density standards to fit their needs. Of course, these scenarios could be totally avoided simply by defining a reliable criterion.

For many types of free-draining, cohesionless soils, ASTM specified test methods cause a moderate amount of degradation (particle breakdown) of the soil (ASTM, 2006a). When degradation occurs, typically there is an increase in the maximum index density/unit weight obtained, and comparable test results may not be obtained when different size moulds are used to test a given soil. This raises the question of comparability of test results, and as will be later discussed, any small changes to the limit indexes will result in dramatic changes in relative density.

Referring to Holtz (1973b), ASTM (2006a, 2006b) also acknowledges that there are published data to indicate that these test methods have a high degree of variability, but proposes that the variability can be greatly reduced by careful calibration of equipment. Of course, calibration of equipment can only reduce systematic errors caused by equipment conditions, but it will have no effect on random errors. The sources of errors and variations of relative density testing require further review.

2.10.2.2.2 Errors in relative density testing

Relative density testing is subject to a combination of systematic errors, random errors and mistakes. Systematic error is a measure of accuracy and the difference between correct value and the measured average of a set of repeated tests. Random error is the precision of a quantity and is measured by the scatter in the results of a group of repeated tests (Selig and

Ladd, 1973). The distributions of these errors around the true value are shown in Figure 2-176.

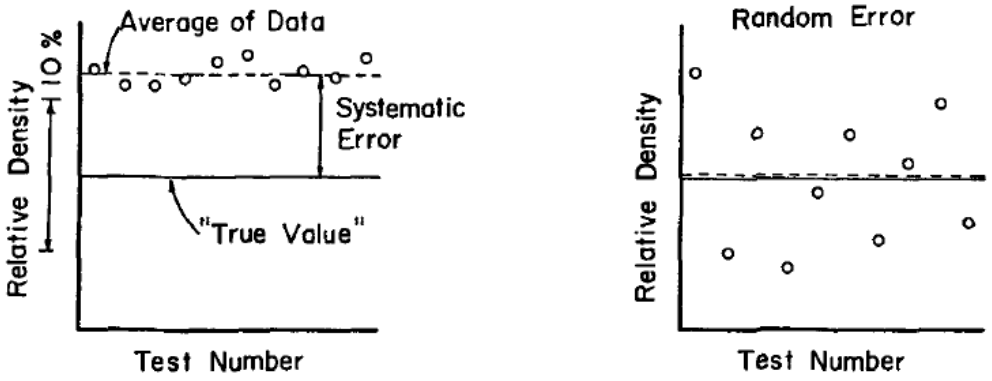

Figure 2-176: Systematic and random errors (Selig and Ladd, 1973)

The reliability of relative density measurements has, for the most part, been taken for granted by most engineers, but not by all. Yoshimi and Tohno (1973) have assumed a statistical approach, and note that since relative density is proportional to (γ_d - γ_{dmin})/ γ_d, even a small variation in γ_d or γ_{dmin} can cause a considerable variation in relative density when γ_d - γ_{dmin} is small; i.e., when relative density is low. For example, when γ_{dmin}= 13.5 kN/m^3, γ_{dmax}= 16.37 kN/m^3, and γ_d= 14.25 kN/m^3, relative density will be 30%. If γ_{dmin} is increased by 1% to 13.635 kN/m^3, D_d reduces to 25.8%, which is 14% less than the initial value. In other words, the relative deviation in relative density is 14 times that of γ_{dmin}.

Yoshimi and Tohno express the influence of dry unit weight random errors on relative density using Equation 2-243:

$$\left(\frac{S_{D_d}}{D_d}\right)^2 = C_{\gamma_{dmax}}{}^2\left(\frac{S_{\gamma_{dmax}}}{\gamma_{dmax}}\right)^2 + C_{\gamma_{dmin}}{}^2\left(\frac{S_{\gamma_{dmin}}}{\gamma_{dmin}}\right)^2 + C_{\gamma_d}{}^2\left(\frac{S_{\gamma_d}}{\gamma_d}\right)^2 \qquad 2\text{-}243$$

The terms in the parentheses are coefficients of variation. S_{Dd}, $S_{\gamma dmax}$, $S_{\gamma dmin}$ and $S_{\gamma d}$ are respectively the standard deviations for D_d, γ_{dmax}, γ_{dmin} and γ_d, and $C_{\gamma dmax}$, $C_{\gamma dmin}$ and $C_{\gamma d}$ are error propagation factors that are expressed in the forms of Equations 2-244 to 2-246.

$$C_{\gamma_{dmax}} = \frac{\gamma_{dmin}}{(\gamma_{dmax} - \gamma_{dmin})} \qquad 2\text{-}244$$

$$C_{\gamma_{dmin}} = \frac{\gamma_{dmax}(1-D_d)}{(\gamma_{dmax}-\gamma_{dmin})D_d} = (C_{\gamma_{dmax}}+1)\frac{1-D_d}{D_d} \quad \text{2-245}$$

$$C_{\gamma_d} = \frac{\gamma_{dmax}}{(\gamma_{dmax}-\gamma_{dmin})D_d} - 1 = \frac{(C_{\gamma_{dmax}}+1)}{D_d} - 1 \quad \text{2-246}$$

As illustrated in Figure 2-177, for the case of $C_{\gamma dmax}$= 4.7 which is a representative value for clean sand with low uniformity, these equations show that while $C_{\gamma dmax}$ is independent of relative density, $C_{\gamma dmin}$ and $C_{\gamma d}$ increase as relative density decreases until they reach infinity when relative density reduces to zero.

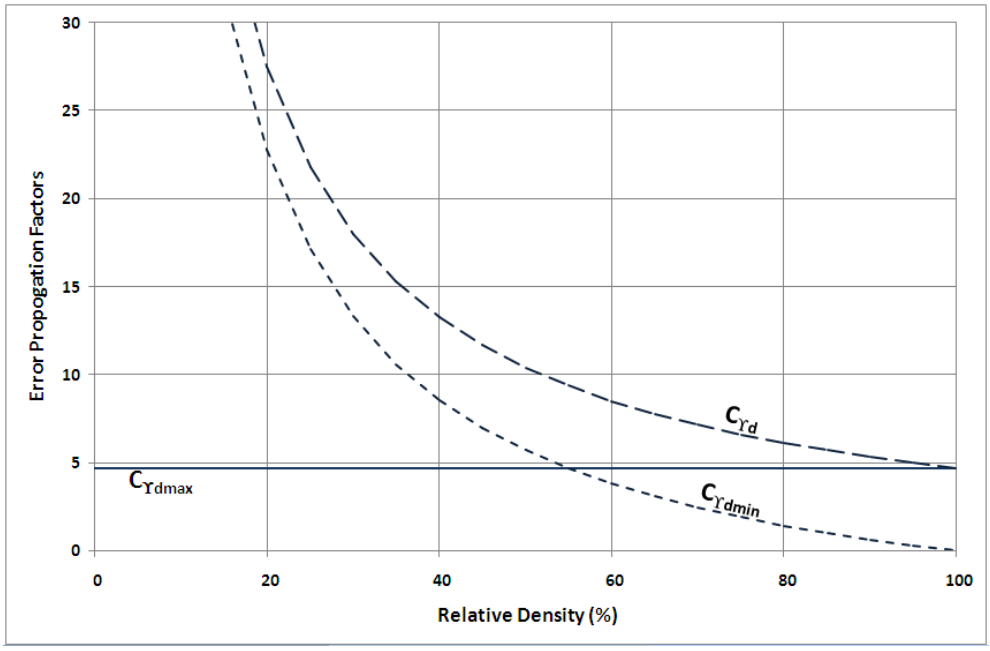

Figure 2-177: Error propagation factors for relative density, redrawn from Yoshimi and Tohno (1973)

Random errors can be reduced to any desired degree by repeating the test and averaging the results (Selig and Ladd, 1973).For the case when the coefficients of variation are equal, for a defined coefficient of variation, the number of measurements, m, for each dry unit weight was calculated by Yoshimi and Tohno (1973) to be as expressed in Equation 2-247.

$$m = \frac{{C_{\gamma_{dmax}}}^2 + {C_{\gamma_{dmin}}}^2 + {C_{\gamma_d}}^2}{\left(\frac{S_{D_d}}{D_d}\right)^2} \quad \text{2-247}$$

For example when $C_{\gamma dmax}$=4.7, if D_d= 50%, (S_{Dd}/D_d)=5% and coefficient of variation equals to 1% then 7 tests must be made for each of the maximum index, minimum index and specimen unit weights. For D_d= 22%, with the previous other parameters, 40 tests for each unit weight will be required. Unfortunately, and even to the acknowledgement of ASTM (2006a, 2006b) it seems that in practice this recommendation of Yoshimi and Tohno has gone unheard of and most commonly, regardless of the value of relative density, only one test for each parameter is carried out.

When studying the influence of dry unit weight systematic errors on relative density, Yoshimi and Tohno (1973) formulate relative deviation in relative density, $\Delta D_d/D_d$, due to a deviation in any one of the dry unit weights; i.e., $\Delta \gamma_{dmax}$, $\Delta \gamma_{dmin}$ and $\Delta \gamma_d$, and express them in the forms of Equations 2-248 to 2-250.

$$\left.\frac{\Delta D_d}{D_d}\right]_{\Delta\gamma_{dmin}=\Delta\gamma=0} = \frac{\gamma_{dmin}}{\gamma_{dmax}-\gamma_{dmin}+\Delta\gamma_{dmax}}\frac{\Delta\gamma_{dmax}}{\gamma_{dmax}} \qquad 2\text{-}248$$

$$\left.\frac{\Delta D_d}{D_d}\right]_{\Delta\gamma_{dmax}=\Delta\gamma=0} = \frac{(1-D_d)\gamma_{dmax}}{D_d(\gamma_{dmax}-\gamma_{dmin}-\Delta\gamma_{dmin})}\frac{\Delta\gamma_{dmin}}{\gamma_{dmin}} \qquad 2\text{-}249$$

$$\left.\frac{\Delta D_d}{D_d}\right]_{\Delta\gamma_{dmax}=\Delta\gamma dmin=0} = \frac{\gamma_d\gamma_{dmin}}{(\gamma_d-\gamma_{dmin})+(\gamma_d+\Delta\gamma_d)}\frac{\Delta\gamma_d}{\gamma_d} \qquad 2\text{-}250$$

For simultaneous errors in γ_{dmax}, γ_{dmin}, and γ_d the resulting values of $\Delta D_d/D_d$ may be added, keeping in mind the correct signs. In view of relatively large values of $\Delta \gamma_{dmax}$ or $\Delta \gamma_{dmin}$ due to the systematic errors of the unit weight measurements, it can be understood that $\Delta D_d/D_d$ may reach tens of per cent.

Referring to Equations 2-8 to 2-242, there are three parameters that must be determined for calculation of relative density; i.e., e_{max}, ρ_{min} or γ_{min} that describes the loosest state of the soil, e_{min}, ρ_{max} or γ_{max} that describes the densest state of the soil and e, ρ_d or γ_d that describes the in-situ state of the soil.

Due to the relative magnitude of the maximum index, minimum index and in-situ dry unit weights, relative density is computed from the ratio of small differences between large numbers (Tavenas et al., 1973). This implies that small variations of large numbers will be

magnified to produce a great variability in the computed result. The simple application of the theory of errors led Tavenas and La Rochelle (1970) to conclude that any laboratory determination of relative density would be affected by a large variability, even if the ASTM standard method was used.

As part of the study of Tavenas et al. (1973) 87 laboratories in the United States and Canada participated in grading tests, minimum and maximum index density tests. Some very important, if not dramatic, conclusions that they were able to draw from their findings included:

- Even though ASTM standard tests for determining the minimum and maximum (index) density of cohesionless materials was considered as "normally accurate" soil mechanics tests with observed coefficient of variability of the order of 2.5 per cent and coefficient of reproducibility of the order of 0.8 per cent, the use of these parameters in the relative density formula leads to a result of poor quality, since it is characterised by coefficients of variability of the order of 15 to 40% and by coefficients of reproducibility of the order of 3 to 15% in most of the usual cases. Thus, and simply due to the formulation of relative density, the variability is multiplied by a factor of 10.

- The variability of the relative density increases as the maximum grain sizes of the tested materials increases. Standard deviations were found to be 60 to 100% larger for gravelly sand than for fine sand. Since the fine sand tested was close to the ideal material with a small maximum grain size and a coefficient of uniformity of the order of 3, and no particles passing sieve 0.075 mm, the variability and reproducibility observed on this material were the best possible with the testing technique. Thus, it cannot be expected to determine any relative density with a width of the 95% interval, less than 10% if the results obtained by one technician only are considered, and less than 40% if the results obtained by different laboratories are analysed. The results obtained by different operators in the same laboratory fell in between.

- A third basic parameter influencing the determination of the relative density is the actual dry unit weight itself. This parameter is also affected by a certain error. In the most important case of the measurement of the in situ unit weight, the methods were such that any value of dry unit weight could not have been defined with an error less than ±30 N/m^3. The error on the in situ dry unit weight had to be combined

to the previously discussed variability to give the final variability of the relative density. As shown in Figure 2-178, Tavenas et al. demonstrate that the width of the 95% interval for the correlation between the in situ dry density and relative density of fine sand and gravelly and is respectively 64% and 94%, which is close to the full range of possible values for the relative density, and assess that under such circumstances the probability of evaluating the correct relative density by a wild guess is at least equal to that of measuring it by the standard method.

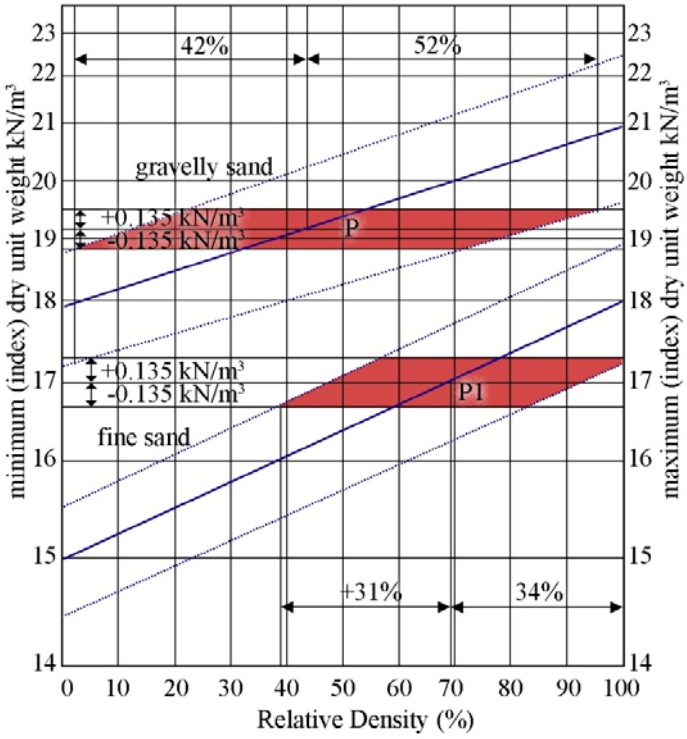

Figure 2-178: Error on the in-situ relative density, redrawn in SI units from Tavenas et al. (1973)

- Due to the very large variability of the relative density between laboratories, the comparison of relative densities measured by different laboratories was totally non-significant. There were important practical implications of this fact: all established correlations between relative density and various properties of cohesionless soils such as standard penetration index, point resistance in a static penetration test, friction angle, modulus of compressibility, shear wave velocity, etc., are useless to anyone but the operator who has established them, since that person is the only one who can reproduce the relative density of the considered soil with sufficient accuracy.

- It appeared that due not so much to the variability of the minimum and maximum unit weights but essentially to the formulation of relative density itself, the resulting accuracy of this parameter was so poor that its use was related to major uncertainties (the best case was of ideal material such as the tested fine sand, and was deemed to be practically meaningless in most of the other cases).

Similarly, Tiedemann (1973) has conducted research on the results of minimum and maximum index unit weight tests performed by 14 US Bureau of Reclamation soil laboratories, and has concluded that based on results obtained from the cooperative test program and other studies, it appeared that the variations associated with the minimum and maximum unit weight tests investigated were approximately the same as, or less than, those associated with the impact-type compaction test. However, when the results are used to compute relative density, large variations can occur. For the extreme variations in both the minimum and maximum density, a dry unit weight of 17.3 kN/m^3 could be reported as a relative density varying from 40 to 76% on a between-laboratory basis or from 52 to 66% if the limiting unit weights were determined by a single operator.

One may argue that in reality the chances of the occurrence of the worst case scenarios as envisaged by Tavenas et al. (1973) and Tiedemann (1973) are quite low. As true as that may be, these worst case scenarios are just an indication that as unlikely as may be, relative density criterion could seriously misrepresent the soil conditions to the point of rejecting a well compacted soil or leading to a total disaster by accepting a loose soil. Of course, there are all the other non-worst case scenarios that nevertheless also lead to misrepresented ground conditions. It would indeed be much more appropriate not to tie a project's destiny to a parameter that is referred to as being as accurate as a guess.

Tiedemann also reports that variatons in duplicate tests were less than for duplicate specimens, indicating that there was considerable variation in the specimen. According to Holtz (1973b) it is usually more difficult to produce uniform samples and specimens of the coarse sand and gravel soils than fine silty and clayey soils. The difficulty usually becomes greater when the soils are cohesionless and as the range of particle sizes increase. This is primarily due to segregation of the material. Segregation can even effect the uniformity of sampling when closely controlled quartering and splitting methods are used. The scooping and placing of cohesionless, coarse-grained soils in moulds for the standard minimum and maximum index density tests can cause segregation, which can produce nonhomogeniety of

gradation within a test specimen and gradation variations between the so-called duplicate specimens.

Similar findings have been also reported by others, such as Gupta and McKeown (1973) who encountered problems for applying relative density criterion for Kettle Generating Station in Canada. In the end they concluded that the effects of variations in minimum unit weight on relative density were startling. They noted that although the variation was decreasing with the increase of relative density, nevertheless, it still created dilemma for effective quality control in the field in terms of enforcing the requirements of 75% relative density as stipulated in the contract.

Gupta and McKeown used four technicians for each test to carry out 10 tests on each soil sample; thus resulting in 40 tests per sample. For the analysis of the tests, they only used those tests that fell within the middle 90% spread. Among the numerous batches of 40 tests, in the best case, relative density at 50% and 75% respectively had errors of ±5% and ±1.6%. In the worst case, a 50% and 75% relative density respectively had errors of ±26% and ±6.6%. This means that a sample with relative density of 50% could have been reported as 64% and a sample with relative density equal to 75% could be reported as 69%. While the true condition of one sample is loose and the other dense, errors may lead to a condition where the material may be practically assumed to have similar test values. Obviously, this may lead to a non-compliance with project specifications solely due to the inherent defaults of the choice of specification. Had Gupta and McKeown not limited the tests to the middle 90% spread, the variations would have been even more concerning.

Reviewing the works of others during the ASTM Symposium for Evaluation of Relative Density and its Role in Geotechnical Projects Involving Cohesionless Soils at the 75th Annual Meeting, Selig and Ladd (1973) assess that the error in γ_{dmax} has the largest effect for high D_d while error in γ_{dmin} has the greatest effect for low D_d and add that, in general, relative density has associated with it a random error of about ±10 to 15 standard deviation and a systematic error of 25 to 30 range. They conclude that in their opinion relative density has value, but that it has frequently been overextended with a false sense of reliability, or improperly used. Ladd and Selig were probably using a mild tone not to upset any supporters of relative density. If there is any value in relative density, with all that has been discussed, the value is not in being an acceptance criterion of ground improvement and it should be sought elsewhere.

2.10.2.2.3 4. A Second Glance at the Standards

After this discussion, it may be interesting to review the ASTM standards (2006a, 2006b) once again. ASTM allows four alternative methods for determination of maximum index density/unit weight of which two methods are on oven dried soil and two are on wet soil. The wet method may be conducted on either oven dried soil to which sufficient water is added or, if preferred, on wet soil from the field.

Although it may be expected that the application of any of the methods should yield the same result, ASTM notes that the wet method can yield significantly higher values of maximum index density/unit weight for some soils, and adds that such a higher maximum index density, when considered along with the minimum index density/unit weight, will be found to significantly affect the value of relative density. ASTM does not define wetness, and it is not clear what would be considered as the minimum water content to be considered as wet.

ASTM notes that although the dry method of testing is often preferred because results can usually be obtained more quickly, as a general rule the wet method should be used if it is established that it produces maximum index densities/unit weights that would significantly affect the use of the value of relative density. However, ASTM does not define what it considers as being significant. Noting that any small changes in limit indexes are magnified several times in changes of relative density, any difference may in fact be significant.

Likewise, ASTM (2006b) specifies three testing methods for determination of minimum index density/unit weight, but allows the individual assigning the test to specify the method to be used. If no method is specified, the provisions of first method shall govern. The two other methods are provided for guidance of testing used in conjunction with special studies, especially where there is not enough material. Once again, surely the application of these three testing methods may yield different results that could result in values of relative density with significant differences.

ASTM (2006a, 2006b) is well aware of relative density deviations and has performed a series of three replicate tests per type and single test per type for poorly graded sand and specifies acceptable ranges of results for it. For single tests, the acceptable range between two results is 1.15 kN/m^3. It has already been discussed that for a much smaller value of 0.135 kN/m^3 Yoshimi and Tohno (1973) calculated 14% change in relative density; hence, it could be expected that the acceptable range of ASTM could result in larger errors.

2.10.2.3 Relative Density Correlations

The unreliability of relative density due to its formulation has complicated its usage as a ground improvement acceptance criterion, but correlation of relative density to other commonly used field tests may appear as an attractive means of applying the philosophy of relative density without the actual implementation of the problematic formulation. Thus, it can be occasionally seen that a project's specification stipulates that the improved ground must exceed a minimum relative density value or curve based on SPT or CPT correlations. Correlations, themselves, are as questionable as the concept of relative density, and have been the subject of discussions by the experts since many years ago. In this section a number of well-established correlations that are commonly referred to will be reviewed, and the unreliability of relative density correlations as acceptance criteria for ground improvement shall be demonstrated.

2.10.2.3.1 Relationship of Relative Density with Soil Characteristics

A fundamental question that crosses the mind is that, irrespective of the limitations and errors that are associated with relative density concept and formulation, would it be true to say that if two soils had the same relative density then they would possess the same physical characteristics and will behave the same? It would have been very satisfying if the reply to this question was positive; however, this is not the case, and the use of relative density correlations based on average sand to predict soil behaviour without considering other parameters can result in poor or misleading predictions.

Youd (1973) conducted a study on the maximum and minimum indexes of 13 specimens of different clean sands with less than 5% fines passing the 0.075 mm sieve, and was able to identify clear relationships between e_{max}, and e_{min}, with particle roundness, grain shape, range of particle sizes defined by the coefficient of uniformity, and the type of gradational curve. Figure 2-179 and Figure 2-180 show the relationship between limit void ratios with roundness and coefficient of uniformity. Youd did not identify a unique relationship between mean particle diameter (D_{50}) and limit void ratios; however, others (Cubrinovski and Ishihara, 1999, Skempton, 1986, Tokimatsu and Yoshimi, 1983) have noted the importance of the effect of particle diameter on relative density-field test relationships.

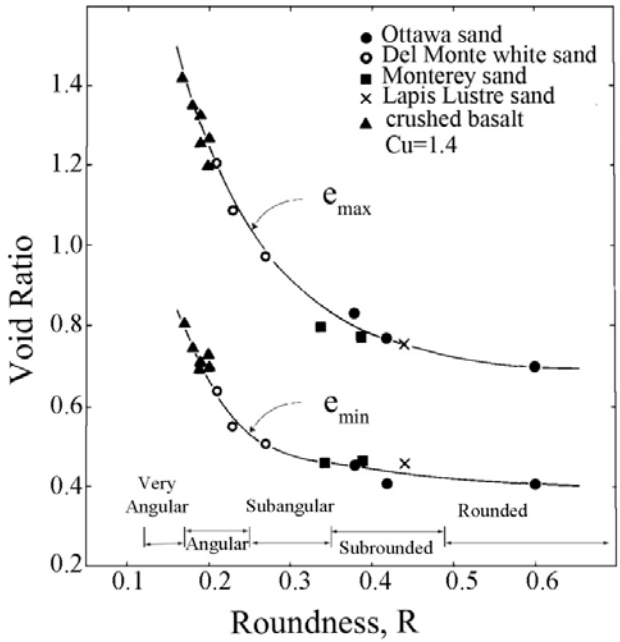

Figure 2-179: Density limits as a function of grain shape for laboratory fractions with Cu=1.4 (Youd, 1973)

Holubec and D'Appolonia (1973) focused their study on the sphericity and the shape of four types of medium to fine sands with the same gradation but varying particle shapes. What they have found is that granular soils at the same relative density can have drastically different engineering properties, and have assessed that the use of relative density criteria in design, without considering particle shape, can result in poor or misleading predictions of soil behaviour. As can be seen in Figure 2-181, Holubec and D'Appolonia show that while both e_{min} and e_{max} increase with the increase of the coefficient of angularity, the increase in e_{max} is considerably more than that for e_{min} and that the difference between these two limits increases with the angularity of the soil particles.

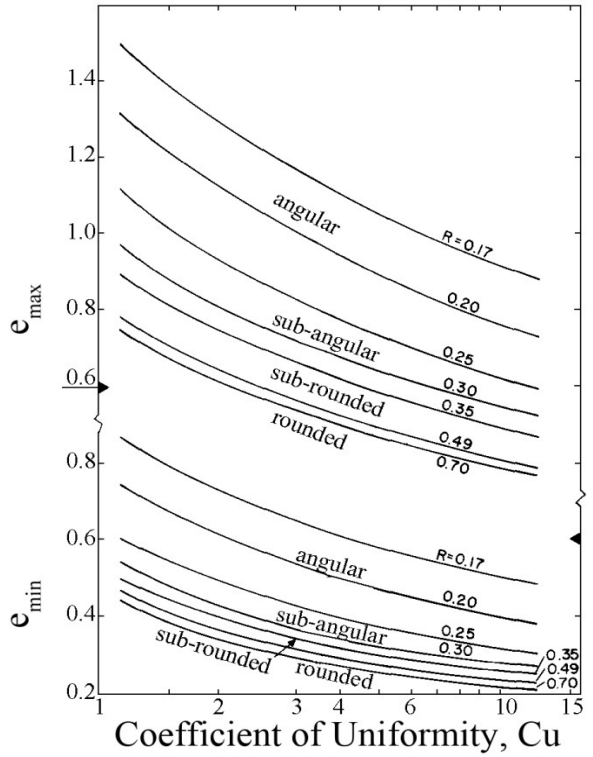

Figure 2-180: Generalized curve for estimating e_{max} and e_{min} from gradational and particle shape characteristics. Curves are only valid for clean sands with normal to moderately skewed grain size distributions. (Youd, 1973)

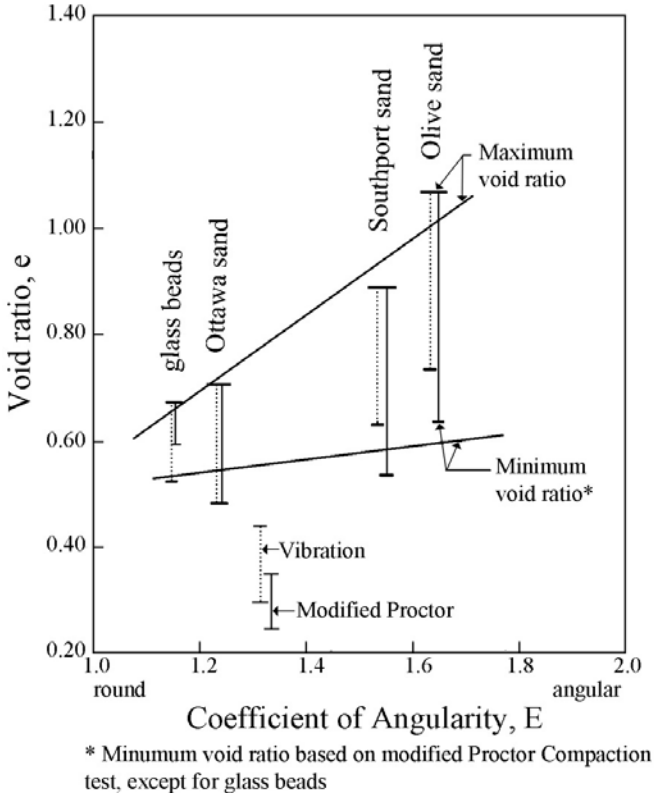

Figure 2-181: Effect of particle shape on minimum and maximum void ratios (Holubec and D'Appolonia, 1973)

It can also been seen from the work of Holubec and D'Appolonia that each of the four sands that they tested had separate and distinct relative density versus friction angle relationships whereas whilst the roundest particles had the least friction angles and exhibited the minimum increase in friction angle with increasing relative density, the sands with angular particles had the highest friction angles with an intermediate increase with increasing relative density. What can be assessed is that friction angle is a function of both relative density and particle shape. In fact, the research suggested that equally large differences in friction angle are possible with variations of particle shape as with changes in relative density.

Stress-strain relations are also influenced by particle shape. Holubec and D'Appolonia show that the more angular the particles are, the greater the failure strain is for a given relative density. They performed a miniature penetration test using a 12.5 mm diameter rod that was driven to a depth of 20 cm in sands that were compacted to selected densities. The data showed a marked increase in the penetration resistance with the increase of angularity of the sand particles. For example, they observed that the required number of blows for sand with angular particles is nearly double the values for sub-rounded sand when relative density is 70%. Conversely, a blow count of 20 indicated a spread in relative densities from 66 to 86%.

More recently, Liu and Lehane (2012) have studied the behaviour of four uniformly graded silica soils with similar mineralogical compositions but with distinctly different particle shapes. The soils were subjected to centrifuge CPT and direct shear tests at different relative densities in dry and saturated states. In these tests gradation and material were controlled to be similar; hence, any differences in test results could be attributed to the grain's sphericity, roundness and roughness.

Figure 2-182 shows the differences between effective peak and critical state friction angles at different effective vertical stresses for the four soils when relative densities were 20%, 50% and 80%. It can be seen that while the general trend is the reduction of friction angle differences at higher effective vertical stresses, the lines fitted to the plotted points of the four soils are distinctly different for any of the three relative densities.

It can be understood from the work of Youd (1973), Holubec and D'Appolonia (1973), and Liu and Lehane (2012) that applying relative density correlations from one type of sand to the other, even if the gradation and mineralogy are similar, could lead to very misleading results.

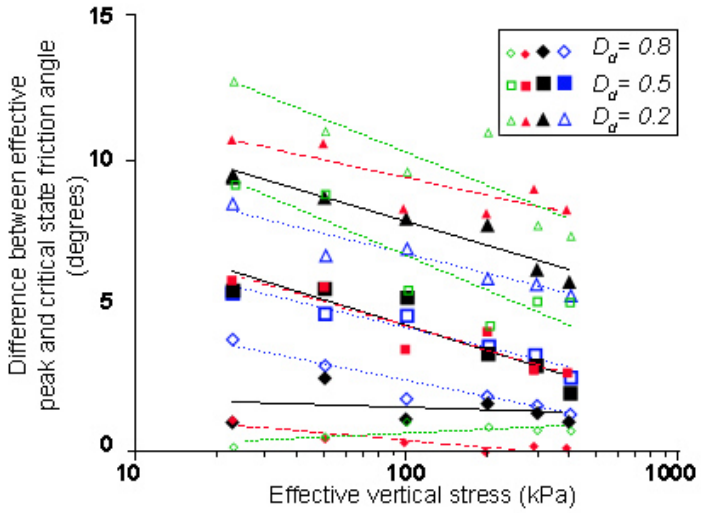

Figure 2-182: Difference between effective peak and critical state friction angles in four different uniformly graded silica soils with similar mineralogical compositions at different relative densities; reconstructed from Liu and Lehane (2012)

2.10.2.3.2 Correlation of relative density with field tests

By definition correlation is a statistical relation between two or more variables such that systematic changes in the value of one variable are accompanied by systematic changes in the other. Correlations are not physical laws or theorems; they are simply statistical relations and only meaningful once their scatters, deviations and variances are known. In general, empirical correlations are derived from a set of specified data under special conditions that are not necessarily applicable to other data, soil and conditions. In addition to the inherent drawbacks and limitations of relative density, when consideration of a correlation's applicable domain is not taken into account, inaccurate and unrepresentative outcomes should be expected.

This section will limit its review and discussion to some of the better known relative density - field test relationships as discussing all research is beyond the scope of this thesis; however, the trend of this discussion and its conclusions is equally applicable to any other such correlations. Also, this discussion and review will not include any limitations and drawbacks that are associated with any of the field testing methods as that is a different issue and not directly associated with the unreliability of relative density.

2.10.2.3.2.1 Relative density – Standard Penetration Test Correlations

While the first correlations between relative density and SPT were qualitatively realised by Terzaghi and Peck (1948), probably the best known and most referenced estimation method has been developed by Gibbs and Holtz (1957) based on data obtained from calibration chamber tests performed at the US Bureau of Reclamation. Gibbs and Holtz performed tests on a fine grained and a coarse grained sand by placing them at controlled densities and moistures in a heavy steel tank, 0.9 m in diameter and 1.2 m in height. Overburden pressure was realised by load plates and loading springs. Maximum density was determined by vibrating the saturated material to constant density or by using extreme compaction hammer blows, whichever gave higher values, in a container of known volume. Minimum density was found by lightly pouring the dry material into the container of known volume.

Gibbs and Holtz carried out this research in 1957; i.e., 12 years before ASTM published its first standard on relative density (ASTM, 1969). Obviously the testing procedure for measuring limit densities could not have been as per a non-existent standard of its time, and even small differences in limit indexes originating from Gibbs and Holtz's testing method could have had significant impacts on the calculated relative densities.

Unlike the rather well known Gibbs-Holtz relative density versus overburden pressure diagram that has been referenced in numerous publications, those who have actually seen Gibbs and Holtz's (1957) paper know that they published a relative density versus penetration resistance chart, as reconstructed in Figure 2-183, not the better known chart of Figure 2-184 that first appeared in Bureau of Reclamation's (1960) Earth Manual in accordance to Gibbs and Holtz. It is noted that the Bureau of Reclamation (1998) does not use the term correlation, but rather refers to the chart as the criterion for predicting relative density of sand. In addition to the limitations that ASTM (2006a, 2006b) has in place for the application of relative density, Bureau of Reclamation also limits the use of its chart to sands containing less than 10% fines and no gravels.

Osterberg and Varaksin (1973) extracted frozen soil samples from Lake Michigan and compared them with what was estimated by Gibbs and Holtz. Predictions were quite different from reality, and it was concluded that relative densities obtained from SPT using Gibbs and Holtz chart had no relationship to the actual relative densities. This study was an indication that relative density correlation of one sand cannot be extended to all other sands.

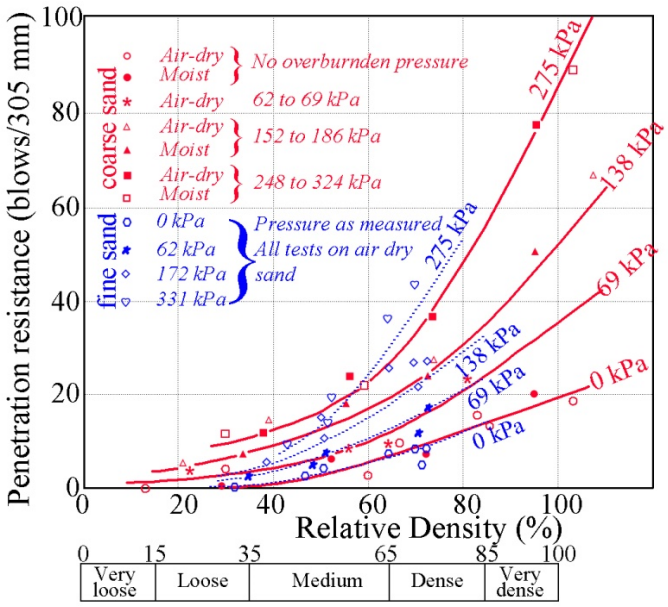

Figure 2-183: Relative density versus penetration resistance curves for fine and coarse sands, reconstructed from Gibbs and Holtz (1957)

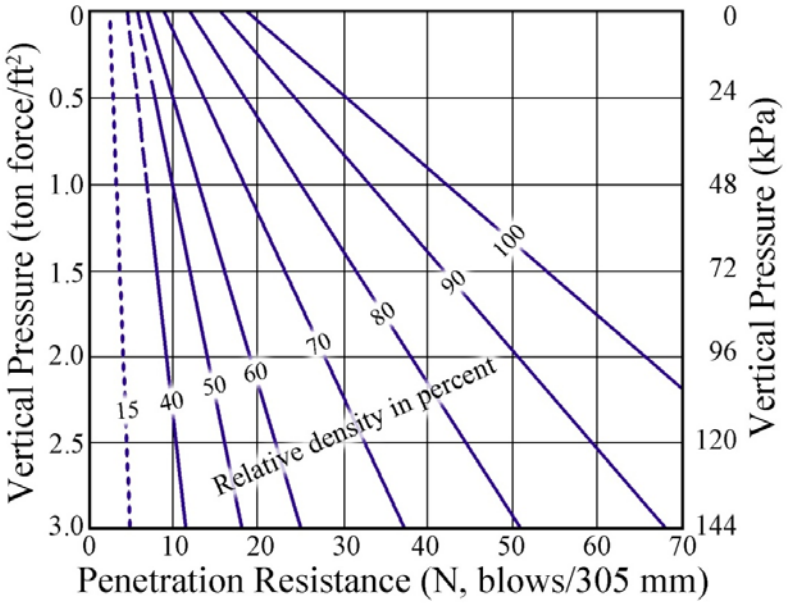

Figure 2-184: Criterion for predicting relative density of sand from the penetration resistance test (Bureau of Reclamation, 1998)

Contrary to the general over confidence by others, Holtz (1973a) does not share the same unconditional and unlimited trust that others have for their chart. In the discussion on the results of Osterberg and Varaksin (1973), Holtz notes that everyone should recognise that the Standard Penetration Test is a relatively crude test, and no one should expect to determine the relative density of sands to the nearest one per cent or anything like that, and further adds that he and Gibbs developed a set of correlations to take into account the effect of overburden pressures, and that they never indicated that the sets of curves developed at

that time were necessarily applicable to all cohesionless soils under all conditions. More importantly he clarifies that they had always stressed on relative density trends indicated by SPT values rather than the specific individual values. This discussion suggests that the research of Gibbs and Holtz may have been blown out of proportion, and rather than acknowledging the trend of relative density versus overburden pressure it is used systematically for something that was never the intention.

Meyerhof (1957) has formulated the coarse sand graph of Gibbs and Holtz (1957) and expressed it in the form of Equations 2-251 or 2-252 (after conversion to SI units); however, in practice this equation is often extended to most types of sands, regardless of the soil particle size and shape, gradation and mineralogy. Obviously, this will further cast doubt on the reliability of the correlation as it is very clear in the original Gibbs and Holtz research that the fine and coarse sand curves do not coincide.

$$N = (17 + 0.25\sigma'_v){D_d}^2 \qquad 2\text{-}251$$

$$D_d = \sqrt{\frac{N}{17 + 0.25\sigma'_v}} \qquad 2\text{-}252$$

N= SPT blow count

D_d= relative density expressed as a ratio (not percentage)

σ'_v= effective vertical stress (kPa)

In lieu of Equation 1-12, Haldar and Tang (1979) have approximated Gibbs and Holtz's relative density correlation using Equation 2-253 (after conversion to SI units).

$$N = 20{D_d}^{2.5} + 0.21\sigma'_v{D_d}^2 \qquad 2\text{-}253$$

Haldar and Tang who note the difficulty of obtaining data that actually includes measurements of D_d, *N* values and σ'_v have plotted measured versus calculated (using Gibbs and Holtz's relationship) relative density of what they could gather (Gibbs and Holtz, 1957, Marcuson III and Bieganousky, 1977, Moretto, 1954, Varaksin, 1970, Wu, 1957) onto the graph of Figure 2-185. It can be seen that there is considerable spread about the 45^o bisecting parity line. The majority of data is above the 45^o line, suggesting that Gibbs and Holtz's

relationship may be non-conservative. Figure 7 also shows a mean line, an upper bound (line B) and a lower bound (line E). For a given value of relative density calculated from Gibbs and Holtz's relationship, the measured relative density may be assumed to follow a triangular distribution between the upper and lower bounds and be symmetrical about the mean line. On this basis, the mean measured relative density is only 75% of the calculated value and the scatter around the mean has a coefficient of variation of 27% which is constant at any relative density calculated. Haldar and Tang conclude that except for sand exhibiting a small difference between the limit indexes, the uncertainty in direct laboratory determination of in-situ relative density (which is prone to large errors) is expected to be less than estimations using Gibbs and Holtz's relationship for normally consolidated deposits, and that a systematic bias appears to exist in Gibbs and Holtz's prediction relationship.

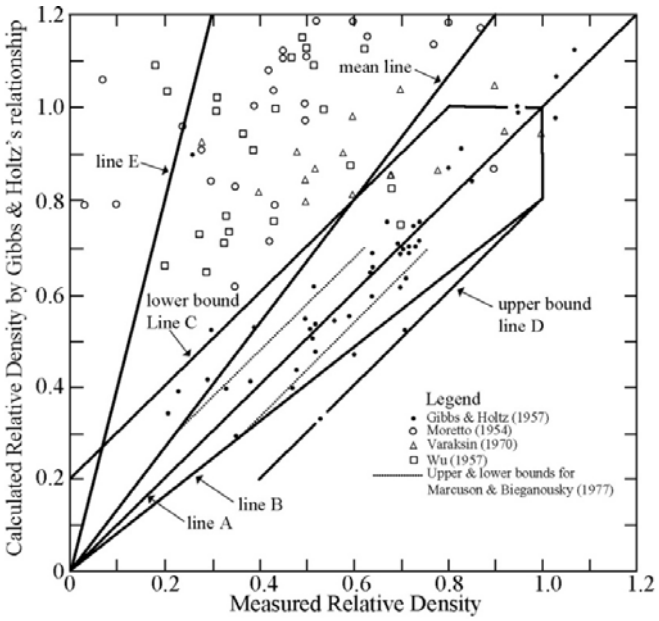

Figure 2-185: Comparison of measured versus calculated relative density using Gibbs and Holtz's relationship (Haldar and Tang, 1979)

Peck and Bazaraa (1969) proposed Equations 2-254 and 2-255 (after conversion to SI Units) for predicting relative density. Comparison of these relations will show that for equal *N* values, these equations will consistently yield higher relative density estimates than Gibbs and Holtz's relationship.

$$D_d = \sqrt{\frac{N}{20 + 0.84\sigma'_v}} \qquad \text{for } \sigma'_v < 72\text{kPa} \qquad \text{2-254}$$

$$D_d = \sqrt{\frac{N}{65 + 0.21\sigma'_v}} \qquad \text{for } \sigma'_v \geq 72\text{kPa} \qquad \text{2-255}$$

Lacroix and Horns (1973) note that it is their experience Gibbs and Holtz's method of predicting relative density yields results that are too high for heavily compacted fill. As noted by Peck and Bazaraa (1969), they also agree that while Gibbs and Holtz greatly underestimate *N* values corresponding to 100% relative density, Bazaraa's (1967) relationship was in better agreement with the blow count data.

Marcuson III (1978) who refers to a study on four sands at various relative densities under overburden pressures in the laboratory of the US Army Waterways Experiment Station (WES) concluded that a simple family of curves relating *N* values, overburden pressure and relative density for all sands under all conditions is not valid. He also concluded that based on comparisons between the relationships presented by Gibbs and Holtz, Bazaraa and WES, SPT is not sufficiently accurate to be recommended for final evaluation of the density or relative density, unless site specific correlations are developed.

Skempton (1986) proposes the relationship between relative density and *N* values in the general form of Equation 2-256, with a and b as two parameters. Skempton tested five different types of sand and proposed values for a and b ranging respectively from 15 to 30 and from 17 to 24 in the imperial system (ton/ft^2). It can be seen that the values for these parameters can be respectively 100% and 40% more than the least values. Inclusion of Bazaraa (1967) would even further increase the figures respectively to 300% and 47%. This clearly suggests that the specific studies of one site cannot be used on other sites so simply.

$$D_d = \sqrt{\frac{N}{a + b\sigma'_v}} \qquad \text{2-256}$$

Among his observations, Skempton (1986) notes that at a given relative density and overburden pressure, *N* values are higher for sands with larger grain sizes (D_{50}). He also assesses that there is direct evidence that aging of sand will increase the SPT blow counts (also refer to Section 2.5.6). This suggests that not only is relative density influenced by numerous other parameters such as gradation, particle size, overburden pressure, mineralogy and particle shape, and hence its correlation in one sand is not reliable for any

other sand, but even the correlation for a soil at a specific time or state may be not valid and applicable at other times and conditions. Skempton also identifies a relationship between the effects of over consolidation and relative density, and introduces an over consolidation coefficient, C_{oc}, into Equation 2-256 to derive Equation 2-257. C_{oc} itself can be calculated from Equation 2-258.

$$D_d = \sqrt{\frac{N}{a + C_{oc} b \sigma'_v}} \qquad 2\text{-}257$$

$$C_{oc} = \frac{1 + 2K_O}{1 + 2K_{ONC}} \qquad 2\text{-}258$$

K_{ONC} and K_O are the ratio of effective horizontal to vertical stresses respectively when the soil is normally consolidated and over consolidated. Skempton refers to Mayne and Kulhawy (1982) for determining these coefficients as a first approximation according to Equations 2-259 and 2-260.

$$K_{ONC} = 1 - \sin \varphi' \qquad 2\text{-}259$$

$$K_O = K_{ONC} (OCR)^{\sin \varphi'} \qquad 2\text{-}260$$

OCR= over consolidation ratio

φ'= effective internal friction angle

Tokimatsu and Yoshimi (1983) who were studying soil liquefaction modified Equation 2-252 to Equation 2-261 by taking into account the effect of fines content, F_c, and introducing ΔN_f as a correction term (refer to Table 2-28). However, they themselves did not demonstrate confidence in their proposed equation, and note that its application had yet to be proven.

$$D_d = 0.21 \sqrt{\frac{N}{0.7 + \frac{\sigma'_v}{98}} + \frac{\Delta N_f}{1.7}} \qquad 2\text{-}261$$

Fines content (%)	ΔN_f

0-5	0
5-10	interpolate
10-	$0.1F_c$+4

Table 2-28: ΔN_f – fines content correlation (Tokimatsu and Yoshimi, 1983)

More recently, Hatanaka and Feng (2006) have carried out a comparative study on high quality undisturbed samples recovered by the in-situ freezing method. The material used in this study was less than 4.75 mm in size and D_{50} was less than 1 mm. They then compared the measured and calculated values of relative density using Meyerhof (1957), Bazaraa (1967) and Tokimatsu and Yoshimi (1983). As shown in Figure 8, the estimated values of relative density based on Meyerhof's method were in the range of +15% to -45% of the measured values. Similar to Haldar and Tang (1979), this research also shows a large scatter of results about the prediction equation; however, contrary to Haldar and Tang, the scatter is mostly concentrated on the lower side of the bisecting parity line, suggesting that Meyerhof's equation is generally underestimating relative density. Similar results were also obtained when the correlation of Tokimatsu and Yoshimi (1983) was used. In this case, the range of estimated to measured relative density was from +25% to -20%.

Tatsuoka et al. (1978) who examined the accuracy of Meyerhof's (1957) expression by studying the results of SPT on normally consolidated sandy deposits and conventional undisturbed samples made a similar assessment, and concluded that Meyerhof's formulation tends to underestimate the relative density of fine sands and silty sands.

For estimating relative density, Cubrinovski and Ishihara (1999) note the importance of grain size and propose Equation 2-262.

$$D_d = \sqrt{\frac{N_{78}(e_{max} - e_{min})^{1.7}}{9}} \sqrt{\frac{98}{\sigma'_v}} \qquad 2\text{-}262$$

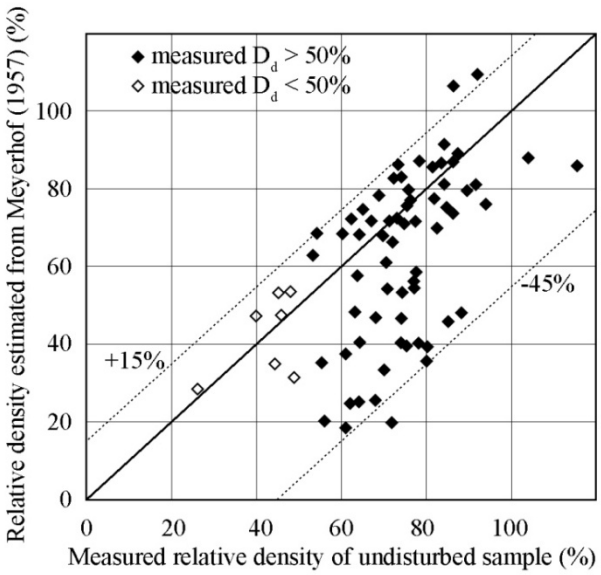

Figure 2-186: Figure 8: Comparison of measured versus calculated relative density using Meyerhof's equation (Hatanaka and Feng, 2006)

N_{78}= SPT blow count corresponding to an energy rod ratio of about 78% from the theoretical free-fall energy.

Cubrinovski and Ishihara report that by using Equation 2-262, in 84% of instances they were able to calculate relative density within a deviation of 20% from the measured values, and more than half the calculations were within 10% deviation. Although this amount of accuracy is by no means sufficient enough to reliably establish an acceptance criterion upon, in any case, here we are dealing with three parameters, two (limit void ratios) of which are included in the original definition of relative density, and the third (N value) is a function of the in-situ density. It may be simply more appropriate to use the definition of relative density (ASTM, 2006a and 2006b) to calculate a value which is prone to error rather than going to the trouble of estimating a value which may be even more erroneous and misleading.

We can review or introduce many other *SPT-D_d* correlations and continue this discussion endlessly; however, what is evident and established is that due to the numerous other parameters that influence the outcome, SPT-relative density correlations will have an unreliably large amount of scatter, and cannot be trusted as ground improvement criteria.

2.10.2.3.2.2 Relative density – Cone Penetration Test Correlations

Many, for example Jamiolkowski et al. (2001), note that the first CPT versus relative density correlation was published by Schmertmann (1976). This is not entirely accurate as the

authors are aware of at least one previous publication by Schmertmann (1975) and a reference by Schmertmann (1978) to Mitchell and Gardner (1975).

Although the author agrees that Schmertmann's 1976 publication should be recognised as an early research on the subject, it has unfortunately been published in the form of a contract report for Waterways Experimental Station and today, this document is not even available in WES's own library (Dolan, 2011). The author has unsuccessfully attempted to obtain a copy of the report through numerous sources, and to date has not met anyone who has actually read the publication. We can only speculate that many researchers who are more recently referring to this publication have also never read the original publication, and are simply citing information from other publications. This can be quite concerning due to possible publication errors, misinterpretations or the fact that each of the intermediate authors only extract that scope of work that is relevant to their own study. By reviewing Schmertmann (1978) and other research such as Villet and Mitchell (1981) the author understands that the updated correlation of Schmertmann (1976) is the same as what was later published in Schmertmann (1978).

Schmertmann (1978) who himself is aware that cone resistance is significantly affected by grain size distribution, cementing, lateral stresses, depth of overburden, compressibility, pore pressure and thin layer effects modifies and updates his earlier work (Schmertmann, 1975) after performing 80 more tests in a calibration chamber with a 1.2 m diameter on two artificial sands with opposite extreme crushabilities, two natural fine sands, and one natural and one artificial medium sand, and proposes a correlation chart which only takes into account the effect of vertical effective stress and is for normally consolidated, recent, uncemented fine SP sands. He also proposes a correction factor for converting over consolidated sands' cone resistances, q_{cOC}, to normally consolidated sands' cone resistances, q_{cNC}. Once simplified, the expression will take the form of Equation 2-263.

$$\frac{q_{cOC}}{q_{cNC}} = 1 + \frac{3}{4}(4OCR^{0.42} - 1) \qquad 2\text{-}263$$

As shown in Figure 2-187, there are significant differences between the relative density estimations of Schmertmann (1975) and Schmertmann (1978). Although the latter publication does not show the scatter of testing results, Schmertmann does note that for clean quartz sands his chart is able to estimate relative density with a standard deviation of

about 10%. The standard deviation of Schmertmann (1975) was 7%. This suggests that irrespective of the scatter that one may experience in one study, there is a strong possibility that the correlation would be almost meaningless for another soil.

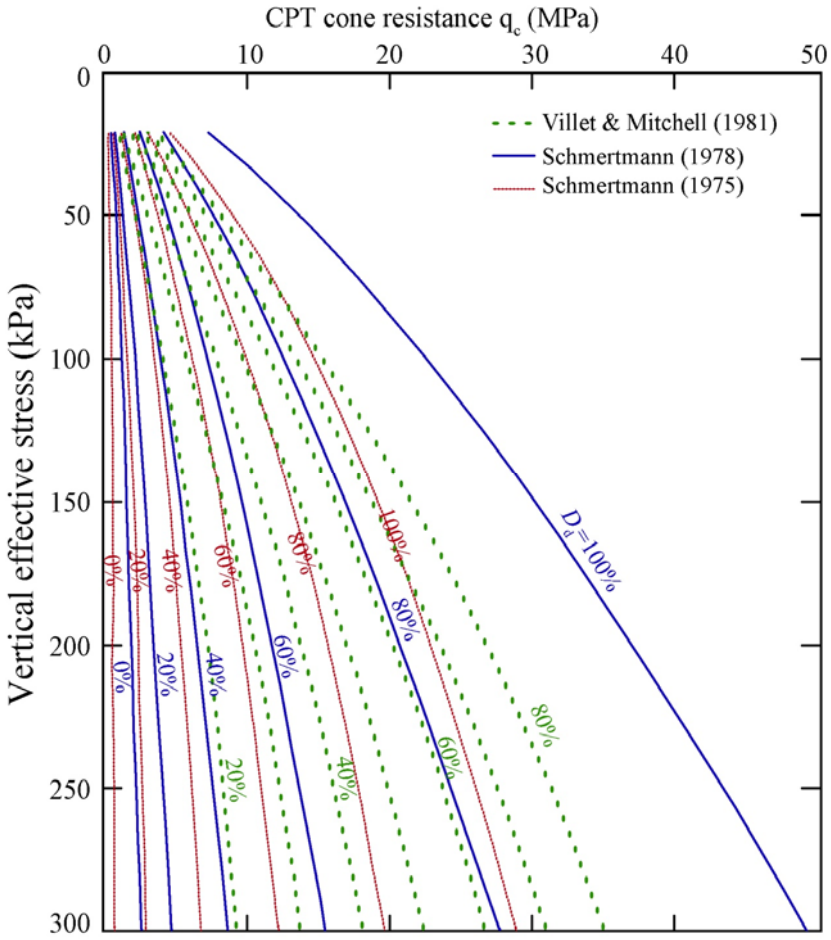

Figure 2-187: Comparison of relative density – CPT cone resistance relationships for Schmertmann (1975), Schmertmann (1978) and Villet and Mitchell (1981)

This has also been observed by Villet and Mitchell who performed a series of tests on four gradations of a commercially available windblown dune sand in a calibration chamber with a diameter of 0.76 m and height of 0.8m. The sands were mainly of quartz and feldspar grains and sub-rounded to sub-angular in shape.

The relationship of Villet and Mitchell is also shown in Figure 2-187. The differences between Villet and Mitchell's measurements and Schmertmann (1978) are significant and from as low as 20% in dense sand with lesser vertical effective stress to 140% for loose sand subject to more vertical effective stress. This is shown in Table 2-29. After comparing their calibration chambers and chamber boundary conditions, Villet and Mitchell conclude that these large differences are due to soil type, thus suggesting that cone resistance, vertical stress, relative

density relationships are not unique and universal for all sands, but rather a function of the sand being penetrated. This conclusion is applicable to any other research that defines a relationship between these parameters.

Vertical effective stress (kPa)	q_c ratios at relative densities of			
	20%	40%	60%	80%
100	1.7	1.9	1.5	1.2
200	2.0	2.1	1.7	1.3
300	2.4	2.2	1.8	1.3

Table 2-29: The ratio of qc measured in Villet and Mitchell (1981) to q_c predicted by Schmertmann (1978) (after Villet and Mitchell)

In fact, had Villet and Mitchell used the same calibration chamber as Schmertmann then the differences would have been even larger. A number of researchers such as Parkin (1977) and Parkin and Lunne (1982) have studied the effects of calibration chamber size and boundary conditions. Parkin's results indicate that calibration chamber diameter ratio to the CPT cone diameter and boundary conditions affect the test results whereas either decreasing diameter ratio or maintaining constant stress rather than constant volume boundary conditions results in lower cone resistance.

In addition to the corrections that may be necessary due to the geometry and boundary conditions of the calibration chamber, Bolton and Gui (1993) mention the simulation method of overburden pressure by surcharging as another limitation of the calibration chamber as the effect of stress gradient due to the self-weight of the soil cannot be simulated in this way. Bolton and Gui conclude that the results obtained from calibration chambers always leave room for questioning, and propose the use of centrifuge testing.

Irrespective of Bolton and Gui's view, calibration chamber testing has remained the dominant approach for developing relative density – CPT correlations. Baldi et al. (1986) who have proposed one of the most popular correlations performed calibration chamber tests on Ticino sand and Hokksund sand. They proposed an expression in the form of Equation 2-264.

$$D_d = \frac{1}{C_2} \ln \left[\frac{q_c}{C_o \sigma'^{C_1}} \right] \qquad 2\text{-}264$$

C_o, C_1, and C_2 = experimental coefficients

Baldi et al. then refer to earlier work by themselves, and define σ' as effective vertical stress if the sand is normally consolidated or as the effective horizontal stress or effective mean stress if the soil is over consolidated. This was based on the fact that using effective vertical stresses in over consolidated sands led to an overestimation of relative density, as also observed for SPT.

Although Baldi et al. propose experimental coefficients for 10 cases of normally consolidated, over consolidated and normally/over consolidated conditions for both Ticino sand and Hokksund sand, for some unknown reason, the normally consolidated Ticino sand has become the better known and popular correlation as expressed in Equation 2-265 and what will generally appear in one form or the other when relative density correlations are used as ground improvement acceptance criteria.

$$D_d = \frac{1}{2.41} \ln \left[\frac{q_c}{157 {\sigma'_v}^{0.55}} \right] \qquad 2\text{-}265$$

Had normally consolidated Hokksund sand gained fame, the expression would have had been as shown in Equation 2-266. The difference between predicted relative density values using Equations 2-265 and 2-266 increases with effective vertical stress and the reciprocal of cone resistance and can be more than 20%. This is yet another example of the fact that relative density correlations are not unique and are dependent on soil type.

$$D_d = \frac{1}{3.29} \ln \left[\frac{q_c}{86 {\sigma'_v}^{0.53}} \right] \qquad 2\text{-}266$$

In line with the above, Jamiolkowski et al. (2001) have proposed Equation 1-28 using Ticino sand, Hukksund sand and Toyoura sand. Here, the data scatter is more for each of the Ticino sand or Hukksund sand equations. Equation 1-28 yields the lowest estimate of relative density as compared to Equations 2-265 and 2-266 in most cases, except in loose sand at high effective vertical stresses.

$$D_d = \frac{1}{3.10} \ln \left[\frac{{q_c}/{98.1}}{17.68 \left({\sigma'_v}/{98.1} \right)^{0.50}} \right] \qquad \text{2-267}$$

It should be noted that Jamiolkowski is well aware of the unreliability of relative density as a criterion, and is merely proposing expressions to better the estimate of relative density. Jamiolkowski and Pasqualini (1992) note that quality control only on values of relative density can be insufficient to evaluate the ground modifications achieved by compaction. Even if effective horizontal stresses are used in the estimation expression, they conclude that important factors such as compressibility, aging, and the presence of fines limits the use of correlations as a guide for evaluating in-situ density of clean, predominantly silica sands of recent, uncemented deposits. Evaluation of relative density in over consolidated sands becomes less reliable because of the inherent difficulties in proper assessment of effective horizontal stresses for improved soils.

Relative density correlations are even more unreliable when it comes to calcareous sands. Almeida et al. (1992) who carry out calibration chamber tests on the calcareous Quiou sand conclude that for the same relative density, cone resistance in the calcareous sand is well up to half the value of q_c measured in the silica Ticino sand. The observed trend in the differences was greater for higher relative densities.

More recently, Al Hamoud and Wehr (2006) report that based on correlation charts of Robertson and Campanella (1985), relative density of 60% was required for land reclamation projects (Palm Jumeira) in Dubai (The authors note that there are no such charts in Robertson and Campallena's cited publication and Al Hamoud and Wehr have probably made a mistake in their reference). Due to the difficulties in achieving the requested penetration resistance in some zones of the compacted fill, a need was felt to verify whether silica sand based correlation was equally applicable to calcareous sand.

Al Hamoud and Wehr refer to the unpublished work of Gudehus and Cudmani who had performed calibration chamber tests on Dubai's calcareous sand and Karlruhe's quartz sand. According to Al Hamoud and Wehr the calibration chamber diameter and height were respectively 0.95 m and 1.5 m. The diameter of the CPT rod used in the test was 36 mm. Without entering into a detailed discussion Al Hamoud and Wehr state that a shell correlation (correction) factor of 1.5 for depths greater than 8 m, 1.6 for depths of 4 to 8 m, and 1.7 for

depths less than 4 m must be applied to Dubai sand. According to this study, these correlation factors should be seen as lower limit and conservative for calcareous sand if the material in the field is much coarser than the soil fractions used in the experiments since larger shells crush easier than very small ones. They also note that penetration resistance for Dubai sand was reported to be about 37% lower than that of Karlsruhe sand for a medium dense state. They also divide the best fit exponential curves of Dubai sand to a number of other silica sands to derive a shell correlation factor f_{shell} which is expressed in Equation 2-268.

$$f_{shell} = 0.46D_d + 1.3629 \qquad 2\text{-}268$$

Comparing Dubai sand with Karlsruhe sand demonstrates that, as previously mentioned, there is no unique relationship between relative density and cone resistance. At the same time, the cone resistance difference between Dubai sand and Karlsruhe sand does not mean that the same difference would have been observed if the same sand (referenced incorrectly by Al Hamoud and Wehr) as the project's acceptance criteria was used for. The same is equally true for the expression that was derived in Equation 1-29. In fact, entering a relative density of 0.6 into Equation 1-29 will yield a correlation factor of 1.6389 which, if used, would have resulted in about 10% overestimation of Dubai sand relative density at depths deeper than 8 m.

Furthermore, the calibration chamber diameter to cone diameter ratio in this testing programme was 26.4. This is almost half of what Parkin and Lunne (1982) propose for boundary effects to become negligible in normally consolidated dense sands. With the small ratio that has been used by Al Hamoud and Wehr, the difference between the calibration chamber test and the project's acceptance criteria may have simply been due to the boundary effects.

2.10.3 Reclamations

It is the author's observation that while most engineers well understand that dumped fills on land are non-engineered fills, and subject to numerous geotechnical problems such as low bearing capacity, creep and excessive settlements under external loads, many do not have an equal comprehension when (sand) filling is done in the sea as reclamation. Perhaps this is due to the fact that those engineers are not acquainted with ground improvement techniques, and hoping that constructing an engineered fill above ground water level will

alleviate future foundation problems. Unfortunately, reclamations systematically realise loose to very loose fills that, as a least, bear the same problems as land based non-engineered fills.

Reclamation can either be by dump trucks tipping fill into the sea or by hydraulic placement from the sea. Sladen and Hewitt (1989), Lee et al. (1999), Lee et al. (2000), Lee (2001) and Na et al. (2005) have studied the effects of placement methods on the geotechnical behavior of sand fills.

Figure 2-188: Dump truck tipping fill into the sea

The density of sand that is dumped by trucks (Figure 2-188), and then pushed into the sea by a bulldozer is usually low, with relative density of about 20%. Exceptions can be thin layers that have been compacted by the traffic of earthmoving equipment. Hydraulic placement can be subaqueous by hoppers or bottom dump barges. When possible sand is discharged by means of a big door located on the bottom of the hull, but when the water is shallow alternative methods; i.e., pipeline discharge or subaerial rainbow discharge will be used. In pipeline discharge low velocity water-sand slurry is pumped; however, in the rainbow method the dredger sprays a high velocity water-sand mixture onto the reclamation. These processes are schematically shown in Figure 2-189.

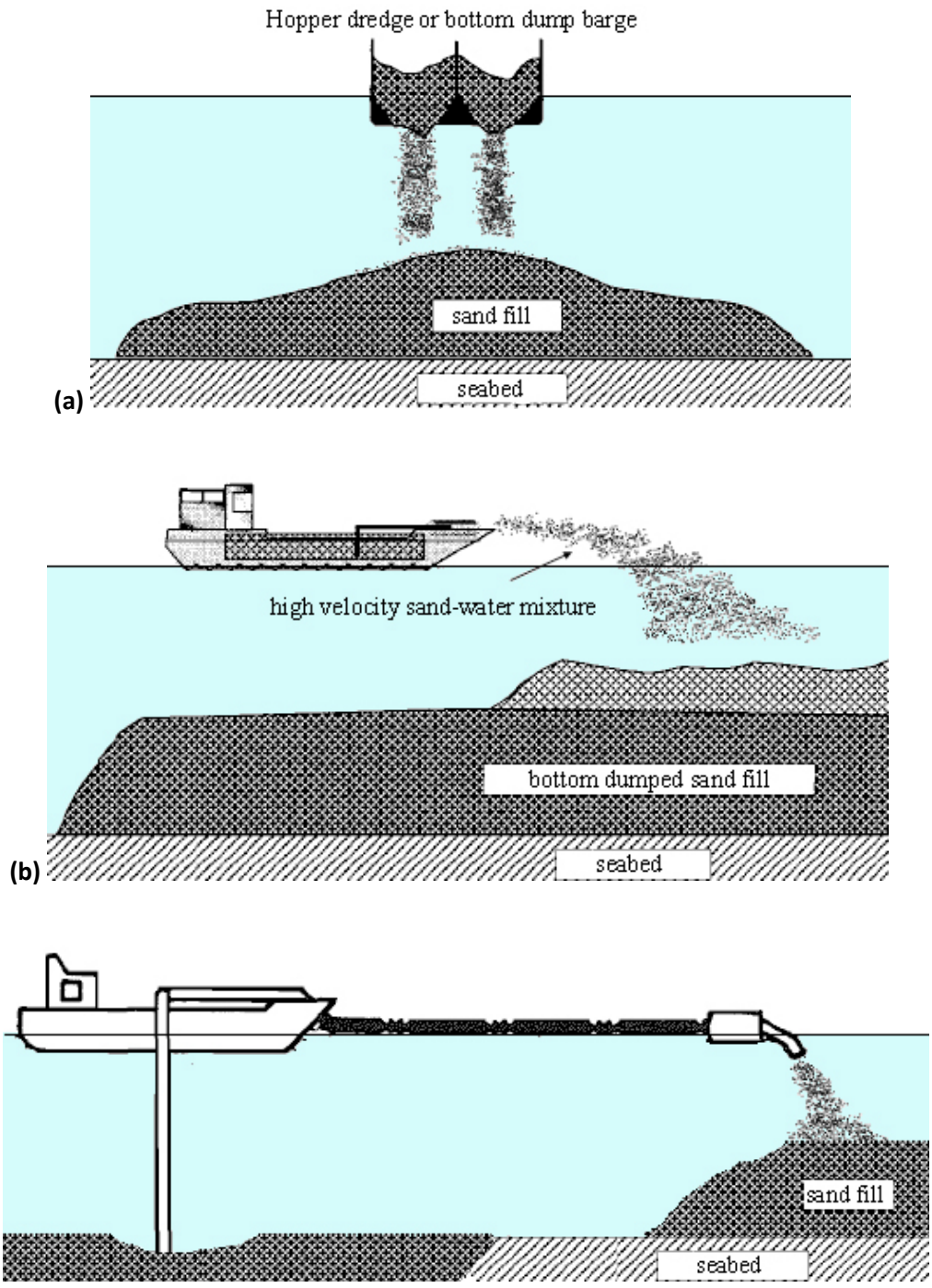

Figure 2-189: (a) subaqueous discharge by hopper or bottom dump barge (b) subaerial rainbow discharge (c) pipeline discharge, redrawn from Lee et al. (1999)

The variation in fill densities achievable by hydraulic placement is large and closely related to the placement method. Hopper placed sand is denser than pipeline placed sand. Sand deposited by hydraulic filling below water level generally has a low to medium relative density of about 20 to 60% due to the loose packing from self-weight sedimentation of sand particles under water. The zone with the least strength could be expected to be just beneath water level if fill is placed by subaqueous discharge through hydraulic pumping. Sand placed

above water table by hydraulic filling tends to have a higher relative density in the range of 60 to 80% because of dense packing from downward seepage and reduction in void ratio as a result of sliding and rolling of the sand particles mixture.

Hopper or bottom dumping achieves a higher density than pipeline discharging for a number of reasons. Firstly, the sand mass stored in a hopper has a higher bulk density than the sand slurry that is discharged from a pipe. Also, dumping a large quantity of sand from a hopper in a short period will result in the sand mass falling as a slug rather than as individual particles. Furthermore, the simultaneous opening of all bottom doors prohibits the entrapment of fresh water into the slug that would reduce the fall velocity and expand the slug size. The fall energy of the slug is likely to be dissipated in compaction of berm through impact and shearing. The loosest possible state would likely be achieved if the pipe discharge was placed near the water surface in such a way to allow maximum fresh water entrapment. In such a case the slurry becomes a clod with falling velocity being close to the falling velocity of individual grains. Each particle will basically come to rest in the position that it makes contact with the previously placed fill. Impact may result in some pushing around of the grains, but the impact velocities and forces can be expected to be small. Subaerial rainbow dredging can be expected to yield similar results to pipe discharging.

Once the process of reclamation is understood, it will not be difficult to be able to foresee that reclaimed sand fills will most probably be loose and potentially subject to a number of geotechnical problems. Hence, project developers and designers must be aware that they may require specific geotechnical solutions such as ground improvement in reclaimed projects.

Menard (1971) was quick to notice the benefits of applying dynamic compaction to reclamation projects, where the fill is usually composed of good quality material such as rock waste, rubble, sand, etc., and the but the reclamation's apparent poor behaviour is merely due to its loose state and low compaction. Dynamic compaction has been used in many noteworthy reclamations; e.g. Changi International Airport (Bo et al., 2009, Choa, 1980, Choa et al., 1979), Nice International Airport (Gambin, 1983), Macau International Airport (Spaulding and Zanier, 1997), Tsing Yi Oil Terminal (Hendy and Muir, 1997), or Port Botany Expansion (Berthier et al., 2009).

2.10.4 Offshore Dynamic Compaction and Dynamic Replacement

It can be observed that the notion of improving the ground for engineering purposes initially developed implicitly to resolve land based foundation problems because the quantity of foundations on land is by far more than what is encountered in marine environments and offshore. However, the 20th century was witness to a number of marine and onshore geotechnical failures such as the 1916 collapse of Gothenburg Harbour's Stigberg Quay in Sweden (Massarsch and Fellenius, 2012), and the 1979 failure of Nice Harbour in France (Dan et al., 2007). Hence, it was inevitable that sooner or later attention would be drawn towards modifying or adjusting ground improvement techniques for application to subaqueous near shore and offshore projects.

The first applications of marine ground improvement can be traced back to the 1970s. Menard carried out the first offshore dynamic compaction project in 1973 as part of the construction of Brest Naval Port's prefabricated dry dock in France. In this project a specially designed 11 ton pounder that is shown in Figure 2-190 was used to compact about 3 m of loose alluvium seabed over an area of 4,500 m^2 (Boulard, 1974, Gambin, 1982, Menard, 1974, Renault and Tourneur, 1974). Dynamic compaction was applied with variable energies ranging from 240 tm/m^2 in one pass, 480 tm/m^2 in two passes, up to 700 tm/m^2 in special cases, and on average applied energy was 400 tm/m^2. PMT parameters before and after dynamic compaction are shown in Figure 2-191.

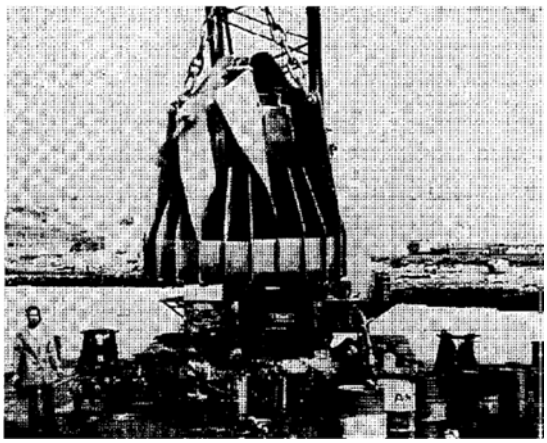

Figure 2-190: Application of dynamic compaction at Brest Naval Base using a specially designed 11 ton marine pounder (Boulard, 1974)

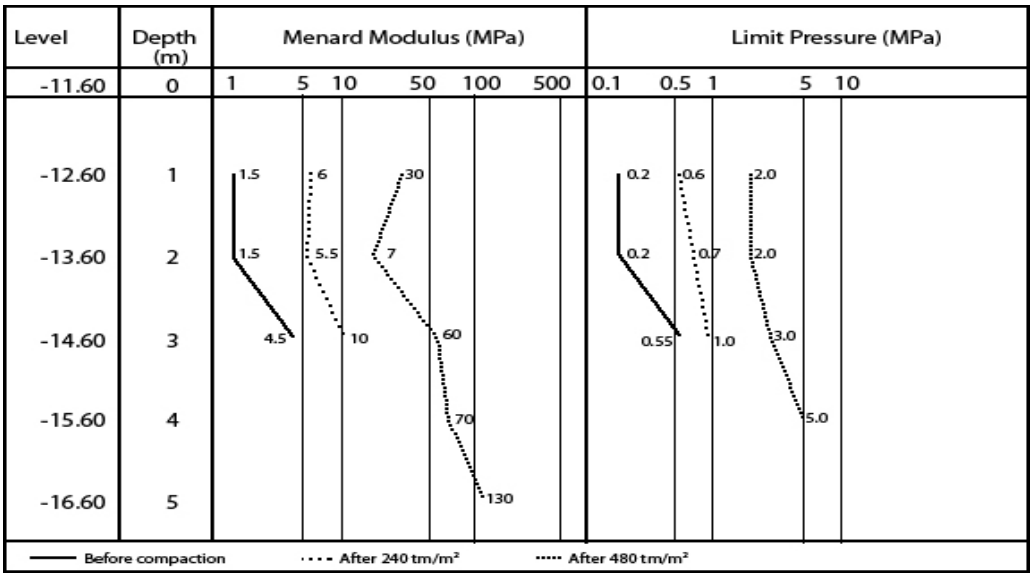

Figure 2-191: E_M and P_{LM} before and after offshore dynamic compaction at Brest Naval Base (Boulard, 1974)

In 1975, offshore dynamic compaction was used at Pointe Noire in Gabon to improve the passive resistance of loose sand in front of a cellular sheet piled wall. The specially designed pounder used in this project weighed 12 tons. Prior to ground improvement a 0.4 m thick blanket of gravelly sand was placed over the seabed, located 13.5 m below sea level. Generally, in this 14,000 m^2 project two phases of dynamic compaction with compaction energy intensity of 240 tm/m^2 were applied to provide an allowable bearing capacity of 400 kPa; however, in one sandy area one phase, and in one very silty sand area three phases of compaction were utilised. P_{LM} before improvement ranged from 250 to 600 kPa in the upper 5 m of seabed. Post improvement tests indicated that the limit pressure had increased by about 100 to 300% (Menard, 1978).

As part of the 50,000 m^2 dynamic compaction project at Udevalla, Sweden in 1975, offshore DC was applied for the treatment of a granite rock fill that was placed below the prefabricated caissons. The rock size was up to 1 m in diameter, the top of the fill was 12 m below sea level, and its thickness was variable from 17 to 20 m. Due to the size of the rock fill, dynamic compaction was performed by using a 40 t pounder that was dropped from 40 m using the Menard's Mega Machine (refer to Section 2.7.1). In this area 20 tm/m^3 of energy was applied to increase E_M in the upper 11 m of rock fill below the casing from 4.85 MPa before DC to about 110 MPa after dynamic compaction (Menard, 1978). The cross section of the project is shown in Figure 2-192.

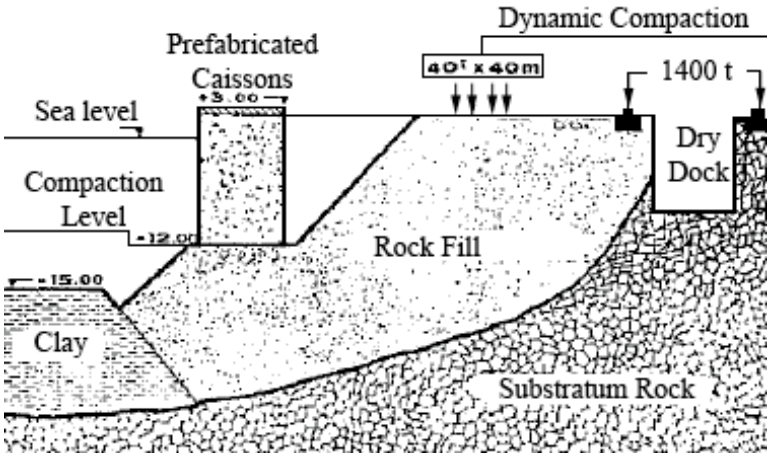

Figure 2-192: Cross section of rock fill at Udevella, Sweden (Menard, 1978)

As shown in Figure 2-193, in 1977 a 32 ton pounder was used to compact a 5 m thick layer of silty sand and a 1.5 to 2 m thick rock fill blanket at the depth of 10 m below seawater level to mitigate the risk of liquefaction of a breakwater foundation at Kuwait Naval Base (Chu et al., 2009, Gambin, 1982, Menard, 1978). Marine ground improvement was carried out over an area of approximately 36,000 m^2.

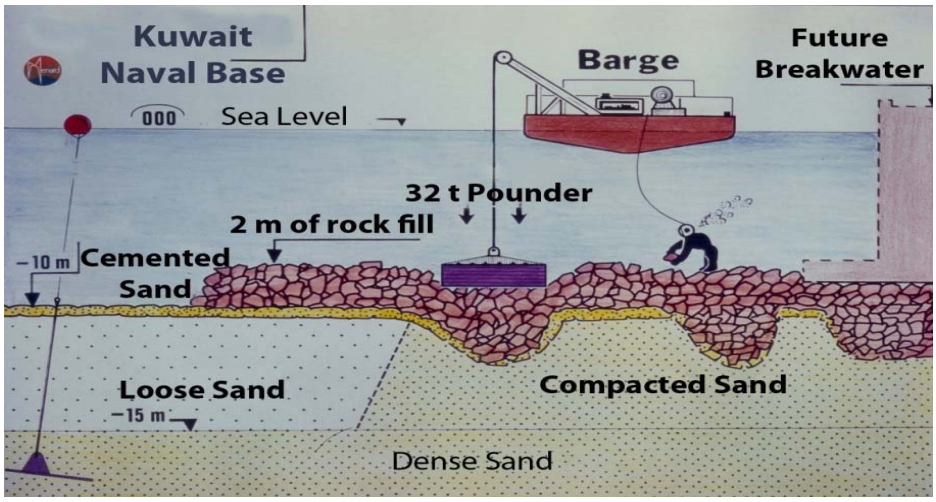

Figure 2-193: Application of offshore dynamic compaction at Kuwait Naval Base

Also in 1977, offshore dynamic compaction was applied for the treatment of seabed at Sfax Fishing Quay in Tunisia (Gambin, 1982, Menard, 1981). In this project water depth was 1 m, and the seabed was composed of 5 m of very soft clay followed by 2 m of silty sand and 3 m of denser clayey sand, and firm clay.

Conventionally, in such projects the solution would have been to remove the soft clay, replace it with sand, drive in the sheet pile wall, and deepen the quay by dredging in front of the quay wall. However, as sand was not available in the required quantity, and the project

owner intended to construct a gravity quay wall, the foundation construction technique consisted of removing the soft clay and replacing it with a rock fill blanket, and improving the silty and clayey sands to provide a an allowable bearing capacity of 300 kPa. Dynamic compaction was performed using a 17 ton pounder with a square grid spacing of 2 m. Compaction was carried out in 3 to 5 phases with 2 to 10 blows per print.

Figure 2-194: Offshore DC at Kuwait Naval Base using a 32 t specially designed pounder

Prior to placement of the prefabricated sections of a dry dock in Lagos, Nigeria, dynamic compaction was carried over an area of 13,800 m^2 in 1979. Initially, the seabed was excavated to -15 m RL (reduced level), and backfilled with 1 m of rock fill. As shown in Figure 2-195, soil improvement was carried out using a 40 t pounder with the intention of treating 15 m of soil. Up to 5 passes of dynamic compaction were applied in some locations. The square compaction grid spacing varied from 2 to 4.5 m. As can be seen in Figure 2-196, large improvement was achieved in the upper 10 m, and a mean soil reaction modulus of 0.82 kPa/m was obtained for a 20x44 m^2 slab (Gambin, 1982).

Figure 2-195: Dynamic compaction at Lagos dry docks, Nigeria

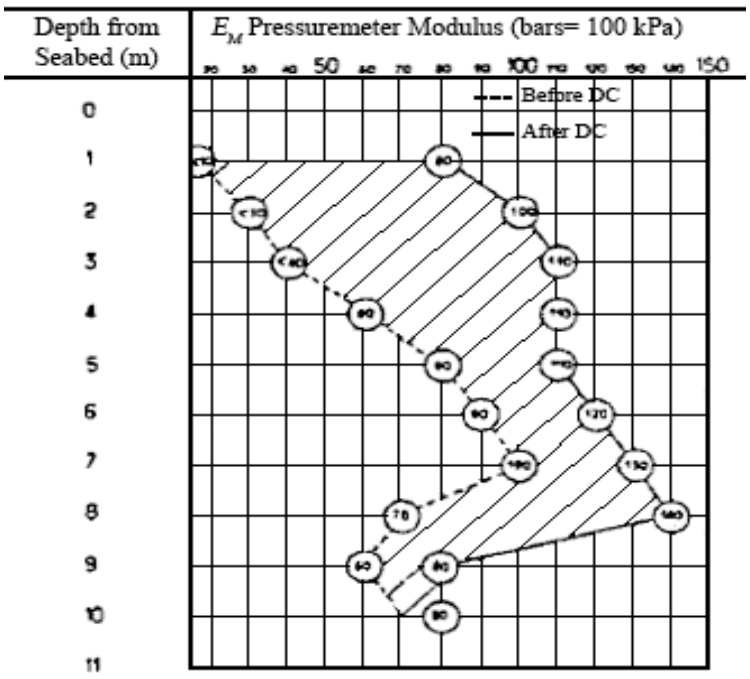

Figure 2-196: Comparison of E_M before and after dynamic compaction at Lagos Dry Docks (Gambin, 1982)

In 1980, a desalination plant was assembled in Japan, towed to Yanbu in Saudi Arabia, and sunk on a seabed foundation prepared by dynamic compaction. The seabed was composed of 8 m of loose silty sand, with the upper 4 m being very heterogeneous. Hence, the top 4 m of seabed was removed, and replaced by crushed coral, and dynamic compaction was applied using a 17 ton pounder that was dropped on a square grid with 8 m spacing. The number of blows per print in the compaction phases varied from 12 to 10. By this means the allowable bearing capacity of the seabed was increased from 30 to 120 kPa (Gambin, 1982). The treated area in this project was 4,000 m^2.

3 Distinguished Dynamic Compaction and Dynamic Replacement Projects

3.1 Choice of Projects

Millions of square metres of ground improvement have been undertaken by dynamic compaction and dynamic replacement since Menard invented and developed these techniques more than 40 years ago. These techniques have generally been used to improve the soil strength, to increase bearing capacity and to reduce external load induced settlements, but many projects have also been undertaken to mitigate soil liquefaction or to prevent settlements originating from the self-weight of the soil.

The author has had the unique opportunity to be involved in numerous state-of-the-art dynamic compaction and dynamic replacement projects that can be of great value for improving our understanding of what to expect by performing these techniques, to optimise design and management procedures, and to develop new methods for quantifying ground and soil behaviour. Hence, a number of such projects with various aspects have been chosen for this purpose, and will be documented, analysed and compared with existing publications in this thesis.

A summary of the projects that are documented and analysed in this research are presented in Table 1. To the knowledge of the author, a number of projects that have been chosen in this research have been world records or first time applications at their time. These include:

Project Name	**Location**	**Area (m^2)**	**Technique**	**Ground**	**Genre**
Al Falah Community	Abu Dhabi UAE	4,840,000	DC	Dry desert sand	Buildings
King Abudulla University of Science and Technology	Jeddah Saudi Arabia	2,600,000	DC, DR	Loose and soft saturated soil	Buildings
Al Quo'a New Township	Al Quo'a UAE	1,130,000	DC	Very thick non-engineered dry fill	Buildings, roads
New Corniche	Abu Dhabi UAE	900,000	DC	Reclamation	Road, infrastructure

Project Name	Location	Area (m^2)	Technique	Ground	Genre
Blue City	Oman	225,000	DC	Saturated loose silty sand	Buildings
Marjan Island Road Corridor	Ras Al Khaimah UAE	198,000	DC	Reclamation	Road
Al Nakhilat Ship Repair Yard	Ras Laffan Qatar	175,000	DC	Reclamation	Quay, dry dock
Ritz-Carlton Hotel	Abu Dhabi UAE	90,000	DR	Saturated soft very silty sands	Building, Embankment, wall foundation
Umm Quwain Marina	Umm Quwain UAE	86,000	DR	Saturated soft very silty sand	Buildings
Al Jazira Steel Pipe Factory	Mussafah, Abu Dhabi UAE	39,000	DR	Saturated soft very silty sands	Industrial building
Fujairah Desalination Plant Phase II	Fujairah UAE	28,000	DC	Loose sand	Industrial
Reem Island Causeway	Abu Dhabi & Reem UAE	8,000	DC	Reclamation	Road
Heavy Fuel Oil Tanks	Ras Laffan Qatar	~ 12,200	DC	Loose sand and sabkha	Tanks
Palm Jumeira Sewage Treatment Plant Tanks	Dubai UAE	~ 2,000	DC	Reclamation	Tanks
Al Khaleej Raw Sugar Silos	Dubai, UAE	~ 3,300	DR	Loose sand	Silos

Project Name	Location	Area (m^2)	Technique	Ground	Genre
Palm Jumeira Trial	Dubai, UAE	~ 900	DC	Reclamation	Building
Quay Expansion	Southeast Asia	~ 550	DR	Disturbed clayey seabed	Offshore

Table 3-1: Case studies used for documentation, analysis and comparison with previous publications

- Abu Dhabi New Corniche, UAE: In this project 900,000 m^2 of ground was reclaimed by hydraulic filling. This project was 6 km long, which makes it the longest dynamic compaction project that has been carried out in a metropolitan area. Figure 3-1 shows the New Corniche against Abu Dhabi's skyline after the completion of the project.

Figure 3-1: Abu Dhabi Corniche: 6 km long project in a metropolitan area

- Al Quo'a New Township, UAE: In this project 1.13 million m^2 of levelled dune sands were treated using dynamic compaction. While, at most, the ground had to support two storey villas, the maximum treatment depth for creep or self-bearing was 28 m. The *MARS* (Menard Accelerated Release System) was invented and used to drop a 35 t pounder in free fall and automatically reconnect it to the DC rig in this project for the first time. Figure 3-2 shows the pounder lifting and dropping phases.

- King Abdulla University of Science and Technology (KAUST), Saudi Arabia: In this project more than 2.6 million m^2 of ground was treated using dynamic compaction, dynamic replacement, and dynamic surcharging. At its time of construction this project was the largest (in size) DC or DR project that was carried out in one contract

by a ground improvement specialist contractor. KAUST also scored the world record for the project with the most number of DC and DR rigs as it implemented 13 rigs working two shifts a day. Consequently, at its peak, production reached approximately 600,000 m^2 per month, which was also a world record at its time. Extreme heterogeneity of the ground conditions over short distances, a very tight programme requiring treatment before completion of architectural and structural designs, and late changes in design have all made this project one of the most challenging projects that has ever been undertaken.

Figure 3-2: First application of MARS pounder release and reconnect mechanism in the world

Figure 3-3: Application of DC and DR at KAUST using 13 (9 shown in the photograph) DC-DR rigs working in two shifts per day.

- Al Falah Community, UAE: This development required application of dynamic compaction for the treatment of loose desert sands over an area of 4.84 million m^2, making it also the largest (in size) DC project that has been performed in one contract by a ground improvement specialist contractor at its time of construction. Although the number of DC rigs used in this project was 11 (working in two shifts) production rate reached 966,000 m^2 per month, which surpassed KAUST's record, and became the new world record. Figure 3-4 shows the application of DC at Al Falah Community.

Figure 3-4: Treatment of 4.84 million m^2 of loose sands at Al Falah Community.

- Quay in Southeast Asia: In this project dynamic replacement was applied to the seabed at the depth of 30 m below sea level, which makes it the world's deepest application of DC or DC in an offshore project. The double sided DC-DR grated pounder that is shown in Figure 3-5 and that was used in this project was also an innovation in pounder construction.

- Abu Dhabi New Corniche, Al Quo'a, KAUST, and Al Falah Community are all mega DC or DR projects, but it is the author's experience that projects larger than 30,000 m^2 can also be considered as large size projects. Thus, Blue City, Marjan Island Road Corridor, Al Nakhilat Ship Repair Yard, Abu Dhabi Ritz-Carlton Hotel, Umm Quwain Marina, Al Jazira Steel Pipe Factory, and Fujairah Desalination Plant can be understood to be large or very large size projects as well.

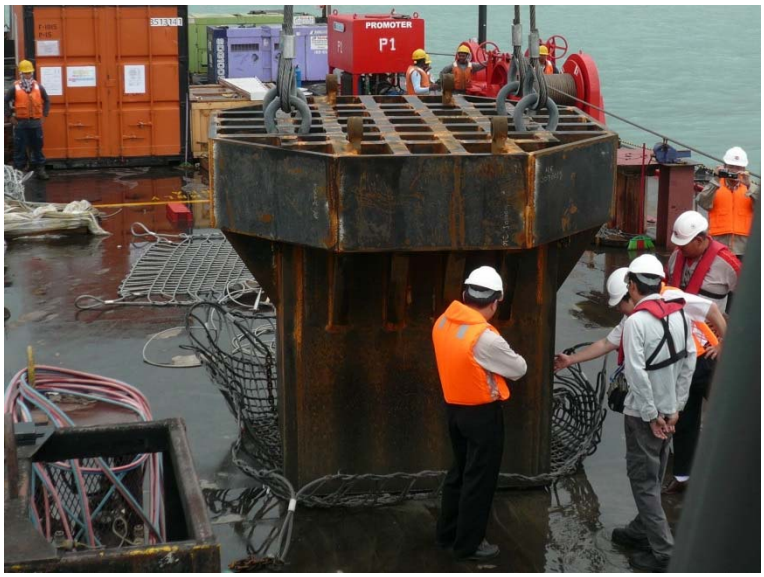

Figure 3-5: First application of a double sided DC-DR grater pounder in the world

3.2 Abu Dhabi New Corniche Road

3.2.1 Project Description

As shown in Figure 3-6 Abu Dhabi New Corniche (Beach Road) is a 6 km long (see Figure 3-6) reclamation with an area of 900,000 m^2 that has been hydraulically reclaimed from the Persian Gulf using the pipeline discharge method (Figure 3-7). The reclamation began at the face of the original beach road, varied in width from zero to 300 m, and on average extended 160 m into the sea. Maximum reclamation thickness was about 12 m at the sea facing, which was to be retained by sheet piles, and average thickness of the fill was 6.5 m. In addition to the leisure areas, pedestrian pathways and bicycle lanes on each side of the road, the road itself was designed to have 4 lanes in each direction that were to be separated in the centre by a variable width median.

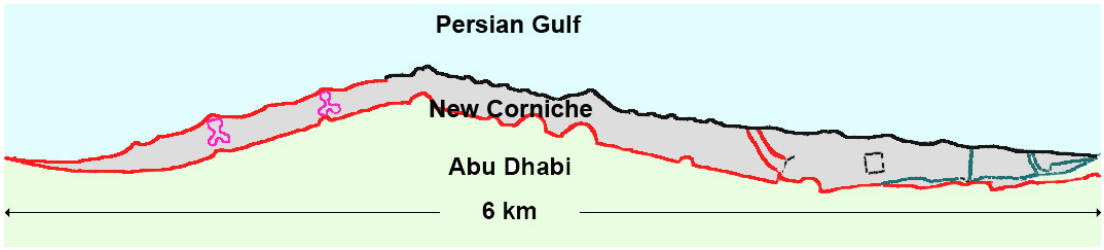

Figure 3-6: Plan of Abu Dhabi New Corniche

Figure 3-7: Reclamation of New Corniche by pipeline discharged hydraulic fill

3.2.2 Ground Conditions

The preliminary geotechnical investigation revealed that the seabed was composed of medium dense fine grained sand followed by a dense layer of sand, shells and ultimately the limestone bedrock.

Project specifications stipulated that fines content in the reclamation material had to be less than 10%, and the fill's relative density had to be at least 80% with an SPT blow count correlation that is shown in Table 3-2.

Depth (m)	N_{SPT}
0- 2	15
2- 5	18
5- 8	20
8-11	22

Table 3-2: SPT blow counts acceptance criteria based on correlation to 80% relative density

Post reclamation testing indicated that the fill, with a maximum thickness of 12 m, was loose to very loose with SPT blow counts in the range of 1 to 10, and that acceptance criteria were not satisfied. Hence, the ground improvement works were tendered, and the project was awarded to a ground improvement specialist contractor who had proposed the implementation of dynamic compaction.

3.2.3 Application of Dynamic Compaction and the Challenges

Further testing upon award of the ground improvement package and during the course of the works revealed that the hydraulic fill had segregated, and in some locations a silty layer with at least 0.5 m thickness was covering the seabed.

This project is an example of one of many problems associated with application of relative density (refer to Section 2.10.2). ASTM (2006a), (2006b) specifies that the concept of relative density is applicable to soils with less than 15% fines; however, as this was not the case throughout the soil profiles of the project, the concept of relative density and thus any correlation with it would become inapplicable.

Additionally, sampling with the split spoon of the SPT device proved to be difficult, and occasionally produced unreliable results. Theoretically, the split should be able to extract 0.45 m long samples from the ground; however, this is not always the case in practice, and in some boreholes the samples were just a few centimetres and sometimes the sampler had total loss of sample.

Thus, in addition to hte criteria of relative density and SPT, pressuremeter testing was also carried out for the design of sheet piles and further verification of the work.

The 900,000 m^2 work area was divided into 22 sequential sub areas along the length of the project. Energy intensity, pounder weight, drop height and number of phases were varied based on the treatment thickness and confirmed by a calibration programme. Pounder weights varied from 12.5 to 25 tons and a maximum drop height of 20 m was implemented. In this project dynamic compaction was carried out only as deep treatment phases without ironing because it was possible to meet project requirements without performing the latter phase.

In areas with less than 6 m thickness, two phases of deep treatment using 12.5 and (14 to) 16 ton pounders were utilised. Depending on the fill thickness Phase 1 had a grid spacing of 6 m, and included 10 to 12 blows per print. Phase two prints were offset in two directions, and were located in the middle of Phase 1's grid. In this phase 8 to 10 blows were applied to Phase 2 prints and an additional 2 blows were also applied to Phase 1 prints.

In deeper areas four phases of dynamic compaction comprising of three phases using 25 ton pounders and one phase using 14 or 16 ton pounders were carried out. When fill thickness was limited to 8 m or was 8 to 12 m it was envisaged that the number of blows per print in the first three phases would be respectively 10 or 16 blows. Grid spacing for Phases 1, 2 and 3 were respectively set at 12 m, 12 m, and 8.5 m. Phase 4 had a grid spacing of 6 m, and each print received 12 blows. Additionally, during this phase, prints of Phases 1 to 3 received another 3 blows.

Figure 3-8: Typical crater size and depth in the deep treatment areas of Abu Dhabi New Corniche

Sometimes due to the buildup of pore pressure the first three phases of areas with more than 6 m had to be performed in sub phases, and sufficient time was permitted for the excessive pore pressure to dissipate to tolerable values. The maximum breakdown of phases occurred in one area where Phase 1, 2 and 3 were respectively performed in 4, 3 and 2 sub phases. After each sub phase the craters were backfilled with sand, time was allowed for the pore water pressure to dissipate, and then the next sub phase was carried out. A typical crater size and depth in the deep treatment areas of the project is shown in Figure 3-8.

While the suitability of dynamic compaction application is well established for saturated granular soils, the author is frequently asked if this ground improvement method can be used for treating saturated sands, and about the minimum distance that should be maintained between the works and the shoreline. As shown in Figure 3-9 the works can be carried out basically at the shoreline itself; however, this must be done with consideration of work safety practices.

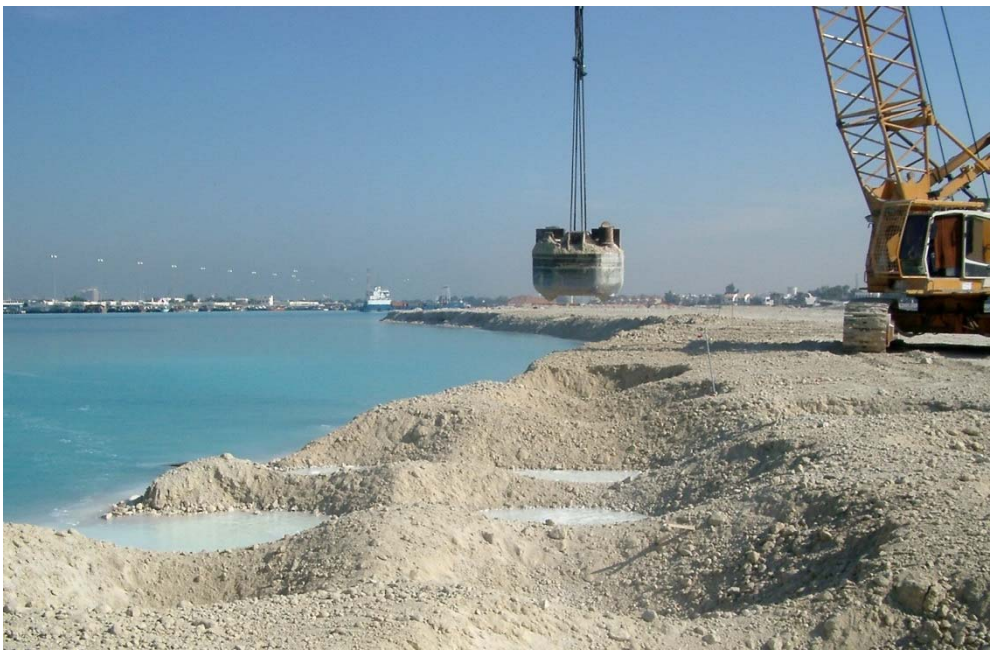

Figure 3-9: Application of dynamic compaction at the shoreline

Generally, a point of concern for application of dynamic compaction in residential areas is noise and vibration disturbance (see Section 2.8.3) due to pounder impact. Although the results of vibration monitoring is not available to the author, as can be seen in Figure 3-10, it was possible to perform dynamic compaction in two shifts per day parallel to the skyline of Abu Dhabi over a length of 6 km. To minimise disturbance during nights, works were scheduled in such a way that the areas closest to the towers were treated only during day time.

Figure 3-10: Application of dynamic compaction in front of Abu Dhabi skyline

The works were carried out with a maximum number of 7 DC rigs in two working shifts over a period of 7 months. The maximum production rate during the course of this project was 200,000 m^2 of improved ground per month.

3.2.4 Testing and Verification

SPTs and PMTs were carried out in this project as part of quality control, quality assurance, and verification of works. P_{LM} and E_M at three points before and after dynamic compaction have been shown in Figure 3-11 to Figure 3-13. For clarity, average P_{LM} and E_M of the same points have also been shown in Figure 3-14 (only Point No 3 in shown for depth of 1 m) .

It can be observed that due to the earthmoving and construction equipment traffic before ground improvement the upper crust of the reclamation was quite dense with P_{LM} exceeding 1,000 kPa, but the soil rapidly became very loose, generally with P_{LM} being less than 300 kPa, and subject to creep under self-weight (see Section 2.9.2.8). After dynamic compaction P_{LM} increased up to 3,000 kPa in the upper sand layers and to at least 750 kPa at depth. Similarly, E_M increased up to 30,000 kPa in the upper sand layers, and to at least 7,000 kPa at depth. It should be noted that improvement of the upper ground layers could have been even better if the ironing phase of dynamic compaction was also performed.

For convenience, the ratio of pressuremeter parameters after dynamic compaction to before dynamic compaction is defined as *improvement ratio*; i.e.

$$P_{LM}\ \text{Improvement Ratio} = \frac{(P_{LM})_{after\ DC}}{(P_{LM})_{before\ DC}} \quad \text{3-1}$$

$$E_M\ \text{Improvement Ratio} = \frac{(E_M)_{after\ DC}}{(E_M)_{before\ DC}} \quad \text{3-2}$$

Figure 3-15 to Figure 3-17 show the improvement ratios of P_{LM} and E_M for the three test points shown in Figure 3-11 to Figure 3-13. Also, the average improvement ratios of P_{LM} and E_M for the same three test points are shown in Figure 3-18. As can be observed that while it is general perception that the most dynamic compaction improvement would be achieved at the upper ground levels, in this project specifications were satisfied without the ironing phase, and consequently improvement at the shallow depths was less than what would be typically encountered if ironing was also performed. It is observed that the improvement ratio of P_{LM} was about 1.5 at the depth of 1 m, but on average approximately 7 and at most nearly 10 at the depth of 3 m. As expected, the ratio then gradually reduced at further depths.

In this project the average peak improvement ratio was 7 (i.e., 600% increase) and the maximum peak in any of the tests under study was approximately 10 (i.e., 900% increase). Comparison of P_{LM} improvement ratios in this project with previous research (Lukas, 1986) that suggests increases would be in the order of 100 to 400% (see Section 2.5.5) indicates that greater peak improvement ratios can be considered. However, the average P_{LM} improvement ratio for all depths in this project was 4.1, which is in the order of magnitude that Lukas has noted. It should be noted that in general the pattern of foundation stress and improvement ratio reduction in depth is similar; hence, assuming an average improvement ratio will probably yield conservative values.

The improvement ratio of E_M appears to have been bounded by a lower value of approximately 4, which matches the order of magnitude that Lukas has observed.

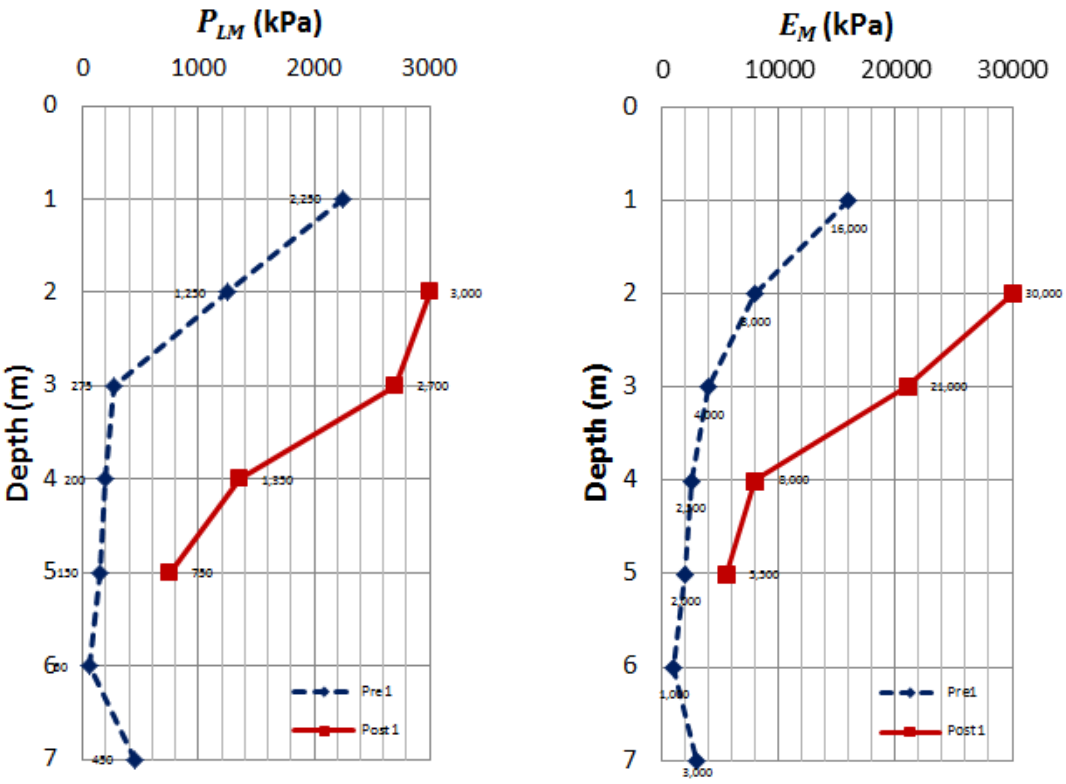

Figure 3-11: P_{LM} and E_M before and after dynamic compaction at test point No. 1

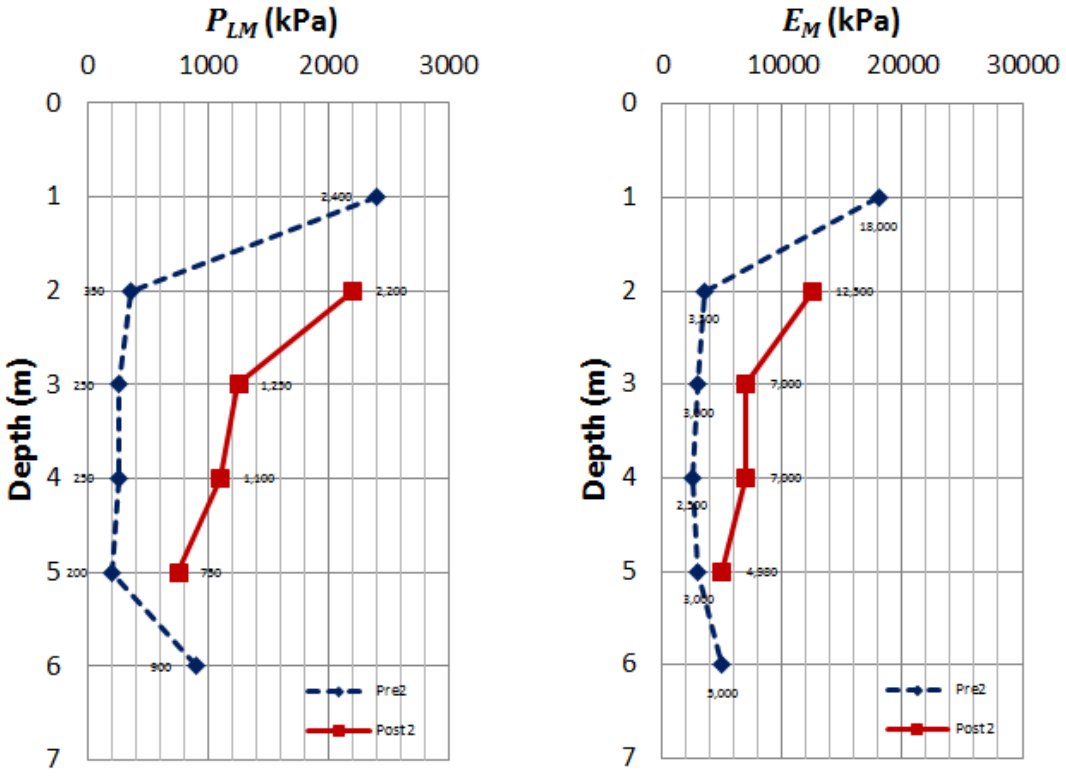

Figure 3-12: P_{LM} and E_M before and after dynamic compaction at test point No. 2

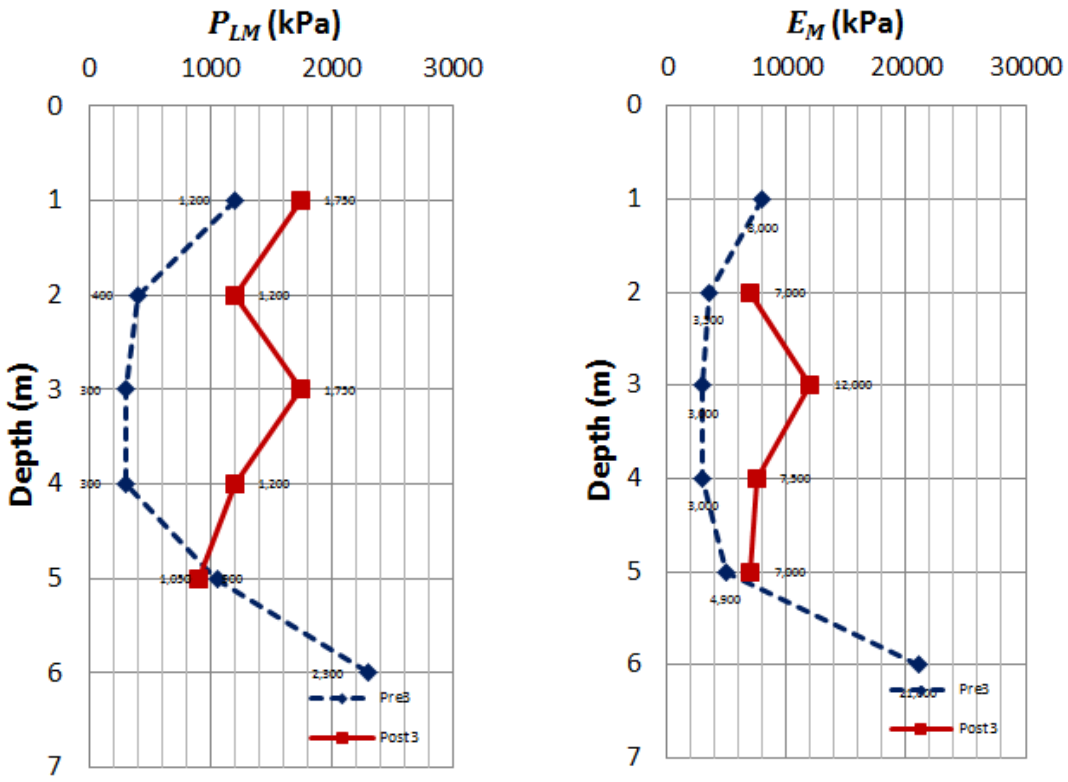

Figure 3-13: P_{LM} and E_M before and after dynamic compaction at test point No. 3

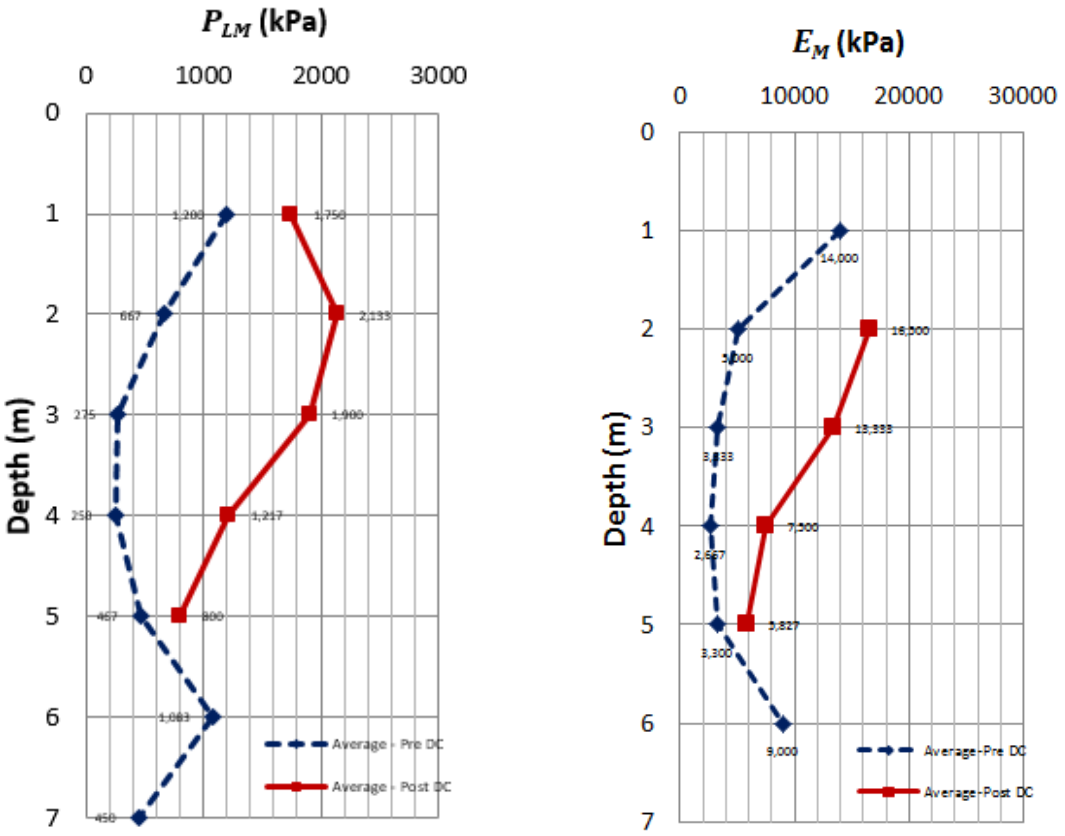

Figure 3-14: Average P_{LM} and E_M before and after dynamic compaction for three points

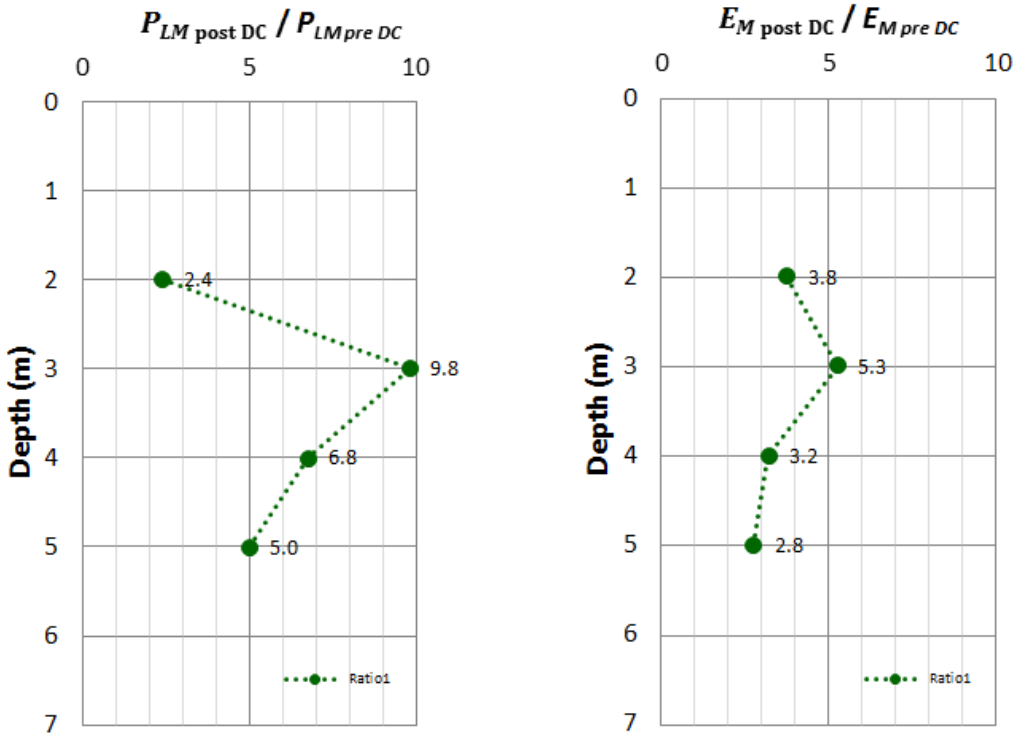

Figure 3-15: P_{LM} and E_M improvement ratios for Point No. 1

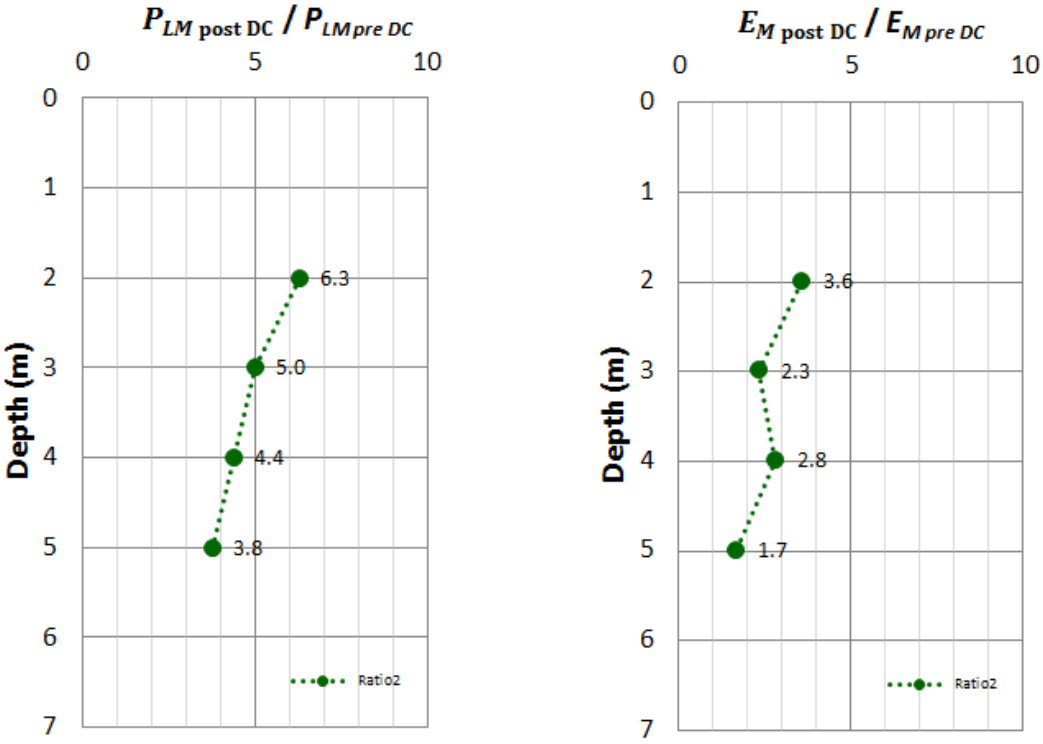

Figure 3-16: P_{LM} and E_M improvement ratios for Point No. 2

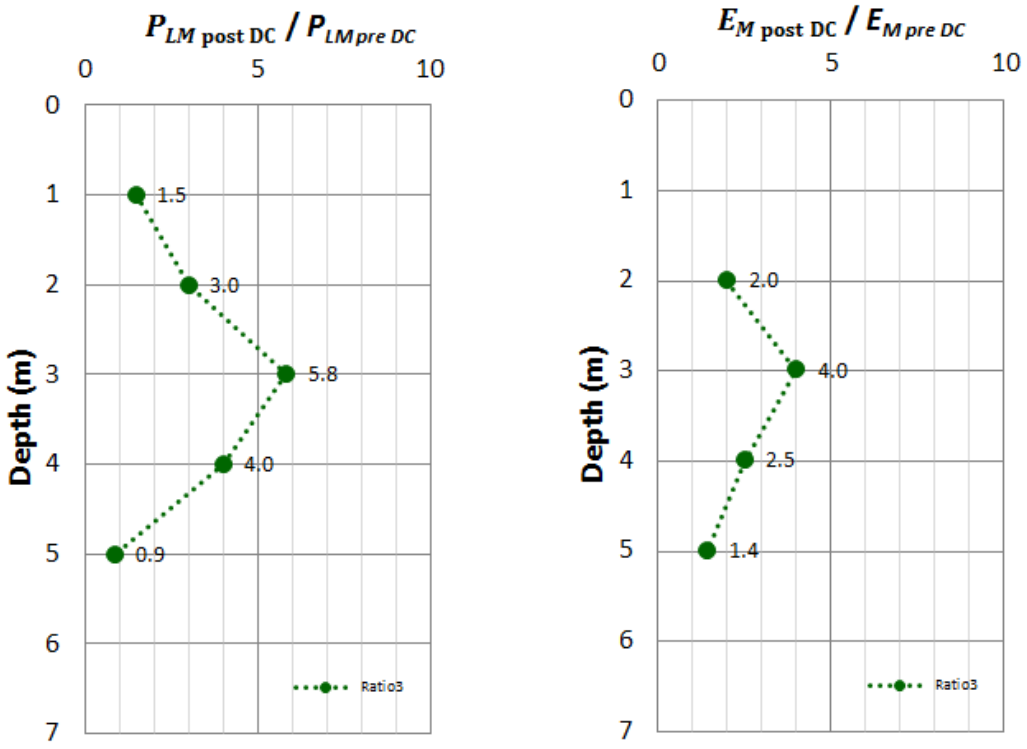

Figure 3-17: P_{LM} and E_M improvement ratios for Point No. 3

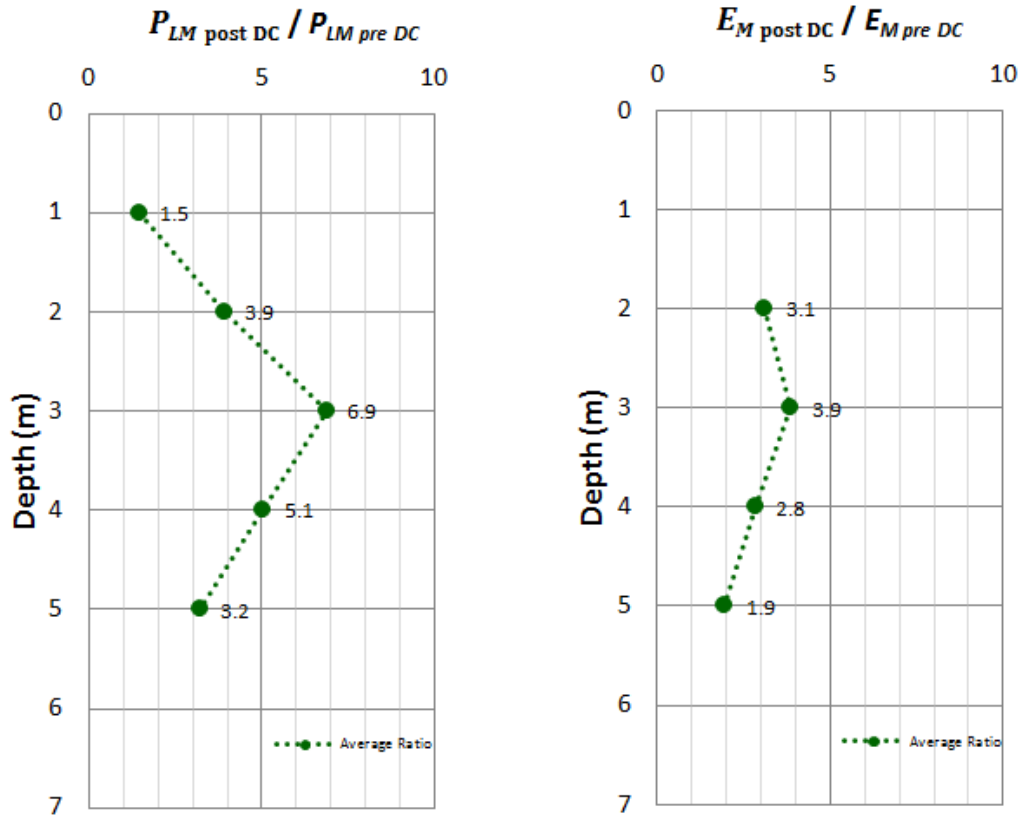

Figure 3-18: Average P_{LM} and E_M improvement ratios

3.2.5 Lessons and Conclusion

1. If project size justifies, in an optimal dynamic compaction design the treatment area should be broken down to sub areas based on design and acceptance criteria, loading, and ground conditions. Pounder weight and drop height, compaction intensity, grid size, and the other design parameters can consequently be determined.

2. Relative density is an unreliable acceptance criterion.

3. It is possible to perform dynamic compaction in populated areas.

4. It is possible to perform dynamic compaction at close vicinity to the shoreline.

5. Average P_{LM} improvement ratios after dynamic compaction were from 1.5 to 7. This suggests that maximum improvement ratio can be more than what has been reported in previous publications.

Figure 3-19 shows Abu Dhabi Corniche after completion.

Figure 3-19: Abu Dhabi Corniche

3.3 Al Quo'a New Township

3.3.1 Project Description

Al Quo'a is a remote desert township that is located about 100 km from Al Ain and on the UEA side of the United Arab Emirates - Oman border (Figure 3-20). The first phase of this town was constructed by creating a levelled platform for the town's foot print by cutting and filling the dune sands. The town structures were built directly on the platform, and although the buildings were only two stories high, most that were built on the fill areas suffered from severe damages and substantial amounts of cracking. Consequently, the town developers became well aware of problems associated with construction on young non-engineered fills, and stipulated that specific measures had to be implemented as part of the construction of later phases of the project to avoid more damage.

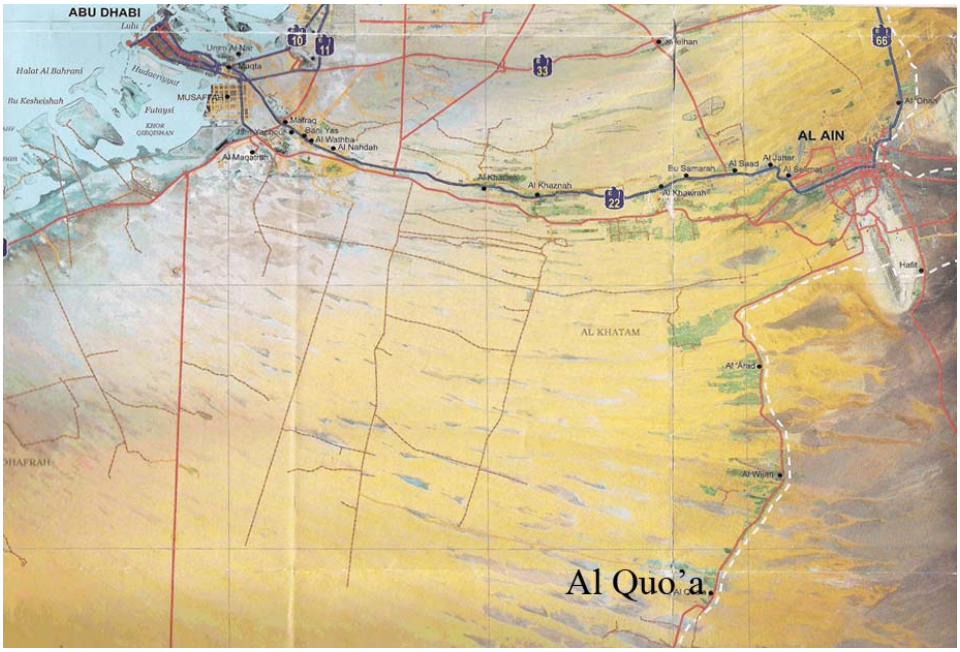

Figure 3-20: Location of Al Quo'a

The second phase of Al Quo'a, consisting of 450 two floor villas and the associated infrastructure was planned to be constructed on a site with a rectangular shape that was 2.3 km long and 1.65 km wide, and that had an area of more than 3.8 million m^2. This phase was also anticipated to be constructed on a relatively flat platform. Thus, as shown in Figure 3-21, the dune hills were once again cut and dumped into the lower level areas as non-engineered fill.

Figure 3-21: Grand size cutting and dump filling of dune sands for the construction of the second phase of Al Quo'a Township.

3.3.2 Ground Conditions

The sieve analysis of the dune sand that was used for constructing the town's platform is shown in Figure 3-22. It can be observed that the soil was poorly graded fine clean sand. As could be expected, groundwater was not observed or recorded in any of the tests that were carried down to a maximum depth of about 30 m below platform level.

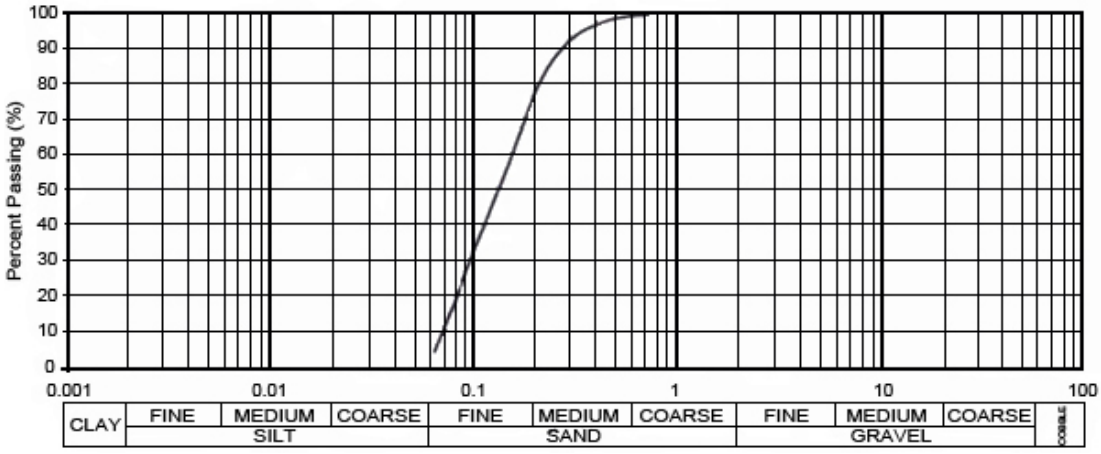

Figure 3-22: Sieve analysis of the dune sand

The fill areas were measured, and it was calculated that they covered an area of 1,135,000 m^2. More detailed assessments revealed that 44% of the fill material was placed at depths less than 6 m, 35% were from 6 to 12 m deep, 13% were from 12 to 16 m deep and the remaining 8% were located at depths greater than 16 m below the finished working platform (±0.0 m RL, reduced level). The maximum depth of the fill was 28 m.

CPT test results indicated that while the ground condition in the cut areas was satisfactory enough to support the structures and infrastructures, as could have been predicted, the dumped dune sands in the fill areas were in a rather loose state and except for the upper 2 m, q_c was constantly in the low range of 2 to 4 MPa. The higher values of the soil strength (q_c in the range of 10 to 15 MPa) in the upper crust was contributed to the effects of the earthmoving equipment traffic. Likewise, pressuremeter tests that were later carried out as part of the post ground improvement programme indicated that P_{LM} was in the range of 100 to 500 kPa, indicating that the young uncontrolled fill would be subject to creep under self-weight (refer to Section 2.9.2.8).

The low strength of the fill indicated that the ground would not be able to safely support the footing loads of the villas. It was expected and calculated that the facilities of this phase of the project would not only have problems with settlement and bearing of structural loads, but would also suffer from creep settlements, cracks and other damages if no specific remedy was anticipated for the loose fill.

Piling was deemed as an unfavourable solution namely because it was only feasible for supporting the structural loads of buildings, and was not applicable for providing a geotechnical solution for creep of the town's platform and non-building areas. Furthermore, although calculations were not made at that phase, the piles had to be longer than the fill thickness to avoid the settlements of the piles themselves in the creeping soil. This would have incurred huge costs and a very long construction time. Consequently, Ground improvement was deemed as a possible solution for the treatment of the very loose fill.

3.3.3 Development of an Alternative Solution

Noting that the maximum depth of ground improvement was 28 m, a figure that appears to be out of dynamic compaction's reach with typical equipment, the ground improvement tender envisaged vibro compaction as the ground improvement method, and acceptance was based on CPT results. While vibro compaction could be viewed as a preferred method of soil improvement when depth of treatment of loose sands is in the order of Al Quo'a project, its application on this jobsite would have been very challenging and difficult due to dry state of the dune sands and the logistics for providing water for jetting. Although vibro compaction can be done without water jetting by utilising compressed air, it is the author's experience that this may also turn into a challenging endeavour if the insertion cavity does not collapse, and the vibroflot vibrations are not transferred to the soil mass. Lukas (1995) has carried out

a cost comparison between different ground improvement solutions. His research shows that when applicable, dynamic compaction is the most affordable ground improvement technique.

If applicable (due to depth constraints), dynamic compaction could have been a more preferable solution with consideration of the below:

- When applicable, dynamic compaction is a very affordable ground improvement solution. As a comparison, the treatment of a unit volume of soil by dynamic compaction costs 42% to 70% that of vibro compaction or 7 to 15% of excavation and replacement (Lukas, 1995).

- Dynamic compaction does not require water (or compressed air) for the works.

- Dynamic compaction requires the minimal amount of equipment; i.e., the DC rig and the pounder, and a loader for levelling the ground after each phase of compaction. On the contrary, vibro compaction requires a rig, the vibroflot, water tanks, water pumps, a generator, and a compressor. Handling a larger pool of equipment in an isolated and remote site such as Al Quo'a was more challenging.

Implementation of dynamic compaction with PMT for verification was proposed as an alternative ground improvement solution by one of the specialist soil improvement contractors, and ultimately accepted. In addition to being the most affordable solution, the alternative proposal had to address the technical objectives and concerns of the designers as well.

The structures in Al Quo'a were only 2 floors, so it could have been envisaged that the stress bulb generated by the structural loads would not extend deeper than about 6 m below ground level. However, the ground was a thick uncontrolled and non-engineered fill that could have further settled under its own weight, external vibrations, and water ingress. These conditions suggested that the specifications could specifically address external and structural loadings on the upper ground layer when there were loads to be considered and self-bearing (refer to Section 2.9.2.8) at other depths.

In villa areas, single footing loads were known to be less than 100 tons, so it was possible to stipulate an allowable bearing capacity (200 kPa) and thus a maximum footing size (2.25 x 2.25 m^2). Total settlements were to be limited to 25 mm, and angular distortions were

required to be less than a very stringent value of 1/1,250 due to the special psychological concerns and the previous disappointing results of the first phase of the project. It was also possible to determine the stress bulb influence depth and to specify self-bearing treatment for further depths. In non-villa areas a nominal bearing capacity of 100 kPa was stipulated for light and unanticipated loads. The bearing capacity safety factor was 3. The approved design criteria of the project are summarised in Table 3-3.

Design Criteria	Villa Areas	Non-Villa Areas
Bearing capacity	200 kPa at -0.75m RL	100 kPa at -0.75m RL
Total settlement	25 mm	25 mm
angular distortion	1/1,250	1/1,250
Creep settlement	To be eliminated	To be eliminated

Table 3-3: Table 1. Design criteria

By implementation of PMT calculation methods (Centre D'Etudes Menard, 1975) that have been described in Sections 2.9.2.6 and 2.9.2.7, acceptance criteria based on design criteria was developed and tabulated as presented in Table 3-4 and Table 3-5.

Criteria for Villa Areas	Safe bearing	Self-bearing
Thickness where parameters prevail	-0.75 to-5.50 m RL	From -5.50 m RL
P_{LM} (kPa)	750	600
E_M (kPa)	4,800	4,000

Table 3-4: Acceptance criteria for villa areas

Criteria for Non-Villa Areas	Safe bearing	Self-bearing
Thickness where parameters prevail	From ±0.00 m RL	From ±0.00 m RL
P_{LM} (kPa)	600	600
E_M (kPa)	4,000	4000

Table 3-5: Acceptance criteria for non-villa areas

3.3.4 Application of Dynamic Compaction and the Challenges

The depth of improvement is mainly a function of ground conditions, pounder weight and drop height (refer to Equation 2-41):

$$D = c\sqrt{WH} \qquad 2\text{-}41$$

The percentage of each treatment area was defined in the project's ground conditions (Section 3.3.2). Assuming the coefficient of depth of improvement for dry sand is 0.7 to 0.8, the required impact energy to reach the bottom of fill for each zone will be as shown in Table 3-6:

Treatment thickness (m)	Percentage of treatment (%)	Required energy (t x m)
treatment thickness < 6 m	44	56 to 74
6 m < treatment thickness < 12 m	35	225 to 294
12 m < treatment thickness < 16 m	13	400 to 522
16 m < treatment thickness < 28 m	8	1,225 to 1,600

Table 3-6: Required treatment energy

It could be understood that it was possible to treat almost 90% of the site using conventional DC rigs that were capable of lifting pounders weighing up to 15 tons using a single cable line or 25 tons using two single cable lines; however, the deepest region required more energy, at least in the order of what could be provided by Menard's 700 tm rig and in the order of what the mega-machine and tripods could provide for the deepest areas (refer to Section 2.7.1).

While Menard's 700 tm rig was available, the mega-machine and tripods had long been decommissioned, and an alternative solution was developed and patented specifically for this project, and later used in other projects, such as Federal Highway BAB A 71 in Germany (Chaumeny et al., 2008).

MARS (Menard Accelerated Release System) is an innovative automated pounder free fall release and grab mechanism. As was discussed in Section 2.7.1, although free fall drops provide more impact energy than cable connected drops, the former is associated with practical difficulties as the disengagement of the pounder from the hook would cause the crane boom to spring back; thereby ramming the hook block forcefully into the boom and potentially damaging it in the absence of reliable shock absorbers. Furthermore, reconnecting the pounder to the hook is a costly activity as it is a slow and time consuming process that also requires manual labour.

In MARS, the pounder is released and allowed to drop in true free fall during its process of pseudo free fall and as it is falling while connected to the hoist line. This unique release mechanism prevents the boom to snap back, and thus, eliminates the risks of the hook block striking the boom. Also, the pounder drop location remains in line with the vertical alignment of the cable; hence, making it possible for the system's mechanism to grab the pounder without the assistance of time consuming labour. Figure 3-23 and Figure 3-24 show the implementation of MARS in Al Quo'a for dropping a 35 ton pounder in true free fall and automatically grabbing it without manual labour.

Figure 3-23: Free fall of 35 ton pounder using MARS

In all, a total of 6 rigs were used for performing the ground improvement works at Al Quo'a over a contract period of 10 months. Of these, 3 were single cable line heavy duty DC rigs with lifting capacities of 15 tons (Figure 3-25), one was a two single line heavy duty DC rig with lifting capacity of 25 tons (Figure 3-26), one was the Menard 700 tm rig (Figure 3-27), and one was a 250 ton rig for lifting the 35 ton pounder using MARS (Figure 3-28).

Dynamic compaction energy intensity was optimised based on the treatment thickness and acceptance criteria. The heavier 35 (free fall using MARS) and 25 ton pounders were used for the first phase of treatment of the deep fill areas, and heavy duty rigs dropping up to 15 ton pounders were utilised for the improvement of subsequent phases of those deep treatment

areas and the remaining areas of the project. By this means, the project was completed within the contracted period of 10 months.

Figure 3-24: Automatic grabbing of a 35 ton pounder by MARS

Figure 3-25: DC rig for lifting 15 ton pounders at Al Quo'a

Figure 3-26: DC rig for lifting 25 ton pounders at Al Quo'a

Figure 3-27: Menard 700 tm rig at Al Quo'a

As the minimum distance between the first and second phases of Al Quo'a developments was 200 m it was not expected that dynamic compaction induced vibrations would become a problem. From Equation 2-150, it can be calculated that PPV generated by a 35 ton pounder that is dropped from 23 m will be about 3 mm/s, which is barely perceptible (see Figure 2-126) and well below the limit that could be damaging to the villas (see Figure 2-122). Actual site measurements confirmed that PPV was less than the estimated value.

Figure 3-28: 250 ton rig for lifting the 35 ton pounder using MARS

3.3.5 Testing and Verification

The tender had stipulated that CPT tests be carried out in advance of the ground improvement works to confirm the treatment depths. This verification programme, itself, would have become a critical activity, and would have impacted the scheduling and progress of works. Noting that the intent of this testing was strictly limited to determining the boundary between loose and dense sand, the specialist ground improvement contractor proposed an innovative solution in which a static penetration machine was developed to perform a quick probing. Similar to a wick drain rig, as shown in Figure 3-29, the main components of this machine included an excavator base, a mast with sufficient height, and a tubular rod to be pushed into the ground in lieu of a wick drain mandrel.

By this means more than 25,000 m of quick probings were carried out at 1,600 points over a 3 week period. The same activity could have required between 25 to 30 weeks using a single CPT rig.

A total of 250 PMTs were carried out at the site. For comparative purposes, 50 tests were carried out before ground improvement, and the remaining 200 tests were performed after dynamic compaction. Depth of testing was based on the fill thickness and depth of dense in-situ soil.

Figure 3-29: Quick probing machine composed of an excavator base, a mast and a penetrating tubular rod.

Figure 3-30 to Figure 3-33 show P_{LM} values before and after dynamic compaction and P_{LM} improvement ratios in four locations. As can be observed that except the upper layer of ground that was relatively dense due to earthmoving equipment traffic, the soil was in a very loose state, with P_{LM} consistently between 200 to 500 kPa. These low values suggest that the soil was indeed subject to creep under self-weight (see Section 2.9.2.8). It can be observed that post dynamic compaction P_{LM} values have substantially increased in an almost classical sickle shaped curve to nearly 2,500 kPa and at least to about 1,400 kPa in the upper 6 m. P_{LM} values then gradually reduced to figures in the order of 700 to 900 kPa. The test results indicate that acceptance criteria defined in Table 3-4 and Table 3-5 have been satisfied. Peak P_{LM} improvement ratios in these tests were as high as 20.5 in Test No. 1 (refer to Figure 3-30) and from 5.2 to 6.6 in other tests. The improvement ratio at depth ranged from 1 to 3.

Average P_{LM} values and P_{LM} improvement ratios for the four tests are shown in Figure 3-34. Averaging the values at each level smoothens out any unusually high or low values and allows a more representative view. It can be seen that before dynamic compaction the upper ground level is relatively dense due to earthmoving equipment, but the soil then becomes very loose and subject to creep under self-weight. The limit pressure values appear to increase linearly and gently with depth. After dynamic compaction P_{LM} values in the upper layers of ground increase substantially, and are about 2,000 kPa over a thickness of about 5 m, and consistently around 800 kPa at the deepest layers. Peak P_{LM} improvement ratio is 6.7

at 4 m, and more than 5 (400% improvement) over a thickness of about 3.5 m). After the peak value, improvement ratio initially declines with a greater slope to 2.6 at the depth of 9 m, but then continues to reduce in value to 1.4 at the depth of 15 m.

As can be observed that all post improvement test results basically follow the variation with depth that Lukas (1986) has suggested. P_{LM} values increase to a peak value at about ⅓ to ½ of the influence depth and then deceases to a point where improvement would be negligible. Lukas (1986) also assumes an upper bound post dynamic compaction P_{LM} value of 1.9 to 2.4 MPa for sands and gravels (refer to Section 2.5.5), which is in line with the results of the works carried out in this project.

Lukas (1986) also suggests an upper bound improvement value of 400% for P_{LM} due to dynamic compaction. The results of Figure 3-30 to Figure 3-34 indicate that it is possible to improve P_{LM} of very loose dune sands by up to 1950% at least in one instance and by up to 570% as an average for peak improvements. In fact, test results show that in the study area of this project, on average, approximately 20% of the treated thickness improved by at least 400%.

In addition to the PMT, 3 zone load tests and 5 plate load tests were also carried out in this project. Plate load tests were performed on a 900 millimeter diameter plate at -0.75 m RL to a maximum pressure of 200 kPa. The objective of the zone load tests was to measure the settlements under an applied load of 25 kN/m^2, similar to the total loading of an average villa, for 7 days. The loading dimensions were equal to the villa dimensions.

Measured site settlements after dynamic compaction were in the range of 0.60 to 0.80 m.

3.3.6 Lessons and Conclusion

The review of this project can provide the geotechnical engineer with a number of lessons to be incorporated in future projects, including:

1. It is more likely that non-engineered backfilling will be loose and potentially subject to low bearing and excessive settlements. It is recommended that ground improvement be envisaged during planning stage to avoid any surprises and disappointments during development.

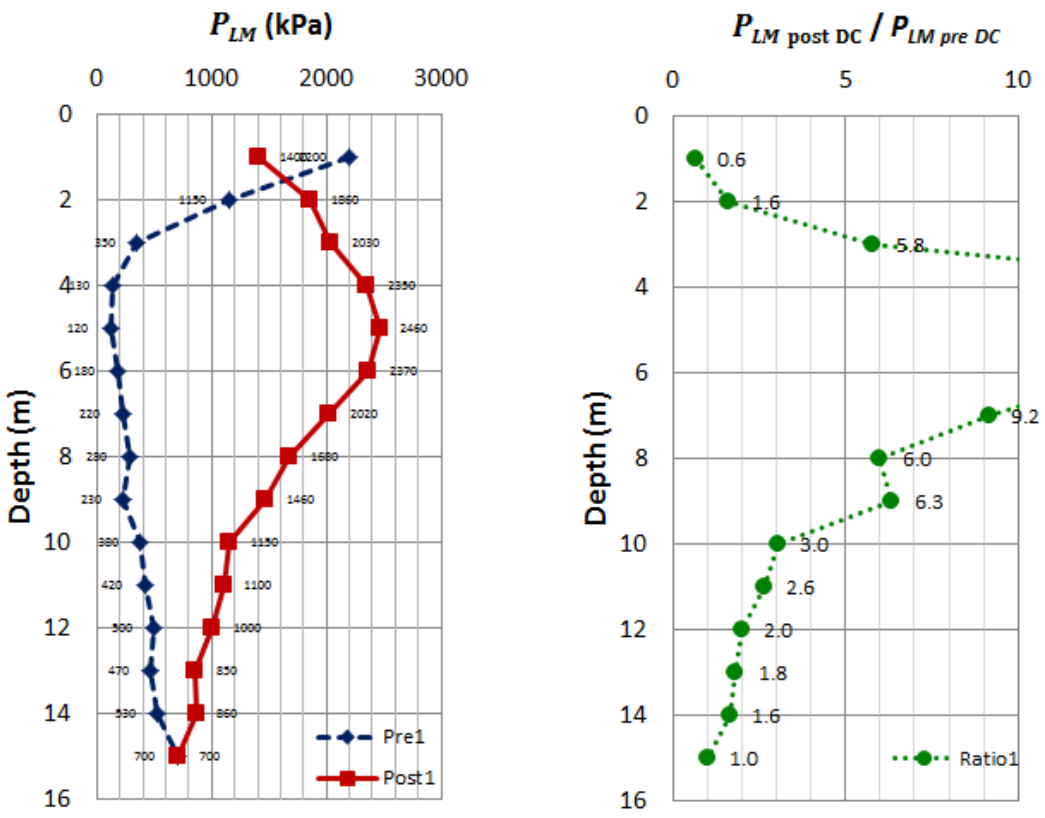

Figure 3-30: P_{LM} and ratio of P_{LM} before and after dynamic compaction at test point No. 1

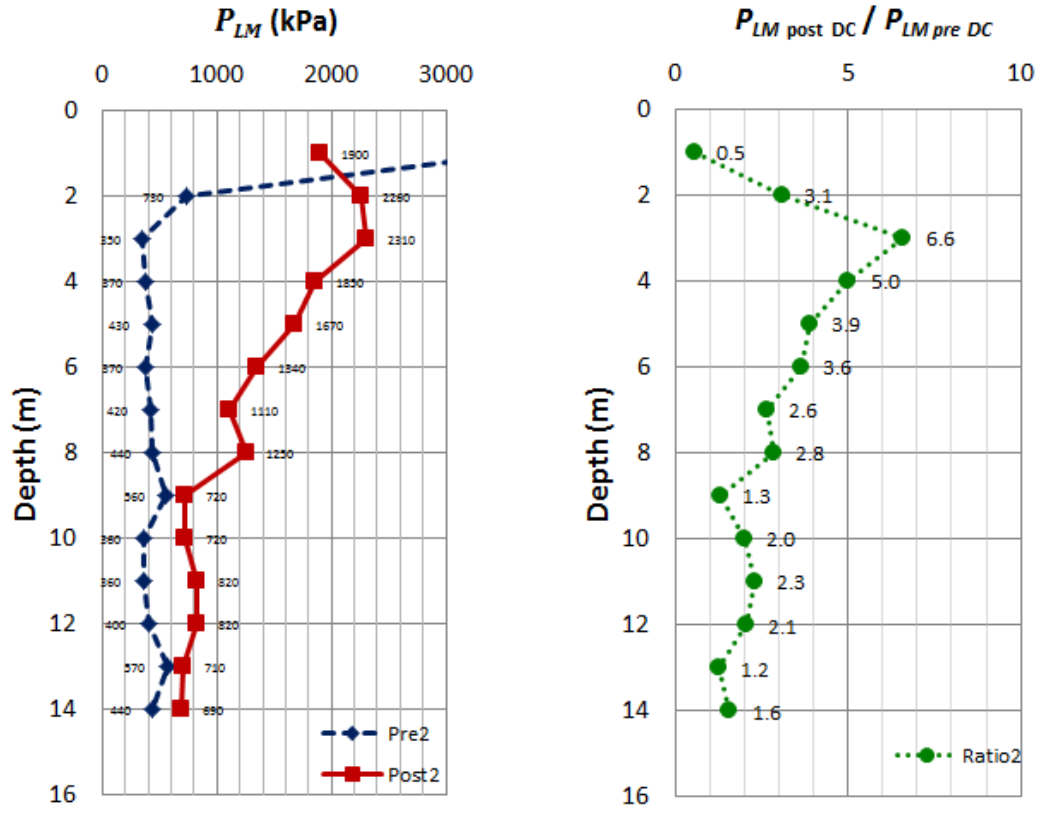

Figure 3-31: P_{LM} and ratio of P_{LM} before and after dynamic compaction at test point No. 2

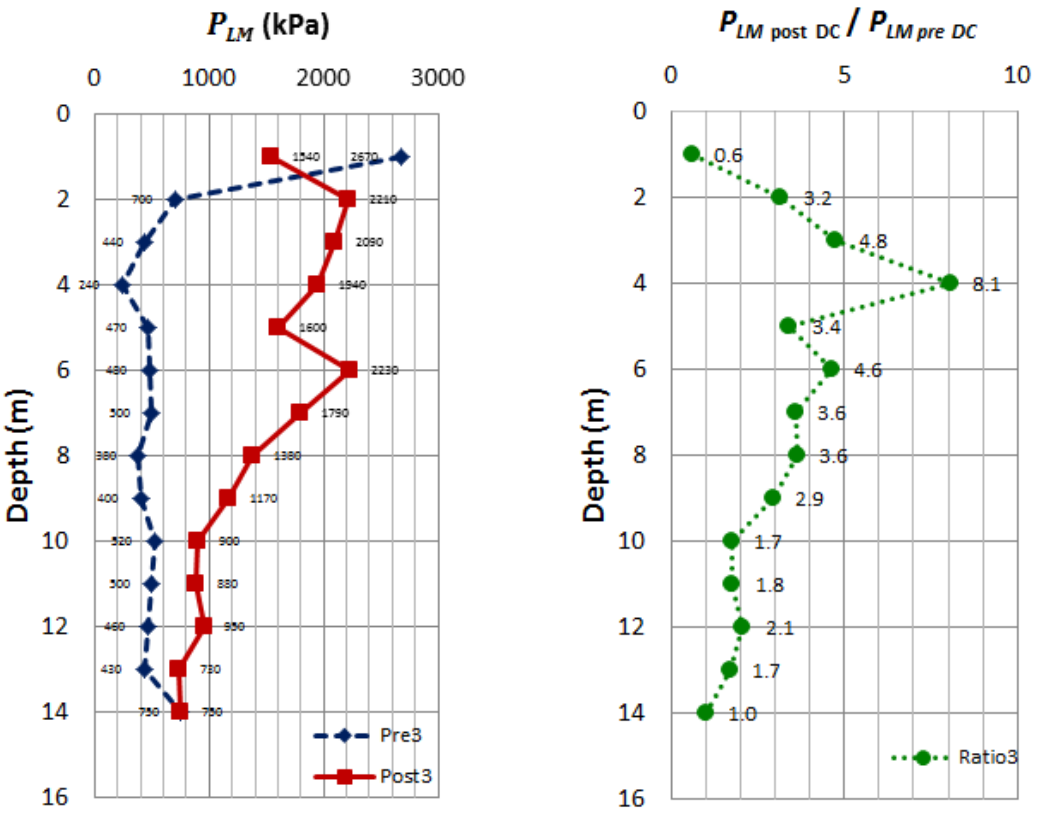

Figure 3-32: P_{LM} and ratio of P_{LM} before and after dynamic compaction at test point No. 3

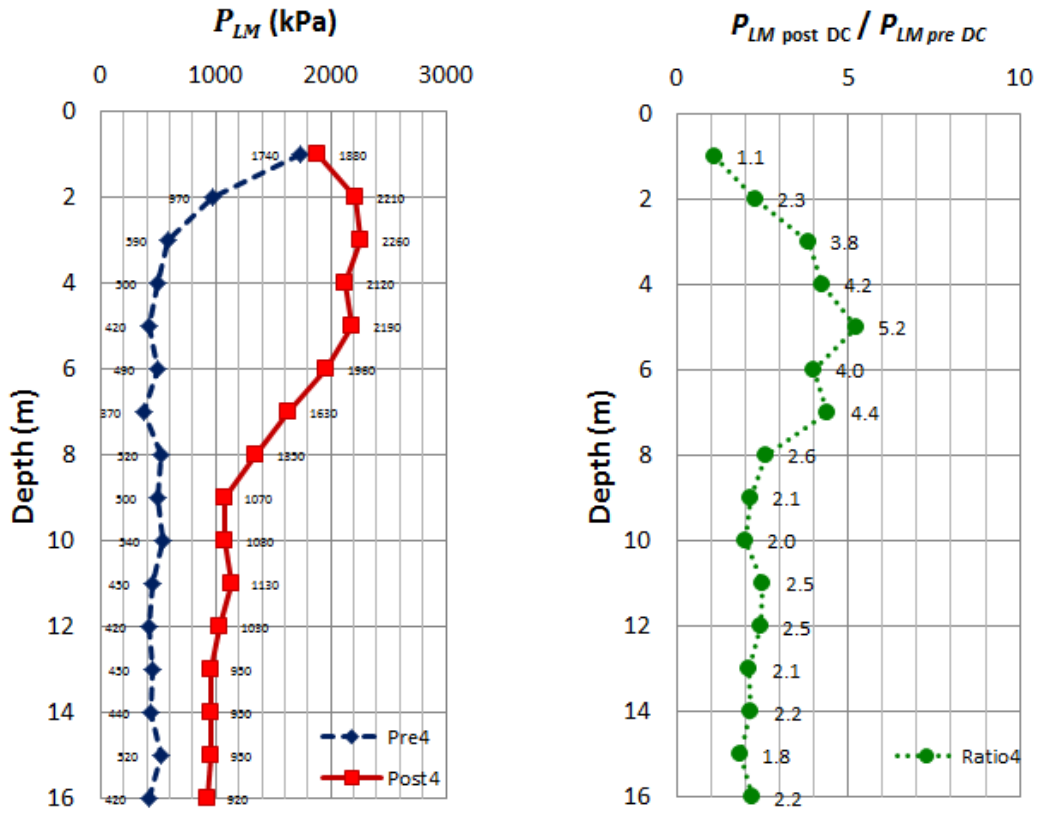

Figure 3-33: P_{LM} and ratio of P_{LM} before and after dynamic compaction at test point No. 4

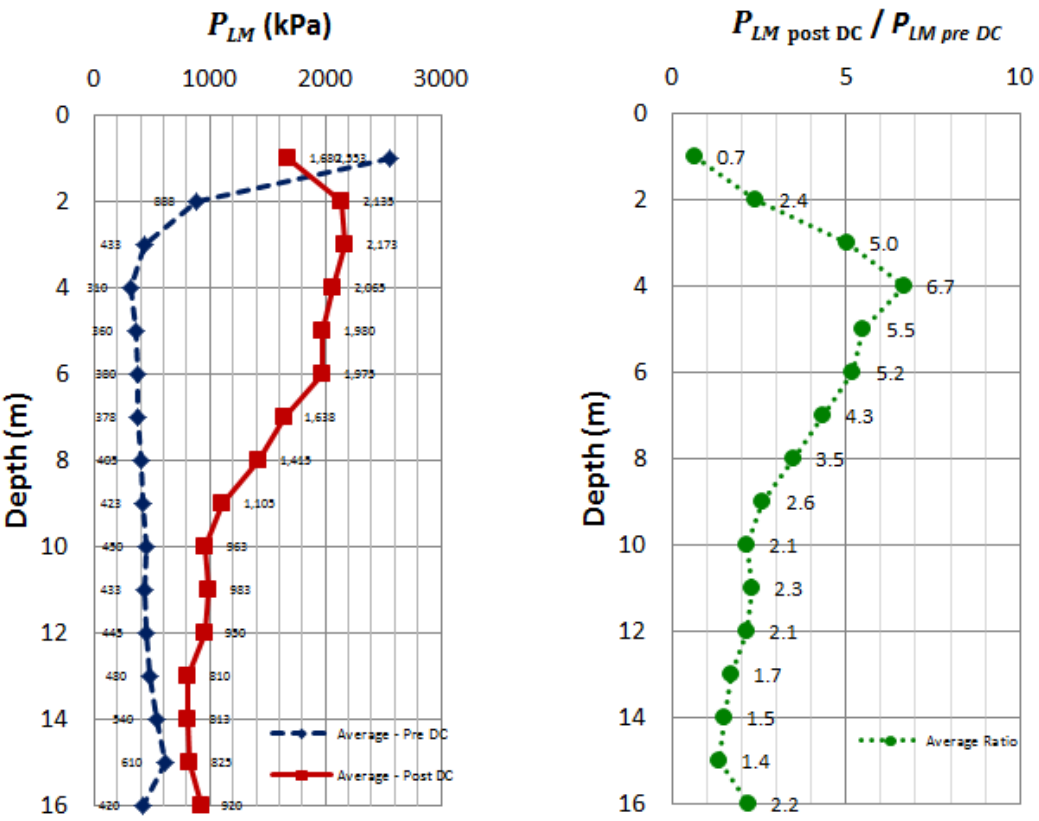

Figure 3-34: Average P_{LM} and ratio of average P_{LM} before and after dynamic compaction

2. Dynamic compaction can be understood to be an affordable and effective ground improvement for thick dry desert dune sands in isolated locations.

3. Proper determination of design criteria is very important, and failure to adopt a suitable specification can lead to unnecessary treatment, additional costs and delay.

4. The most suitable acceptance criteria are based on design criteria. It is not necessary to specify minimum test results as proper testing should be able to verify that design criteria have been satisfied. Also, one criterion does not have to govern throughout the depth of treatment. In Al Quo'a the upper layers were treated for bearing capacity and settlement under structural loads while the deeper soils were treated for self-bearing.

5. In large projects, it is preferable to mobilise dynamic compaction rigs with different capacities and to optimise treatment by applying various energy intensities based on the requirements of each zone.

6. It is possible to efficiently improve the depth of influence in dynamic compaction by implementation of the free falling and automatic grabbing MARS technology.

7. It is possible to improve maximum P_{LM} values of dune sands on average by up to 570% and at least in one instance by up to 1950%. Improvement beyond 400% was observed over a thickness of 20% of treatment depth.

3.4 King Abdulla University of Science and Technology

3.4.1 Project Description

The 5.6 million m^2 King Abdulla University of Science and Technology (KAUST) is located in Rabigh, on the Red Sea coast and near the city of Jeddah, in Saudi Arabia. KAUST, originally anticipated to have buildings with at most two to three stories, includes the university campus and academic administration core, a desalination plant, wind turbines, residential neighbourhoods, a research park, a commercial centre, a waste water treatment plant and a beach club. The university plan is shown in Figure 3-35.

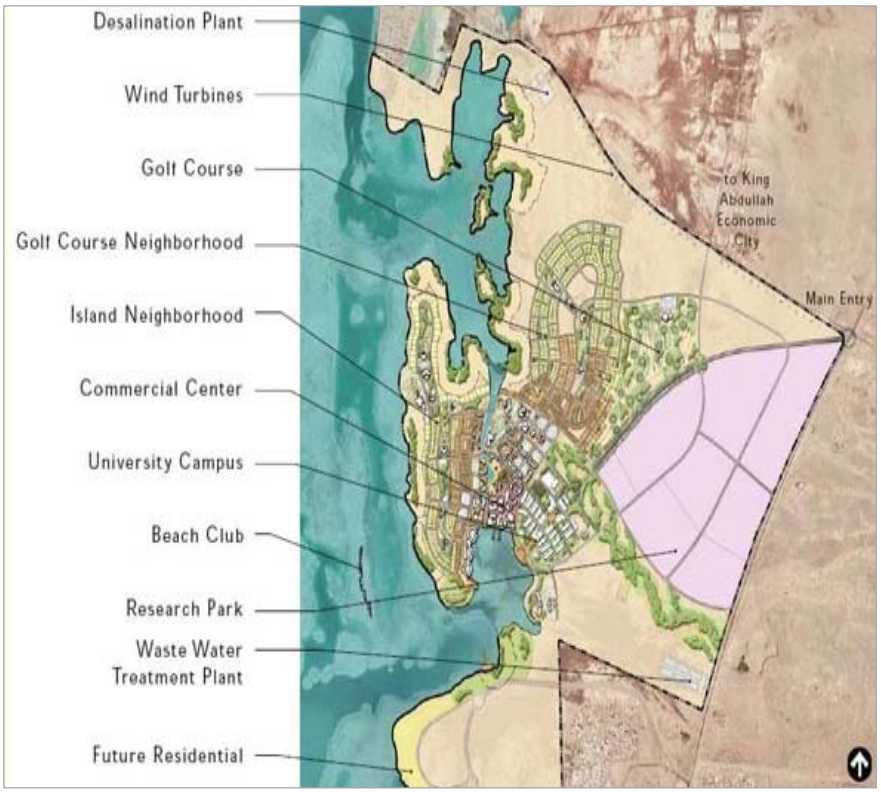

Figure 3-35: Plan of KAUST

The concept of the project was developed in 2006. According to the schedule, master planning, architectural and structural design and construction had to be completed in less than three years and handover date was set at September 2009.

3.4.2 Ground Conditions

The preliminary geotechnical investigation that was carried out at a relatively wide grid indicated that the ground was very heterogeneous and composed of a combination of loose

or soft soils with rapid variations within short distances. For example, q_c of two test locations that were 30 m apart are shown in Figure 3-36. It can be observed that in the first test q_c was approximately 5 MPa in the upper 1.5 m, but then dropped to almost null for the next 4 m until the ground strength increased and ultimately reached more than 20 MPa at the depth of 8.5 m. However, in the second test q_c in the upper generally sandy 2.5 m of ground is about 7 MPa, but drops to about 4.5 MPa (which is much more than the values of the first test at the same depths) in the finer soil that extends down to the depth of about 5.5 m, and then further reduces to about 2 MPa (which is much less than the values of the first test at the same depths).

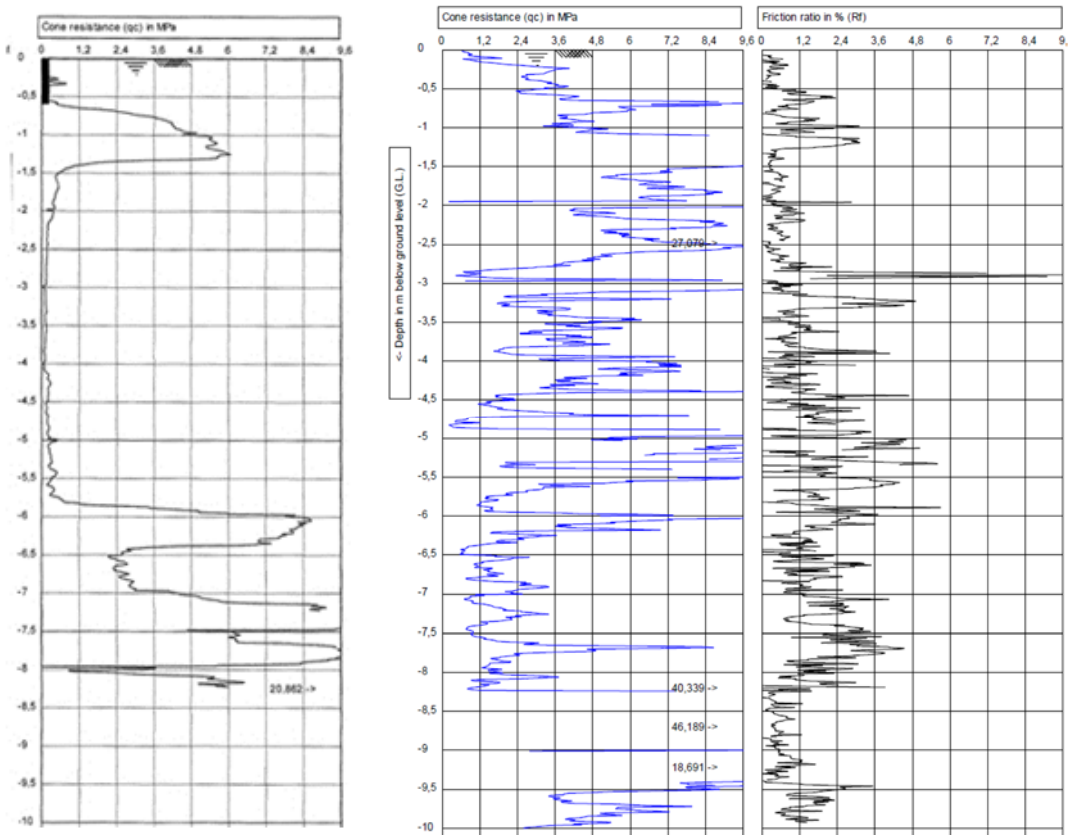

Figure 3-36: Variation of ground conditions for two test locations that were 30 m apart.

This investigation and further testing during the works revealed that more than 2.6 million m^2 of the construction area was to be built on soil consisting of up to 9 m of loose silty sand or soft sandy silt, which is locally called *sabkhah*, and originates from storms or eolien actions that have resulted in tidal lagoon deposits, and contain high concentrations of salt.

A generalised schematic profile of the ground and a summary of the test results for each soil layer are respectively shown in Figure 3-37 and Table 3-7.

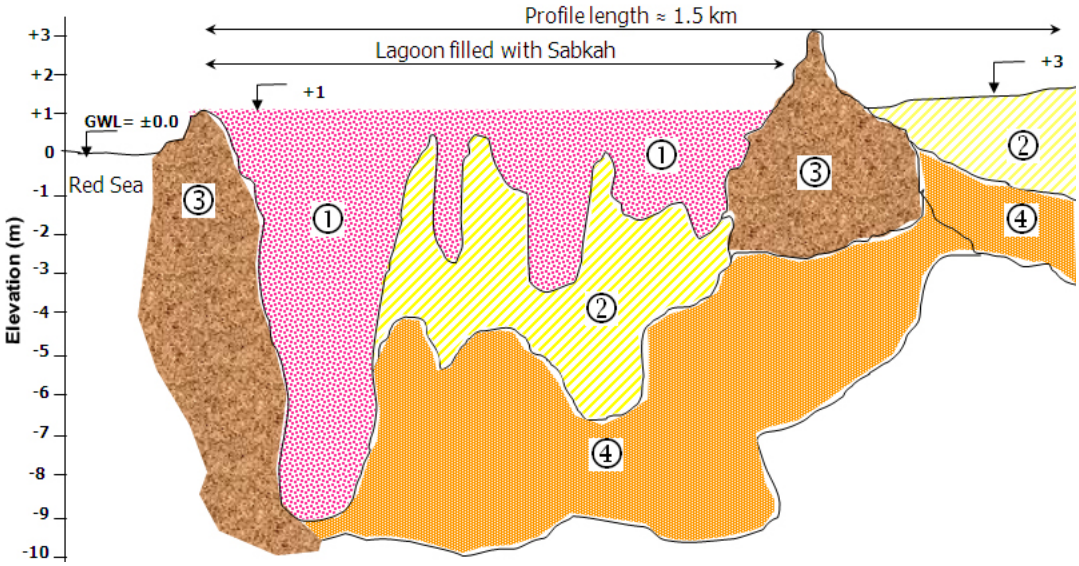

Figure 3-37: Ground profile at KAUST

Layer & USC	Water Content	Fines Content	N_{SPT}	CPT		PMT	
				q_c (MPa)	f_r (%)	P_{LM} (kPa)	E_M (MPa)
1- Sabkhah: Silty Sand and low plasticity Silt	35-48%	28-56%	0-2	0-0.2	1.2-4.0	40-190	0.4-1.7
2- Silty Sand	-	15-28%	3-9	1.2-4.5	0.5-1.2	210-400	1.8-3.5
3- Coral	26-35%	-	6-12	-	-	510-720	3.5-6.0
4- Silty Sand	-	12-37%	3-18	1.5-1.8	0.5-1.8	400-1200	2.8-8.5

Table 3-7: Ground conditions at KAUST

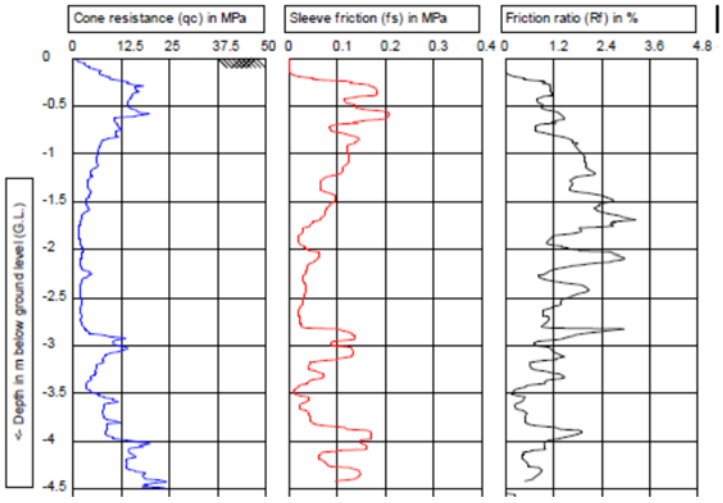

Figure 3-38: CPT-19

A number of CPTs that demonstrate the variation of ground conditions are shown in Figure 3-38 to Figure 3-43.

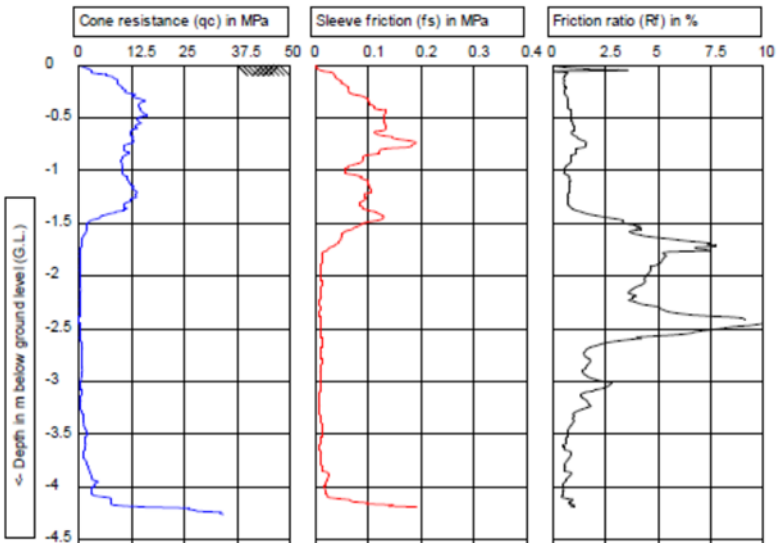

Figure 3-39: CPT-178

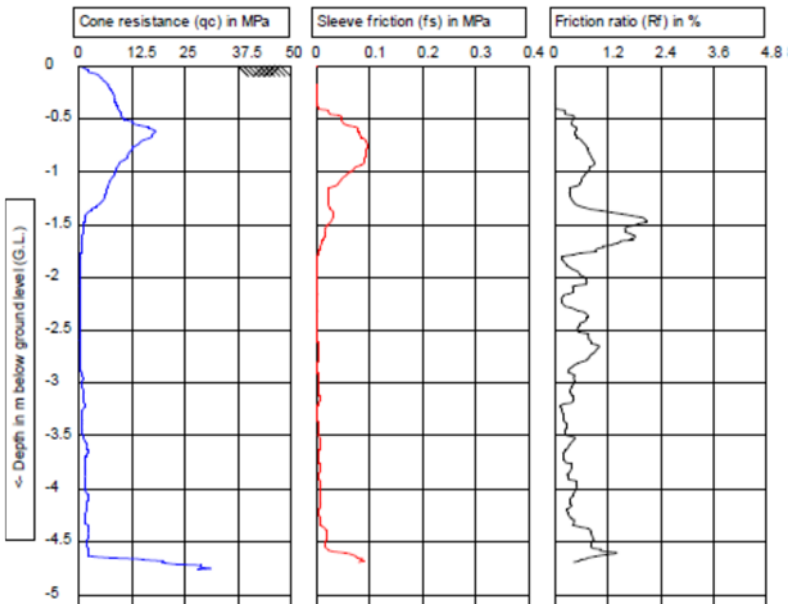

Figure 3-40: CPT-27

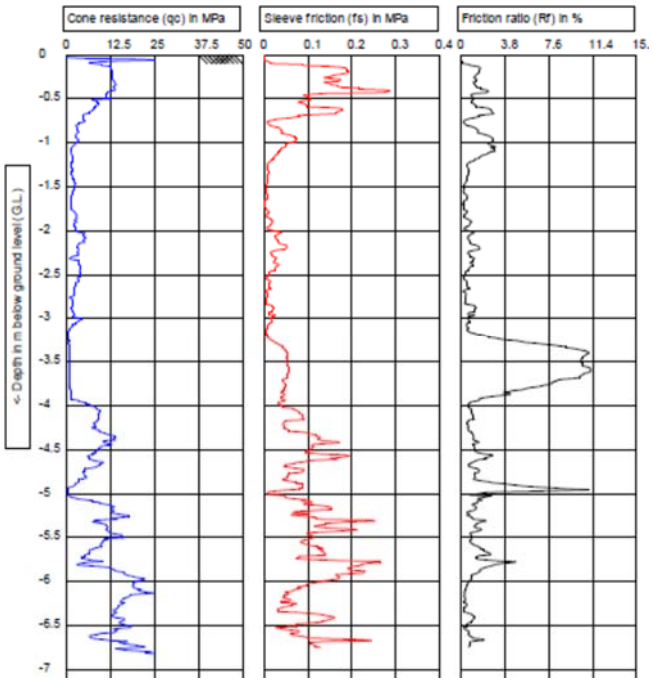

Figure 3-41: CPT-12

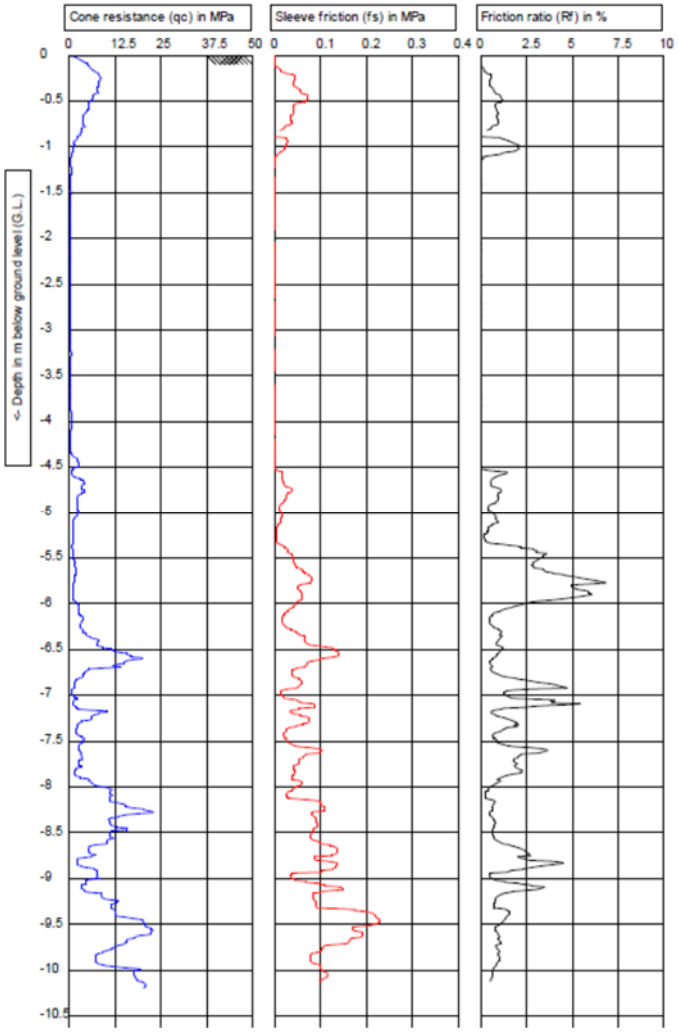

Figure 3-42: CPT-138

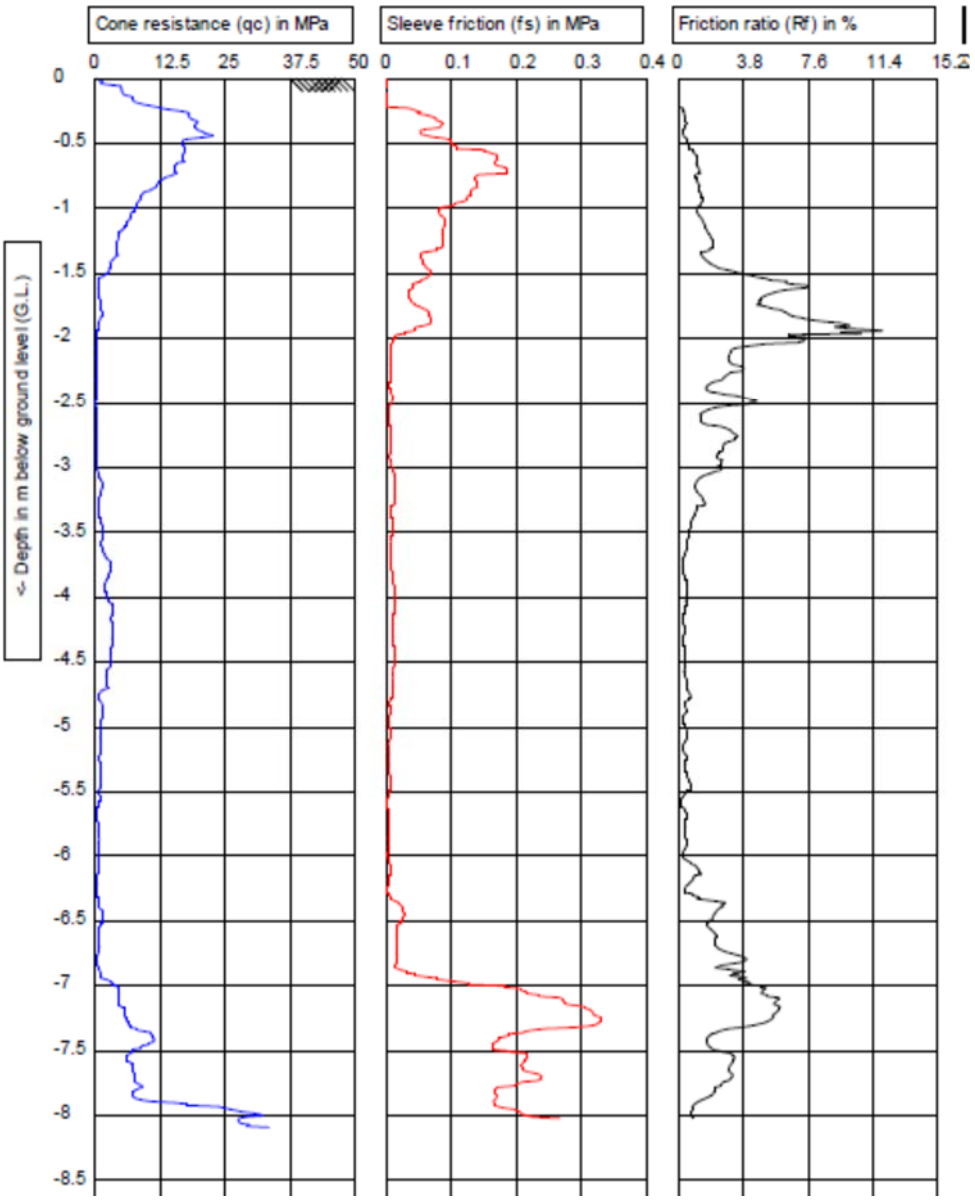

Figure 3-43: CPT-206

As groundwater level was less than 1 m below in-situ ground level it was decided to raise the ground by about 3 m to be safely above high tide. Approximately 1 to 1.5 m of this granular fill was placed before ground improvement.

The unsuitable ground conditions was a warning to the project team that they should be expecting foundation problems, and with the objective to complete the project in due time, it was decided to develop and apply a ground improvement plan while design was proceeding.

3.4.3 Development of the Ground Improvement Solution

While it was evident that only a well worked out schedule that incorporated design and construction could meet the project's deadline, the problematic soil that covered an area of approximately 2.6 million m^2 posed a serious threat to this programme as it was not possible to design the foundations without the finalisation of the buildings' locations and architectural drawings. The size of the area containing the problematic soil was so large that if ground improvement was to be undertaken in a single package (which became the case), then to the knowledge of the author, it would have become the world's largest ground improvement project of its time.

All possible foundation solutions were considered. Piling was immediately deemed as infeasible because without architectural and structural design it was not possible to define the pile locations. Thus, only ground improvement remained as a potential solution. Ultimately, the record breaking (to the knowledge of the author) ground improvement design and construction package was awarded to a specialist contractor that had proposed the application of dynamic compaction and dynamic replacement.

Design criteria were stipulated as:

- Footing location: Any place within the treatment area
- Maximum footing load: 1,500 kN
- Allowable bearing capacity: 200 kPa
- Maximum total settlement: 25 mm
- Maximum differential settlement between two adjacent footings: 1/500
- Liquefaction mitigation for an earthquake with (peak ground acceleration) *PGA*= 0.07g
- Foundation level: 0.8 m below final ground level, but in any case at least 2 m above sabkhah level.

While it was possible to construct a footing at any location without any concerns in the sandy zones that were to be treated by dynamic compaction, *per se* the same was not true after treatment of the zones consisting of sabkhah by dynamic replacement. In the latter case the structural loads would have had to distribute between the in-situ soft soils and dynamic replacement columns by arching (refer to Sections 2.4.9.12.4.9 and 2.6.1). Consequently and as shown in Figure 3-44 to Figure 3-46, finite element analyses was undertaken to determine the DR grid size for safely distributing the footings' loads without punching into the ground

in between the DR columns. Based on a minimum P_{LM} value of 180 kPa in the sabkhah layer, the optimised column grid was determined to be a square grid of 3.8 m with minimum DR column diameters of 2.2m.

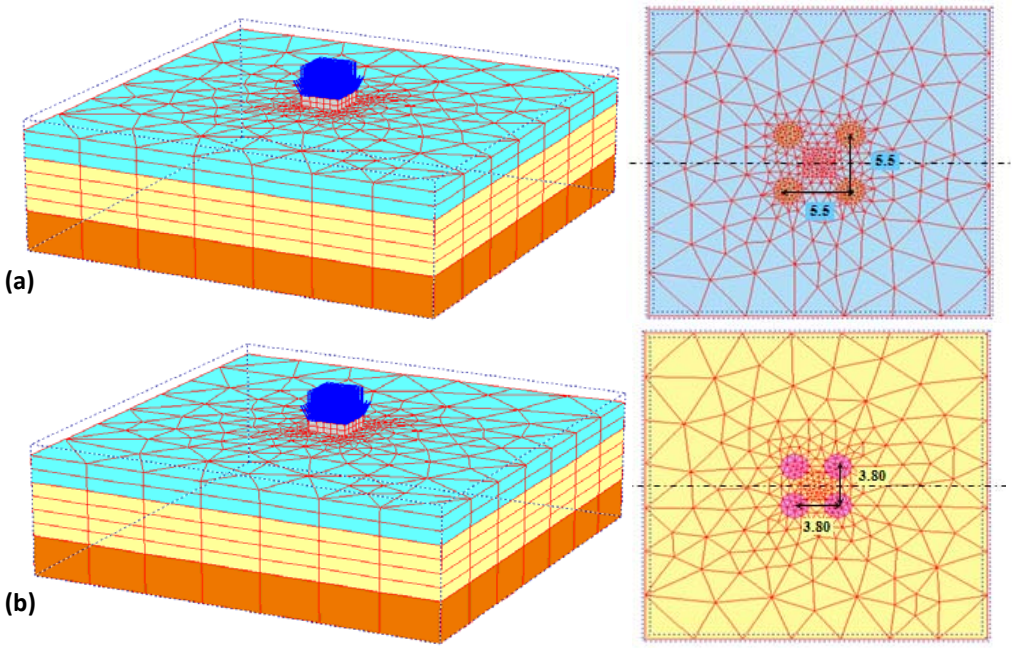

Figure 3-44: Finite element modelling for DR columns at (a) 5.5 m grid and (b) 3.8 m grid

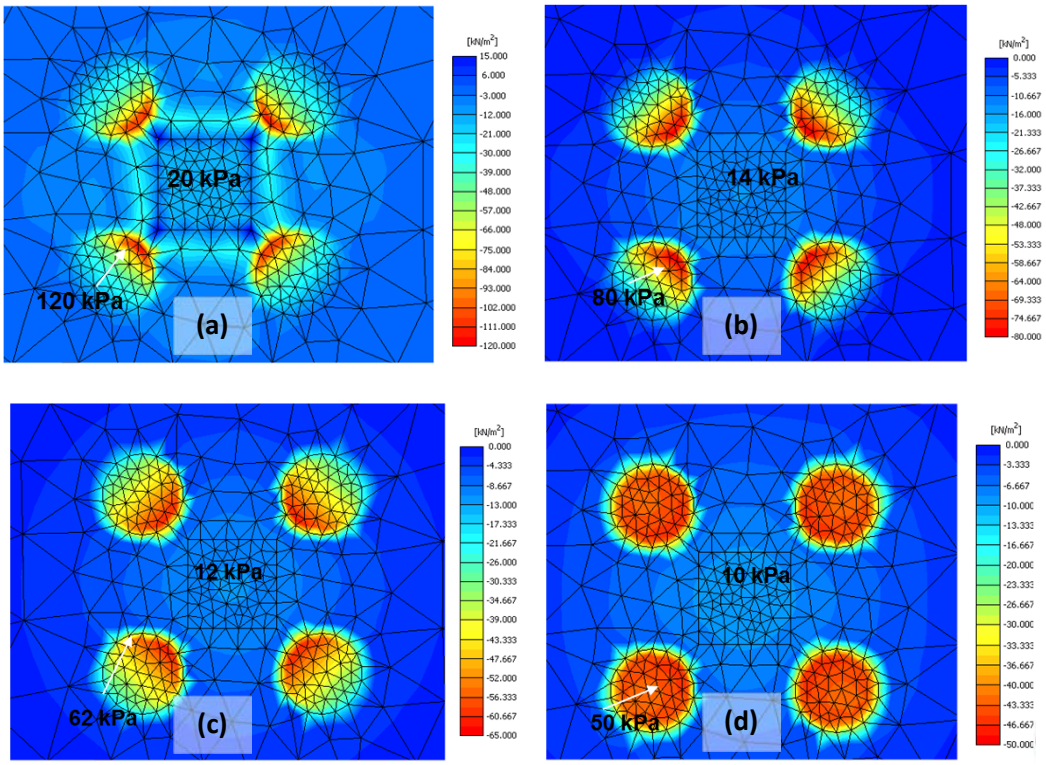

Figure 3-45: Vertical effective stresses for 5.5 m spaced DR grid elevations (a) 0.0 m RL, (b) -1 m RL, (c) -2 m RL and (d) -3 m RL

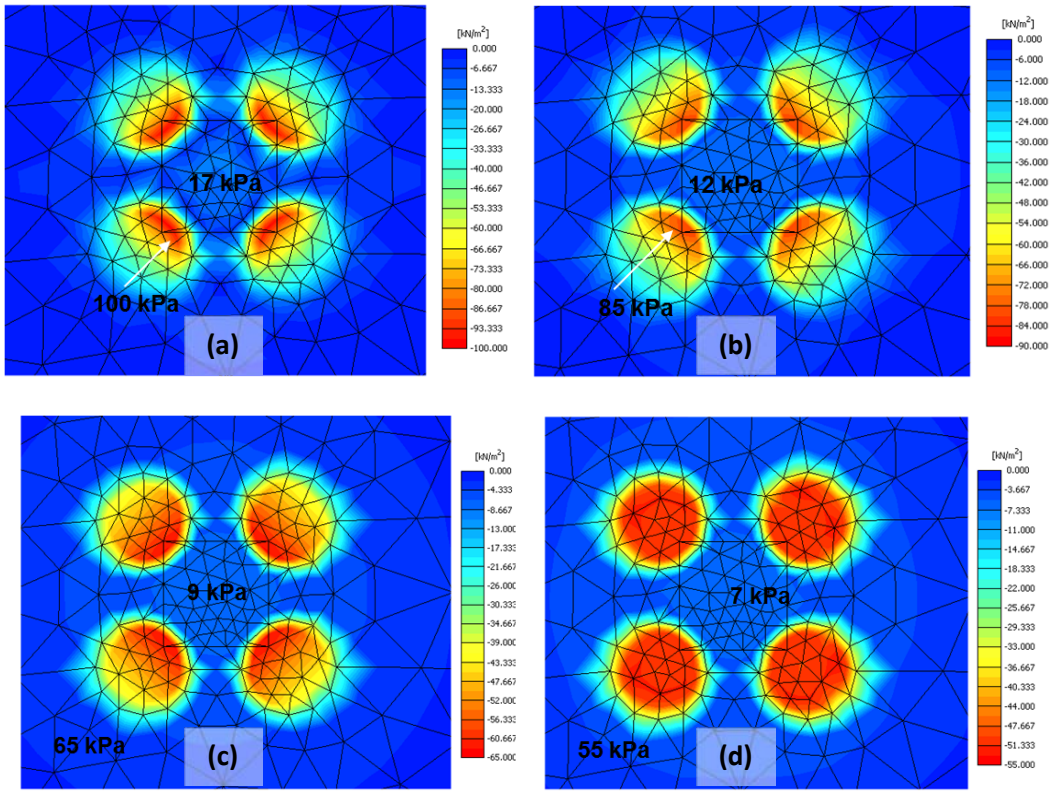

Figure 3-46: Vertical effective stresses for 3.8 m spaced DR grid elevations (a) 0.0 m RL, (b) -1 m RL, (c) -2 m RL and (d) -3 m RL

The foundation concept is shown schematically in Figure 3-47.

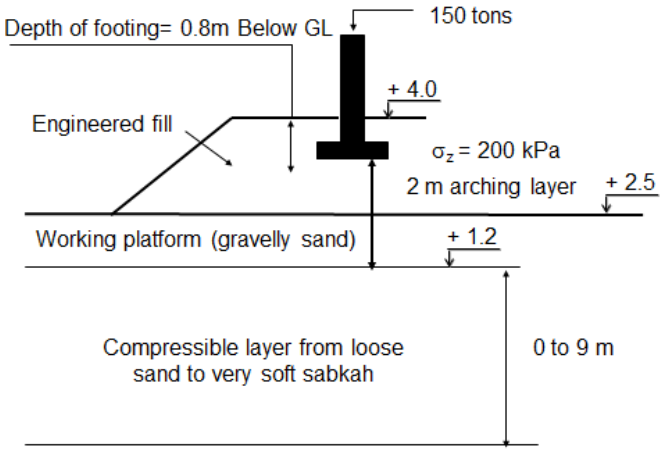

Figure 3-47: Foundation concept

3.4.4 Application of Dynamic Compaction and Dynamic Replacement

Prior to application of ground improvement by a combination of dynamic compaction and dynamic replacement techniques the working platform was constructed by dumping and levelling 1 to 1.5 m of granular fill. Roller compaction was not necessary as the platform

material was to be compacted in the process of soil improvement works. This was advantageous because not only was the cost of levelling in layers, watering, removal of oversize material, mixing and roller compaction eliminated, but more importantly precious construction time was saved.

In this project pounders weighing up to 25 tons were used to compact soils with fines content up to about 30 to 35% using dynamic compaction. Dynamic replacement was used in areas where the maximum depth of sabkhah was 5 m. When the depth of sabkhah was more than 5 m, high energy dynamic replacement (*HDR*) was used in conjunction surcharging the areas for a period of 6 weeks. The surcharge was placed to 3 m above final grade level.

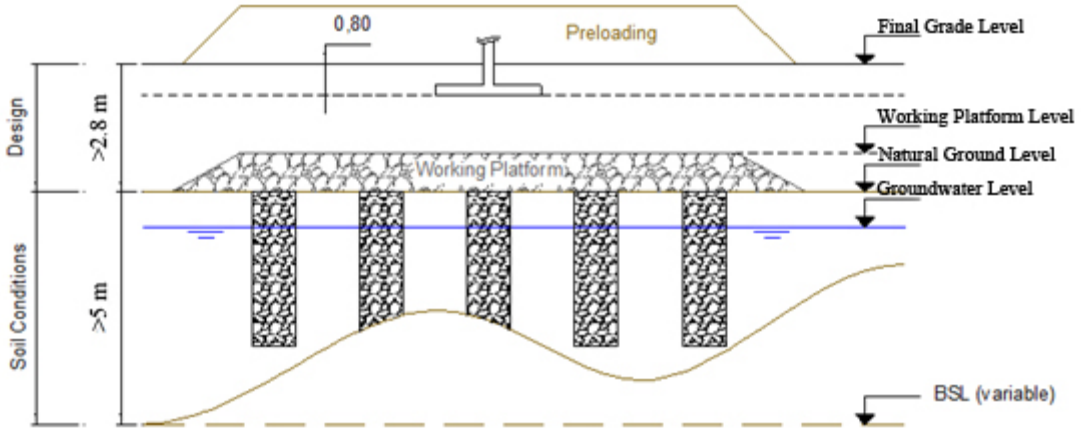

Figure 3-48: Application of 3 m surcharge above final grade level after dynamic replacement in areas with sabkhah being deeper than 5 m.

After completion of ground treatment in specific areas, it became known that the revised master plan incorporated 36 buildings with more floors and heavier loads. Consequently, a derivative of dynamic compaction called *dynamic surcharging* was also used to consolidate the deep sabkhah layers. In this technique the combination of preloading and vibration is used to re-introduce pore pressure in the soil-water system and consequently to accelerate settlement rates. It is the author's experience (Varaksin, 2014) that dynamic surcharging is applicable to silts, but not to clays, and additionally the degree of consolidation must be roughly in the range of 50 to70%.

Hence, in addition to the engineered fill required for reaching final grade level, a 3 m high surcharge was placed, and as shown in Figure 3-49, dynamic compaction was performed on top of the surcharge. The surcharge was left in place for 3 weeks.

Figure 3-49: Dynamic Surcharging in KAUST

As previously noted, variations in ground conditions occurred quite rapidly, within short distances and the field geotechnical tests were performed in a relatively wide grid; hence, it was necessary to develop a method for determining the ground condition, and applying the relevant ground treatment method. Although performing additional field tests would have been the first logical choice, the introduction of hundreds of additional tests would have delayed the project. Therefore, a highly accurate observational approach was implemented.

In this approach the trend of sabkhah depth was initially identified by the field tests. Differences in ground behaviour due to pounder impact enabled the site supervisors to assess the rapidly varying ground conditions, and to apply the appropriate ground improvement technique as needed. It was observed that while the first DC pounder impact penetrated the ground by about 0.25 m, the DR pounder penetration was substantially more and in the range of about 1 m. Also, performing DC frequently resulted in the seepage of groundwater to the surface, but this phenomenon was rarely encountered in the DR areas. Ground rest periods in between DC phases were 1 to 3 days. However, this period was considerably longer and from 7 to 21 days when DR was utilised. Furthermore, ground heave due to pounding was not observed in DC areas, but was evident in DR zones.

A pilot test was realised with pressuremeter testing and SPT (for grain size analysis) to define the boundaries of application of the dynamic compaction and dynamic replacement techniques as a function of grain size, P_{LM} and applied energy. Furthermore, a spread sheet

based on PMT interpretation rules (Centre D'Etudes Menard, 1975) was prepared for the quick estimation of the bearing capacity and settlement by the site engineer.

Figure 3-50 shows the flow chart for determining the applicable ground improvement technique.

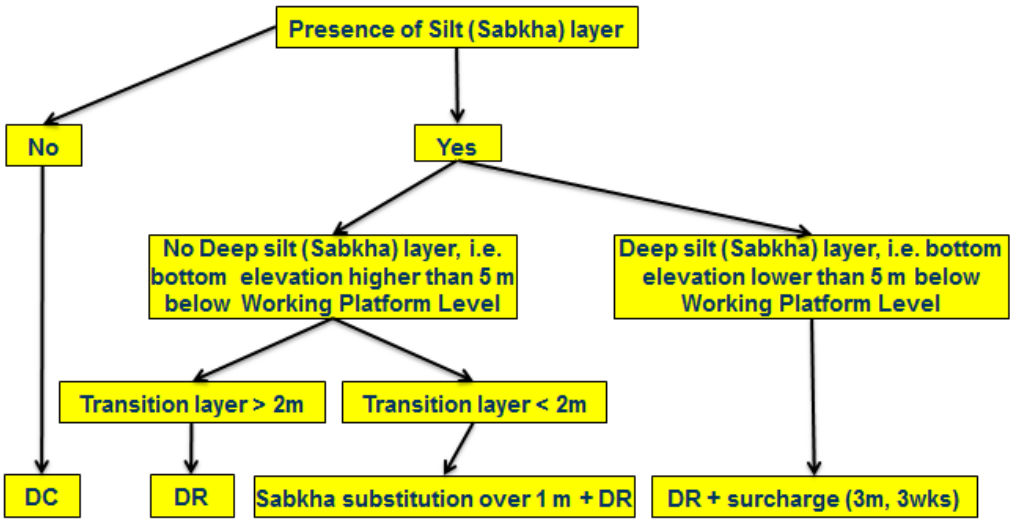

Figure 3-50: Flow chart for determining applicable ground improvement technique

The allocated time frame for mobilisation, execution and testing of ground improvement works was 10 months. Ground improvement was carried out over a period of 8 months using a total of 13 rigs working two shifts per day. To the knowledge of the author, this is the world record for the number of DC rigs working at the same time on a single project. A review of production data shows that at its peak, the rate of ground improvement was about 600,000 m^2 per month, which to the knowledge of the author was the world record at that time. Figure 3-51 shows 12 rigs symbolically lifting their pounders. The 13^{th} rig was used for providing the necessary elevation for taking the photograph.

Figure 3-51: Utilisation of 13 DC-DR rigs in two shifts (photograph taken from the 13^{th} rig)

In addition to the 13 rigs, other equipment that were implemented in the project included 15 pounders weighing from 12 to 25 tons, 30 vehicles, 1 truck equipped with a crane, 1 forklift, 3 CPT rigs, 3 SPT rigs, and 3 PMT rigs.

3.4.5 Testing and Verification

During the course of ground improvement works a total of 76 test pits, 122 SPTs boreholes, 672 CPTs, and 403 PMTs were carried out for determination of the appropriate ground improvement method, fines content, liquefaction mitigation, bearing capacity and settlements.

P_{LM} before and after dynamic compaction in one of the test locations is shown in Figure 3-52. It can be observed that while P_{LM} was as low as 200 kPa at some depths before dynamic compaction, P_{LM} increased by 3 to more than 4 times after dynamic compaction. P_{LM} improvement ratio can be seen to be variable from as low as 1.9 to 4.5 with an average value of 2.9.

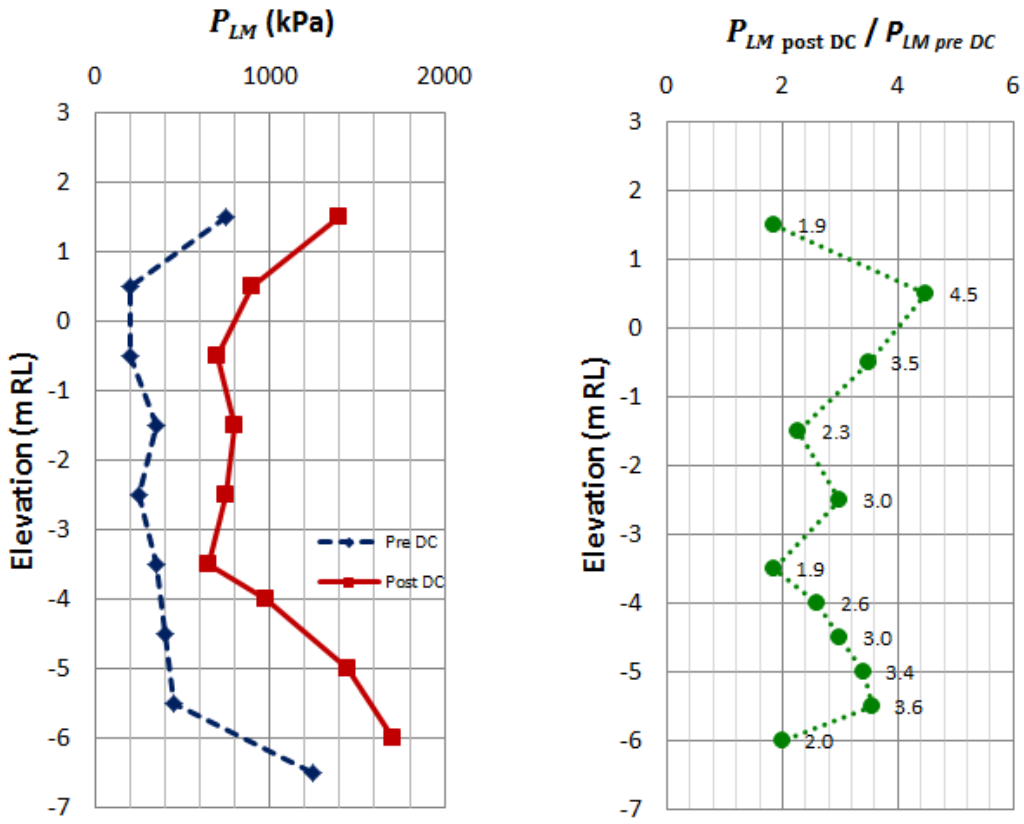

Figure 3-52: P_{LM} before and after dynamic compaction and P_{LM} improvement ratio

Figure 3-53 shows P_{LM} before and after (between DR columns and inside one of the DR column) dynamic replacement in one of the test locations. It can be observed that dynamic

replacement has been able to the improve the sabkhah layer in between the DR columns throughout the testing depth to at least 190 kPa and that average P_{LM} improvement ratio of the in-situ is approximately 2.3; however, this amount of improvement would not have been sufficient to satisfy the design requirements without the DR columns. The peak and average P_{LM} improvement ratio of the DR column were respectively 18.56 and 10.2, which demonstrate a massive improvement in the ground conditions.

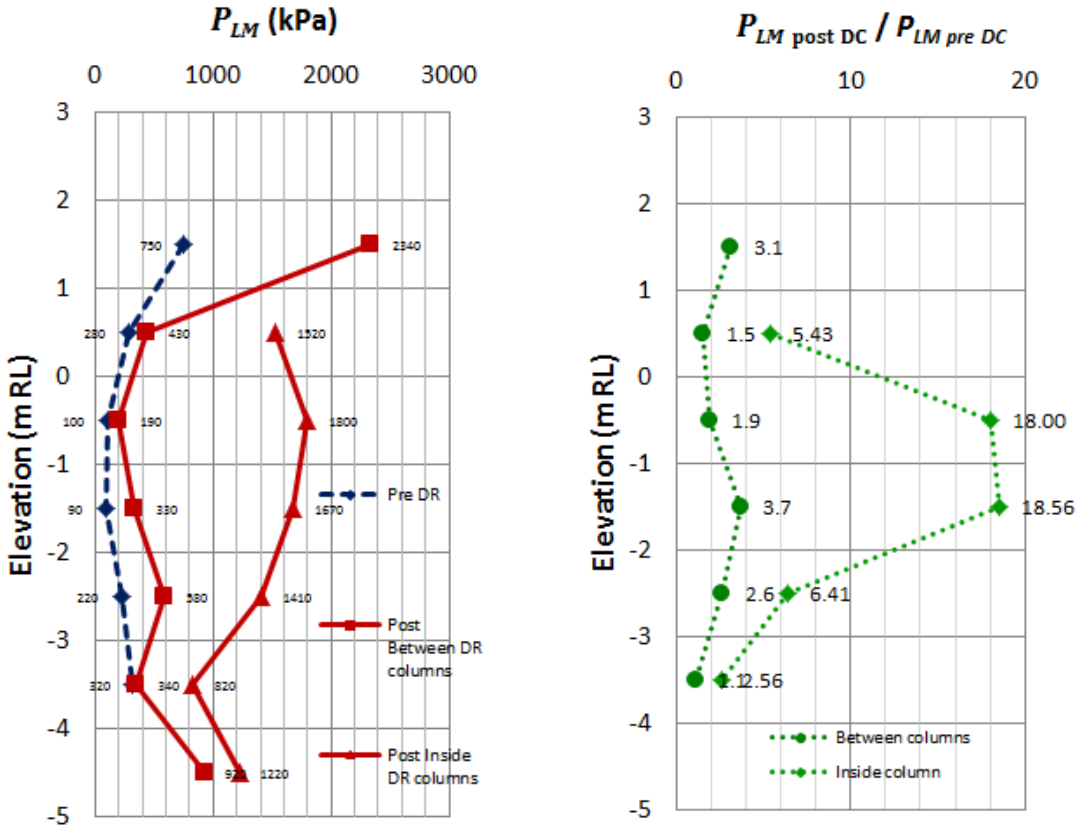

Figure 3-53: P_{LM} before and after dynamic replacement and P_{LM} improvement ratio

Due to the wide range of ground conditions, including soil classification, strength, and thicknesses of layers, test results showed a wide range of results. Although the results clearly demonstrated that design criteria had been satisfied, it is interesting to note that it is possible to classify the test results according to the amount of dynamic energy applied to the ground and the amount of improvement. Figure 3-54 shows the relation between the net pressuremeter limit pressure (P_{LM}-P_o) and the energy per volume of improved soil. As expected, it can be observed that the improvement factor (*I*) or the ratio of after to before soil improvement net limit pressure (only the in situ soil without the DR columns) is higher and more efficient when the soil is more granular and contains lesser fines. Furthermore, it can be noted that the DR columns play a vital role in providing the required ground properties in the sabkhah soils, and their exclusion will result in failure of satisfying the design criteria.

Figure 3-54, which has been realised by Serge Varaksin, also indicates that the boundary between the application zones of DC and DR is at about 30% fines content.

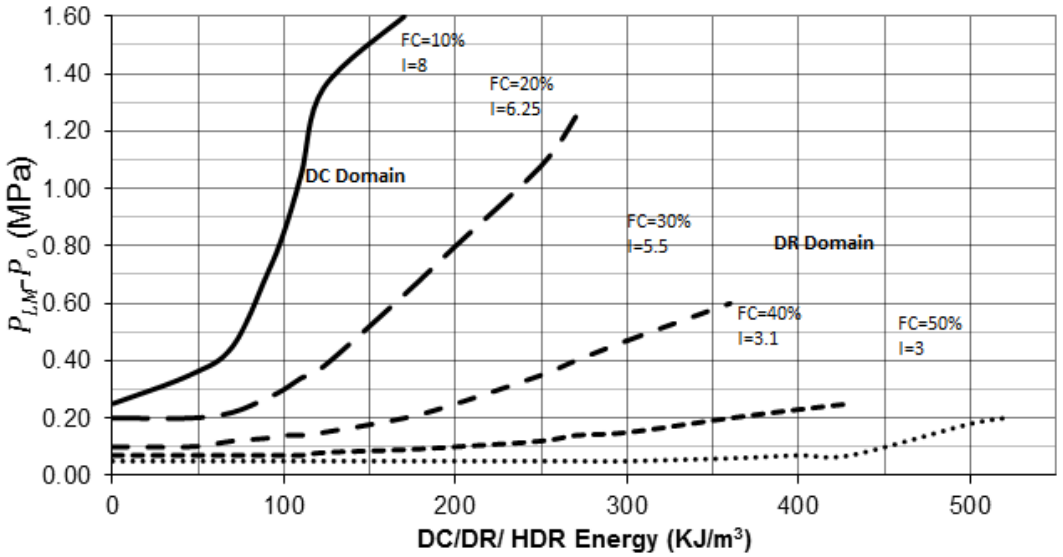

Figure 3-54: The relationship between net limit pressure, fines content and improvement energy

The effect of surcharging in one of the areas where the depth of sabkhah exceeded 5 m is shown in Figure 3-55. As can be observed, even though dynamic replacement columns had strengthened the ground in this area, settlement of the deep soft soils would have potentially remained a geotechnical concern, and could have resulted in damaging settlements without the application of surcharging.

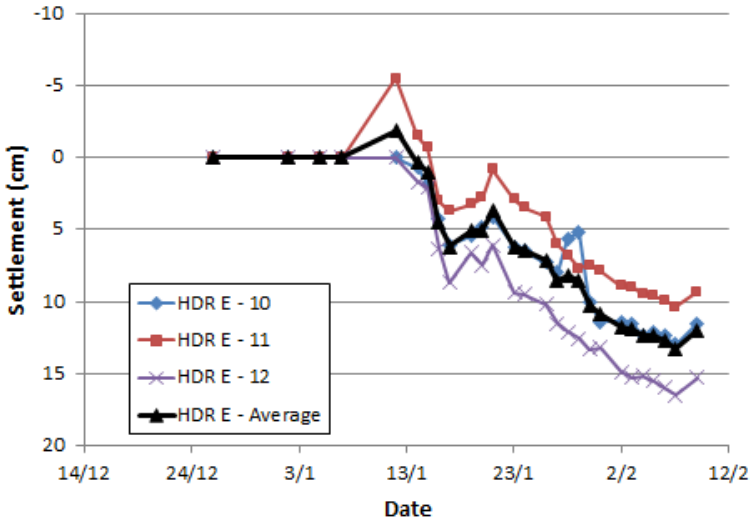

Figure 3-55: Settlement induced by surcharging after implementation of DR in areas where sabkhah depth exceeded 5 m.

More interesting than inducing settlement of deep sabkhah layers in areas that have been treated by dynamic replacement is the pattern of induced settlements realised by dynamic surcharging. As can be seen in Figure 3-56, prior to the commencement of the first phase of dynamic surcharging the ground was gently settling due to the static preload that had been placed on the ground. However, contrary to classical consolidation theories that predict a reduction of rate of consolidation as time progresses, application of the first phase and second phases of dynamic surcharging suddenly increased both the magnitude and rate of settlement.

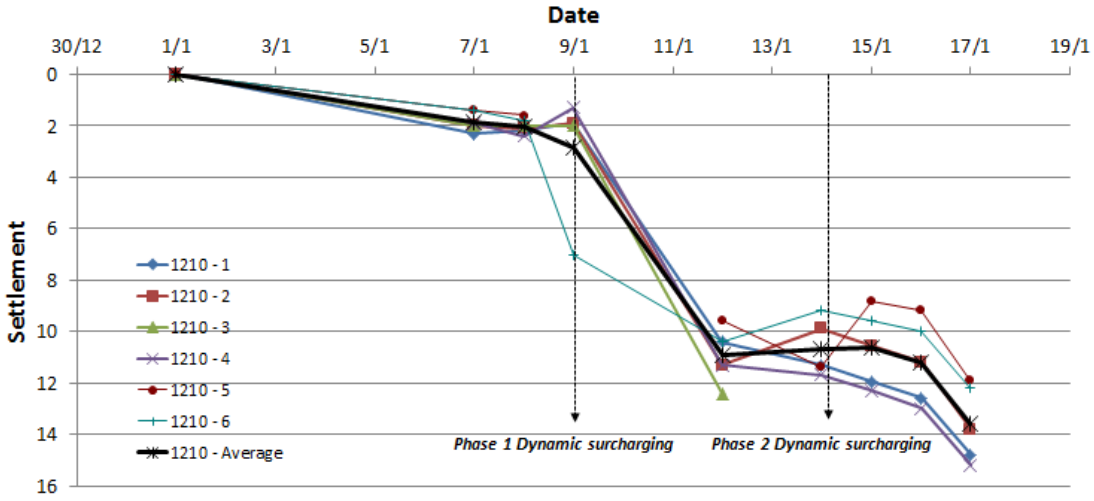

Figure 3-56: Settlement induced by static and dynamic surcharging

3.4.6 Lessons and Conclusions

This project demonstrates that classical solutions are not able to meet the requirements of special projects in which the site is unusually large, preliminary field tests are most probably insufficient, design and construction period is relatively short, and construction must commence in parallel to the preparation of the architectural and structural drawings. However, it is possible to construct such a project successfully if:

1. Design and construction phases are merged smartly and efficiently.

2. Design and acceptance criteria are specified based on the actual project requirements.

3. A combination of ground improvement techniques are used for treating different ground conditions rather than forcefully trying to implement one technique to a

variety of different conditions. Furthermore, it may be more efficient to provide different amounts of treatment for each technique.

4. The limits of each technique are well understood. The efficiency of dynamic compaction rapidly deteriorates with the increase of fines content. It appears that the limit of efficiency is when fines content reaches approximately 30%.

5. It is the author's experience that dynamic surcharging is applicable to silts, but not to clays, and additionally the degree of consolidation must be roughly in the range of 50 to70%.

6. Possible production rates are well understood and sufficient amounts of plant and equipment are mobilised.

7. Site observations are given value and changes in actual ground conditions are taken into account during the process of the works.

8. Furthermore, combination of treatment methods; e.g. dynamic replacement and surcharging or dynamic surcharging can expand the applicability limit of the ground improvement techniques.

Figure 3-57 shows King Abdulla University of Science and Technology after construction.

Figure 3-57: King Abudulla University of Science and Technology

3.5 Al Falah Community

3.5.1 Project Description

As part of the development of Abu Dhabi, Aldar Properties launched the 12.7 million m^2 Al Falah Community Development project in 2008 in the outskirts of the capital city of UAE. The project was anticipated to include 5,000 villas, 2,300 townhouses, 2,100 apartment houses, 14 schools, a hospital, a shopping mall, a number of hotels, restaurants, and health clubs. The town's master plan is shown in Figure 3-58.

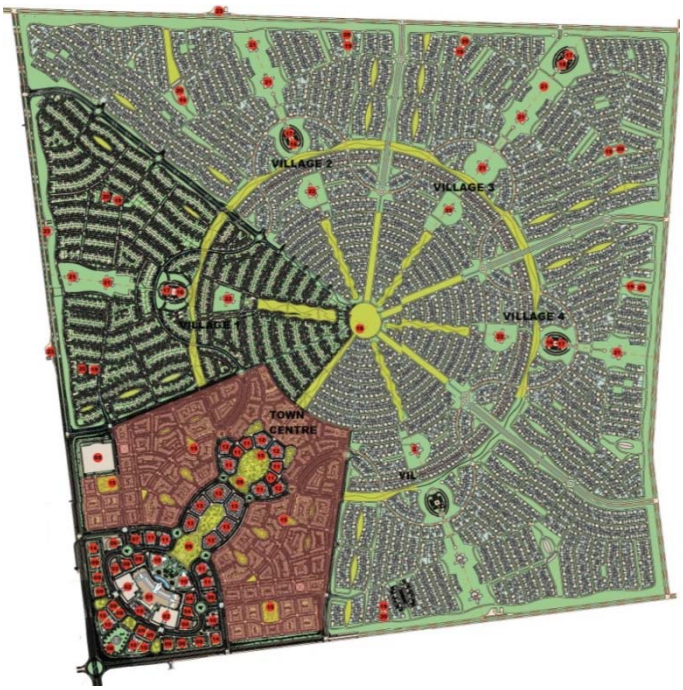

Figure 3-58: Master plan of Al Falah Community

3.5.2 Ground Conditions

The geotechnical investigation of the project indicated that the site was covered with a superficial layer of silty sand that had a variable thickness of only several centimetres to more than 18 m, and which was underlain by sandstone or siltstone bedrock.

As illustrated in Figure 3-59 (white areas), the major portion of ground at the site was very dense, and it was possible to construct shallow foundations without any geotechnical issues. The SPT blow counts in these areas were consistently more than 50, and CPT penetration would generally reach refusal within the first metre.

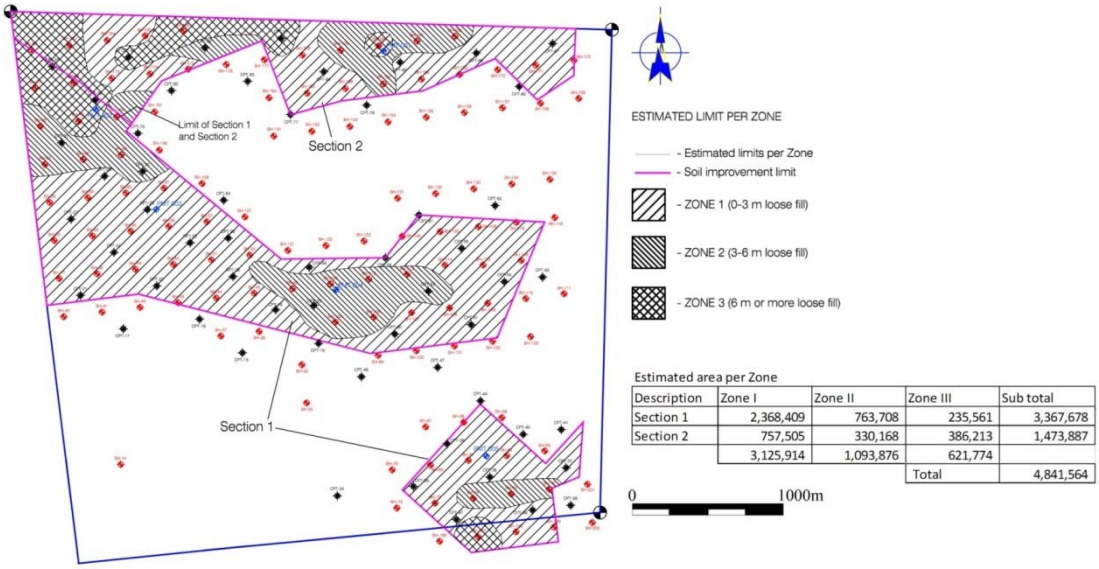

Figure 3-59: Site plan and limit of loose silty sands (hatched areas)

However, the ground conditions were not suitable for foundation construction throughout the entire site, and the test results indicated the presence of loose soil, shown as hatched zones in Figure 3-59, that approximately covered a total area of 4.84 million m^2. SPT blow counts in the superficial layer of these areas were generally from 7 to 12 and occasionally as low as 2. Similarly, q_c was mostly 2 to 3 MPa. Fines content of these loose soils were usually less than 25% but occasionally higher. CPT friction ratio was generally less than 1%, but occasionally increased to as high as 3%. Typical SPT and CPT results are shown in Figure 3-60.

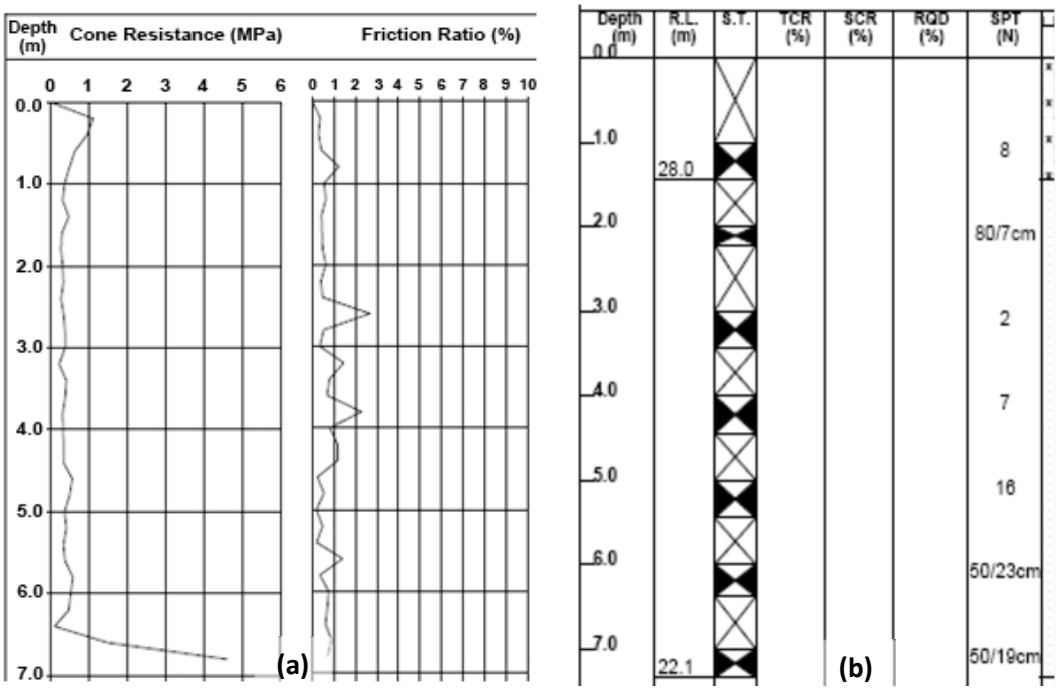

Figure 3-60: Two typical test results of initial ground conditions (a) CPT, (b) SPT

Further study and analyses of the data indicated that the thicknesses of loose soil deposits were less than 3 m in 66% of the site. 20% of the loose soils had thicknesses of 3 to 6 m, 8% had thicknesses of 6 to 10 m and 6% had thicknesses of more than 10 m and exceptionally up to 18 m.

It was observed that while the groundwater level was relatively deep and from 11 to 18 m below ground level, moisture content of the ground varied from 8 to 35% in the non-saturated layers.

The study, analyses and assessment of the geotechnical investigation and preliminary calculations demonstrated that the areas with poor ground conditions could not meet the project's foundation design criteria, which was defined as:

- Allowable bearing capacity: 150 kPa for conventional strip or pad foundations with maximum dimensions of 1.5m$\times$1.5m^2 (villa areas) or 3$\times$3 m^2 (heavy loads).
- Maximum total settlement: 25 mm for a maximum pressure of 150 kPa applied to the above mentioned footings
- Differential settlement: 1:500 measured between surface points not closer than 8 m apart.
- Liquefaction mitigation: for an earthquake with magnitude 6 and PGA= 0.15g

It was assessed that piling could not be included among the optimised foundation solutions as it was not only costly, but could not be carried out within the allocated time frame for foundation works; hence, ground improvement was identified as the preferred method for foundation construction.

3.5.3 Application of Dynamic Compaction and the Challenges

Based on the experiences of a number of mega size ground improvement projects local to the Middle East, such as the 2.6 million m^2 King Abdulla University of Science and Technology (Section 3.4), the 1.13 million m^2 Al Quoa New Township (Section 3.3), and the 0.9 million m^2 Abu Dhabi New Corniche (Section 3.2), one of the ground improvement specialist contractors proposed the implementation of dynamic compaction, and was awarded a 240 day design and construct contract to carry out the ground improvement works.

To the knowledge of the author, this project was the largest (in size) single soil improvement contract that had ever been undertaken at its time. Furthermore, the schedule was very tight,

and it was expected that the average ground improvement production rate during the contract period had to exceed 700,000 m^2 per month for the project to reach completion on time. As production rate was expected to increase gradually with the mobilisation of additional DC rigs, peak production rate was expected to exceed 900,000 m^2 per month for reaching the defined milestones. This, itself, was a challenge as the peak production rate world record was understood to be 600,000 m^2 per month (refer to Section 3.4) at that time.

It was evident that meeting the design specifications for the world's most demanding dynamic compaction project required the optimisation of impact energy by selecting the best combination of DC parameters. As a first step, it was decided to divide the treatment zones according to treatment thicknesses (0 to 3 m, 3 to 6 m, 6 to 10 m, and more than 10 m) and loading intensity (low rise villas or more heavily loaded apartments).

A total of 11 DC rigs were mobilised to complete the project within the contract period. Figure 3-61 shows six DC rigs during execution of the works. Heavy steel pounders weighing up to 23 tons were implemented to reduce the required number of drops per print.

Figure 3-61: Implementation of 11 special cranes for DC (not all shown in this photograph)

To facilitate site verification of tes results without detailed calculations and comparison of results with design criteria, a quick verification method that is shown in Table 3-8 was developed. It can be calculated by using Menard's method (Centre D'Etudes Menard, 1975) that safe bearing capacity and settlement of villas with the PMT parameters of Table 3-8 will

be respectively 360 kPa and 5 mm. For the heavily loaded structures safe bearing capacity and settlement can be calculated to be respectively 310 kPa and 7 mm.

Depth	PMT P_{LM} (kPa)	PMT E_M (kPa)	CPT q_c (MPa)
Above 9 m	800	7,500	6
Below 9 m	600	5,500	4

Table 3-8: Quick verification criteria

If test values exceeded the defined parameters, then acceptance would have definitely been achieved; otherwise detailed calculations would have been necessary.

The optimisation of the DC design and ability to provide sufficient number of rigs allowed the completion of the project before the due handover date; i.e., within a period of 7 months. It can be observed from Figure 3-62 that the maximum ground improvement production rate per month was 966,000 m^2, which to the knowledge of the author is the world's current ground improvement production rate record.

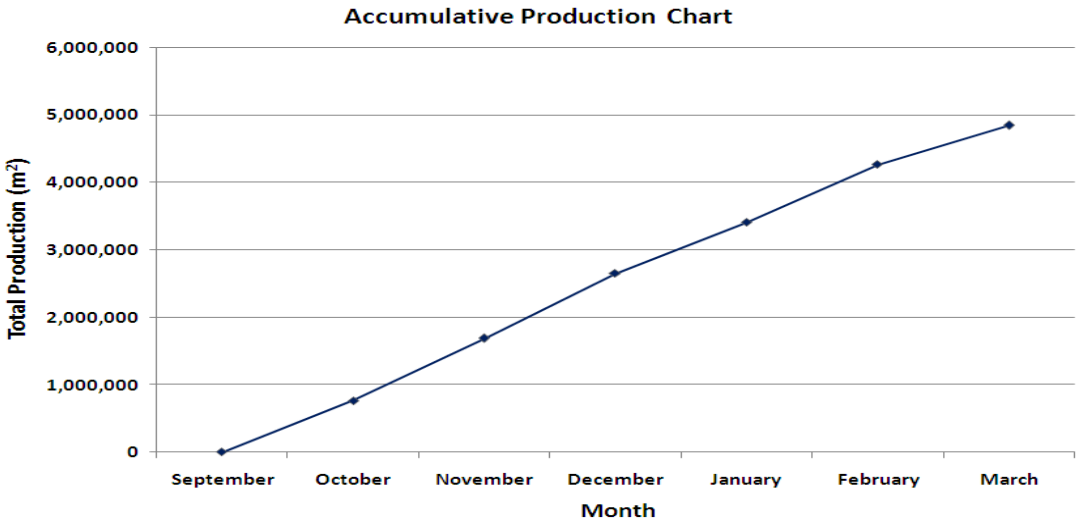

Figure 3-62: Accumulative treated area

3.5.4 Testing and Verification

3.5.4.1 Calibration

Due to the scale of the project and benefits of optimising the DC parameters as much as possible, prior to commencement of dynamic compaction a number of calibration programmes were carried out in areas with different thicknesses. The results of one of these

studies is discussed and analysed hereunder. In this programme the weight of the pounder was 20 tons, its base dimensions were 2x2 m^2, and the drop height was 20 m.

Figure 3-63 shows the preliminary stage of the calibration programme where the pounder was dropped 4 to 8 times on 5 prints. The distance between the centres of the prints were selected at 14 m to eliminate the effect of compacting one print on the other. In this part of the calibration programme a CPT was carried out next to (7 m away from the centre of) each print, and one CPT in the centre of each print after compaction. Preliminary calibration as undertaken in this project is, if ever, seldom, performed on typical projects as the potential benefits do not justify the required time and effort to perform it; however, the size of this project was an opportunity to perform this additional activity.

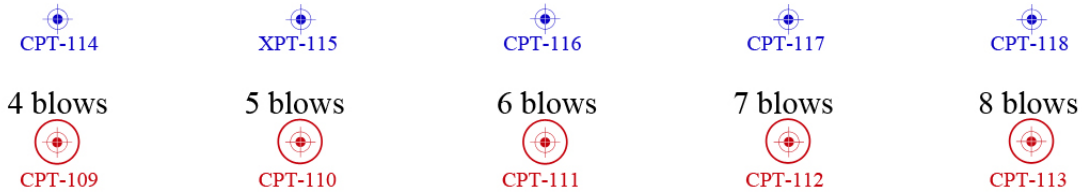

Figure 3-63: Calibration of phase 1 number of blows

CPT cone resistance before and after dynamic compaction for 6, 7 and 8 blows are compared in Figure 3-64. It can be observed that prior to dynamically compacting the prints the upper surface of the ground was very dense, but the sand then became loose to very loose. Application of the minimum number of 3 blows has met the quick criteria of Table 3-8, and this calibration suggests that there is no need to apply more than 3 blows to satisfy the project requirements at depth in the print location. Although the magnitude of q_c suggests that the quick criteria may have been also satisfied in between the prints, the results of this preliminary calibration *per se* do not definitively make such a conclusion and further testing during the calibration programme will be required.

It can be seen that DC blows have improved the soil strength at depths lower than about 1.2 to 1.5 m in the order of 3 to 5 times. The thicknesses of the superficial loosened sands were somewhat more than the pounder penetration depths. This is not very unexpected as the impact points were backfilled with sand from the platform, and ironing was not carried out.

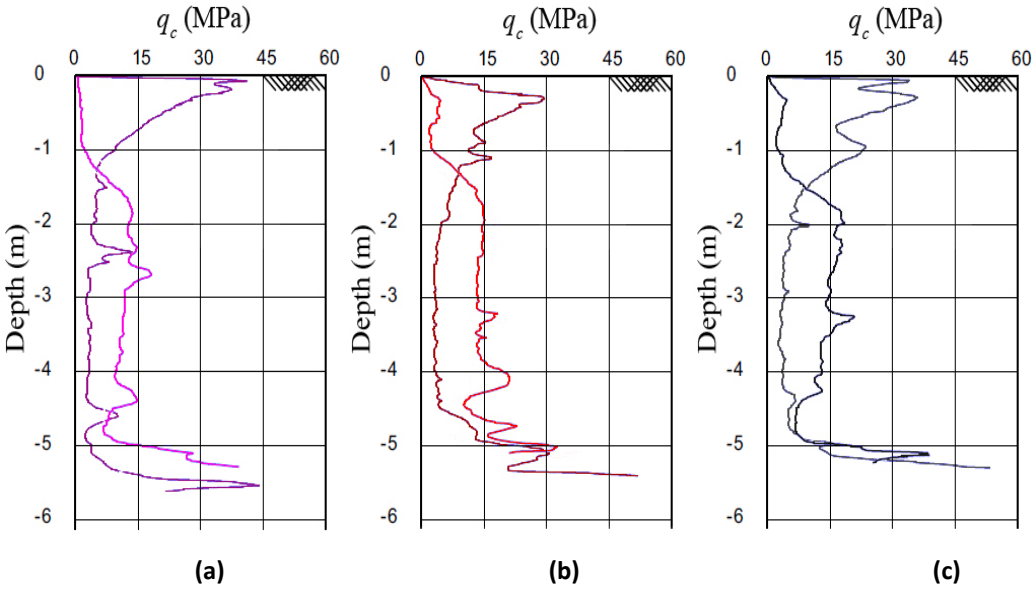

Figure 3-64: CPT cone resistance before and after DC (a) 6 blows, (b) 7 blows, (c) 8 blows

Cone resistance of CPTs performed in the prints after dynamic compaction is shown in Figure 3-65. Although it appears that the sequential increase of blows at some depths has led to progressive improvement, the variation of the CPT profiles does not lead to such a conclusive observation.

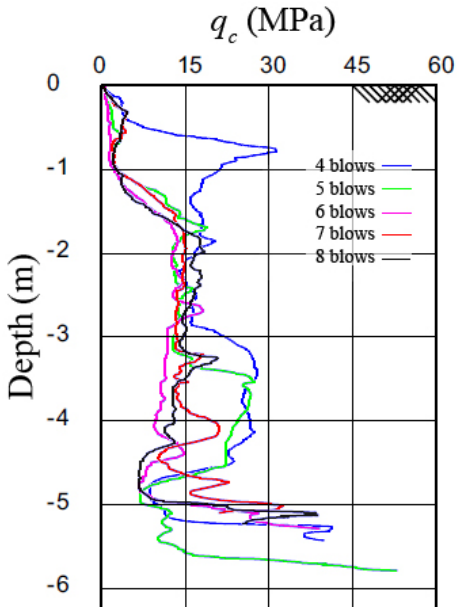

Figure 3-65: CPT cone resistance after compaction of prints

The layout of one of the calibrations is shown in Figure 3-66. In this part of the programme the same pounder (with a base area of 2x2 m^2 and weighing 20 tons) was also dropped from 20 m in 4 compaction patterns that have been shown in Figure 3-66. In the first phase of compaction the pounder was dropped 3 to 6 times on 4.95x4.95 m^2 grids. In the second phase of compaction the in between prints that were on a 3x3 m^2 grid were each subjected to 3

blows, and each of the prints of phase 1 received one more blow. A penetration test was also carried out using 20 blows.

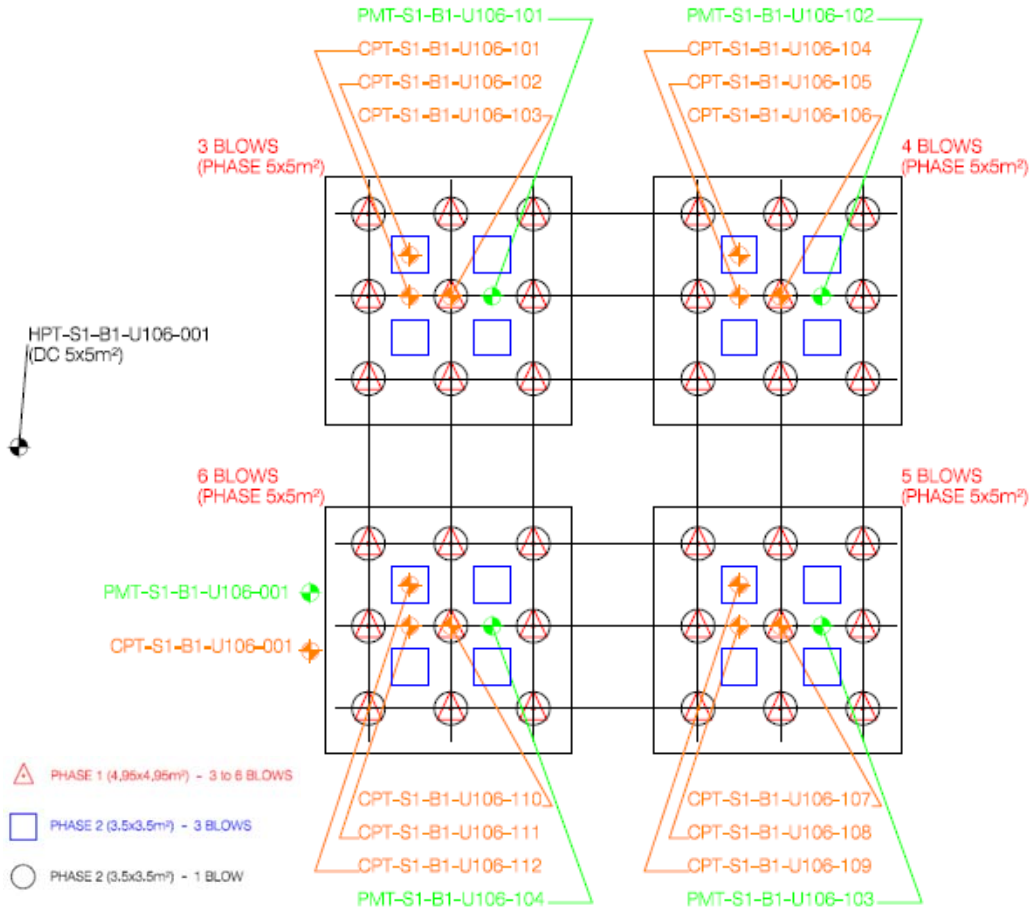

Figure 3-66: Dynamic compaction calibration layout

Prior to dynamic compaction a CPT was carried out at the calibration area, and 3 CPTs were also carried out after execution of dynamic compaction in each of the compaction patterns shown in Figure 3-66. These latter CPTs were carried out inside phase 1 print centres (with varying blow counts depending on the pattern), inside phase 2 print centres (with 3 blows) and in between the prints. For each pattern, one PMT was also performed in between the prints.

Figure 3-67 shows q_c values of the preliminary calibration (3 tests), the patterns (1 test) and the average q_c of all 4 tests before dynamic compaction. As before, it can be observed that the superficial ground layer is very dense, but the soil then becomes loose with q_c in the range of 2.5 to 3.5 MPa.

Cone resistances and average q_c improvement ratio, calculated as the ratio of average q_c after dynamic compaction to average q_c before DC, are shown in Figure 3-68 to Figure 3-71. It can

be seen that even the pattern with the least amount of energy intensity (3 blows in phase 1) is able to satisfy the quick criteria. More interestingly, the variation of q_c in phase 1 prints, phase 2 prints and in between prints is small, in particular below the depth of about 1.5 to 2m, and can be assumed to be practically the same as the average. At depth above approximately 1.5 to 2 m, although the quick criteria are still satisfied in all CPT profiles, it seems that the lowest q_c occurs in between the prints. No specific relationship can be observed in this superficial layer between phase 1 and phase 2 prints as q_c values are sometimes higher in phase 1 prints, sometimes higher in phase 2 prints, and sometimes appear to be practically equal.

In all patterns q_c improvement ratio is greatest at depths of about 3 to 4 m, and in the range of about 4.5 to 5.5, which is in the order that has been proposed by Lukas (1986).

Comparison of the average q_c and average q_c improvement ratio in Figure 3-72 indicates that the maximum amount of improvement has been achieved in the pattern with the maximum energy intensity (6 blows in phase 1), but the overall q_c improvement ratio of the four patterns seem to be very close, and it cannot be immediately concluded that applying additional blows has improved the ground strength.

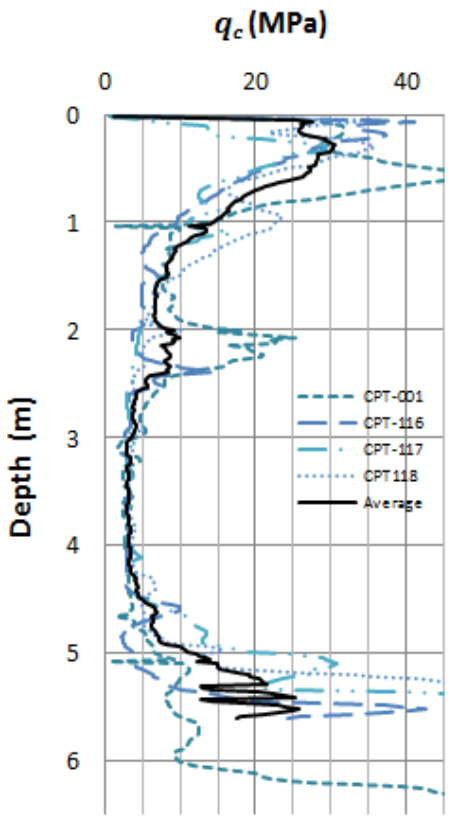

Figure 3-67: CPT cone resistances before dynamic compaction

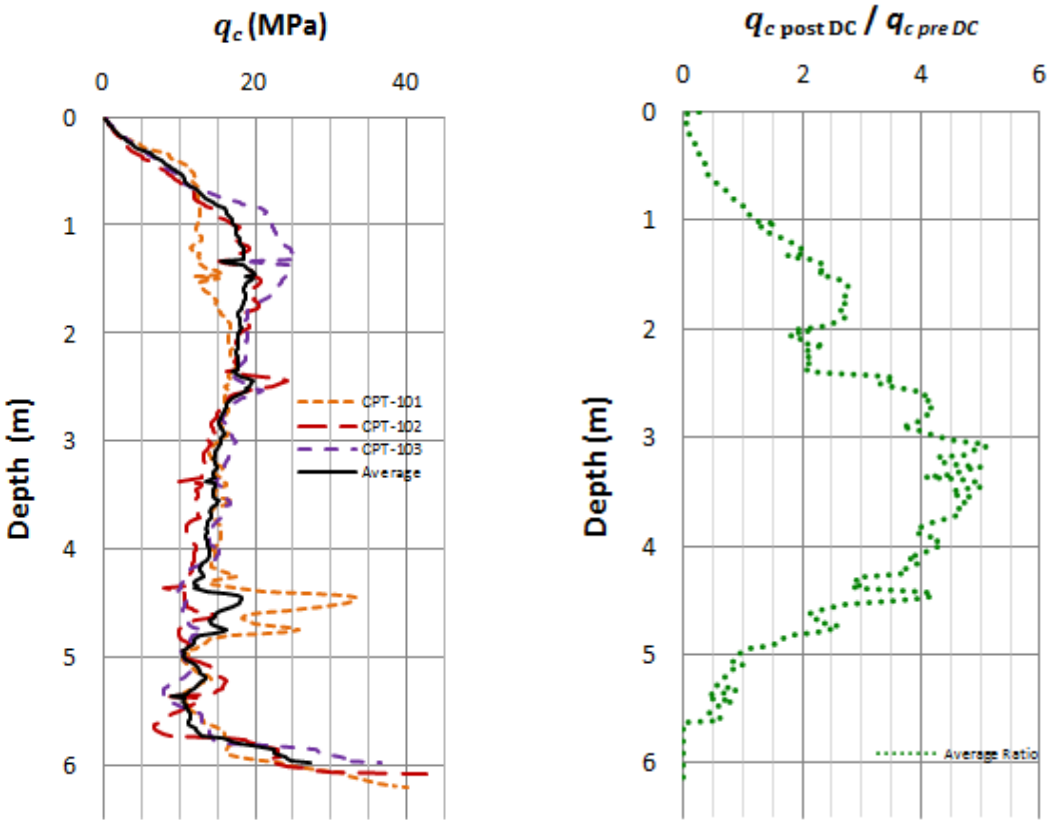

Figure 3-68: q_c and average q_c improvement ratio for pattern with 3 blows per print in phase 1

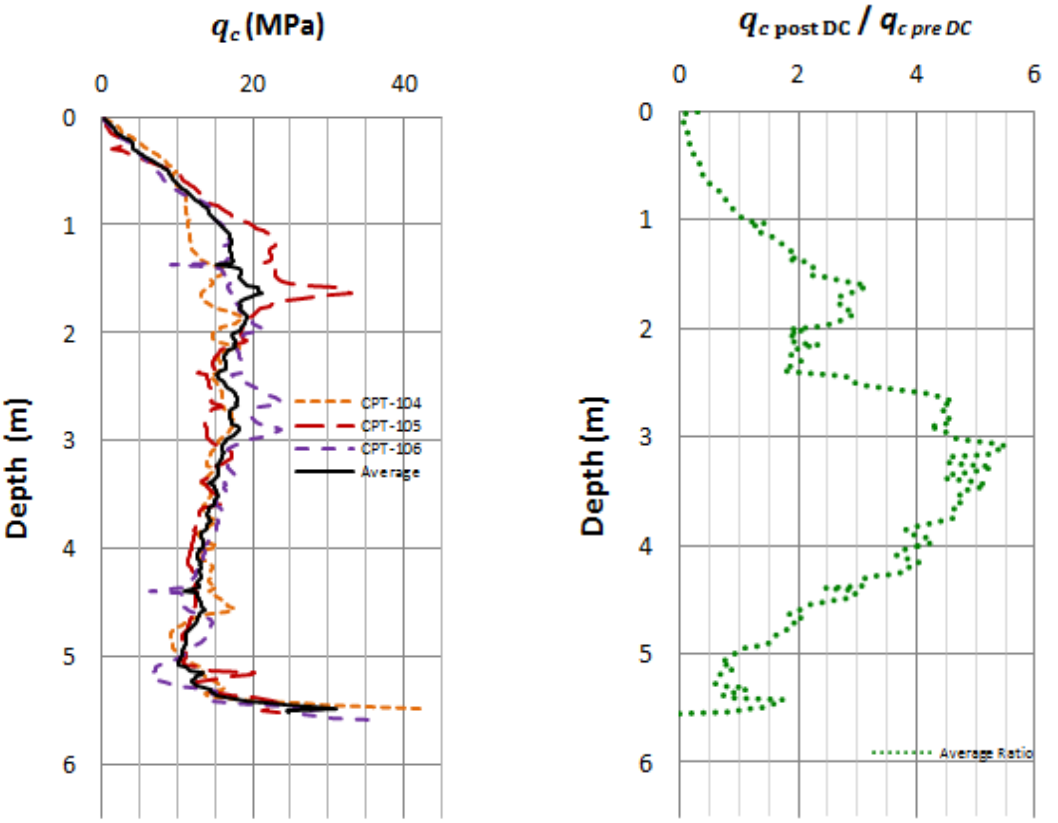

Figure 3-69: q_c and average q_c improvement ratio for pattern with 4 blows per print in phase 1

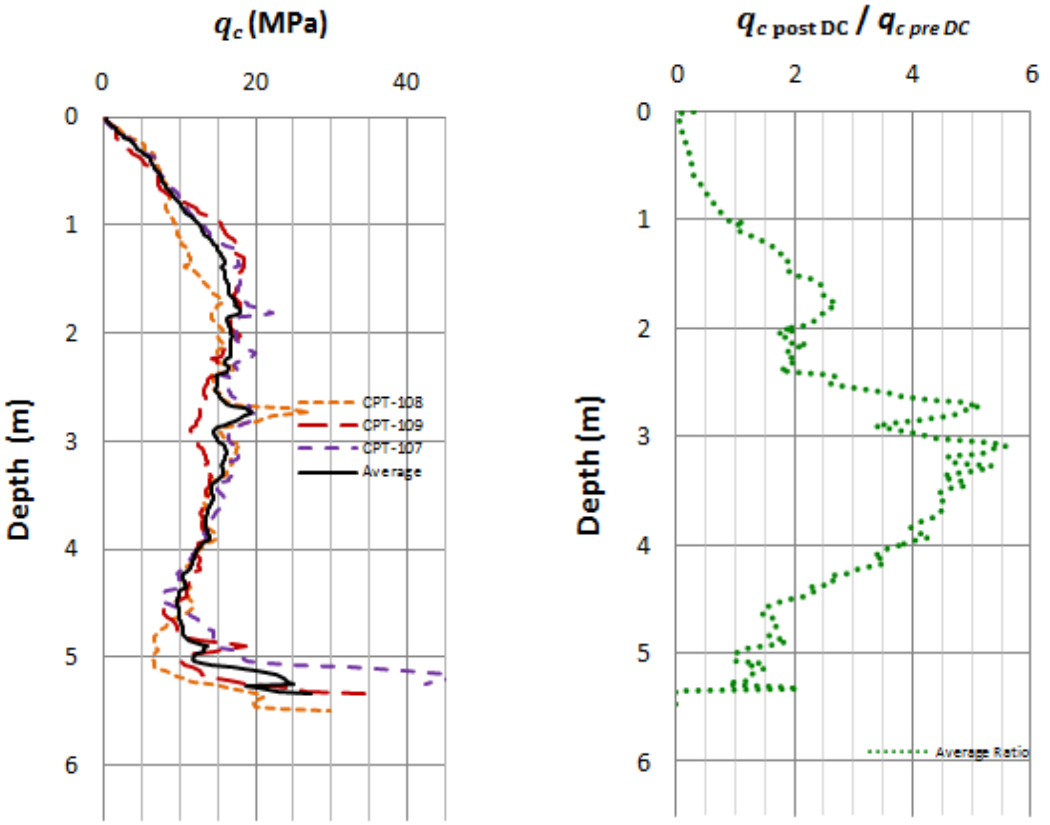

Figure 3-70: q_c and average q_c improvement ratio for pattern with 5 blows per print in phase 1

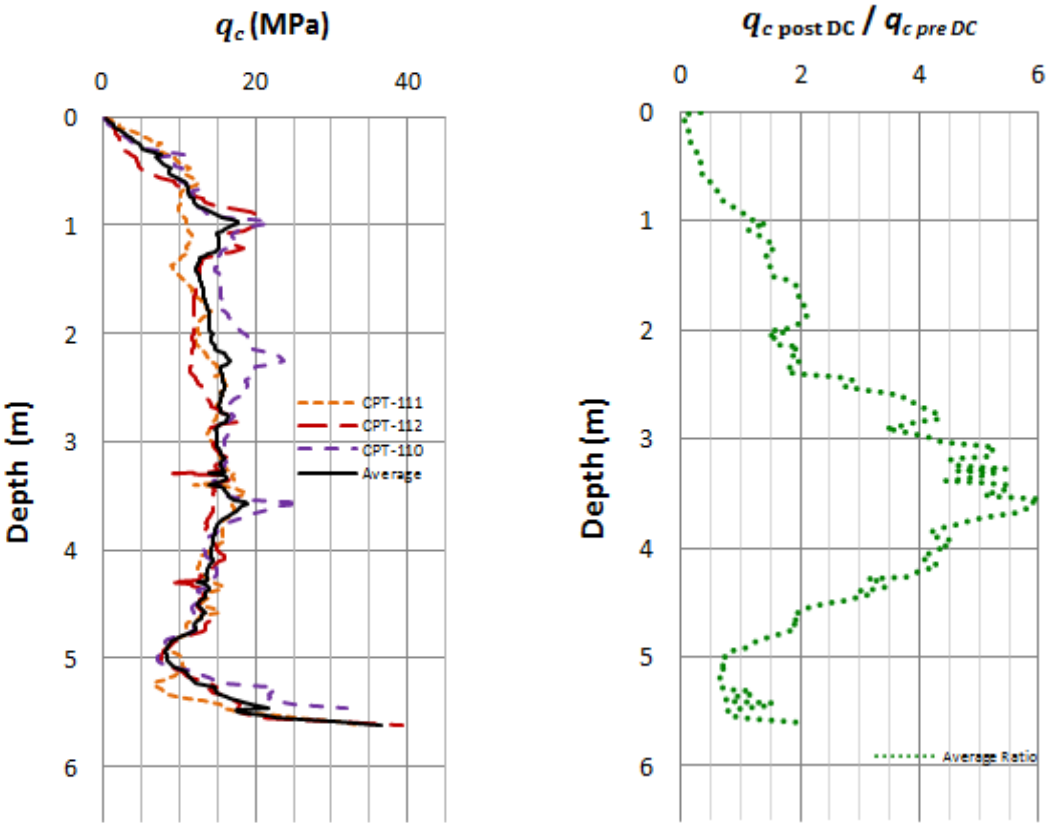

Figure 3-71: q_c and average q_c improvement ratio for pattern with 6 blows per print in phase 1

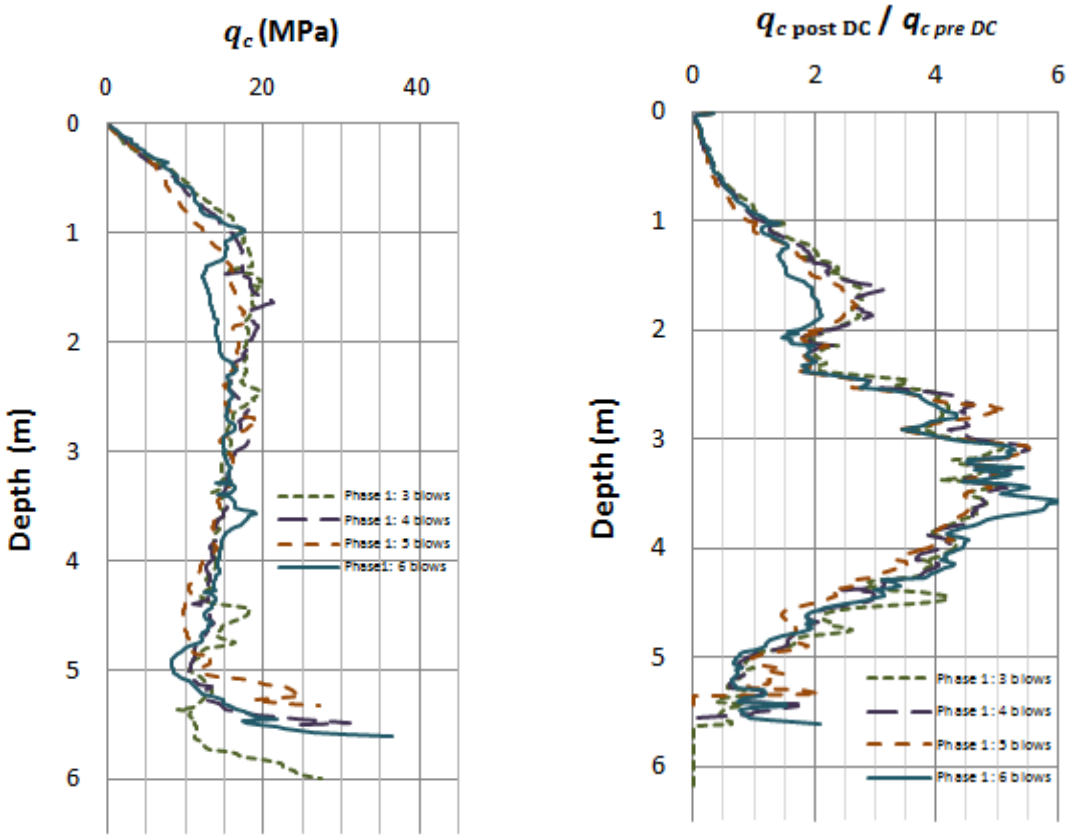

Figure 3-72: average q_c and average q_c improvement ratios of all four patterns

In addition to the PMT that was performed before dynamic compaction, one PMT was carried out in between the prints after DC in each pattern. Due to project requirements and gage limitations tests were terminated for P_{LM} of 2,500 kPa and E_M of 20,000 kPa (assuming E_M /P_{LM}= 8, refer to Table 2-22). Figure 3-73 to Figure 3-76 compare P_{LM} and E_M values in the four patterns before and after dynamic compaction. As before, it can be observed that even the pattern with the least amount of energy intensity is able to satisfy the quick criteria with a margin of almost 100%. Comparison of P_{LM} and E_M values of the four patterns in Figure 3-77 is more oriented than the CPT results, and the trend of increasing soil strength with application of additional energy appears to be more obvious. However, even in the PMT results there is a fluctuation, and the pattern with the most blows does not yield the highest P_{LM} and E_M values.

P_{LM} and E_M improvement ratios of the patterns are shown in Figure 3-78 to Figure 3-81. While at first glance it appears that the magnitude of PMT improvement ratio is less than CPT improvement ratio, it is reminded that PMTs were terminated at 2,500 kPa, and higher improvement ratios would have been achieved if the tests were continued. P_{LM} and E_M improvement ratios of the patterns are compared in Figure 3-82. As with the P_{LM} and E_M values themselves, while the general trend of improvement indicates that additional blows

further increase PMT parameters, the pattern with the most energy intensity does not yield the highest parameters.

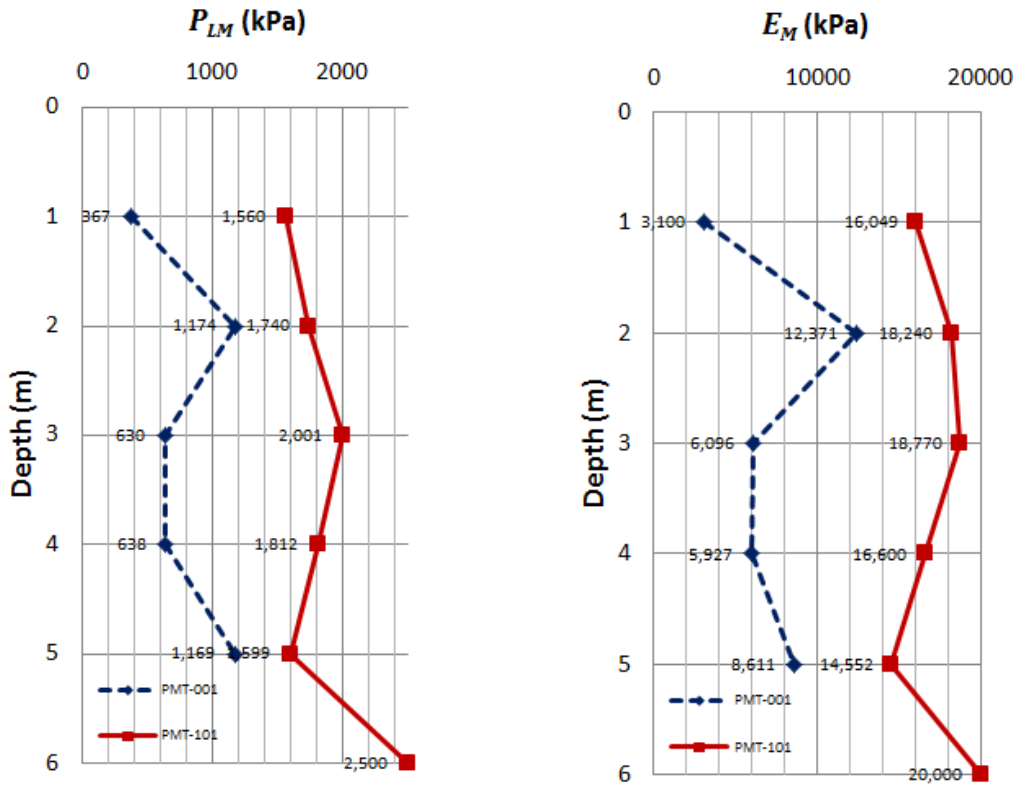

Figure 3-73: P_{LM} and E_M for pattern with 3 blows per print in phase 1

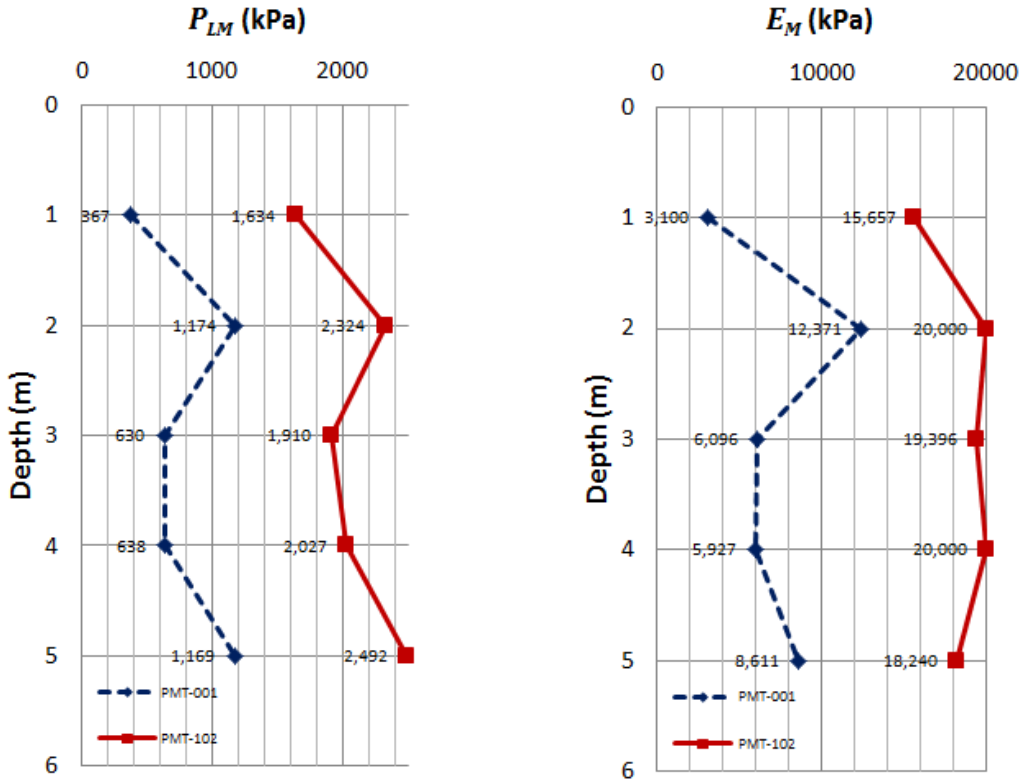

Figure 3-74: P_{LM} and E_M for pattern with 4 blows per print in phase 1

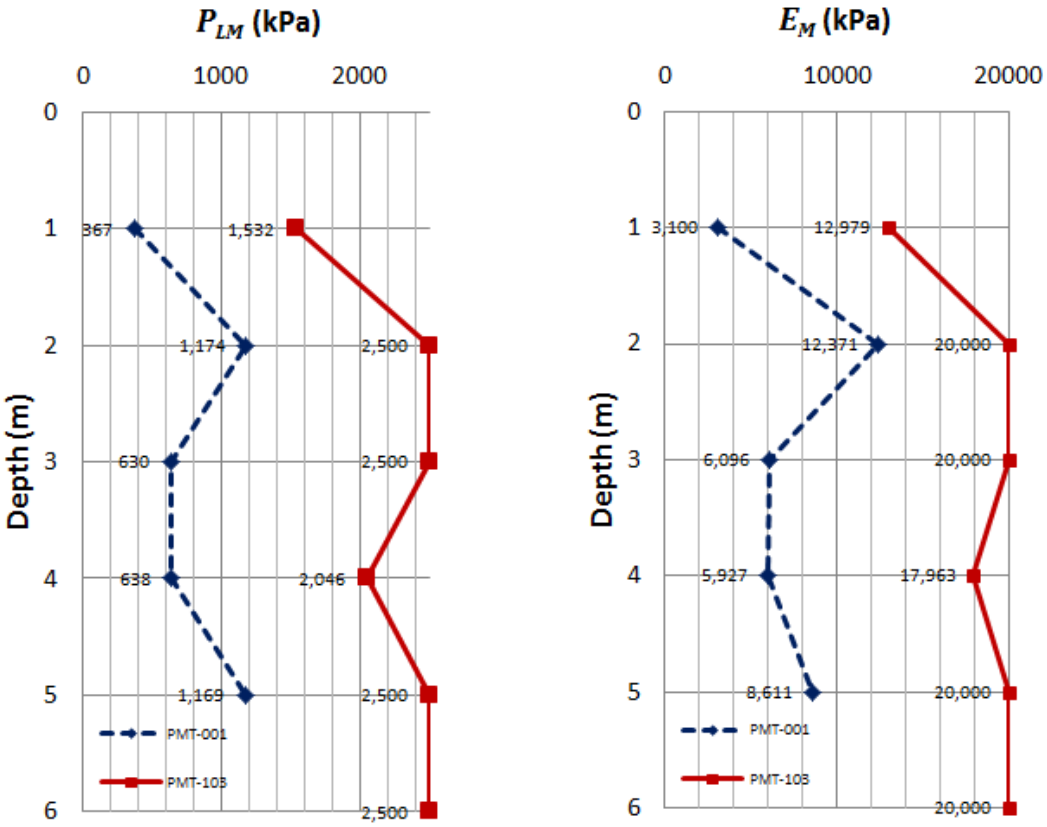

Figure 3-75: P_{LM} and E_M for pattern with 5 blows per print in phase 1

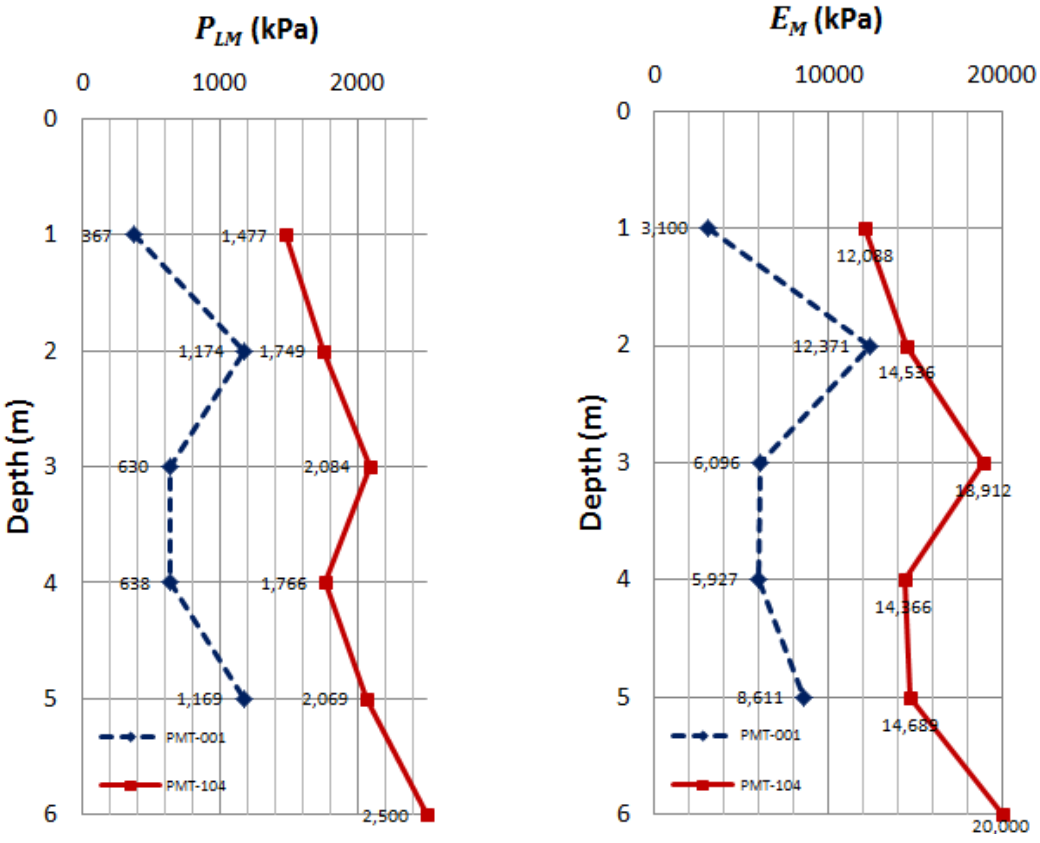

Figure 3-76: P_{LM} and E_M for pattern with 6 blows per print in phase 1

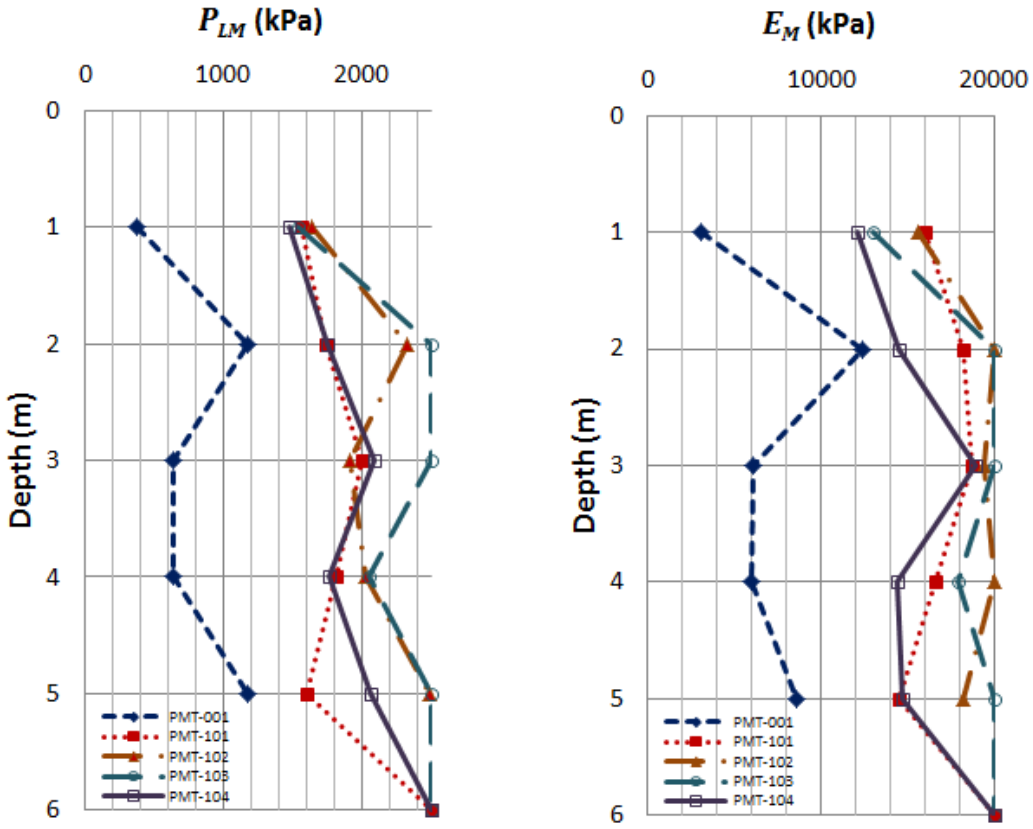

Figure 3-77: Comparison of P_{LM} and E_M before and after dynamic compaction

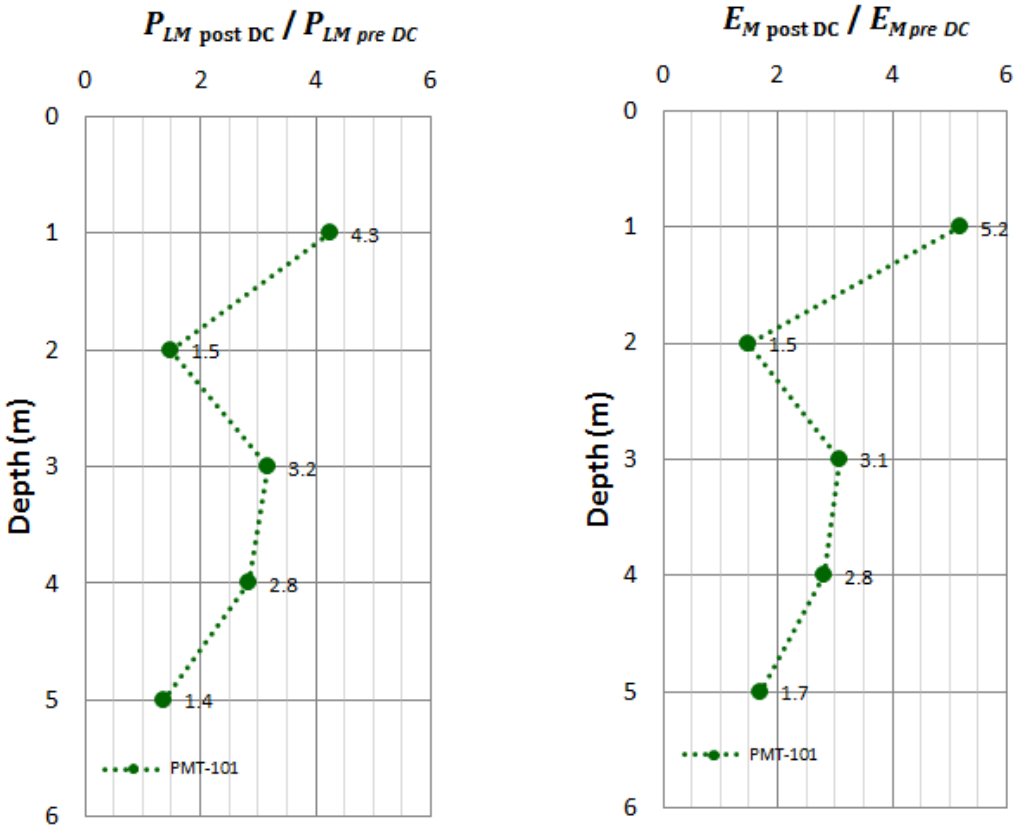

Figure 3-78: P_{LM} and E_M improvement ratios for pattern with 3 blows per print in phase 1

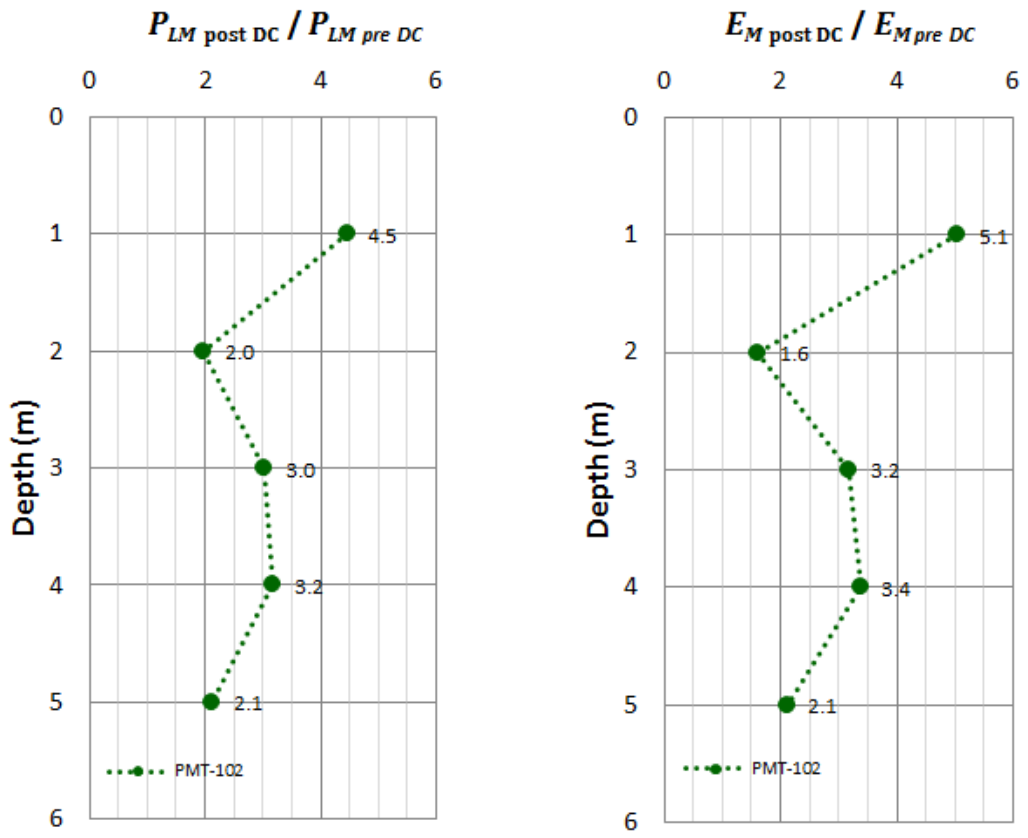

Figure 3-79: P_{LM} and E_M improvement ratios for pattern with 4 blows per print in phase 1

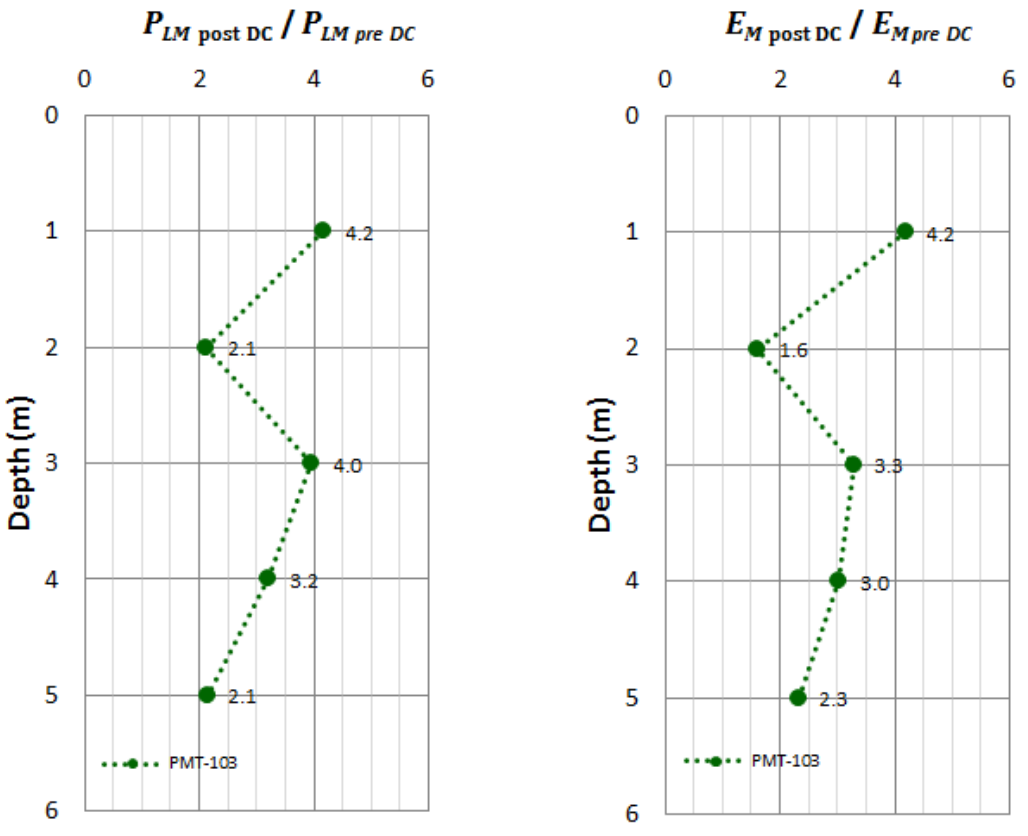

Figure 3-80: P_{LM} and E_M improvement ratios for pattern with 5 blows per print in phase 1

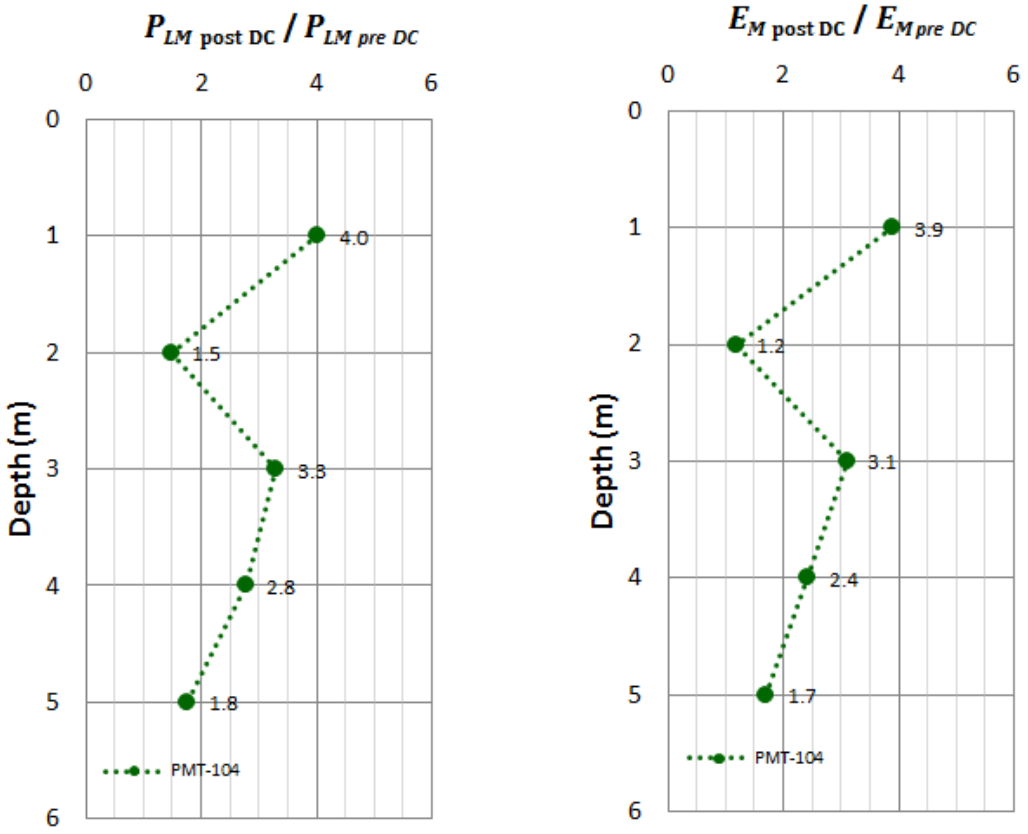

Figure 3-81: P_{LM} and E_M improvement ratios for pattern with 6 blows per print in phase 1

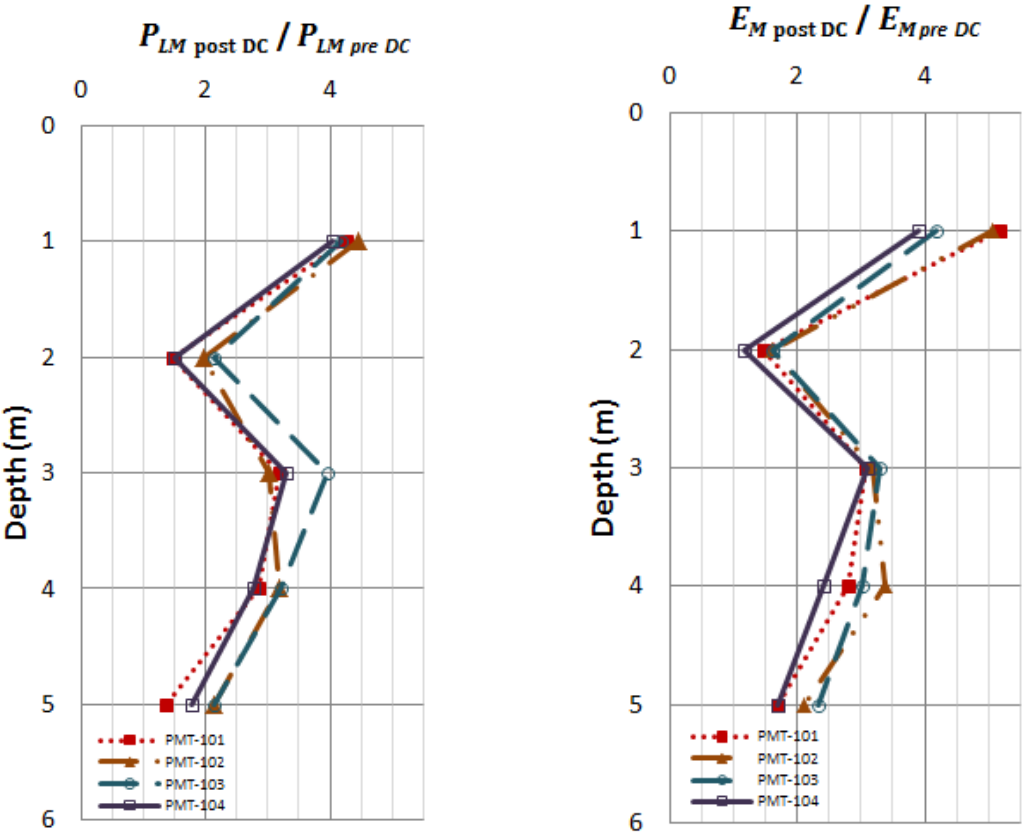

Figure 3-82: Comparison of P_{LM} and E_M improvement ratios of all 4 patterns

After dynamic compaction, the 4 patterns were levelled, and the amount of settlement measured. It was observed that the ground settlement in the first (with the least energy intensity of 3 blows in phase 1) to fourth pattern (with the most energy intensity of 6 blows in phase 1) were respectively 0.16, 0.25, 0.26, and 0.32 m.

Blow No.	Upper Diameter of crater (m)	Penetration (m)			Crater volume (m^3)
		Per blow by surveying	Accumulative		
			Surveying	Rig	
0	0	0.00	0.00	0.00	0.00
1	2	0.31	0.31	0.40	0.33
2	2.2	0.21	0.52	0.60	0.66
3	2.5	0.17	0.69	0.70	1.12
4	2.8	0.10	0.79	0.80	1.61
5	3	0.10	0.89	0.80	2.09
6	3.2	0.04	0.93	0.90	2.49
7	3.2	0.09	1.01	1.00	2.72
8	3.2	0.04	1.05	1.00	2.82
9	3.4	0.07	1.12	1.10	3.38
10	3.5	0.05	1.16	1.10	3.73
11	3.6	0.04	1.21	1.20	4.09
12	3.6	0.04	1.24	1.20	4.22
13	3.6	0.03	1.27	1.20	4.32
14	3.6	0.04	1.31	1.30	4.46
15	3.6	0.02	1.34	1.30	4.54
16	3.6	0.05	1.38	1.40	4.70
17	3.7	0.02	1.40	1.40	5.03
18	3.7	0.02	1.42	1.40	5.10
19	3.7	0.04	1.46	1.40	5.23
20	3.8	0.02	1.48	1.40	5.60

Table 3-9: Penetration test

The crater diameter, pounder penetration, and crater volume for every pounder blow during the heave and penetration test is shown in Table 3-9. Pounder penetration was measured by both surveying four points on the pounder (the average penetration is presented here only)

and implementing the drop line measuring device of the rig. It can be observed that the measurements using these two methods are fairly similar in the practical sense.

The accumulative penetrations that were measured by surveying and the crater volume are plotted against the number of blows in Figure 3-83. It can be observed that the shapes of accumulative penetration and crater volume curves are very similar, and the slope of both curves reduce as the number of blows increases. This can be better observed in Figure 3-84, which shows the percentages of final accumulative penetration and final crater volume against the number of blows. It can be seen in this plot that 80% of the final pounder penetration was achieved in the first 10 blows while the pounder only penetrated the last 20% of the total penetration in the second 10 blows. Likewise 80% of the crater volume was achieved during the first 10 blows, and the second 10 blows only contributed to 20% of the crater volume.

3.5.4.2 Final Testing

The project specification required that bearing and settlements to be verified by performing PMTs. Also, it was anticipated to carry out CPTs for verification of liquefaction mitigation and as an additional control measure. Consequently, in addition to the 18 PMT and 32 CPT that were carried out as part of the full scale DC calibration program, a total of 282 PMT and 1,029 CPT were also carried out to confirm that the project requirements had been met. As the final test results are comparable and compatible with the calibration results further tests will not be presented.

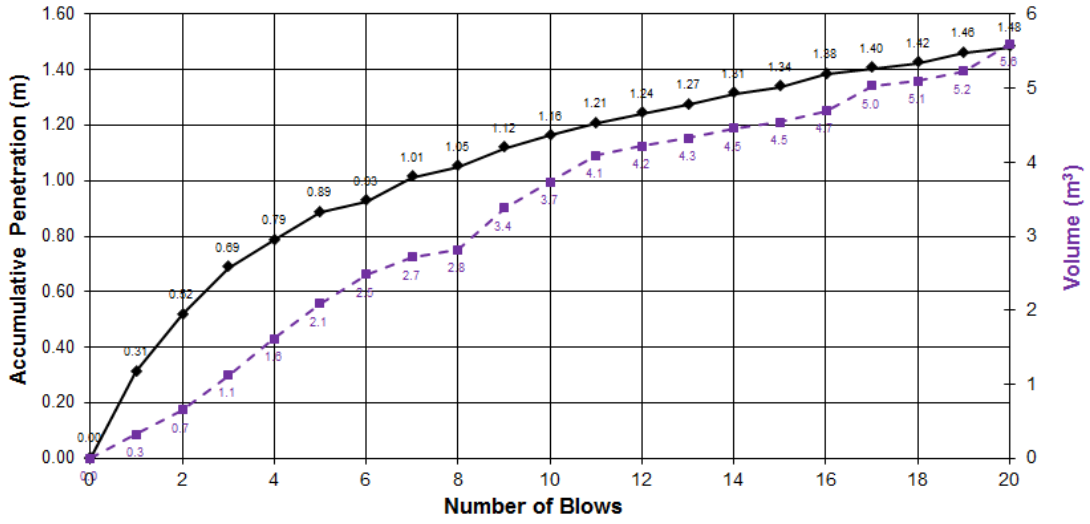

Figure 3-83: Accumulative penetration and crater volume against number of blows

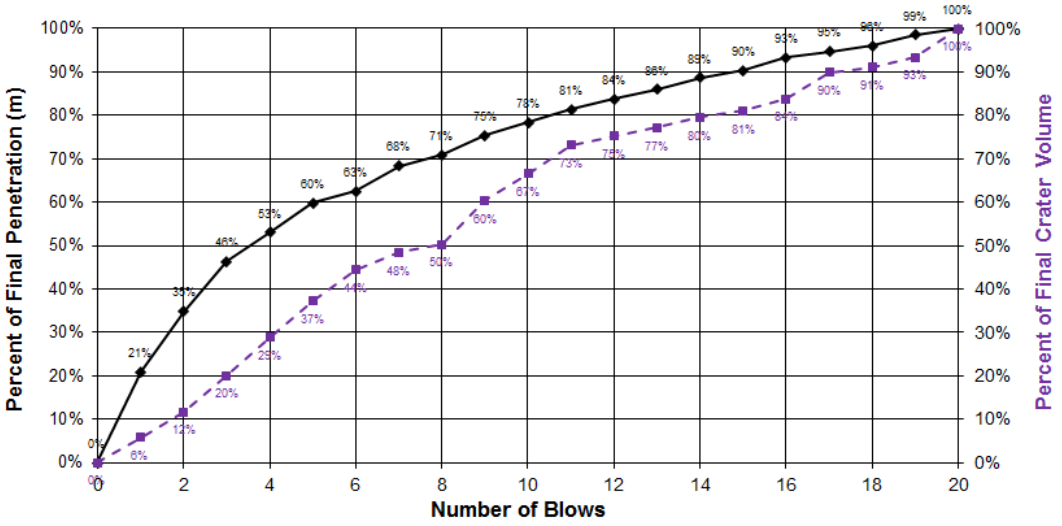

Figure 3-84: Percentages of accumulative penetration and crater volume against number of blows

3.5.5 Lessons and Conclusion

To the knowledge of the author, at the time Al Falah Community Development was under construction, it held the world records for largest (in size) single ground improvement contract at 4.84 million m^2 and highest ground improvement production rate of 966,000 m^2 per month.

Worthwhile points in this project are:

1. The site was broken down to sub-areas, and treatment was performed based on ground conditions and structural loads.

2. It is possible to meet the project specifications in a shorter time by using high heavy pounders with high drops rather than using lighter pounders with the same energy intensity.

3. Early planning will allow mobilisation of sufficient numbers of plant and equipment to perform grand size projects in relatively short periods.

4. The improvement ratio in the calibration programme was in the order that has been suggested by Lukas (1986). However, it could be cautiously expected that higher energy intensities will result in better results.

Figure 3-85 shows Al Falah Community Development after dynamic compaction and completion of villas and roads.

Figure 3-85: Al Falah Community

3.6 Marjan Island Road Corridor

3.6.1 Project Description

Marjan Island is the first manmade group of island(s) of its kind that has ever been undertaken in the northern emirate of Ras Al Khaimah in the United Arab Emirates. This project is located approximately 27 km southwest of Ras Al Khaimah city and 54 km northwest of Dubai city.

Marjan is the Arabic word for coral, and as can be seen in the project's master plan that is shown in Figure 3-86, the reclamation is composed of a peninsula followed by four coral shaped islands that are connected together via bridges. Upon completion Marjan Island will include various structures including low rise villas, townhouses, apartment buildings, retail and leisure areas, utilities, hotels, resorts, and open spaces.

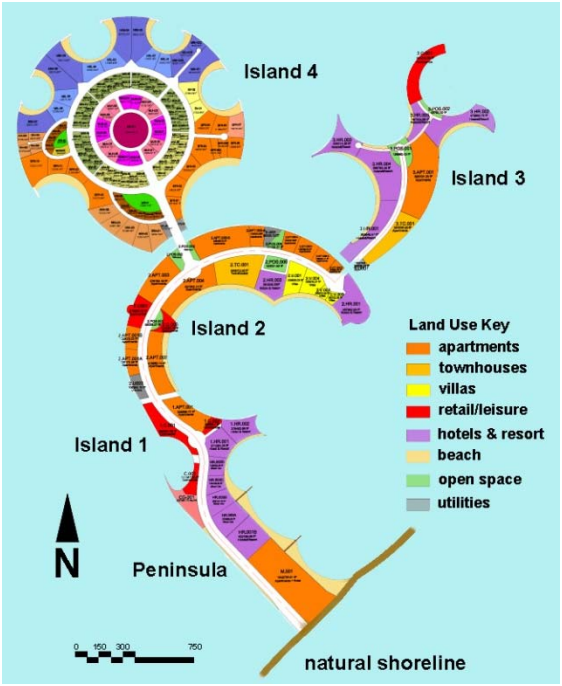

Figure 3-86: Master plan of Marjan Island (main road corridor shown in white)

3.6.2 Ground Conditions

Unlike most manmade islands in the UAE where land has been reclaimed from the sea by hydraulic filling, in Marjan Island trucks were used to cart and dump soil more than 3 km into the Persian Gulf to an average elevation of +4 m ACD (Admiralty Chart Datum) that is 2 m above average groundwater level.

The preliminary geotechnical investigation on the Island's main road (shown as a red strip in Figure 3-87) that passes through the Peninsula, Island 1 and Island 2 consisted of 37 SPT boreholes drilled down to depths of 2.5 to 16 m. These tests indicated the presence of a heterogeneous fill. On average, in the top 7 m that extended down to -3 m ACD the fill was composed of very loose to medium dense sand that was occasionally interbedded with boulders at different depths. Fines content was variable from 13% to 30%, and SPT blow counts were generally low, sometimes as low as 4, but rarely exceeding 50. The second layer of soil, extending down to -12 m ACD, appeared to possess better mechanical properties. This layer was composed of medium dense to very dense silty sand with occasional interbedded pockets of sandy silt. Fines content was generally from 5% to 30%, and SPT blow counts were from 10 to more than 50.

Figure 3-87: Marjan Island satellite image (taken in 2009) with the main road identified in red

Marjan Island's SPT borehole layout plan of the Peninsula and Island 1 are shown in Figure 3-88. Figure 3-89 shows the blow counts of the upper 8.5 m of the Peninsula's first 5 SPT boreholes that were spread out at distances of approximately 70 to 80 m from one another. It can be observed that not only was the soil generally in a loose state, but also that the scatter of blow counts at any one depth was considerable, which indicated that in addition to bearing and total settlement issues, the ground could have also been subject to excessive differential settlements.

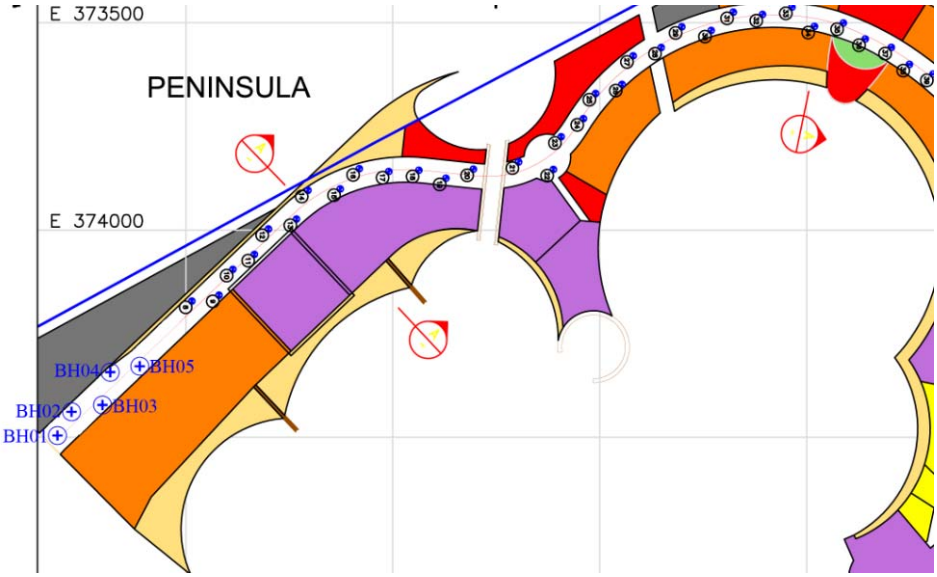

Figure 3-88: SPT borehole layout

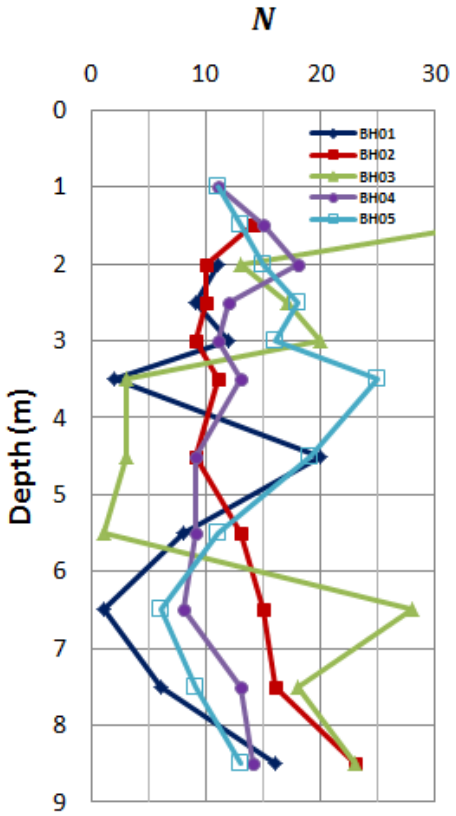

Figure 3-89: SPT blow counts of several boreholes at Marjan Island before dynamic compaction

Later, 16 PMTs were also carried out as part of a supplementary geotechnical investigation. P_{LM} in these tests also indicated that the ground was sometimes very loose in the upper 7 m, in such a way that the lowest measured P_{LM} was as low as 50 kPa. Although due to the traffic of the earthmoving equipment the upper 1 to 2 m of ground was generally very dense and P_{LM} of more than 1,000 kPa was commonly observed, the limit pressure of the deeper layers

was usually less than 600 kPa. Similarly, while E_M was generally 4 to 8 MPa at depths of 2 to 7 m, values of less than 1 MPa were also occasionally encountered. The layout plan of the PMTs on the Peninsula, P_{LM} and E_M of the first three tests of the Peninsula are respectively shown in Figure 3-90 and Figure 3-91. The distances between these three test locations were about 200 to 250 m.

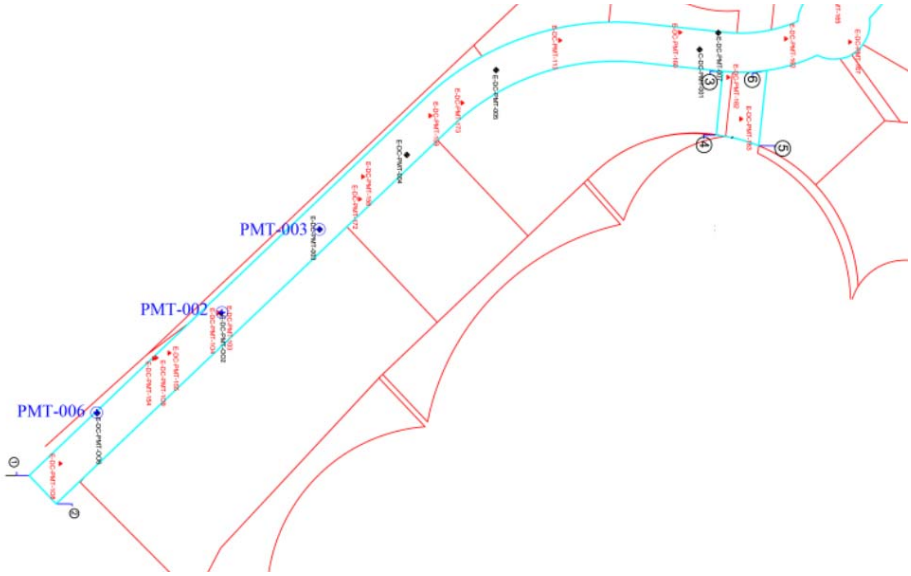

Figure 3-90: PMT layout plan on the Peninsula

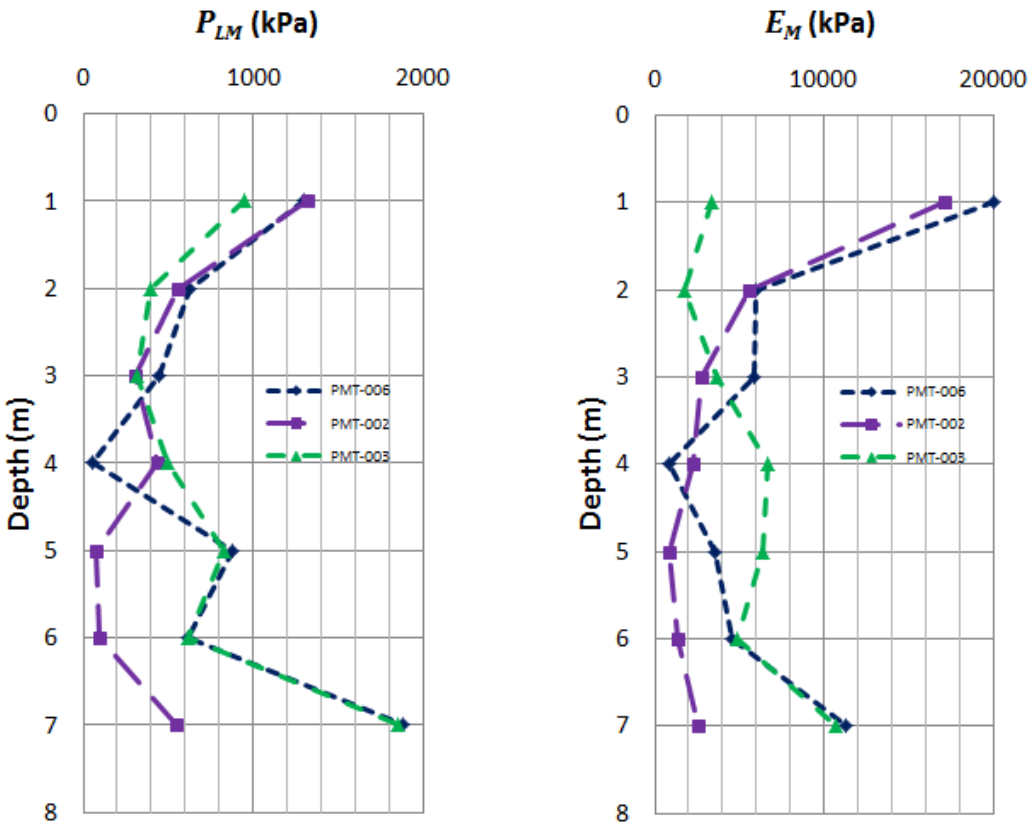

Figure 3-91: Several PMT results at Marjan Island before dynamic compaction

As explained in Section 2.9.2.8, natural unconsolidated soil or young fills will undergo large settlements with time, even if they are very lightly loaded. The self-bearing condition of a soil; i.e., the minimum value of the soil parameters that a soil must have so as not to settle under its own weight, can be related to physical or mechanical properties of the soil. Menard's experience shows that the limit pressure is a suitable characteristic, and for sand and sand with gravel the P^*_{LM} at depths less than 10 m must be at least respectively 600 kPa and 800 kPa to prevent creep settlement (refer to Section 2.9.2.8). Menard proposes to estimate the self-weight settlement of soft or loose soils during a period of one year as a first approximation using Equation 2-211.

$$\text{For } P_{LM} < \frac{200}{\alpha} \text{ (kPa)} \qquad s = \frac{h \text{ (cm)}}{1000} \frac{1 - \alpha \frac{P_{LM}}{200}}{\alpha \frac{P_{LM}}{200}} \qquad \text{2-211}$$

Assuming creep due to the soil's self-weight will reach stabilisation after t years according to a logarithmically decreasing curve, self-weight settlement, s_n, in year n will be:

$$s_n = s_{year\ 1} \frac{\ln\left(\frac{t+1}{n}\right)}{\ln(t+1)} \qquad \text{3-3}$$

Thus, it can be estimated that a one metre thick layer of sand with an initial limit pressure of 400 kPa will undergo 18 to 25 mm of creep settlement depending on whether the stabilisation period is assumed to be 10 or up to 20 years.

The heterogeneity in soil strength and the presence of loose spots near dense spots indicated that it was possible for the ground to undergo large differential settlements due to the self-weight of the soil without external loading. Structural and traffic loads further increased the risks of excessive ground deformations.

The geotechnical concerns were considered to be of high priority for the main road corridor that passed through the Peninsula, Island 1 and Island 2 (refer to Figure 3-87). Hence, the project management team approached geotechnical specialist contractors to propose solutions for mitigating the geotechnical problems.

3.6.3 Development of Solution and Application of Dynamic Compaction

After reviewing the proposals the project's management team and consultant awarded the 198,000 m^2 ground improvement works of the main road corridor to a specialist ground improvement contractor who had proposed the application of dynamic compaction. 123,000 m^2 of the works was in the Peninsula and Island 1, and 75,000 m^2 was located in Island 2.

Ground improvement design criteria were specified to be:

- Maximum total settlement: 25 mm under a uniform load of 20 kPa on the road area
- Maximum differential settlement: 1:500 between any two points on the road with a distance of 10 m under a uniform load of 20 kPa.

Verification and acceptance of the works was defined to be by PMT.

As can be observed bearing capacity was not a requirement of this project as it was expected that the ground loaded over a large area would cease to function by excessive settlement rather than by bearing failure.

Dynamic compaction was carried out by 3 DC rigs using 17 and 20 ton pounders. Each print location was subjected to 5 to 8 blows dropped from 20 m using a final grid size of 5x5 m^2. In the ironing phase the 17 and 20 ton pounders were dropped from 12 m or a 12 ton pounder was dropped from 17 m.

The author is frequently asked about the effect of dynamic compaction and vibrations generated by DC on non-sensitive structures and facilities. It is important to note that while application of dynamic compaction at close distances creates displacements and vibrations that can crack buildings and damage structures, the level of tolerance for different structures and facilities varies (refer to Section 2.8.1and 2.8.4). Figure 3-92 shows the application of dynamic compaction at the vicinity of the reclamation slope's rock armour. As can be observed the rock armour is able to remain intact even when works are performed at close proximity.

Mobilisation of equipment, ground improvement works and testing by PMT were carried out during a period of 5 months.

Figure 3-92: Application of dynamic compaction at the vicinity of slope armour protection

3.6.4 Testing and Verification

3.6.4.1 Calibration

At the beginning of the works a calibration dynamic compaction programme was performed in two zones to verify and to optimise the ground improvement parameters. The results of the first zone, which included two patterns is discussed hereunder.

Figure 3-93 and Figure 3-94 respectively show the location and layout of the dynamic compaction calibration programme in which a 20 ton pounder was used to compact the prints of phases 1 and 2 from 20 m height, and dropped once from 12 m height on each print of the ironing phase. The grids of the first and second phases of Pattern 1 and Pattern 2 were respectively 7x7 m^2 and 5x5 m^2. In addition to the 4 HPTs, one PMT was performed before dynamic compaction and 6 PMTs were carried out in phases 1 and 2, and in between the prints of the two patterns (refer to Figure 3-94). Figure 3-95 and Figure 3-96 respectively show the measurement of the crater's depth and upper diameter during the heave and penetration test. Pounder diameter, crater diameter and amount of heave (or subsidence) were not available to the author, and volumes reported herein are from project reports.

The results of the heave and penetration tests in the first and second phases of Patterns 1 and 2 are shown in Figure 3-97 to Figure 3-100. In each pattern, the first HPT was carried out in the first print of the pattern's first compaction phase. After completion of compaction of the first phase prints, the second HPTs were performed in the first print of the second phase

prints of the two patterns. 11 blows were applied in the first HPT of Pattern 1, but all other HPTs were subjected to 10 blows.

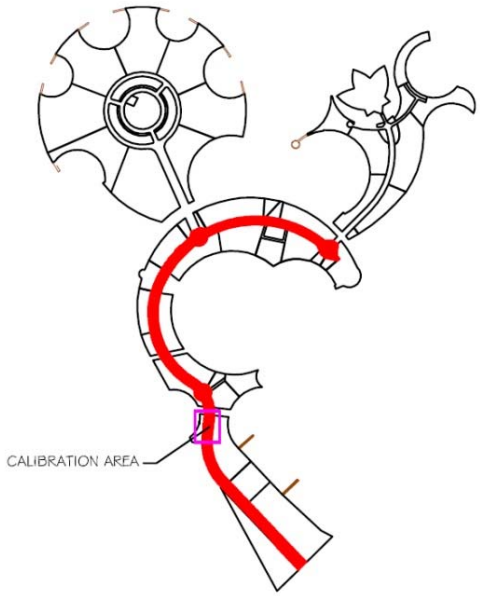

Figure 3-93: Location of calibration area

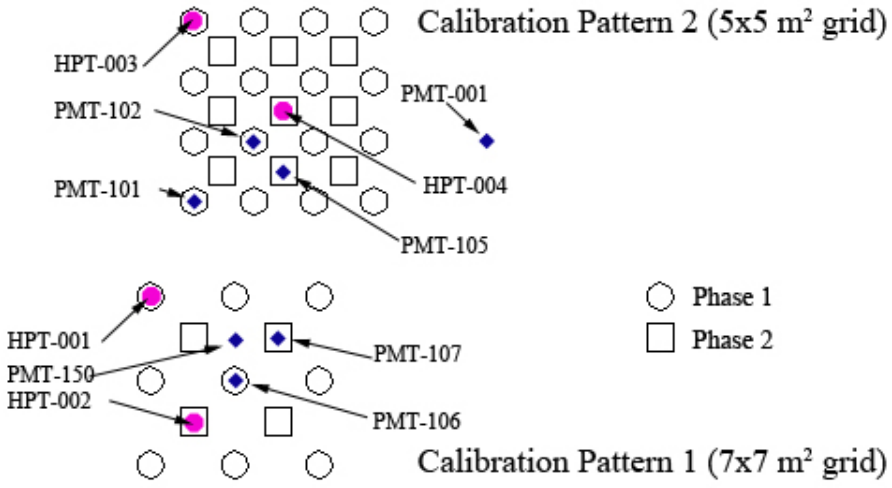

Figure 3-94: Dynamic compaction calibration layout

It can be observed that in both patterns the accumulative pounder penetration and compaction volume of the first phase HPT is greater than the second phase HPT. This indicates that, similar to the laboratory scale tests of Hajialilue-Bonab and Zare (2014), which were discussed in Section 2.5.4, the soil in the zone of influence of phase 2 was already somewhat improved due to the compaction carried out during phase 1; hence, the amounts of penetration, reduction in void ratio and volume reduction were less in the second DC phase.

Figure 3-95: Measurement of crater depth in the heave and penetration test

Figure 3-96: Measurement of the crater's upper diameter in the heave and penetration test

Figure 3-101 shows the ratio of phase 2 to phase 1 accumulative penetrations and compaction volumes. It can be seen that the ratios are fluctuating within a limited band that, except for one data set, is less than one for both penetration and compaction volume ratios. While it could be expected that the tighter grid should yield lower penetration and compaction volume ratios (because the ground strength in the zone of influence of the second phase has been improved more due to the compaction of the tighter first phase grid), this cannot be concluded for the HPT results of this project. This may be explained when the penetration of the first phases of the two patterns are compared. While both HPTs were performed on virgin ground that were not influenced by any ground improvement activities, and the measured penetrations should have logically been approximately the same figures

for both patterns, the penetrations of the first pattern are greater than the second pattern. This suggests that the original ground conditions of the latter pattern could have been better, which consequently, led to a larger decrease of phase 1 penetrations compared to phase 2 crater depths.

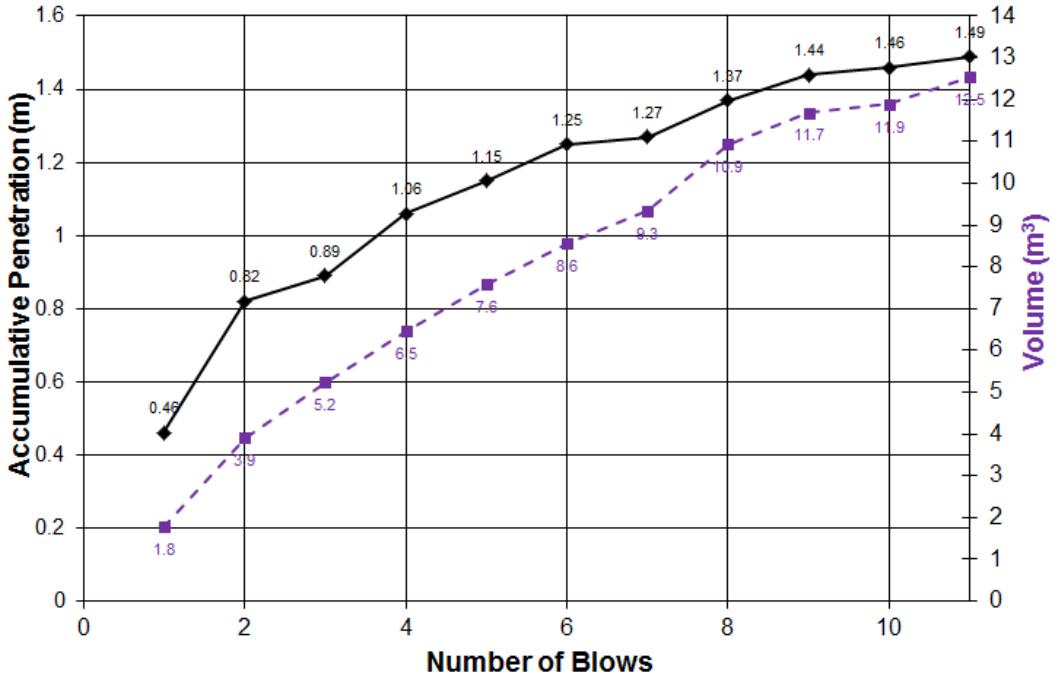

Figure 3-97: Heave and penetration test in phase 1 print of 7x7 m^2 grid pattern

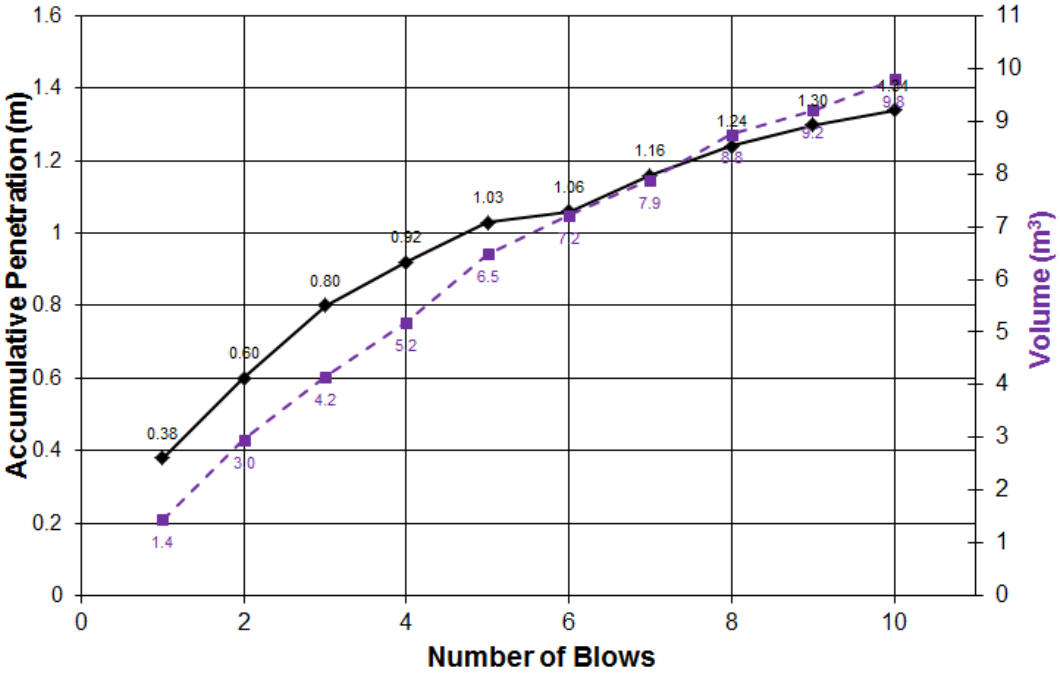

Figure 3-98: Heave and penetration test in phase 2 print of 7x7 m^2 grid pattern

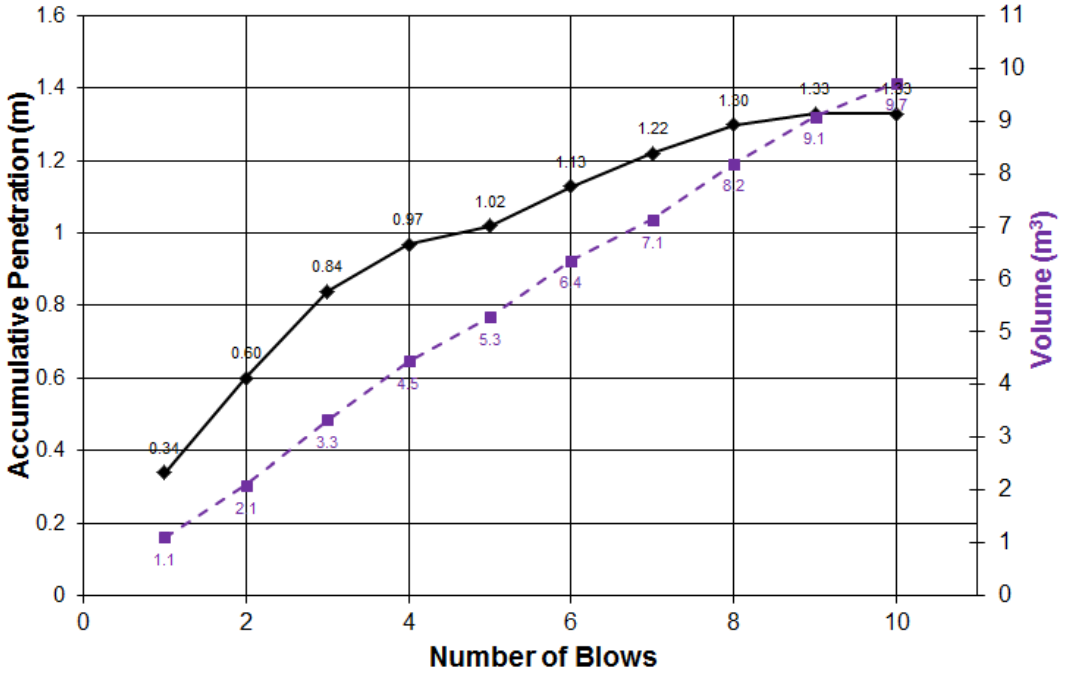

Figure 3-99: Heave and penetration test in phase 1 print of 5x5 m^2 grid pattern

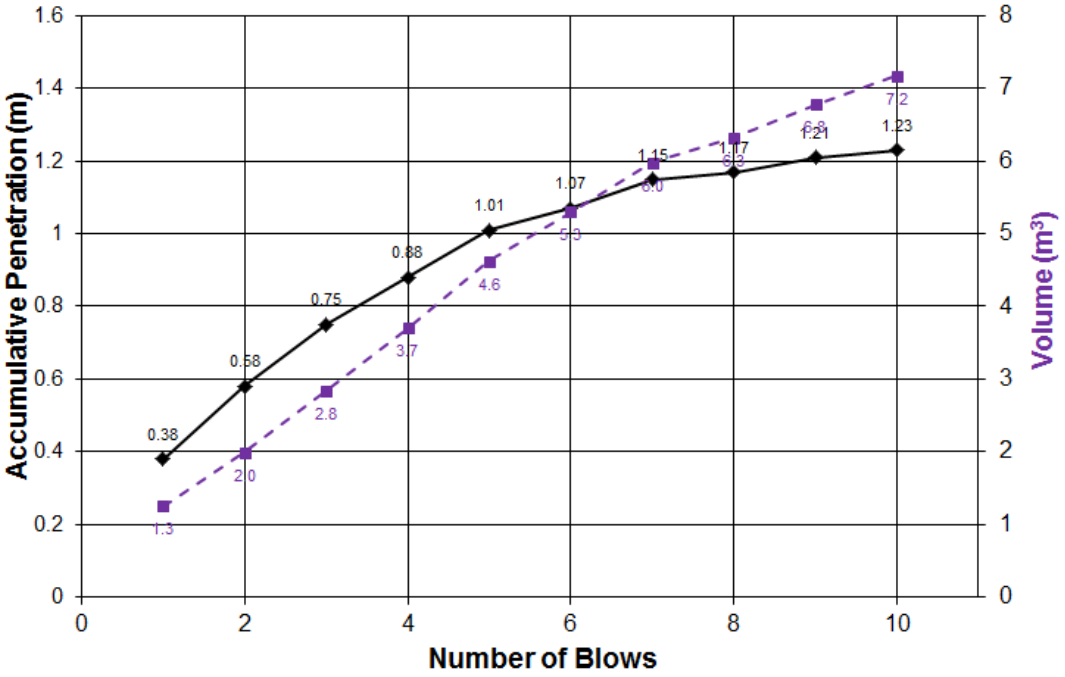

Figure 3-100: Heave and penetration test in phase 2 print of 5x5 m^2 grid pattern

The ratios of the compaction volume to accumulative heave of the four HPTs are shown in Figure 3-102. It can be observed that the ratios increase with the number of blows. Noting that the dimension of the ratios are length squared, the ratios of the four HPTs were fitted to second degree polynomials, and it was observed that, within the range of calibration blow counts, compaction volume to accumulative heave ratios of all four HPTs can be formulated by second degree polynomials with very high coefficients of determination.

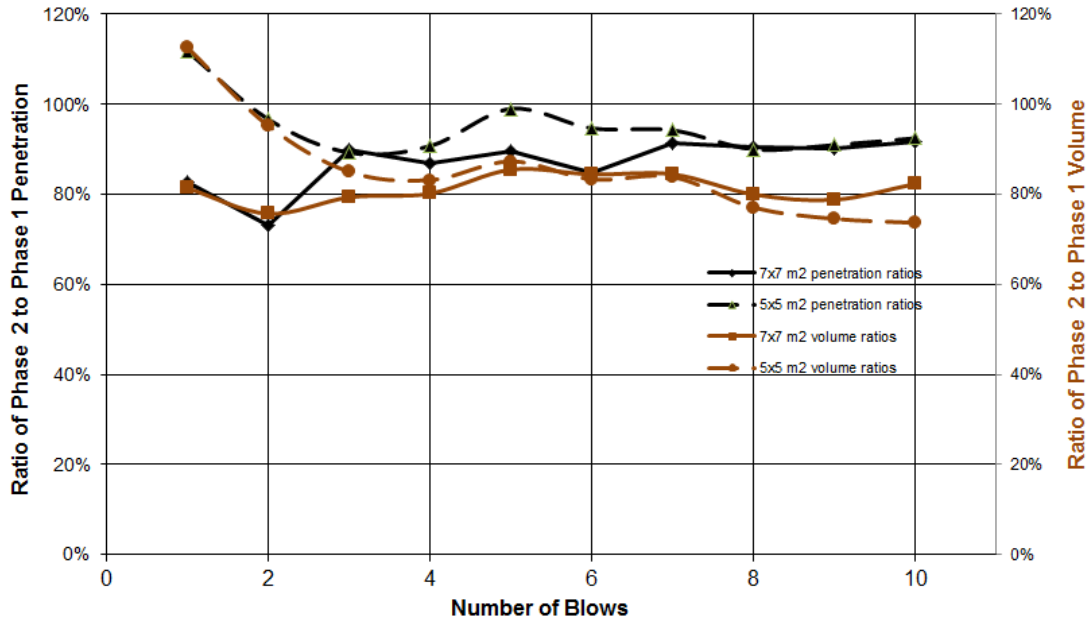

Figure 3-101: Ratio of Phase 2 to Phase 1 penetration and volume reduction in the two patterns

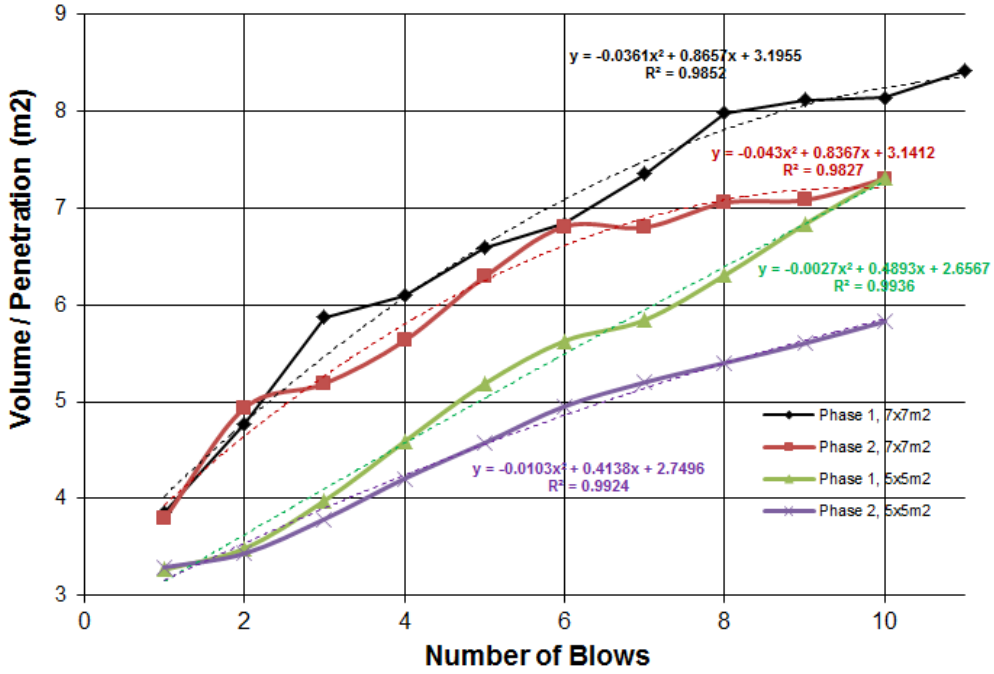

Figure 3-102: Ratio of compaction volume to accumulative penetration in HPTs

Replotting the same data of Figure 3-102 with the ratio of the square root of the compaction volume to accumulative penetration yields Figure 3-103, which shows that after the first several (3) blows the ratio is generally between 2.15 to 2.4. Thus:

$$\frac{\sqrt{V}}{D_c} = 2.15 \; to \; 2.4 \qquad 3\text{-}4$$

V= compaction volume (m^3)

D_c= crater depth (m)

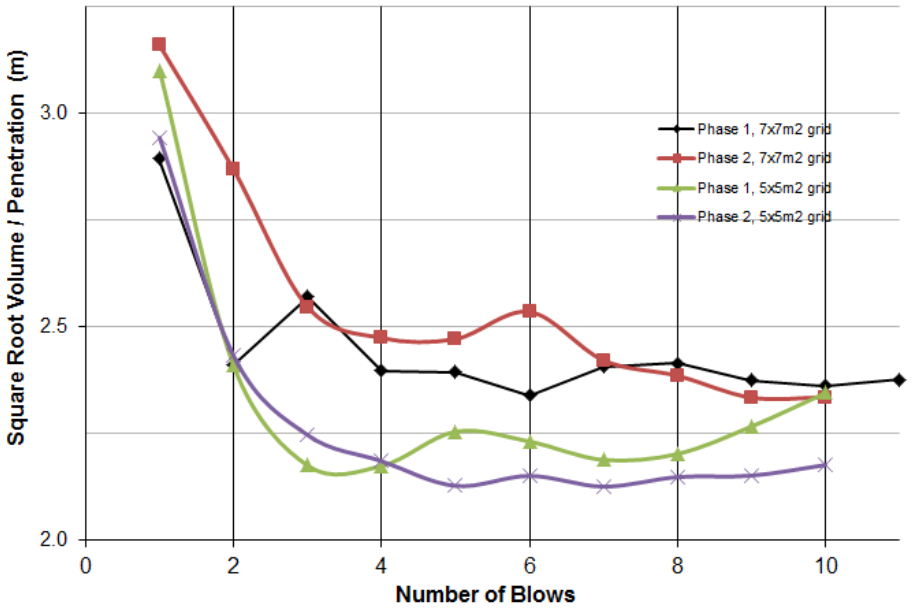

Figure 3-103: Ratio of square root of compaction volume to accumulative penetration in HPTs

The range shown in Equation 2-40 should be dealt with caution at this phase as compaction volume is a function of the pounder base's area (bottom of crater), and it is not known if the basis of calculations in this project was the customary assumption that crater base diameter was equal to the pounder's diagonal length or the equivalent pounder diameter (which in the author's opinion is the more reliable assumption).

Based on the result of the HPT 6 blows were applied from the height of 20 m using a 20 t pounder in both the first and second DC phases of pattern 1 with 7x7 m^2 grid. For the latter pattern with 5x5 m^2 grid the blows in the second phase was reduced to 5. Ironing was performed by dropping the same pounder from 12 m height.

P_{LM} and E_M before and after dynamic compaction inside two prints of compaction phases 1, in between the prints, and their average values for Pattern 1 are shown in Figure 3-104. It can be observed that the variation of the results inside phase 1 prints and in between the prints are practically insignificant, and in fact the difference between the two inside print P_{LM} values is greater than the difference between them and the in between print test. The average test values that are also shown in Figure 3-104 are suitably representative of the compacted ground condition.

Figure 3-105 shows P_{LM} and E_M improvement ratios for inside phase 1 prints, in between the prints, and their averages. While the peak P_{LM} improvement ratio of all tests is approximately 6, the peak average P_{LM} improvement ratio was about 5, which is compliant with 400% improvement that has been proposed by Lukas (1986). Peak average E_M improvement ratio appears to be slightly more and approximately 6, which is still in the magnitude that has been noted by Lukas. Peak improvement ratios were observed at depth of about 2 m to 3 m, and as expected, the amount of improvement then decreased with depth.

Ground settlement after the final levelling in the area with 5x5 m^2 grid pattern was measured to be 0.29 m. Although final settlement is the accumulative effect of phases 1 and 2 of deep compaction and ironing, using Equation 2-40, the crater depth can be estimated to have been 1.12 m to 1.25 m, which reasonably agrees with Figure 3-99 and Figure 3-100.

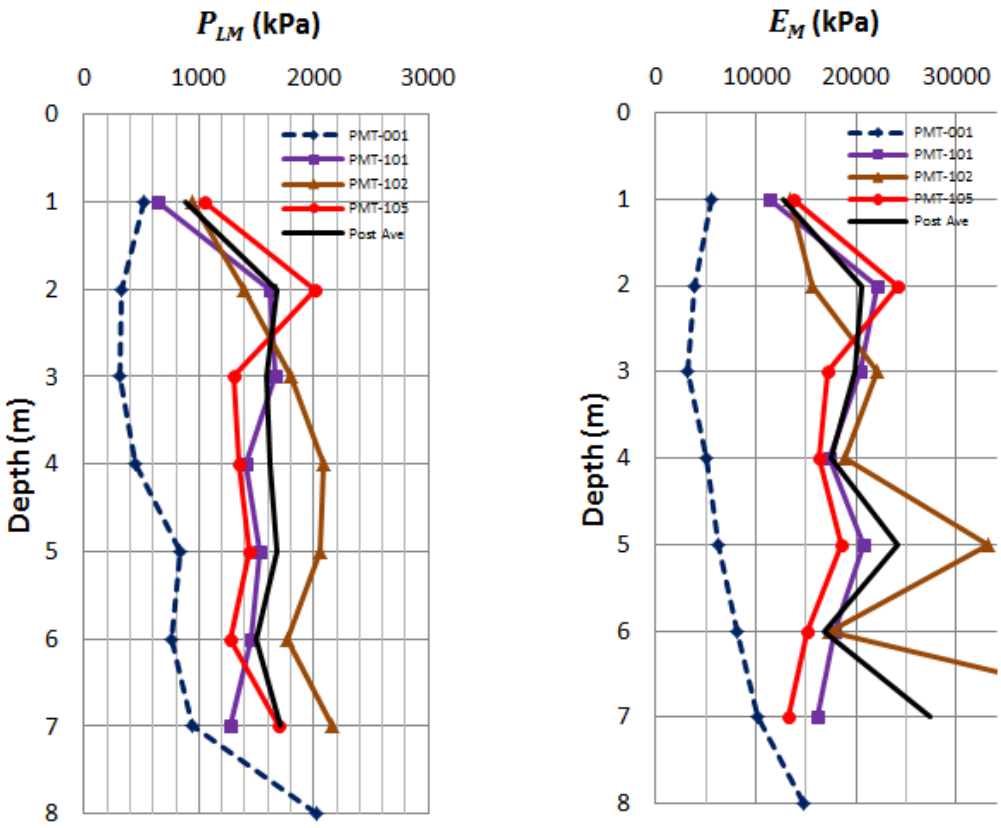

Figure 3-104: P_{LM} and E_M values before and after dynamic compaction in pattern with 7x7 m^2 grid

In the second pattern with 5x5 m^2 grid, one PMT was performed in each of the deep phases' prints, and one PMT was carried out in between the prints. P_{LM} and E_M values of these tests and the average test values are shown in Figure 3-106. It can be observed that in this pattern the improvement of the ground in phase 1, phase 2 and in between the prints is reasonably close and the average test values are representative of the ground's mass improvement.

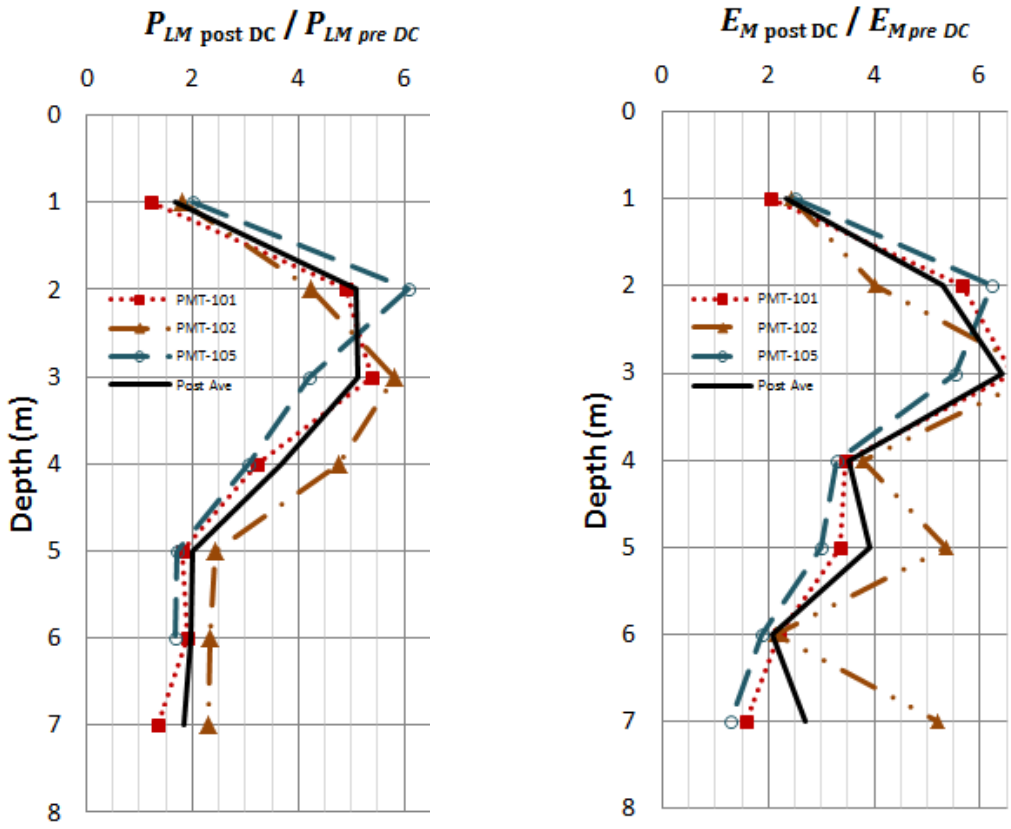

Figure 3-105: P_{LM} and E_M improvement ratios in pattern with 7x7 m^2 grid

Figure 3-107 shows P_{LM} and E_M improvement ratios for inside phase 1 and phase 2 prints, in between the prints, and their averages. The peak P_{LM} improvement ratio of all tests is about 5.2, and the peak average P_{LM} improvement ratio is about 4.2, which is somewhat less than an improvement of 400% that has been proposed by Lukas (1986).

Figure 3-108 and Figure 3-109 respectively show the ratio of Phase 1 (average of two prints for Pattern 1) to Phase 2 limit pressure values for Patterns 1 and 2 and the same ratio and the ratio of Phase 1 to in between the prints P_{LM} for Pattern 2. It can be observed that, except of the variations on the most upper testing level, Phase 1 to Phase 2 ratios for both patterns are very similar, and it appears that in general the ground strength is up to 30% more in Phase 1 prints. Interestingly, Figure 3-109 suggests that at some depths the strength of ground is more in between the prints that in Phase 1 prints.

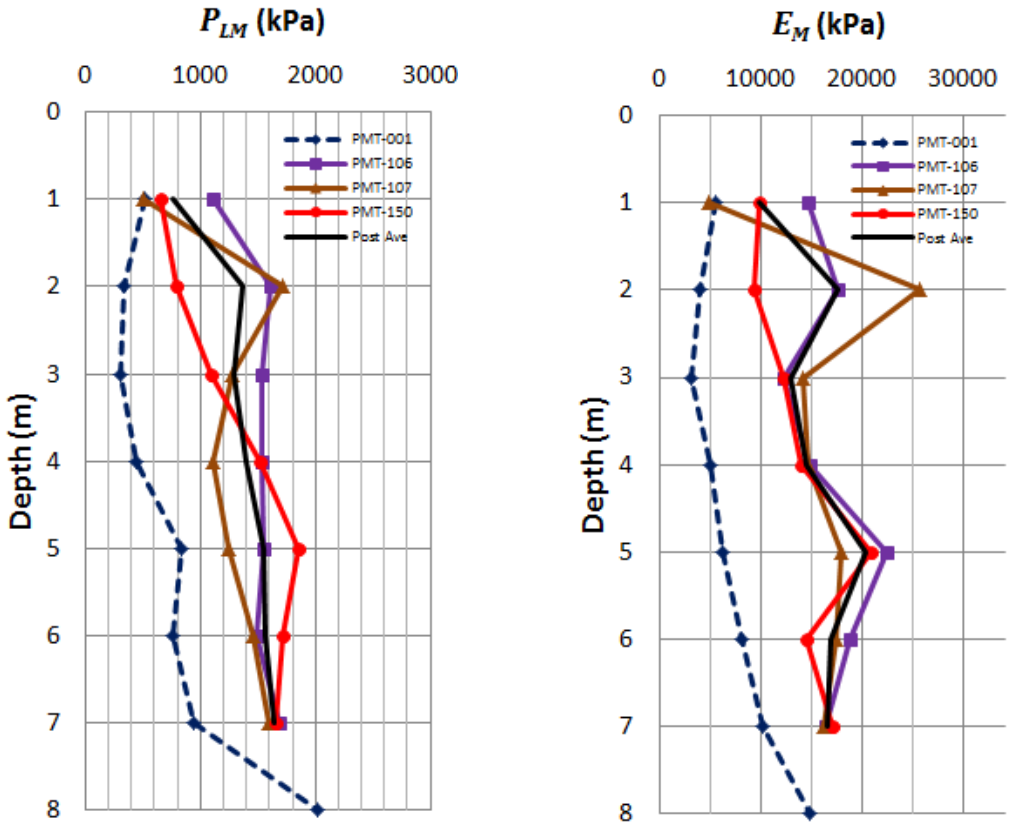

Figure 3-106: P_{LM} and E_M values before and after dynamic compaction in pattern with 5x5 m^2 grid

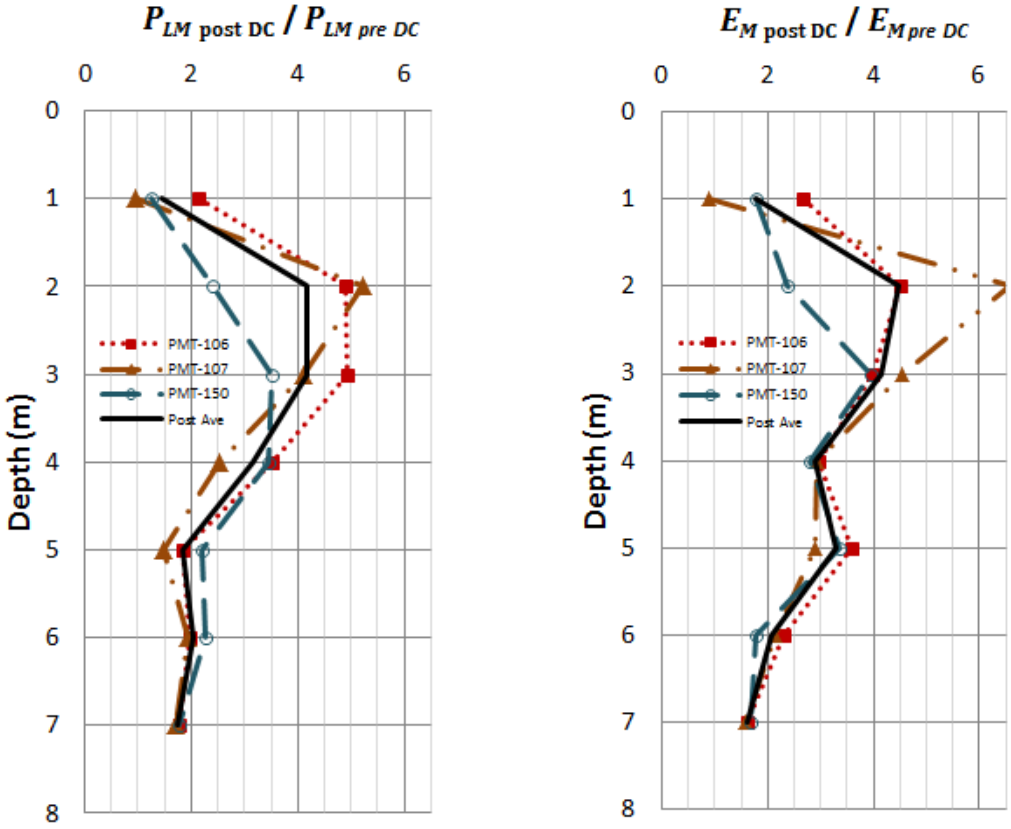

Figure 3-107: P_{LM} and E_M improvement ratios in pattern with 5x5 m^2 grid

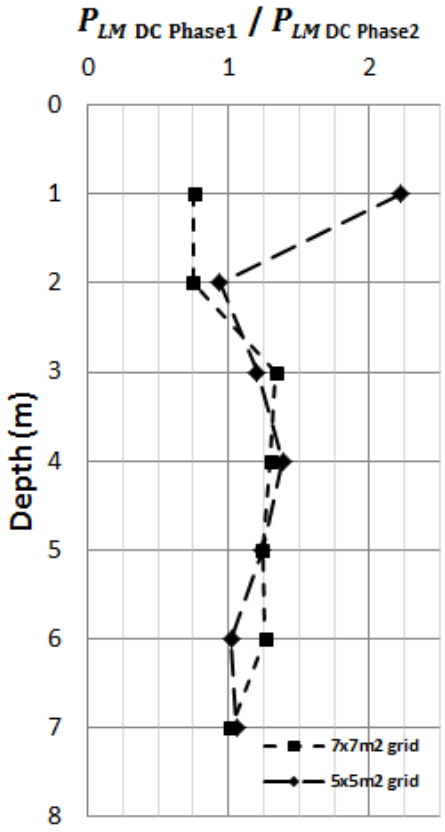

Figure 3-108: Ratio of Phase 1 to Phase 2 P_{LM} values for Patterns 1 and 2

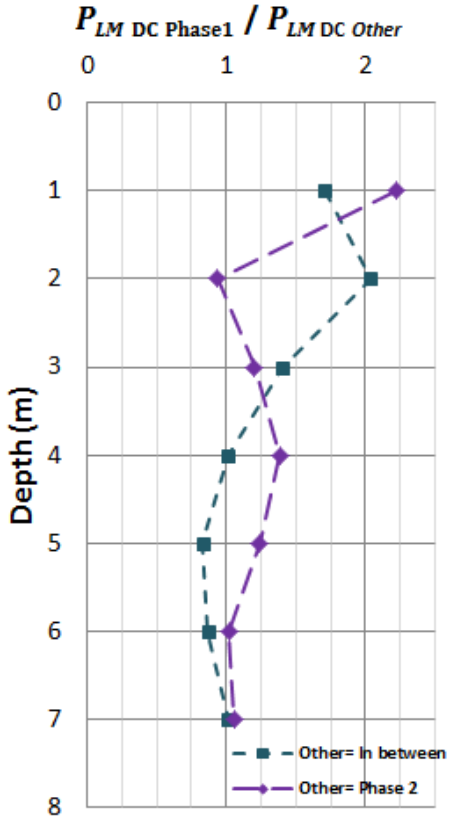

Figure 3-109: Ratio of Phase 1 to Phase 2 and in between prints P_{LM} values for Pattern 2

3.6.4.2 Final Testing

16 PMTs were carried out before dynamic compaction. A further 32 PMTs were also carried out after ground improvement to verify the ground conditions and to confirm that acceptance had been achieved. Of these, 14 tests were on the Peninsula, 5 were on Island 1 and 13 were on Island 2.

For comparative purposes E_M values of two test locations that were substantially different are shown in Figure 3-110. In these tests E_M values were assumed to have a maximum value of 25 MPa due to equipment gauge limitations. Although in reality the distance between these two tests was much more than 10 m, it is of interest to study the total settlements.

Settlements can be calculated using Equation 2-198:

$$s = (q - \sigma_{vo})\left[\frac{2}{9}\frac{B_0}{E_d}\left(\lambda_d \frac{B}{B_o}\right)^{\alpha} + \frac{\alpha\lambda_c}{9E_c}B\right] \qquad 2\text{-}198$$

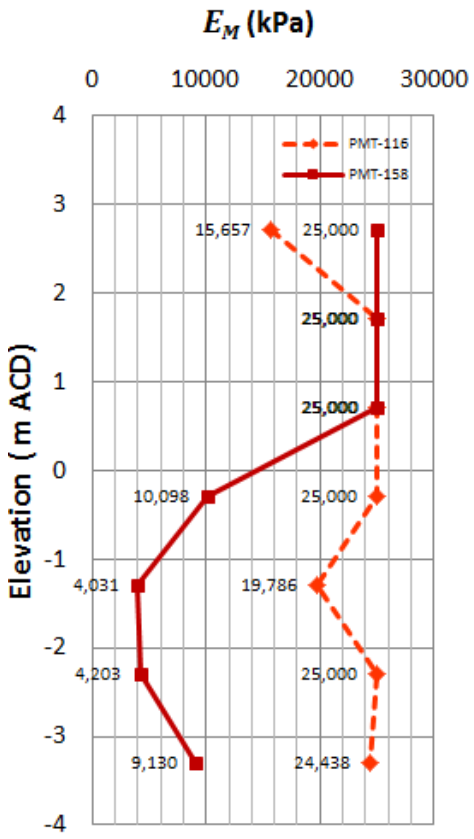

Figure 3-110: Two post dynamic compaction E_M logs

Assuming a loading area of 100 m by 10.5 m subject to a uniform load of 20 kPa, and conservatively assuming E_M= 20 MPa for all layers below testing levels, it can be seen that the total settlement of the testing point with lower moduli will result in only 2.2 mm of settlement. This figure itself is much less than the acceptable differential settlement between two points, and demonstrates that acceptance has been achieved.

Figure 3-111 shows average E_M before and after dynamic compaction. It can be seen that while it is generally expected for the improved test profile to be sickle shaped, in this case because average E_M before dynamic compaction was least where the improvement was most, the improvement profile appears to be more linear and only slightly curved. Figure 3-111 also shows the average E_M improvement ratio, and it can be observed that the ratio appears to be in the shape of a sickle with maximum improvement at about half the depth of improvement. The maximum average E_M improvement ratio was 5.31, which is quite compatible with the indicative upper bound figure of 400% that has been proposed by Lukas (1986) as a guideline.

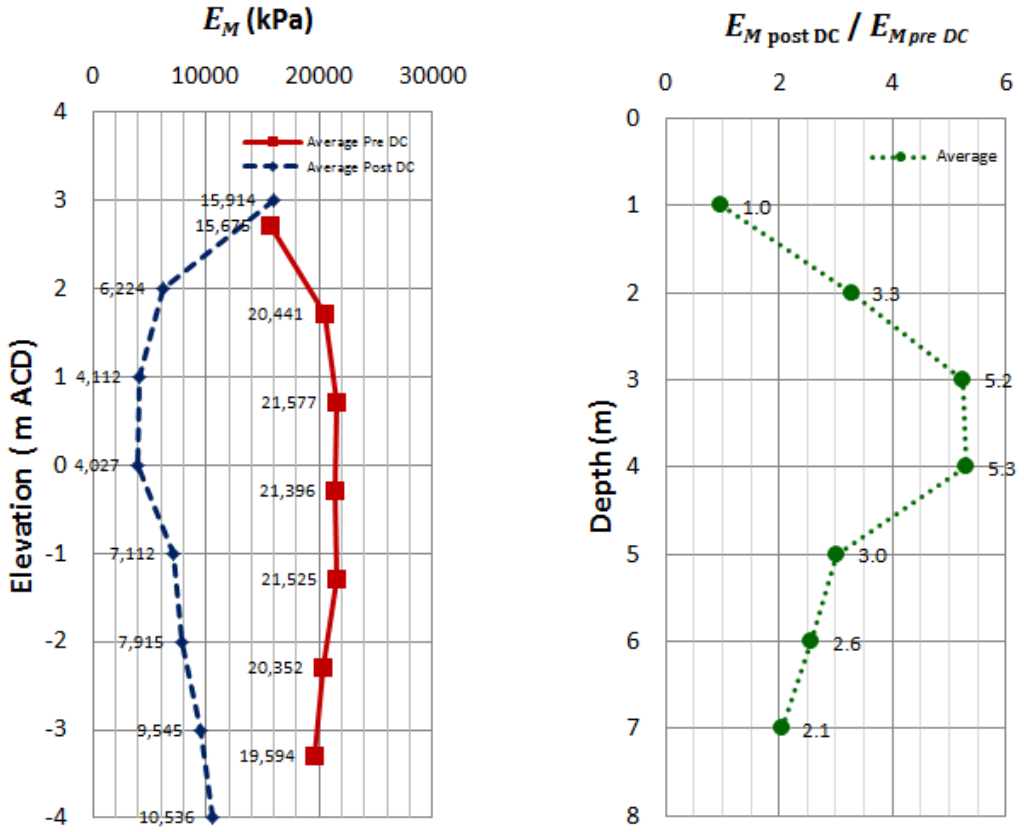

Figure 3-111: Average E_M before and after dynamic compaction and average E_M improvement ratio

3.6.5 Lessons and Conclusions

Marjan Island is a reclaimed site that has been realised by dumping sand into the sea by trucks. The geotechnical investigation showed that the soil was of variable strength and generally very loose down to the depth of about 7 m, and preliminary analysis indicated that the ground was subject to creep settlement due to self-weight and differential settlements. Dynamic compaction was implemented to improve the main road of the Peninsula, Island 1 and Island 2.

Post ground improvement PMTs were carried out, and were able to demonstrate that ground settlements due to the project's uniformly distributed design load was negligible and much less than the acceptance criteria.

In summary, it was observed that:

1. Ground reclaimed by dumping sand into the sea was in a loose state.

2. Should the grid pattern be close enough, compaction of first phase prints will also somewhat densify the ground influenced by the second phase prints. Consequently, it may be possible to apply lesser amounts of energy in the second phase of compaction.

3. In this project, the PMT parameters' improvement ratios were in the order suggested by Lukas (1986).

4. In this project (reclamation by dumping sand), the square root of the compacted volume (in m^3) of ground is about 2.15 to 2.4 times the crater depth (in m).

Figure 3-112 shows Marjan Island Road Corridor after completion of dynamic compaction works.

Figure 3-112: Marjan Island road after completion of dynamic compaction works

3.7 Al Nakhilat Ship Repair Yard

3.7.1 Project Description

Ras Laffan, located on the southern coast of the Persian Gulf and approximately 70 km north of Qatar's capital city, Doha, houses the onshore facilities of the world's largest gas field. Nakhilat Ship Repair Yard that is shown in Figure 3-113 is part of Port of Ras Laffan's expansion programme, and has been constructed on land that was hydraulically reclaimed.

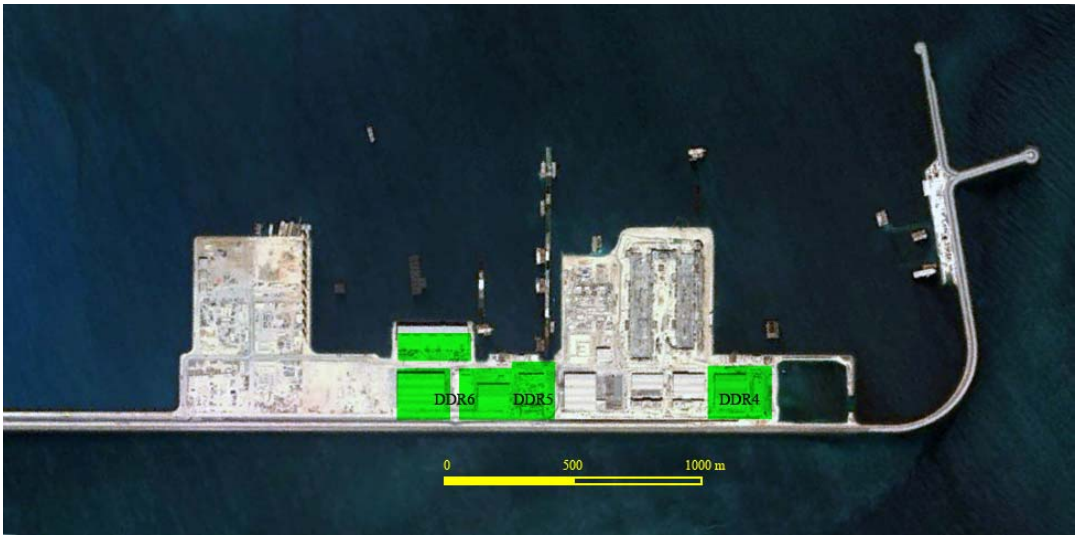

Figure 3-113: Plan of Nakilat Ship Repair Yard

3.7.2 Ground Conditions

Seabed level at the location of the project was variable from -9.1 m to -13.2 m CD (chart datum). Design (final platform) level was set at +3.5 m CD; however, it was envisaged that the hydraulic fill would be placed in a loose state, ground improvement would be required, and the platform level would consequently reduce. Ground subsidence due to treatment was estimated to be in the range of 0.6 to 0.8 m; hence, the working platform was reclaimed approximately to +4.1 to +4.3 m CD.

Reclamation was carried out using carbonate sand and gravel that were dredged from the sea for deepening the port. The fill's grain size was generally less than 75 mm, but stones as large as 500 mm in diameter were also present. The maximum fines content of the fill was mostly less than 10% in the upper elevations, but there were occasional lenses of silt at depth with thicknesses varying from 0.2 to 0.4 m. Carbonate content of the reclamation material was approximately 90% as $CaCO_3$.

CPTs were carried out as part of the geotechnical investigation after reclamation. In areas DDR4 (57,064 m^2), DDR5 (35,643 m^2) and DDR6 (82,962 m^2) of the dry dockyards (see Figure 3-113) the soil in the upper 3 m to 5 m was medium to very dense with q_c ranging from as low as 5 MPa to more than 20 MPa. The soil then became loose to medium dense with q_c fluctuating between 1 MPa to 7 MPa. Dense seabed was encountered at depths of 13 m to 17 m, and CPT friction ratio was understood to be generally well below 1%. Three typical CPT q_c logs are shown in Figure 3-114.

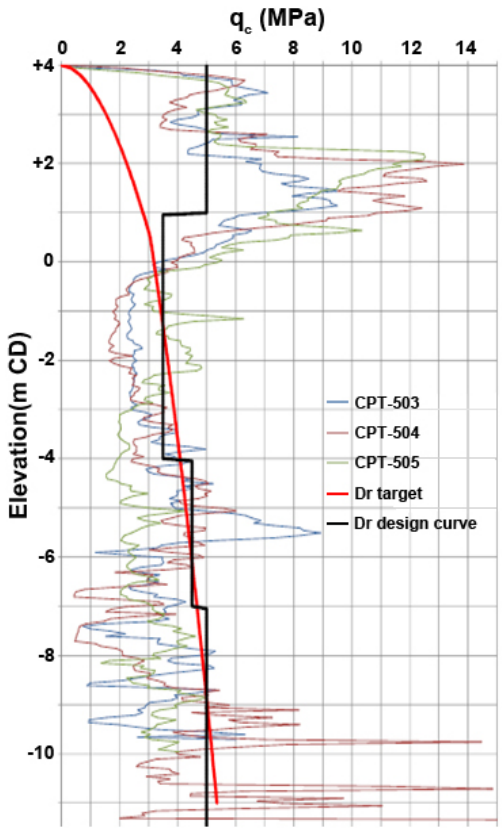

Figure 3-114: Comparison of CPT cone resistance before ground improvement with target relative density

3.7.3 Design and Acceptance Criteria

While it was understood that less sensitive areas of the project would require lesser ground treatment, areas DDR4, DDR5 and DDR 6 with a total area of more than 175,000 m^2 were deemed to be sensitive, and project specifications stipulated that minimum relative density, D_d, in these areas had to be 60% based on the correlation of Baldi et al. (1986), which has been derived for normally consolidated Ticino sand (see Equation 2-265).

$$D_d = \frac{1}{2.41} \ln \left[\frac{q_c}{157 {\sigma'_v}^{0.55}} \right] \quad \text{2-265}$$

As discussed in Section 2.10.2.3.2.2, the penetration resistance of calcareous sands is lower than quartz sands with similar grain size distributions. Thus, in this project a correction factor of 1.94 was defined in the specifications for application to the cone resistances of the calcareous soil. For the purpose of calculations it was specified that the saturated and unsaturated densities of the soil were to be assumed to be respectively 18.7 kN/m^3 and 15.2 kN/m^3. Average groundwater level was assumed to be at +0.5 m CD.

By also plotting Baldi's 60% relative density curve (red line) in the CPT logs of Figure 3-114 it can be seen that the hydraulically reclaimed fill was not able to satisfy the project's acceptance criterion, and it was confirmed that ground improvement would be required. Figure 3-114 also shows the relative density design curve, which takes the soil's better characteristics in the upper layers into account, and assumes a number of line segments in lieu of the actual relative density correlation curve.

3.7.4 Development of Solution and Application of Dynamic Compaction

The ground improvement works of the project was awarded to a specialist geotechnical contractor who had proposed the application of dynamic compaction. With consideration of the numerous draw backs of relative density as a ground improvement criterion (refer to Section 2.10.2), and with the knowledge that foundation requirements could be satisfied more affordably by using alternative criteria that were directly based on design requirements, (refer to Section 2.10.1.12.10.1), the specialist contractor proposed alternative criteria based on a worst case isolated footing scenario:

- Footing load: 4000 kN
- Allowable bearing capacity: 200 kPa
- Maximum settlement: 50 mm

The project's schedule stipulated that mobilisation, ground improvement and testing to be completed according to the below milestones:

- DDR4: 154 days after issuance of notice to proceed
- DDR5: 63 days after issuance of notice to proceed

- DDR6: 91 days after issuance of notice to proceed

Based on the fill thickness and the phase of dynamic compaction, soil improvement was carried out in areas DDR4, DDR5 and DDR6 using a combination of 15, 25, 28 and 35 ton pounders. As shown in Figure 3-115, the 35 ton pounder was dropped in free fall from 25 m using *MARS* that had previously been used successfully in Al Quo'a (refer to Section 3.3.4).

Figure 3-115: Free fall drop of a 35 ton pounder using MARS technology

3.7.5 Testing and Verification

3.7.5.1 Heave and Penetration Test

Prior to the commencement of dynamic compaction production a number of heave and penetration tests were carried out, of which one that was carried out in DDR6 has been selected for review, analyses and discussion. In this HPT a 25 ton pounder was dropped 20 times from 20 m. The pounder was square with each side being 2 m. The assumption that the pounder's diagonal length of 2.82 m should be taken as the crater's bottom diameter does not seem justified in this project because firstly the pounder was lifted using two parallel single cable lines; hence, the pounder could not have rotated as it was lifted and dropped onto the print with different orientations, and secondly the crater's upper diameter in the first few blows was less than the pounder's diagonal length. Therefore, for calculation purposes, it is assumed that the diameter of the crater's base is the equivalent pounder diameter of 2.25 m.

Crater depth, which is equal to the accumulative pounder penetrations, crater, heave and the net compaction volumes are shown in Figure 3-116. As also observed in the HPT of Al Falah Community (Section 3.5.4.1) and Marjan Island Road Corridor calibrations (Section 3.6.4.1) the rate of crater depth increase is initially higher, but then reduces.

Except for the first several blows where heave volumes are negligible, additional blows generated negative heave volumes; i.e., additional settlement and compaction around the print. The rate of negative heave volume appears to be constant and not reducing noticeably with the increase of the number of blows. However, the net compaction volume rate seems to be declining. Thus, it can be envisaged that while the soil directly within the pounder print is reaching an asymptote value, the soil in the periphery is still able to undergo further compaction. Comparison of crater, heave (subsidence in this case) and net volume changes suggest that approximately 80% of the compaction volume originates from the crater and 20% can be contributed to the peripheral subsidence. Of course, this should not be necessarily interpreted as the crater volume being the result of the sole compaction of the soil directly beneath the crater.

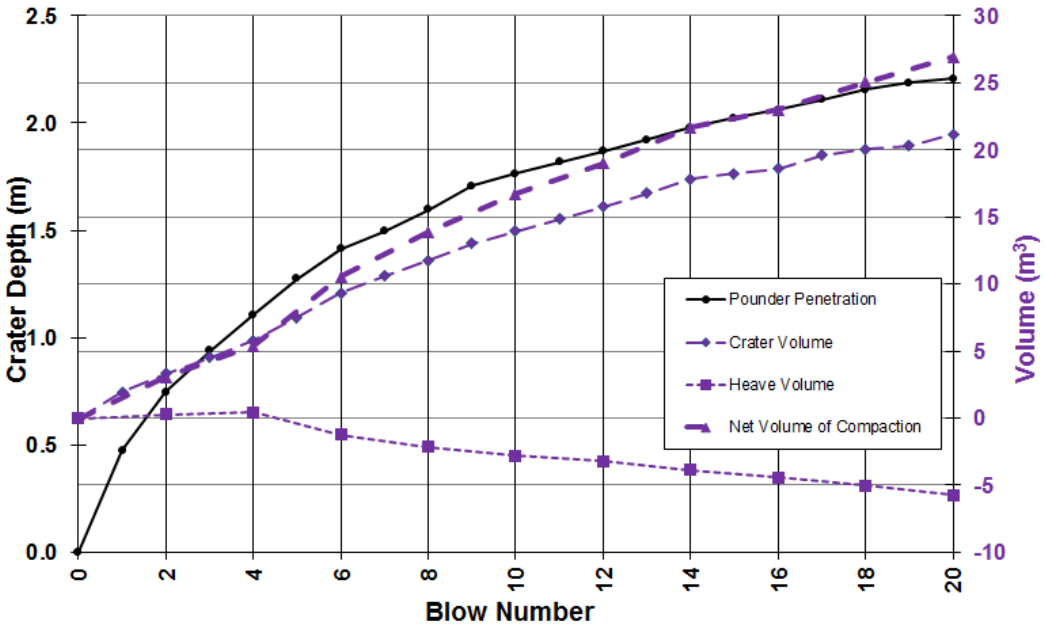

Figure 3-116: Heave and penetration test results

Figure 3-117 shows the relationship between the number of blows and the ratio of the square root of the compaction volumes to the crater depth. It appears that after the first several blows the ratio becomes independent of the number of blows. The ratio is approximately 2.32 when the net compaction volume, being the resultant of the crater and periphery volume changes, is considered, and is about 2.11 when only the crater volume is considered.

This suggests that the ratio of the square root of the crater volume to penetration is approximately 90% of square root of the net volume to penetration.

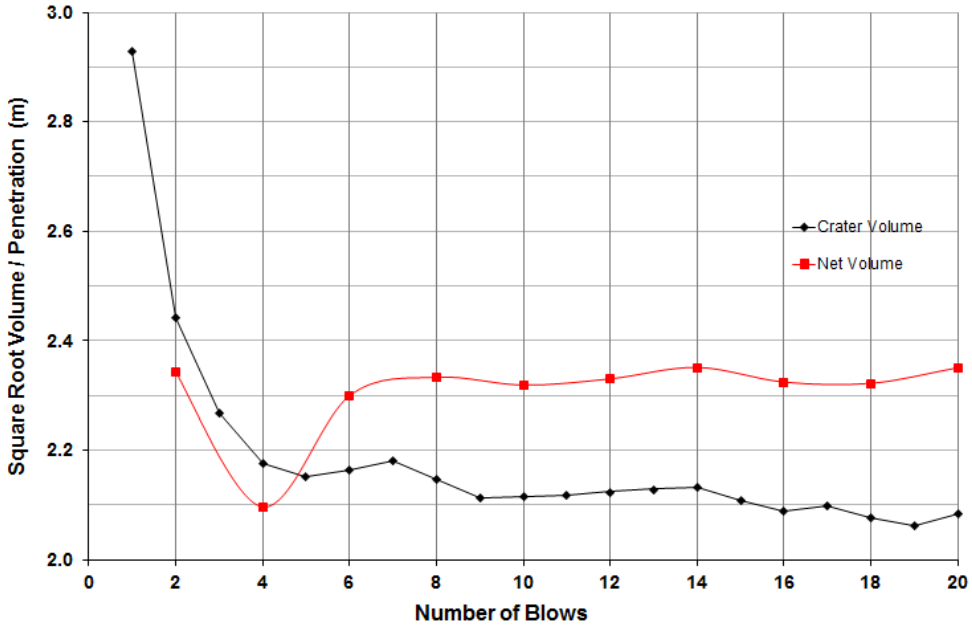

Figure 3-117: Ratio of square root of compaction volumes to penetration

A similar conclusion can be made when the compaction volume of the crater and each of the concentric rings around the crater are compared with the total volume of compaction for 6, 10 and 20 blows in Figure 3-118. It can be seen that the ratio of crater compaction volume to total compaction volume reduces with the number of blows from approximately 90% for 6 blows to about 80% for 20 blows. Compaction volume rapidly reduces with radius whereas 98% of the compaction volume occurs within a radius of 5 m for 6 blows, and within a radius of 10 m for 20 blows. Also, it can be noted that approximately 8% of the compaction has been realised within the concentric circle with 3 m radius. Noting that final grid sizes are usually about 4 to 6 m, an educated guess would suggest that compaction of second phase prints could increase the compaction volume of the soil within the zone of the first phase prints by about another 3 to 5%.

Figure 3-119 shows the ratio of the difference between the crater top diameter, D_T, and base diameter, D_B, to the crater depth. It can be observed that for the first 7 blows the ratio increases almost linearly with a gradient of approximately 14%; however, it then almost suddenly reaches a constant value of about 1.05. This suggests that the crater sides are initially steeper, possibly and partially due to the pounder side retaining the soil, but reach equilibrium at an angle of about 28^o from the vertical after several blows when the crater becomes deep (about 1.5 m at 7 blows).

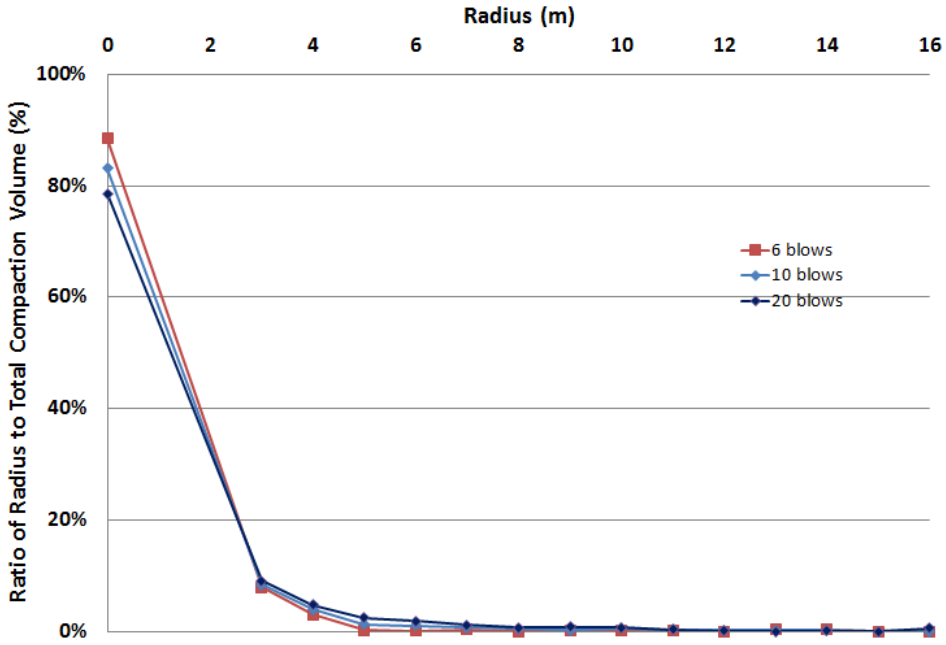

Figure 3-118: Percentage of compaction share of the crater and the peripheral concentric rings

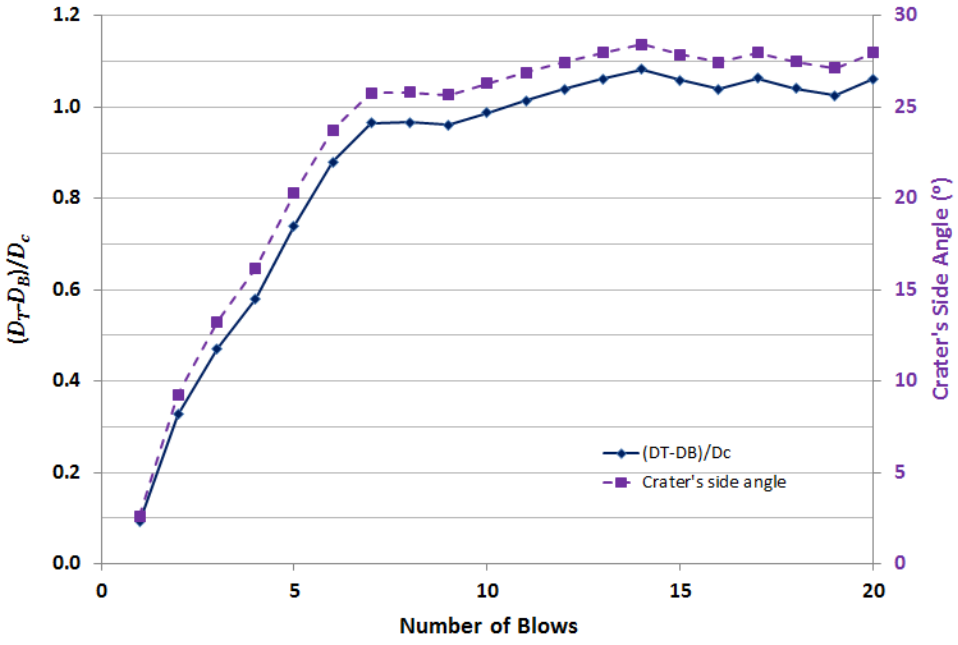

Figure 3-119: Variation of $(D_T\text{-}D_B)/D_c$ and crater side angle with number of blows

A penetration test (only crater measurements without recording peripheral heave) was also carried out in DDR-5 using a 35 ton pounder that was dropped from 25 m in free fall using MARS. The pounder was 2.4x2.4 m^2, and had an equivalent diameter of 2.7 m.

Figure 3-120 shows the ratio of the square root of the crater compaction volume to crater depth. Once again, it can be observed that after the first several blows the ratio levels off at approximately 2.36. Noting from Figure 3-117 that about 90% of the compaction volume

originates from the crater itself, it could be envisaged that the ratio for the total compaction volume would have been in about 2.6, which would have been higher than what was observed in Al Falah Community, Marjan Island, and for the 25 ton pounder calibration in this project. Thus, Equation 2-40 can be modified to become:

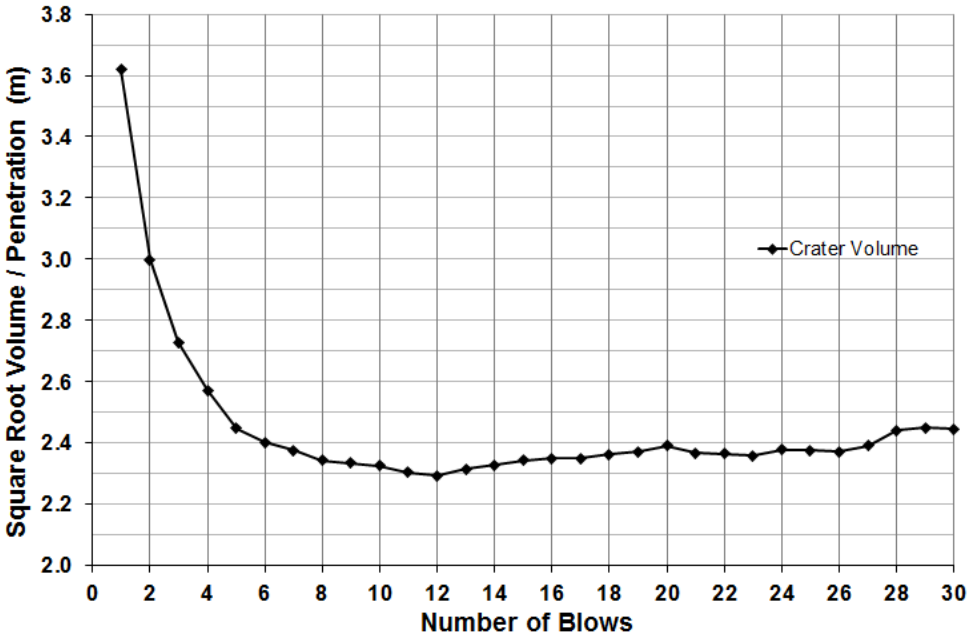

Figure 3-120: Ratio of square root of crater compaction volume to penetration

$$\frac{\sqrt{V}}{D_c} = 2.15 \; to \; 2.6 \qquad 3\text{-}5$$

Similar to Figure 3-119 and as shown in Figure 3-121, changes in $(D_T\text{-}D_B)/D_c$ and crater side angle values are higher for the first several blows, but then the rate reduces with more blows. However, in this calibration there does not seem to be an asymptote value, and it appears that $(D_T\text{-}D_B)/D_c$ and crater side angle diagrams follow logarithmic curves.

Changes of $(D_T\text{-}D_B)/D_c$ become more meaningful when they are studied against the changes of impact energy. Figure 3-122 shows the changes of $(D_T\text{-}D_B)/D_c$ against impact energy for two calibrations that were presented in this Section, and suggests that the variations of $(D_T\text{-}D_B)/D_c$ are almost linear against the logarithm of the impact energy. The comparison of only two curves is not sufficient to conclude anything concrete and definite, but one of the below scenarios is likely:

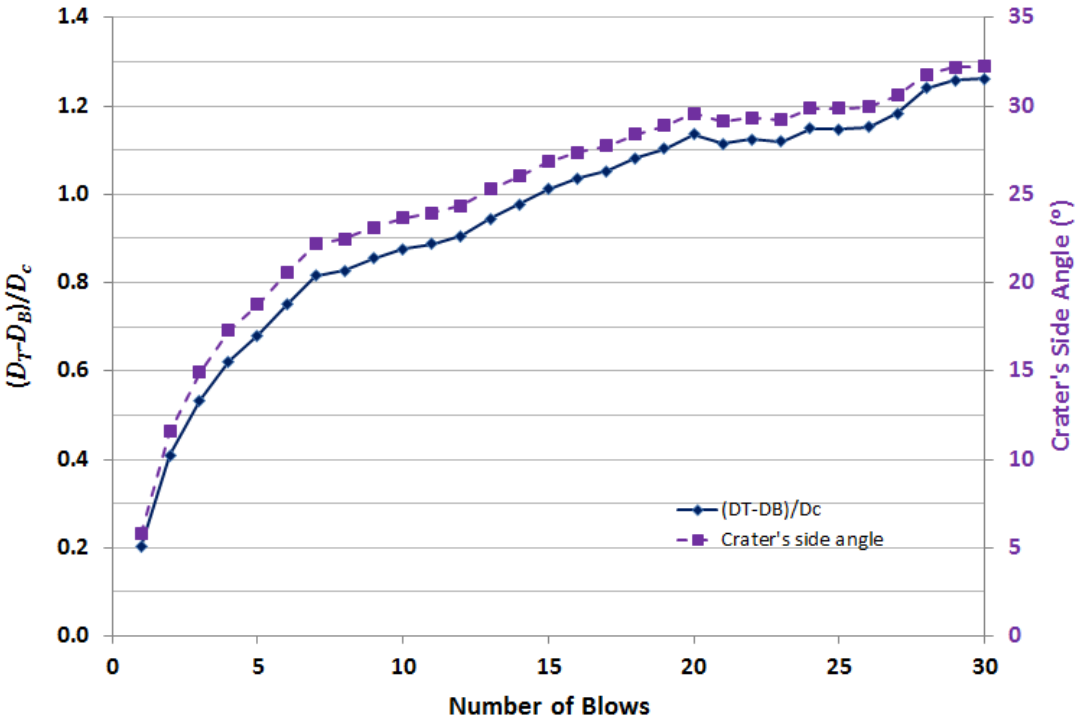

Figure 3-121: Variation of $(D_T\text{-}D_B)/D_c$ and crater side angle with number of blows

1. These two curves should be the same, there is only a single curve that explains the relationship between $(D_T\text{-}D_B)/D_c$ and impact energy, and the two curves in Figure 3-122 have not fallen on top of each other due to testing accuracy. This scenario appears reasonable as it is possible that crater proportions are independent of the energy of a single impact.

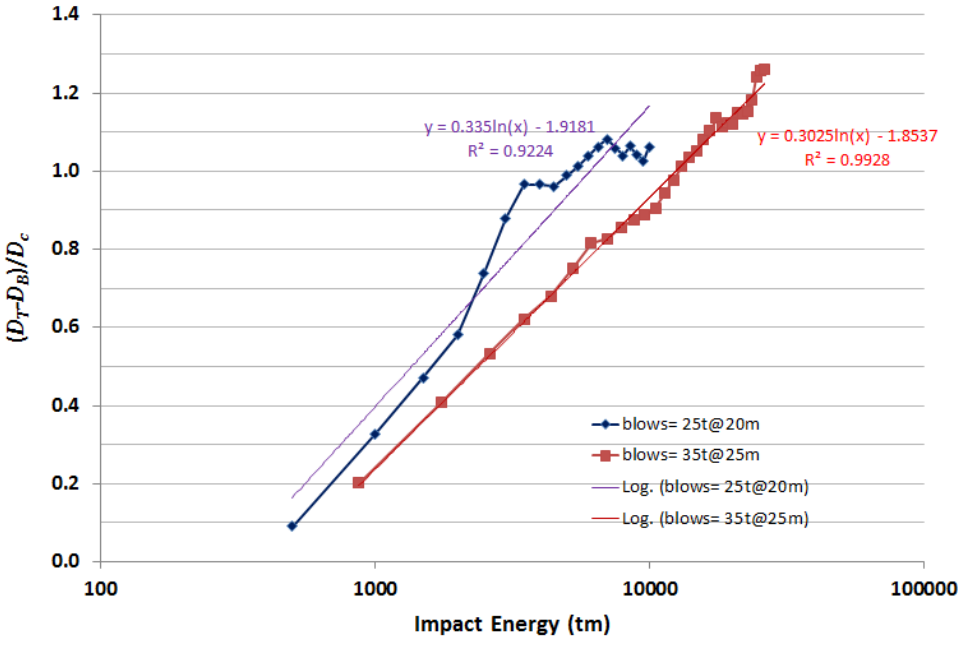

Figure 3-122: Variation of $(D_T\text{-}D_B)/D_c$ with impact energy

2. These two curves that are for two different impact energies per blow are different, and are part of a family of parallel curves that define the relationships between (D_T-D_B)/D_c and impact energy. This scenario appears to be equally reasonable as it is possible that crater proportions are dependent on the energy of each drop.

3.7.5.2 CPT

In order to verify that the project requirements had been satisfied one CPT was carried out per every 600 m^2 of improved ground. A number of PMT were also carried out for comparative purposes.

Two commonly encountered post ground improvement soil profiles (using a 28 ton pounder) in area DDR4 and four commonly encountered post ground treatment soil profiles in area DDR6 are respectively shown in Figure 3-123 and Figure 3-124. The soil compositions of these profiles are summarised in Table 3-10. It can be well seen that while the fines content of the upper layers in all areas and the entire fill thickness in some areas is composed of clean sand as per the project specifications, the post treatment tests were able to identify substantially siltier soil (fines content greater than 10%) at depth in some areas. Fines content in some layers were considerably higher than expected, and even reached 100%. Similarly, the CPT friction ratio in some locations was measured to be up to 7%.

For design purposes, a worst case scenario of the q_c curve was chosen from DDR4 Profile 1 (the black line segments in Figure 3-123a), and simplified into a number of segments. The same line has been copied onto Figure 3-123b and Figure 3-124 for comparison purposes. It can be observed that the actual ground improvement is considerably better in the other profiles.

Irrespective of all the serious drawbacks and ambiguities that the application of relative density can have on a project (refer to Section 2.10.2), it is still possible to draw the relative density curve (knowing that it does not apply when fines content exceeds 15%) and to compare it with the worst case scenario design curve. Figure 3-123c compares the q_c design curve, developed in Figure 3-123a, with the target relative density curve and relative density curve, developed in Figure 3-114. It can be seen that while the worst case scenario design curve has higher values in the upper soil layers, the relative density curve has greater values at depth.

Soil Profile	Ground Levels (m CD)		Layer information		Friction Ratio (%)	Fines Content (%)
			Description	bottom level (m CD)		
DDR4- Profile 1	+3.5 to +4	-13.5	clean sand	-13.5	0.2	0 to 5
DDR4- Profile 2	+3	-13	clean sand	-4.5 to -7	0.2	0 to 5
			silty sand	-7 to -9.5	1 to 3	15 to 50
			clean sand	-13	0.2	0 to 5
DDR6- Profile 1	+2.5	-11	clean sand	-6 to -9	0.2	0 to 5
			silty sand	-11	0.2 to 0.5	5 to 10
DDR6- Profile 2	+3	-10.5	clean sand	-8.5 to -9.5	0.2	0 to 5
			silty sand	10.4	0.2 to 0.5	5 to 10
			silt (0.5 m thick) inter-bedded in silty sand layer		4 to 5	50 to 70
DDR6- Profile 3	+2.5 to +3	-10.5	clean sand	-5 to -6.5	0.2	0 to 5
			silty sand	-10.5	0.5 to 1	20 to 30
			silty sand/ silt three bands, each 0.2 to 0.4 m thick		1.2 to 5	30 to 70
DDR6- Profile 4	+1.5 to +3.2	-10.5	clean sand	-3.5 to -8	0.2	0 to 5
			silty sand	-10.5	0.5 to 1	20 to 30
			silty sand/ silt four bands, each 0.2 to 0.6 m thick		4 to 7	70 to 100

Table 3-10: Soil profiles in areas DDR4 and DDR6

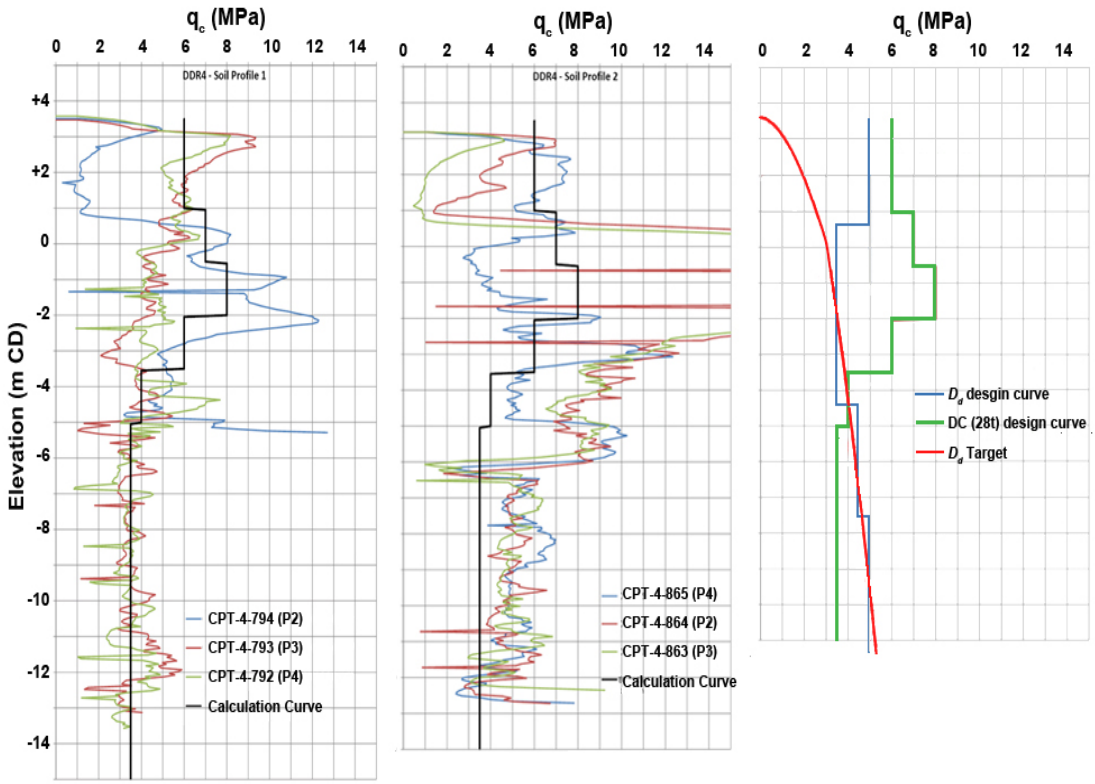

Figure 3-123: Post ground improvement soil profiles in DDR4

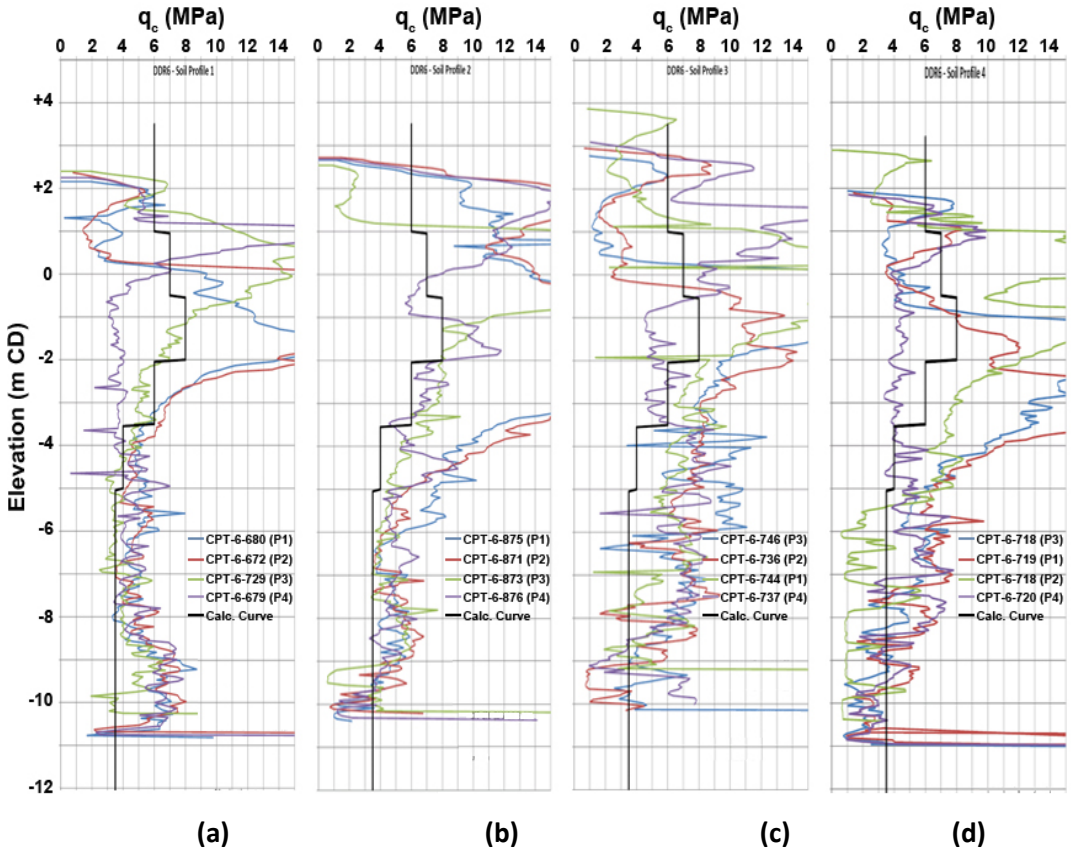

Figure 3-124: Post ground improvement profiles in DDR6

Ultimate bearing capacity, q_u, for a square footing on a cohesionless soil can be estimated from Bowles (1996):

$$q_u = 4800 - 0.9(300 - q_c)^{1.5} \quad \text{(kPa)} \qquad 3\text{-}6$$

Jullienne (2008) calculated the allowable bearing capacity for each of the q_c curves with a factor of safety of 3. The allowable bearing capacity for the relative density design curve and worse scenario design curve are respectively 400 and 414 kPa, which are both much more than 200 kPa.

Likewise, using the method proposed by Schmertmann (1970) and Schmertmann et al. (1978), Jullienne also calculated the settlements for the relative density design curve and each of the soil profiles that have been shown in Figure 3-123 and Figure 3-124. In his calculation Jullienne assumed that the square footing is subject to 4,000 kN and subject to 200 kPa of pressure (a 4.5 x 4.5 m^2 footing). The result of the calculations is summarised in Table 3-11. It can be seen that it is in fact the relative density design curve that will result in the maximum amount of settlement.

Profile	settlement (mm)
DDR4- Profile 1	35.52
DDR4- Profile 2	30.67
DDR4- D_d design curve	50.16
DDR6- Profile 1	28.33
DDR6- Profile 2	33.66
DDR6- Profile 3	33.66
DDR6- Profile 4	35.06
DDR6- D_d design curve	50.16

Table 3-11: Settlements of the D_d design curve and the soil profiles subject to a load of 4,000 kN

The above calculations show that q_c values after dynamic compaction at depth may have been less than the relative density curve; however, all soil profiles have performed better than the relative density specification, and regardless of the drawbacks and unreliability of relative density as a ground improvement criterion, it can be seen that application of specifications that unnecessarily limit the acceptance zone by defining a hypothetical minimum passing value can result in failure to meet acceptance without failure to meet

design requirements. Indeed, as discussed in Section 2.10.1.3, acceptance criteria that are based on design criteria without proxy will yield the most efficient result and consequently the shortest construction programmes with the least construction costs.

3.7.5.3 CPT-PMT Correlation for Carbonate Sand

After execution of dynamic compaction in DDR5 using a maximum pounder weight of 28 tons (without ironing) it was decided to perform a dynamic compaction trial to study the improvement effects using a 35 ton pounder that was dropped by *MARS*. This process included 3 deep compaction phases and an ironing phase.

As shown in Figure 3-125, 3 PMTs were carried out next to 3 CPTs in the below order:

- Before phase 1: PMT-007 and CPT-551 (in between impact points)
- After phase 1: PMT-009 and CPT-576 (in between impact points)
- After phase 3: PMT-010 and CPT-595 (in impact point)

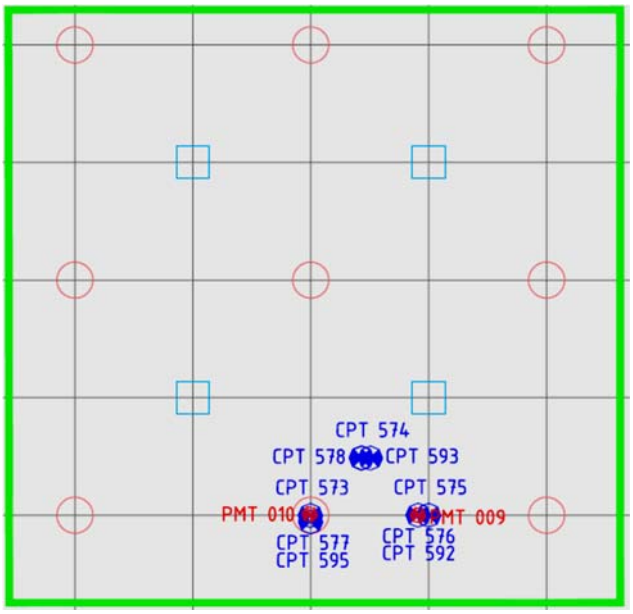

Figure 3-125: CPT and PMT layout

CPT q_c values are shown in Figure 3-126. Likewise, PMT P_{LM} and E_M are respectively shown in Figure 3-127 and Figure 3-128.

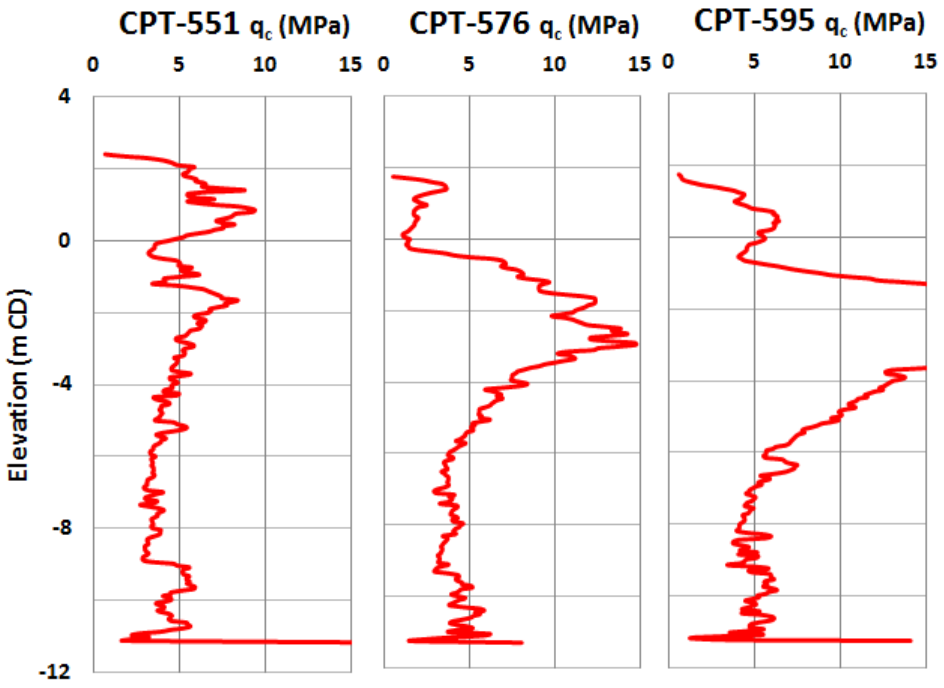

Figure 3-126: CPT cone q_c used in the correlation

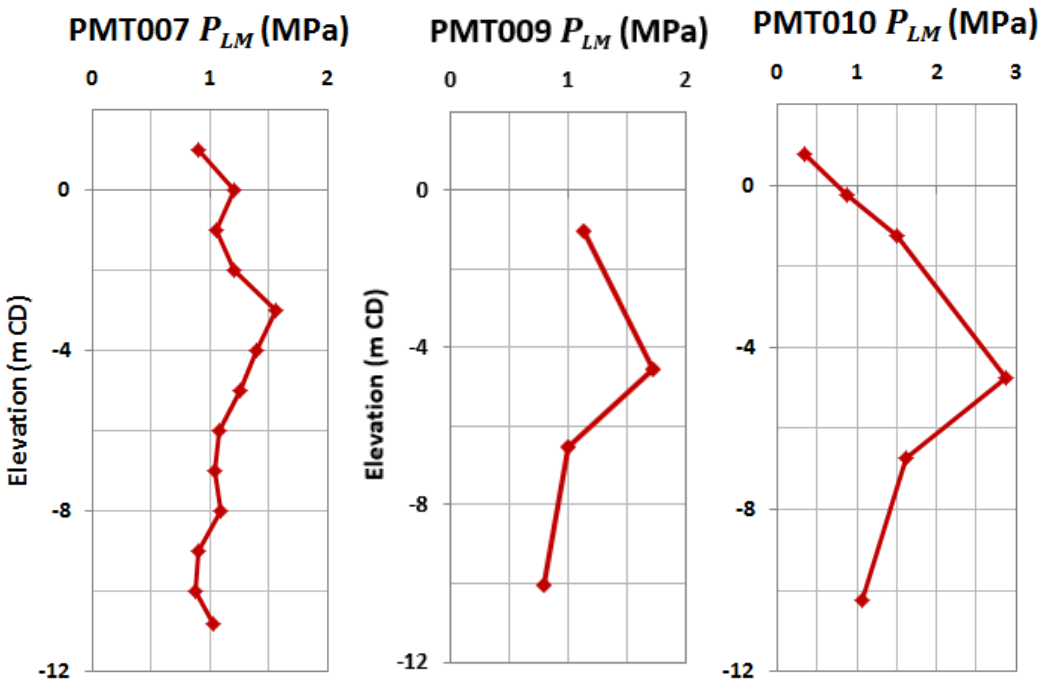

Figure 3-127: PMT P_{LM} values used in the correlation

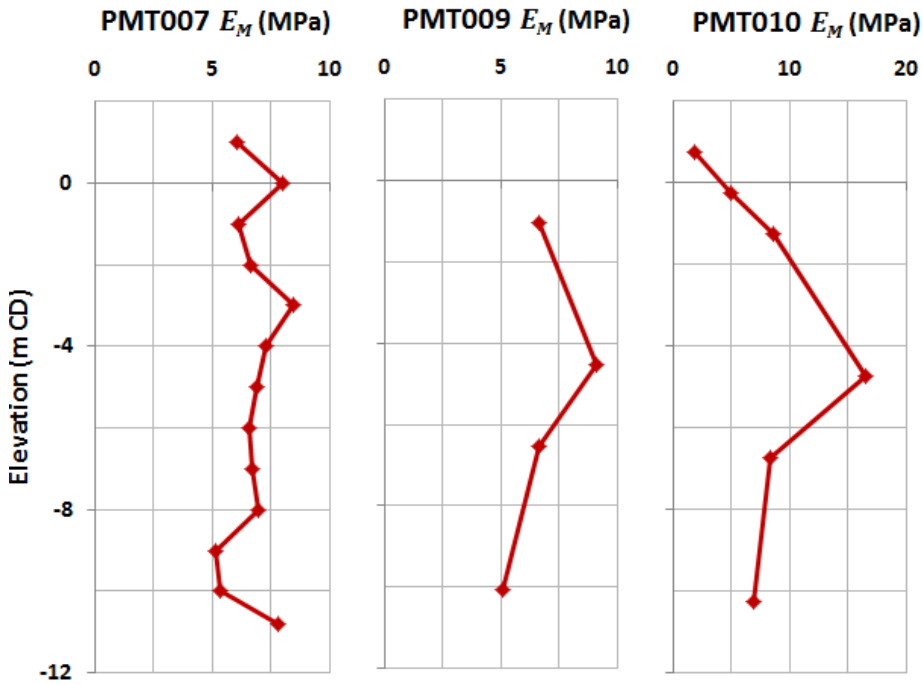

Figure 3-128: PMT E_M values used in the correlation

The ratios of q_c/P_{LM} are shown in Figure 3-129. It can be observed that the average q_c/P_{LM} values for 21 tests points, which exclude the uppermost test points of PMT007 and PMT010 due to the differences in between the shallow and deep failure modes, are equal to 4.54 (the average q_c/P_{LM} value is 5.20 when the top two ratios of PMT007 and PMT010 are also included). The average q_c/P_{LM} value for the three correlations on Ras Laffan carbonate sand are 4.1, 5 and 5.3 excluding the mentioned uppermost points. Minimum and maximum q_c/P_{LM} values were respectively 2.9 and 9.1 for the 21 points. Briaud et al. (1985), see Table 2-27, have proposed the correlation to be P_{LM} =0.11q_c, which is equivalent to q_c/P_{LM}= 9. This is almost twice the average q_c/P_{LM} value that was derived in this project[1].

As shown in Figure 3-130, q^*_c/P^*_{LM} plots are identical in shape and very close in value to the q_c/P_{LM} ratios, and indicate that implementation of q_c/P_{LM} ratios has yielded the same results as q^*_c/P^*_{LM} in this saturated sand. The average q^*_c/P^*_{LM} value for the 21 tests points is equal to 4.82, which is just below the range of 5 to 12 that has been proposed by Baguelin et al. (1978) that was presented in Table 2-26. The average q^*_c/P^*_{LM} values for the three

[1] The author has previously published a paper (Hamidi, B., Varaksin, S. & Nikraz, H. (2010) Correlations between CPT and PMT at a Dynamic Compaction Project. *2nd International Symposium on Cone Penetration Testing (CPT10)*, Huntington Beach, California, 9-11 May, paper 2-04.) The interpretation of that paper is erroneous as there has been a mistake in the comparison of results. The interpretation in the thesis is correct.

correlations are 4.3, 5.4 and 5.2 excluding the mentioned uppermost points. Minimum and maximum q^*_c/P^*_{LM} values for the 21 points were respectively 3 and 9.3.

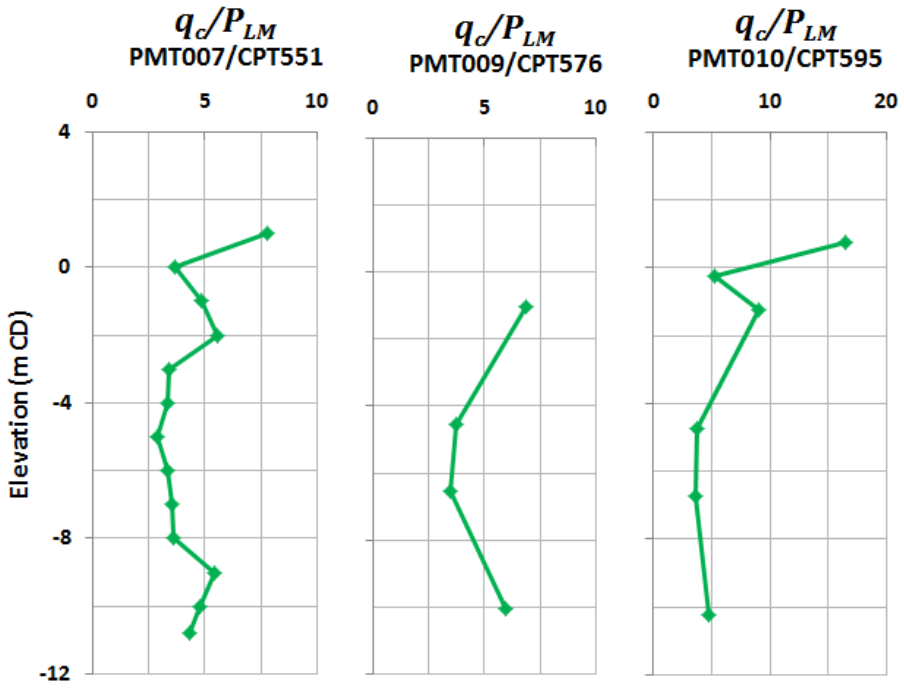

Figure 3-129: q_c/P_{LM} for Ras Laffan carbonate sand

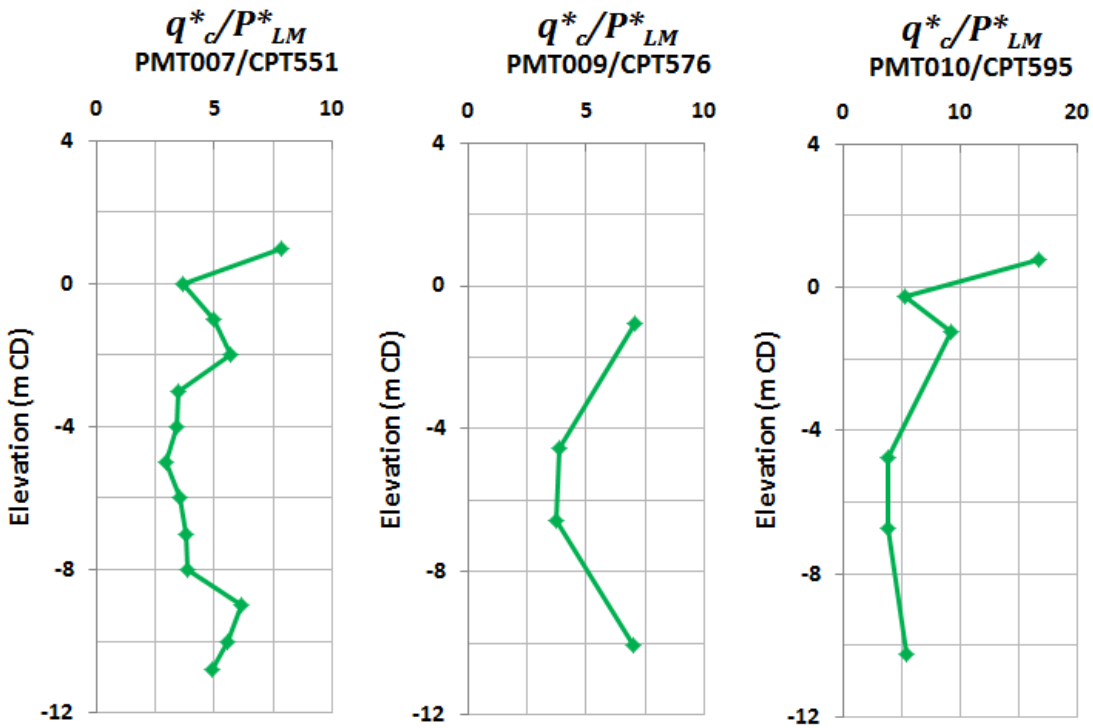

Figure 3-130: qc*/P*LM for Ras Laffan carbonate sand

As shown in Figure 3-131, E_M/q_c values of the two uppermost shallow points do not seem to correlate differently with the deeper points as the result of differences between the shallow

and deep failure modes. The average E_M/q_c value for the 23 test points is 1.35. The average E_M/q_c values for the three tested locations on Ras Laffan carbonate sand were 1.5, 1.3 and 1.1. Minimum and maximum E_M/q_c values for the test points were respectively 0.3 and 1.91. Briaud et al. (1985) have proposed a correlation of E_M=1.15q_c (see Table 2-27), which is almost 85% of what has been measured in this project.

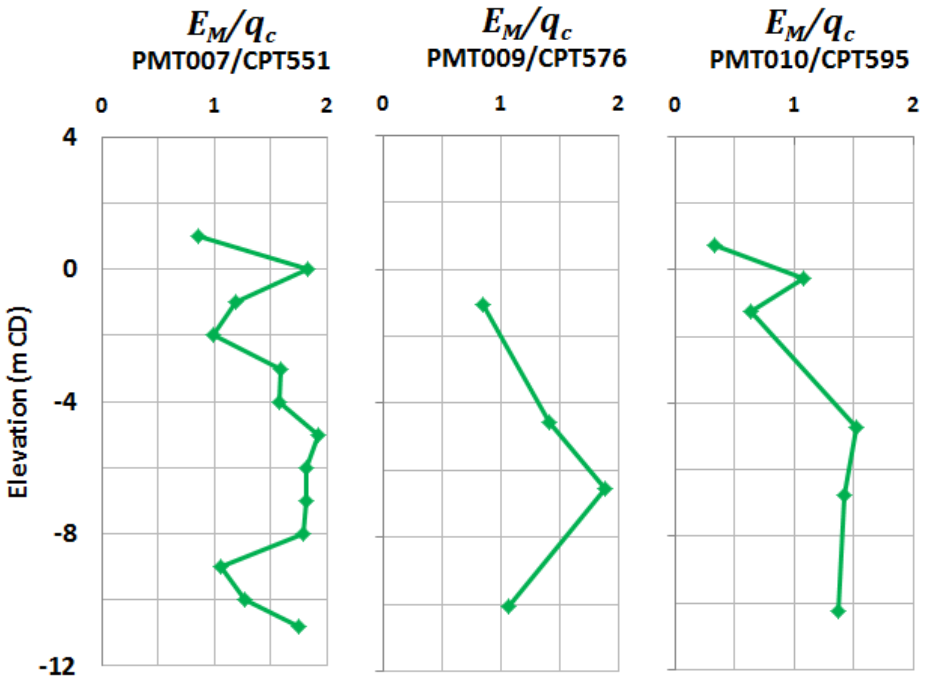

Figure 3-131: E_M/q_c for Ras Laffan carbonate sand

With consideration of the two uppermost points, it can be concluded that for Ras Laffan saturated carbonate sand, after dynamic compaction:

$$q_c/P_{LM} = q^*_c/P^*_{LM} = 5 \qquad 3\text{-}7$$

$$E_M/q_c = 1.35 \qquad 3\text{-}8$$

3.7.5.4 Zone Load Testing

Sieve analyses and hydrometer tests carried out on samples extracted from boreholes that were drilled as part of the geotechnical investigation during ground improvement indicated the presence of bands of fine soils in the area of the skid beams in DDR6. Fines content in these layers were considerably higher than the specified 10% limit and up to 97%. As shown in Figure 3-132, clay content of some layers was up to 38%.

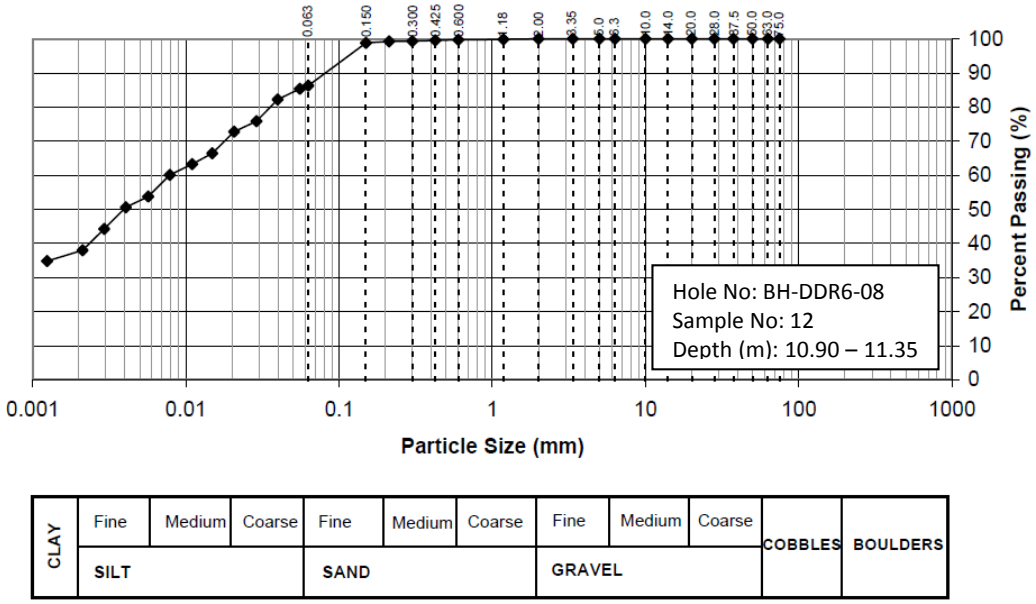

Figure 3-132: Fines content of reclaimed soil with very high fines content

The CPT profiles of a test that was carried out before and a test that was performed after dynamic compaction in the same area is shown in Figure 3-133. The CPT friction ratio also confirmed the presence of the same fine layers.

A PMT that was also performed in the area with fine soil layers is shown in Figure 3-134. While this test does not identify fine soil layers, a noticeable reduction of PMT parameters is seen at the depth of the fine soil layers.

The presence of a potentially soft clayey soil at depth raised concerns about the long term settlement of the ground under external loads. Therefore, a full scale zone load test was performed at the location of tests shown in Figure 3-132 to Figure 3-134 that appeared to have the most amount of silty or clayey layers with a thickness of 4 m from approximately -5 m to -9 m CD, and which has been marked with a circle in Figure 3-135.

As shown in Figure 3-136 (relative to the DC grid and test locations) and Figure 3-137(a) (relative to one another, the loading units and settlement measuring locations), similar loading to the skid beams was carried out using 1.5 m^3 concrete blocks (3.75 tons) placed in two parallel strips, each composed of 3 rows and up to 5 columns. For the first layer, 18 blocks, spaced at 0.2 m distances from edge to edge, were placed over a length of 25.7 m. The second to fifth layers each had from 17 to 14 blocks. Maximum height of the blocks (from ground level to the top of the fifth layer) was 5.7 m. The centres of the strips were 6 m apart.

It can be assumed that the boundary influence will be eliminated between block rows number 5 to 13. Hence, on an area of 53.6m^2 (14.3x3.75 m), the load intensity was assumed to be 105 kPa.

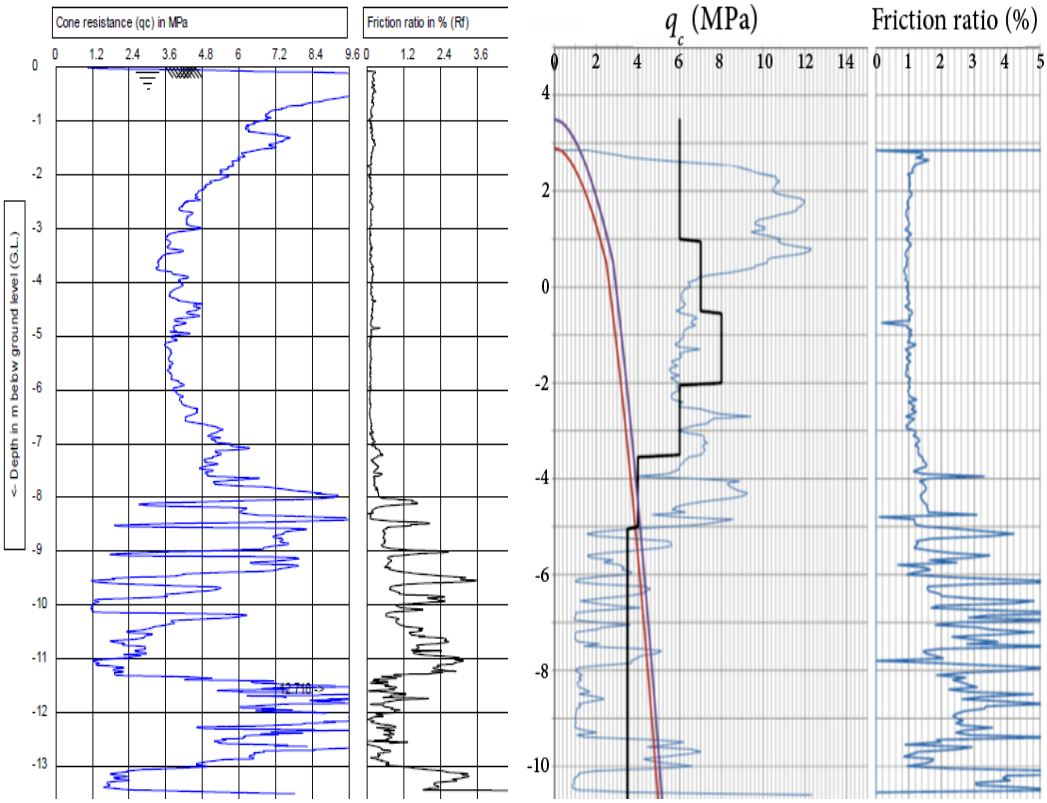

Figure 3-133: results of CPT-615 (before DC) and CPT-828 (after DC)

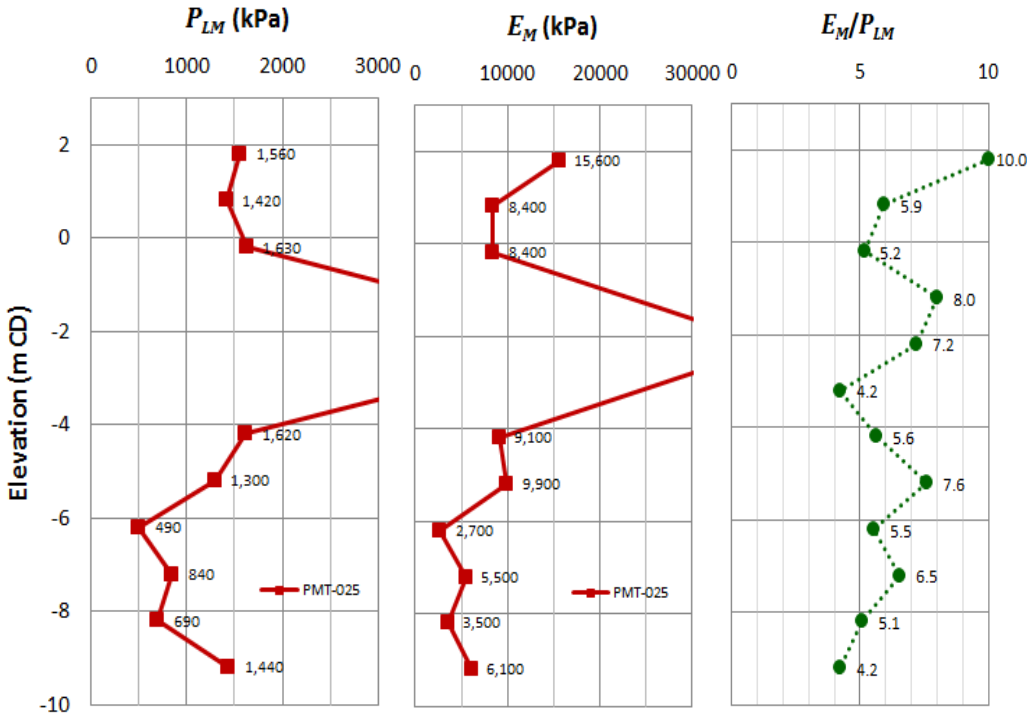

Figure 3-134: Results of PMT-025

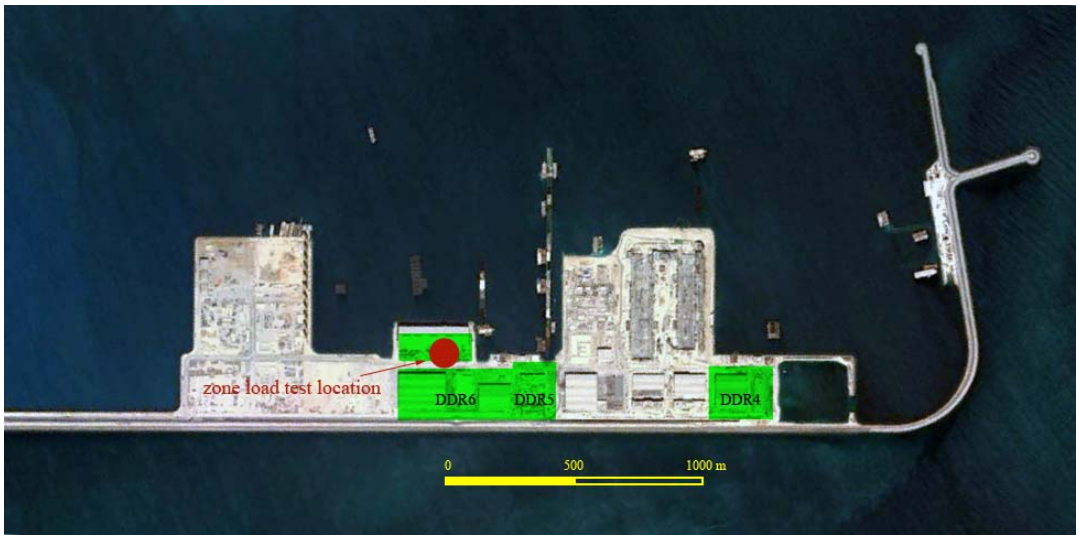

Figure 3-135: Location of zone load test in area with the most amount of fine soil

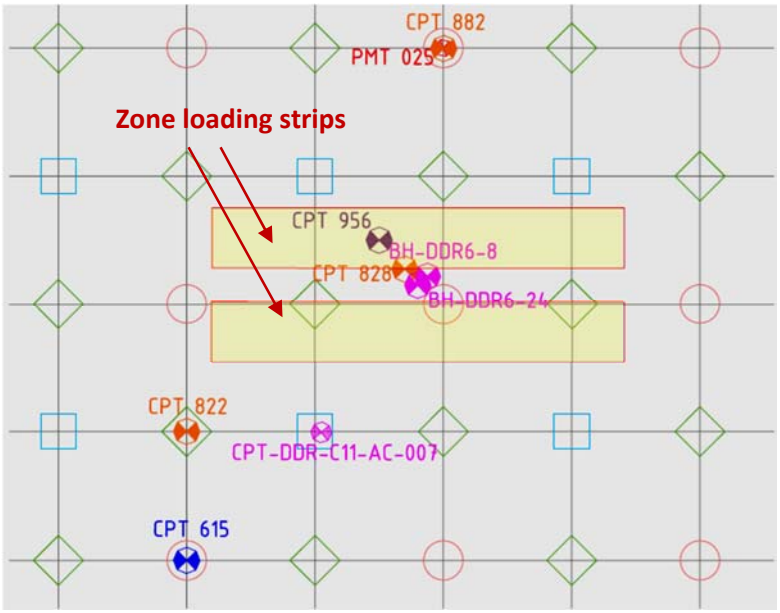

Figure 3-136: Location of zone load test and field tests shown in Figure

After levelling the areas to +3.5 m CD, four settlement monitoring beacons (the blue monitoring points in Figure 3-137) were installed as in-survey points. These were measured immediately before and right after the test loading. After the first layer of blocks was placed and all monitoring points (red points at the edge of the blocks) were established and measured, the remaining four block layers were also placed on the strips. The placement was done layer by layer. Upon completion of loading, the red monitoring points shown in Figure 3-137 were immediately measured. The blocks were removed after the testing period.

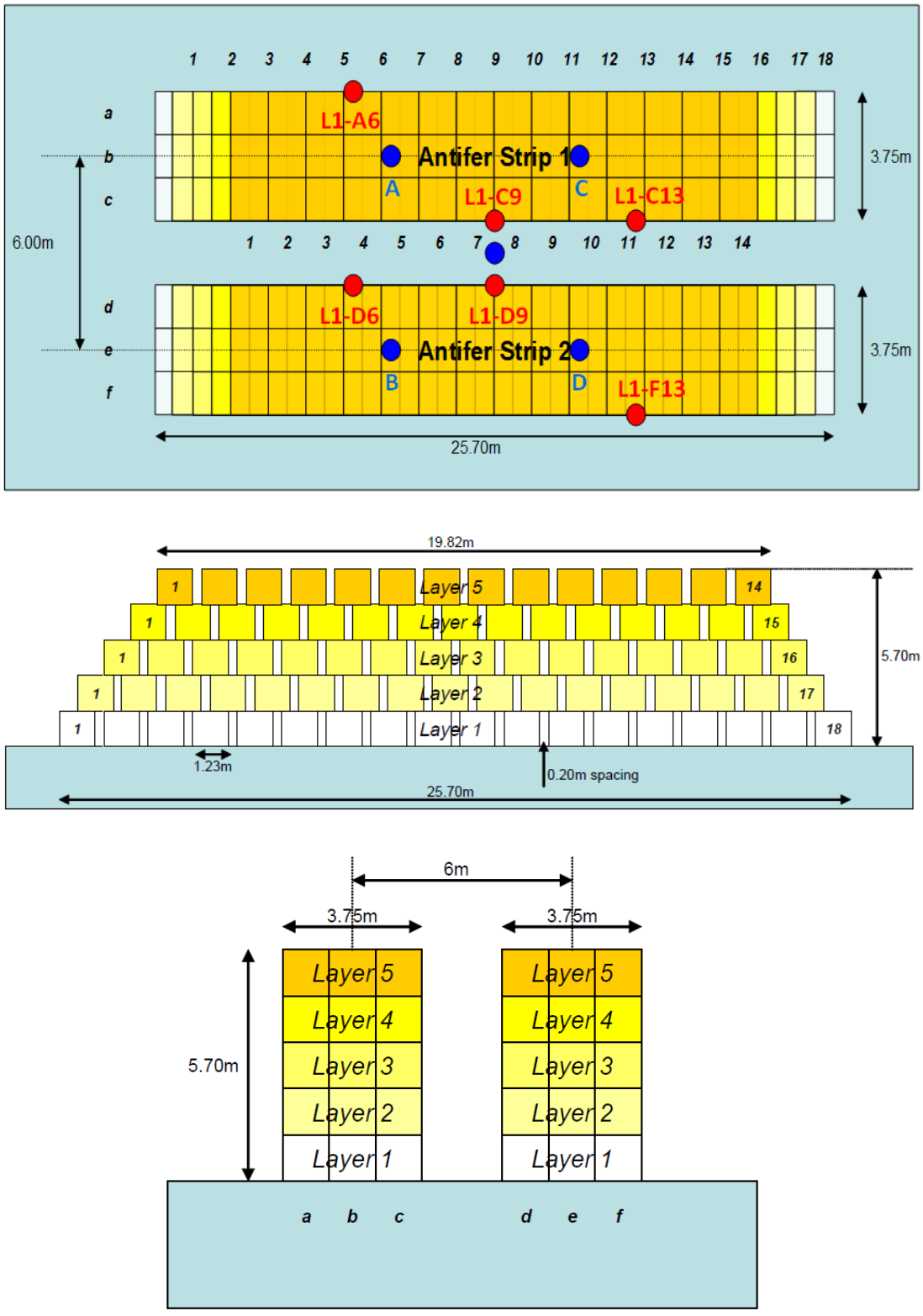

Figure 3-137: Skid beam zone load test details (a) plan view, (b) side view, (c) front view

The non-processed (red) monitoring point settlements for a duration of 41 days are shown in a semi logarithmic chart in Figure 3-138. It can be observed that while the settlements have undergone some oscillations due to the accuracy of the surveying, maximum ground settlement at the end of the monitoring ranged from 9 mm to 16 mm. It can be extrapolated

that the average settlement of the ground 10 years after monitoring will remain less than 18 mm, which is still significantly less than the design criterion of 50 mm.

A similar surcharging was repeated in a second area. Results of this monitoring were quite compatible with the first area, with final settlements after 40 days being in the range of 6 mm to 20 mm. The maximum settlement probably occurred due to a movement of the blocks as the first day settlement of this point itself was 14 mm, which was more than double the of the next largest measured settlement. Further settlement rates then followed the same pattern as all other points.

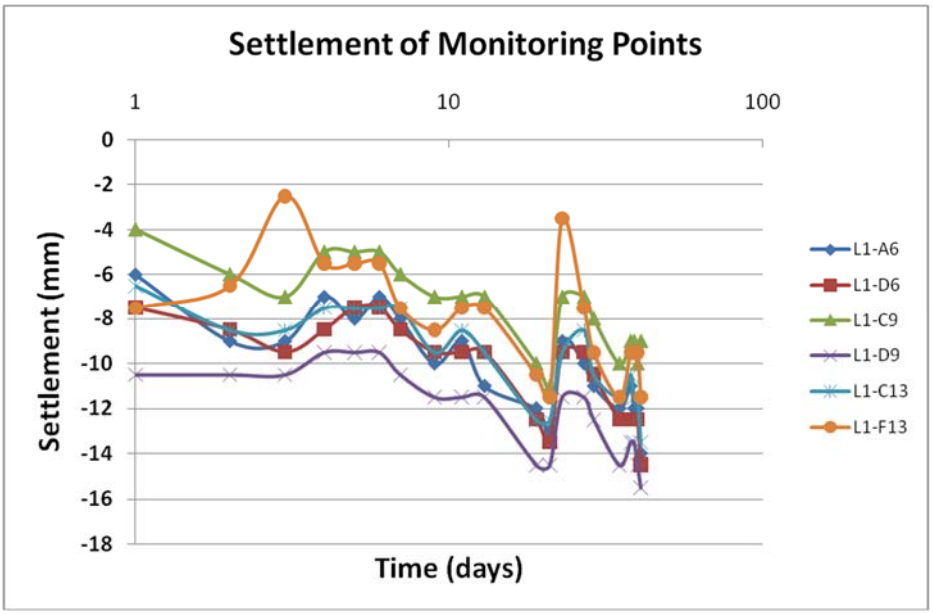

Figure 3-138: Settlement monitoring of settlement monitoring points

3.7.6 Lessons and Conclusion

The review of this project can provide the geotechnical engineer with a number of lessons to be incorporated in future projects, including:

1. It can be envisaged before reclamation that young hydraulic fills will most likely be placed in a loose state and potentially subject to low bearing, excessive settlements and creep.

2. Project specifications should be defined appropriately.

    a. Relative density is an unsuitable quality control criterion (also refer to Section 2.10.2), and this parameter should not be used as an acceptance criterion.

b. It is possible to reach better results without meeting relative density specifications. This means that while it is likely that ground improvement works can satisfy a project's technical and design requirements, it may appear as non-conforming with relative density specifications due to the poor choice of defining acceptance criteria.

c. Further to the in-situ tests that showed a reduction of strength and deformation modulus at depth, the monitoring of settlements under a full scale zone load test showed that it is not necessary to have the same amount of improvement in all soil layers. Ground behaves as a mass with each layer contributing to the settlement according to its physical and mechanical properties. It is the summation of the settlement increments that must be less than design and acceptance settlements, not the settlement of each individual layer.

3. This project has demonstrated the ability of dynamic compaction to treat loose hydraulic fills as deep as 16 m. The technique has been successful even when fines content was more than what was originally expected.

4. It was observed that for Ras Laffan saturated carbonate sand the relationship between the CPT cone resistance and PMT parameters are:

   a. $q_c / P_{LM} = q^*_c / P^*_{LM} = 5$

   b. $E_M / q_c = 1.35$

   The above correlations did not appear to be influenced by depth

5. In this project (hydraulic fill), the ratio of the square root of the compacted volume of ground (in m^3) to the crater depth (in m) is about 2.11 (when only the crater volume is considered) to 2.32 (when the net compaction volume, being the resultant of the crater and periphery volume changes is considered). This suggests that approximately 90% of the compaction volume has originated from the crater and 10% from the ground around the crater.

6. There appears to be a linear relationship between the logarithm of impact energy and $(D_T - D_B)/D_c$. More research is required to determine if the relationship is unique for a given soil type or whether it is also a function of the drop energy.

3.8 Abu Dhabi Ritz-Carlton Hotel

3.8.1 Project Description

Ritz-Carlton Hotel is a luxurious resort constructed on the southern coastlands of Abu Dhabi, UAE. It is constructed on a plot of land with an area of 210,000 m^2 that includes the previous site of the now demolished Gulf Hotel and the virgin site, which was situated on its southern border. An 11 storey hotel with an underground parking is located in the middle of the resort. This structure is encompassed on the north and south by two man-made hills gradually elevating to about 8 m above street level. 100 single storey chalets were designed to be spread out throughout the hills and the original ground. The hills are retained on the outer perimeter with mechanically stabilised earth (MSE) walls and slope inwards towards a large pond (originally envisaged to be a man-made lagoon) that is excavated in front of the hotel. The project was originally commenced as J W Marriott Hotel, but was later rebranded as the Ritz-Carlton. Figure 3-139 shows the project's layout.

Figure 3-139: Layout of Abu Dhabi Ritz-Carlton Hotel

3.8.2 Ground Conditions

Noting that the site was located in a part of the city with a known history of soft soils and with the recognition that the two floor buildings of the original Gulf Hotel were built on piles, it was expected that the project would also be situated on problematic soils. This speculation was confirmed by the preliminary soil investigation.

The original ground level in the undeveloped southern part of the site was mostly from +1.6 m to +2.1 m RL (reduced level= Abu Dhabi Datum); however, the level in the eastern portion of this area was even lower and at +0.9 m RL. The original ground level in the location of the previous Gulf Hotel was about +2 m RL. Groundwater depth was recorded to be from 0.5 m to 1.8 m below borehole levels, and groundwater level was from +0.4 to +1.30 m RL.

During the preliminary geotechnical investigation 23 SPT boreholes were drilled down to depths of 15 m and 30 m. The testing layout is shown in Figure 3-140. It was observed that the upper 1 to 2 m of soil was loose silty sand with fines content ranging from 5 to 25% and generally less than 15%. The upper sandy layer was underlain by very soft silty to clayey sand to sandy silt that was 3 to 4 m thick, and had fines content ranging from 35 to 70%. The bottom of that layer was generally at the depth of 4 to 5 m and exceptionally as deep as 6 m. SPT blow counts were consistently low, often as low as 1. The very soft layer was followed by a medium to very dense silty to very silty sand layer with SPT blow counts commencing from at least 18 and rapidly increasing to 30 and even more than 50. The bottom of this layer was at the depth of 12 m. Mudstone with occasional layers of crystalline gypsum or sandstone was encountered in all boreholes. Figure 3-141 shows the profiles of four SPT boreholes in a section through the site.

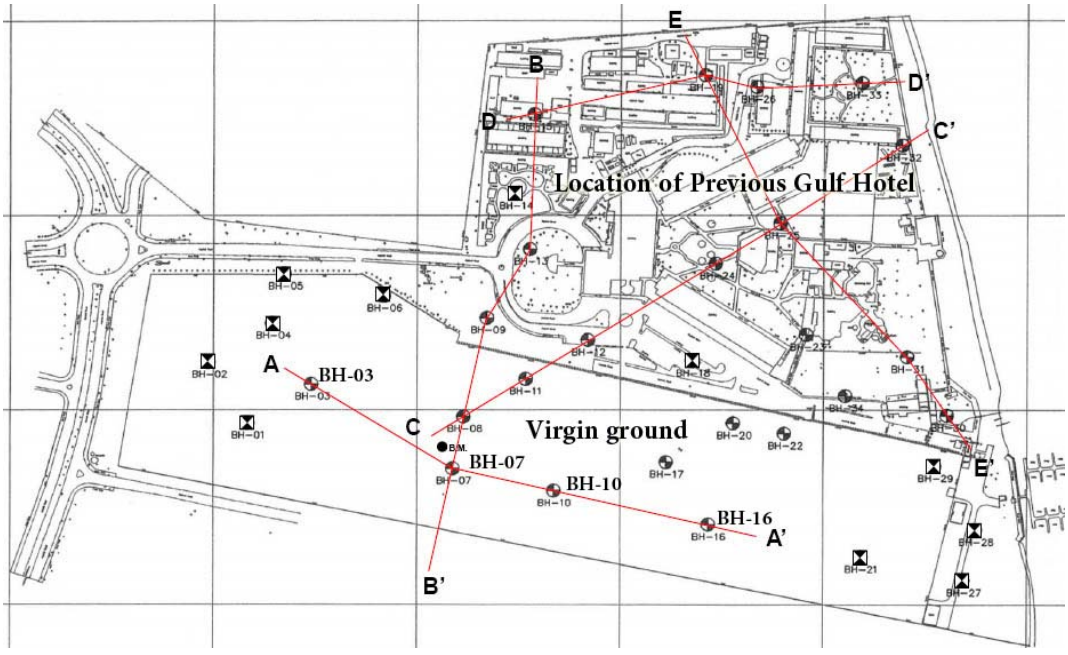

Figure 3-140: Layout of SPT tests

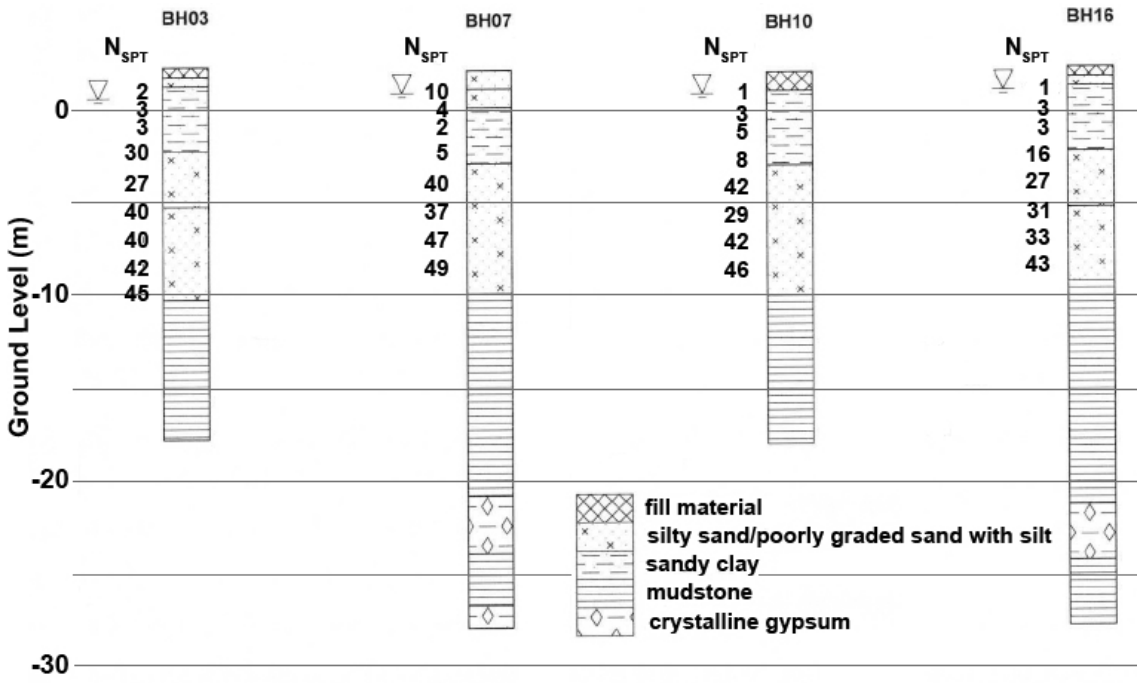

Figure 3-141: The profiles of four SPT boreholes in a section through the site

PMT carried out during later phases of the project as part of a supplementary geotechnical investigation also indicated the presence of a very soft layer with P_{LM} as low as 110 kPa. The ground profile is summarised in Table 1.

Description	Bottom Depth (m)	thickness (m)	Fines content (%)	N	P_{LM} (kPa)
Silty sand	1-2	1-2	5-25%	5-10	500-1000
Silty sand/sandy silt	5	3-4	35-70	1-3	110-230
Silty sand	12			18-50	2500-4000
Mudstone	-	-	-	-	-

Table 3-12: Summary of the ground profile

Further to the geotechnical investigation, it became even more evident that the ground conditions would be challenging for construction when the equipment mobilised for demolition of Gulf Hotel began sinking in areas where the top of the soft soil was at shallow depth. Figure 3-142 shows an excavator that sunk into the clay during the works, and was ultimately pulled out with a crane.

Figure 3-142: Construction equipment sinking into the ground due to poor ground conditions

The construction of the original Gulf Hotel on piles, the local failures of the ground under the load of the construction equipment, the poor results of the soil investigation, and the preliminary calculations all indicated that the site was situated on soft compressible soil and unable to support the loads that the new project.

3.8.3 Development of Solution and Application of Dynamic Replacement

The project team decided that very heavy structures such as the 11 storey hotel and the underground car parks (that were in fact buried under the hills) were to be built on piles; however, piling did not seem to be a solution of interest for an area of approximately 90,000 m^2 that covered the hills, MSE walls, chalets and roads as it would have taken too much time to execute, and would have been very costly. Thus, ground improvement was concieved as an economical solution for treating the ground under the mentioned above.

As a first step it was required to develop appropriate design criteria based on the special requirements of the embankments, walls, and chalets. The stipulated design criteria were:

1. Allowable Bearing capacity:
    a. Chalets: 100 kPa under raft footings located 1 m below finished floor level (variable) of the structure.
    b. Man-made landscape hills: To support fill compacted to 95% proctor dry density (assumed to have a unit density equal to 18 kN/m^2) for a slope less than 2V:3H.
    c. Retaining walls: To support 1.3 times the fill weight within a strip behind the wall with a width equal to 70% of the wall height.
2. Total settlement

    a. Chalets: 25 mm under actual footing loads (on average 20 kPa).
3. Differential settlement
    a. Chalets: 1/500 between adjacent columns under footing loads
    b. Added fill: 1/500 after 90% consolidation for two points located 10 m apart under fill load
4. Consolidation ratio: 90% after 90 days of constructing the full fill height.

As can be observed that although the design criteria could have been further optimised, they have still been able to concisely address each of the designer's concerns. The required allowable bearing capacity of the chalet does not appear to be in line with the actual 20 kPa load of the chalet; however, as this bearing can be usually achieved under a raft footing without extra work and cost, it was accepted. On the other hand stipulating settlement criterion for 100 kPa uniform load over the chalet foot print would be very irrational because that load is several times larger than the actual load, will never be realised in a one storey chalet, and is in the magnitude of multi-storey buildings. Relating settlements to a load equivalent to the bearing capacity would needlessly increase construction energy and cost, to a point where ground improvement may no longer be a feasible solution due to poor and unsuitable specifications. Bearing or shear failure for the walls has been addressed, but as the wall design was not completed during design of ground improvement it was not possible to optimise design criteria by comprehensively stipulating wall stability as well. Total hill settlement was rightfully deemed as unimportant during construction phase, and was not incorporated in the criteria; however, total and differential settlements had to be defined after a certain amount of time to ensure that the walls, chalets, utilities and roads on the embankments would not be subject to damage.

The design and construct ground improvement tender was based on achieving the mentioned design criteria, and any ground improvement method was deemed as acceptable. In the opinion of the author this is the preferred method of performing ground improvement projects as specialist contractors are given an equal opportunity to propose any technique that will meet the requirements with the lowest cost. Furthermore, soil improvement is a technology that is usually driven by specialist contractors who are continuously developing enhancements to their methods to improve performance.

The project was awarded to a specialist contractor who had based ground treatment on the dynamic replacement method.

If necessary and possible, soft soil may be excavated at the location of the print and backfilled with granular material prior to implementation of dynamic replacement. This may be due to the existence of a stiff superficial layer or to facilitate deeper penetrations. In this project due to the availability of redundant sand in the lagoon area and affordable sand resources in the vicinity of the project it was decided to pre-excavate the DR prints and to backfill them with sand. The pre-excavation of a DR print is shown in Figure 3-143.

Figure 3-143: Pre-excavation of DR prints

In order to provide a minimum thickness of granular material as the working platform that was sufficiently above groundwater level, the lowlands and areas with thin layers of superficial sand were backfilled with sand in such a way that the thickness of the granular layer was at least 1.5 m and the platform level was at least 1.3 m above groundwater level.

High energy impacts such as what is experienced in dynamic replacement increase the pore water pressure. In cohesive soils that do not allow the rapid dissipation of pore water pressure, each consecutive blow increases the pressure to the point where the soil liquefies. In some soils only one blow is enough to liquefy the soil, and to hinder the application of additional blows. In such a case, additional blows can (or should) only be applied when the pore water pressure has sufficiently decreased. As can be seen in Figure 3-144, built up of pore pressure and its release in the form of sand boiling was observed in prints surrounding the impact location during the soil improvement works.

Figure 3-144: Release of excess pore water pressure in the form of sand boiling

Application of pre-excavation and backfilling of DR prints with sand was able to accelerate the pore water pressure distribution in the soil; however, even the implementation of this technique was not able to prevent the liquefaction of soil during the first few poundings, and work had to be continued in sub-phases once the pore water pressure had reduced sufficiently.

Experience gained during the works suggests that the liquefaction of the soil can be retarded by minimising the time interval between backfilling pre-excavated prints and pounding. This may be somewhat expected as increasing the time interval between the different stages of the work process will allow the backfill material's water content to increase.

While design calculations indicated that execution of dynamic replacement columns would be able to satisfy the design criteria in most areas, the wall stability analyses suggested that additional measures may be required. MSE walls were 3 m, 5 m, 5.5 m and 8 m above finished road level (+2 m RL). Calculations using numerical analyses showed that it was necessary to install DR trenches in lieu of DR columns to reach a safety factor of 1.5 (see Figure 3-145). For walls higher than 7.5 m, the trench had to extend 5.25 m and 2 m respectively behind and in front of the MSE wall. For shorter walls, the treatment zone required only 50% replacement. Hence, while maintaining the original band width, the excavation was done as alternative segments within the trench setout path with a total coverage of 50%.

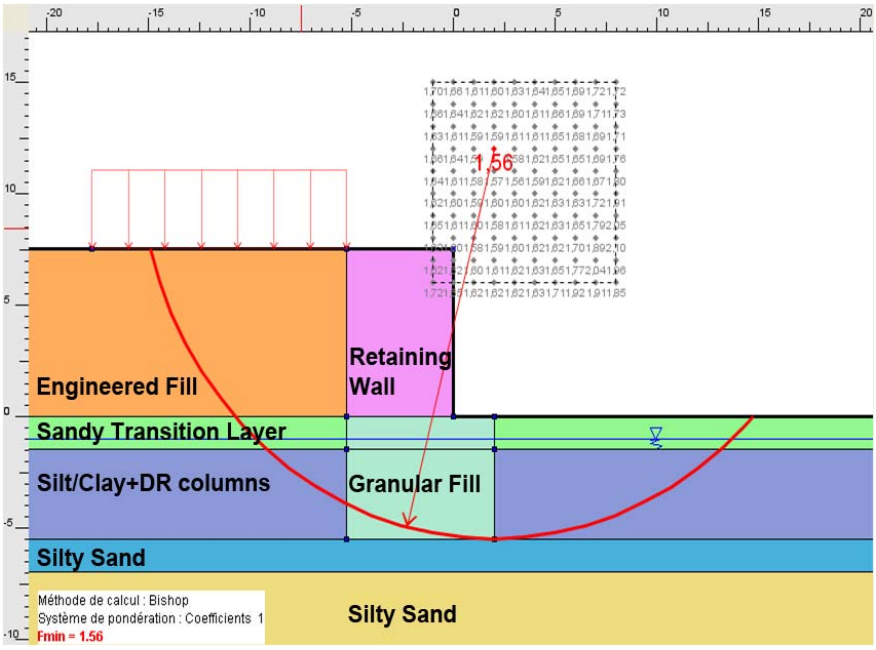

Figure 3-145: Stability analysis of MSE Wall on pre-excavated DR trench

In order to ensure that the bottom of the trenches or segments would have a high friction angle for stability assessment, the excavations were originally backfilled with demolished concrete pieces and then with sand that was similar to what was utilised in the DR columns. Excavation of trenches and execution of dynamic replacement for the walls are shown in Figure 3-146.

Figure 3-146: Backfilling of the lower part of the trenches beneath the wall with demolished concrete debris

Two DR rigs were allocated to the project to complete the works within 150. DR pounders weighing 12 to 14 tons were used for the works. Based on the ground conditions and project requirements, drop heights were variable from 5 to 15 m, and grid spacing was 5 m or 6 m.

3.8.4 Testing and Verification

22 pressuremeter tests (PMT) were carried out after dynamic replacement to verify that acceptance had been achieved. P_{LM} and E_M values before ground improvement, after ground improvement in between the prints and after ground improvement in a DR column are shown in Figure 3-147. It can be observed that while P_{LM} in between the DR columns increased by about 100% from 110 kPa to 220 kP after dynamic replacement, the magnitude of improvement has still remained insufficient, and calculations can demonstrate that this amount of treatment on its own would not have been enough to satisfy acceptance, and it was in fact the substantial increase of strength in the DR columns that made acceptance achievable. The same discussion is valid for E_M, and it can be seen that the moduli in between the prints have improved marginally, but the improvement inside the DR columns is substantial. Figure 3-147 shows a reduction in parameters at depth, but this is interpreted as the better properties of the in-situ ground at the testing location before DR compared to the post DR testing locations, and is not considered to be the result of applying dynamic replacement.

P_{LM} and E_M improvement ratios in between and inside prints are shown in Figure 3-148. It can be observed that while limit pressure improvement in between the columns was at best 100%, the maximum amount of improvement inside the columns exceeded 900%, and was 5.15 times more than improvement in between the columns. The same approximate order of difference is also noticeable for the modulus.

Bearing capacity acceptance was confirmed by using the method proposed by Centre D'Etudes Menard (1975) (refer to Section 2.9.2.6).

While calculations confirmed that settlement criteria had been satisfied, 15 settlement plates were additionally installed to measure the ground subsidence due to construction of the hills (see Figure 3-149). Fill height and the associated settlements of one of the settlement plates are shown in Figure 3-150. The diagram has not been corrected for possible errors in surveying, vibrations caused by construction equipment, etc., and it appears that the true settlement at the 90th day may have been more than what was recorded.

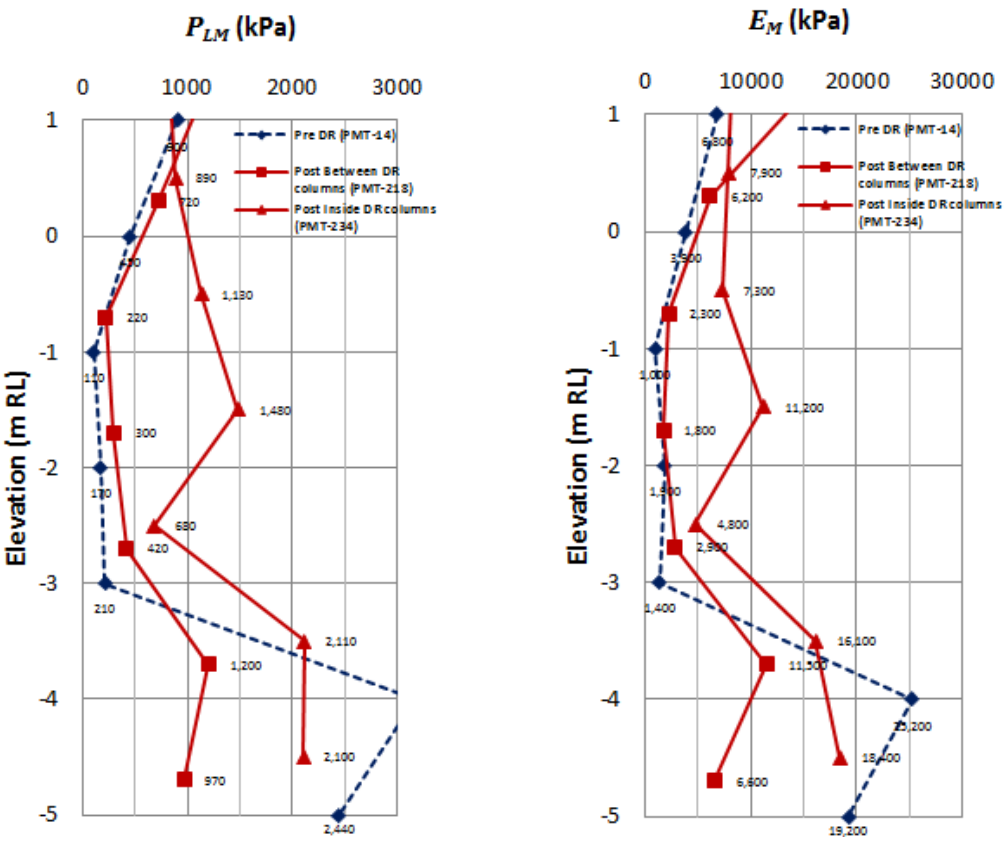

Figure 3-147: Comparison of PMT parameters before and after DR (in between and inside DR columns)

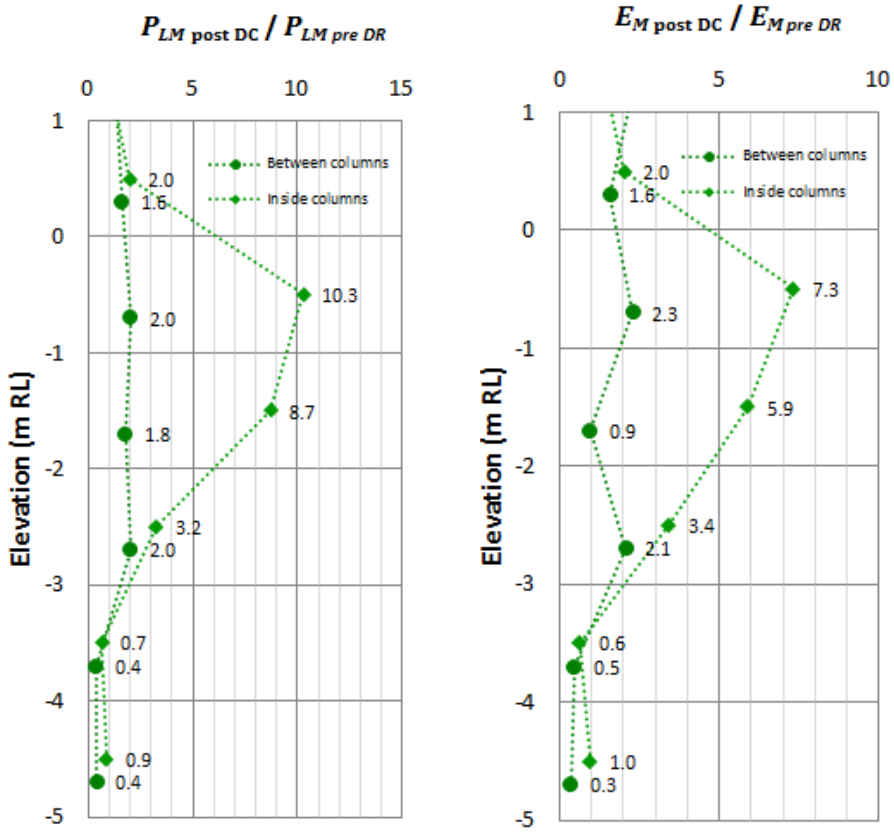

Figure 3-148: Comparison of PMT parameters ratios in between and inside DR columns

Figure 3-149: Construction of hills supported by MSE walls on one side

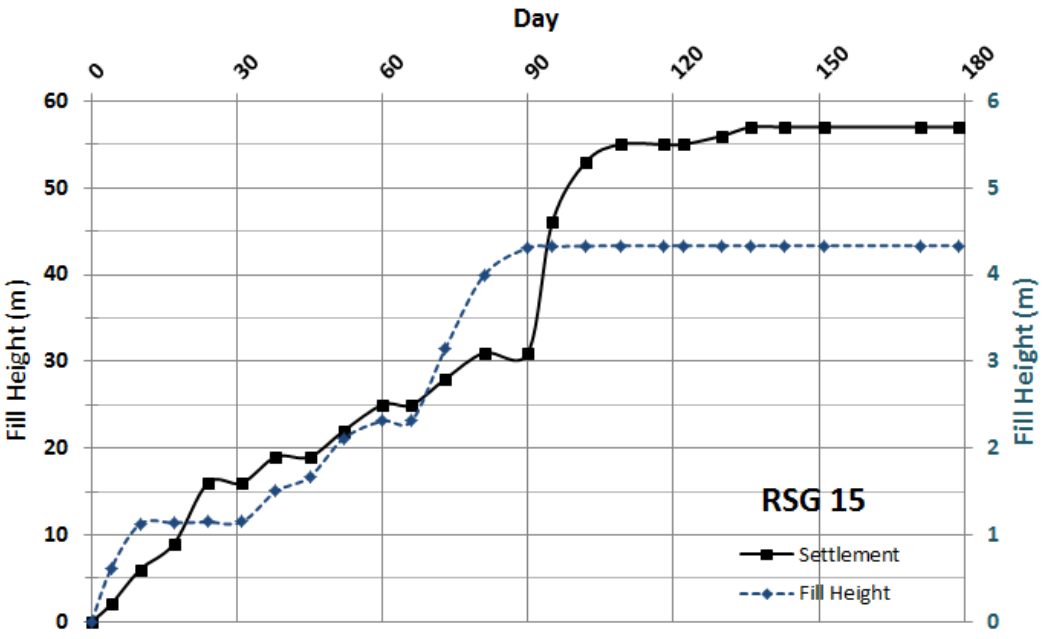

Figure 3-150: The measurements of fill height and ground settlement under the fill during a time interval

Consolidation ratio and the maximum ground settlement under the weight of the hill at the location of each plate was estimated using the method of Asaoka (1978) in which ground settlement at a specific point is measured at constant time intervals, and settlements are plotted on both coordinates. The abscissa of each point on the graph is the settlement, S_n, and the ordinate is the next settlement, S_{n+1}. At 100% consolidation the settlements plot must intersect the bisector. As shown in Figure 3-151 the consolidation ratio of the settlement plate that was shown in Figure 3-150 reached 99% after 90 days, and the stipulated 90% criterion was achieved about 6 weeks before 90 days.

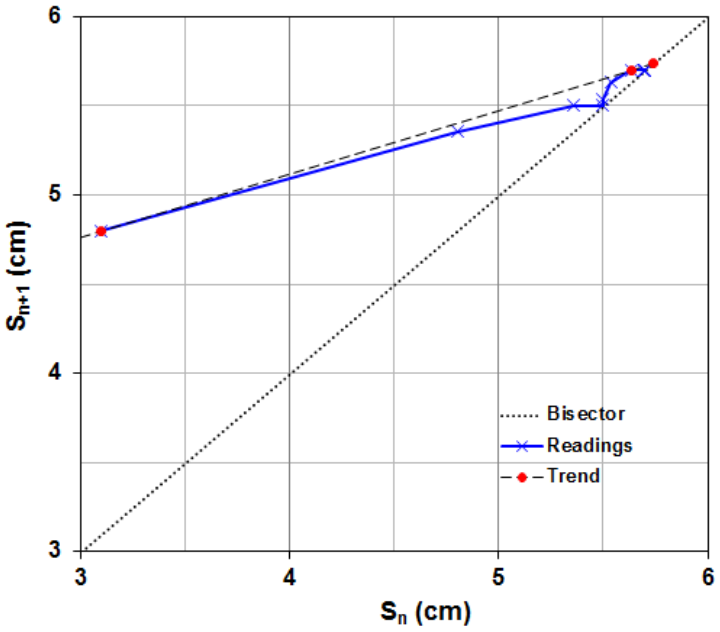

Figure 3-151: Estimation of settlement and consolidation ratio using Asaoka's method

3.8.5 Lessons and Conclusion

In this project dynamic replacement was used to successfully improve the ground for the construction of hills (embankments), MSE walls, chalets and roads based on a package of design criteria. PMTs were used to verify the works. Additionally, settlement plates were able to prove that the ground had consolidated under the hill load to more than 90% before the contractually specified period of 90 days. Points worth noting are:

1. Pre-excavation was used to accelerate pore water pressure dissipation and to allow the application of more pounder blows during each sub-phase of DR. At critical locations pre-excavation was further adopted in the form of DR trenches.

2. By pre-excavation and allowing accelerated dissipation of pore water pressure it is possible to use sand for backfill material.

3. While PMT parameters of the soft layer increased after DR by up to 100%, the improvement was not sufficient to satisfy acceptance criteria without the introduction of compacted granular material in the form of DR columns. P_{LM} improvement inside the DR column was more than 900% the value of the original ground, and 5.15 times more than the improvement in between the columns.

Figure 3-152 shows the completed Abu Dhabi Ritz-Carlton Hotel.

Figure 3-152: Completed chalets at Abu Dhabi Ritz-Carlton Hotel

3.9 Al Jazira Steel Pipe Factory

3.9.1 Project Description

Al Jazirah Steel Pipe Factory (AJSPF) is constructed on Plot 203ER6 of Industrial City Abu Dhabi (ICAD) Phase 1 Extension in the UAE. The plot is approximately a chamfered square with an area of 397,889 m^2. As can be seen in Figure 3-153, six buildings were considered for the first phase of AJSPF. These included the 31,200 m^2 main and annexed building, the 2,700 m^2 workshop, the 3,300 m^2 hot bending building, the 1,700 m^2 administration building, a mosque with associated washrooms, and the fire water tank and pump room.

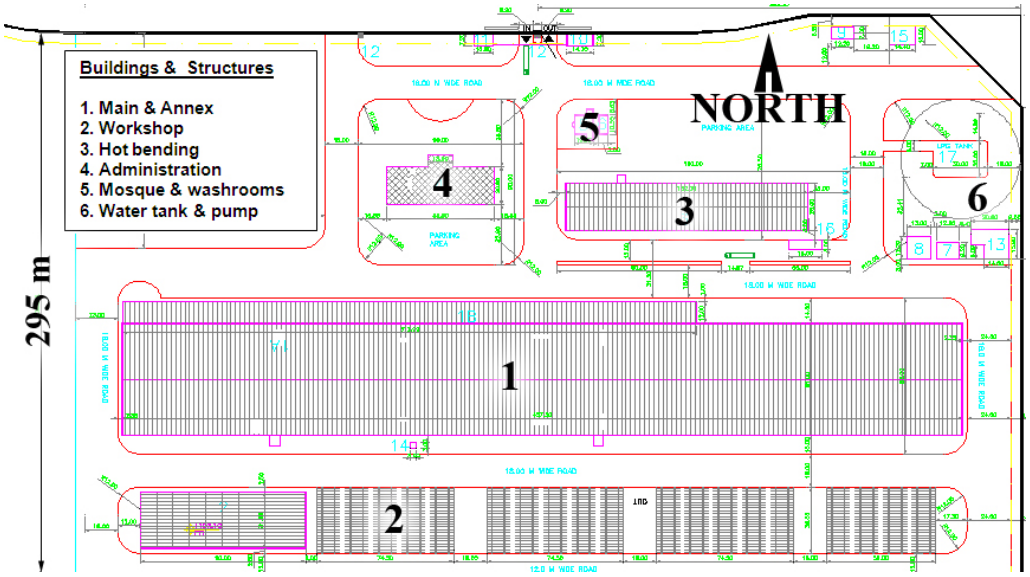

Figure 3-153: Layout of Al Jazira Steel Pipe Factory structures

Different activities including plate stacking, preparing, rolling and bending, welding, inspecting and controlling are undertaken in the main building, and the maximum vertical load on a stanchion of this building was estimated to be 2,500 kN. As shown in Figure 3-154 floor loads ranged from as low as 40 kPa to as high as 200 kPa. The annexed building mainly consists of storage areas, laboratories and changing rooms, and the maximum vertical column load was estimated to be 300 kN. The workshop and hot bending buildings each have 50 columns that carry crane loads and support vertical loads of up to 1,000 kN. The administration building was the only two storey structure on site with column loads of up to 1,500 kN.

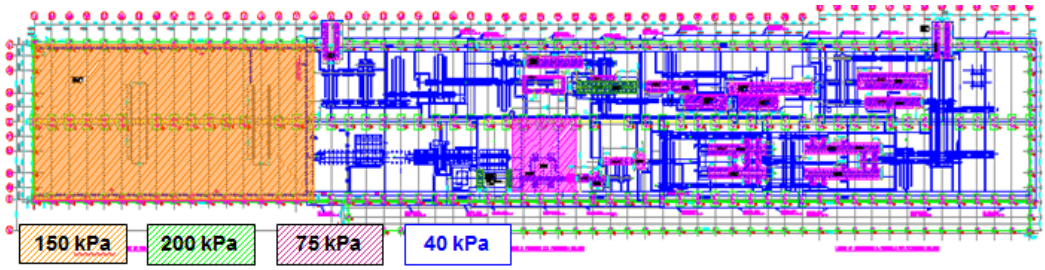

Figure 3-154: Loading patterns in the main building

3.9.2 Ground Conditions

The developer of ICAD Phase 1 Expansion A undertook a preliminary geotechnical investigation that included a number of SPT boreholes and CPTs of which two SPTs and one CPT fell within the limits of AJSPF.

Ground level was generally 1 m below final finished levels of the buildings, and groundwater level was 1.8 to 1.6 m below site level.

SPT results suggested that the geotechnical profile of the site was composed 11 to 12 m of soil followed by bedrock. SPT blow counts in the upper 5 m were generally as low as 10 and up to 15, but then the soil became very dense with blow counts occasionally exceeding 50. It appeared that up to 2 m of the compressible soil at the depth of 1.5 to 2 m was high in fines.

CPT results illustrated a more problematic condition with the presence of a soft layer of silty or clayey material that commenced at the depth of about 1.5 to 2 m, was approximately 2 m thick, generally had q_c in the range of 1.5 to 4 MPa but sometimes as low as of 0 MPa. Figure 3-155 shows the typical soil profile.

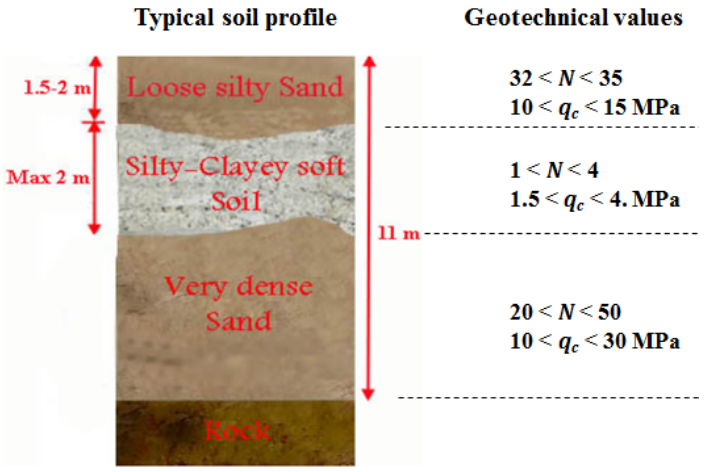

Figure 3-155: Soil profile

Supplementary PMTs that were later carried out proved that the CPT was more representative of the ground conditions. P_{LM} in the soft layer was generally in the range of 0.2 MPa and E_M was as low as 15 kPa.

The history of almost all projects in ICAD using piles as their foundation system and the poor ground conditions was enough evidence for the project's developer to conclude that the project required the implementation of special measures for safely transferring the loads to the ground.

3.9.3 Development of Solution and Application of Dynamic Replacement

The developer of AJSPF considered the alternatives of piling or performing ground improvement and utilising shallow footings. Piling was well established in the region and was a method that was technically acceptable; however, the cost study revealed that installation of 2,500 piles was more expensive than ground improvement. Among possible soil improvement technologies stone columns and dynamic replacement were proposed, but after weighing the technical and financial aspects of each method, it was the latter that was deemed as the more appropriate of the two techniques, and a design and construct contract was awarded to the specialist geotechnical contractor who had proposed DR.

Due to the variation of loading and the deformation tolerances of the different components of the project the design and acceptance criteria consisted of a number of bearing capacity and settlement requirements that have been summarised in Table 3-13, and quality control was based on PMT. Footings in the main building were from 1.5 x 1.5 m^2 to 4.25 x 5.5 m^2.

Type	Allowable Bearing Capacity (kPa)	Maximum Settlement	
		Total (mm)	Differential
Building footings	200 kPa, 1.5 to 3.5 m below finished floor levels	25	1/1,000 to 1/500
Equipment footings	generally 75, locally up to 200	25	1/1,000
Ground slabs			
Steel plate storage	100	75	1/500
Water tank	150	50	1/500
Other industrial	40	35 to 50	1/500
Other non-industrial	15 to 25	25	1/500

Table 3-13: Summary of design criteria

Initial calculations suggested that heavy point loads would require a number of DR columns to safely transfer the loads to the foundations, and a cost study suggested that it would be more economical to pre-excavate the soft soils, backfill the foundation with granular material and to compact the backfill dynamically rather than to create a group of individual DR columns under the load. It should be noted that this decision was made attractive because the excavated material did not contain any contaminants that would have required treatment, and it was possible to distribute the excavated material throughout the vacant factory boundaries at very low cost (ironically, while the excavated material was deemed as waste material, the project's developer was later approached by other organisations who were interested in buying the excavated material). Thus the soft soil was pre-excavated and replaced with granular material under the stanchion and equipment footings. In the storage areas with 100 and 150 kPa of uniform loading and smaller footing locations the excavation and removal was limited to the DR column locations. The schematic illustration of this process is shown in Figure 3-156.

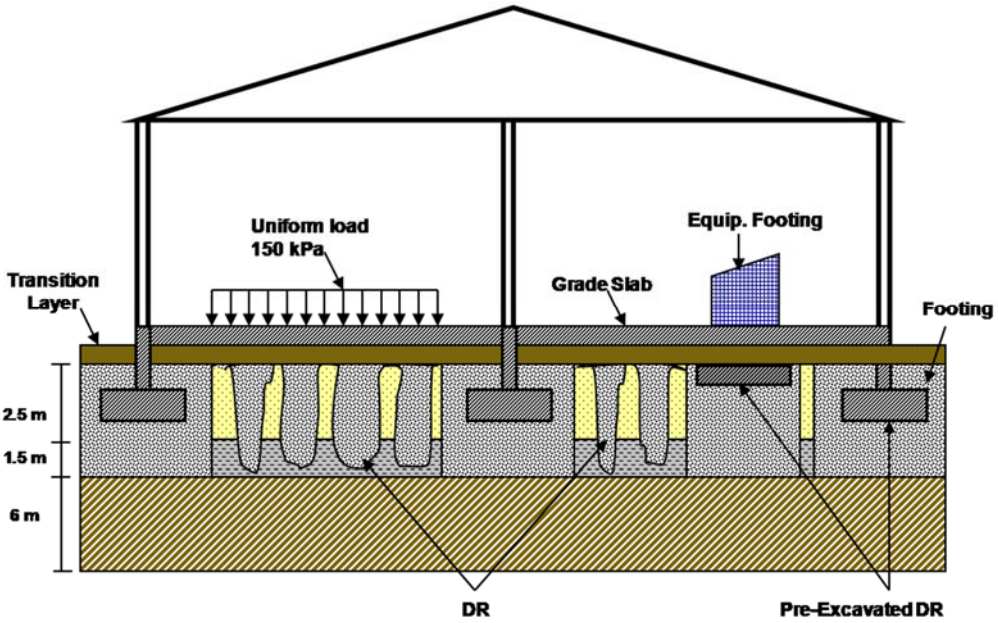

Figure 3-156: Schematic illustration of the dynamic replacement process

Although dynamic replacement is frequently carried out using crushed stone because it can provide better properties, any granular material including construction debris and demolished concrete that will not rapidly liquefy under dynamic loading conditions can be used for creating DR columns. As the closest stone quarries were about 300 km away from the project, in addition to the high price of crushed stone, transportation of the material would have also been costly. Calculations indicated that it would be possible to meet the

design and acceptance criteria by using locally sourced sand. The emirate of Abu Dhabi is basically flat ground and suitable sand quarries were still about 100 km away; thus, as a further step towards optimisation, sand was supplied from excavation sites within the metropolitan areas. The portions of the upper sandy soil that were not mixed with the fine soils during pre-excavation of the DR columns were also used for backfilling.

Figure 3-157(a) shows the excavation of a stanchion down to the depth of about 5 m. As shown in Figure 3-157 (b) the excavations were then backfilled with sand and compacted with a 13 ton pounder that was dropped from heights of 10 to 20 m.

(a) (b)

Figure 3-157: (a) Pre-excavation, (b) backfilling with sand

Mobilisation, calibration, completion of 37,000 m^2 of dynamic replacement and testing was performed during a period of less than 4 months.

3.9.4 Testing and Verification

3.9.4.1 DR Calibration

Prior to the commencement of ground improvement works two heave and penetration tests were carried out of which one test was for dynamic replacement and the other was for pre-excavated dynamic replacement. The results of the first test is described, reviewed and analysed in this section.

The testing layout is shown in Figure 3-158. For the purpose of the calibration programme a 13 ton pounder was dropped from 10 to 20 m.

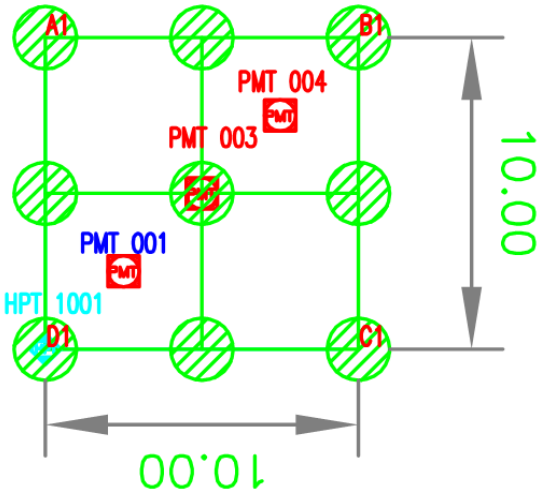

Figure 3-158: Dynamic replacement HPT test layout

Pounder penetration and volumetric changes versus the number of pounder blows are shown for HPT-1001 in Figure 3-159. During the HPT the pounder was dropped consequtively 8 times when crater depth reached 1.74 m, and the crater was backfilled with sand before additional blows were applied. Both crater depth (penetration reset at backfill) and accumulative penetration depth are shown in Figure 3-159. It can be observed that introduction of backfill in a loose state after the 8th blow has resulted in a sharp increase in the rate of penetration at the 9th blow, but the penetration curve returns back to the previous logarithmic trend at the 10th blow.

Contrary to HPT in sand (e.g. Marjan Island Road Corridor Project described in Sectoin 3.6.4.1) where successive blows created settlement (negative heave) around the pounder's impact point, it can be observed in Figure 3-159 that pounder blows are creating heave at the periphery of the impact point. The compaction, heave and net compaction volumes (difference between compaction and heave volumes) rates appear to be relatively linear, and compaction has not reached a stage where the soil has liquefied, and additional blows simply result in volumetric displacement with little or no compaction, such as was observed during the ground improvement works of the saturated very silty sand to sandy silt section of Dubai Airport Runway that is shown in Figure 3-160 (Serridge, 2002).

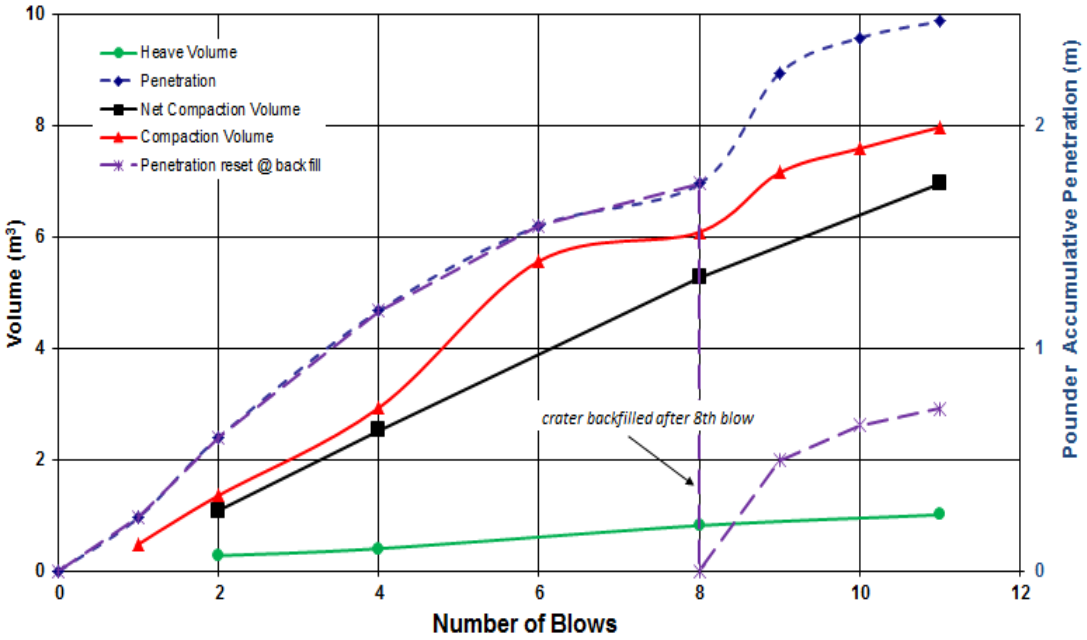

Figure 3-159: Pounder penetration and volumetric changes during the DR HPT

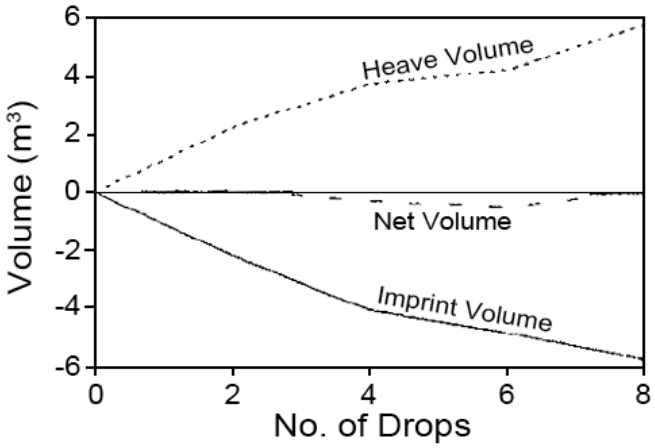

Figure 3-160: Heave and penetration test at Dubai Airport (Serridge, 2002)

The result of the HPT becomes more meaningful when before and after dynamic replacement PMTs are compared in Figure 3-161 and Figure 3-162. It can be observed that PMT parameters have increased both in between and inside DR prints down to the depth where the ground becomes very dense; however, the amount of improvement inside the prints are larger. The initial PMT parameters at the depth of soft soil, the amount of improvement and that depth, and the amount of ground heave suggests that supposedly soft cohesive layer at the testing location was probably higher in sand content than the typical location encountered at site; hence, the amount of improvement in the soft layer was comparable to other layers.

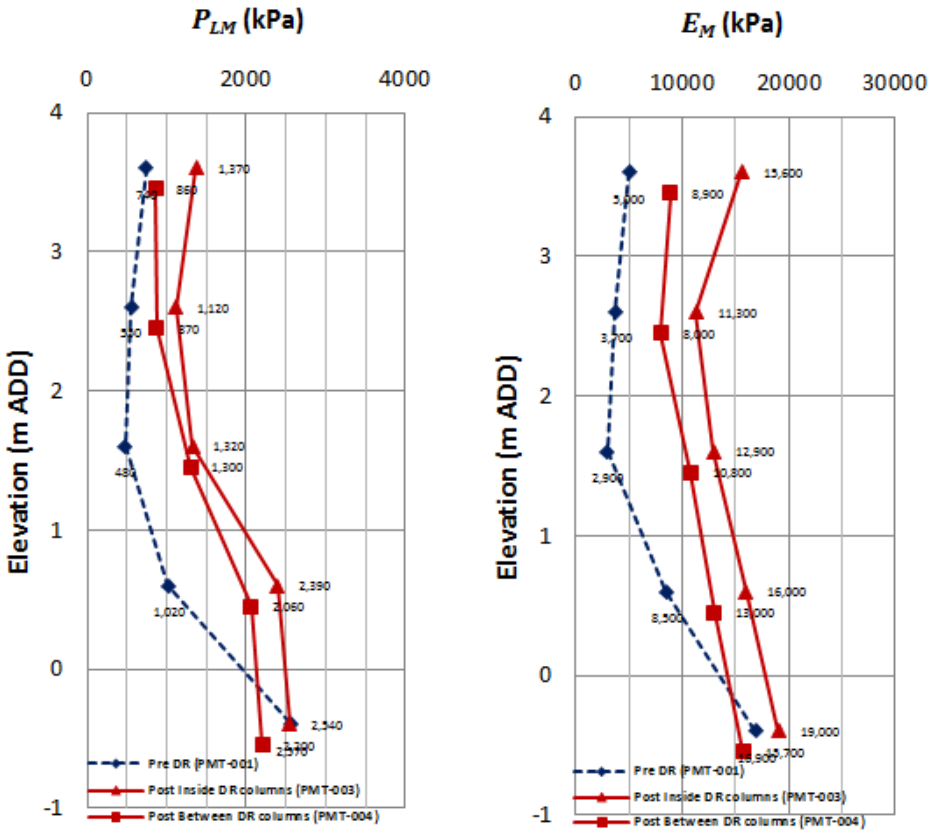

Figure 3-161: DR calibration PMT results

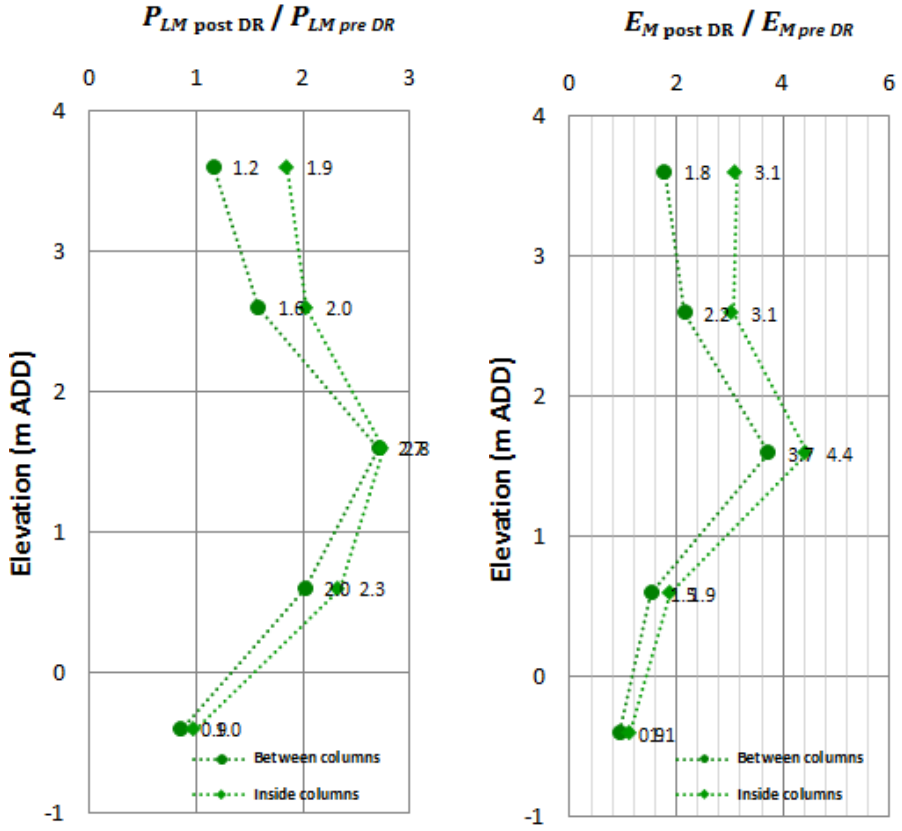

Figure 3-162: DR calibration PMT improvement ratios

3.9.4.2 Final Testing

In addition to the six PMTs that was performed during calibration, 41 PMTs were also carried out during the works. 37 of these tests were performed after ground improvement for verification purposes.

The results of three PMTs are shown in Figure 3-163. For comparative purposes a PMT was performed before dynamic replacement. The test was located in between pre-excavated DR prints, and was re-tested after ground improvement, and a PMT was also performed in one of the print locations next to the location that had been tested earlier. Ground level at the testing points was +4.4 m ADD (Abu Dhabi Datum). It can be seen that the soft layer was approximately from elevation +1.5 to +2.5 m ADD in the test area. After dynamic replacement P_{LM} and E_M increased both inside and outside of the DR columns in the first several upper metres until very dense sand was encountered. Improvement was also observed in the soft layer that would typically be assumed to remain unimproved in calculations; however, the magnitude of improvement in the soft soil was noticeably less than the sand and what was observed in Figure 3-161 and Figure 3-162. The soft layer has somewhat improved because in reality it was not pure silt and clay, and it did contain an amount of sand in its grading. Hence, asa also observed in KAUST (see Figure 3-54 in Section 3.4.5) the impact did not only lead to plastic displacement and heave, and the impact energy was able to improve this layer to an extent as well.

The effectiveness of dynamic replacement is more observable when P_{LM} and E_M improvement ratios in between and inside DR prints are compared with each other. It can be seen that improvement ratios in the sand layers are of the same order, but there is a pronounced difference at the level of the soft soil. In this band the P_{LM} and E_M improvement ratios of in-situ ground are respectively 3.9 and 2.6, but the replacement sand's P_{LM} and E_M improvement ratios are respectively 12.2 and 12.4; i.e., respectively 3.1 and 4.8 times more than that of the in-situ cohesive soil.

The harmonic mean of P_{LM} in the pre-excavated DR column is 2,817 kPa. Assuming that the lower layers also have the same limit pressure, it can be calculated using the method proposed by Centre D'Etudes Menard (1975) (refer to Section 2.9.2.6) that a sandy soil with a footing that is on ground surface will be able to provide a safe bearing of 800 kPa with a safety factor of 3. Bearing will be even higher for embedded footings; however, in that case it will be the settlement criteria that will govern. For example, calculation for a 3.5x4.5 m^2

stanchion footing demonstrates that settlement will be 9 mm when the foundation is subjected to a load of 2,500 kN. Clearly, settlement under a load of 12,600 kN (800 kPa x3.5 m x4.5 m) will greatly exceed the settlement criterion.

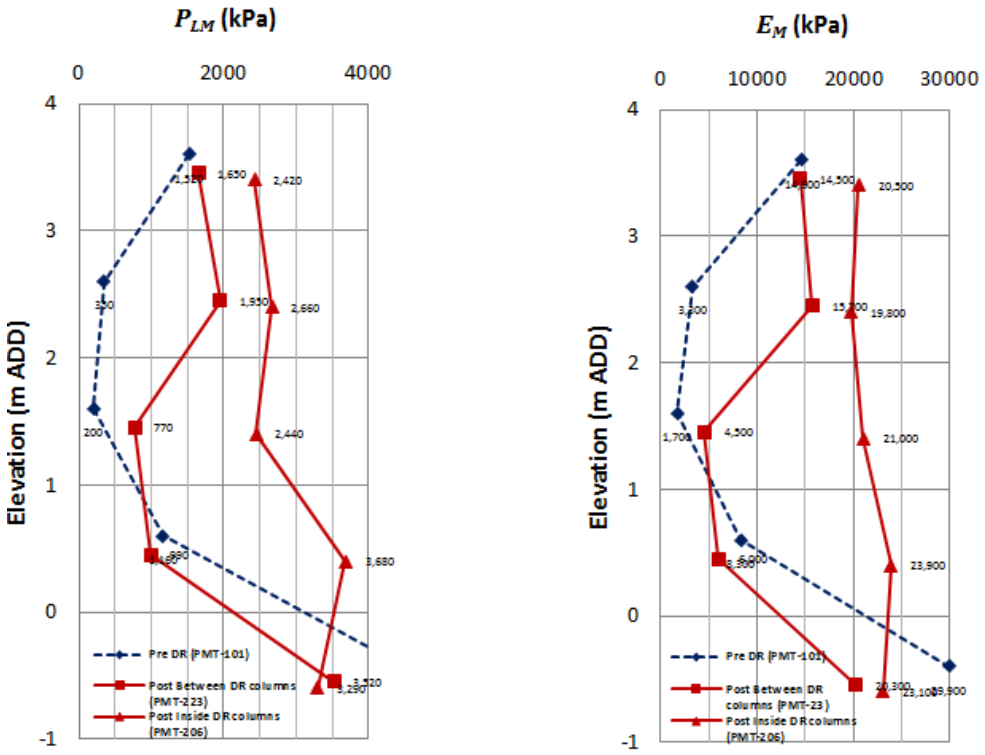

Figure 3-163: Comparison of PMT parameters before and after DR

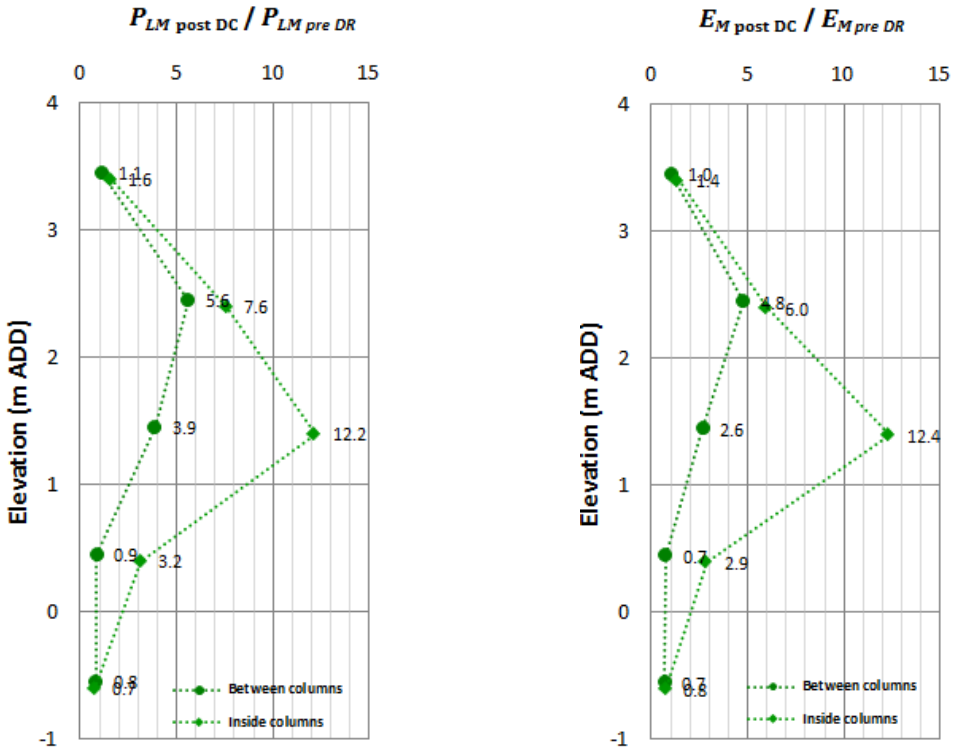

Figure 3-164: Comparison of improvement ratios in between and inside DR columns

The author notes to have observed that some engineers are in the habit of using formulas for predicting bearing capacity that are based on a 25 mm settlement. This project, where settlement criteria are variable and not necessarily equal to 25 mm, is a very good example of how this approach could provide erroneous results. Bearing capacity and settlement are two different phenomena. Each should be individually assessed; however, in the end it will be one of them that will govern the design.

Detailed calculations were carried out using the PMT results to verify that all design criteria had been satisfied.

3.9.5 Lessons and Conclusion

Al Jazira Steel Pipe Factory was the first of a series of ground improvement projects in the Industrial City of Abu Dhabi. In this project dynamic replacement and pre-excavated DR were successfully used to provide foundations for footings and slabs on a site that contained a layer of saturated soft soil.

It was noted that:

1. Acceptance criteria should be based on design criteria.

2. Sand can be used in lieu of commonly used crushed stone for DR column material to reduce material and transportation costs.

3. Pounder impacts create heave when the ground contains saturated cohesive soils.

4. Although DR was able to improve the PMT parameters of the soft soil layer, the amount of improvement in the soft layer was noticeably less than the other layers. However, inside the DR column, the replacement backfill improved as much as the other layers.

Figure 3-165 shows the completed main building.

Figure 3-165: Al Jazira Steel Pipe Factory

3.10 Reem Island Causeway

3.10.1 Project Description

Reem Island, previously called Abu Shaoum, is a small island that is located approximately 0.4 km north of Abu Dhabi, United Arab Emirates. The island was basically vacant until 2005 when it was decided to develop it into a modern suburb of UAE's capital city.

One of the first requirements of the new development was the construction of a causeway to link the island to the mainland. According to the design, the causeway was to be composed of approach roads on the two sides and a bridge structure in the centre. The approaches on each side were to be approximately 150 m in length. As can be seen in Figure 3-166, the reclamation was anticipated to be approximately 135 m and 50 m long respectively on Abu Dhabi and Reem Island sides.

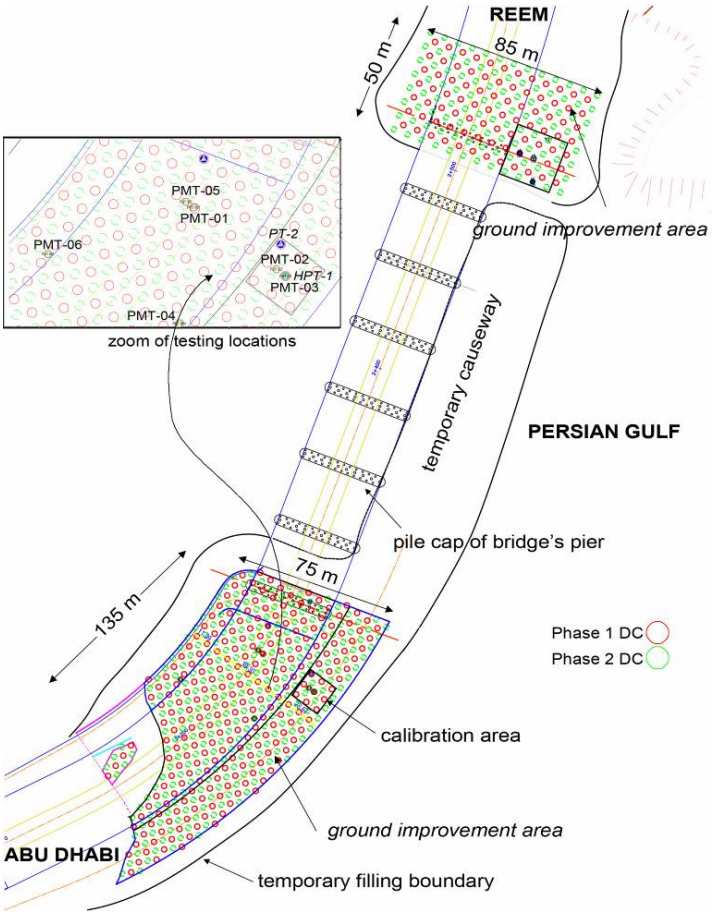

Figure 3-166: Site plan of Reem Island Causeway

The approach road was to be constructed on coastal grounds and on reclamation. The road level was anticipated to be from +2.0 m RL (Reduced Level= mean sea level) to +7.0 m RL at bridge level. The maximum elevation difference between the low and high points of the approach road was 5 m, and the road slope was 3.25%. The longitudinal profile of the project (Abu Dhabi side) is shown in Figure 3-167.

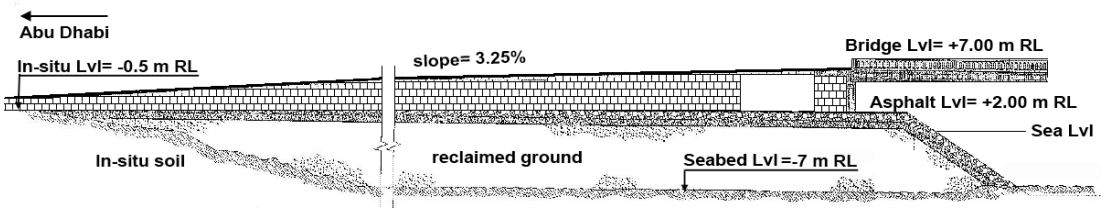

Figure 3-167: Longitudinal profile of the approach road

The approach road and bridge were designed to have four lanes in each direction. The width of the approach road leading to the bridge was 28 m. An additional lane was envisaged on each side for drivers who intended to turn back without crossing the bridge. In order to limit the total width of the road to 38 m the stability of the two sides of the bridge's access road was to be provided by an MSE (mechanically stabilised earth) wall. The cross section of the project at bridge level is shown in Figure 3-168.

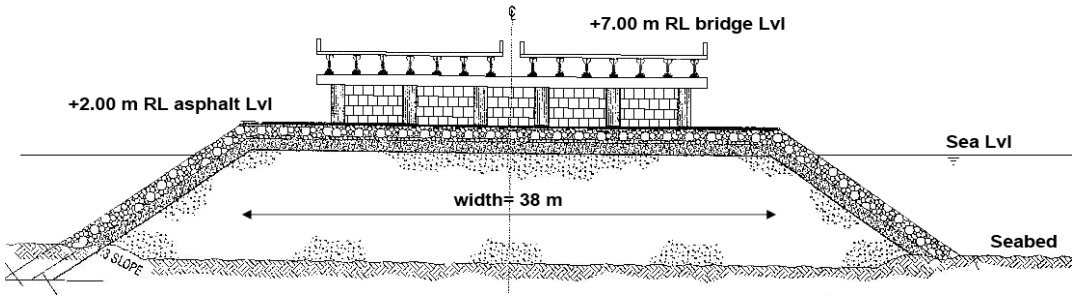

Figure 3-168: Project cross section at bridge level

3.10.2 Ground Conditions and Fill Description

Natural ground levels (NGL) in Abu Dhabi and Reem Island approaches were respectively at about -0.5 m and +1 m RL, but rapidly dropped to about -7 m and -5.5 m RL on the sides of the bridge. Groundwater level in the boreholes varied from +0.7 to -0.7 m RL.

Although NGL in the marine boreholes differed, as summarised in Table 3-14, the in-situ ground profile was generally the same within the project's area. The upper 0.8 to 1.5 m of soil was soft sandy silty clay. This layer was followed by a very loose to very dense sandy layer with a variable thickness of 0 to 2 m that contained less than 20% fines. This latter layer

overlaid bedrock. The bottom elevation of the loose sandy layer was from about -6 m to -8 m RL.

Description	thickness (m)	N	fines content	P_{LM} (kPa)	Comment
Fill (reclaimed by dumping)	up to 9	-	< 20%	250 to 400	PMT values after reclamation and before ground improvement
marine mud (sandy silty clay)	0.8 to 1.5	0-2	50 to 80%	-	removed before ground improvement
loose in-situ sand	0 to 2	4 to 30	< 20%	500 to 700	
bedrock	-	-	-	-	encountered at elevation -6 to -8 m RL

Table 3-14: Ground profile of reclamation area before ground improvement

Although the marine mud thickness was at most 1.5 m, it was understood that the consolidation of this layer during the life time of the project could cause excessive settlements; hence, it was removed by dredging the seabed prior to filling and reclamation.

With similar intent to minimise foundation settlements due to poor ground conditions and the marine environment in which the bridge piers had to be constructed in, the foundations of the piers were designed as bored piles.

As shown in Figure 3-169, reclamation was anticipated to be done by dumping sand and pushing it into the sea. Soil layers above the sea level were to be compacted using vibratory rollers; however, the submerged fill mass and existing loose sand would have remained in a loose and uncompacted state. Although it was expected that the sand fill would consolidate in a relatively short period under the embankment loads, it was also recognised that the fill could pose a number of problems such as insufficient bearing capacity, creep settlement under self-weight, excessive differential settlements of the MSE walls, and excessive total and differential settlements under vibratory traffic loads. These problems could be most evident in the form of unpleasant bumps at the interface of the approach road and the bridge abutment (Li, 2005).

Figure 3-169: Reclamation by dumping sand and pushing it into the sea

3.10.3 Development of Solution and Application of Dynamic Compaction

Based on the above concerns, ground improvement of the submerged fill was envisaged to be carried out in the form of a design and construct package, and the contract for soil treatment was awarded to a specialist contractor who had proposed the application of optimised design criteria, and implementation of dynamic compaction along with an objective testing method based on PMT.

3.10.3.1 Design and Acceptance Criteria

The criteria that were defined to address the geotechnical concerns of the project were:

1. Safe bearing capacity under the approach road: 120 kPa with a safety factor of 3.
2. Total settlement of the fill in the approach road with a uniform loading of 20 kPa: 30 mm
3. Differential settlement of the fill in the approach road with a uniform loading of 20 kPa: 1:500

The maximum required bearing capacity of the fill is at the location where the approach road reaches the bridge elevation at +7 m RL, which is realised by constructing 5 m of embankment in between the MSE walls. Conservatively assuming that the unit weight of the engineered fill is 20 kN/m^3 and adding an further 20 kN/m^2 for traffic loads, the required bearing capacity will be 120 kPa. At the same time the pavement of the road was designed to be able to sustain

a maximum total settlement with a condition that differential settlements did not exceed 1:500.

It is noted that in this project the settlement criterion was defined for the actual post construction loading, not for a load that was equal to the bearing capacity. Once the ground has been stabilised, and the project has been constructed, the road will be subject only to traffic loads that at most will be 20 kPa, and will never reach an extraordinary road loading of 120 kPa that is approximately equivalent to a 12 m high oil tank or 10 storey building spread out over the project's area. Indeed, specifying the same load for the bearing capacity and settlement criteria would have been poor engineering and meaningless.

3.10.3.2 Application of Dynamic Compaction

Due to the requirements of the main contractor, ground improvement works were carried out with one mobilisation and demobilisation for each end of the bridge, and each part was executed within two weeks.

Based on the recommendations of the ground improvement specialist contractor, the fines content of the fill that was used for reclamation was limited to 20% to remain compatible with the in-situ sand and within the range of dynamic compaction treatment.

The fill was tipped into the sea to an average elevation of +1.35 m RL using dump trucks. In addition to the road's 38 m width, an extra 5 m was also initially reclaimed on each side of the approach road to ensure that the slopes of the embankment would also receive sufficient compaction. The extra width was later further increased to allow temporary passage of traffic between Abu Dhabi mainland and Reem Island. The extra width was removed after ground improvement at a later stage of the project, and replaced with geotextiles and rock armour to protect the reclamation against wave action and erosion.

A 15 ton steel pounder with an area of 2x2 m^2 and a drop height of 20 m was used for dynamic compaction. Other compaction parameters; i.e., grid size, number of impacts per print location and number of phases were optimised during a calibration program that was carried out at the beginning of the works. Based on the HPT and PMT results, a total energy of 240 tm/m^2 was applied in three phases. Figure 3-170 shows the application of dynamic compaction at the second end (Reem Island side) of the project. Also visible in the left hand side of Figure 3-170 is the rig used for installing the bored piles.

Figure 3-170: Application of dynamic compaction at Reem Island Causeway

3.10.4 Testing and Verification

3.10.4.1 DC Calibration

As part of the calibration programme two PMTs (before and after improvement), a HPT and a penetration test were carried out during phase 1 of dynamic compaction (see Figure 3-166). HPT-1, shown in Figure 3-171, and PT-2, shown in Figure 3-172, were carried out respectively with 12 blows and 20 blows. It can be observed that implementation of consecutive blows not only created a crater under the impact point but caused the ground at the periphery of the print to subside (negative heave) in a progressive manner as well. It can be observed that initially the amount of pounder accumulative penetration (crater depth) and compaction volume per blow follows a higher rate, but after about 6 blows the rate decreases, and it can be extrapolated and expected that asymptotes will be reached at about 35 to 40 blows.

It is generally neither necessary nor justifiable to apply the number of blows for reaching the asymptote. It is much more preferable to be able to implement the feasible heaviest pounder and highest drop height to make use of the higher rates of improvement with lesser blows. Further blows realise less achievement with the same impact energy.

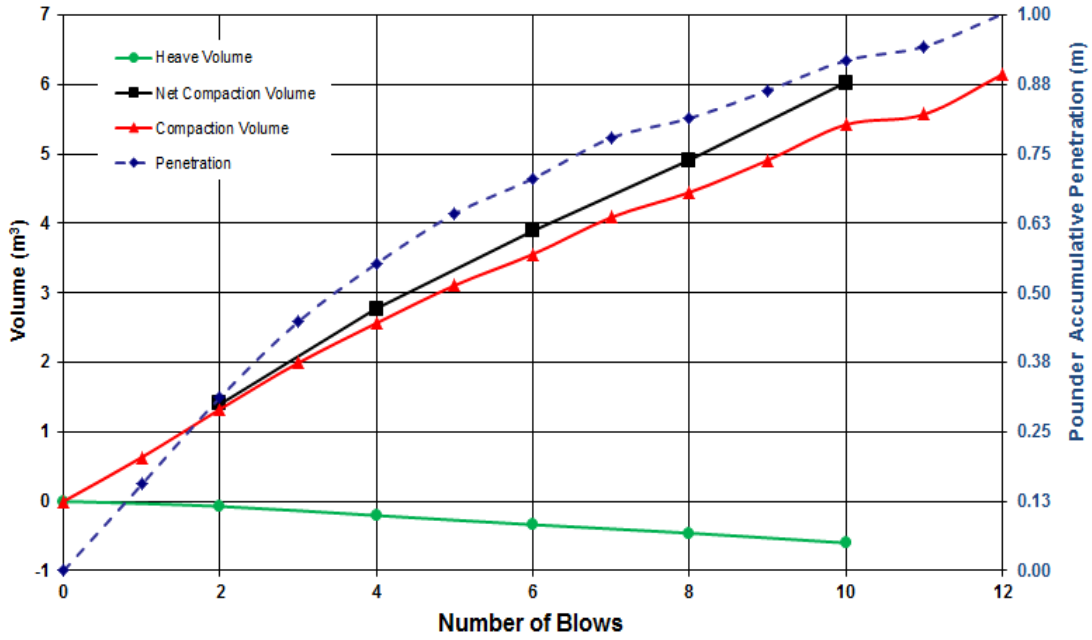

Figure 3-171: Heave and Penetration Test results

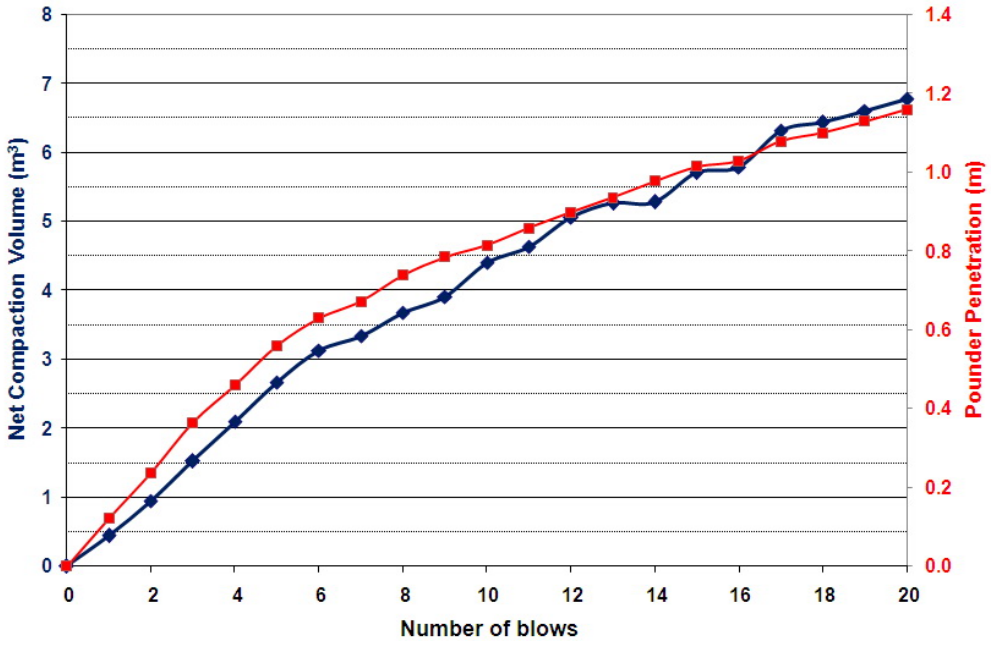

Figure 3-172: Penetration Test results

It should be noted that optimisation of dynamic compaction is based on both the HPT results and the verification testing that follows. It is possible to optimise the number of blows by reviewing the penetration and volume changes of HPT, but the amount of penetration, even if considerable, does not necessarily imply that design criteria have been satisfied. Design requirements can be confirmed only by proper testing and measuring the parameters that are able to demonstrate that specifications have been satisfied. In this project PMT was used for this purpose.

The square roots of the crater volume and net compaction volume (summation of crater and periphery subsidence volumes) are shown in Figure 3-173. It can be observed that similar to the results achieved in Marjan Island Road Corridor (refer to Section 3.6.4.1) and Al Nakhilat Ship Repair Island (refer to Section 3.7.5.1) the square root of the net volume to penetration curve initially commences with larger values, but slopes down and levels off after the first several blows to a value that is about 2.6. Therefore, Equation 1-5 is still able to formulate the relationship; however, it seems that the contribution of the peripheral subsidence is less (10% in Al Nakhilat Ship Repair Yard) and about 5%.

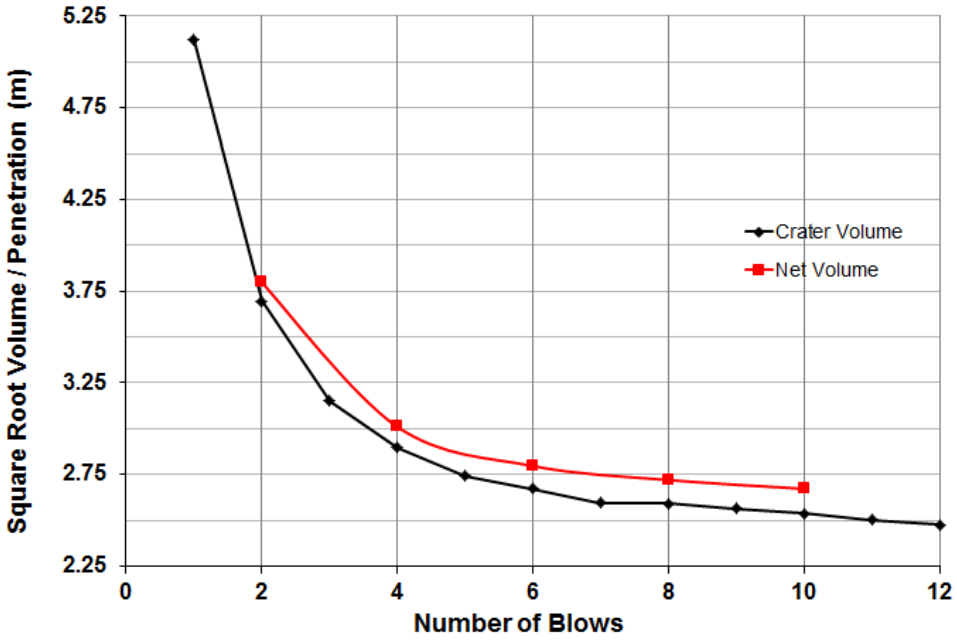

Figure 3-173: The relationship between the square root of volume to penetration and number of blows

The curves of $(D_T\text{-}D_B)/D_c$ and crater side angle versus number of blows are shown in Figure 3-174. The form and values of these curves appear similar to what was observed in Nakhilat Ship Repair Yard (refer to Section 3.7.5.1).

3.10.4.2 PMT and Acceptance

Figure 3-166 shows the location of PMT-001 and PMT-004 that were carried out before dynamic compaction and PMT-i05 and PMT-i06 that were performed respectively in DC phase 1 and phase 2 prints. P_{LM} and E_M of these tests are shown in Figure 3-175, and the P_{LM} and E_M improvement ratios are shown in Figure 3-176. It can be observed that while construction equipment traffic had improved the PMT parameters of the upper meter of soil

crust, deeper layers were initially very loose with P_{LM} values generally less than 600 kPa and as low as 220 kPa.

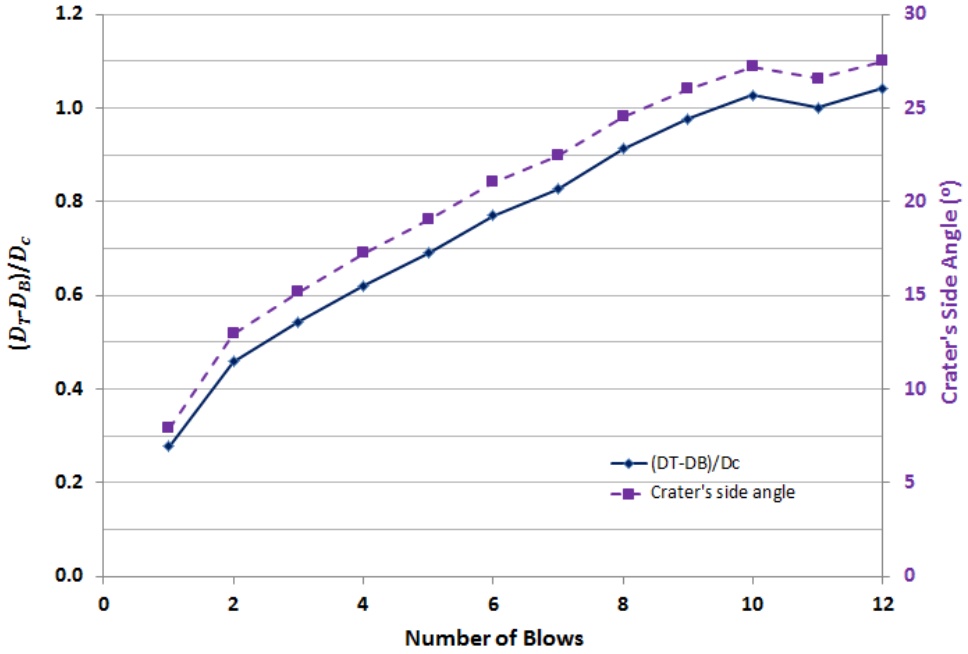

Figure 3-174: The relationship between $(D_T\text{-}D_B)/D_c$ and number of blows

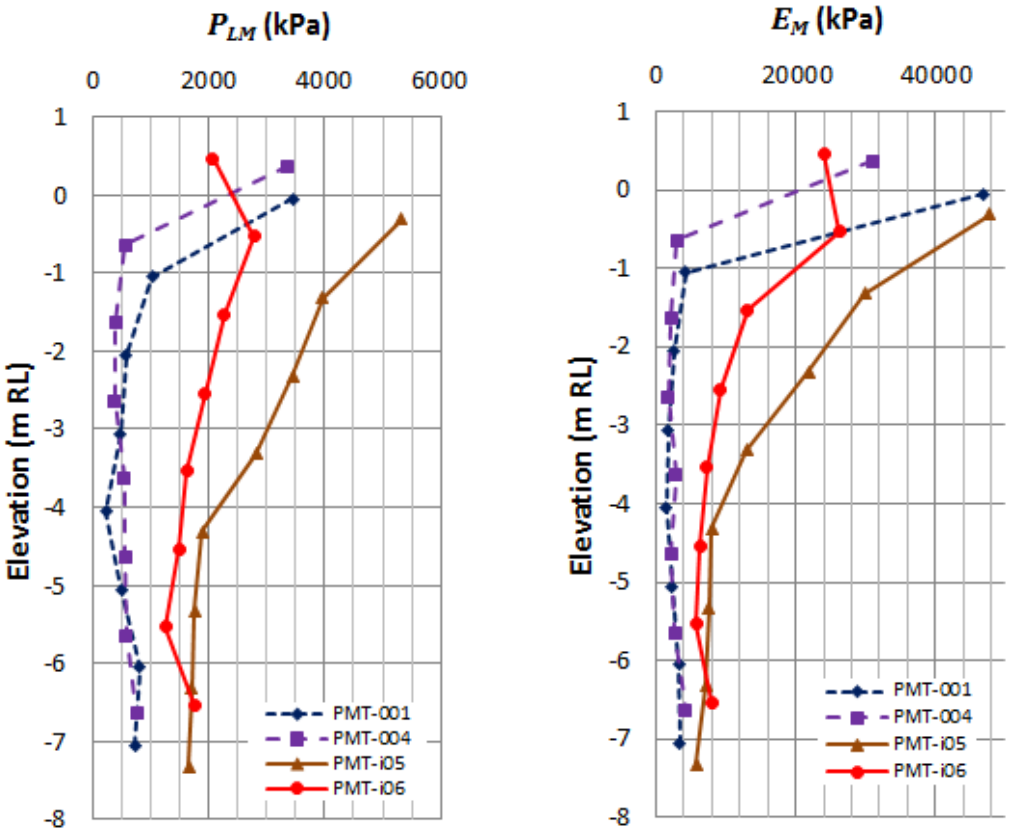

Figure 3-175: P_{LM} and E_M values before and after dynamic compaction

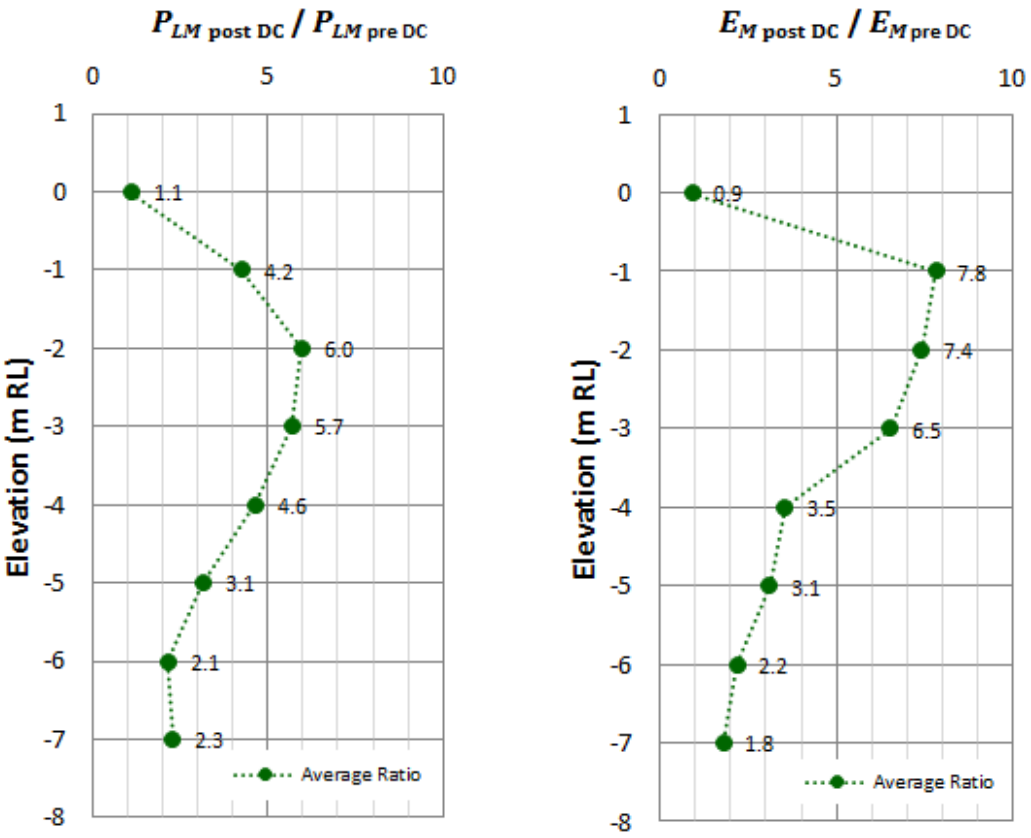

Figure 3-176: P_{LM} and E_M improvement ratios

Post treatment testing demonstrates that the soil parameters improved significantly throughout the fill layer whereas maximum P_{LM} and E_M improvement ratios were respectively 6 (500% increase) and 7.8 (690% increase). Comparison of P_{LM} improvement ratio in this project with previous research (Lukas, 1986) that proposes an increase in the order of 100 to 400% (see Section 2.5.5) suggests that greater peak improvement ratios can be considered.

Lukas has reported that the upper bound for P_{LM} after dynamic compaction in sands and gravels will be 1.9 to 2.4 MPa. It can be seen that the maximum P_{LM} value achieved in this project has exceeded that expectation in one of the test locations. The P_{LM} values are also higher than what Mayne et al. (1984) have reported for a number of sites. However, tests carried out in other projects that have been studied in this thesis, e.g. Al Quo'a New Township (refer to Section 3.3.5) are in line with the results of the PMT carried out in this project and indicate that it is possible to achieve larger values than the mentioned range. Case studies by others such as Spaulding and Zanier (1997) also indicate that higher P_{LM} values of up to 4 MPa can be achieved after dynamic compaction.

It is interesting to note that improvement at depth and at the bottom of the subgrade fill is still substantial and in the range of 80 to 130%. This massive improvement may have been

due to the fact that the very young fill was placed only a short period before ground improvement works and in a very loose state.

The ultimate bearing capacity of a foundation can be conservatively calculated using Equation 2-168 by assuming a value of 0.8 for bearing factor (k) and not considering q_o and P_o. It can be calculated that the geometric mean of the P_{LM} the two post treatment PMTs are respectively 2,640 kPa and 1,890 kPa; thus, with a safety factor of 3, the allowable bearing capacity will be respectively 704 kPa and 505 kPa, which exceeds the design criterion of 120 kPa by far.

Similarly, the harmonic mean of the E_M for the two post treatment tests can be calculated to be respectively 10.7 MPa and 9.3 MPa. E_{oed} can be calculated from E_M with α= 1/3 for sands (refer to Equation 2-214). Thus, the harmonic E_{oed} for two test locations can be calculated to be respectively 32.1 MPa and 27.9 MPa.

Once again, the settlement can be conservatively calculated with the assumption that load intensity does not reduce as stresses distribute in the ground. It can be then readily calculated with Hooke's law that the settlement will be respectively 5 mm and 6 mm.

The above figures show that while the settlements are much less than the design criterion in reality, had the settlement requirements been inappropriately tied to the required bearing capacity, which is 6 times more than the actual design load, then the settlements calculated from the second post treatment test would have exceeded acceptance. This comparison demonstrates the importance of developing proper design criteria.

As a result of the ground improvement works by dynamic compaction the fill settled about 40 cm on average. Should this amount of dynamic compaction induced ground subsidence be plotted against the applied energy of 240 tm/m^2, and compared with previous research (Mayne et al., 1984) that is shown in Figure 3-177, it can be observed that the amount of subsidence in this project falls approximately in the middle of other sites for the same amount of energy. Thus, it can be anticipated that P_{LM} values of this site are not extraordinary either, and it may be possible to obtain higher post DC P_{LM} values than what Lukas (1995) had conceived.

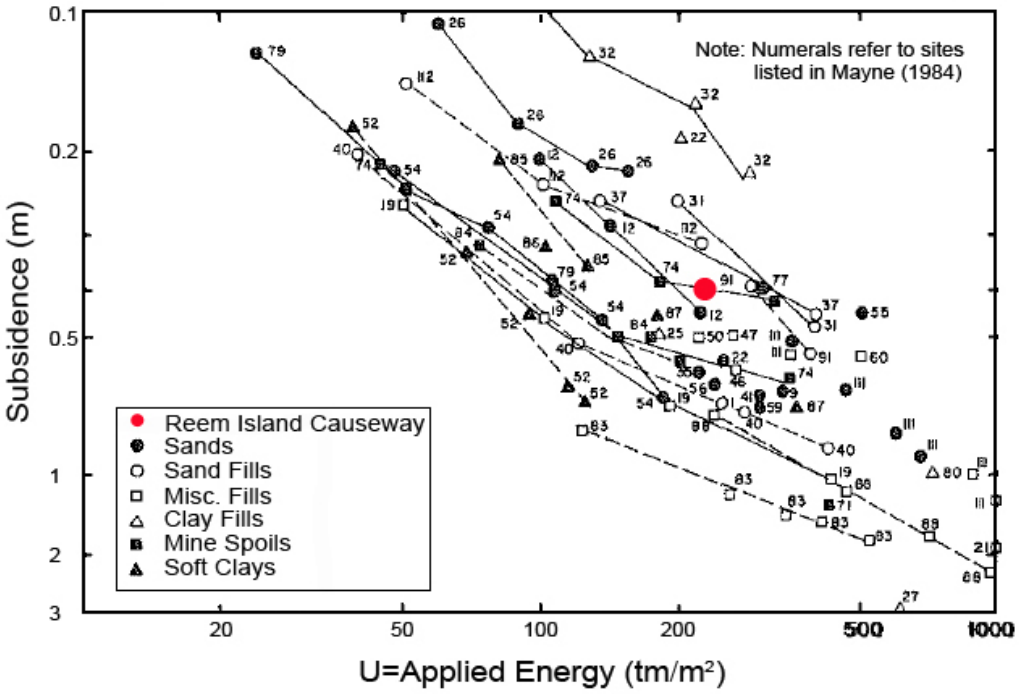

Figure 3-177: Comparison of ground subsidence versus energy with previous research (Mayne et al., 1984)

3.10.5 Lessons and Conclusion

The proper stipulation of specifications benefited the project by allowing the engineers to introduce an affordable ground improvement method with a short construction schedule. The application of dynamic compaction for the treatment of a submerged fill has proven to be very successful, and PMTs were able to demonstrate that the design criteria were readily satisfied. P_{LM} improvement ratio in the upper several metres of soil was 500 to 700%. The parameters' improvements was still substantial and in the range of 80 to 130% at depth.

Useful lessons that can be noted include:

1. Stipulating specifications and project criteria based on requirements is a superior and an optimised approach. This allows works to be carried out in the shortest possible duration and with the most affordable cost while satisfying the project's requirements without introducing technical drawbacks or sacrifices.

2. It would be realistic to assume that reclaimed fills will be in a loose state, and most will require of ground treatment for most construction projects. Although the soil above groundwater level may be dense due to construction equipment traffic or

other reasons, it is highly likely that there will be loose layers of soil below groundwater level.

3. There are numerous methods for improving saturated fills; it is the responsibility of the engineer to identify the best feasible solutions and to implement the one or ones that can provide the most benefits to the project. In this project the thin layer of saturated clayey soil was removed by dredging. Dynamic compaction was used to improve a relatively thick submerged subgrade with fines content up to 20%.

4. It is not necessary to compact the ground until reaching the asymptote of ground settlement (or compaction) versus number of drops (or accumulative energy). What is relevant is to demonstrate that design criteria (settlements, bearing capacity, etc) have been satisfied.

5. It is possible to achieve P_{LM} values greater than 2.4 MPa after dynamic compaction in saturated sands; however, the peak value decreases with depth.

6. Noting that the amount of improvement is a function of impact energy, it is possible to improve P_{LM} of saturated sands by 500%. However, the peak amount of improvement decreases with depth. The maximum amount of improvement appears to be in the upper half of the depth of improvement.

7. The square root of net compaction to crater depth was measured to be approximately 2.6 m after the first several blows.

8. Measurements suggest that 95% of the net compaction volume originated from the crater.

As shown in Figure 3-178, Abu Dhabi – Reem Island Causeway has been completed, and is operational. As a result of ground improvement the dumped fill is performing as per the project requirements and no settlements or indications of cracking due to poor foundation or bumping has been reported.

Figure 3-178: Abu Dhabi – Reem Island Causeway after completion

3.11 Ras Laffan Heavy Fuel Oil Bunkering Facility

3.11.1 Introduction

The Qatari industrial city of Ras Laffan, located on the southern shores of the Persian Gulf and 80 km from Doha, is one of the world's largest oil and gas hubs. This industrial complex is continuously and rapidly expanding to increase the production of gas from the North Field.

One of the projects that has been constructed in Ras Laffan is the Heavy Fuel Oil (HFO) Bunkering Facility for Qatar Fuel (WOQOD). The project included the design and construction of an import line, the storage and process area and an export line, along with the necessary utilities and civil works. The storage and process area includes three HFO tanks, a sub-station, a pump shed and other equipment, piping, shelters and other allied facilities. The project location and site plan can be seen and Figure 3-179.

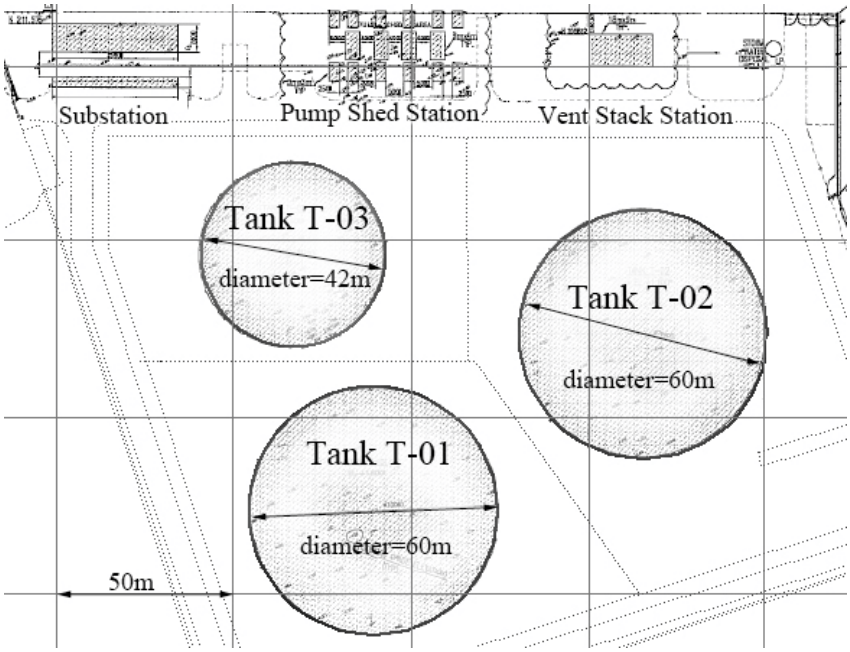

Figure 3-179: HFO Bunkering Facility site in Ras Laffan

The tanks were all designed as steel tanks with fixed roofs. The diameters of Tanks T-01 and T-02 were 60 m while Tank T-03 had a smaller diameter of 42 m. The bottoms of all tanks were to be at +3.2 m QNHD (Qatar National Height Datum), and the foundations were to be subjected to a uniform pressure of 170 kPa.

3.11.2 Ground Conditions

As can be seen in Figure 3-180, the HFO Bunkering Facility is located in a reclaimed area of Port of Ras Laffan. Site survey and initial tests indicated that ground level was generally flat and from +1.2 to +1.8 m QNHD. Groundwater was recorded to be 0.95 to 2.3 m below ground level.

Figure 3-180: Location of HFO Bunkering Facility in Ras Laffan

13 boreholes, 4 per tank and one in the pump station, were drilled and SPTs were carried out. The upper 12 m of ground appeared to be silty sand and gravel with cobbles. The limited information suggested that fines content was from 8 to 23%. While the SPT blow counts in all boreholes were generally high and in the range of 25 to 50, layers of 1 to 2 m thick with lower blow counts of 11 to 14 were encountered from depths of 5 to 8 m. The SPT blow counts of borehole BH2B is shown in Figure 3-181. It can be noted that testing was aborted for unrecorded reasons at depths of 2.5, 3 and 5 m. The ground then became limestone with UCS values mostly recorded to be from 10 to 30 MPa.

At later stages of the project, supplementary PMTs were carried out that appeared to be in disagreement with the results of the initial SPTs. While SPT blow counts were quite high and suggested the presence of very dense layers, PMTs indicated that the soil composition and the presence of cobbles had resulted in misleading and unrepresentative blow counts.

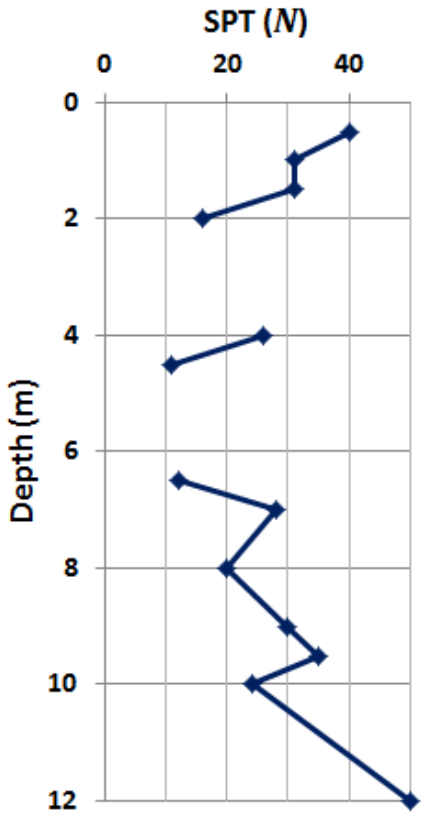

Figure 3-181: SPT blow counts in borehole BH2B

For comparative purposes, PMT T2-01 was carried out in the same location as BH2B. P_{LM} and E_M values of this test along with PMT T1-01 and PMT T1-03 that were performed in the other tanks are shown in Figure 3-182. As can be seen, while the SPT blow counts were indicative of dense to very dense soil, P_{LM} readings were high only in the upper most soil layer, possibly due to traffic and movement of construction equipment. P_{LM} in deeper layers of the reclamation was from approximately 100 to 250 kPa, which indicated the presence of loose sand subject to creep under self-weight (refer to Section 2.9.2.8).

The comparison of the results of the SPT and PMT can be an oblique reminder of the fact that SPT was originally developed for sampling soil (Rogers, 2004) rather than assessing its strength, and that higher blow counts in gravel and cobble strewn formation grounds are recorded when gravel or cobbles plug the end of the split-spoon (Abramson et al., 2002). This can lead to false and very misleading interpretations and can result in dangerously under designed foundations.

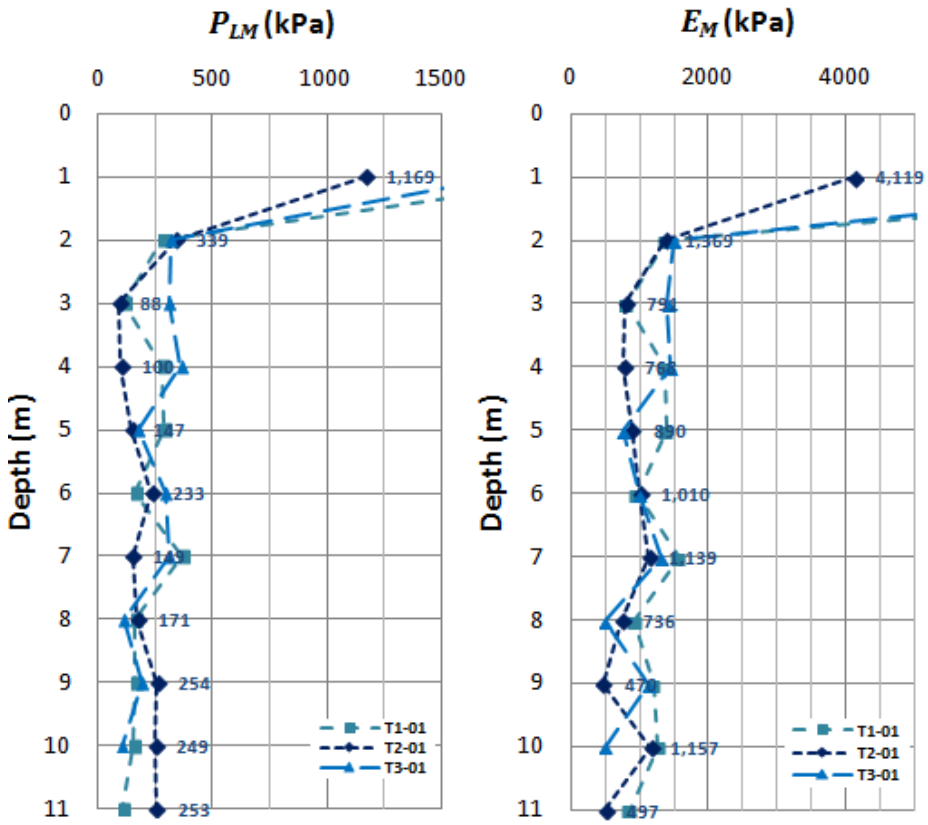

Figure 3-182: P_{LM} and E_M values in PMT T2-01

3.11.3 Development of Solution and Application of Dynamic Compaction

Before the supplementary PMTs were carried out and the presence of loose soils throughout the reclaimed site was established, the medium dense sandy layer at the depth of approximately 5 to 8 m was sufficient reason for applying applying specific geotechnical measures to ensure the safe transfer of loads from the structures to the ground. Piling, although applicable, was deemed as an expensive solution and ground improvement was preferred as a more competitive alternative.

The ground improvement package was awarded to a specialist geotechnical contractor who had proposed the application of dynamic compaction. For the tanks, bearing capacity was determined based on the tank loading. Total and differential settlement acceptance criteria were proposed based on Mobil (1990) specifications. Thus the criteria that had to be sastified became:

- Bearing capacity: 170 kPa
- Total settlement: 300 mm under a uniformly distributed load of 170 kPa
- Differential settlement: 1:180 under a uniformly distributed load of 170 kPa

PMT and finite element analyses were to be used for the verification of design criteria. Interpretation of PMT was carried out using the method of Menard (Centre D'Etudes Menard, 1975).

The total ground improvement works are summarised in Table 3-15.

No.	Item description	Dimensions (m)			Over width (m)	Unit area (m²)	Qty	Total Area (m²)
		L	w	D				
1	HFO Tanks T-01 & T-02			60	4	3,632	2	7,263
2	HFO Tank T-03			42	4	1,963	1	1,963
3	Sub-Station	35.9	8		4	702	1	702
		35.9	8		4	702	1	702
4	Pump shed area	40	16		4	1,152	1	1,152
5	Vent stack	18	9		4	442	1	442
Total Area								12,226

Table 3-15: Dynamic compaction treatment area

3.11.3.1 Preliminary Design

Noting that the risk of a large diameter tank failing in bearing is very unlikely, especially when deeper layers are limestone bed rock, failure could be expected to be either by local shear beneath the tank wall or due to excessive settlements. Therefore, it was defined that bearing capacity as calculated using Menard's (Centre D'Etudes Menard, 1975) equation (refer to Equation 2-168), had to be satisfied in the superficial upper 5 m that could be subject to shear failure.

$$q_u = q_o + k(P_{LM} - P_o) \qquad 2\text{-}168$$

With a safety factor of 3, assuming that the base of the tank is at ground level and with k=0.8, it can be calculated that the required geometric mean value of P_{LM} will be 638 kPa. At greater depths it was defined that P_f had to be greater than the extra stress; i.e.

$$\Delta\sigma' \leq P_f \qquad 3\text{-}9$$

Equation 2-168 yields: $P_f \geq 170$ kPa

It can be conservatively assumed that $P_{LM} \geq 170$ kPa with consideration that creep pressure is one half to two thirds of the limit pressure (Centre D'Etudes Menard, 1975); i.e.

$$P_f \approx \frac{1}{2} \; to \frac{2}{3} P_{LM} \qquad 3\text{-}10$$

Settlements were calculated using numerical analysis software. In the model whose geometry is shown in Figure 3-183, it was assumed that the bottom plates of the tank were represented by a beam with flexural rigidity E_yI and axial stiffness E_yA. The Young modulus of steel was assumed to be 210,000 MPa, and the thickness of the bottom plates was considered to be 2 cm. The radii of the tank and dynamic compaction were respectively assumed to be 30 m and 35 m, and the uniform load applied to the tank was 170 kPa. The parameters used in the model are shown in Table 3-16.

The numerical analysis whose results are shown in Figure 3-184 indicated that maximum settlements at the centre and edge of the tank were respectively 14.9 cm and 9.0 cm that are less than 300 mm. The centre to edge differential settlement can be calculated to be 5.9 cm, which is equivalent to 0.1475% (0.26/180) and is less than 1:180.

3.11.3.2 Application of Dynamic Compaction

Prior to dynamic compaction the ground was raised to +2.3 m QND by backfilling the site with sandy soil.

Based on the depth of treatment it was decided to apply heavy dynamic compaction using a 23 ton pounder that was dropped from 22 m. Compaction was applied in three deep phases for the tank foundations. Based on the results of the calibration, it was originally decided to apply 15, 11 and 8 blows respectively in deep compaction phases 1, 2 and 3; however, to

further increase the safety factor and to achieve even more improvement than necessary to meet design the number of blows in phases 1, 2 and 3 were respectively increased to 25, 15 and 8. A further 7 blows were then applied to phase 3 prints to homogenise the compaction of phases 2 and 3. As shown in Figure 3-185 the first and second phases of deep compaction were carried out in a rectangular pattern of 8.3 m by 9.6 m, and the third deep compaction phase's grid was designed in such a way that the overall deep compaction grid became an equilateral triangle with 4.8 m sides. Ground improvement was carried out with on offset width of about 5 m beyond the tanks' boundaries.

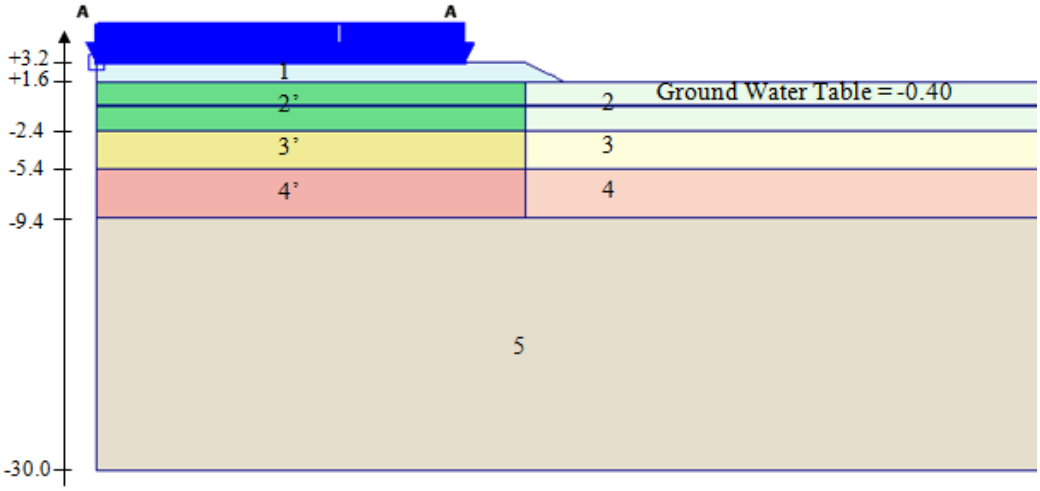

Figure 3-183: Numerical analysis model geometry

Layer ID	1 - Backfilling	2	2'	3	3'	4	4'	5
Top level (m)	+3.2	+1.6		-2.4		-5.4		-9.4
Bottom level (m)	+1.6	-2.4		-5.4		-9.4		-30
E_y (kPa)	60,000	15,000	60,000	7,500	10,500	3,500	5,500	300,000
c (kPa)	0							
φ (°)	35	33	38	30	32	28	30	38
γ (kN/m^3)	18							
ν	0.33							

Table 3-16: parameters used in the numerical analysis model

Dynamic compaction of the buildings was performed using 2 deep compaction phases, with 15 blows in each phase.

Upon mobilisation and completion of calibration, dynamic compaction works for the three tanks and three buildings were completed in less than 4 weeks.

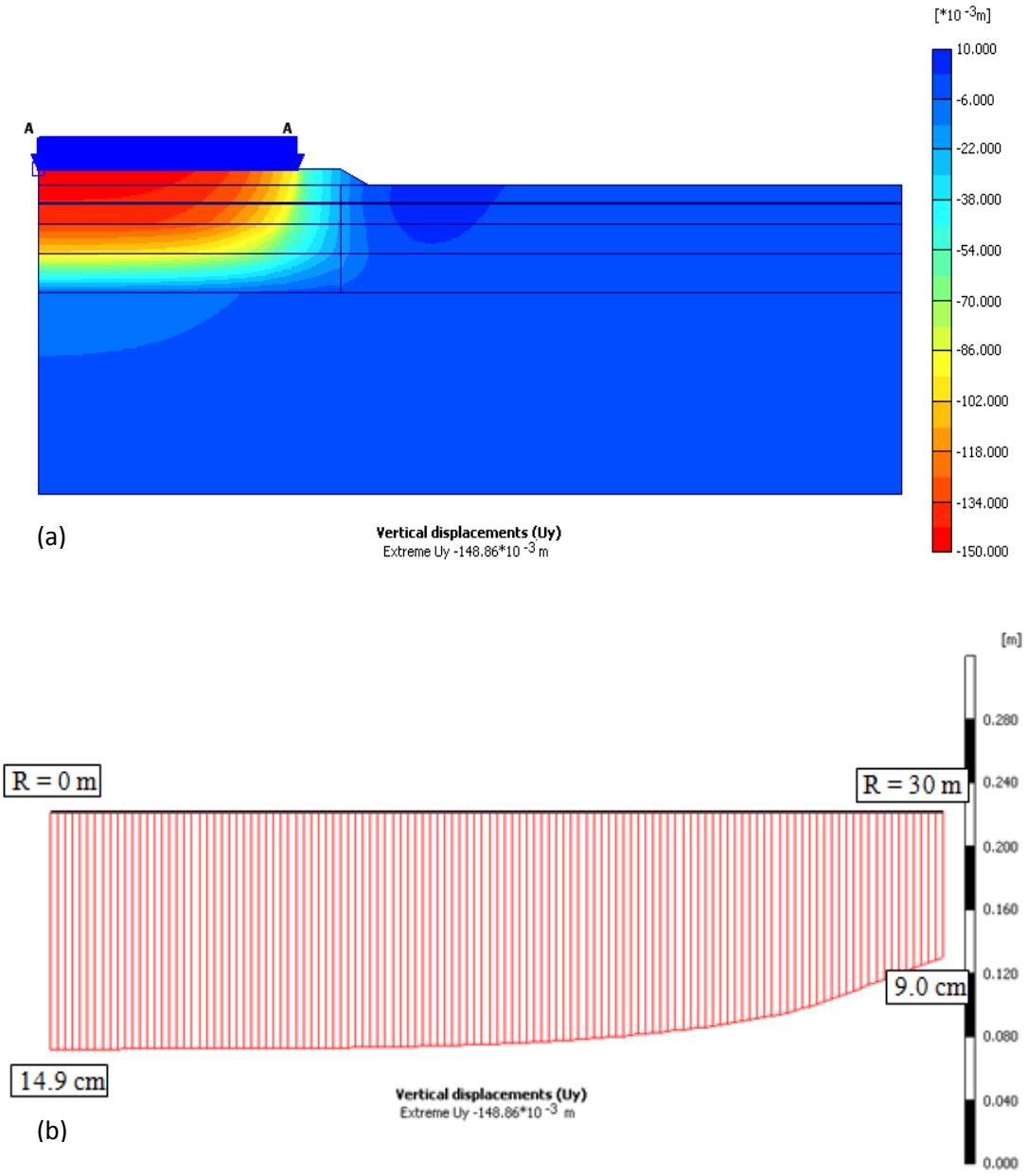

Figure 3-184: (a) Vertical displacement contours, (b) vertical displacement at the ground surface

3.11.4 Testing and Verification

3.11.4.1 DC Calibration

Prior to commencing ground improvement a calibration programme that included 3 heave and penetration tests was carried out respectively in the prints of deep compaction phases 1, 2 and 3 of Tank T-02. Although it is common practice to carry out the calibration outside the project's treatment area, due to space limitations, in this project the calibration was performed within the tank's boundary.

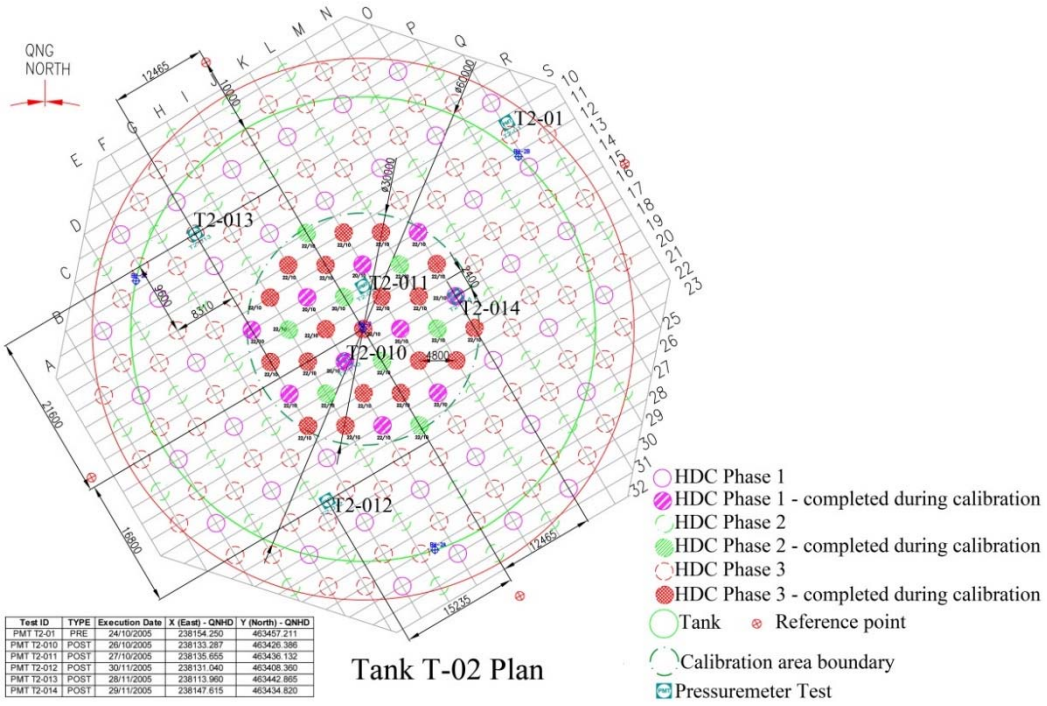

Test ID	TYPE	Execution Date	X (East) - QNHD	Y (North) - QNHD
PMT T2-01	PRE	24/10/2005	238154.250	463457.211
PMT T2-010	POST	26/10/2005	238133.287	463426.386
PMT T2-011	POST	27/10/2005	238135.655	463436.132
PMT T2-012	POST	30/11/2005	238131.040	463408.360
PMT T2-013	POST	28/11/2005	238113.960	463442.865
PMT T2-014	POST	29/11/2005	238147.615	463434.820

Figure 3-185: Layout of Dynamic Compaction works and PMTs

Ground surface settlements measured during HPT-01 in deep compaction phase 1 due to 22 pounder drops is shown in Figure 3-186. The 23 ton pounder that was dropped from 22 m had a base area of 1.9x1.9 m^2. In addition to measuring the crater's upper diameter and depth in four corners, changes in ground elevation were also measured up to 6 m away from the print centre in three directions.

It can be observed that while the ground around the pounder impact point has also settled, most of the deformation has occurred either directly around the pounder or at its vicinity. Yet, irrespective of the vibration magnitude, the ground deformation at even the farthest measured distance is sufficient to cause damage to most structures. Therefore, it can be concluded that at very close distances, both vibrations and ground deformation can result in cracking and damage to buildings.

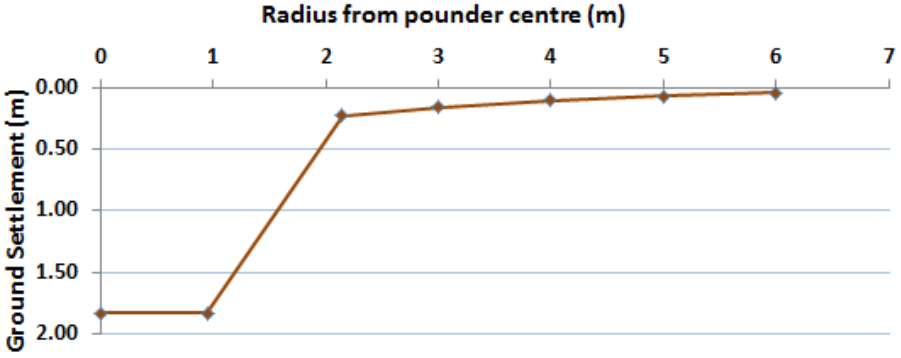

Figure 3-186: Measured ground settlement during HPT-01

Figure 3-187 shows the increase in crater depth, crater volume, heave volume and net volume of compaction due to the increase of pounder blows in HPT-01. It can be observed that similar to the previous projects that have been studied in this thesis, the ground around the print has also undergone settlement (negative heave) due to pounding. However, it appears that while about 90% of net compaction volume originated from the crater in Nakhilat Ship Repair Yard (Refer to Section 3.7.5) that was also in Ras Laffan, and about 95% of net compaction volume in Reem Island Project was realised from the crater, in this project only about 60 to 65% of the net compaction volume was measured as crater volume.

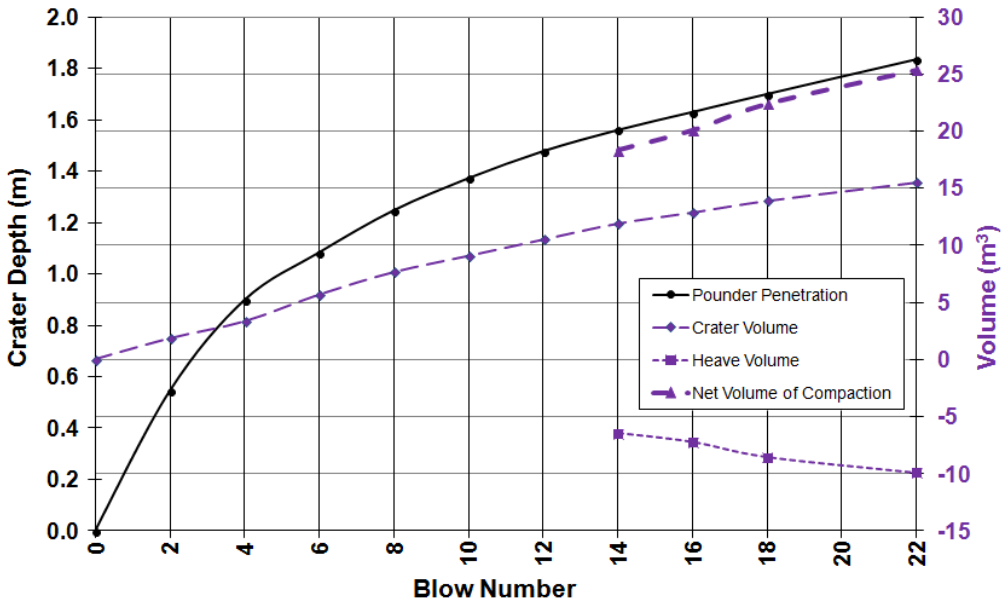

Figure 3-187: crater depth, crater, heave and net compaction volume changes due to consecutive pounder blows during HPT-01

Figure 3-188 shows that the square root of the crater volume to penetration was measured to be approximately 2.2 after the first several blows, which is similar to the other projects that have been reported in this thesis, but the same ratio for net volume is higher than the previous projects and about 2.75. Therefore, the range of Equation 3-5 can be extended to 2.75; i.e.

$$\frac{\sqrt{V}}{D_c} = 2.15 \; to \; 2.75 \qquad 3\text{-}11$$

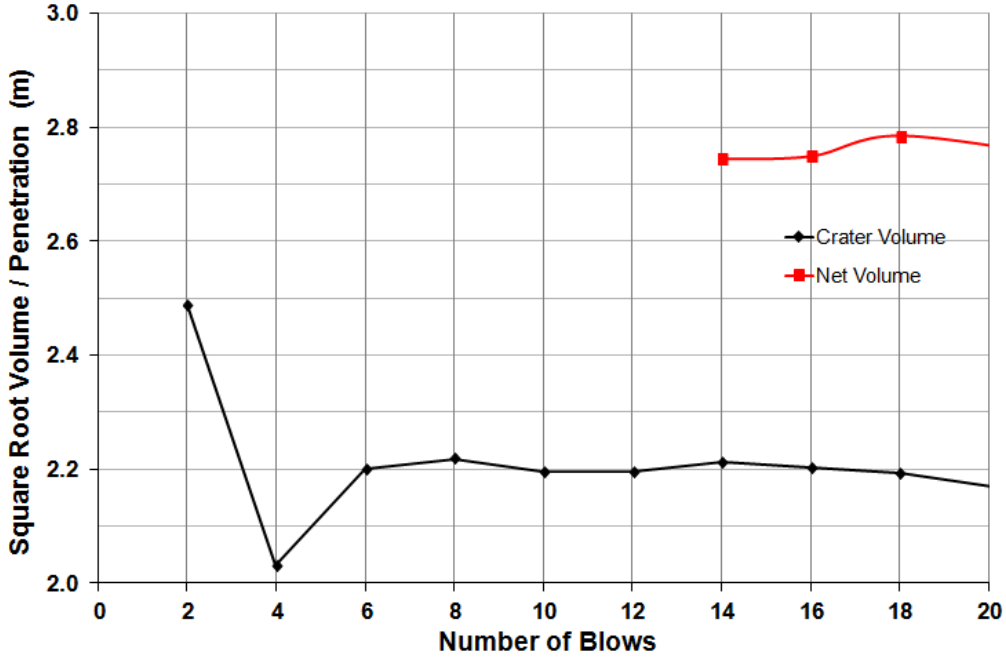

Figure 3-188: Variation of the square root of compaction volumes with consecutive pounding

Measurement of ground levels after dynamic compaction in Tank T-02 indicated that the ground level had dropped by about 0.85 m from +2.3 m QND to +1.45 m QND. With consideration that phase 1 prints amounted to 27% of all deep phase prints, by applying a factor of 0.8 based on the observation that the ratio of phase 2 to phase 1 compaction in Marjan Island Road Corridor Project was about 0.8 (refer to Section 3.6.4.1), it can be estimated that the average blow count per print (25 blows per phase 1 print and 0.8 times 15 blows per phase 2 and 3 prints) would be 16. The crater depth for 16 blows is 1.63 m in Figure 3-187. By assuming that the ratio of the square root of net compaction volume to crater depth is 2.75, it can be estimated that the volume of compaction per print is approximately 20 m^3. The unit cell for a triangular grid of 4.8 m is 19.94 m^2, which suggests that the ground should have settled about 1 m. This estimate is about 17% more than reality (0.85 m), and suggests that the ratio of 0.8 for the ratio of phase 2 to phase 1 compaction volume may have been too high when the ratio of crater compaction volume to net compaction volume is about 0.6 to 0.65; however, it may still be a suitable way to make a first estimate of the amount of ground subsidence due to dynamic compaction.

3.11.4.2 PMT and Acceptance

PMT parameters in Tank T-02 before and after dynamic compaction are shown in Figure 3-189. T2-01 demonstrates the ground condition before application of dynamic compaction. T2-010 was carried out in a phase 1 print during the calibration programme after

14 pounder blows, T2-011 and T2-012 were performed in between the prints during calibration (T2-011 after 22 blows in phase 1 and 21 blows in phase 2), T2-013 was conducted in a phase 3 print after 15 blows, and T2-014 was executed in a phase 1 print.

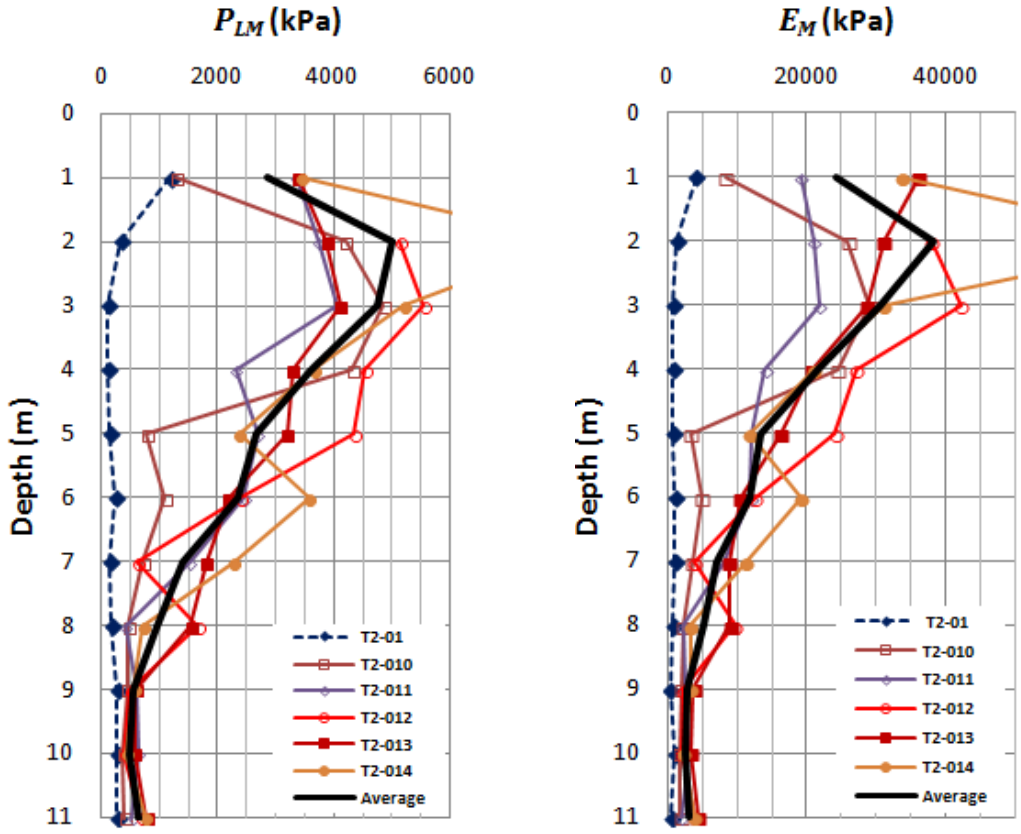

Figure 3-189: P_{LM} and E_M values before and after dynamic compaction

The effect of increasing the impact energy intensity is observable in Figure 3-189. It can be seen that the PMT parameters in a phase 1 print after 14 blows is similar to when higher energy was implemented in the upper and lower depths of the soil. However, there is a noticeable difference in the intermediate treatment depth. The scatter of results between tests carried out in the compaction prints and in between the prints suggests that, on average, in between prints have improved as much as the prints.

It is interesting to note that while Lukas (1995) suggests that dynamic compaction can increase P_{LM} values to 2,400 kPa and improved limit pressure values in previously studied projects in this thesis were generally less than 3,000 kPa, it seems that in this project the maximum value of P_{LM} exceeds the more common observations and, on average, is about 5,000 kPa.

PMT parameters' improvement ratios based on T2-01 and the average values after dynamic compaction are shown in Figure 3-190. As can be observed P_{LM} and E_M improvement ratios are both extremely high (possibly due to the very low PMT parameters before ground improvement), and by far larger than what has been observed in other projects. For example, peak values for both P_{LM} and E_M improvement ratios are in the order of 40 while the peak figures in the previously studied projects of this thesis were in the order of 6 to 12.

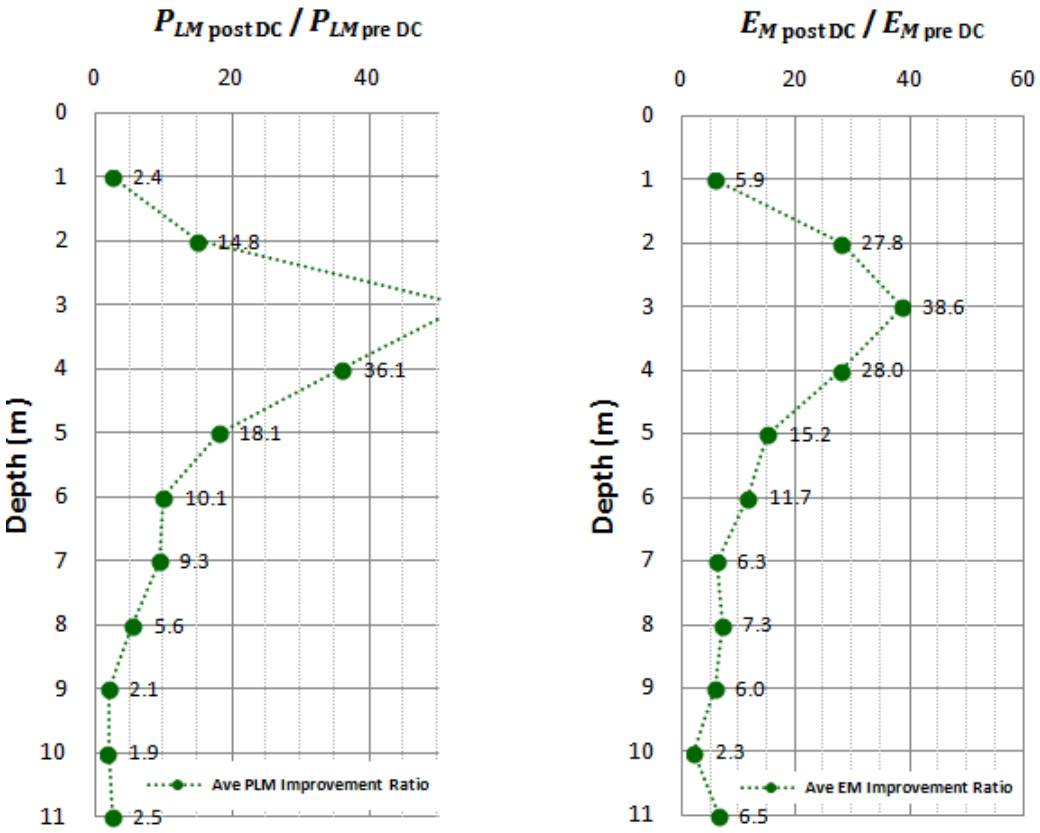

Figure 3-190: Ratio of P_{LM} and E_M before and after dynamic compaction

It can be observed from the test results that bearing capacity and settlement criteria have been well satisfied.

Hydro testing was performed after completion of ground improvement and the fabrication of the tanks. Of the 32 points on the shell of Tank T-02, maximum and minimum total settlements were 13 and 26 mm, and differential settlement between any two consecutive points that were 5.89 m apart was less than 4 mm that equated to less than 1 in 1,472, and was considerably less than the design criterion of 1:180.

3.11.5 Lessons and Conclusion

In this project it was observed that:

1. SPT can result in misleading interpretations when the ground is composed of large size particles.

2. Compaction results very impressive and it was seen that even at the deepest layers, at 11 m, improvement was still significant.

3. Maximum percentage of improvement was much more than what is suggested by earlier literature and observed values for other projects that have been studied in this thesis. PMT parameters' improvement ratios were in the order of 40 and maximum P_{LM} was in the order of 5,000 MPa.

4. In addition to the PMTs and finite element calculations, a full scale hydro test was performed for each tank. These tests were able to demonstrate that both total and differential settlements were considerably less than design criteria.

5. Buildings that are at very close distances from dynamic compaction works may sustain damage not only due to vibrations, but also due to DC induced ground deformations.

6. Crater volume was about 60 to 65% of net compaction volume. This is much less than about 90% that was recorded in Al Nakhilat Ship Repair Yard Project.

7. The ratio of the square root of net compaction to crater depth was measured to approximately 2.75 after the first several blows. This figure is higher than the other projects that have been studied in this thesis prior to this project.

8. It may be possible to make a first estimation of the amount of ground subsidence due to dynamic compaction by measuring crater depth and applying the value to the ratio of the square root of compaction volume to crater depth.

Figure 3-191 shows the HFO tanks during construction.

Figure 3-191: HFO tanks under construction

3.12 Palm Jumeira Sewage Treatment Plant Tanks

3.12.1 Project Description

Palm Jumeira is a group of man-made reclaimed islands off the coast of Dubai in the United Arab Emirates and the first of the three famous and world renowned palm shaped reclamations that lead to the notion of figure shaped reclamation projects. The Palm consists of a tree trunk, a crown with 17 fronds, three surrounding crescent islands that form an 11 km long breakwater and two identical smaller islands on the sides of the trunk that are in the shape of the logo of The Palm. The island itself is 5 km by 5 km, and has added about 78 km to Dubai's original 72 km coastline.

In total, 94 million m^3 of sand and 7 million m^3 of rock have been used in the construction of Palm Jumeira. Calcareous sand was dredged from the Persian Gulf using trailing suction hopper dredgers (Dowdall Stapleton, 2008). During the dredging process the dredger initially lowered the suction pipes on both sides of the ship all the way to the seabed. Sand pumps transferred the sand dredged up by the suction head into the hold or hopper, and the excess water was drained off via the overflow pipes. When the hopper was full, the ship sailed off to the reclamation area. When possible, the hopper was discharged by means of a big door located on the bottom of the hull, but when the water was shallow, that was not possible and the dredger sprayed the sand and water mixture onto the reclamation by rainbow discharge. The process of rainbow discharge that was utilised on Palm Jumeira is shown in Figure 3-192.

Figure 3-192: Reclamation by rainbow discharge at Palm Jumeira

In general, the reclamation at Palm Jumeira was about 12 to 14 m thick of which about 3 to 4 m was above sea level. It was observed that CPT cone resistance of the deposited calcareous sand above water level was very high and in the range of 20 to 40 MPa. The soil then became very loose in the rainbow discharged sand layer below water level with q_c as

low as 1 MPa in the next 4 to 5 m of soil. Loose to medium dense sand with q_c varying from 4 to 8 MPa was encountered down to depths of about 12 to 14 m where the soil became very dense. Carbonate content of the sand, measured as $CaCO_3$, varied from as approximately 60% to more than 90%.

Due to the low strength and high compressibility of the soil, almost the entire reclamation was treated using vibro compaction. Heavily loaded structures were additionally constructed on piles. The two sewerage treatment plant (STP) tanks were the only heavily loaded structures that were neither treated with vibro compaction nor were supported on piles.

As shown in Figure 3-193, a sewerage treatment plant has been constructed at the tip of each of the lower crescents of Palm Jumeira. The SPT lots were denoted A-A and G-G, and each plant includes one reinforced concrete tank that has a diameter of 35.1 m.

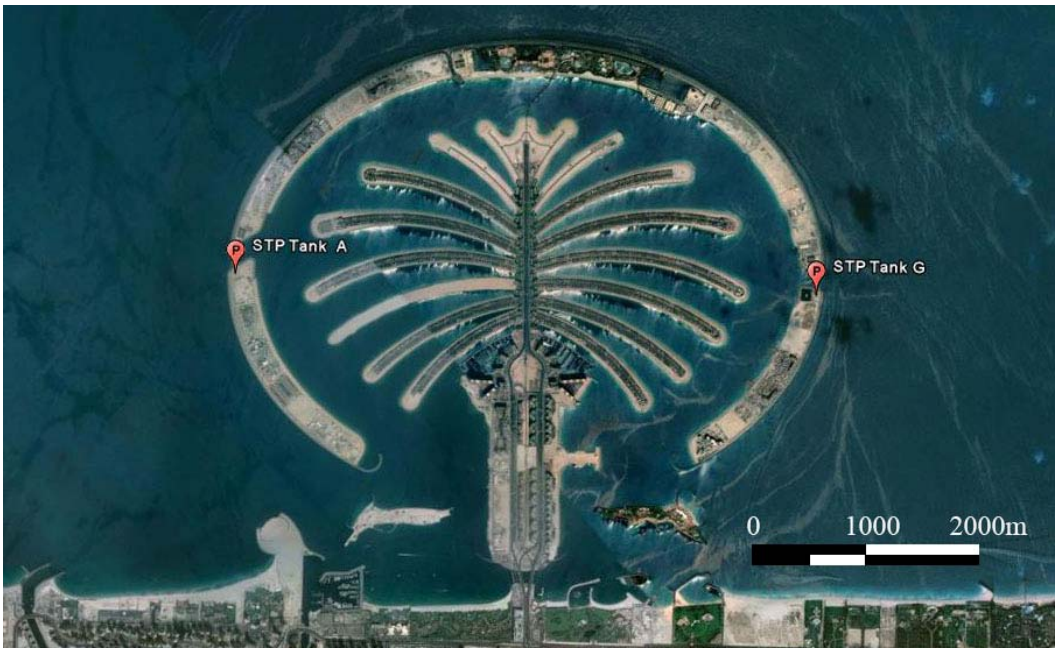

Figure 3-193: Location of the two sewerage treatment plant on Palm Jumeira

Each tank was subject to the below loads:

- Dead load corresponding to the reinforced concrete structure: 41 kPa
- Dead load corresponding to steel structures: 8 kPa
- Live load corresponding to the liquid inside the tank: 71 kPa
- Total dead and live load: 120 kPa

3.12.2 Preliminary Geotechnical Investigation

While no geotechnical investigation was available for Lot G-G, two SPT boreholes and two CPTs were carried out not very far from Lot A-A's tank location.

The boreholes indicated that the upper crust of the soil was generally very dense with SPT blow counts up to 28; however, the deeper layers of soil were less dense, with minimum blow count in the upper 8 m of the reclamation dropping to as low as 5. The soil then appeared to become denser with a minimum blow count value of 18 below 8 m depth and exceeding 50 at the depth of 13 m. The fines content of the soil in these two boreholes was from 2 to 10% in the upper 13 m of soil, but increased to 22% at the depth of 14.5 m. Ground level was at +4 m RL (reduced level) and groundwater was at the depth of about 3 m.

CPT readings also suggested that the upper 2 m of soil was composed of very dense sand with q_c as high as 25 MPa. The soil then became loose with q_c as low as 3 to 4 MPa down to the depth of approximately 13 m where great resistance was encountered and testing was terminated.

Although the SPT and CPT results suggested that the soil was clean sand, fines content as high as 30% was observed in a number of boreholes that were not very far from the project.

3.12.3 Development of Solution

In the absence of conclusive and definite geotechnical information, the limited and somewhat contradicting geotechnical data from nearby boreholes and the general pre-ground improvement conditions of Palm Jumeira was enough evidence to indicate that specific foundation measures were required.

Although piling was deemed as a feasible method the costs associated with the execution of deep foundations made this solution unattractive. Steel piles were both uncommon and expensive in the UAE. Cast in place concrete piles were very common; however, providing concrete to the crescent islands by marine transportation made this method very inefficient and costly.

In the event that a suitable ground improvement solution was developed, acceptance criteria at tank foundation level (+2.5 m RL) were specified to be:

- Bearing capacity: 160 kPa with a safety factor of 3

- Differential settlement: 1/750 for a uniformly distributed load of 120 kPa

During that period vibro compaction was the commonly practiced method of ground improvement on Palm Jumeira, but the possible presence of silty sand placed doubt on the applicability of this technique. Stone columns (vibro replacement) were another feasible solution, but also proved to be costly.

One of the ground improvement specialist contractors proposed the application of dynamic compaction.

Using Equation 2-41 with c= 0.7 and a drop height of 20 m, it can be estimated that treating a loose sand layer that is about 13 m thick would require a pounder that weighs 18 tons; however, at that time, and the heaviest pounder that was available to the specialist contractor weighed 15 tons.

As a supplement to dynamic compaction it was decided to implement dynamic surcharging (also refer to Section 3.4.4) to improve the results by combining the effect of static loading and high energy impacts to generate acceleration in the soil under static loading in such a way as to produce a shearing process around the surcharge fill. This process was to reduce the spreading of the load that was initially caused by the high strength of the upper layers. Generation of vibrations and increasing the pore pressure under the tank was to result in a reduction in friction between the granular particles of the soil and to ultimately lead to the collapse of the foundation soil under the influence of dynamic surcharging.

To realise this process, a surcharge was to be initially placed onto the treatment area and dynamic compaction was to be performed. Although granular materials settle under static loads, as dynamic shear modulus has been found to decrease significantly with increasing values of shear strain amplitude (Silver and Seed, 1971), it can be expected that introducing vibration will increase the amount of settlement under the surcharge. Furthermore, the rate of consolidation of fine soils is greatest when pore water pressure is high, and as was observed in King Abdulla University of Technology (refer to Section 3.4) it is possible to increase the rate of consolidation back to previously high values by inducing pore water pressure through vibration.

3.12.4 Supplementary Geotechnical Investigation in Lot A-A

In order to verify the ground conditions before finalising the treatment scheme, four SPT boreholes were drilled, and tested in the centre and three sides of Lot A-A's tank. These boreholes also indicated that the upper 3 m of sand was very dense, but the soil then became very loose to medium dense at groundwater level. SPT blow counts at depths of 3 to 8 m varied from as low as 4 to as high as 14, recorded N values were then from 11 to 20 to depths of approximately 12 to 13 m where the ground became very dense, and blow counts exceeded 50. Fines content of the 38 samples that were extracted from the four boreholes ranged from 16% to 21%. This was much more than the average 5% that was indicated by the preliminary geotechnical investigation. Also, although no silt pockets were identified under the tank, as fines content was observed to be more than 20% in almost half of the samples and as high as 30%, it was understood that the tank's location was probably one of the siltiest areas of the reclamation. SPT blow counts and fines content in the preliminary and supplementary boreholes are shown in Table 3-17.

Furthermore, two PMTs were also carried out in the tank area. As it was already established that the ground was very dense above water table level, testing was done at 1 m intervals below sea level. These tests also reconfirmed that the submerged soil was in a loose state. In this zone P_{LM} was less than 100 kPa to about 700 kPa, and E_M was measured to be from less than 1 MPa to 6 MPa.

3.12.5 Ground Improvement in Lot A-A & Verification of Results

3.12.5.1 Dynamic Surcharging

As shown in Figure 3-194 and prior to the placement of any surcharge material four settlement monitoring plates were installed at the tank location. One plate was installed in the centre of the tank, and the remaining three were installed at 120 degrees angles from one another on a ring with a radius of 17.5 m.

The surcharge was provided by scraping sand from the vicinity of the tank and placing it evenly over the loading area with a base diameter of 44.2 m. The fill height was 4 m with a lateral slope of 1V:1.5H; thus the top diameter of surcharge was 32.2 m. The surcharge is schematically shown in Figure 3-195.

Depth	Supplementary SPT								Preliminary SPT			
	BH-1		BH-2		BH-3		BH-4		BH-13		BH-14	
	SPT	fines	SPT	fines	SPT	fines	SPT	fines	SPT	fines	SPT	fines
0.0									28			
0.5											22	
1.0									18		17	4%
1.5									8		8	
2.0									15		17	
2.5									13		21	
3.0									14		29	
3.5									19		5	
4.0			4	11%	13	14%	13	12%	9	5%	7	
4.5	6	9%							7		11	
5.0			7	15%	7		11	20%	15		12	
5.5	10	30%										
6.0			7	15%	15	17%	14	16%	8	6%	12	
6.5	13	30%										
7.0			12	10%	22	30%	14	20%	18		11	6%
7.5	9	30%										
8.0			5	22%	14	30%	10	15%	38	10%	16	
8.5	5	27%										
9.0			14	21%	12		21	22%	55		36	
9.5	18	17%										
10.0			11	6%	13	17%	13	22%	26		41	
10.5	11	17%										
11.0			24	14%	17	17%	23	22%	18		20	2%
11.5	11	17%										
12.0			37	29%	20	23%	64		20	3%	200	
12.5	11	22%										
13.0			36	17%	24		33	22%	133		26	5%
13.5	38	15%										
14.0			38	14%	53		52	20%	25		47	
14.5										22%		
15.0											200	

Table 3-17: SPT blow counts and fines content in the preliminary and supplementary boreholes

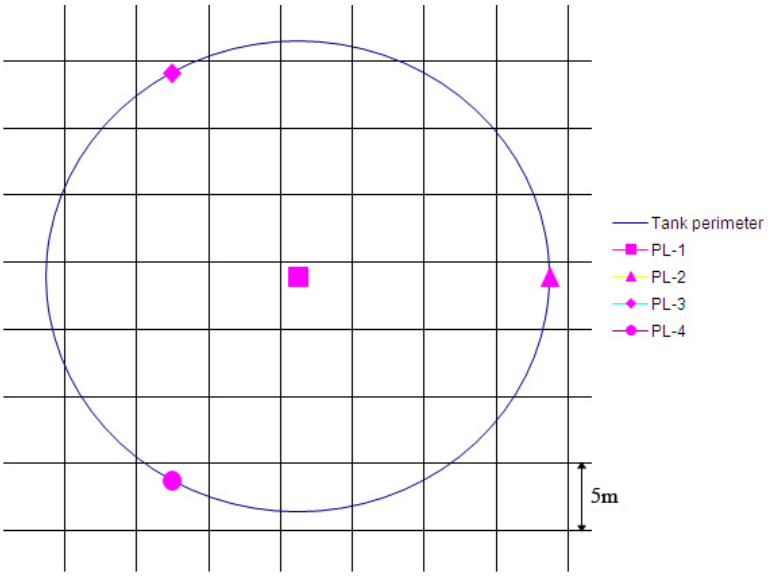

Figure 3-194: Layout of settlement monitoring plates

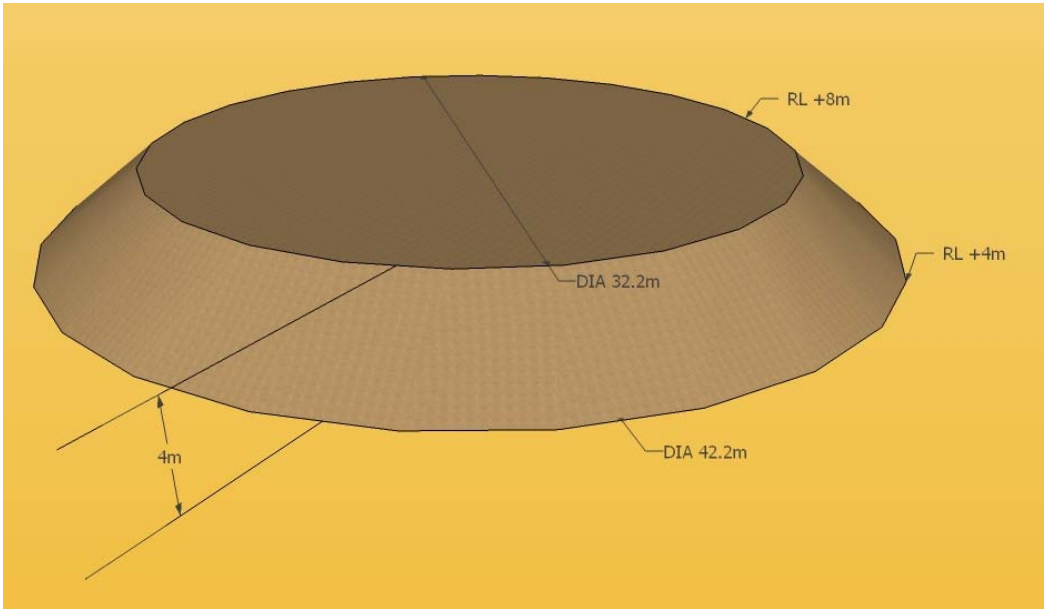

Figure 3-195: Schematic illustration of the surcharge

It can be estimated that the approximate volume of the surcharge was 4,700m^3. Assuming that the in-situ unit weight of the surcharge was 17 kN/m^3, the total weight of the surcharge material can be estimated to be 80 MN. Noting that ground and tank levels were respectively at +4 m RL and +2.5 m RL, that overburden will be the equivalent of an additional surcharge load of approximately 25 MN. Although the uniformly distributed load acting specifically on the tank's area was 93.5 kPa (4 m of surcharge plus 1.5 m of over burden pressure), which is equivalent to 78% of the tank's total load, the 105 MN of load applied over the tank's area and its periphery equates to approximately 90% of the tank's total load. Hence, it would be

fair to assume that this amount of surcharge would have been able to well consolidate the deep layers of silty sand satisfactorily.

As graphically shown in Figure 3-196 and numerically presented in Table 3-18, the monitoring plates' settlements were recorded during the stages of the surcharge. Ignoring the errors in recording, it can be seen that the plates settled prorate with surcharge placement. Once backfilling was completed, the surcharge was left in place for 5 additional days. It can be predicted from the settlement trend that the ground could have settled an additional maximum settlement of 5 mm in the long run.

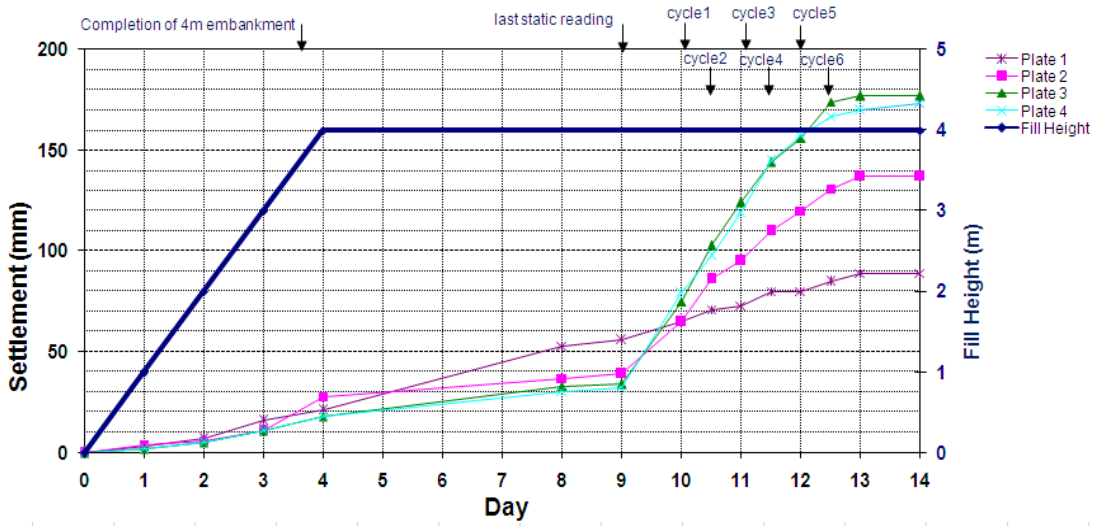

Figure 3-196: Ground settlement in Tank A-A during static and dynamic surcharging

Status	Plate 1	Plate 2	Plate 3	Plate 4
Completion of static surcharge	21	28	18	18
Static surcharge, end of Day 5	56	39	34	32
Dynamic surcharge cycle 1	65	65	75	79
Dynamic surcharge cycle 2	71	86	103	98
Dynamic surcharge cycle 3	73	95	124	119
Dynamic surcharge cycle 4	80	110	144	145
Dynamic surcharge cycle 5	80	120	156	157
Dynamic surcharge cycle 6	85	131	174	167
End of surcharging	89	137	177	173

Table 3-18: Ground settlement during static and dynamic surcharging

Before commencement of dynamic surcharging, as shown in Figure 3-197, 26 DC print locations were pre-excavated by approximately 1 m at 5.95 m intervals on a ring around the

tank with a diameter of 49.2 m. The excavation was carried out to increase the pounder's depth of influence by lowering the impact level and also reducing the amount of energy absorption in the very dense superficial layer. Then, as shown in Figure 3-198, a 15 ton pounder was dropped a total of 30 times per print in 6 consecutive cycles.

Figure 3-197: Pre-excavation of dynamic surcharging prints

Figure 3-198: Dynamic surcharging

It can be assessed from Figure 3-196 and Table 3-18 that dynamic surcharging has increased ground settlements by 1.6 to 5.2 times the value of the static settlements. As could have been anticipated, the maximum effect and increase was on the periphery where impact wave amplitudes were greatest. It can also be observed that by the sixth cycle, the efficiency of

dynamic surcharging seems to be diminishing and additional cycles would have yielded a non-linearly lower rate of induced settlement.

Although the maximum differential settlement of outer monitoring plates were 7 mm at the end of static surcharging, the maximum differential settlements during dynamic surcharging increased by 4 times to 40 mm. This suggests the possibility of large differential settlements under seismic and vibratory loads in untreated areas of the same ground.

3.12.5.2 Dynamic Compaction of the Tank Foundation

After completion of dynamic surcharging the surcharge was removed, and the ground was excavated to working platform level at +2.8 m RL. This elevation was defined with the intention of allowing for 0.3 m of induced settlement due to dynamic compaction, approximately reaching the tank's base level of +2.5 m RL at the end of the ground improvement works, and sufficiently and safely remaining above groundwater level without destabilising the platform or delaying the works due to ground liquefaction and water seepage to the surface.

The diameter of the working platform level after excavation and top of excavation were respectively 41.2 m and 46 m, and the excavation cross section is shown in Figure 3-199.

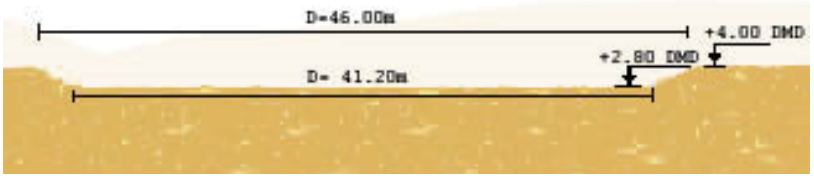

Figure 3-199: Cross section of excavation for reaching working platform level

Dynamic compaction was carried out on prints located in the centre of the working platform and on 4 concentric rings around the central print. The description of the print rings is summarised in Table 3-19. As with the dynamic surcharging prints, each DC print was pre-excavated by approximately 1 m to facilitate pounder penetration and to increase the depth of influence.

Approximately 150 m^3 of crushed rock and cobbles were added to the total of 58 DC prints. This amount equates to about 2.6 m^3 of rock per print or an equivalent of approximately 0.13 m of rock per every metre of ground within the treatment zone. This amount of stone is

insufficient to effectively increase the ground strength, and was rather used to increase soil permeability.

Ring	radius (m)	No. of prints
Centre	0.0	1
R1	5.5	6
R2	10.5	11
R3	15.5	20
R4	19.5	20

Table 3-19: Description of prints

Due to the small size of the project and consequently the limited number of prints, in the first phase of compaction each print received between 28 to 35 blows from a drop height of 20 m. In the second phase of compaction, each print received an additional 3 to 5 blows. During ironing stage the pounder was dropped with low energy once onto the points of a of 2x2 m^2 grid. A photograph of the works is shown in Figure 3-200(a). As shown in Figure 3-200(b), due to soil liquefaction and an increase in pore water pressure during dynamic compaction, water was observed to boil out from the craters.

(a) **(b)**

Figure 3-200: (a) Dynamic compaction of the tank's foundation, (b) water boiling into the craters

As shown in Figure 3-201, pounder penetration and the outer crater diameter for each print location were measured during the first two phases of dynamic compaction. In the first phase, the average pounder penetration depth and average upper diameter of crater were respectively 1.7 m and 5 m. In the second phase, these numbers significantly reduced and respectively dropped down to 0.4 m and 2.3 m. The diameter of the crater at the base could be assumed to be equal to the pounder's dimension; i.e., 1.7 m.

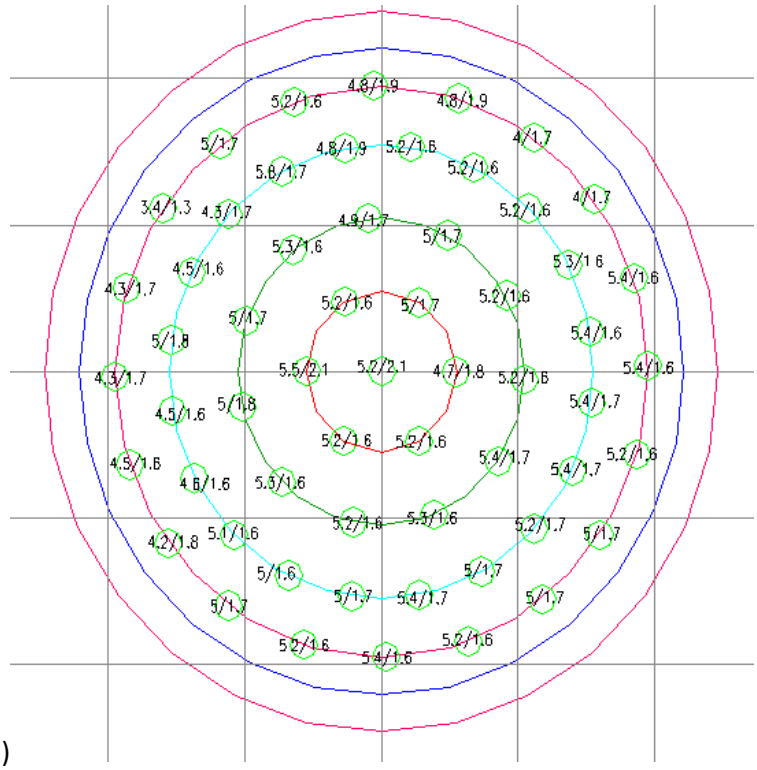

(a)

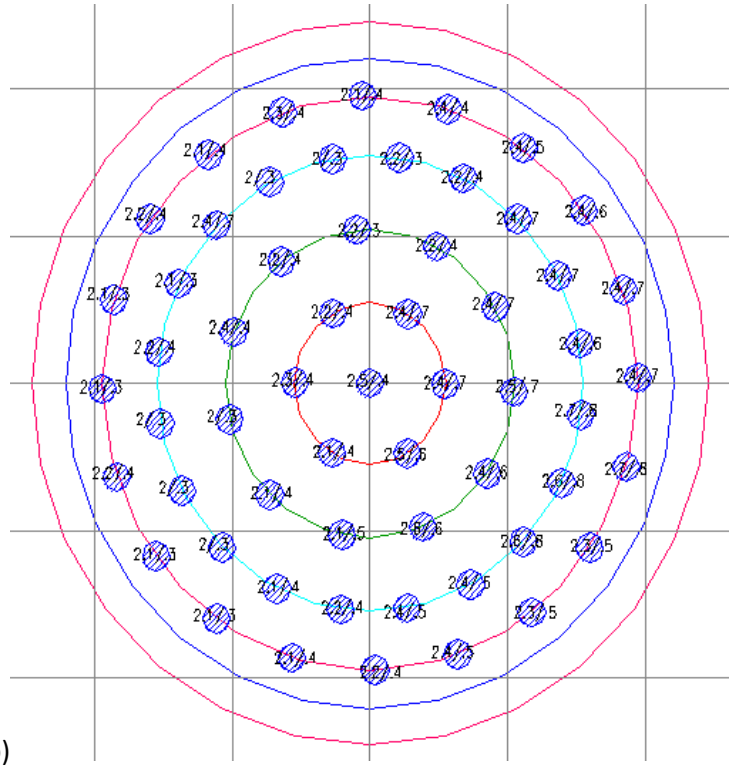

(b)

Figure 3-201: Crater top diameter and depth in (a) the first and (b) the second phase of DC

At the end of dynamic compaction, the ground level dropped to +2.25 m RL. Noting that 150 m^3 of stone that equated to a thickness of 0.13 m had been added, it can be calculated that

the ground had settled 0.68 m in addition to the settlements induced by dynamic surcharging.

Noting that the treatment diameter was 41.2 m, it can be calculated that the compaction volume was 906 m^3. Assuming $\sqrt{V}/D_c = 2.26$ (refer to Equation 3-11) for each of the two phases of the 58 prints will yield the same volume. Assuming the ratio to be equal to 2.15 and 2.75 will respectively result in total compaction volumes of 775 and 1268 m^3, which respectively underestimate the compaction volume by 15% and overestimate the compaction volume by 40%. $\sqrt{V}/D_c = 2.5$ will result in 16% overestimation in this case.

Comparison of the above figures suggests that Equation 3-11 has sufficient accuracy for a first estimate or at least as a rule of the thumb estimation of the compaction volume, and thus the average induced strain in the soil.

Although the magnitude of this settlement is much larger than what was measured during dynamic surcharging, it should be reminded that dynamic surcharging was aimed at reducing the settlement of the deeper and siltier layers that may have been too deep to effectively reach with dynamic compaction using a 15 ton pounder or too silty for dynamic compaction to be efficiently effective.

3.12.5.3 Post Improvement Verification in Lot A-A

Upon completion of dynamic compaction and levelling of the site, 4 PMTs were carried out within the treatment area to assess the ground conditions. P_{LM} before and after ground improvement are shown in Figure 3-202. As could have been predicted, maximum improvement occurred to depths of about 8 where, excluding the highest values of one of the tests(A2), P_{LM} ranged from approximately 2 to 4 MPa that is quite more than 1.9 to 2.4 MPa that Lukas (1986) has expected. E_M ranged from 23 to 30 MPa at depths of about 4 m to 8 m. Due to the combination of dynamic surcharging and pre-excavated dynamic compaction with high number of blows improvement can still be observed at greater depths. Furthermore, the minimum P_{LM} value after improvement is greater than 600 kPa, which demonstrated that the young hydraulic fill was no longer subject to creep due to self-weight (see Section 2.9.2.8).

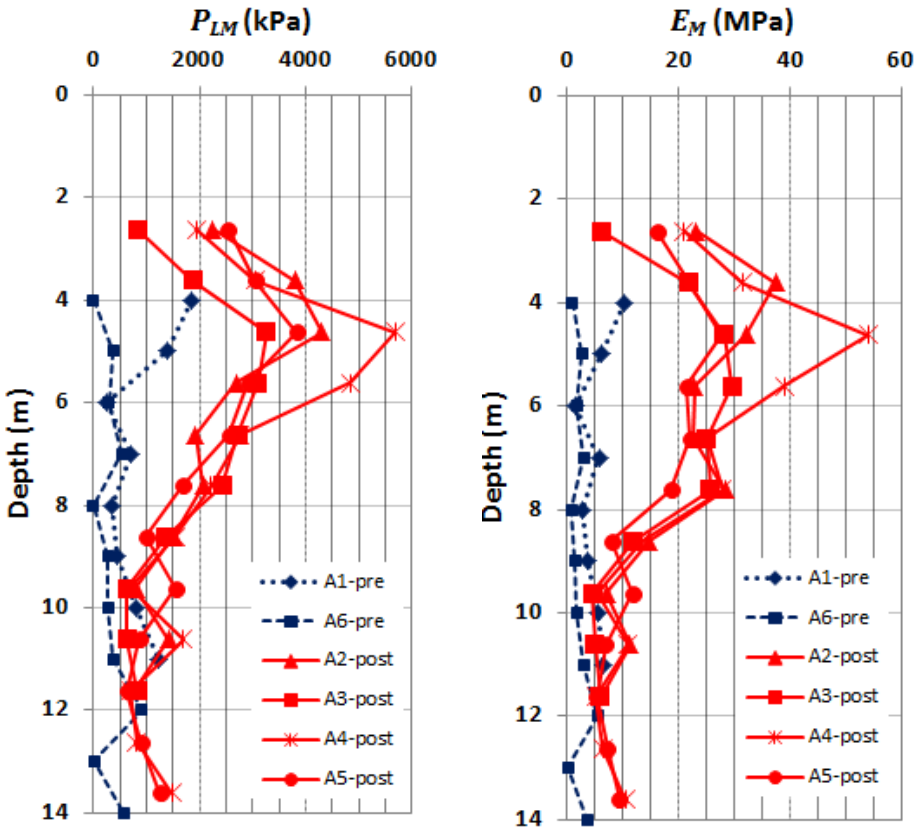

Figure 3-202: Pre and post ground improvement PMT P_{LM} and E_M values

Figure 3-203 shows the average P_{LM} and E_M improvement ratios. It can be seen that while the lower bound of improvement ratio at depths of 4 to 8 m is about 4 to 5, which is compatible with the upper bound values suggested by Lukas (1986), upper bound values are quite higher and in the range of 10 to 18.

Bearing capacity can be calculated by using Equation 2-168. The geometric mean of the average of the 4 post ground improvement PMTs is 1,684 kPa. Conservatively assuming that the deeper layers also have the same geometric value and that the foundation is on ground level, with k=0.8 and safety factor= 3, the allowable bearing capacity can be calculated to be 449 kPa, which is more than the required 160 kPa.

Although it could have been possible to calculate the tank settlements using hand calculations, it was decided to study the total and differential settlements by using finite element analysis. Therefore, a three dimensional model consisting of 41,920 elements and 45,979 nodes was realised (refer to Figure 3-204(a)). Loads consisted of the weight of tank and concrete raft that were assumed to be about 1800 kN and a uniform pressure of 63.8 kN/m² on the raft that represented 6.5 m of water height in the tank.

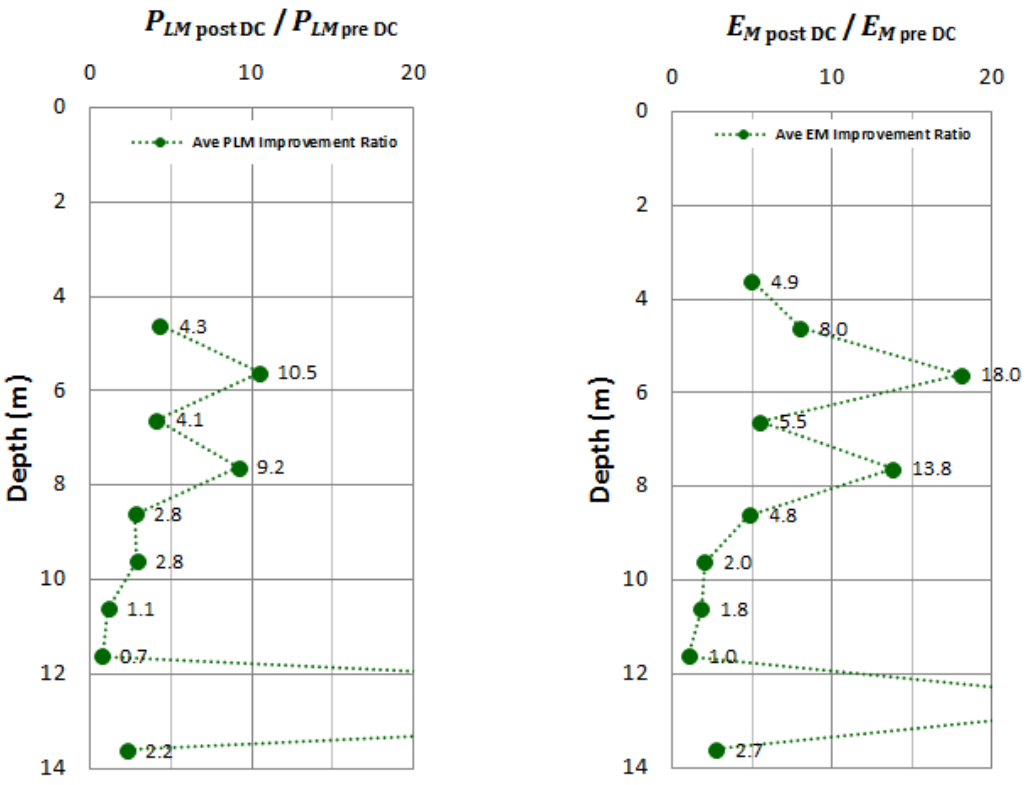

Figure 3-203: Average P_{LM} and E_M improvement ratios

The model was developed in half space due to symmetry. In this model the tank was placed on a 0.5 m thick concrete raft and two layers of sand of which the upper layer had higher values for its geotechnical parameters. Also, in order to assess differential settlements, the ground in the model was made more stiff on one side of the tank by assuming that the thickness of the upper and lower sand layers in the left and right sides of the tank were respectively 7.5 m and 3.5 m. On the right side, the upper and lower sand layers were respectively assumed to be 6.5 m and 6.5 m. An enlarged image of the model is shown in Figure 3-204(b).

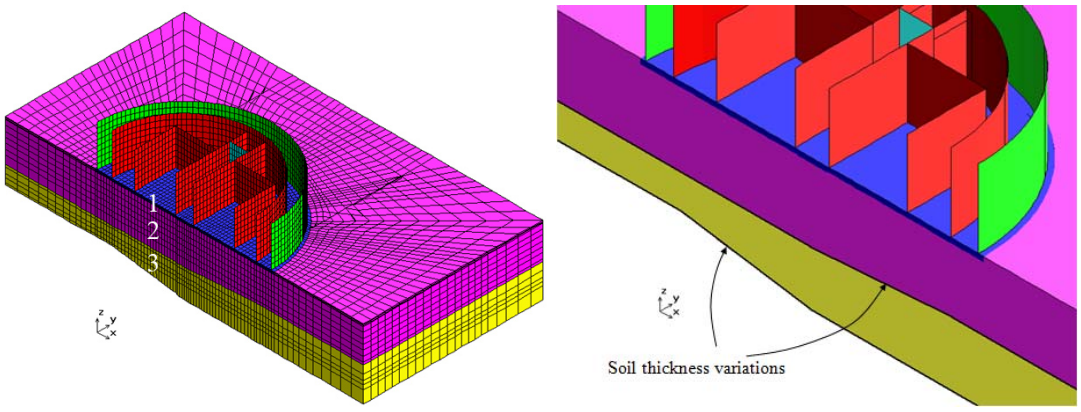

(a) **(b)**

Figure 3-204: (a) Finite element model, (b) zoom of model details

The principal characteristics of the material (see Figure 3-204(a)) and dimensions for the model are shown in Table 3-20.

Material ID	1	2	3
E_y (MPa)	11 000	59.7	22.5
Thickness (m)	0.50	6.5 – 7.5	3.5 - 6.5

Table 3-20: The principal characteristics and dimensions for the model

The result of the finite element analysis is shown in Figure 3-205 and Figure 3-206. As can be observed the maximum settlement at the tank's centre was calculated to be 21.35 mm. Minimum tank settlement at the shell was 10.91 mm. Thus, differential settlement over the radial length of 17.55 m was 10.44 mm or less than 1/1,681, which was much smaller than the allowed value of 1/750. Differential settlement from one side to the other side of the tank can be calculated to be 3.13 mm or less than 1/11,200.

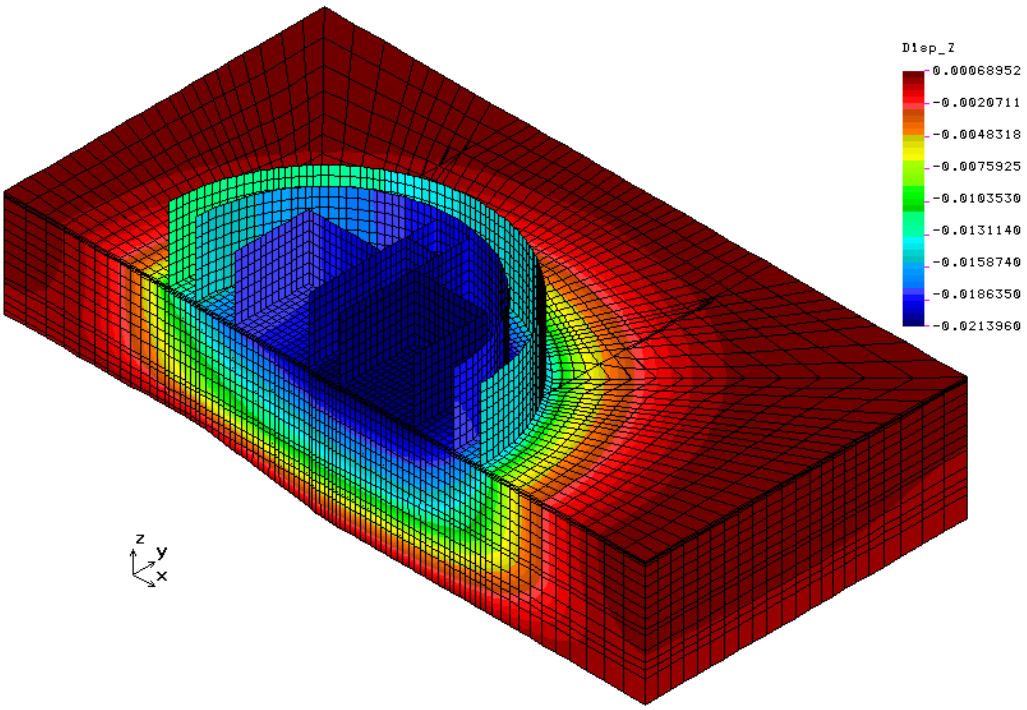

Figure 3-205: Settlement contours

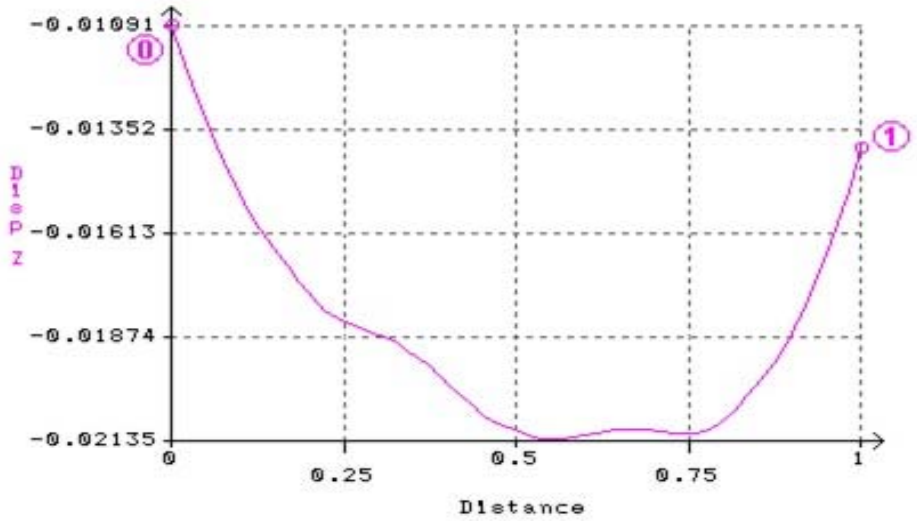

Figure 3-206: Settlement variation under Tank A-A

3.12.6 Ground Improvement in Lot G-G & Verification of Results

Based on the general understanding of the project and the experience gained in Lot A-A, similar works were carried out in Lot G-G. Here, only a summary of Tank G-G will be presented as the results are very similar to what has been already reported in Lot A-A.

Geotechnical tests comprising of 5 SPTs and 3 PMTs were carried out before ground improvement. SPTs were carried out from the depth of 4 m. The soil was identified to be loose to medium dense sand with blow counts in the range of 6 to 16 down to depths of about 9 to 12 m. The sand then became denser with blow counts falling within the range of about 16 to 40. Fines content ranged from 5 to 25% and with an average of 13%, indicating that the soil in this Lot contained lesser fines than Lot A-A.

P_{LM} from the depth of 4 to 13 m ranged from as low as 100 kPa to 1,500 kPa. P_{LM} and E_M are shown in Figure 3-208.

Once the ground conditions were confirmed, the surcharge was placed in the same manner as has already been explained for Lot A-A. However, in this Lot, the surcharge was placed over a longer period due to logistics difficulties, and only 5 cycles of dynamic surcharging was performed. The static and dynamic settlements are shown in Figure 3-207. It can be observed that the magnitudes of both static and dynamic settlements are larger in Tank G-G. The ratios between last measured static settlements and final settlements were from 1.3 to 3 that are less than both the maximum and minimum ratios of Tank A-A.

After removal of surcharge and excavation to platform level dynamic compaction was carried out. Settlement induced by dynamic compaction in the foundation of Tank G-G was 0.64 m, which is very similar to the 0.68 m figure of Tank A-A. Post ground improvement PMT results are shown in Figure 3-208.

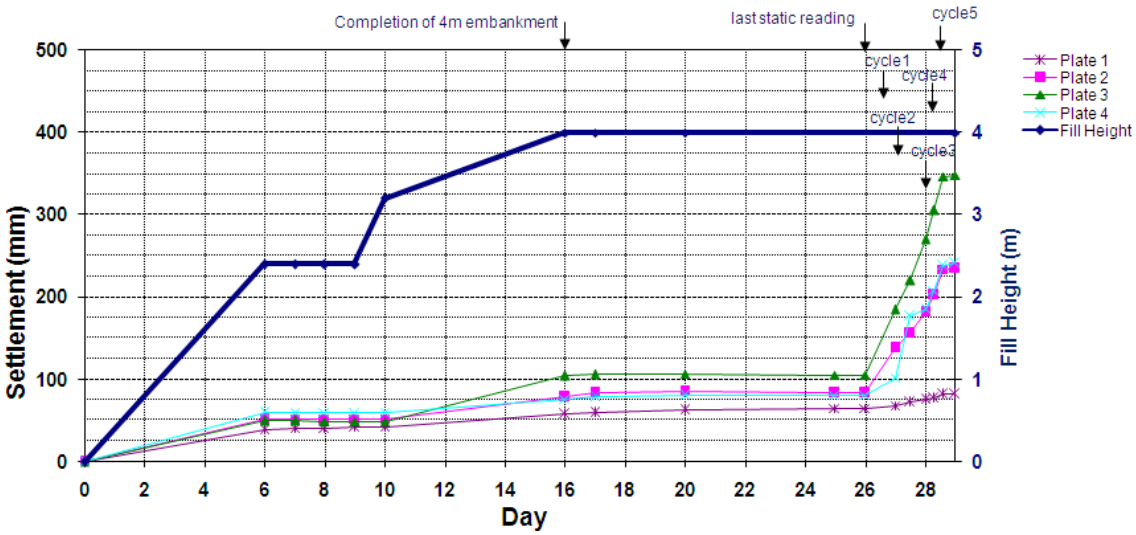

Figure 3-207: Ground settlement in Tank G-G during static and dynamic surcharging

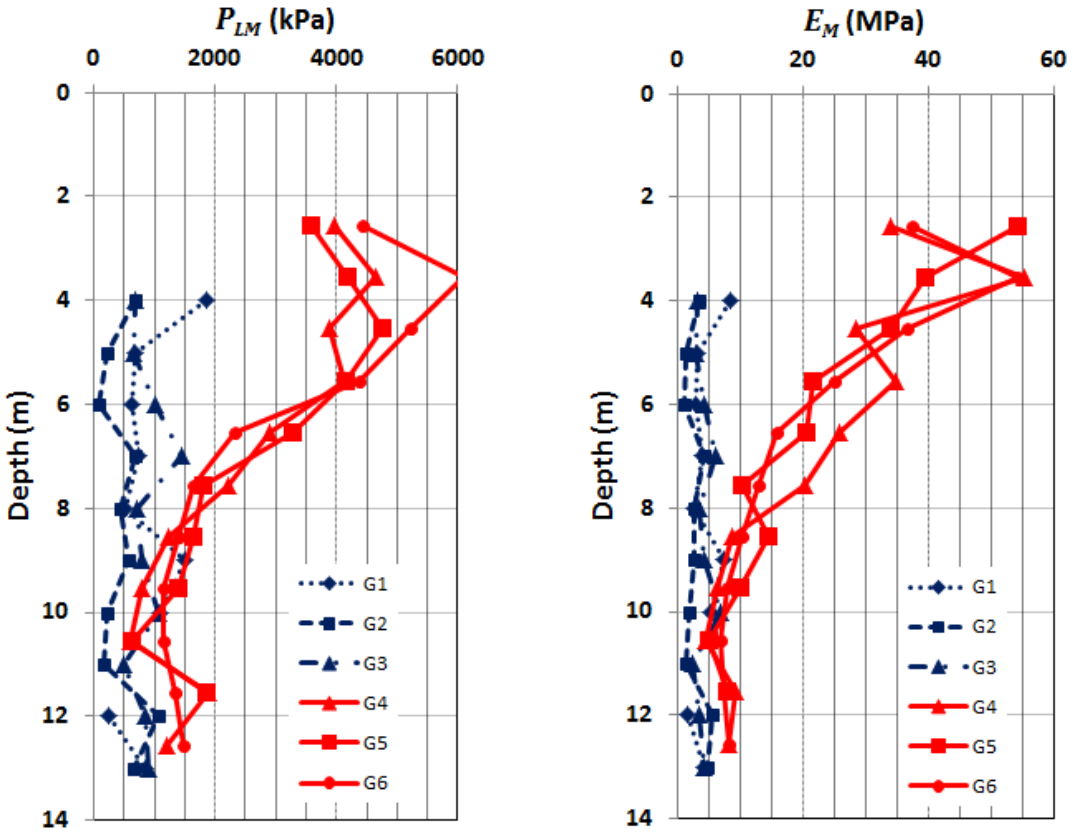

Figure 3-208: Pre and post ground improvement PMT P_{LM} and E_M values

Similar to Tank A-A, the ground in this Lot also had the most amount of improvement down to depths of about 8 to 9 m; however, improvement is observable and rather uniform throughout the remainder of the testing depth. The deeper layers may have improved uniformly due to the effects of dynamic surcharging. As can be seen, P_{LM} and E_M values have improved rather similarl to Lot A-A whereas they are respectively from approximately 2 to 5 MPa and from 15 to 50 MPa at depths of about 3.5 to 7.5 m.

The geometric mean of the average P_{LM} of the 3 post ground improvement PMT is 2,199 kPa, which is 30% higher than the geometric mean of Tank A-A, and bearing capacity criterion can be deemed to have been satisfied without further calculation.

Finite element for the calculation of Tank G-G was also done using the same principles as Tank A-A; however, in this tank the upper and lower sand layers were assumed to be respectively 5 m and 6 m with equal thickness throughout the treatment zone. Here, E_y for the upper and lower sand layers were assumed to be respectively 69.6 MPa and 24 MPa. As shown in Figure 3-209, maximum settlement in the centre of the tank was 18.39 mm. Shell settlement was calculated to be 11.61 mm; thus differential settlement from the centre to the shell of the tank can be calculated to be 1/5,177 that is much less than 1/750.

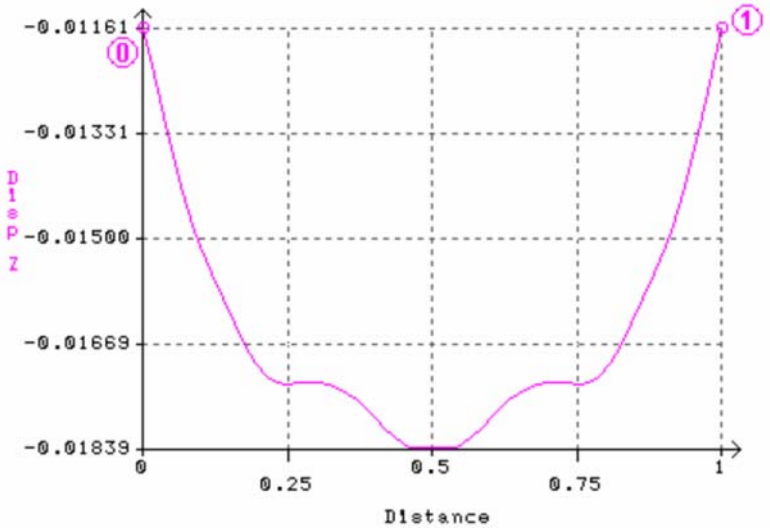

Figure 3-209: Settlement profile under Tank G-G

3.12.7 Lessons and Conclusion

This project has been able to demonstrate the effectiveness of combining two techniques; i.e., dynamic surcharging and dynamic compaction, to improve the ground and achieve results that would have been otherwise infeasible with the available equipment.

Dynamic surcharging was able to induce additional settlement compared to what was realised under static loading conditions. This has not only shown the value of dynamic surcharging for increasing induced settlements and reducing soil porosity, but is also a reminder that even if settlements are acceptable under static loading conditions, vibration of the ground due to earthquakes or any other sources can generate more settlement.

Some lessons that can be concluded from this project include:

1. Dynamic surcharging can be used to increase induced foundation settlement under static surcharge by 1.3 to 5 times, depending on the distance from the pounder impact point, to treat siltier material that would normally not be treatable by dynamic compaction, and to increase the depth of treatment.

2. Although the settlement magnitude of dynamic compaction was much more than dynamic surcharging, the latter has induced critical settlement at depths that were treated less effectively with the allocated pounder.

3. Equation 3-11 was able to estimate the compaction volume in this project the equation equaled 2.26; i.e., when $\sqrt{V}/D_c = 2.26$. The upper and lower bound values of 2.15 and 2.75 in Equation 3-11 resulted in 15% underestimation and 40% overestimation. $\sqrt{V}/D_c = 2.5$ will result in 16% overestimation in this case.

4. It may be possible to make a first estimation or at least a rule of thumb estimation of the induced strain in the treated sand using crater depth.

5. Excluding the highest values, average P_{LM} and E_M respectively ranged from approximately 20 to 40 MPa and from 23 to 30 MPa at depths of about 4 m to 8 m. These values are significantly higher than what has been suggested by Lukas (1986).

6. Due to the combination of dynamic surcharging and pre-excavated dynamic compaction with high number of blows improvement can still be observed at greater depths.

7. Maximum improvement ratios were in the range of 10 to 18 that are significantly higher than the range that has been suggested by Lukas (1986).

Figure 3-210 shows Tank A-A after construction.

Figure 3-210: Tank A-A after construction

3.13 Al Khaleej Raw Sugar Silos

3.13.1 Introduction

Al Khaleej Sugar Factory is located on the southern coast of the Persian Gulf in Jebel Ali Free Zone, Dubai, UAE (see Figure 3-211). As part of the company's development programme, it was decided to construct two identical 72 m high reinforced concrete sugar silos, each 34 m in diameter and 3.5 m apart from one another.

Figure 3-211: Satellite image of location of Al Khaleej Sugar Factory

3.13.2 Ground conditions

The geotechnical investigation report indicated that ground level on site was variable from +4.2 to +4.8 m RL (reduced level). Mean High High Water (MHHW) and Mean Low Low Water (MLLW) were respectively at +1.7 m and +0.5 m RL, indicating a relatively high groundwater level at all times.

As part of the soil investigation, six boreholes were drilled and SPTs were carried out in them. These boreholes indicated that the first layer of soil, extending down to approximately +2 m RL, was loose to medium dense silty fine sand fill. Occasional high fines content in this layer suggested the presence of bands or pockets of silts and clay. The top soil layer was followed by 4 m of medium dense to dense slightly silty sand that terminated at -2 m RL. Fines content in this layer was less than 20%.

The subsequent layer was 6 m of weak sandstone or cemented sand extending down to approximately -8 m RL. Then, a very weak to weak layer of sandstone that was 4 m thick and extended to -12 m RL was encountered. The next layer that was only 1 m thick and

terminated at -13 m RL was very weak to very stiff calcisilite. Then, very weak calcisiltite or conglomerate, 4 m thick, and extending down to -17 m RL was identified. Finally, weak to moderately weak calcisiltite or conglomerate was observed down to the end of boring at -35 m RL. Ground layers and their assumed design properties are summarised in Table 3-21.

Layer No.	Level (m RL)	Description	E_y (MPa)	ν
1*	ground level to +2.5	Loose to medium dense silty, fine sand fill with silts and clay	25	
2	+2.5 to –2	Medium dense to dense slightly silty sand	25	0.25
3	-2 to –8	Weak sandstone or cemented sands	540	0.3
4a	-8 to –12	Very weak to weak sandstone	132	0.3
4b	-12 to –13	Very weak to very stiff calcisilite	132	0.3
4c	-13 to –17	weak calcisiltite or conglomerate	132	0.35
5	-17 to –35	weak to moderately weak calcisiltite or conglomerate	360	0.35
6	+2.5 to +0.5	shear ring, crushed stone	-	

* Later removed

Table 3-21: Ground layers and E_y values before ground improvement

Calculations showed that due to the presence of the superficial loose layers of soil, it was not possible to construct the silos without the implementation of specific geotechnical solutions.

3.13.3 The Foundation Solution: Dynamic Replacement

Preliminary studies suggested that safe foundations for the silos could be provided by using piles and concrete rafts. Depending on the design pile diameter, pile lengths were calculated to be from 29 to 37 m.

Although piles and raft footings were technically acceptable solutions, the cost of installing long piles in rock was estimated to be very high, and the project engineers began considering the option of ground improvement. Thus, several specialist contractors were approached, and subsequently a design and construct contract was awarded to the company that had proposed the implementation of dynamic replacement at approximately one fifth of the price of piling.

As shown in Figure 3-212, in order to optimise the ground improvement solution, the geometry of the project was reviewed, and silo dimensions and distances were revised. In the new design silo heights were reduced to 55 m, diameters were increased to 40 m, and the distance between the silos was increased to 25 m to reduce the side loading effect of one silo on the other.

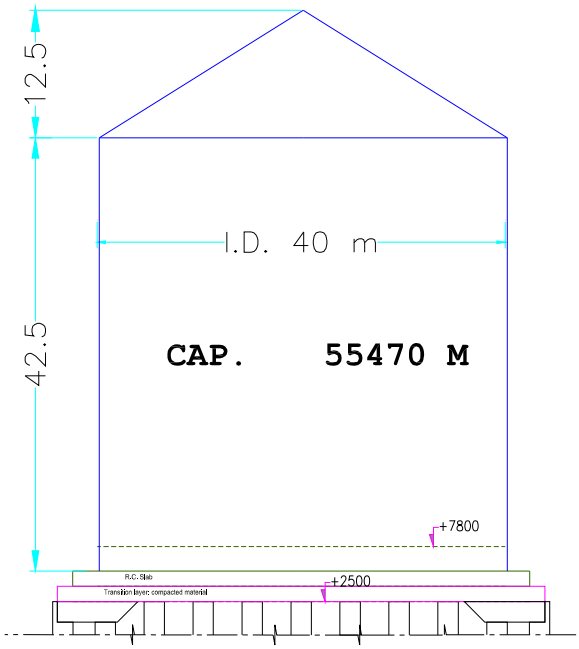

Figure 3-212: Schematic cross section of the sugar silos

Description	1 Load transfer platform	2 Compacted Sand	3 Rock	4 Weaker Rock	5 Substratum	6 Replacement
Thickness (m)	1.50	4.00	6.00	9.00	13.00	2.00
First loading E_y (MPa)	80	60	540	132	360	100
Reloading E_y (MPa)	104	78	700	264	720	130
Cohesion (kPa)	0	0	0	0	0	0
Friction angle (°)	35	38	40	40	40	40
Unit weight (kN/m^3)	18	18	18	18	18	18

Table 3-22: Design parameters for numerical analyses

The concept of applying dynamic replacement was realised based on excavating the unsuitable man-made top soil layer down to working platform level at +2.5 m RL, carrying out ground treatment and improving the properties of the sandy layer down to -2 m RL and finally constructing an engineered fill from finished soil improvement level to bottom of raft level. The ground improvement concept was based on application of dynamic compaction for compacting the sandy layer and reinforcing it with crushed stone inclusions that were backfilled into excavated pits within the tank area, and installing a crushed stone shear ring trench for supporting the shell. The depth of the ring was assumed to be 2 m. Top and bottom widths of the trench were designed to be respectively 8 and 6 m. Design parameters that were used in the numerical analyses of Figure 3-213 using finite element software are presented in Table 3-22.

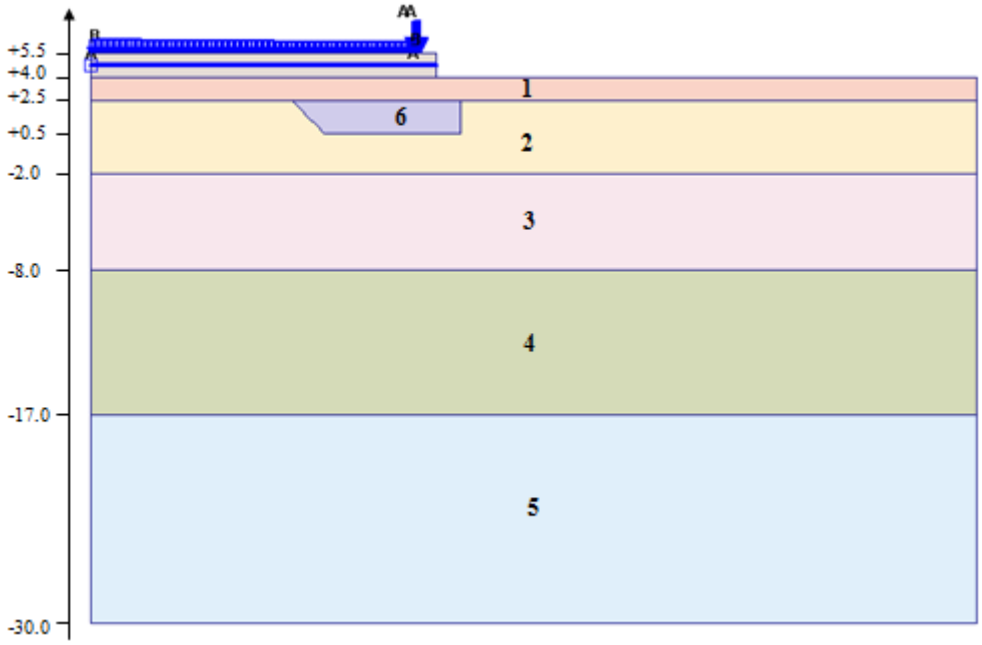

Figure 3-213: Model used for the numerical analysis of the sugar silo

In the numerical analyses the thickness and unit weight of the raft were respectively assumed to be 1.5 m and 25 kN/m^3. The 0.45 m thick shell was modelled by a 1,222 kPa load spread over the shell thickness, and an additional 25 kPa of uniform load was used to model the tunnel and slab below the raft. Sugar heights in the centre and at the shell were assumed to be respectively 52.7 m and 40.2 m, and unit weight of sugar was taken as 9 kN/m^3. The Sugar's dynamic load during the unloading phase was taken as 2,444 kPa spread over the wall and with a reduction factor of 2 with consideration of the dynamic modulus of soil being higher than the static modulus.

In the calculations 3 load cases were analysed; i.e., after construction (empty silo), after full loading and upon unloading (inclusive of sugar dynamic loading). Vertical displacements for these load cases are shown in Figure 3-214 to Figure 3-216.

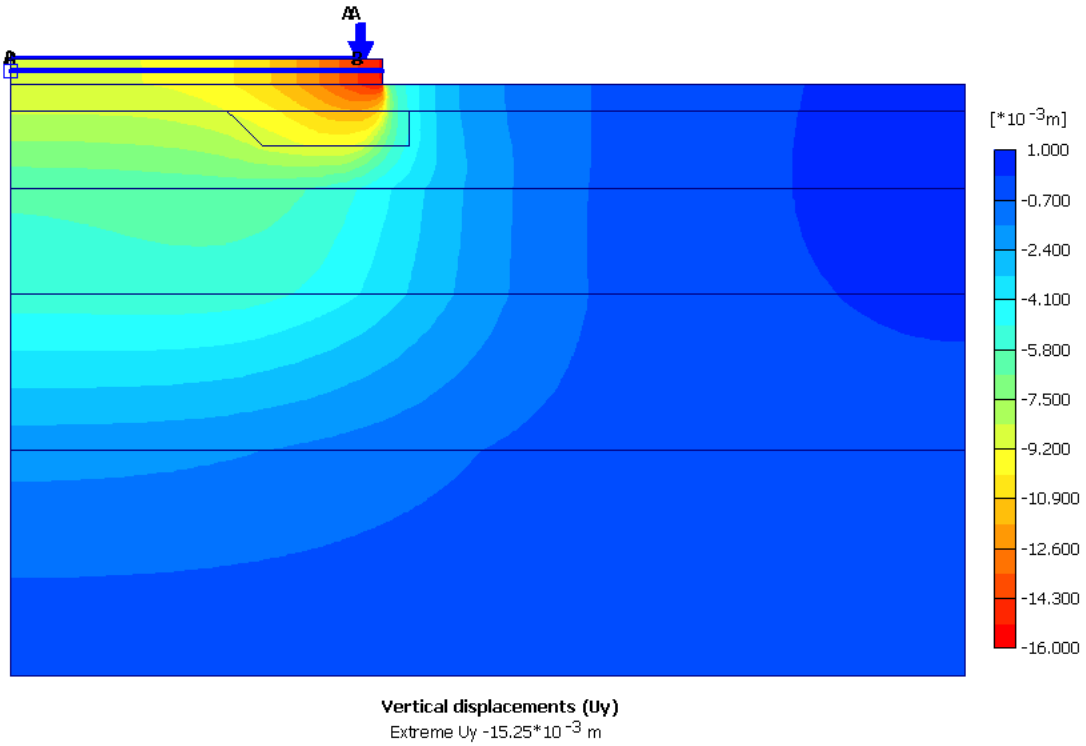

Figure 3-214: Total settlement after construction

Vertical displacements along the ground surface of the model are plotted in Figure 3-217. As can be seen, calculations showed that maximum settlement of approximately 71 mm was realised in the centre of the silo when it was fully loaded. While it was calculated that maximum settlement would increase negligibly to 71.5 mm in the centre at the beginning of sugar unloading, it can be observed that settlement at the shell increases by about 70% during that phase. It can also be seen that the effect of one silo loading on the other is negligible at 25 m.

The finite element analysis also showed that approximately 70% of the ground settlements were due to the compression of the engineered fill and the improved ground below it.

Figure 3-218 to Figure 3-220 show horizontal stresses (tensile stresses are positive) in the concrete raft. The values in the boxes are the maximum tensile stresses. It can be seen that the maximum tensile stresses reach 1.8 MPa, and occur on the top fibre of the concrete raft.

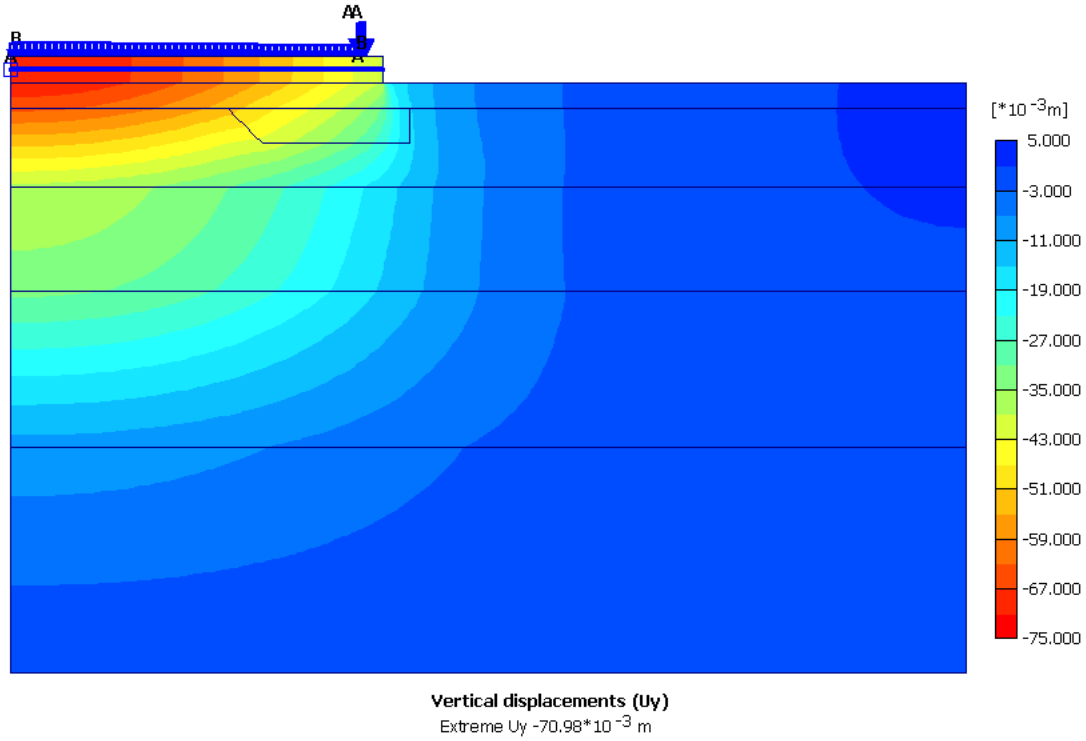

Figure 3-215: Total settlement after first loading

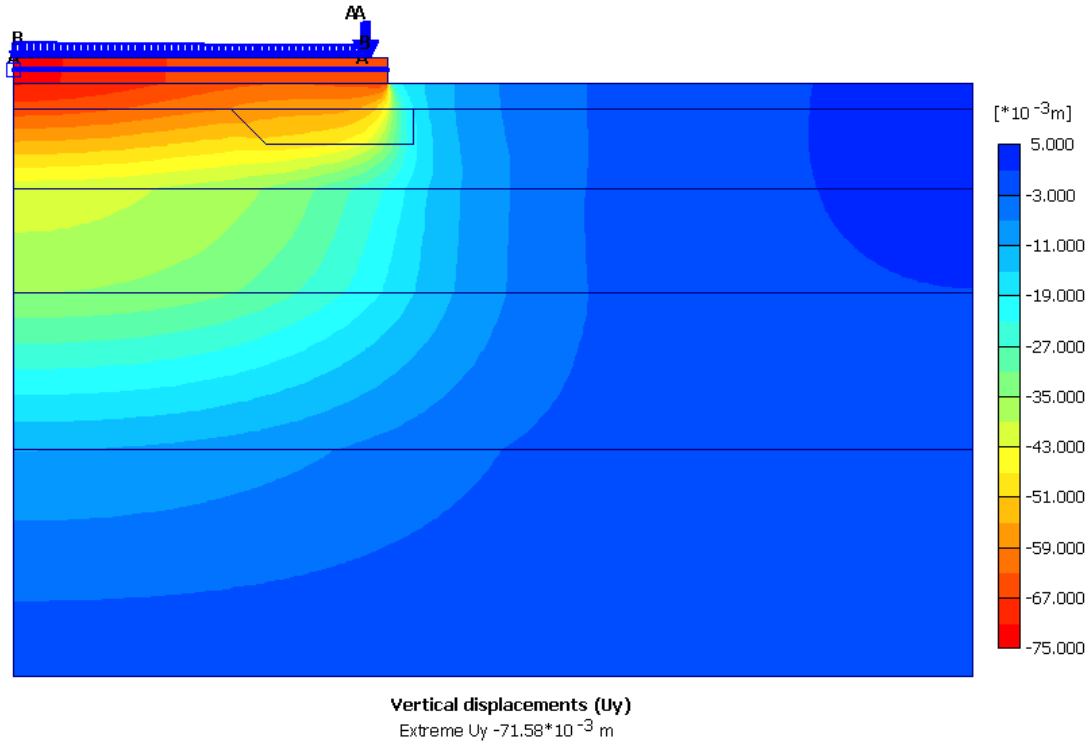

Figure 3-216: Total settlement after beginning of first unloading

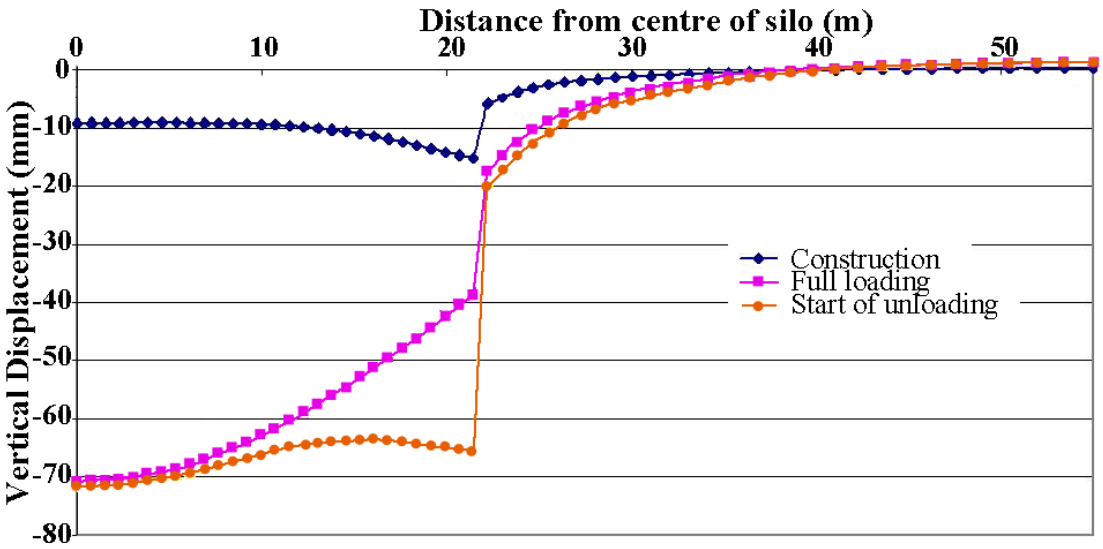

Figure 3-217: Vertical displacement of the ground due to different load cases

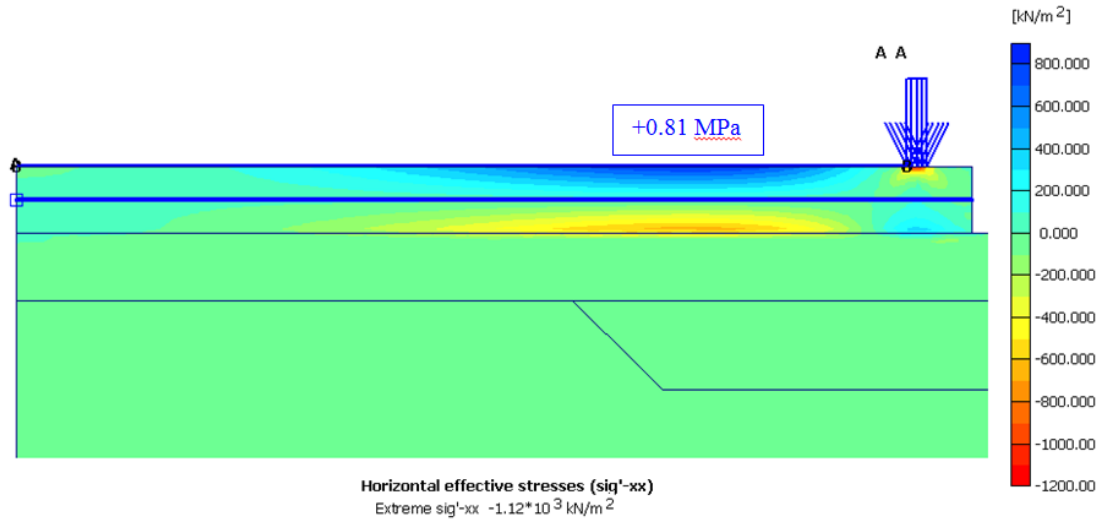

Figure 3-218: Maximum horizontal stresses after construction

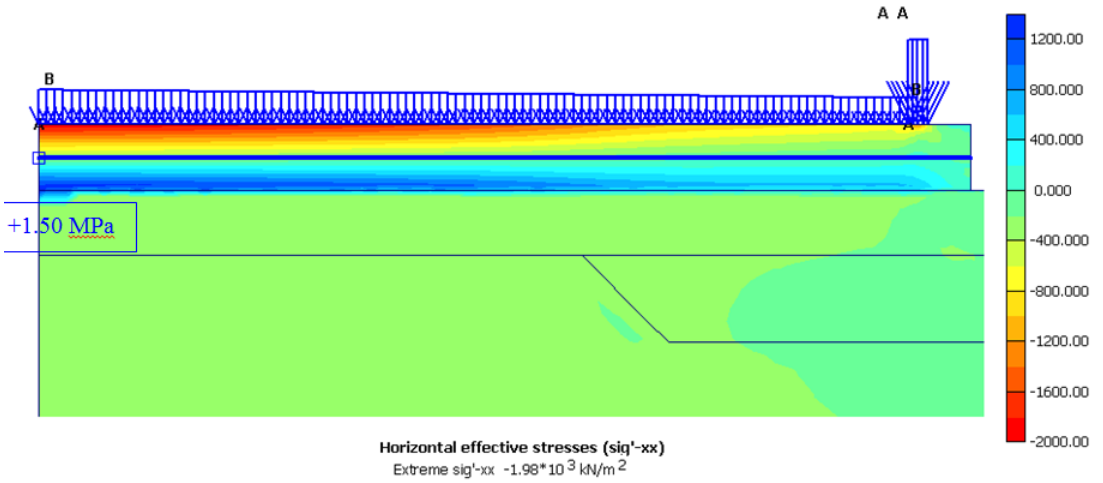

Figure 3-219: Maximum horizontal stresses after first loading

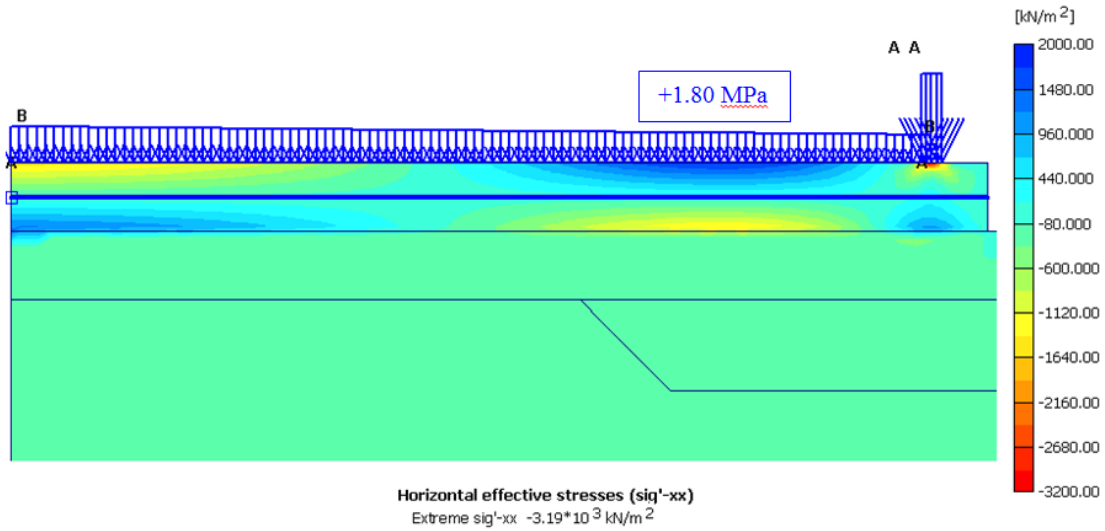

Figure 3-220: Maximum horizontal stresses after beginning of first unloading

A similar set of calculations were also undertaken for the reloading of the silo using the reload moduli that have been presented in Table 3-22. Figure 3-221 shows that the maximum displacement is 46 mm during reloading. Similarly, the maximum tensile stresses after unloading with reload moduli will reach 2.3 MPa on the top fibre of the concrete raft due to the dynamic effect of unloading.

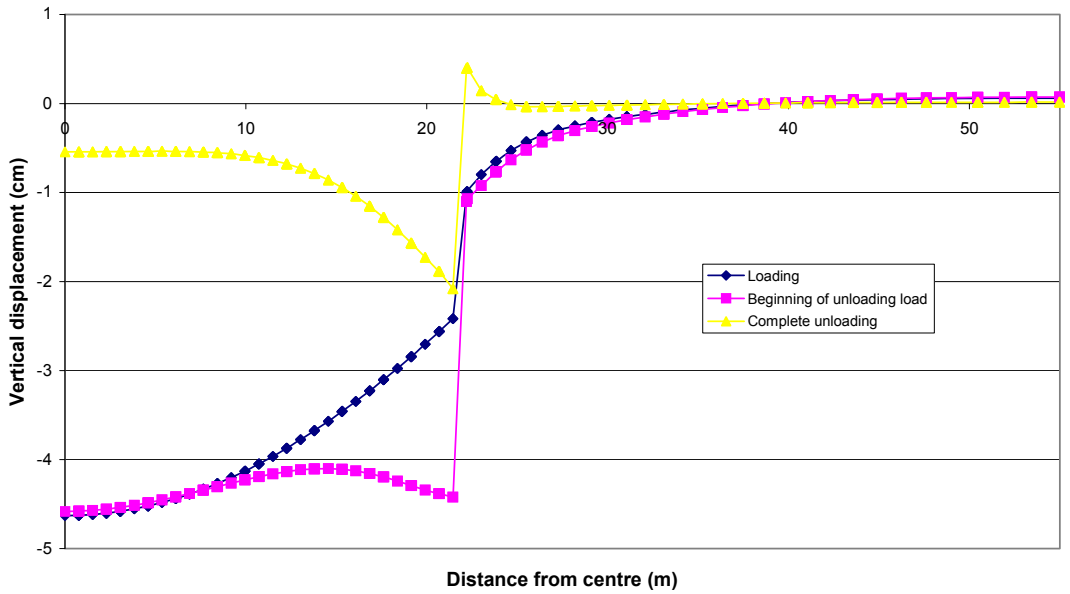

Figure 3-221: Vertical displacement of the ground due to different reloading cases

The curves of Figure 3-222 allow the assessment of the behaviour of the soil under the cyclic loadings. The last curve corresponds to the vertical displacements of complete unloading with reload moduli minus beginning of unloading with reload moduli plus beginning of first unloading with initial moduli. These curves show that maximum differential settlement

occurs during the first loading and is equal to approximately 1/500. During complete unloading, differential settlement does not exceed 0.94/1000.

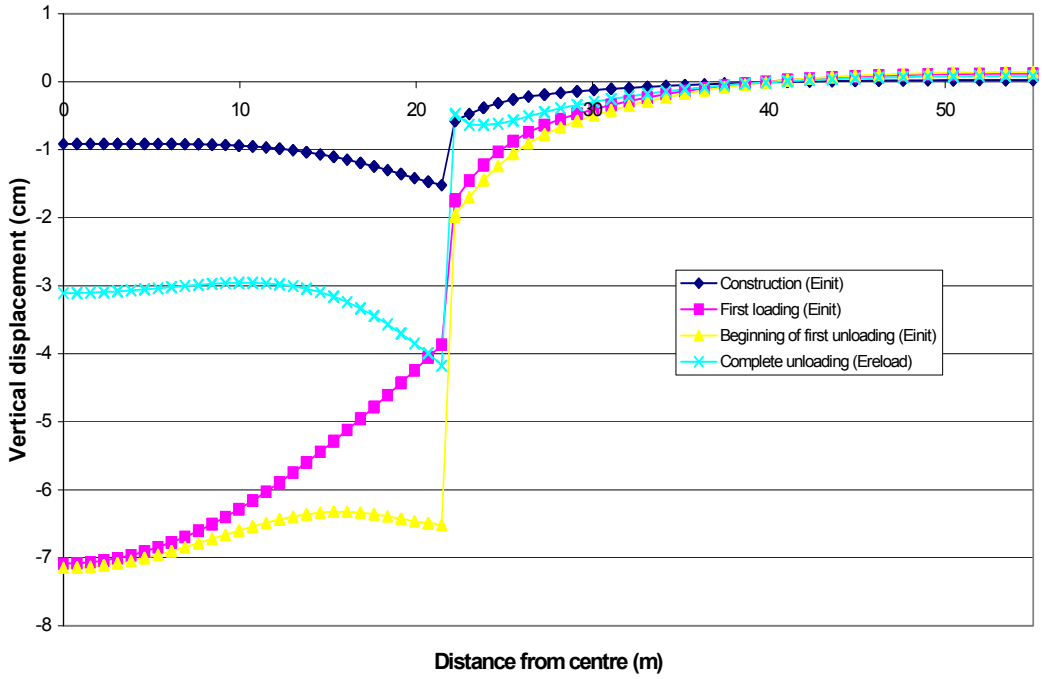

Figure 3-222: Vertical displacement of the ground due to different loading and reloading cases

Taking into consideration the ground deformation shapes and the bending moments that would be realised in the reinforced concrete raft, the application of dynamic replacement was approved with target values of E_y being 60 MPa and 100 MPa respectively under the silo and the shell.

In practice, the location of the DR columns in each silo was excavated and backfilled with crushed stone with a replacement ratio of 13% using a grid that was approximately 4.9x4.9 m^2. On average, each print was subjected to 12 blows. Dynamic compaction of the shear ring is shown in Figure 3-223.

The presence of an already existing concrete silo at a minimum distance of 10 m from the dynamic replacement works (see Figure 3-224) presented a challenge as it was expected that at such distances peak particle velocity would exceed what is recommended by USBM (Siskind et al., 1980). When distances were at a minimum a constant dilapidation survey was performed during dynamic compaction, to observe the behaviour of the existing silo, and if necessary, to devise an alternative work procedure. However, the survey demonstrated that no specific procedures had to be introduced.

Figure 3-223: Dynamic compaction of the shear ring

Figure 3-224: Dynamic replacement next to an existing concrete silo

During the works it was observed that, as shown inFigure 3-225 , a very dense layer that was 0.5 to 1 m thick had capped a portion of the loose sand in the second silo. This layer damped the energy transmitted to the loose layer beneath. Hence, in this zone the pounder was dropped in total 25 to 30 times to break through the very dense layer and to achieve the desired compaction.

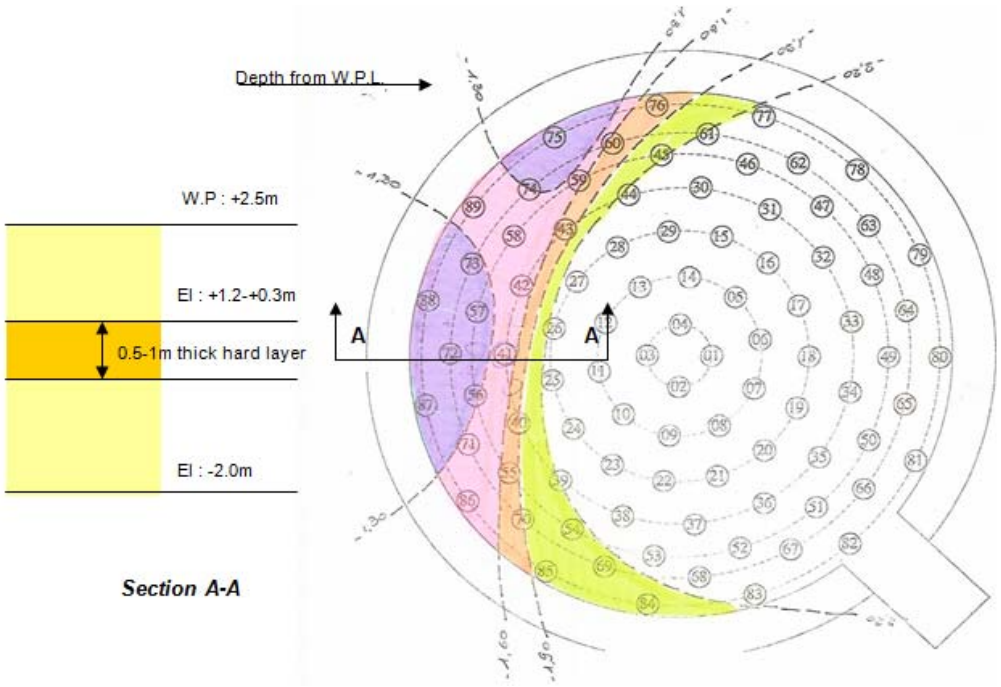

Figure 3-225: Presence of very hard damping layer

After completion of soil improvement works, at the end of dynamic replacement, the project's client and consultant decided to reduce foundation level to +2.5 m RL to eliminate the cost of constructing the engineered fill; thus calculated settlements were further reduced due to the elimination of this layer.

3.13.4 Testing and Verification

PMTs were performed inside the DR columns, in between the columns and in the shear ring trench before and after the ironing phase of dynamic replacement. The summary of test locations for the first silo has been tabulated in Table 3-23, and E_M values are shown in Figure 3-226. All tests before ironing were intended to be carried out to the depth of 4 m below working platform level; however, some tests reached refusal before that depth.

It can be understood from the PMTs that ironing has been able to increase E_M values at the depth of 1 m by 2.6 to 3.5 times. However, calculations show that it would have been possible to meet acceptance criteria even without application of the ironing phase.

The harmonic mean values of E_y for each test location can be calculated from E_M values using Equations 2-212 and 2-214 with rheological factors of 1/3 for sand and 1/4 for gravel to demonstrate that acceptance E_M values have been achieved.

PMT	Location	Time
1	in DR column	before ironing
1B	in DR column	before ironing
2	in between DR columns	before ironing
3	in between DR columns	before ironing
4	in shear trench, in DR print	before ironing
4B	in shear trench, in DR print	after ironing
5	in between DR columns	before ironing
6	in shear trench, in DR print	before ironing
6B	in shear trench, in DR print	after ironing
7	in shear trench, in between DR prints	before ironing
8	in shear trench, in between DR prints	before ironing
9	in DR column	after ironing

Table 3-23: PMT Schedule

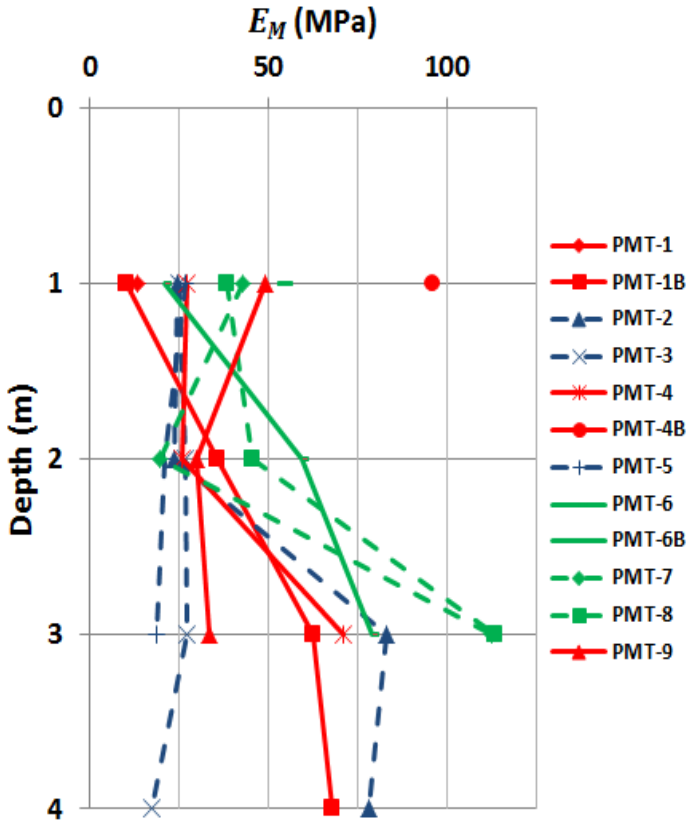

Figure 3-226: PMT modulus before and after ironing in the first silo

3.13.5 Lessons and Conclusion

In this project two sugar silos, each 55 m high, have been constructed on improved soil. This project faced numerous challenges including the very heavy loading of the silos, the insufficient distance between the silos, the presence of an existing nearby silo, a high groundwater level, and several metres of loose soil. Lessons learned in this project include:

1. By reviewing and redesigning the silos' layout, adopting appropriate design procedures and acceptance criteria, and implementing state-of-the-art ground improvement techniques it may be possible to construct very heavy structures on improved ground.

2. The mass mechanical properties of sand layers can be further improved by introducing dynamically compacted crushed stone inclusions.

3. Application of ironing phase of DC will improve the superficial ground parameters.

Figure 3-227 shows Al Khaleej raw sugar silos after completion of construction.

Figure 3-227: Al Khaleej raw sugar silos after completion of construction

3.14 Trail for Quay Expansion in Southeast Asia

3.14.1 Introduction

Recently, dynamic replacement was carried out in Southeast Asia to treat soft marine deposits more than 30 m below seawater level for the construction of a container terminal using caisson seawalls. According the original design the soft marine clay at the seabed was to be dredged to the depth of 30 m below sea level where the shear strength of the stiff clay exceeded 250 kPa. The excavated key was to be then backfilled with sand and compacted using vibro compaction under 3 m of additional overburden sand fill. Next, the surcharge had to be removed, a rubble mound was to be placed over the sand key, and as shown in Figure 3-228, caissons were to be then sunk onto the mound.

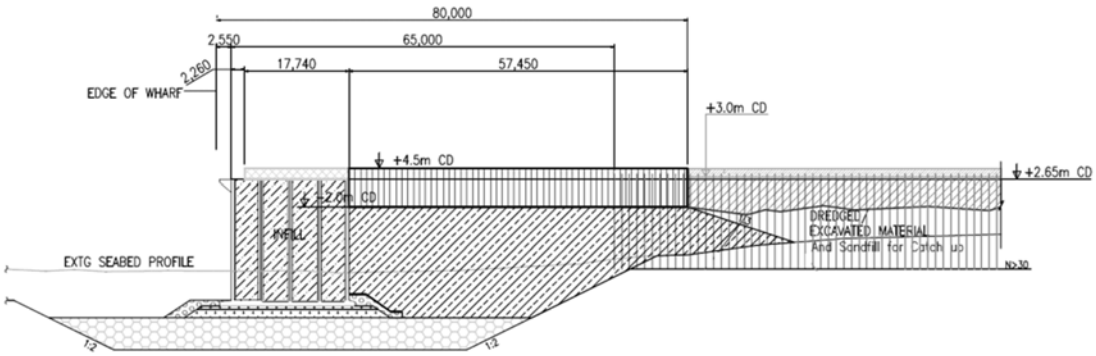

Figure 3-228: Cross section of container terminal based on original foundation concept

3.14.2 Soil Softening

As SPT blow counts exceeded 50 and the assumed clay shear strength of 250 kPa was achieved at dredge level, works progressed by backfilling sand and compacting the fill using vibro compaction.

While the clay at dredge level was initially very stiff, dredging works and cutting into the clay softened the upper 1 to 1.5 m of the exposed clay surface and post dredging CPT tests performed before the removal of the overburden sand fill indicated that the clay's shear strength had dropped to about one third of its original value; i.e., to approximately 80 kPa. PMTs carried out at later stages suggested that the shear strength had even further reduced at some points to a mere 16 kPa.

3.14.3 The Solution: Offshore Dynamic Replacement

Further dredging of the softened clay and replacing it with more sand fill did not appear to be an effective method because it was expected that this would lead to the disturbance of deeper clay layers and the persistence of the problem.

Due to the nature of the soft soil and its thickness, marine dynamic replacement was envisaged as a possible treatment solution. Based on previous experiences (refer to Section 2.10.4), it was anticipated that if proper equipment; i.e., a large stable barge, a specialised crane with a sufficiently powerful winch system for lifting a heavy pounder and resisting tidal action, and a special pounder for transmitting sufficient impact energy to the seabed were available, it would then be possible to drive granular material into the soft clay and improve its properties.

Unlike land based dynamic replacement where suitable material can be pushed into the crater by a loader, this method is not possible in offshore dynamic replacement, and material can only be punched in from the load transfer platform. Hence, a stone blanket was used to feed the DR columns and to create the load transfer platform. This layer also prevented the contamination of seawater by the flow and dispersion of suspended clay particles produced by the pounder's impacts.

In the proposed dynamic replacement methodology it was assumed that a 1.8 m thick granite rock fill layer would be placed over the soft clay layer. The blanket material was chosen in such a way that 30% of the stone diameters were from 150 to 200 mm and the remaining 70% were from 200 to 300 m. The DR rock columns were designed to be 2 m in diameter, in a 4.5 m grid and with a replacement ratio of 15%.

As shown in Figure 3-229, in this project a specially designed grater shaped marine pounder weighing 38.5 tons was used to drive the rock into the ground to form the DR columns, and to dynamically compact the rock blanket. The pounder's dimensions were 1.7 m by 1.7 m on the DR side and 2.3 m by 2.3 m on the DC side. Figure 3-230 and Figure 3-231 show the pounder being used respectively for dynamic replacement and dynamic compaction works from a barge that was 15x50 m^2 in platform area.

Previous experiences by the working team suggested that water resistance could greatly reduce the effect of significantly high drops. Hence, the drop heights during the trial were set to 5 m above seabed level. Records of the crane's winch speed during the works indicate

that the maximum drop speeds were in the order of 430 m per minute. This speed is equivalent to a free fall with a drop height of 2.6 m (in air), and verifies the original assumption that a great portion of the drops' kinematic energies would have been lost due to water resistance.

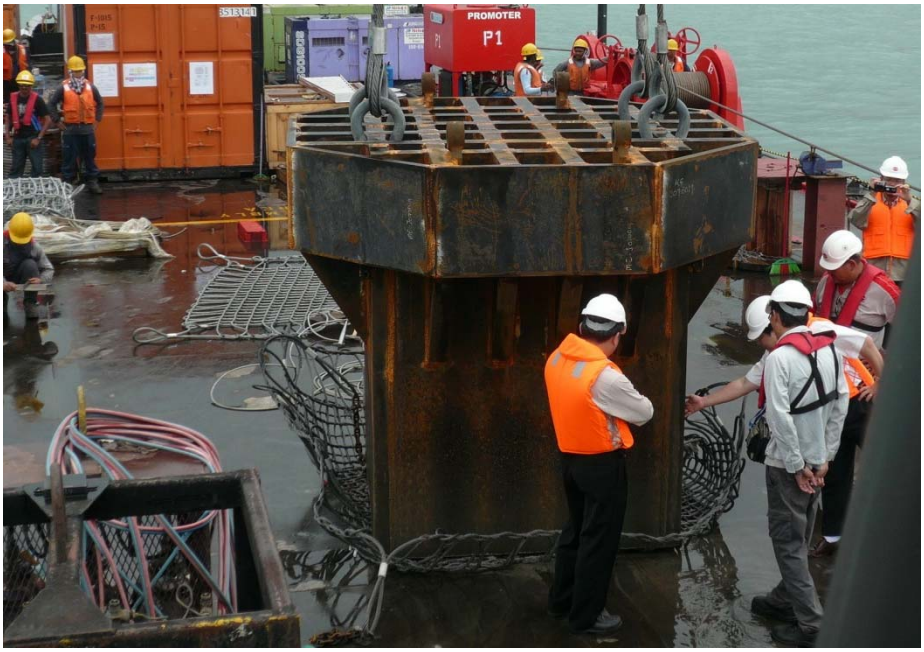

Figure 3-229: Marine DR (bottom side) - DC (top side) pounder

Figure 3-230: Marine pounder being utilised for dynamic replacement

Each dynamic replacement print location was subjected to 30 blows. Furthermore, 3 to 6 blows were applied as ironing using the larger end of the pounder. As shown in Figure 3-232 the penetration of the pounder into the ground was measured for every blow. It can be

observed that while the pounder penetrated the ground at a more pronounced rate during the first four blows, the penetration rate then rapidly decreased to the point where it appears that no penetration was practically observed after the 15th blow. The amount of pounder penetration was variable from 1.1 to 1.7 m. Comparing these figures with the thickness of the soft soil prior to dynamic replacement, it can be interpreted that the pounder impact was able to effectively drive the granular material of the blanket to the end of the soft soil layer with the first 4 to 12 blows and then to further compact the granular rock fill. It can also be observed that the maximum penetration values per print were sometimes more than the assumed soft soil layer's thickness. This indicates that either the DR columns have penetrated into the stiffer clay or that the actual soft layer's thickness was more than originally anticipated at some locations.

Figure 3-231: Marine pounder used for dynamic compaction

The total ground settlement was measured by echo sounding and the survey showed that the top of the blanket dropped by 0.38 m as a result of the ground improvement works.

3.14.4 Testing and Verification

Divers were used to visually inspect the impact results at seabed level. Based on the larger amounts of crushed rock at the DR column location, it was determined that the columns were 2.4 m in diameter, which equates to the diagonal length of the pounder's base on the DR side. It can be interpreted that the larger DR columns' diameter as compared to the pounder's base may have been formed by a combination of soft soil being pushed away

laterally due to the high horizontal stresses exceeding the soil's strength at impact location and possible rotations of the pounder during the impacts (although the latter is less likely due to the implementation of synchronised double winches in the drop mechanism). Thus, the actual DR replacement ratio was 22.3% in lieu of the originally assumed 15%. Target rock friction angle was 45 degrees.

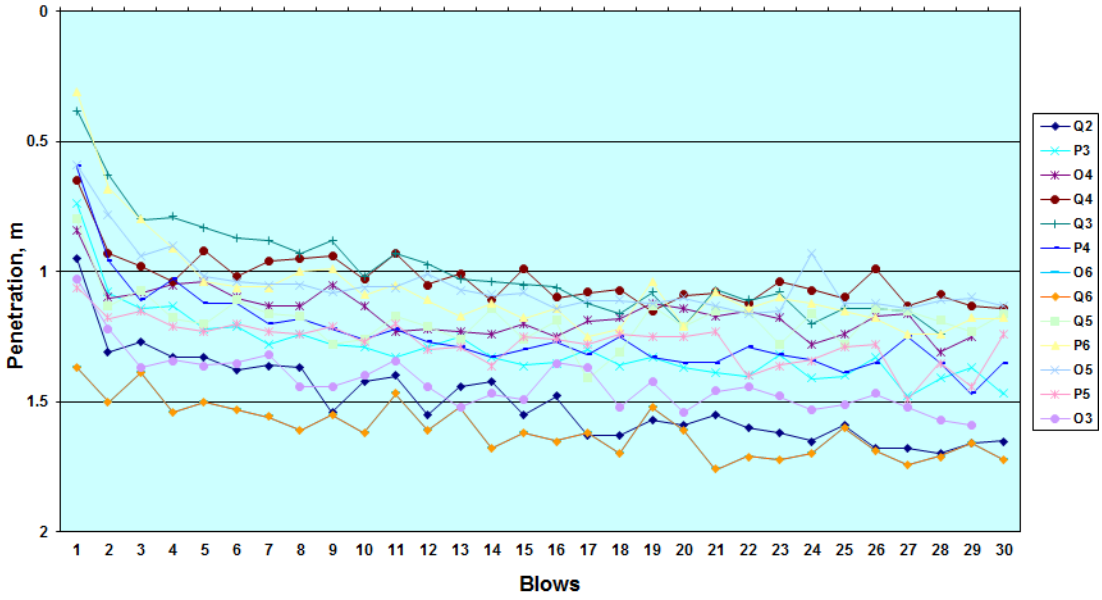

Figure 3-232: Pounder penetration at several DR print locations

Due to the large water depths and open sea working conditions 63 mm slotted casing PMTs were carried out using 100 mm guide tubes followed by the 60 mm PMT tube. During testing visual observation on the return of drilling fluid was recorded. No return of drilling fluid indicated that the test was carried out in the free-draining rock material whereas testing in impervious clay was identified by the return of the drilling fluid.

Figure 3-233 shows the trial zone and PMT locations. Two PMTs (Pre-2 and Pre-8) were carried out prior to dynamic replacement and six (Post-2, 2a, 2b, 2c, 8 and 9) were carried out after treatment. E_M and P_{LM} before and after treatment values are tabulated in Table 3-24. It can be observed that Post-8 registered a non-yielding curve with a high value of P_{LM}, probably due to a localised closer matrix of rock pieces in the vicinity of the slotted casing, and as such, was deemed as non-representative and excluded.

The comparison of PMT Pre-2 and Post-2a that were done in the almost same location indicates that while the rock fill has been driven into the soft clay, its E_M and P_{LM} values have also increased respectively by 118% and 132%. The average values of E_M and P_{LM} after improvement were respectively 8.05 MPa and 1.40 MPa. The maximum P_{LM} that was

recorded during the test exceeded 2.2 MPa. It can also be calculated that the harmonic mean of E_M in the rock fill after improvement is equal to 6.03 MPa.

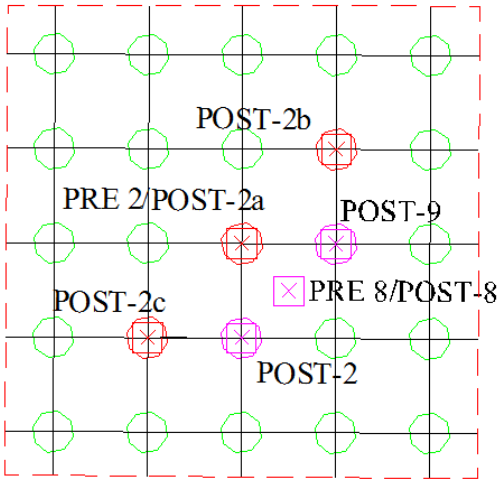

Figure 3-233: Trial zone and PMT locations

Test No.	Depth (m)	E_M (MPa)	P_{LM} (MPa)	Comment
Pre-2	-29.1	1.63	0.34	rock fill
	-29.9	0.17	0.09	clay
Pre-8	-28.7	3.75	0.63	rock fill
	-29.9	11.34	1.44	clay
Post-2a	-29.2	3.56	0.79	rock fill
	-30.0	6.34	1.17	rock fill
Post-2b	-29.1	22.22	2.82	rock fill
Post-2c	-29.1	6.86	1.32	rock fill
	-29.9	2.64	0.78	rock fill
	-30.7	7.98	1.40	rock fill
Post-2	-29.3	7.04	0.99	rock fill
	-30.2	7.34	1.63	rock fill
Post-9	-29.0	9.13	1.36	rock fill
	-29.8	7.37	1.78	rock fill

Table 3-24: Pre-treatment and post treatment PMT results

The Young modulus of the clay and rock fill can also be calculated using Equation 2-214 with α equal to 1/4 for rock fill and 1/2 for altered clay.

The shear strength parameters can also be estimated from the pressuremeter test using Equation 2-222; however, Equation 2-224 or 2-225 have been proposed for estimation of

drained friction angle of sands, and it is the experience of the author that their application will underestimate the friction angle in rock fill. As shown in Figure 3-234, during the project Yee and Varaksin proposed to extend Menard's line (see Figure 2-168) to φ = 38° and 40° (presumably the indicative φ angle for uncompacted crushed rock), suggested that the relationship lies within this range, and proposed[2] Equation 2-224:

$$P^*_{LM} = 4 \times 2^{\frac{\varphi - 40}{7}} \qquad 3\text{-}12$$

Based on these values presented, a finite element model can be constructed with the parameters of Table 3-25.

Layer	elevation below seabed level (m)	E_M (MPa)	c (kPa)	φ°
rock fill	0 to -1.3	24.1	0	49
composite	-1.3 to -2.8	18.7	12	47

Table 3-25: Equivalent parameters for finite element model

3.14.5 Lessons and Conclusion

The offshore dynamic replacement trial has demonstrated that it is possible to perform this technique and to verify the results by implementing the pressuremeter test at depths of 30 m. Test results can be used for constructing suitable models for required analyses.

Specific lessons and conclusions for this project can be summarised as:

1. The barge must be large enough to safely support the personnel and equipment. The barge size will be influenced by the location of the project and the sea conditions.

2. Water resistance reduces the pounder's dropping velocity, and consequently the impact energy.

[2] The author has previously published a paper (Hamidi, B., Yee, K., Varaksin, S., Nikraz, H. & Wong, L. T. (2010) Ground Improvement in Deep Waters Using Dynamic Replacement. *20th International Offshore and Polar Engineering Conference*, Beijing, 20-26 June, 848-853) in which Equation Equation 2-224 has been mistyped, and appears in the corrected form in this thesis.

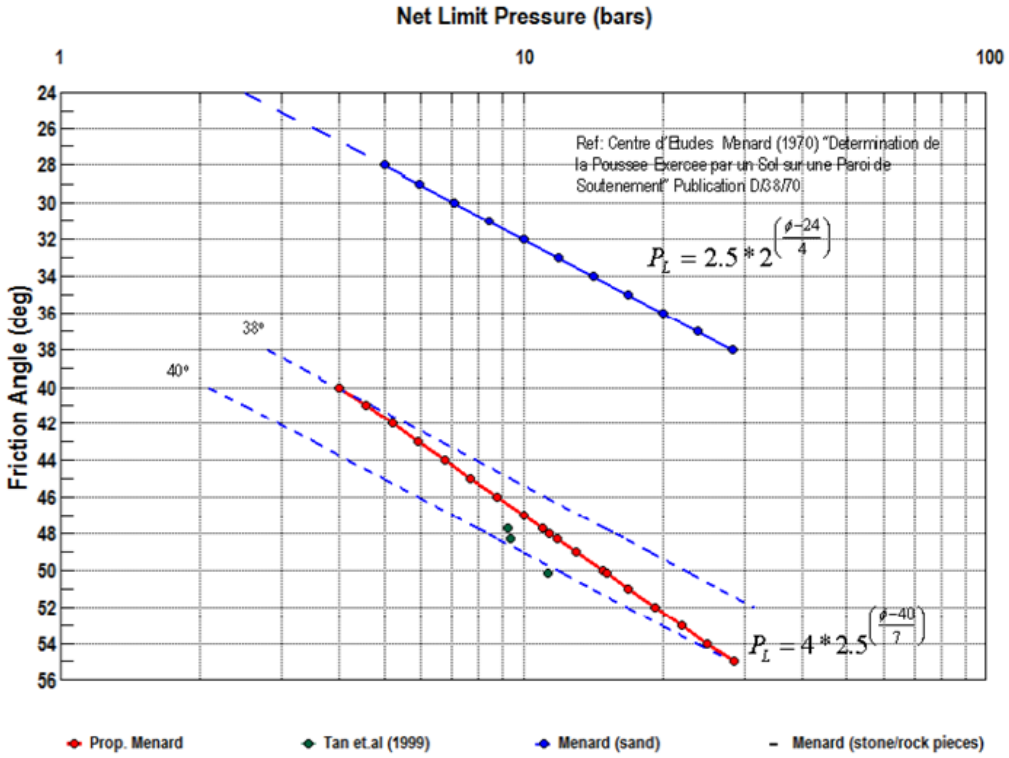

Figure 3-234: Proposed method for estimation of rock fill friction angle from PMT

3. Offshore pounders must be designed to minimize water resistance. As water resistance reduces impact energy, marine pounders are generally heavier than land pounders.

4. The DC rig should be large enough to provide the required stability and winch capacity.

5. Suitable material (rock fill) must be placed on the seabed prior to commencement of works. In this project rock size ranged from 150 to 300 mm.

6. Grid size and number of blows appear not to be very different from the parameters that would be used for land based DR; however, water resistance reduces impact efficiency, and equations developed for estimation of depth of improvement in land based DC are not applicable to marine DC.

7. Friction angle of rock fill can be estimated from PMT by using Equation 2-224.

3.15 Palm Jumeira Trial

3.15.1 Project Description and Ground Conditions

As described in Section 3.12.1 Palm Jumeira is a reclamation off the coast of Dubai in the United Arab Emirates, and consists of a tree trunk, a crown with 17 fronds, three surrounding crescent islands and two identical smaller islands on the sides of the trunk that are in the shape of the logo of The Palm.

After it was established that the reclamation was in a loose state the project's engineers stipulated that ground improvement had to be undertaken to increase the soil strength. Initially, the specifications required that relative density be at least 60%, and CPT q_c be (Al Hamoud and Wehr, 2006):

- Depth < 4 m: $q_c \geq 6$ MPa
- 4 m > depth > 8 m: $q_c \geq 8$ MPa
- Depth > 8 m: $q_c \geq 10$ MPa

Later, in consideration of the carbonate content of the soil (refer to Section 3.12.1) the specification was revised to $q_c \geq 6$ MPa for all depths.

In order to demonstrate the ability of dynamic compaction to satisfy this requirement, a DC trial was performed at Chainage +300 m of Frond N, which has since been renamed to Al Naghal, at the location shown in Figure 3-235.

Figure 3-235: Location of dynamic compaction trial on Frond N (Al Naghal)

3.15.2 Ground Conditions

PMTs were carried out at the trial location to establish the existing ground conditions.

Pre-treatment PMT results at intended print and in between print locations are shown in Figure 3-236. It can be observed that the approximately 3 to 4 m thick superficial crust of the reclamation was very dense, but the sand then became loose to medium dense. P_{LM} and E_M in the upper 4 m were respectively dominantly ranging from 1.4 to 2 MPa and from 4.5 to 20 MPa. At greater depths down to 11 m P_{LM} and E_M were respectively from 0.4 to 0.8 MPa and from 3 to 4.5 MPa.

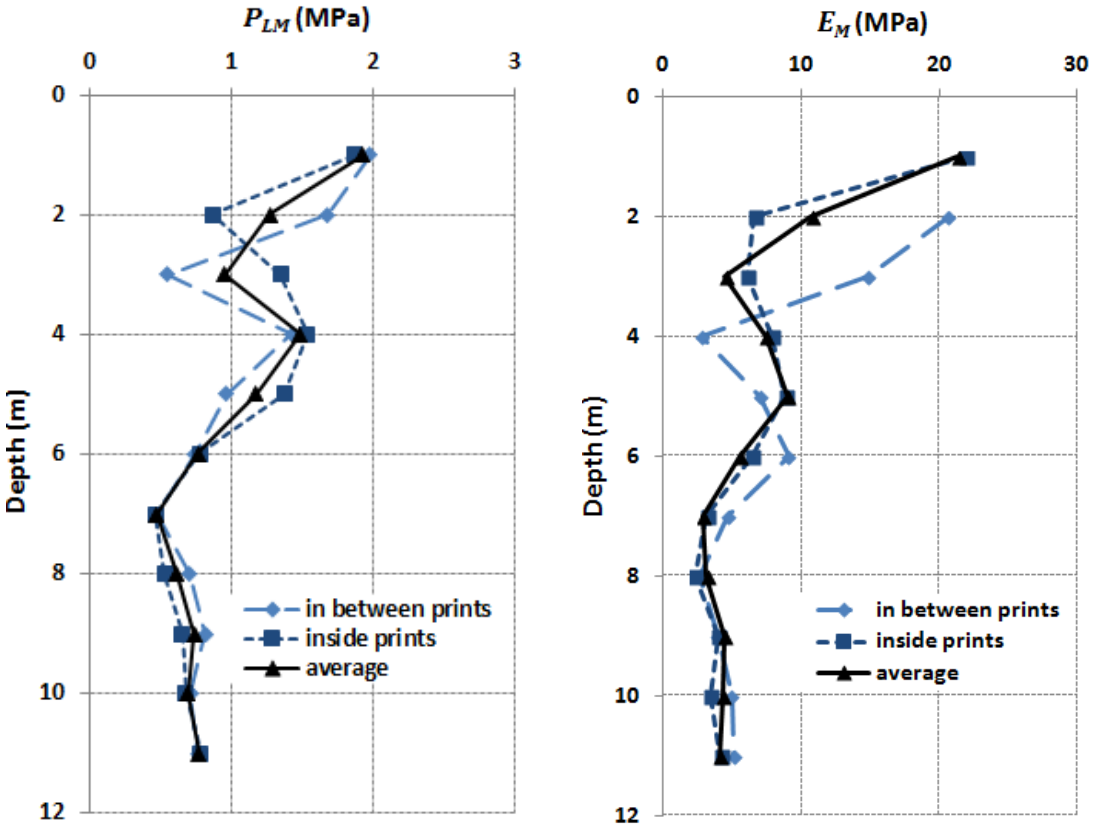

Figure 3-236: Pre-treatment P_{LM} and E_M values in the DC trial area

3.15.3 Dynamic Compaction Trial

The dynamic compaction trail was carried out in a 30 x 30 m^2 area that is shown in Figure 3-237using a 25 ton pounder that was dropped from 20 m. Three compaction phases were performed based on grids of 11 x 11 m^2. As a first step the locations of Phase 1A were pre-excavated by approximately 2 m, with material retained on site for backfilling the craters.

Then 30 blows were applied per print (additional blows were implemented during the HPTs), and the site was levelled using the excavated sand. The same procedure was also followed for Phases 1B and 2 (with the grid size reduced to 7.8 x 7.8 m^2), also with 30 blows per print. As a last step 3 blows were applied to each print (with the final grid size of 5.5 x 5.5 m^2) to compact the backfilled and levelled sand.

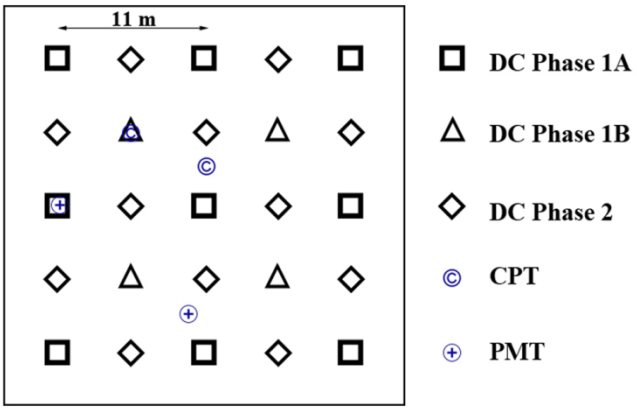

Figure 3-237: Dynamic compaction trial area

3.15.4 Testing and Verification

As shown in Figure 3-237 and as part of the trial, PMTs and CPTs were carried out inside and in between the DC prints after dynamic compaction. Figure 3-238 shows P_{LM} and E_M values after dynamic compaction. It can be observed that the improvement profile of the average PMT parameters have sickle shapes with the average maximum P_{LM} and E_M values at the depth of about 4 m. Figure 3-239 shows that in the absence of ironing and with consideration of the original strength of the topsoil, the soil parameters of uppermost layer of sand has remained almost unchanged, but both P_{LM} and E_M improvement ratios are above 1, up to 5, and approximately 2 at the depth of 11 m. Average P_{LM} and E_M improvement ratios throughout the 11 m of fill was respectively 2.7 and 3.1. This suggests that dynamic compaction with blows inside pre-excavated prints has significantly improved the PMT parameters at even the deepest depths of the hydraulic fill.

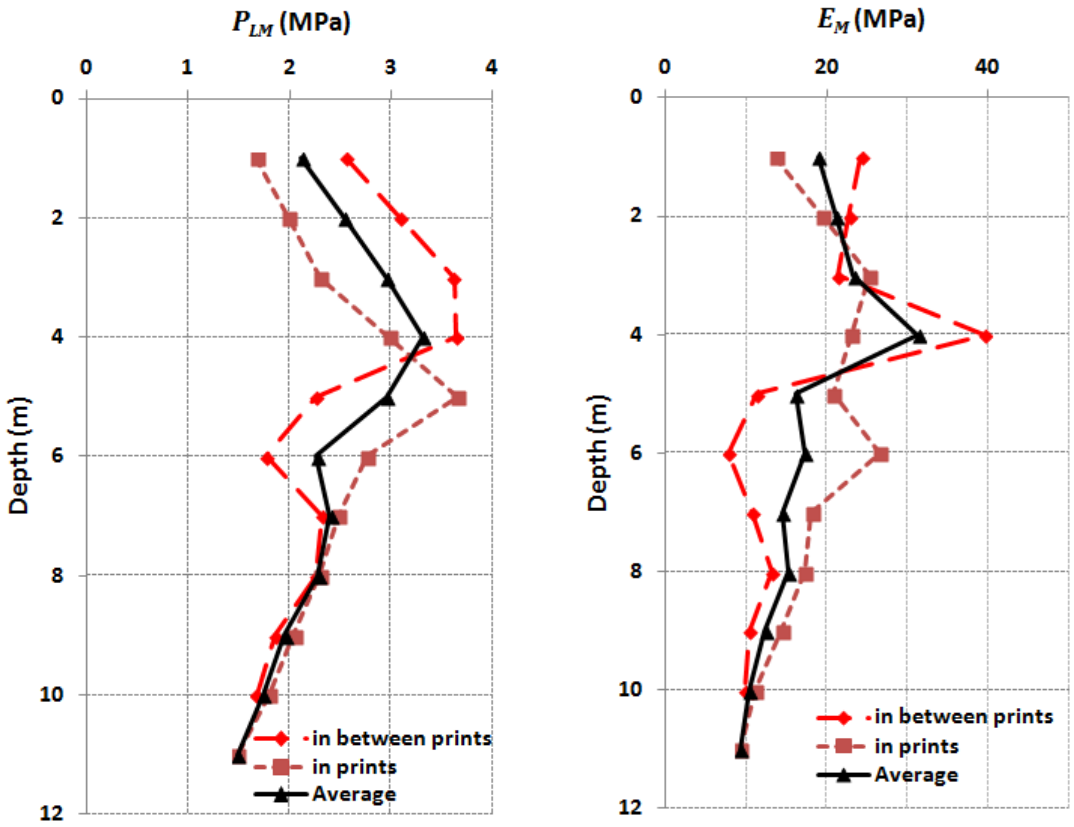

Figure 3-238: After dynamic compaction P_{LM} and E_M values in the DC trial area

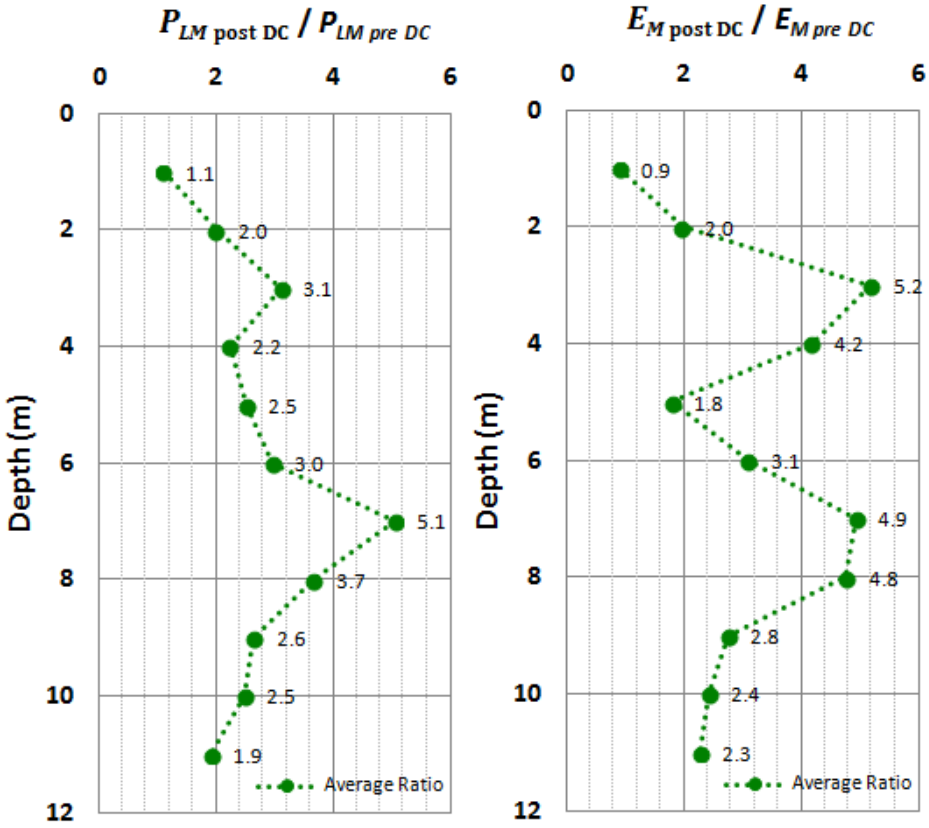

Figure 3-239: P_{LM} and E_M improvement ratios

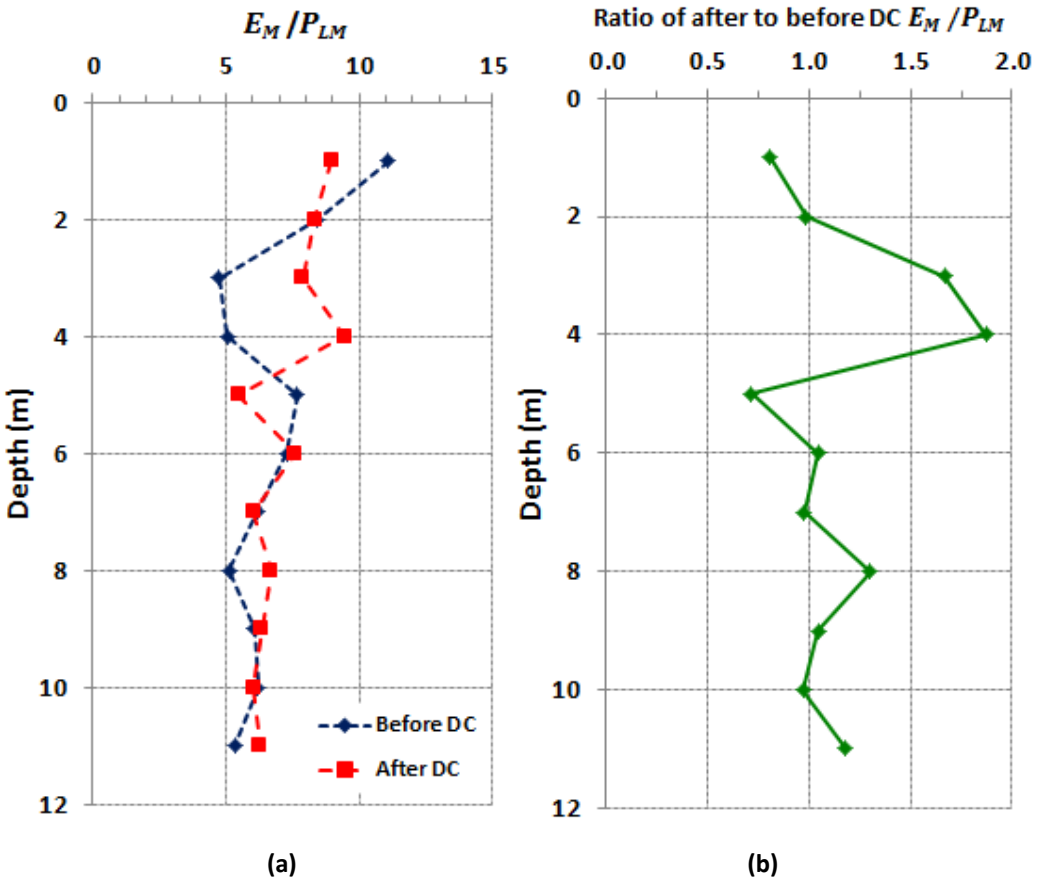

Figure 3-240: (a) E_M/P_{LM} before and after dynamic compaction, (b) Ratio of after to before dynamic compaction E_M/P_{LM}

E_M/P_{LM} values before and after dynamic compaction are shown in Figure 3-240(a). As can be observed except for the layer between the depths of approximately 3 to 4 m that initially had a lower E_M/P_{LM} value, but whose value increased to an over consolidated status (see Table 2-22), average E_M/P_{LM} has remained unchanged. This can be better understood in Figure 3-240(b) that shows the ratio of after to before dynamic compaction E_M/P_{LM}. As can be seen for most of the test points the ratio fluctuates around unity. Calculation shows that the average ratio of all points is 1.14, but the average drops to 1.0 if the points at depths of 3 and 4 m are excluded.

CPT q_c values inside and in between DC prints after dynamic compaction are shown in Figure 3-241. It can be seen that the q_c profiles are also sickle shaped with maximum values at depths of about 3 to 4 m. It can also be observed that while the minimum value of q_c is about 6 MPa at the bottom of the test profile, it was constantly much higher than the acceptance value of 6 MPa throughout the depth and more than 20 MPa at its peak.

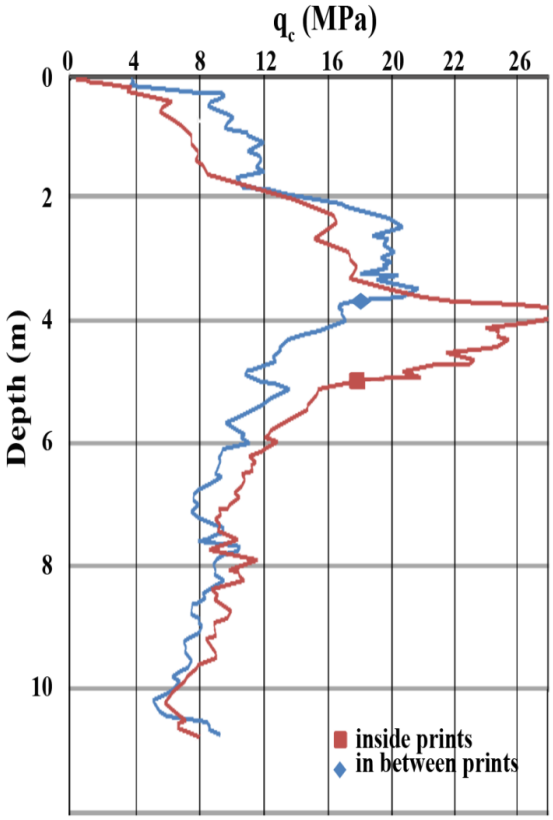

Figure 3-241: After dynamic compaction CPT qc values

The result of these tests show that while the soil profile has improved several times more than acceptance throughout its depth and calculations can readily demonstrate that bearing capacity and settlement performance are better than what could have been achieved if the soil strength was strictly as per the acceptance criterion of $q_c \geq 6$ MPa, in the event that cone resistance had dropped to slightly less than 6 MPa at depth, then improvement would have been non-compliant. The results of this test is a good example of why it was emphasised in Section 2.10.1 that acceptance should be based on design criteria rather than minimum test results.

3.15.5 PMT-CPT Correlations for Calcareous Sand

q_c/P_{LM} and E_M/q_c correlations for in between prints, in prints and for average values at various testing depths are shown in Figure 3-242. As can be seen, it does not appear that q_c/P_{LM} is affected by the shallow and deep failure modes that were observed in Al Nakhilat Ship Repair Yard (refer to Section 3.7.5.3). As in Al Nakhilat project, q_c/P_{LM} does not seem to be influenced by depth.

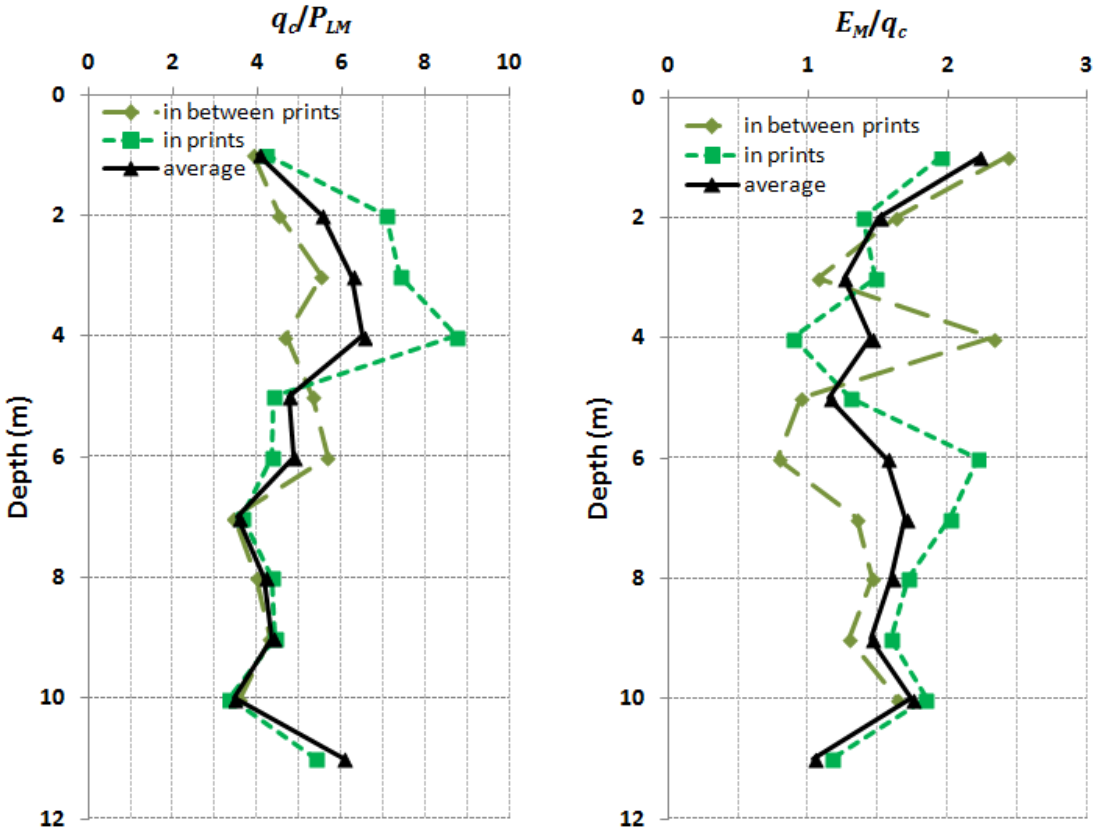

Figure 3-242: q_c/P_{LM} and E_M/q_c correlations

Average q_c/P_{LM} in between prints, in prints and for all tests, including tests carried out at the uppermost levels, can be calculated to be respectively 4.50, 5.20 and 4.86. These figures are either just below or just above the minimum q^*_c/P^*_{LM} value of the 5 to 12 range that has been proposed by Baguelin et al. (1978), see Table 2-26, but substantially less than q_c/P_{LM} = 1/(0.11) that has been suggested by Briaud et al. (1985), see Table 2-27.

Baguelin et al. have related q^*_c/P^*_{LM} values to dilatancy (see Section 2.9.2.9.4) possibly non-dilant when q^*_c/P^*_{LM} is about 5 to 6 and dilant if it is 8 to 12, but as confirmed by the test results the treated sand in the trial was well compacted and a higher ratio should have been predicted. Noting that the location of the sands that were considered by Baguelin et al. are in a region where sands are not calcareous (see Section 2.9.2.9.4), with the available data it can be speculated that the low q_c/P_{LM} values originate from the soil mineralogy rather than compaction and the potential of soil dilatancy in shear.

Standard deviations of these points were respectively 0.80, 1.75 and 1.08. Comparison of the overall q_c/P_{LM} average and standard deviation with Al Nakhilat (respectively 4.54 and 1.48) suggests that while the standard deviation in this project has been less and thus the results can cautiously be deemed as having lesser fluctuation, the difference between the average q_c/P_{LM} of the two studies is less than 8%.

q_c versus P_{LM} values of Palm Jumeira Trial and Al Nakhilat Ship Repair Yard have been plotted in Figure 3-243. Best fit linear, second and third degree polynomials and power curves were compared within the data range. Although these different mathematical functions produced non-coinciding curves, they all appeared to be pseudo linear, which suggests that the best curve correlation can be assumed to be a linear function. By forcing the function to pass through the origin of the axes, the best curve can be expressed by:

$$q_c = 4.82 P_{LM} \qquad 3\text{-}13$$

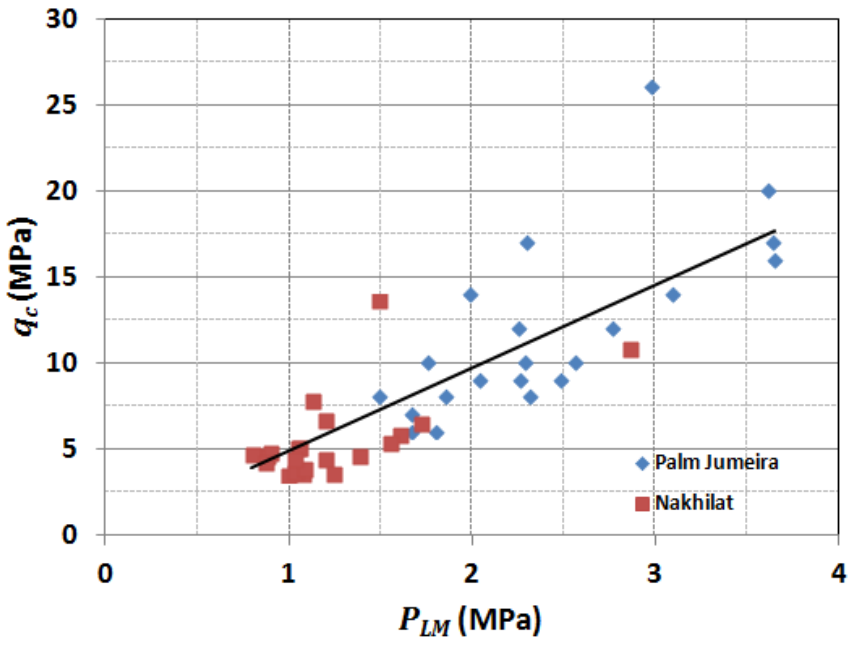

Figure 3-243: q_c versus P_{LM} values of Palm Jumeira Trial and Al Nakhilat Ship Repair Yard

E_M/q_c correlations at depth for in between prints, in prints and average values are also shown in Figure 3-242. Here, E_M/q_c for the average of all points at the uppermost level seems to be

greater than deeper points, but the deviation seems to be equal in magnitude to some deeper points of the in between prints and in print locations.

Average E_M/q_c of in between prints, in prints and all tests, including tests carried out at the uppermost levels, can be calculated to be respectively 1.49, 1.60 and 1.52. Standard deviations were respectively 0.54, 0.40 and 0.32. Comparison of the overall E_M/q_c average and standard deviation with Al Nakhilat Ship Repair Yard (respectively 1.42 and 0.38 for 21 points) shows that the results of the two studies are compatible whereas there is less than 8% difference in the average E_M/q_c.

Similar to Al Nakhilat Ship Repair Yard, the average value of E_M/q_c in Palm Jumeira Trial is somewhat higher than what Briaud et al. (1985) have proposed (1.15, see Table 2-27).

E_M versus q_c values of Palm Jumeira Trial and Al Nakhilat Ship Repair Yard have been plotted in Figure 3-244. Best fit linear, second and third degree polynomials and power curves were compared within the data range. While the power curve also appeared to be pseudo linear, the polynomials slightly bent downwards towards the end of the range. In the studied range, the linear curve still seems to be the best curve, and by forcing the function to pass through the origin, the best curve can be expressed as:

$$q_c = \frac{E_M}{1.54} \qquad 3\text{-}14$$

From Equations 2-212 and 2-214, the relationship between Young and oedometer moduli are:

$$E_{oed} = \frac{1-\nu}{(1+\nu)(1-2\nu)} E_y \qquad 2\text{-}212$$

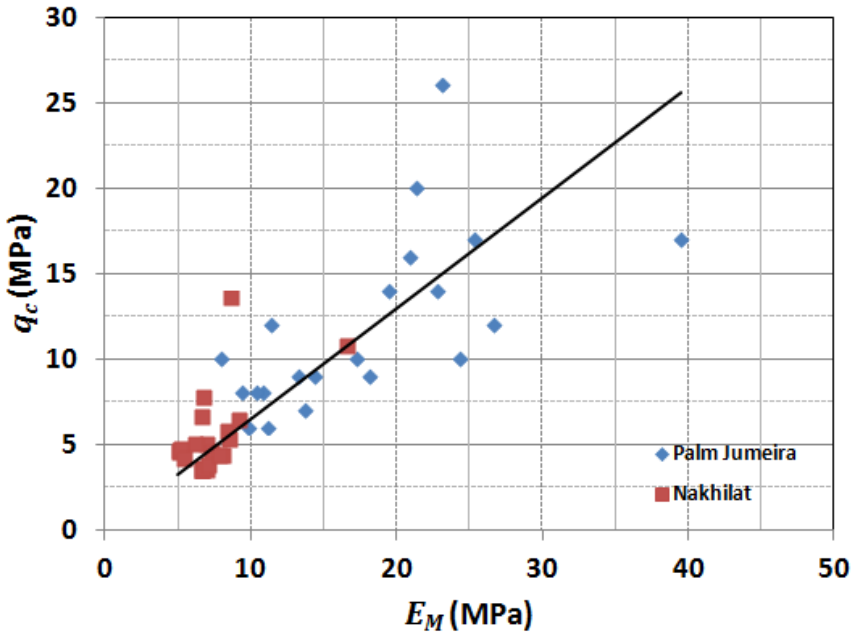

Figure 3-244: q_c versus E_M values of Palm Jumeira Trial and Al Nakhilat Ship Repair Yard

$$E_{oed} = \frac{E_M}{\alpha} \qquad 2\text{-}214$$

From Equations 2-212 and 2-214 and 3-14, for the calcareous sands of Palm Jumeira and Al Nakhilat Ship Repair Yard:

$$q_c = \frac{\alpha}{1.54}\frac{1-\nu}{(1+\nu)(1-2\nu)}E_y \qquad 3\text{-}15$$

Also from Table 2-22, α= 1/3 for sand with 7< E_M / P_{LM} <12. With an arbitrary value of ν=0.33 (see Section 2.9.2.5), for saturated calcareous sands:

$$E_y = 3.12q_c \qquad 3\text{-}16$$

Lee and Salgado (2002) have cited from Schmertmann et al. (1978) and Robertson and Campanella (1989):

For young normally consolidated silica sand:

$$E_y = 2.5q_c \quad \text{3-17}$$

For aged normally consolidated silica sand:

$$E_y = 3.5q_c \quad \text{3-18}$$

For over consolidated silica sand:

$$E_y = 6q_c \quad \text{3-19}$$

The factor of 3.12 in Equation 3-16 is in between the factors for young normally consolidated and aged normally consolidated silica sands, and suggests that silica sand correlations are not suitable for carbonate sands.

3.15.6 Lessons and Conclusion

1. It is possible to improve the strength of loose saturated carbonate sand at depth using dynamic compaction.
2. Depth of improvement can be improved by performing dynamic compaction in pre-excavated prints.
3. Ironing is required to improve the strength of the superficial strength.
4. Acceptance should be based on design criteria rather than minimum test results.
5. It appears that compared to before dynamic compaction, average $E_{M/}P_{LM}$ after dynamic compaction can be considered to remain unchanged if points with initially low $E_{M/}P_{LM}$ are excluded from the calculation.
6. It was observed that for the saturated carbonate sands of Palm Jumeira and Al Nakhilat Ship Repair Yard the relationship between q_c and PMT parameters was not influenced by depth and could be formulated as:

a. $q_c = 4.82\ P_{LM}$

b. $q_c = E_M / 1.54$

7. It was observed that for the saturated carbonate sands of Palm Jumeira and Al Nakhilat Ship Repair Yard the relationship between the CPT cone resistance and Young modulus is $E_y = 3.12\ q_c$.

8. Silica sand correlations for E_y versus q_c are not suitable for carbonate sands.

3.16 Dynamic Compaction Vibration Monitoring

The focus of this section of the thesis is not the actual ground improvement works themselves, but rather the assessment and interpretation of the results of vibration monitoring.

3.16.1 Fujairah Desalination Plant Phase 2

3.16.1.1 Project Description and Ground Conditions

As shown in Figure 3-245, Fujairah Power and Desalination Plants are located in Qidfa in the United Arab Emirates, and have been subject to an expansion project to meet the increasing power and potable water requirements of the UAE. The new desalination plant includes a pumping station, reverse osmosis, lime re-mineralisation, CO_2, chemical, sludge, and electrical buildings.

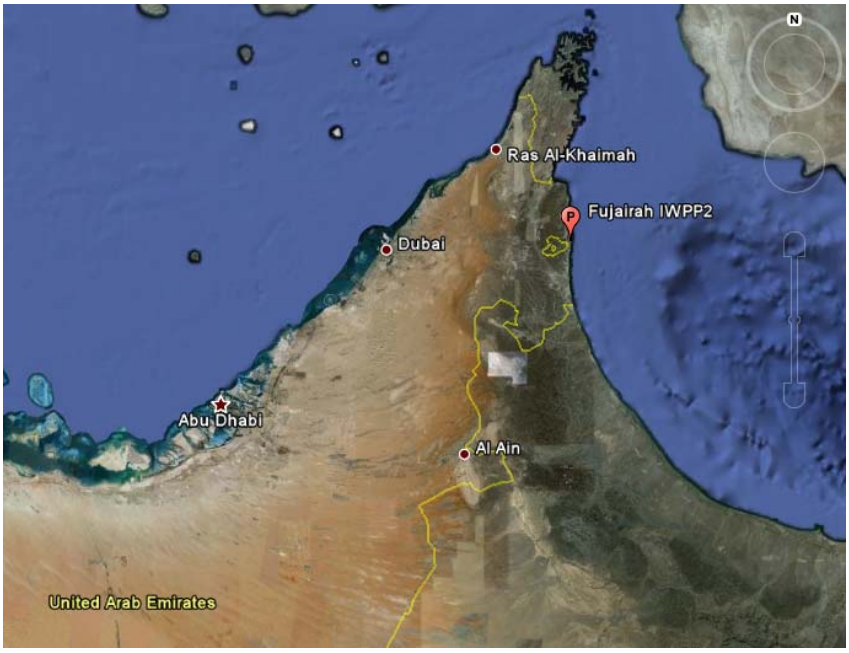

Figure 3-245: Location of Fujairah Power and Desalination Plant

The geotechnical investigation reported that the ground was composed of multiple layers of sandy soil. The top soil was composed of about 1.5 m of well compacted sand backfill that was placed as the working platform. This man-made layer was followed by about 9 m of loose to very dense sand with SPT blow counts in the range of 11 to 30 and sometimes more. Fines content was usually less than 10%, but occasionally higher and up to 15%. The ground then became very dense sand with infrequent layers of very stiff silty soil down to the end of the

boreholes at the depth of about 30 m. SPT blow counts were constantly more than 50 and fines content was generally less than 10% but as high as 55% in the very stiff deep silt layers. The CPT log of one of the test locations is shown in Figure 3-247.

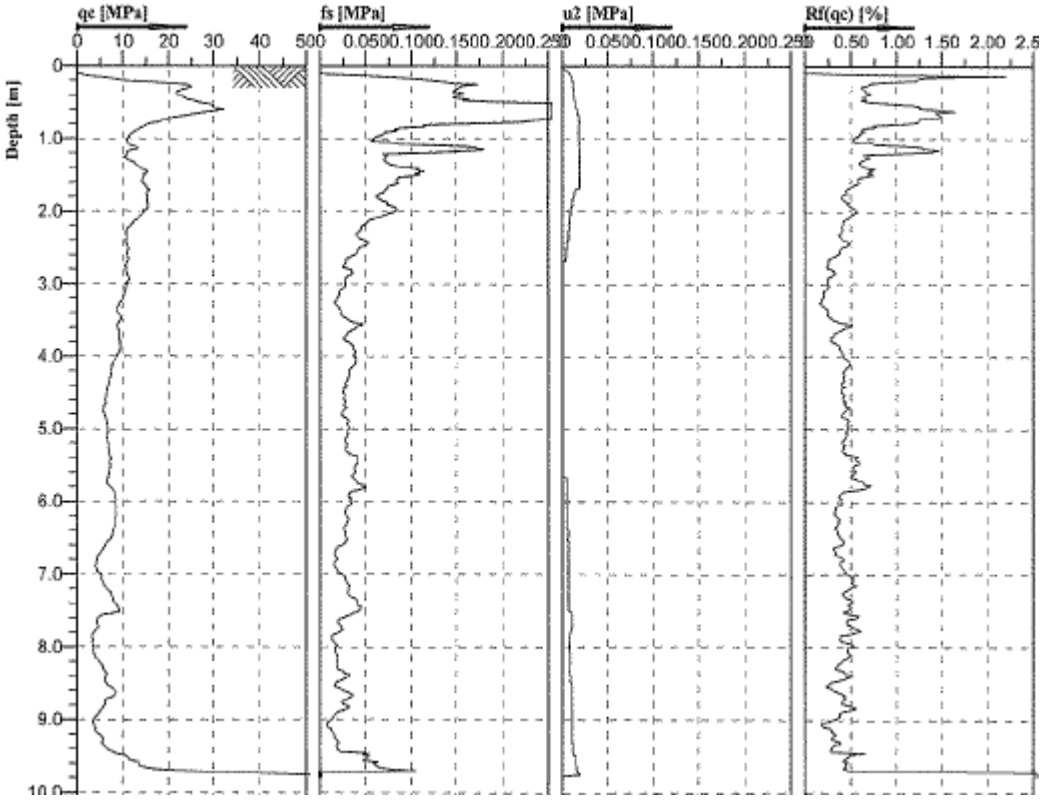

Figure 3-246: Before dynamic compaction CPT at Fujairah Desalination Plant

Groundwater level was approximately 6 m below working platform level.

Calculations by the engineering team suggested that the project requirements were not met, and ground improvement with the below criteria were stipulated for an area of 28,000 m^2:

- Bearing capacity: 150 to 170 kPa for mat foundations and 250 kPa for single footings
- Total settlement: 25 mm
- Differential settlement: 10 mm

Dynamic Compaction was proposed and implemented to increase the soil's mechanical properties and to satisfy the design criteria. The 15 ton pounder that was used for the works had a base that was made of 2x2 m^2 steel plates that were chamfered at the corners.

3.16.1.2 Vibration Monitoring

As shown in Figure 3-247, dynamic compaction was sometimes carried out in the vicinity of plant and pipelines; hence, there were concerns about the magnitude of induced vibrations and the potential effects that they could have.

Figure 3-247: Dynamic Compaction at Fujairah Desalination Plant

For informative purpose the vibrations were monitored and measured in three directions (dir. 1= radial, dir. 2= vertical, dir. 3= transverse) during the project. The results of 22 readings are presented in Table 3-26. These measurements were carried out without the utilisation of vibration reducing trenches. It can be observed that the registered vibration frequencies associated with the peak particle velocities were most often in the range of 7 to 12 Hz and occasionally up to 27 Hz. Vibration frequencies for all three directions are shown in Figure 3-248. It can be observed that the registered frequencies in the other two directions were 11 to 21 Hz and are also within the same range order. The most occurring frequencies appear to be in the range of 10 to 20 Hz.

Table 3-26 is graphically presented in Figure 3-249. For demonstrative purposes the multiple equations proposed by Mayne et al. (1984), Mayne (1985), and Varaksin (1981) have also been plotted onto the same figure. Mayne's upper limit and conservative equation (Equation 2-150) has the largest overestimation and estimates the PPV values by 3 to 5 times of what was measured on site. Although Mayne's earlier proposed relationship (Equation 2-149) is less conservative, it is never-the-less still overestimating PPV by 3 to 4 times. It appears that Equations 2-149 and 2-150 predict relatively similar particle velocities at greater distances from pounder impact point, but the calculated values divert when PPV is predicted closer to the source of vibration.

PPV (mm/s)	Frequency (Hz)	Distance (m)	Drop Height (m)
4.57	7.5	46.6	20
5.33	7.6	46.6	20
5.84	7.4	46.6	20
5.97	7.4	46.6	20
6.22	7.3	46.6	20
5.97	7.2	46.6	20
5.97	10.6	36.6	20
6.60	12.1	36.6	20
7.11	12.4	36.6	20
7.62	26.9	36.6	20
7.49	12.8	36.6	20
7.62	20.4	36.6	20
10.80	11.3	26.6	20
11.94	11.6	26.6	20
12.32	12.1	26.6	15
11.05	12.1	26.6	15
12.95	12.8	26.6	15
11.18	12.1	26.6	15
10.67	11.9	16.6	10
11.81	12.1	16.6	10
12.70	11.6	16.6	10

Table 3-26: Results of vibration monitoring

Mayne's final relationship (Equation 2-152) that is independent of the pounder weight, but that takes into consideration the pounder's drop height and radius appears to be closer to the measured PPV values on site. This equation predicts PPV by an overestimation of 1.2 to 2.8 times. It appears that the larger variations are when prediction is made closer to the vibration source.

Varaksin (Equation 2-153) appears to be the closest to the site's PPV measurements. However, Equation 2-153 sometimes underestimates PPV. This has also been noted by

Romana Ruiz and Jurado (1999) for dynamic compaction vibrations that were monitored for an onshore fill project in the Canary Islands.

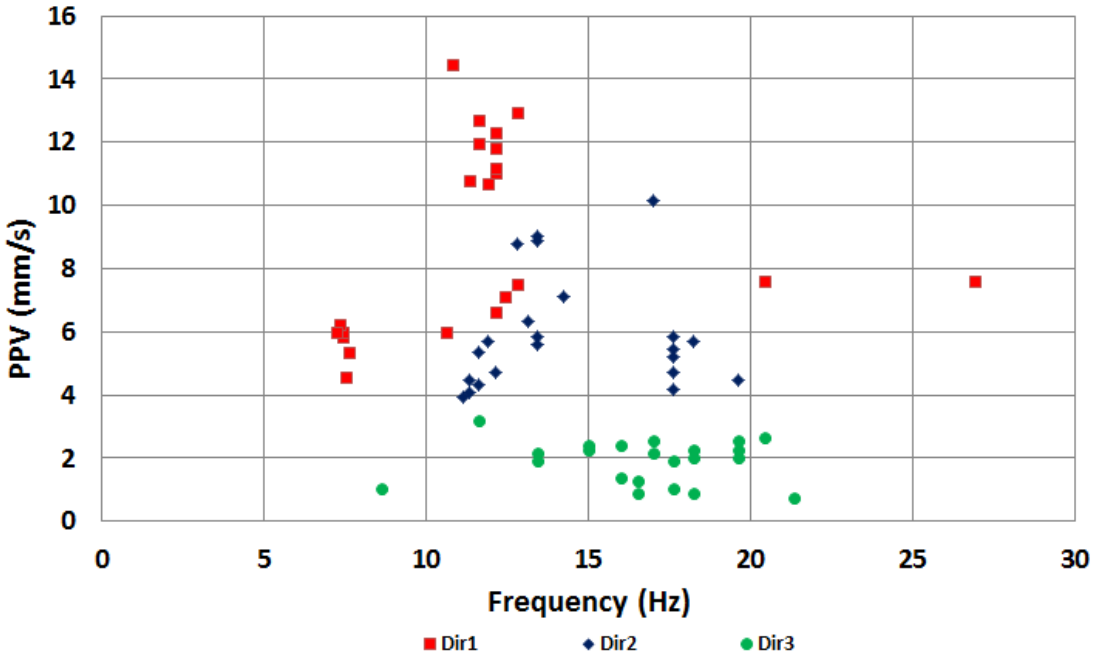

Figure 3-248: *PPV* and vibration frequencies

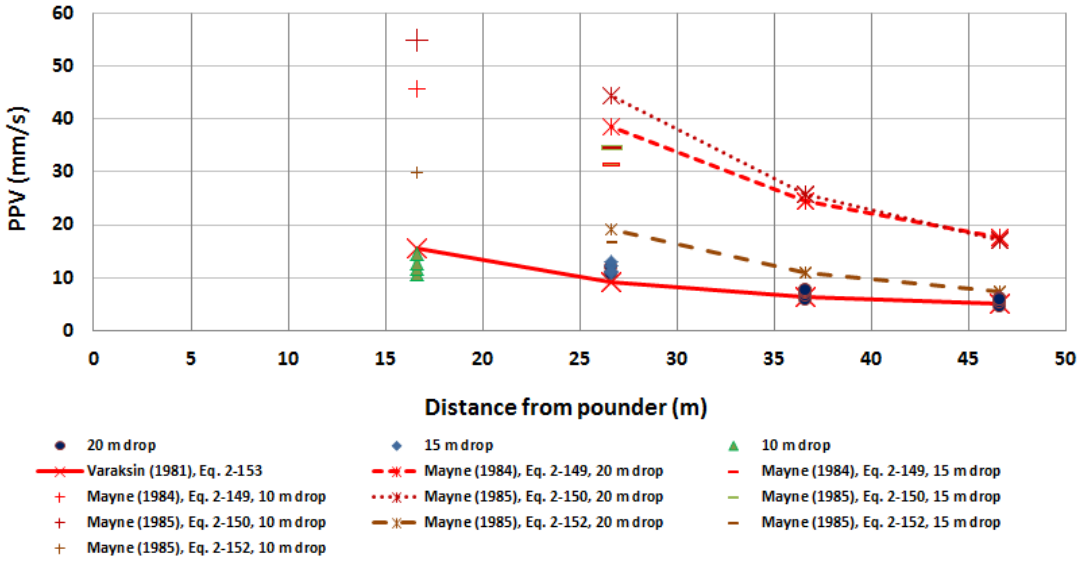

Figure 3-249: Comparison of *PPV* measurements with various methods for estimating *PPV*

3.16.1.2.1 Improving PPV Estimation Accuracy

Although Equation 2-153 appears to predict *PPV* values quite reasonably, in some occasions it may unsafely underestimate the actual field values. As underestimation of *PPV* can lead to unanticipated problems during the execution of the works, the author proposes a

modification to this equation in the form of Equation 2-153 that overestimates measured PPV by 1.2 to 2.4 times in this case study.

$$PPV = 560d^{-1.1} \text{ mm/s} \qquad 3\text{-}20$$

Instead of solely a function of distance as presented in Equation 2-153, PPV values of Table 3-26 can be formulated in the form of Equation 2-148 to yield:

$$PPV \leq 25\left(\frac{\sqrt{WH}}{d}\right)^{1.1} \qquad 3\text{-}21$$

The comparison of the field data with Equations 2-152 and 2-153 and 3-21 are graphically shown in Figure 3-250. It appears that while providing a more reasonable estimate of PPV, Equation 3-21 can still sufficiently overestimate PPV during the planning stage of a project.

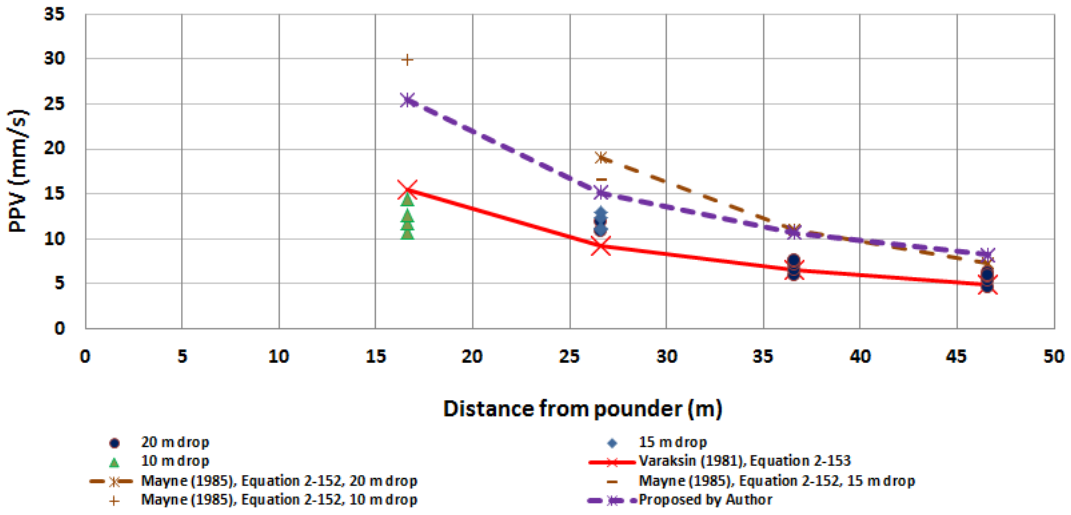

Figure 3-250: Comparison of field measured *PPV* values with equations proposed by Mayne (Equation 2-152), Varaksin (Equation 2-153) and the author (Equation 3-21).

3.16.2 Medina A'Zarqa (Blue City)

3.16.2.1 Project Description and Ground Conditions

Al Medina A'Zarqa, translating to Blue City, is a multibillion dollar megacity project that has been planned in Oman, and is to spread over an area of 32 km^2 with 16 km of coastline southeast of Al Sawadi and along the Gulf of Oman. The general location of the project is

shown in Figure 3-251. The multiple phases of the project are to be built over a period of several years. Phase 1 of this project is located within an area that measures 3 km along the coastline and 2 km inland. Figure 3-252 shows the plan of the various phases of Medina A'Zarqa.

Figure 3-251: Location of Medina A'Zarqa

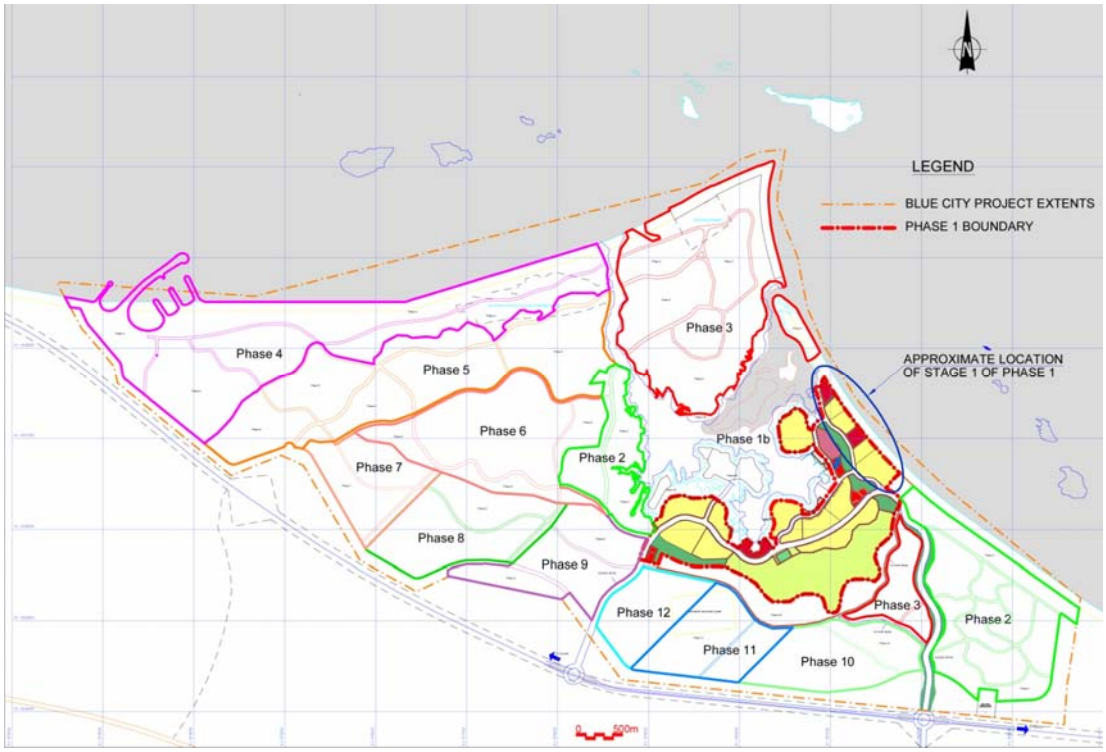

Figure 3-252: Plan of various phases of Medina A'Zarqa

The plan of Phase 1 of Medina A'Zarqa is shown in Figure 3-253. Plots No. 1.1.2, 1.4.2, 1.3.1 and 1.3.2 with an approximated area of 225,000 m^2 are to be the first construction areas. Based on the topographical survey, as a whole, the original ground level of the site was from

+0.8 m to +2.7 m MSL (Mean Sea Level). Average ground level was approximately +1.5 m MSL in Plots No. 1.1.2 and 1.4.2, and approximately +2.3 m MSL in Plot No. 1.3.1 and 1.3.2. Minimum, maximum and average groundwater levels were reported to be respectively -0.4 m, +0.25 m and ±0.0 m MSL.

Excluding their partial basements, the buildings in the mentioned plots were anticipated to be 2 to 7 stories.

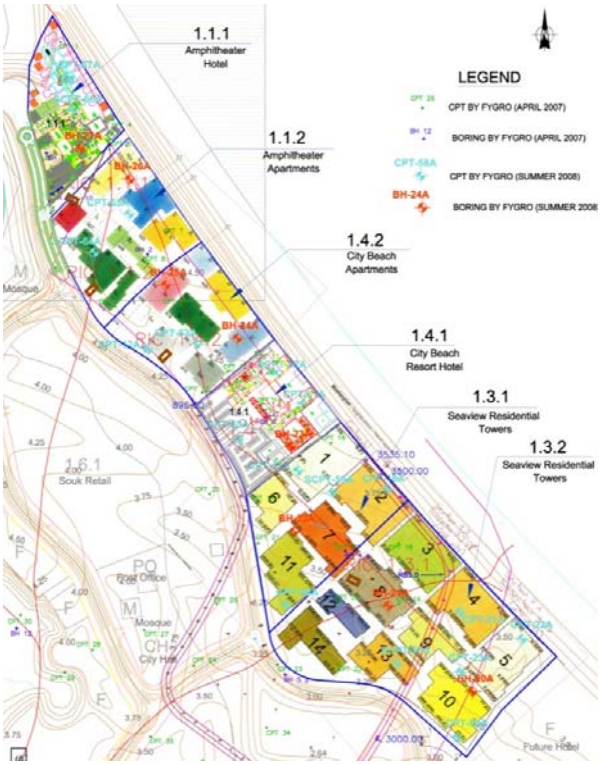

Figure 3-253: Plan of Medina A'Zarqa Phase 1

Description	Top elevation (m MSL)	Average Thickness (m)	q_c (MPa)	R_f (%)	N_{SPT}
Medium dense slightly silty sand	2.5	8.5	2-12	0.5-1	2-35
Soft very silty sand to sandy silt and clay	-6	2.5	2	2	
Interbedded medium dense silty sand and firm to stiff silt and clay	-8.5	15.5	3-20	1-4	
Substratum	-24		refusal		

Table 3-27: Summary of ground conditions

A summary of the generalised ground conditions is tabulated in Table 3-27.

Preliminary calculations indicated the presence of loose sand layers in the upper 8.5 m of ground, and stipulated the application of ground improvement to allow the construction of raft foundations. Ground improvement works were tendered, and the accepted proposal was based on the implementation of dynamic compaction.

Dynamic compaction was carried out from elevation +1.8 m MSL in three deep phases using a 23 t pounder that was dropped from 20 m, followed by ironing using a 15 t pounder that was dropped from 15 m. Figure 3-254 shows the application of dynamic compaction during one of the deep phases.

Figure 3-254: Application of dynamic compaction at Medina A'Zarqa using a 23 t pounder

3.16.2.2 Vibration Monitoring

As shown in Figure 3-255 vibration monitoring by recording the peak particle velocities and associated frequencies in the radial (Dir R), vertical (Dir V) and tangential (Dir T) directions was performed using a seismograph. Measurements were carried out at different distances, from 10 m to 100 m during the three deep and ironing phases for drops that was applied to a specific print.

Figure 3-255: Dynamic compaction vibration monitoring at Medina A'Zarqa

PPV versus the blow number for deep DC phases 1 and 3 are respectively shown in Figure 3-256 and Figure 3-257 at various distances. As can be observed that regardless of the blow number, distance to pounder impact point and phase of dynamic compaction, peak particle velocity was always in the radial direction. Similarly, particle velocity in the tangential direction was always the least value among the three directions. The comparison of the two figures also indicates that at equal distances, *PPV* in phase 3 is higher than phase 1. The *PPV* ratio of the two phases appears to be less at closer distances and more at further distances.

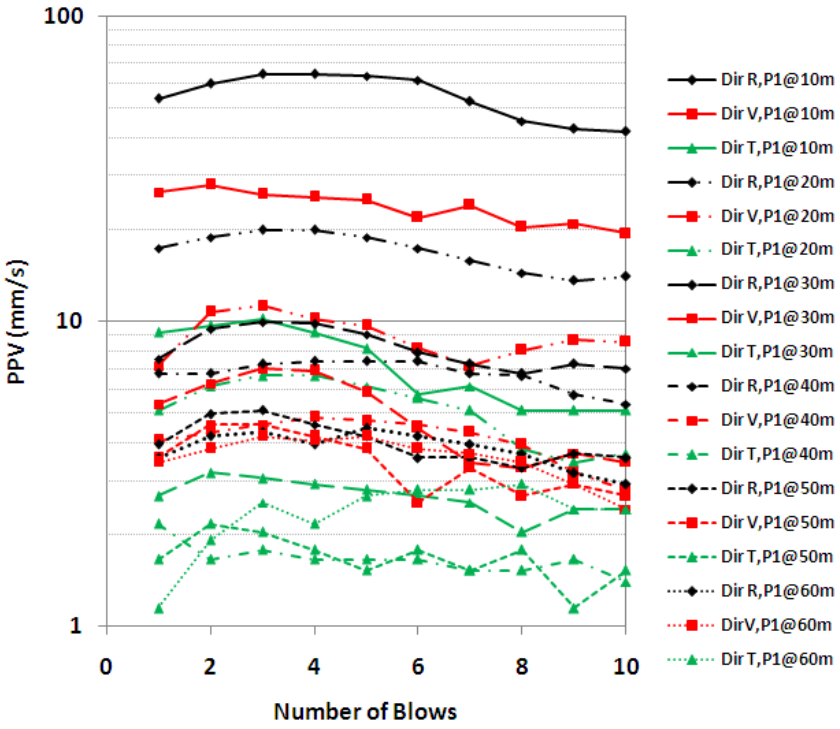

Figure 3-256: *PPV* versus number of blow in DC phase 1

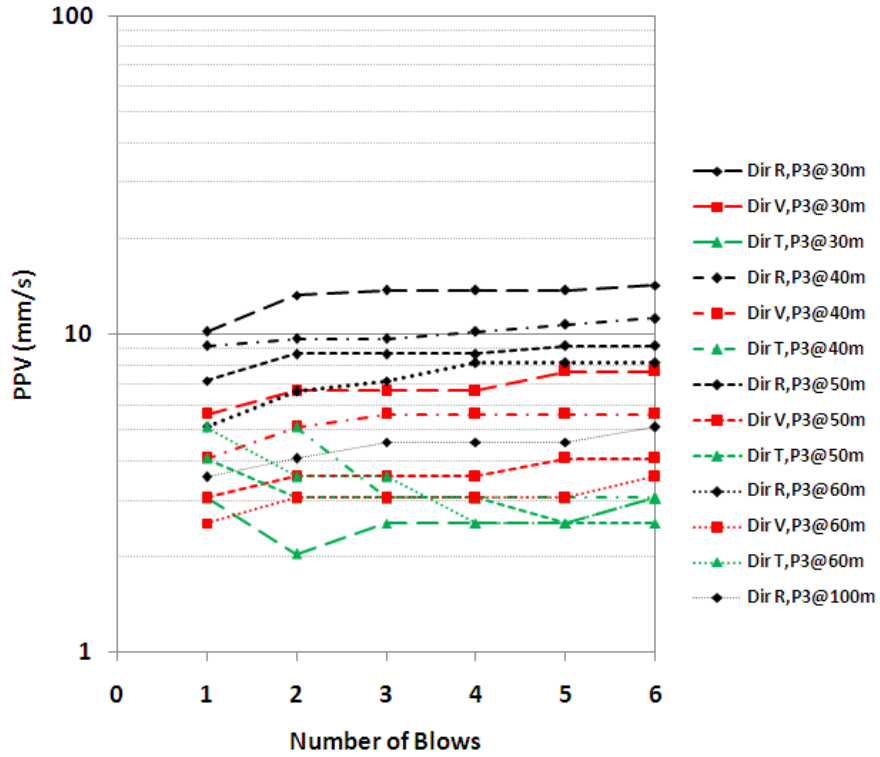

Figure 3-257: *PPV* versus number of blow in DC phase 3

It can also be seen in Figure 3-256 that in most instances of phase 1 monitoring, when distance is kept constant, *PPV* initially increases with the number of blows, but then reduces to values lower than what was measured in the first blow. This is most observable in all three directions in the closest distances. As lesser blows were applied per impact point in phase 3 it cannot be said that the same has happened in the later phase, but Figure 3-257 shows that *PPV* of the first blow in this phase was also smaller than subsequent blows.

Figure 3-258 shows the plot of peak particle velocity of each direction against frequency for phases 1, 3 and ironing at various distances. It can be observed that almost all plotted points are between the frequency range of 5 to 9 Hz.

Plotting *PPV* against distance for DC phases 1, 2 and 3 produces interesting results. It can be seen that although there is *PPV* scatter for records made at the same distance during each phase, the upper limit value of *PPV* for each phase appears to fit reasonably well with a line drawn in a semi logarithm scale. It can also be understood that the slope of *PPV* attenuation in the earlier phases is more than the later phases. This suggests that there is greater material damping in loose soils than dense soils. As already noted for Figure 3-256 and Figure 3-257, Figure 3-259 also clearly indicates that the difference between *PPV* values of premier and subsequent phases of dynamic compaction becomes greater as distance from impact point

increases. Also, it appears that at distances closer than a critical distance, seemingly about 19 m in this study, PPV becomes insensitive to the compaction phase.

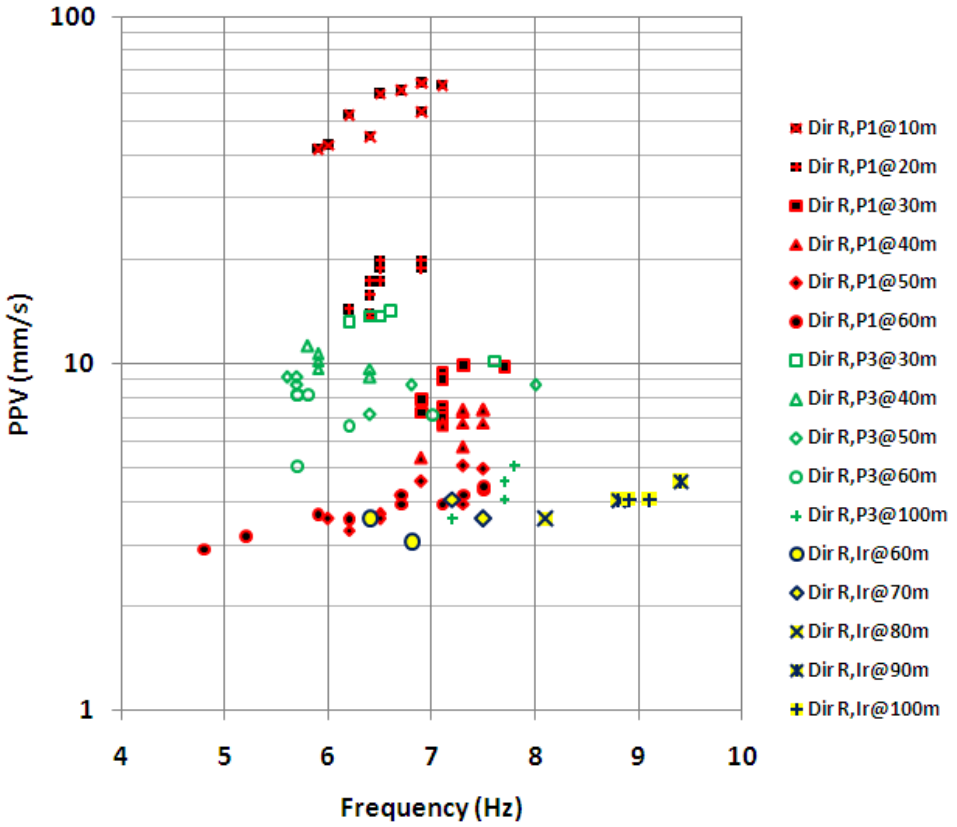

Figure 3-258: PPV versus frequency in phase 1, phase 3 and ironing

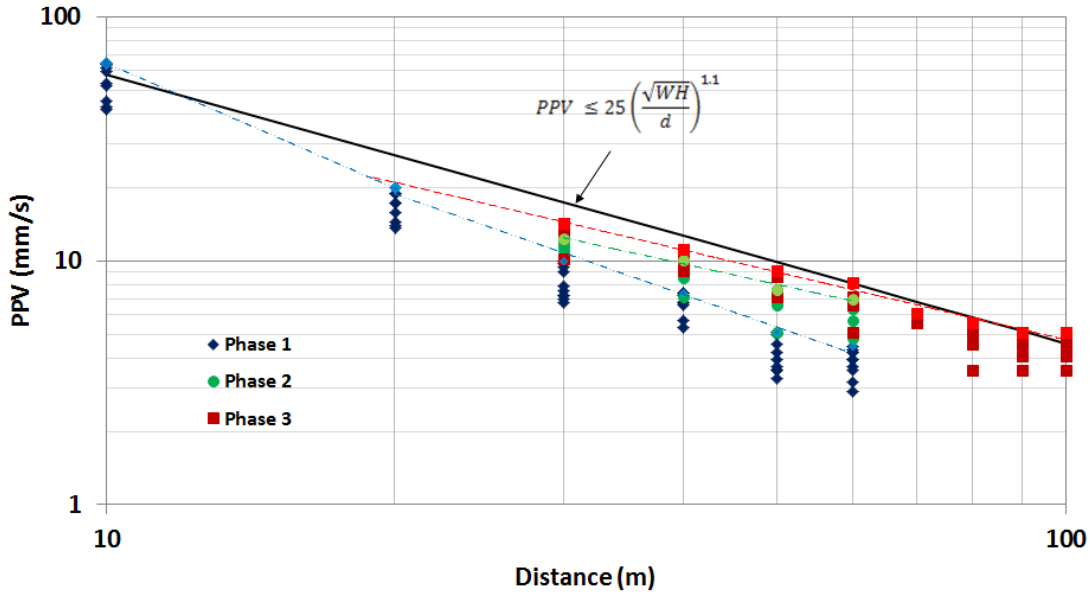

Figure 3-259: PPV versus distance and comparison with prediction equations

Comparison of measured PPV in Figure 3-259 with Equation 2-151 indicates that this empirical formula is able to predict PPV with sufficient accuracy in this project as well.

3.16.3 Um Quwain Marina

3.16.3.1 Project Description and Ground Conditions

Umm Al Quwain (UAQ) Marina is a master-planned community in the northern emirate of Umm Al Quwain in the UAE (refer to Figure 3-260). The plan of the project envisages 6,000 villas, 2,000 townhouses, 1,200 resort and hotel rooms, super markets, shopping centres, schools and health clinics. UAQ Marina Phase 1 consists of 277 two floor (ground and first floor) villas in Community 16 of which 127 villas are within the area (86,000 m^2) that will be reviewed in this thesis.

Figure 3-260: General location of UAQ Marina

Groundwater was recorded to be 1 to 3 m below ground level. The preliminary geotechnical investigation that was based on SPT boreholes suggested that the site was composed of 2 m of very loose to medium dense silty sand with SPT blow counts ranging from 2 to 28 and with fines content less than 10%. This stratum was followed by 4.5 m of very loose to dense silty sand with blow counts ranging from 0 to 35 and fines content of less than 15%.The next 3.5 m of soil was silty sand with SPT blow counts ranging from 16 to more than 50 and with fines content of less than 20%.

Based on the geotechnical investigation the project engineers designed strip footings on improved ground. Maximum footing width was 1.5 m under a uniform load of 140 kPa. Footing depth was defined as 1 m below ground level. Consequently, the project was tendered and the design and construction ground improvement package was awarded to a

ground improvement specialist contractor who had proposed the implementation of dynamic compaction.

Once the contractor was on site, further geotechnical testing revealed a different soil profile and the presence of a previously unidentified 0.3 m thick layer of very soft very silty sand to sandy silt (fines content in the range of 40 to 60%) at an upper depth of approximately 1.7 m to 2.1 m. P_{LM} in this layer was 200 kPa.

Therefore, the ground improvement technique was modified to pre-excavated dynamic replacement. The saturated soft material was excavated from below groundwater level, the excavated pits were backfilled with sand to groundwater level, and mixed soil was placed above groundwater level.

3.16.3.2 Vibration Monitoring

As dynamic replacement works were to be carried out as close as 20 m from existing and under construction structures concerns were raised that vibrations generated by the ground improvement works could damage the buildings. Hence, a vibration monitoring programme was developed to study the vibration parameters with and without the installation of vibration isolators.

In this programme initially a 14.5 ton pounder was dropped from 20 m, and radial, transversal and vertical particle velocities and associated vibration frequencies were measured at distances of 10 to 40 m, see Figure 3-261(a).

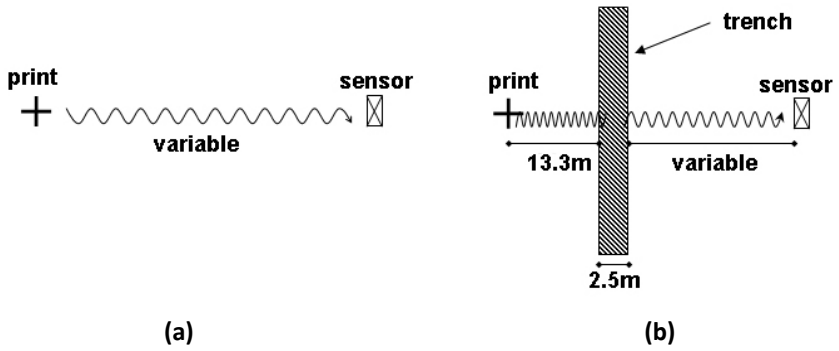

Figure 3-261: (a) Vibration monitoring without a trench, (b) vibration monitoring with a trench

Next, as shown in Figure 3-261 (b), a trench that was 25 m long, 2.5 m wide and 2.5 deep (to groundwater level) was excavated 13.3 m away from the pounder's drop point and the same

parameters were measured again. In this phase the pounder used was 13 tons and the pounder drop height varied from 5 m to 18 m.

Vibration Monitoring without an Isolation Trench

The measured PPVs and their corresponding frequencies for the case with no trench are tabulated in Table 3-28, which also shows PPV values that have been estimated by using Equation 2-151 and the ratio of estimated PPV to measured PPV. It can be observed that the frequencies corresponding to peak particle velocity are within the range of 12 to 24 Hz. It can also be seen that in this monitoring programme the frequency of the peak particle velocity increases with distance.

Distance (m)	Frequency (Hz)	PPV (mm/s)		Ratio of estimated to measured PPV
		Measured	Estimated	
10	10.6	65.0	44.9	0.69
15	12.4	33.5	28.7	0.86
20	13.1	22.9	20.9	0.91
25	15.0	14.0	16.4	1.17
30	22.2	10.7	13.4	1.25
35	24.3	7.2	11.3	1.57
40	22.2	6.0	9.8	1.63

Table 3-28: Vibration monitoring summary for the case without the trench

While Equation 2-151 has underestimated PPV at close distances (by 31% at 10 m and by 14% at 15 m), it has been able to conservatively estimate PPV at other distances. The underestimations at 10 m and 15 m are not of major concern as they are still above what would be statistically deemed as non-damaging (Siskind et al., 1980). Underestimation at 20 m is approximately 9%, but the predicted values become an overestimation of 63% at 40 m.

Measured and estimated PPVs plotted against distance are shown in Figure 3-262 for the case with no vibration isolation trench. Noting that PPV is dependent on a number of parameters other than those appearing in Equation 2-151, such as number of pounder drops, the reliability of Equation 2-151 can be deemed as satisfactory as a starting point.

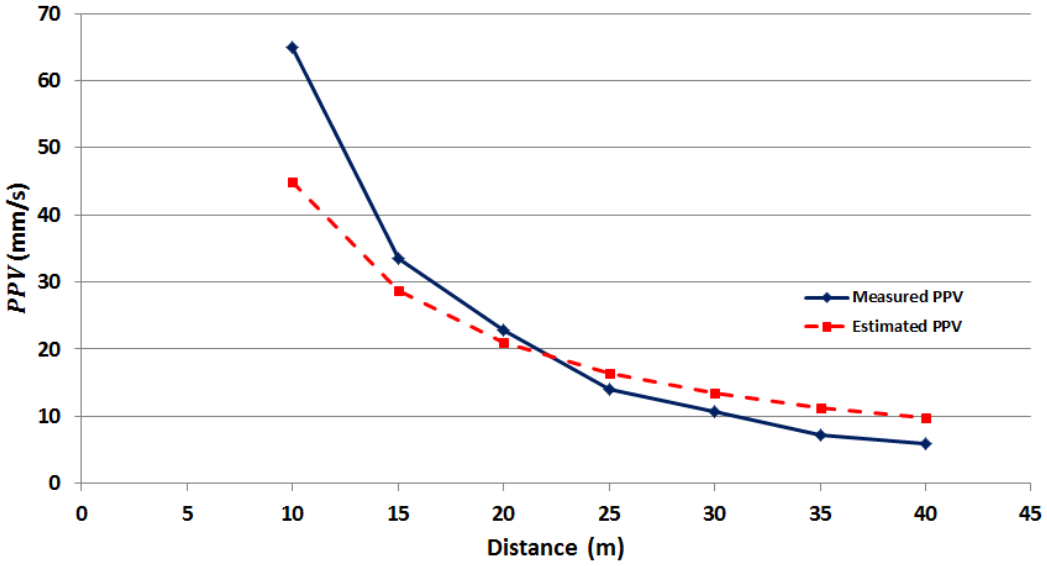

Figure 3-262: Comparison of measured and estimated *PPV*

Vibration Monitoring with an Isolation Trench

The measured *PPV*s and their corresponding frequencies for the case with a trench are tabulated in Table 3-29, which also shows the estimated *PPV*s had there been no trench.

The ratios of estimated *PPV* (without a trench) to measured *PPV* for the two cases of monitoring with and without an isolation trench have also been included in Table 3-29. It can be seen that the ratio of estimated to measured *PPV* is considerably higher when a trench has been excavated. For example at the distance of approximately 35 m the ratio of estimated to measured *PPV* is 1.57 without a trench but 2.91 and 5.46 when a trench has been excavated. The ratios of estimated to measured *PPV* for the trenched case are not demonstrative of the true efficiency of the trench as these ratios were also not unity when there was no trench. To obtain a more accurate estimation of the efficiency of the trench it is more proper to calibrate the results by dividing the ratios of estimated to measured *PPV* (last column in Table 3-29).

The division of the ratios indicates that the trench has been efficient with *PPV* possibly having been 1.09 to 3.47 times more had there not been any trench. Graphically presenting the trench efficiency, Figure 3-263 shows that while the data scatter does not allow a conclusive interpretation of any specific trend of the *PPV* reduction factor, it can still be observed that the best linear fit is almost a horizontal line with an average value of 2.05.

Distance (m)	Drop height (m)	Frequency (Hz)	*PPV* (mm/s)		Ratio		
			Measured (trench at 13.3 m)	Estimated without trench	Estimated to measured		trenched to no trench
					trenched	no trench	
10.0	5	5.2	35.6	19.7			
10.0	8	10.0	47.2	25.5			
16.3	8	18.2	7.4	14.9	2.02	0.86	2.35
25.8	12	16.5	5.7	11.3	1.97	1.17	1.69
25.8	15	18.9	7.9	12.7	1.61	1.17	1.38
30.8	12	24.3	3.2	9.3	2.89	1.25	2.31
30.8	15	24.3	3.7	10.5	2.83	1.25	2.26
35.8	10	28.4	1.3	7.1	5.46	1.57	3.47
35.8	12	23.2	2.7	7.9	2.91	1.57	1.85
35.8	18	22.2	5.7	9.8	1.72	1.57	1.09
40.8	5	10.2	1.4	4.2	3.00	1.63	1.84
40.8	10	12.1	1.7	6.2	3.62	1.63	2.22

Table 3-29: Vibration monitoring summary for the case with the isolation trench

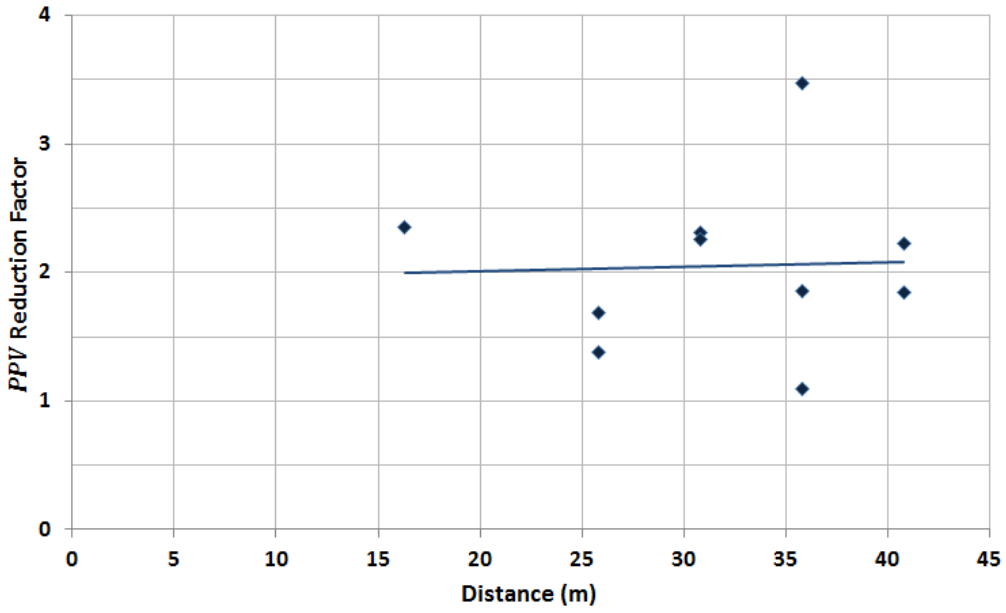

Figure 3-263: *PPV* reduction factor when using a vibration reduction trench

3.16.4 Comparison of Vibrations Generated by Dynamic Compaction and Vibro Compaction

Vibro compaction, also known as vibroflotation, is a deep ground compaction technique that was developed almost 80 years ago (Mitchell, 1981) with the invention of the first vibroprobe by Degen and Steuermann (Better Ground) in Germany.

This technique is best suitable for the treatment of soils with limited amounts of fines. Mitchell (1981) proposes that the best desirable soils for vibro compaction are when the soil's fines content is limited to 18%. Woodward (2005) suggests that best results can be achieved when fines content is less than 10%.

The vibroflot, also referred to as vibroprobe or vibrating poker is a hollow steel tube containing an eccentric weight mounted on a vertical axis in the lower part so as to give a horizontal vibration. The vibroflot itself is connected to extension tubes that are supported by a rig, which is usually a crane.

The vibroflot is either flushed down to the required depth in the soil using water jets or vibrated dry with air jets. When the vibroprobe reaches the required depth, material is added from the ground surface during withdrawal, and the vibroflot is moved in an up and down motion at certain intervals. The horizontal vibrations form a compacted cylinder of soil with a depression at the surface due to the reduction of void ratio in the ground. Depending on the vibroflot power, the zone of improved soil extends from 1.5 m to more than 4 m from the vibrator.

Similar to dynamic compaction, application of vibro compaction also generates vibrations. The intent of this section of this thesis is to develop a method using a case study to estimate vibro compaction generated vibrations and to compare the peak particle velocity with estimated dynamic compaction PPV (using Equation 2-151.

3.16.4.1 Previous Research on Vibro Compaction Generated Vibrations

Unfortunately not much research is available on particle velocity generated by vibro compaction. Without providing details about the measurements and the scatter of data, Woods and Jedele (1985) have presented the graph of peak vertical velocity (which may have been PPV) for vibroflots with motor powers of 22 kW (30 hp) and 75 (100 hp). Similarly, Dowding (2000) has presented the graph for a vibroflot with a motor power of 120 kW, 18

mm vibration amplitude and 30 Hz frequency. Neither of the publications has referred to the depth of the vibroflot during particle velocity measurements. Figure 3-264 shows the results of Woods and Jedele's and Dowding's publications.

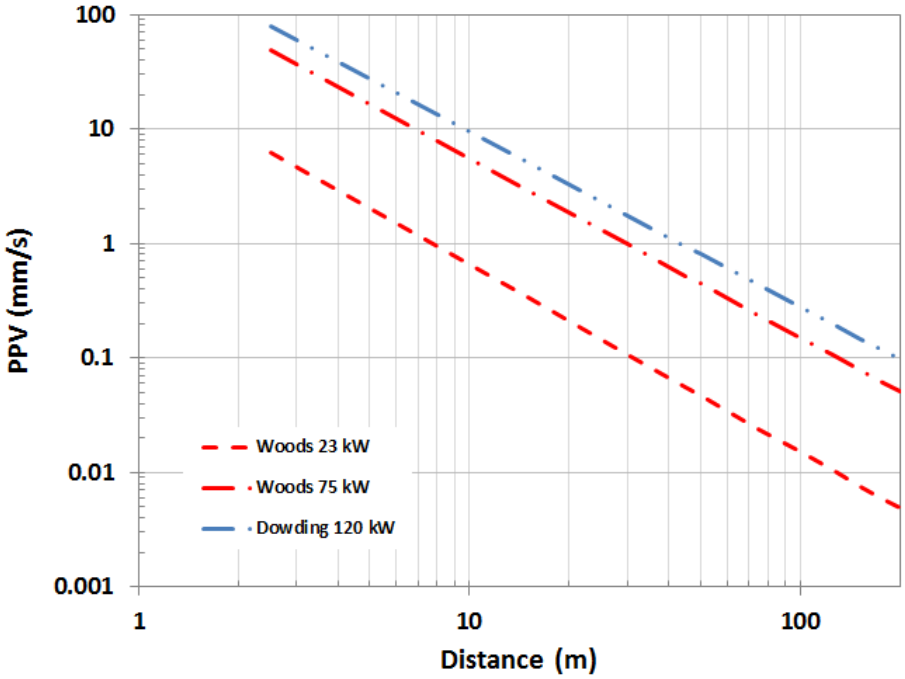

Figure 3-264: : *PPV* generated by vibro compaction as per previous research

3.16.4.2 This Study: Vibration Monitoring of Vibro Compaction on Palm Jumeira

As shown in Figure 3-265, vibration monitoring was carried out on points located on Plot 106 of Frond D, now renamed to Al Barhi, of Palm Jumeira whose general description and ground conditions were presented in Section 3.12.1.

The power of the vibroflot's motor that was used in this study was 96 kW. The amplitude at the tip of the vibro probe was rated at 6 mm. Centrifugal force and eccentric moment were respectively 193 kN and 17 Nm. Vibration frequencies were up to 53 Hz.

Vibration monitoring was carried out using an accelerometer at distances of 5, 10, 15, 20, 30, 40 and 70 m along 4 lines for two treatment points. *PPV* was recorded at depths ranging from seabed at approximately 12.5 m to 2 m below the ground surface.

Measured *PPV* at various depths and distances from the vibroflot are shown in Figure 3-266. Although the scatter of data does not allow the realisation of curve fitting processes with high amounts of reliability, it can be observed that *PPV* reduces not only with distance, but also with depth. The lines that are shown in Figure 3-266 are not the best fitted curves for

PPV versus vibroflot depth, but are drawn to visualise the trend of changes. What is noticeable is that the rate of *PPV* reduction with depth increases as distance reduces.

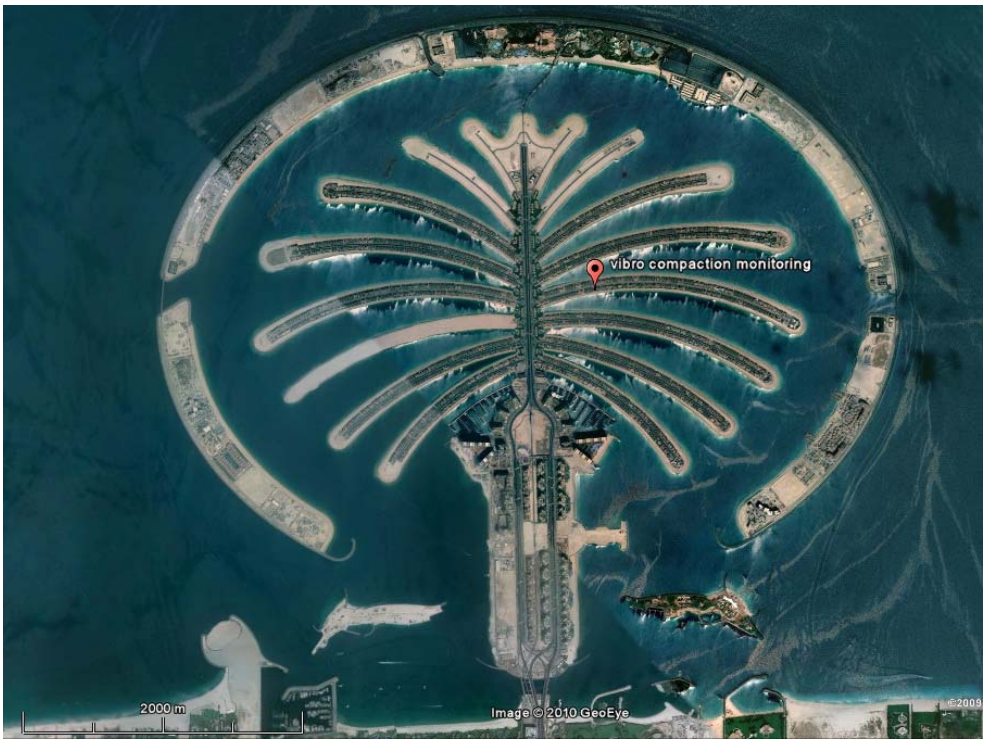

Figure 3-265: Location of vibro compaction vibration monitoring on Frond D of Palm Jumeira

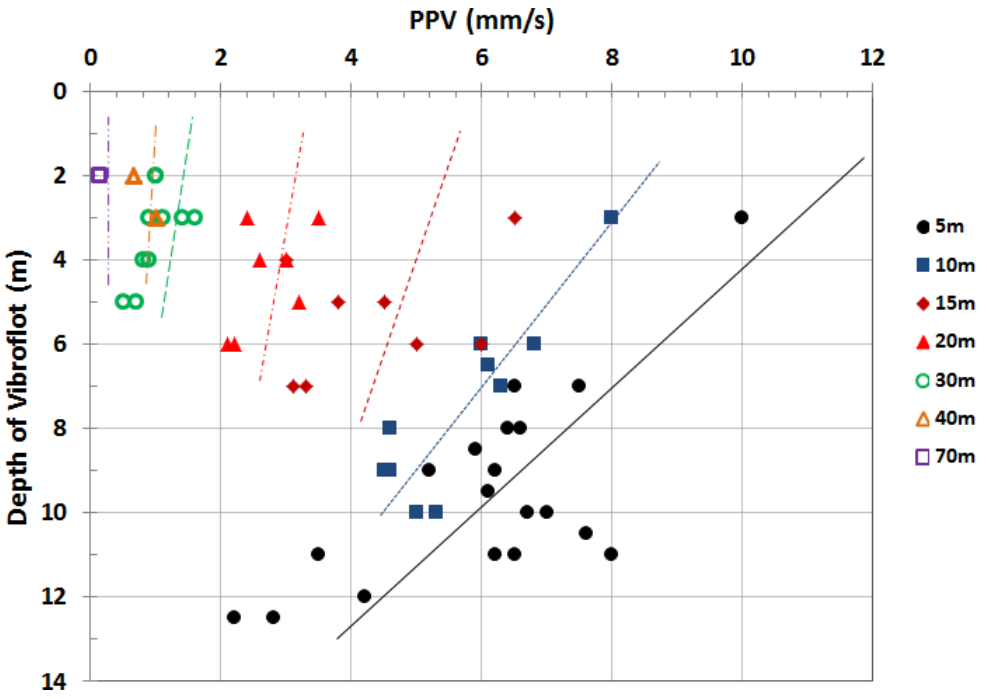

Figure 3-266: *PPV* at various depths and distances from the vibroflot

As *PPV* monitoring has not included data above the depth of 2 m, extrapolation must be carried out to predict *PPV* at shallower depths. Considering the amount of data scatter, this

approach is justifiable. Using this concept, it is possible to develop a curve for PPV when the vibroflot nose is at ground level. This is shown as a dotted curve in Figure 3-267. It can be seen that even though the plot of the extrapolated PPV values on ground surface is not strictly parallel to the other curves, the curve that best fits these points (the solid line in Figure 3-267) is parallel with the other lines and falls in between the 75 and 120 kW vibroflots. This suggests that earlier research may have also measured PPV at ground surface.

Figure 3-267 also suggests that while the magnitude of vibro compaction generated vibrations can be expected to be less than dynamic compaction vibrations at the same distance, implementation of vibro compaction can also lead to exceeding proposed vibration limits (Siskind et al., 1980) at distances that are less than 10 m.

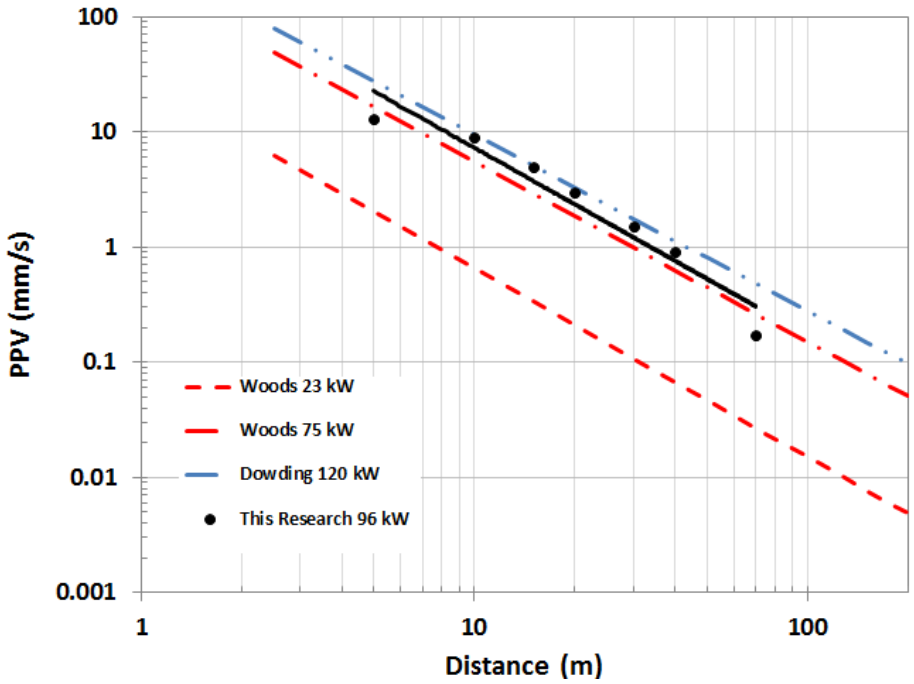

Figure 3-267: vibro compaction generated *PPV* versus distance

In Equation 2-148 Wiss (1981) expressed PPV as a direct function of distance, d, and reciprocal function of energy, E:

$$PPV = K\left(\frac{d}{\sqrt{E}}\right)^{-n} \qquad 2\text{-}148$$

K is the intercept with the ordinate and n is the slope or attenuation rate.

As power, P, is energy per unit of time, it is possible to express vibro compaction generated PPV in terms of vibroflot power and distance. By applying Equation 2-148 to the PPV measurements by Woods and Jedele (1985), Dowding (2000) and this study, it can be calculated that n is from 1.52 to 1.64 with an average value of 1.59. Calculation shows that K ranges from 2.08 to 8.16 with an average value of 6.2 for the four set of curves. Noting that the lowest K value is for the 24 kW vibroflot, the average K for the remaining 3 vibroflots will be 7.5 when the value of the 24 kW vibroflot is excluded. As the 24 kW vibroflot, if ever at all, is less commonly used than the other types of vibro probes, and since using a larger K value is more conservative (as it over estimates); thus, when P is in kW and d is in metres:

$$PPV = 7.5\left(\frac{d}{\sqrt{P}}\right)^{-1.59} \quad \text{mm/s} \qquad \text{3-22}$$

It can be observed that while the attenuation rate for vibro compaction is 1.59 the same parameter for dynamic compaction was 1.1 in Equation 2-151. This signifies that the attenuation rate of dynamic compaction is less than vibro compaction. In other words, dynamic compaction vibrations will reduce over a longer distance.

3.16.5 Lessons and Conclusion

In the projects that were studied in this Section, vibrations were monitored during dynamic compaction works. Measurements included vibration frequencies and peak particle velocities for various pounder weights, drop heights and at various distances. From the results it can be understood that:

1. Vibration frequencies were generally in the range of 5 to 20 Hz.

2. Measured PPVs were 3 to 5 times less than Equation 2-150. Equation 2-152 also appeared to be conservative, but was able to estimate more accurate results.

3. Equation 2-153 was able to predict reasonably close values to field-measured PPVs; however, the equation sometimes underestimated the results.

4. Equation 2-153 suggests that without application of specific vibration reduction techniques, it may be possible to carry out dynamic compaction as close as 25 to 35

m from structures without exceeding the maximum PPV values that have been recommended by USBM (Siskind et al., 1980).

5. Equation 2-151 is able to predict PPV reasonably well and with sufficient accuracy; however, it may underestimate PPV at distances less than 20 m. As both measured and predicted vibrations within the underestimation zone are probably above recommended tolerances and specific vibration reduction measures have to be adapted, Equation 2-151 can still be used for distances that are further away than 20 m and with caution and as a first assessment at closer distances.

6. Vibration parameters have been monitored for different number of blows and distances during several phases of dynamic compaction. It has been observed that peak particle velocities are greater during later phases of compaction as compared to the premier phases. The differences are greatest at farther distances, and it appears that when the distance is closer than a critical value, compaction phase influence becomes unnoticeable.

7. Vibration frequency associated with PPV increases with distance.

8. Excavation of a trench that was 25 m long, 2.5 m deep (to groundwater level), 2.5 m wide, and that was approximately 13 m away from a DC print was able to reduce PPV on average to half of its value when there was no trench. This experiment suggests that isolation trenches can be an effective means for reducing dynamic compaction vibrations.

9. The result of this study indicates that maximum PPV can be expected to be highest when the vibroflot is closest to the ground surface. In other words, the most critical time that vibroflot vibrations can damage a nearby structure is when it is just penetrating the ground or being pulled out of the treatment point.

10. Vibro compaction generated PPV can be estimated as a function of vibroflot power and distance from Equation 3-22.

11. It appears that while the magnitude of vibro compaction generated vibrations can be expected to be less than dynamic compaction vibrations at the same distance, vibro compaction generated vibrations can also exceed vibration limits (Siskind et al., 1980) at distances that are less than 10 m.

12. The attenuation rate of dynamic compaction is less than vibro compaction. In other words, dynamic compaction vibrations will reduce over a longer distance.

3.17 Predicting P_{LM} and E_M from Dynamic Compaction Induced Subsidence

3.17.1 Introduction

Common practice in dynamic compaction to carry out a calibration programme before production and execution of actual ground improvement works to optimise the design parameters. The ground is tested before soil treatment to provide an understanding of its condition and geotechnical parameters. Then, dynamic compaction is carried out on a predefined grid size with a number of blows that are thought to provide the best post improvement data. A number of heave and penetration tests may be carried out during the calibration to provide an understanding of the trend and amount of compaction and heave during the pounder impacts.

Upon completion of dynamic compaction the ground will be tested again to ensure that the desired parameters have been achieved. Occasionally, a number of patterns may be tried in the calibration to provide the engineer with more design options and sometimes poor test results force the repetition of the calibration with alternative patterns. Testing consumes time, and it would be very displeasing to realise that the results were not acceptable after the completion of the tests and interpretation of the data. Thus, it would be beneficial to be able to predict the amount of post treatment soil condition and to take possible corrective measures if the prediction indicates that the tests will not meet the design criteria.

In this section of this thesis a new method is proposed for the estimation of post dynamic compaction P_{LM} and E_M based on the amount of induced ground subsidence by dynamic compaction.

Ground subsidence due to treatment, *per se*, is not a criterion that should be used for assessing or verifying soil improvement, but can be used as an indication of the amount of improvement. With the same amount of energy, loose soil will subside more than dense soil. Likewise, the greater the applied energy is, the larger the induced subsidence will be. However, large or small amounts of settlements do not necessarily mean that design criteria have or have not been satisfied.

If it was possible to relate subsidence to the amount of improvement of the measurable soil parameters, then subsidence could be used in conjunction with actual pre-treatment test results to predict and to estimate the ground condition after dynamic compaction.

3.17.2 The Relation between Induced Strain and Subsidence with P_{LM} and E_M

Varaksin et al. (2005) have developed a relationship between dynamic compaction induced strain and P_{LM} improvement for the dune sands of Al Quo'a (refer to Section 3.3). The hypothesis used was that P_{LM} will double for every 3% of strain. Thus:

$$\varepsilon = na \tag{3-23}$$

$$(P_{LM})_j \Big/ (P_{LM})_i = 2^n \tag{3-24}$$

ε= strain

$(P_{LM})_i$= limit pressure before soil improvement

$(P_{LM})_j$= limit pressure after soil improvement

n= number of times the limit pressure has doubled

a= percentage of strain induced for doubling P_{LM} (3%)

Solving Equation 3-24 for n, and replacing its result in Equation 3-23 will yield:

$$\varepsilon = \frac{log\left((P_l)_j \Big/ (P_l)_i\right)}{log\ 2} a \tag{3-25}$$

Further expanding this notion will result in a relationship between ground subsidence and the increase in limit pressure:

$$s = \sum_{k=1,m} h_k \varepsilon_k = \frac{a}{log\ 2} \sum_{k=1,m} h_k\ log\left((P_l)_j \Big/ (P_l)_i\right) \tag{3-26}$$

m= number of pressuremeter tests in the borehole within the improvement zone (i.e., the depth where P_{LM} has increased), and h_k is the testing spacing. If $(P_{LM})_j/(P_{LM})_i$ is denoted by r ($r \geq 1$), then the subsidence can be calculated to be:

$$s = \sum_{k=1,m} h_k \frac{log(r)_k}{log\ 2} a \qquad 3\text{-}27$$

Replacing the values of a =0.03 and log 2 in Equation 3-27 will yield:

$$s = 0.1 \sum_{k=1,m} h_k\ log(r)_k \qquad 3\text{-}28$$

3.17.3 Strain Distribution in Dynamic Compaction

As illustrated in Figure 2-63, Lukas (1986) studied lateral ground movement due to dynamic compaction, and measured lateral movements in three types of soils at distances of 3 and 6 m from the pounder. Figure 2-63 suggests that the magnitude of ground movement initially increases to some depth, but then reduces and eventually becomes negligible. Noting that we have already established a relationship between strain and P_{LM} in Equation 3-25, it would be rational to assume that the soil's post dynamic compaction P_{LM} profile will also follow a similar trend. This has been observed by Lukas as well (refer to Figure 2-62).

Similar results have also been achieved by Hajialilue-Bonab and Rezaei (2009) (refer to Figure 2-64) who carried out laboratory scale dynamic compaction using particle image velocimetry techniques. A sickle shape curve characterises the soil displacement profile along vertical lines of soil, and the curves become flatter as they go farther away from the impact centre. It was observed that the displacement of soil in any given horizontal plane has a bell shaped curve.

Berry et al. (2004) proposed that for simplicity a Rayleigh distribution be used for void ratio reduction. The probability density function Rayleigh distribution can be mathematically written in the form of Equation 3-29:

$$\varepsilon(z) = \frac{z}{\sigma^2} e^{-z^2/2\sigma^2} \quad \text{3-29}$$

z= depth from ground surface

σ= depth of maximum strain. Lukas (1986) assumes maximum improvement to be a depth between one third to one half the depth of improvement.

3.17.4 Developing the Procedure

The procedure that is proposed in this Section is subject to the below conditions and assumptions:

1. A pre-treatment pressuremeter test has been carried out in the calibration area.
2. The material grading in the ground is relatively uniform throughout the treatment depth.
3. The soil parameters are fairly uniform before treatment; i.e., there are not any very loose or very dense layers.
4. Average ground settlement is measured; either by levelling the ground after dynamic compaction or by using the average measured settlement of the heave and penetration test for the pounder's cell.
5. As geometric mean values are used in bearing capacity calculations (see Section 2.9.2.6), even if prediction of P_{LM} at individual points varies from reality, the difference in bearing capacity calculations would remain within acceptable derivations.

Ground subsidence due to dynamic compaction is the accumulation of the vertical deformation of the layers within the depth of improvement; thus:

$$s = \sum_{k=1,m} \varepsilon_{DC\_k} h_k \quad \text{3-30}$$

ε_{DC_k}= dynamic compaction induced strain in layer (test spacing in borehole) k

If we assume that test spacing is the same throughout the borehole, then Equation 3-30 can be re-written as:

$$\sum_{k=1,m} \varepsilon_{DC\_k} = \frac{s}{h} \qquad 3\text{-}31$$

h= test spacing in borehole

If all layers had the same initial P_{LM} value, then it could have been said that dynamic compaction induced strain could have been defined in a simplistic approach to follow the Rayleigh distribution; however, P_{LM} values will most probably vary in reality. Thus, it is necessary to introduce a pre-strain, ε_{o_k}, for each layer that demonstrates the strain difference of that layer compared to the lowest P_{LM} value. In other words, considering the pre-treatment loosest soil level as the local origin of computations, it can be assumed that all other layers have undergone a strain to reach their initial pre-treatment state. As shown in Figure 3-268, the summation of ε_{o_k} and ε_{DC_k} will form the Rayleigh distribution strain, ε_R:

$$\varepsilon_{o\_k} + \varepsilon_{DC\_k} = \varepsilon_R \qquad 3\text{-}32$$

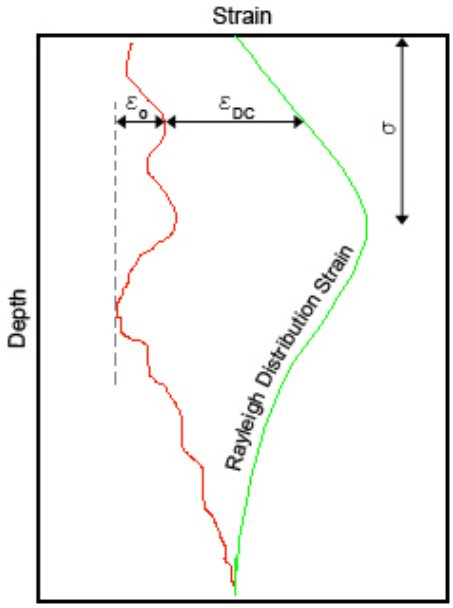

Figure 3-268: Rayleigh distribution strain as a function of pre-treatment and DC induced strain

ε_R follows and is proportional to the Rayleigh distribution, thus:

$$\varepsilon_{o\_k} + \varepsilon_{DC\_k} = \varepsilon_R = c_R \frac{z}{\sigma^2} e^{-z^2/2\sigma^2} \qquad 3\text{-}33$$

σ= scale parameter of the distribution

c_R= proportion coefficient

ε_{o_k} is not known, but can be back calculated by determining the amount that each layer had strained to reach its pre-improvement limit pressure, P_{LM_k}, as compared to the minimum pre-treatment limit pressure value, P_{LM_min}. This calculation can be done using Equation3-25, re-written below:

$$\varepsilon_{o\_k} = \frac{log\left(\left(P_{l\_k}\right)/P_{l\_min}\right)}{log\,2}a \qquad 3\text{-}34$$

Once ε_{o_k} and ε_{DC_k} for each layer has been determined, it is then possible to add them all up, and determine the coefficient:

$$\sum \varepsilon_{o\_k} + \sum \varepsilon_{DC\_k} = \sum \varepsilon_R = \sum c_R \frac{z_k}{\sigma^2} e^{-z_k{}^2/2\sigma^2} \qquad 3\text{-}35$$

or:

$$\sum \frac{log\left(\left(P_{l\_k}\right)/P_{l\_min}\right)}{log\,2} 0.03 + \frac{s}{h} = c_R \sum \frac{z_k}{\sigma^2} e^{-z_k{}^2/2\sigma^2} \qquad 3\text{-}36$$

$$c_R = \frac{\sum \frac{log\left(\left(P_{l\_k}\right)/P_{l\_min}\right)}{log\,2} 0.03 + \frac{s}{h}}{\sum \frac{z_k}{\sigma^2} e^{-z_k{}^2/2\sigma^2}} \qquad 3\text{-}37$$

σ can be assumed to be an arbitrary value between one half to one third of the depth of influence. However, experimenting with this parameter in this research suggested that predicted post improvement limit pressures are very sensitive to σ, and lesser σ values tend to result in unrealistically high limit pressure values at depths that are in the vicinity of σ. It appears that a value of 0.45 to 0.5 times the depth of influence can predict more rational P_{LM} peak values. It is recommended that peak values be controlled and the value of σ be reviewed accordingly.

Once c_R has been determined, Equation 3-35 can be used to calculate ε_{DC_k} for each layer:

$$\varepsilon_{DC\_k} = \frac{\sum \frac{log\left(\left(P_{LM\_k}\right)/P_{LM\_min}\right)}{log\ 2} 0.03 + \frac{s}{D}}{\sum \frac{z_k}{\sigma^2} e^{-z_k{}^2/2\sigma^2}} \frac{z}{\sigma^2} e^{-z^2/2\sigma^2} - \frac{log\left(\left(P_{LM\_k}\right)/P_{LM\_min}\right)}{log\ 2} 0.03 \quad 3\text{-}38$$

As a final step, using Equations 3-23 and 3-24 in conjunction with Equation 3-38, the post improvement P_{LM} value of each layer can be computed to be equal to:

$$\left(P_{LM\_k}\right)_{post} = \left(P_{LM\_k}\right)_{pre} 2^{\varepsilon_{DC\_k}/0.03} \quad 3\text{-}39$$

If calculations yield a negative value for ε_{DC_k}, then the calculation procedure is predicting a negative strain or expansion of soil, which signifies a reduction in P_{LM}. In such a case the calculation should be repeated without considering the rows associated with the negative strain values.

Menard (Centre D'Etudes Menard, 1975) has identified a correlation between P_{LM} and E_M for different soil types (refer to Table 2-22); hence, it seems rational to be able to predict post dynamic compaction E_M values using a similar approach.

E_M will double in value every time the soil is strained by a certain percentage, b, which does not necessarily have to be 3%. Equations 3-34, 3-37, 3-38, and 3-39 can be re-written in terms of b and E_M:

$$\varepsilon_{o\_k} = \frac{log\left(\left(E_{M\_k}\right)/E_{M\_min}\right)}{log\ 2} b \quad 3\text{-}40$$

$$c_R = \frac{\sum \frac{log\left(\left(E_{M\_k}\right)/E_{M\_min}\right)}{log\,2} b + \frac{s}{h}}{\sum \frac{z_k}{\sigma^2} e^{-z_k{}^2/2\sigma^2}} \left(P_{LM\_k}\right)_{post} = \left(P_{LM\_k}\right)_{pre} 2^{\varepsilon_{DC\_k}/0.03} \quad 3\text{-}41$$

$$\varepsilon_{DC\_k} = \frac{\sum \frac{log\left(\left(E_{M\_k}\right)/E_{M\_min}\right)}{log\,2} b + \frac{s}{D} \frac{z}{\sigma^2} e^{-z^2/2\sigma^2}}{\sum \frac{z_k}{\sigma^2} e^{-z_k{}^2/2\sigma^2}} - \frac{log\left(\left(E_{M\_k}\right)/E_{M\_min}\right)}{log\,2} b \quad 3\text{-}42$$

$$\left(E_{M\_k}\right)_{post} = \left(E_{M\_k}\right)_{pre} 2^{\varepsilon_{DC\_k}/b} \quad 3\text{-}43$$

3.17.5 Verification

Al'Quo'a New Township (Section 3.3) and Marjan Island Road Corridor (Section 3.6) projects have been chosen for verification of the proposed method for predicting P_{LM} and E_M from dynamic compaction induced ground subsidence.

In Al Quo'a New Township PMTs were used for quality control and verification purposes. Before and after dynamic compaction P_{LM} values for four locations are shown in Figure 3-30 to Figure 3-33. Measured site settlements after dynamic compaction were in the range of 0.60 to 0.80 m. For the purpose of verification calculations and as summarised in Table 3-30, settlements have been calculated according to Equation 3-28, and depths of improvement have been assumed to be testing termination depth. Also shown in Table 3-30 are the σ values and the ratio of actual to predicted geometric mean P_{LM} within the depth of influence.

Figure 3-269 shows the ratios of actual and predicted limit pressure improvements for the PMTs presented in Figure 3-30 to Figure 3-33. As can be observed that in all diagrams the predicted ratio of improvement is initially less than the actual ratio of improvement, and becomes greater after the depth of maximum improvement ratio has been reached, and

ultimately reverses back to being less at the deepest treatment zones. In all tests the geometric mean of the limit pressure within the improvement depth was quite close to reality with a maximum over estimation of about 5%.

Test ID	Figure 3-30	Figure 3-31	Figure 3-32	Figure 3-33
D (m)	15	14	14	16
s (m)	0.88	0.50	0.59	0.66
σ/D	0.45	0.43	0.43	0.47
Ratio of actual to predicted $P_{LM\_\text{geometric mean}}$	0.97	0.95	0.96	1.00

Table 3-30: Calculation for prediction of post dynamic compaction limit pressures

Ground subsidence due to dynamic compaction at Marjan Island Road Corridor was 0.29 m, and the P_{LM} and E_M values before and after dynamic compaction are shown in Figure 3-104. While it could have been expected that the improvement profiles would look like sickles, which could be defined with a Rayleigh distribution, that was not exactly the case, and improvements seem to have been more uniform in depth with occasional points of higher strength. Due to the non-classical shape of the improvement profiles it is interesting to study the applicability of the proposed calculation procedure for the prediction of P_{LM} and E_M.

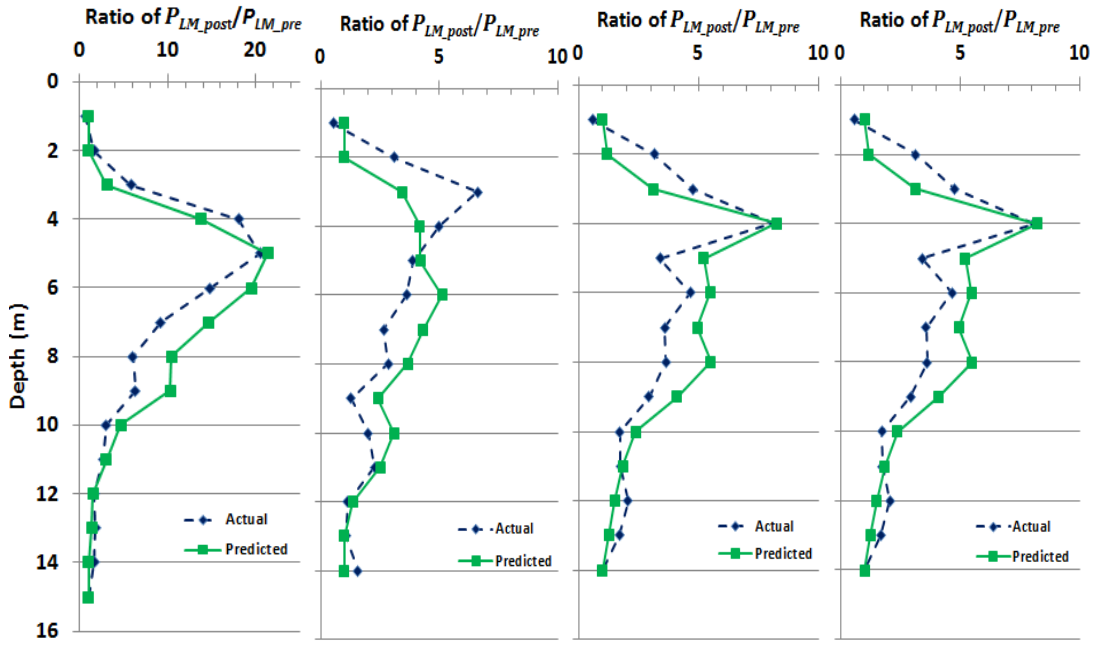

Figure 3-269: Ratios of actual and predicted limit pressure improvements for PMTs of Figure 3-30 to Figure 3-33

For calculation purposes it is assumed that depth of improvement was 10 m (any strain in the deeper denser layers has been assumed to be negligible), σ= 4.5 m, and a= b= 3%.

While subsidence calculated P_{LM} values was from 0.27 to 0.34 m, which is close to the actual average subsidence, E_M based settlement calculations were larger and from 0.33 to 0.42 m. This is not necessarily inaccurate as all tests were performed in print locations. The greatest difference was observed in PMT-102 with the most fluctuating profile.

Actual and predicted P_{LM} and E_M improvement ratios are shown in Figure 3-270. For both P_{LM} and E_M, the general shape of the ratios of predicted post improvement to initial values are rather similar to the ratios of actual post improvement to initial values; however, the actual harmonic mean P_{LM} is 94% to 117% of predicted harmonic mean. In line with the predicted settlements based on E_M, the actual geometric mean E_M is 112% to 144% of the predicted geometric mean. It appears that in general the largest variation in the ratios is in the level where improvement is maximal. This may be due to the fact that all tests were carried out in the print itself; however, more research is required to confirm this explanation. The biggest difference is once again observed in PMT-102. Also, the review of E_M to P_{LM} ratios in the post improvement tests shows that the range of values in PMT-102 has had the most amount of variation.

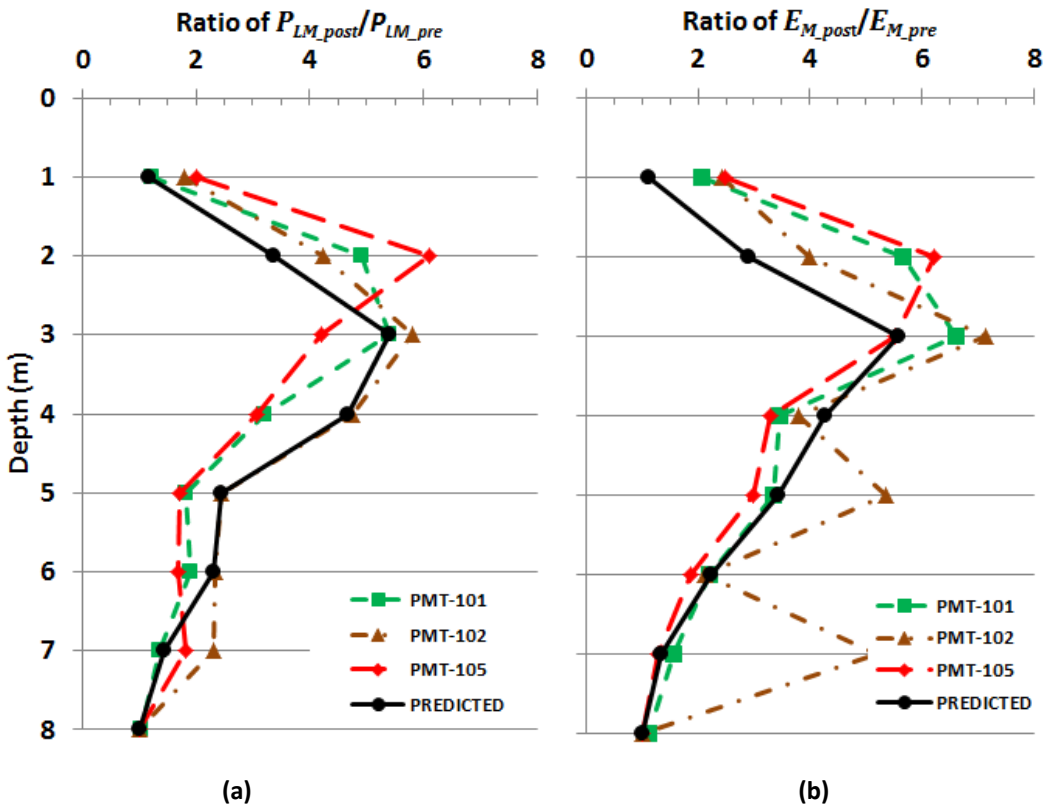

Figure 3-270: Actual and predicted improvement ratios for (a) P_{LM}, (b) E_M

3.17.6 Conclusions

Although it is the belief of the author that actual field tests are the best means for verification of ground improvement works, a calculation procedure has been proposed that can be used as a tool for a first estimation of P_{LM} and E_M values after dynamic compaction. It is noted that:

1. In the proposed procedure it is assumed that P_{LM} and E_M double for every 3% of strain. It is also assumed that the final induced strain in the ground has a Rayleigh distribution.

2. Eliminating the errors of correctly predicting the depth of improvement and ground settlement, it was observed that the Rayleigh distribution is quite sensitive to the scale parameter of the distribution, which is the depth at which strain is maximal. It has been observed that the shallower this depth is the more strain is predicted. It appears that the depth of maximum strain should be assumed to be about 0.45 to 0.5 times the depth of improvement.

3. It has also been observed that the Rayleigh distribution initially underestimates the ratio of P_{LM} improvement; however, beyond the point of maximum ratio of improvement the ratio is overestimated and at the lowest depths the ratio is once again underestimated. Furthermore, in the PMTs that have been studied the predicted geometric limit pressures after dynamic compaction were very close to reality.

4. Application of the proposed procedure was also implemented to PMTs inside DC prints that did not have a sickle shaped improvement profile. Predicted harmonic means P_{LM} in the treatment depth were reliably close to measured harmonic mean P_{LM} values. Back calculated settlement based on measured E_M was more than reality and predicted geometric mean E_M values were less than measured geometric mean values; however, the profile shapes were still reasonably similar to reality. The biggest differences between predicted and measured parameters occurred in PMTs that had the least resemblance to the shape of the sickle.

4 Conclusion

Dynamic compaction and dynamic replacement were respectively patented by Louis Menard in 1970 and 1975. Menard died in 1978, but his legacy was continued by his first generation of engineers. It has been the author's privilege to have been exposed to dynamic compaction and dynamic replacement through the mentoring and guidance of Mr Serge Varaksin who is the first engineer that was employed by Louis Menard and who is the world's leading expert on the subject.

It has come to the author's attention that while dynamic compaction and dynamic replacement have become popular ground improvement techniques due to cost, execution speed, reliability and ability to meet specifications, information about these methods are scattered, and to the knowledge of the author, no attempt has been made since the comprehensive publications of Lukas (1986, 1995) to gather, compile and update previous research and experience on the subject. Hence, Chapter 2 of this thesis was allocated to a thorough and comprehensive literature review.

Chapter 3 focused on distinguished and sometimes globally renowned projects in which the author was directly involved in or indirectly associated with. This provided the author with the opportunity not only to record the approach, construction and quality control methodology in these projects as reference for future studies, but also to compare the results with previous research, and to develop new formulations that were previously not available.

In conclusion it can be noted that:

1) It is more likely that non-engineered backfilling will be loose and potentially subject to low bearing and excessive settlements. Experience in the projects that have been studied in this thesis indicates that regardless of the filling process being on land or at sea, all dumping methods, either tipped or hydraulically placed, result in a range of densities of loose sand fills. It is recommended that ground improvement be perceived during planning stage to avoid any surprises and disappointments when construction commences.

2) Proper determination of design criteria is very important, and failure to adopt a suitable specification can lead to unnecessary treatment, additional costs and delay.

3) The most suitable acceptance criteria are based on design criteria and actual project requirements. It is not necessary to specify minimum test results as verification of satisfying design criteria can be achieved without this limitation. One criterion does not have to govern throughout the depth of treatment. In Al Quo'a the upper layers were treated for bearing capacity and settlement under structural loads while the deeper soils were treated for self-bearing.

4) It was observed in Abu Dhabi New Corniche Road and Al Nakhilat Ship Repair Yard projects that relative density is not a reliable acceptance criterion. It has been seen that in practice fines content can exceed the acceptable limits defined for applicability of relative density, which will result in the project becoming criteria-less in those conditions. Also, it was observed that it is possible to improve the ground more and provide better results (higher bearing capacity and lesser settlements) without necessarily satisfying relative density requirements. The ground works as a mass, not in individual layers, and not satisfying the requirement at one level does not necessarily lead to inferior results.

5) Dynamic compaction is an affordable and effective ground improvement technique for treating thick dry desert dune sands or saturated sands.

6) If the project size justifies, in an optimal dynamic compaction design the treatment area should be broken down to sub areas based on design and acceptance criteria, loading, and ground conditions. Pounder weight and drop height, compaction intensity, grid size, and the other design parameters can consequently be determined. In large projects, it is preferable to mobilise dynamic compaction rigs with different capacities to optimise the relationship between equipment capacity and required impact energy.

7) Classical approaches where activities are clearly separated into preliminary works, design and construction may not yield desirable results in special projects in which the site is unusually large, preliminary field tests are most probably insufficient, and design and construction period is relatively short. In these projects construction may have to commence simultaneously with the preparation of architectural and structural drawings. It is possible to successfully proceed in such projects if design and construction phases are merged smartly and efficiently, a combination of ground improvement techniques are used for treating different ground conditions rather than attempting to implement one technique with its limitations to a variety of different conditions, possible production rates are well understood and sufficient amounts of plant and equipment are mobilised,

and site observations are given value and changes in actual ground conditions are taken into account during the process of the works.

8) The mass mechanical properties of sand layers can be further improved by introducing dynamically compacted crushed stone inclusions.

9) Early planning will allow mobilisation of sufficient numbers of plant and equipment to perform grand size projects in relatively short periods.

10) Energy intensity can be optimised based on the calibration programme results.

11) It is not necessary to compact the ground until reaching the asymptote of ground settlement (or compaction) versus number of drops (or accumulative energy). What is relevant is to demonstrate that design criteria (settlements, bearing capacity, etc) have been satisfied.

12) It is possible to meet the project specifications in a shorter time by using heavy pounders with high drops rather than using lighter pounders with the same energy intensity.

13) The combination of treatment methods; e.g. dynamic replacement and surcharging or dynamic surcharging can expand the applicability limits of the ground improvement techniques.

14) Pre-excavation of soft saturated soils can be used to accelerate pore water pressure dissipation and to allow more repetition of pounder dropping during each sub-phase of dynamic replacement before creating the state of liquefaction. At critical locations pre-excavation can be further adopted in the form of DR trenches.

15) By pre-excavation of soft saturated soils and allowing accelerated dissipation of pore water pressure it is possible to use sand for backfill material; otherwise pounder impact will liquefy the sandy backfill material.

16) Dynamic surcharging can be used to accelerate the consolidation of saturated silty sands and sandy silts. It is the author's experience that dynamic surcharging is applicable to silts, but not to clays. Additionally the degree of consolidation must be roughly in the range of 50 to70%. This technique was used successfully in King Abdulla University of Science and Technology when building loads were considerably increased during the period at which ground improvement works were proceeding. In Palm Jumeira Sewage

Treatment Plant dynamic surcharging was used to increase induced foundation settlement under static surcharge by 1.3 to 5 times depending on the distance from the pounder impact point. Although the settlement magnitude of dynamic compaction was much more than dynamic surcharging, the latter induced critical settlement at depths that were treated less effectively with the allocated pounder.

17) It is possible to perform dynamic compaction at close vicinity to the shoreline. Dynamic compaction was literally carried out to the edge of the reclamation in Abu Dhabi New Corniche.

18) It is possible to efficiently improve the depth of influence in dynamic compaction by implementation of the free falling and automatic grabbing MARS technology. This technology was used in Al Quo'a New Township and Al Nakhilat Ship Repair Yard to drop a 35 ton pounder.

19) To the knowledge of the author, the world record for the most number of DC and DR rigs was achieved in King Abdulla University of Science and Technology with 13 rigs working in double shifts.

20) To the knowledge of the author, at the time Al Falah Community Development was under construction, it held the world records for largest (in size) single ground improvement contract at 4.84 million m^2 and highest production rate of 966,000 m^2 of soil improvement in one month.

21) Should the grid pattern be close enough, compaction of first phase prints will also somewhat densify the ground influenced by the second phase prints. Consequently, it may be possible to apply lesser amounts of energy in the second phase of compaction.

22) The efficiency of dynamic compaction rapidly deteriorates with the increase of fines content to a point where dynamic compaction may no longer be able to satisfy acceptance criteria, and the technique must be switched to dynamic replacement. It was observed in King Abdulla University of Science and Technology that increase of fines resulted in lesser improvement with the same amount of impact energy intensity, and it appeared that the limit of efficient dynamic compaction is 30% fines content. In Abu Dhabi Ritz-Carlton Hotel, while PMT parameters of the soft layer increased after DR by up to 100%, the improvement was not sufficient to satisfy acceptance criteria without the introduction of compacted granular material in the form of DR columns. P_{LM}

improvement inside the DR column was more than 900% the value of the original ground, and 5.15 times more than the improvement in between the columns. A similar behaviour was also observed at Al Jazira Steel Pipe Factory.

23) Pounder impacts create heave around the crater when the ground contains saturated cohesive soils, but the periphery of the crater also settles (negative heave) when the soil is granular.

24) Depth of improvement can be increased by applying DC blows to pre-excavated prints.

25) Application of ironing phase of DC will improve the superficial ground parameters.

26) For marine DC, the barge must be large enough to safely support the personnel and equipment. The barge size will be influenced by the location of the project and the sea conditions.

27) Water resistance reduces the pounder's dropping velocity, and consequently the impact energy.

28) Offshore pounders must be designed to minimise water resistance. As water resistance reduces impact energy, marine pounders are generally heavier than land pounders.

29) Suitable material (rock fill) must be placed on the seabed prior to commencement of dynamic compaction works. In the Quay Expansion in Southeast Asia rock size ranged from 150 to 300 mm.

30) Grid size and number of blows for marine application of DC and DR does not appear to be very different from the parameters that would be used for land based DC and DR; however, water resistance reduces impact efficiency, and equations developed for estimation of depth of improvement in land based DC are not applicable to marine DC.

31) In Abu Dhabi New Corniche average P_{LM} improvement ratios after dynamic compaction were from 1.5 to 7. In Al Quo'a New Township it was observed that it is possible to improve maximum P_{LM} values of dune sands on average by up to 570% and at least in one instance by up to 1950%. Improvement beyond 400% was observed over a thickness of 20% of treatment depth. In Al Falah Community Development improvement ratio in the calibration programme was in the order that has been suggested by Lukas (1986). However, it could be cautiously expected that higher energy intensities will result in

better results. In Marjan Island Road Corridor PMT parameters' improvement ratios were in the order suggested by Lukas (1986). In Reem Island Causeway P_{LM} improvement ratio in the upper several metres of soil was 500 to 700%. The parameters' improvements were still substantial and in the range of 80 to 130% at depth. It is possible to achieve P_{LM} values greater than 2.4 MPa after dynamic compaction in saturated sands; however, the peak value decreases with depth. Noting that the amount of improvement is a function of impact energy, it is possible to improve P_{LM} of saturated sands by 500%, but the peak amount of improvement decreases with depth. The maximum amount of improvement appears to be in the upper half of the depth of improvement. In HFO Tanks the maximum percentage of improvement was much more than what is suggested by earlier literature and observed values for other projects that have been studied in this thesis. PMT parameters' Improvement ratios were in the order of 40 and maximum P_{LM} was in the order of 5,000 MPa. In Palm Jumeira STP project, excluding the highest values, average P_{LM} and E_M respectively ranged from approximately 20 to 40 MPa and from 23 to 30 MPa at depths of about 4 m to 8 m. These values are significantly higher than what has been suggested by Lukas (1986). Maximum improvement ratios were in the range of 10 to 18, which are significantly higher than the range that has been suggested by Lukas. In summary, it appears that while post improvement upper bound values of 1900 to 2400 kPa is a reasonable range, it is possible to exceed these values if sufficient energy is applied. Likewise, while Lukas proposes that properties of soils will improve in the order of 100 to 400% after dynamic compaction, it has been observed in the research conducted in this thesis that it is possible to substantially exceed these figures.

32) SPT can result in misleading interpretations when the ground is composed of large size particles.

33) It is possible to perform dynamic compaction in populated areas. DC works were carried out in an urban area that was highly populated with high rise buildings throughout the length of Abu Dhabi New Corniche, and a 35 ton pounder was dropped in free fall not far away from town houses in Al Quo'a New Township.

34) Buildings that are at very close to dynamic compaction works may sustain damage not only due to vibrations, but also from DC induced ground movements.

35) Dynamic compaction generated vibration frequencies were measured to be generally in the range of 5 to 20 Hz.

36) Measured PPVs in the projects that were studied in this thesis were 3 to 5 times less than what is estimated from Equation 2-150 (Mayne, 1985). Equation 2-152 also appeared to be conservative, but was able to estimate more accurate results.

37) Equation 2-153 (Varaksin, 1981) was able to predict reasonably close values to field-measured PPV; however, the equation sometimes underestimated the results.

38) Peak particle velocity can be estimated for more commonly used impact energies by

$$PPV = 560d^{-1.1} \text{ mm/s} \qquad \text{2-1533-20}$$

Or more generally by

$$PPV \leq 25\left(\frac{\sqrt{WH}}{d}\right)^{1.1} \qquad \text{2-1513-21}$$

39) Equation 2-1533-20 suggests that without application of specific vibration reduction techniques, it may be possible to carry out dynamic compaction as close as 25 to 35 m from structures without exceeding the maximum PPV values that have been recommended by USBM (Siskind et al., 1980).

40) Equation 2-1513-21 is able to predict PPV reasonably well and with sufficient accuracy; however, it may underestimate PPV at distances less than 20 m. As both measured and predicted vibrations within the underestimation zone are probably above recommended tolerances and specific vibration reduction measures will have to be adapted, Equation 3-21 can still be used for distances that are further away than 20 m and with caution and as a first assessment at closer distances.

41) Vibration parameters have been monitored for different number of blows and distances during several phases of dynamic compaction. It has been observed that, with the same impact energy, peak particle velocities are greater during later phases of compaction as compared to the premier phases. The differences are greatest at farther distances, and it appears that when the distance is closer than a critical value, compaction phase influence becomes unnoticeable.

42) Vibration frequency associated with PPV increases with distance.

43) Excavation of a trench that was 25 m long, 2.5 m deep (to groundwater level), 2.5 m wide, and that was approximately 13 m away from a DC print was able to reduce PPV on average to half of its value compared to when there was no trench. This experiment suggests that isolation trenches can be an effective means for reducing dynamic compaction vibrations.

44) A study carried out for comparative purposes on vibro compaction indicates that maximum PPV can be expected to be highest when the vibroflot is closest to the ground surface. In other words, the most critical time that vibroflot vibrations can damage a nearby structure is when it is just penetrating the ground or being pulled out of the treatment point.

45) Vibro compaction generated PPV can be estimated as a function of vibroflot power and distance from Equation 3-22:

$$PPV = 7.5\left(\frac{d}{\sqrt{P}}\right)^{-1.59} \quad \text{mm/s} \qquad \text{3-22}$$

46) While the magnitude of vibro compaction generated vibrations can be expected to be less than dynamic compaction vibrations at the same distance, implementation of vibro compaction can also exceed the proposed vibration limits (Siskind et al., 1980) at distances that are less than 10 m.

47) The attenuation rate of dynamic compaction is less than vibro compaction. In other words, dynamic compaction vibrations will reduce over longer distances.

48) At very close distances, both vibrations and ground deformation can result in cracking and damage to buildings.

49) The analyses of the data from the projects that were studied in this thesis suggest that there is a relationship between the square root of compaction volume and crater depth after the first few pounder blows. In Marjan Island corridor this ratio was about 2.15 to 2.4 (in SI units). In Palm Jumeira STP the ratio was 2.26. The upper and lower bound values of 2.15 and 2.75 in Equation 3-11 resulted in 15% underestimation and 40% overestimation in that case. A ratio of 2.5 resulted in 16% overestimation. In Al Nakhilat Ship Repair Yard the ratio was about 2.11 (when only the crater volume is considered) to

2.32 (when the net compaction volume, being the resultant of the crater and periphery volume changes is considered). In Reem Island Causeway the ratio was approximately 2.6 m after the first several blows. In HFO Tanks the ratio was measured to be approximately 2.75. This figure was higher than the other projects that have been studied in this thesis. In summary, it was observed that:

$$\frac{\sqrt{V}}{D_c} = 2.15 \; to \; 2.75 \qquad \text{3-11}$$

50) In Al Nakhilat Ship Repair Yard it was observed that 90% and 10% of the compaction volume respectively originated from the crater and the ground around the crater. In Reem Island Causeway measurements suggest that 95% of the net compaction volume originated from the crater, and in HFO Tanks project the crater volume was about 60 to 65% of net compaction volume.

51) There appears to be a linear relationship between the logarithm of accumulative impact energy and $(D_T\text{-}D_B)/D_c$. More research is required to determine if the relationship is unique for a given soil type or whether it is also a function of the drop energy.

52) It was observed from Al Nakhilat Ship Repair Yard in Ras Laffan and Palm Jumeira Trial in Dubai that the relationship between CPT cone resistance and PMT parameters was not influenced by depth in saturated carbonate sands, and could be formulated by:

$$q_c = 4.82 P_{LM} \qquad \text{3-13}$$

$$q_c = \frac{E_M}{1.54} \qquad \text{3-14}$$

53) Silica sand correlations for Young modulus – cone resistance are not suitable for carbonate sands. It was observed that for the saturated carbonate sands of Palm Jumeira and Al Nakhilat Ship Repair Yard the relationship between CPT cone resistance and Young modulus is:

$$E_y = 3.12 q_c \qquad \text{3-163-16}$$

54) Friction angle of rock fill can be estimated from PMT by:

$$P^*_{LM} = 4 \times 2^{\frac{\varphi - 40}{7}} \qquad \text{2-2243-12}$$

55) A calculation procedure has been proposed that can be used as a tool for a first estimation of P_{LM} and E_M values after dynamic compaction. It is noted that:

a) In the proposed procedure it is assumed that P_{LM} and E_M double for every 3% of strain. It is also assumed that the final induced strain in the ground has a Rayleigh distribution.

b) Eliminating the errors of correctly predicting the depth of improvement and ground settlement (by adopting the actual depth of improvement), it was observed that the Rayleigh distribution is quite sensitive to the scale parameter of the distribution, which is the depth at which strain is maximal. It has been observed that the shallower this depth is the more strain is predicted. It appears that the depth of maximum strain should be assumed to be about 0.45 to 0.5 times the depth of improvement.

c) It has also been observed that the Rayleigh distribution initially underestimates the ratio of P_{LM} improvement; however, beyond the point of maximum ratio of improvement the ratio is overestimated and at the lowest depths the ratio is once again underestimated. Furthermore, in the PMTs that have been studied the predicted geometric limit pressures after dynamic compaction were very close to reality.

d) Application of the proposed procedure was also applied to PMTs inside DC prints that did not have a sickle shaped improvement profile. Predicted harmonic means P_{LM} in the treatment depth were reliably close to measured harmonic mean P_{LM} values. Back calculated settlement based on measured E_M was more than reality and predicted geometric mean E_M values were less than measured geometric mean values. However, the profile shapes were still reasonably similar to reality. The biggest differences between predicted and measured parameters occurred in PMTs that had the least resemblance to the shape of the sickle.

References

Aboshi, H., Ichimoto, E. & Harada, K. (1979) The Compozer: A Method to Improve Characteristics of Soft Clays by Inclusion of Large Diameter Sand Columns. *International Conference on Soil Reinforcement; Reinforced Earth and Other Techniques,* 2, Paris, 20-22 March, 211–216.

Aboshi, H., Mizuno, Y. & Kuwabara, M. (1991) Present State of Sand Compaction Pile in Japan. *Deep Foundation Improvements: Design, Construction and Testing, ASTM STP 1089-EB*, Philadelphia, 32-46.

Abramson, L. W., Lee, T. S., Sharma, S. & Boyce, G. M. (2002) *Slope Stability and Stabilization Methods, 2nd Edition*, John Wiley & Sons

Adalier, K. & Elgamal, A. (2004) Mitigation of Liquefaction and Associated Ground Deformations by Stone Columns. *Engineering Geology,* 72, 3-4, 275-291.

Adam, D. & Brandl, H. (2009) Innovative Dynamic Compaction Techniques & Integrated Compaction Control Methods. *17th International Conference on Soil Mechanics and Geotechnical Engineering*, Alexandria, Egypt, 5-9 October, 2216-2219.

Adam, D., Brandl, H., Kopf, F. & Paulmichl, I. (2007) Heavy Tamping Integrated Dynamic Compaction Control. *Ground Improvement,* 11, 4, 237-243.

Ahmad, S. & Al Hussaini, T. M. (1991) Simplified Design for Vibration Screening by Open and in-Filled Trenches. *Journal of Geotechnical Engineering, ASCE,* 117, 1, 67-88.

Airey, D., Nazhat, Y., Moyle, R. A. & Avalle, D. L. (2012) Dynamic Compaction - Insights from Laboratory Tests. *International Conference on Ground Improvement and Ground Control - Transport Infrastructure Development and Natural Hazards Mitigation (ICGI2012)*, Wollongong, NSW, Australia, 30 October - 2 November, 987-996.

Akiyoshi, T., Fuchida, K., Matsumoto, H., Hyodo, T. & Fang, H. L. (1993) Liquefaction Analysis of Sandy Ground Improved by Sand Compaction Piles. *Soil Dynamics and Earthquake Engineering,* 12, 299-307.

Al Hamoud, A. S. & Wehr, W. (2006) Experience of Vibrocompaction in Calcareous Sand of Uae. *Journal of Geotechnical and Geological Engineering,* 24, 3, 757-774.

Almeida, M. S. S., Jamiolkowski, M. & Peterson, R. W. (1992) Preliminary Result of CPT Tests in Calcareous Quiou Sand. *Calibration Chamber Testing: First International Symposium on Calibration Chamber Testing (ISCCT1)*, Potsdam, NY, 28-29 June 1991, 41-53.

Amar, S., Clarke, B. G. F., Gambin, M. P. & Orr, T. L. L. (1991) The Application of Pressuremeter Test Results to Foundation Design in Europe - Part 1: Predrilled Pressuremeters/ Self-Boring Pressuremeters. International Society of Soil Mechanics and Foundation Engineering, European Regional Technical Committee No. 4 - Pressuremeter, 1-23.

Amar, S. & Jezequel, J. F. (1972) Essais En Place Et En Laboratoire Sur Sols Coherents, Comparaison Des Resultats. *Bulletin de Liaison des Laboratoires des Ponts et Chaussées,* 58, March.

Anderegg, R. & Kaufmann, K. (2004) Intelligent Compaction with Vibratory Rollers - Feedback Control Systems in Automatic Compaction and Compaction Control. *Transportation Research Record: Journal of the Transportation Research Board,* 1868, 124-134.

Arslan, H., Baykal, G. & Ertas, O. (2007) Influence of Tamper Weight Shape on Dynamic Compaction. *Ground Improvement,* 11, 2, 61-66.

Asaoka, A. (1978) Observational Procedure of Settlement Prediction. *Soils and Foundations, Japanese Society of Soil Mechanics and Foundation Engineering,* 18, 4 (December), 87-101.

ASTM (1969) Test Method for Relative Density of Cohesionless Soils. *D 2049-69.*

ASTM (2006a) Standard Test Methods for Maximum Index Density and Unit Weight of Soils Using a Vibratory Table. *D4253–00 (Reapproved 2006).* 15.

ASTM (2006b) Standard Test Methods for Minimum Index Density and Unit Weight of Soils and Calculation of Relative Density. *D 4254–00 (Reapproved 2006).* 9.

ASTM (2007) Standard Methods for Prebored Pressuremeter Testing in Soils. *D 4719-07.*

Atherton, G. H., Polensek, A. & Corder, S. E. (1976) Human Response to Walking and Impact Vibration of Wood Floors. *Wood Product Journal,* 26, 10 (October), 40-47.

Avalle, D. L. (2004) Ground Improvement Using the Square Impact Roller - Case Studies. *5th International Conference on Ground Improvement Techniques*, Kuala Lumpur, March 2004.

Baez, J. & Martin, G. R. (1993) Advances in the Design of Vibro Systems for the Improvement of Liquefaction Resistance. *7th Annual Symposium of Ground Improvement*, Vancouver, 27-28 May, 1-16.

Baguelin, F., Jezequel, J. F. & Shields, D. H. (1978) *The Pressuremeter and Foundation Engineering,* Aedermannsdorf, Trans Tech Publications,617.

Balaam, N. P. & Booker, J. R. (1981) Analysis of Rigid Rafts Supported by Granular Piles. *International Journal for Numerical and Analytical Methods in Geomechanics,* 5, 4, 379-403.

Baldi, G., Bellotti, V. N., Ghionna, N., Jamiolkowski, M. & Pasqualini, E. (1986) Interpretation of Cpt's and Cptu's - 2nd Part: Drained Penetration of Sands. *4th International Geotechnical Seminar Field Instrumentation and In-Situ Measurements*, Nanyang Technological Institute, Singapore, 25-27 November 1986, 143- 156.

Banerjee, P. K. (1994) *The Boundary Element Methods in Engineering,* London and New York, McGraw Hill Book Co

Barkan, D. D. (1962) *Dynamics of Bases and Foundations (Translated from Russian by L Drashevska and Edited by G P Tschbotarioff),* New York, McGraw Hill Book Co,434.

Barksdale, R. D. & Bachus, R. C. (1983) Design and Construction of Stone Columns, Volume 1, FHWA/Rd-83/026. 194.

Bazaraa, A. R. (1967) Use of Standard Penetration Tests for Estimating Settlements of Shallow Foundations on Sand. University of Illinois at Urbana,

Bely, L. D., Doudler, I. V., Mosiakov, E. F., Potapov, A. D. & Julin, A. N. (1975) Research Methods and Evaluation of Various Genesis Sand Grain Morphology Role in Formation of Their Geological-Engineering Properties. *Bulletin of International Association of Engineering Geology,* 11, 27-31.

Bergado, D. & Long, P. V. (1994) Numerical Analysis of Embankment on Subsiding Ground Improved by Vertical Drains and Granular Piles. *13th International Conference on Soil Mechanics and Foundation Engineering*, New Delhi, 1361-1366.

Berry, A., Visser, A. & Rust, E. (2004) A Simple Method to Predict the Profile of Improvement after Compaction Using Surface Settlement. *International Symposium on Ground Improvement*, Paris, 9-10 September 2004, 371-386.

Berthier, D., Debats, J. M., Shcarff, G. & Vincent, P. (2009) Marine and Land Based Compaction Works at the Port Botany Project, Sydney. *Coasts and Ports 2009 Conference*, Wellington, 16-18 September.

Better Ground History of Equipment Development, Viewed 8 December 2010, http://www.betterground.com/index.php?option=com_content&view=article&id=59:history&catid=37:home&Itemid=65.

Biot, M. A. (1956) Theory of Propagation of Elastic Waves in Fluid-Saturated Porous Solids. *Journal of Acoustical Society of America,* 28, March, 168-191.

Bishop, R. F., Hill, R. & Mott, N. F. (1945) The Theory of Indentation and Hardness Tests. *The Proceedings of the Physical Society,* 57, 321, Part 3, 147-159.

Bo, M. W., Na, Y. M., Arulrajah, A. & Chang, M. F. (2009) Densification of Granular Soil by Dynamic Compaction. *Ground Improvement,* 162, August, 121-132.

Bolton, M. & Lau, C. K. (1993) Vertical Bearing Capacity Factors for Circular and Strip Footings on Mohr-Coulomb Soil. *Canadian Geotechnical Journal,* 30, 1024-1033.

Bolton, M. D. & Gui, M. W. (1993) The Study of Relative Density and Boundary Effects for Cone Penetration Tests in Centrifuge. Technical Report CUED/D-Soils TR 256, Cambridge University, 31.

Bornitz, G. (1931) *Uber Die Ausbreitung Der Von Groszkolbernmaschinen Erzeugten Bodenschwingungen in Die Tiefe,* Berlin, J. Springer

Boulard, J. (1974) La Forme De Radoub Prefabriquee No. 10 Du Port Militaire De Brest. *Travaux*, October, 17-29.

Bowles, J. E. (1996) *Foundation Analysis and Design, 5th Ed.,* New York, McGraw Hill,1175.

Bozbey, I. & Togrul, E. (2010) Correlation of Standard Penetration Test and Pressuremeter Data: A Case Study from Istanbul, Turkey. *Bulletin of Engineering Geology and the Environment,* 69, 4, 505-515.

Briaud, J. L. (1992) *The Pressuremeter,* Rotterdam, A A Balkema,322.

Briaud, J. L. (2011) Email to Varaksin, S. Board Decision on "Louis Menard" Lecture.

Briaud, J. L., Noubani, A., Kilgore, J. & Tucker, L. M. (1985) Correlation between Pressuremeter Data and Other Paramaters, Research Report. Texas A&M University,

Briaud, J. L. & Saez, D. (2012) Soil Compaction: Recent Developments. *International Conference on Ground Improvement and Ground Control - Transport Infrastructure Development and Natural Hazards Mitigation (ICGI2012),* 1, Wollongong, NSW, Australia, 30 October - 2 November, 3-30.

British Standards Institution (1990) Evaluation and Measurement for Vibration in Buildings. Part 1. Guide for Measurement of Vibrations and Evaluation of Their Effects on Buildings. *BS 7385-1:1990.* London, British Standards Institution,

British Standards Institution (1992) Evaluation of Human Exposure to Vibration in Buildings (1 Hz to 80 Hz). *BS 6472: 1992.* London, British Standards Institution,

British Standards Institution (1993) Evaluation and Measurement for Vibration in Buildings. Part 2. Guide to Damage Levels from Groundborne Vibration. in INSTITUTION, B. S. (Ed.) *BS 7385-2:1993.* London, British Standards Institution,

British Standards Institution (1995) Strengthened-Reinforced Soils and Other Fills. *BS 8006:1995.* London, British Standards Institute,

British Standards Institution (2009) Code of Practice for Noise and Vibration Control on Construction and Open Sites. Part 2. Vibration. *BS 5228-2:2009.* British Standards Institution,

British Standards Institution (2010) Mechanical Vibration and Shock. Vibration of Fixed Structures. Guidelines for the Measurement of Vibrations and Evaluation of Their Effects on Structures *BS ISO 4866:2010.* London, British Standards Institution,

British Steel Piling (Bsp) Rapid Impact Compaction, Viewed 7 Feb 2009, http://www.bsp-if.com/RICS.html.

Broons Hire Square Impact Rollers, Viewed 11 March 2009, http://broons.com/impact/broons_impact.pdf.

Bureau of Reclamation (1960) *Earth Manual,* Denver, US Department of the Interior

Bureau of Reclamation (1998) *Earth Manual, Part 1, 3rd Edition,* Denver, US Department of the Interior,329.

Burmister, D. M. (1948) The Importance and Practical Uses of Relative Density in Soil Mechanics. *American Society for Testing and Materials,* 48, Philadelphia, PA, USA, 1249-1268.

Campanella, R. G., Berzins, W. E. & Shields, D. H. (1979) *A Preliminary Evaluation of Menard Pressuremeter, Cone Penetrometer and Standard Penetration Tests in the Lower Mainland, British Colombia,* Vancouver, University of British Colombia,49.

Cascante, G. & Santamarina, J. C. (1996) Interparticle Contact Behavior and Wave Propogation. *Journal of Geotechnical Engineering, ASCE,* 122, 10, 831-839.

Cassan, M. (1968) Les Essais in Situ En Mécanique Des Sols. *Construction,* 10 (October), 337-347.

Cassan, M. (1969) Les Essais in Situ En Mécanique Des Sols. *Construction,* 7-8 (July - August), 244-256.

Castro, J. & Sagaseta, C. (2009) Consolidation around Stone Columns. Influence of Column Deformation. *International Journal for Numerical and Analytical Methods in Geomechanics,* 33, 7, 851–877.

Cattaneo, C. (1938) Sul Contatto Di Due Corpi Elastici. *Accademia die Lincei Rendiconti,* 27, 6, 342-348, 434-436, 474-478.

Centre D'etudes Menard (1975) The Menard Pressuremeter, D60. *Sols Soils*, 26, 5-43.

Chang, F. (1973) Human Response to Motion in Tall Buildings. *Proceedings, ASCE,* 99, 2, 1259-1272.

Chapot, P. & Et Al. (1981) Revue Francaise De Geotechnique (from Queyroi D, Chaput D, and Pilot G: Amelioriation Des Sols De Fondation. *Note Technique de Labratoire Central des Ponts et Chaussées*, 55.

Chaumeny, J. L., Hecht, T., Kirstein, J., Krings, M. & Lutz, B. (2008) Dynamic Consolidation for the Intersection of an Active Sinkhole Area in the Course of the Federal Highway Bab a 71. *4th Hans Lorenz Symposium*, Berlin.

Chen, J. W. & Lin, C. Y. (2002) Effects of the Fines Content in Soil on Stress Attenuation During Dynamic Compaction. *12th International Offshore and Polar Engineering Conference*, Kitakyushi, Japan, 26-31 May 2002, 616-621.

Chen, W. F. (1969) Soil Mechanics and Theorems of Limit Analysis. *Journal of Soil Mechanics and Foundations Division, ASCE,* 95, 2, 493-518.

Chen, W. F. (1975) *Limit Analysis and Soil Plasticity,* New York, Elsevier

Choa, V. (1980) Geotechnical Aspects of a Hydraulic Fill Reclamation Project. *6th Southeast Asian Conference on Soil Engineering*, Taiwan, 469-484.

Choa, V., Karunartne, G. P., Ramaswamy, S. D., Vijaratnam, A. & Lee, S. L. (1979) Compaction of Sand Fill at Changi Airport. *6th Asian Regional Conference on Soil Mechanics and Foundation Engineering*, Singapore, 137-140.

Chow, Y. K., Yong, D. M., Yong, K. M. & Lee, S. L. (1994) Dynamic Compaction of Loose Granular Soils: Effect of Print Spacing. *Journal of Geotechnical Engineering, ASCE,* 120, 7 (July), 1115-1133.

Chu, J., Varaksin, S., Klotz, U. & Mengé, P. (2009) State of the Art Report: Construction Processes. *17th International Conference on Soil Mechanics & Geotechnical Engineering: TC17 meeting ground improvement*, Alexandria, Egypt, 7 October 2009, 130.

Communication Department of Menard (2007) *Menard - Half a Century of History - Un Demi Siècle D'histoire*, Mame à Tours,176.

Cooke, H. G. & Mitchell, J. A. (1999) *Guide to Remedial Measures for Liqufaction Mitigation at Existing Highway Bridge Sites, Mceer Technical Report No 99-0015*,216.

Cubrinovski, M. & Ishihara, K. (1999) Empirical Correlation between SPT N-Value and Relative Density for Sandy Soils. *Soils and Foundations, Japanese Society of Soil Mechanics and Foundation Engineering,* 39, 5, 61-71.

D'appolonia, D., Poulos, H. & Ladd, C. (1971) Initial Settlement of Structures on Clay. *Journal of Soil Mechanics and Foundations Division, ASCE,* 97, SM10, 1359-1377.

Dan, G., Sultan, N. & Savoye, B. (2007) The 1979 Nice Harbour Catastrophe Revisited: Trigger Mechanism Inferred from Geotechnical Measurements and Numerical Modelling *Marine Geology,* 245, 1-4, 40-64.

Dauvisis, J. P. & Menard, L. (1964) Etude Expérimentale Du Tassement Et De La Force Portante De Fondations Superficielles. *Sols Soils*, 10, September, 11-32.

Dayte, K. R. (1982) Note on Design Approach and Calculations for Stone Columns. *Indian Geotechnical Journal*.

Denisov, N. Y. & Reltov, B. F. (1961) The Influence of Certain Processes on the Strength of Soils. *5th International Conference on Soil Mechanics and Foundation Engineering,* 1, Paris, 17-22 July, 75-78.

Deresiewicz, H. (Ed.) (1974) *In R D Mindlin and Applied Mechanics,* New York.

Dggt (2004) Ebgeo: Bewehrte Erdkörper Auf Punkt- Oder Linienförmigen Traggliedern, Chapter 6.9.,

Dimaggio, J. A. (1987) *Stone Columns for Highway Construction. Demonstration Project No. 46. Report No. FHWA-Dp-46-1, Federal Highway Administration,*

Dimaggio, J. A. (2009) Technical Question Regarding Calculation of Equivalent Tangent of Soil - Column. in HAMIDI, B. (Ed.).

Dobson, T. & Slocombe, B. (1982) Deep Densification of Granular Fills. *2nd Geotechnical Conference, ASCE National Convention*, Las Vegas, April 1982.

Dolan, J. (2011) Request for Report Dacw 38-76-M 6646 by Schmertmann. in HAMIDI, B. (Ed.). ERDC Library,

Dowdall Stapleton, M. (2008) Helping to Create a New Map. *Gulf News.* Dubai,

Dowding, C. H. (2000) *Construction Vibrations,*

Duvall, W. I. & Fogelson, D. E. (1962) *USBM Report of Investigation 5968 - Review of Criteria of Estimating Damage to Residences from Blasting Vibrations*, US Bureau of Mines

Edwards, A. T. & Northwood, T. D. (1960) Experimental Studies of the Effects of Blasting on Structures. *The Engineer,* 260, 30 September, 538-546.

Enoki, E., Yagi, N., Yatabe, R. & Ichimoto, E. (1991) Shearing Characteristic of Composite Ground and Its Application to Stability Analysis. *Deep Foundation Improvements: Design, Construction and Testing, ASTM STP 1089-EB*, Philadelphia, 19-31.

Etude Pressiometrique Louis Menard (1967) *Interpretation D'un Essai Pressiometrique. D31/67.,*

Etude Pressiometrique Louis Menard (1970) *Détermination De La Pousée Exercée Par Un Sol Sur Une Pario De Soutènement, D38/70,*

European Standard (2000) Dd Env 1997-3:2000, Eurocode 7: Geotechnical Design - Part 3: Design Assisted by Field Testing 149.

European Standard (2004) En 1997-1: 2004, Eurocode 7: Geotechnical Design - Part 1: General Rules 171.

Ewing, W. M., Jardetzky, W. S. & Press, F. (1957) *Elastic Waves in Layered Media,* New York, McGraw Hill Book Co

Federal Aviation Administration (1995) Advisory Circular Ac150/5320-6d. in FEDERAL AVIATION ADMINISTRATION (Ed.).

Fei, X. Z., Wang, Z. & Zhou, Z. B. (2002) Model Test of Improvement Depth of Dynamic Compaction. *Chinese Journal Sichuan University,* 34, 4, 56-59.

Feng, T. W., Chen, K. H., Su, Y. T. & Shi, Y. C. (2000) Laboratory Investigation of Efficiency of Conical-Based Pounders for Dynamic Compaction. *Geotechnique,* 50, 6, 667-674.

Feng, T. W. & Ke, C. C. (2005) A Study on Using Conical Bottom Tamper for Dynamic Compaction in Platy Sand. *15th International Offshore and Polar Engineering Conference*, Seoul, 19-24 June 2005, 674-678.

Feng, T. W. & Yuan, C. (2009) Discussion: Influence of Tamper Weight Shape on Dynamic Compaction by Arslan Et Al. *Ground Improvement,* 162, GI3, 153-154.

Forssblad, L. (1980) Compaction Meter on Vibrating Rollers for Improved Compaction Control. *International Conference on Compaction,* 2, Paris, 541-546.

Gambin, M. (1979) Utilisation Du Module Pressiométrique Et De La Pression Limite Pour Le Calcul Des Fondations. *Sols Soils*, 28, 14-25.

Gambin, M. & Frank, R. (2009) Direct Design Rules for Piles Using Menard Pressuremeter Test. *International Foundation Congress and Equipment Expo: Contemporary Topics in In Situ Testing, Analysis, and Reliability of Foundations, ASCE Geotechnical Special Publication No 186*, Orlando, Florida, 15-19 March.

Gambin, M. P. (1982) Menard Dynamic Compaction, a New Method for Improving Foundation Beds Off-Shore. *International Symposium*, Brugge, 5-7 May, 3.91-93.95.

Gambin, M. P. (1983) The Menard Dynamic Consolidation at Nice Airport. *8th European Conference on Soil Mechanics and Foundation Engineering*, Helsinki, 231-239.

Gambin, M. P. (1997) Le Compactage Profond Des Sables, Idées Des Base. *3rd International Conference on Ground Improvement Geosystems: Densification and Reinforcement*, London, 3-5 June 1997, 1-27.

Gazetas, G. (1982) Vibrational Characteristics of Soil Deposits with Variable Wave Velocity. *International Journal for Numerical and Analytical Methods in Geomechanics,* 6, 1-20.

Geoquip Geoquip Note: I-01 - What Defines an Impact Roller and What Is It's Purpose, Viewed 8 Feb 2009, http://www.geoquip.com.au/pub-impact-roller-purpose.html.

Geoquip Geoquip Note: I-02 - Comparing Impact Rollers Viewed 8 Feb 2009, http://www.geoquip.com.au/pub-comparing-impact-rollers.html.

Ghassemi, A., Pak, A. & Shahir, H. (2009a) A Numerical Tool for Design of Dynamic Compaction Treatment in Dry and Moist Sands. *Iranian Journal of Science & Technology,* 33, B4, 313-326.

Ghassemi, A., Pak, A. & Shahir, H. (2009b) Validity of Menard Relation in Dynamic Compaction Operations. *Ground Improvement,* 162, 1 (February), 37-45.

Gibbs, K. J. & Holtz, W. G. (1957) Research on Determining the Density of Sands by Spoon Penetration Testing. *4th International Conference on Soil Mechanics and Foundation Engineering,* 1, London, 35-39.

Gibson, R. E. & Anderson, W. F. (1961) In Situ Measurements of Soil Properties with the Pressuremeter. *Civil Engineering and Public Works Review,* 56, 658.

Goh, S. H., Lee, F. H. & Tan, T. S. (1998) Effects of Lateral Constraints and Inertia on Stress Wave Propagation in Dry Soil Columns. *Geotechnique,* 48, 4, 449-463.

Goldman, D. E. (1948) *A Review of Subjective Responses of Vibration Motions of the Human Body in the Frequency Range, 1 to 70 Cycles Per Second, Naval Medical Research Institute Report No. 1 Project Nm 004001,*

Goughnour, R. R. & Bayuk, A. A. (1979) Analysis of Stone Column-Soil Matrix Interaction under Vertical Load. *International Conference on Soil Reinforcement; Reinforced Earth and Other Techniques (Colloque International sur le Renforcement des Sols),* 2, Paris, 20-22 March, 271 – 278.

Goughnour, R. R. & Pestana, J. M. (1998) Mechanical Behavior of Stone Columns under Seismic Loading. *2nd International Conference on Ground Improvement Techniques*, Singapore, October, 157-162.

Greenwood, D. A. (1991) Load Tests on Stone Columns. *Deep Foundation Improvements: Design, Construction and Testing, ASTM STP 1089-EB*, Philedelphia, 148-171.

Gu, Q. & Lee, F. H. (2002) Ground Response to Dynamic Compaction of Dry Sand. *Geotechnique,* 52, 7, 481-493.

Gupta, R. C. & Mckeown, J. D. (1973) Effect of Variations in Minimum Density on Relative Density. *Evaluation of Relative Density and its Role in Geotechnical Projects Involving Cohesionless Soils: ASTM STP523-EB.7744-1*, Los Angeles, 25-30 June 1972, 85-97.

Hajialilue-Bonab, M. & Rezaei, A. H. (2009) Physical Modelling of Low-Energy Dynamic Compaction. *International Journal of Physical Modelling in Geotechnics,* 3, 21-32.

Hajialilue-Bonab, M. & Zare, F. S. (2014) Investigation on Tamping Spacing in Dynamic Compaction Using Model Tests. *Ground Improvement,* 167, GI3, 219–231.

Haldar, A. & Tang, W. H. (1979) Uncertainty Analysis of Relative Density. *Journal of Geotechnical Engineering, ASCE,* 107, 7 (July), 899-904.

Hamidi, B., Varaksin, S. & Nikraz, H. (2010) Correlations between CPT and PMT at a Dynamic Compaction Project. *2nd International Symposium on Cone Penetration Testing (CPT10)*, Huntington Beach, California, 9-11 May, paper 2-04.

Harada, M. & Suzuki, M. (1984) Improvement of Sandy Soil and Measurement of Socking Earth Pressure by Dynamic Consolidation (in Japanese). *16th Soil Engineering Research Seminar*, Tokyo, 1689-1692.

Hardin, B. (1985) Crushing of Soil Particles. *Journal of Geotechnical Engineering, ASCE,* 111, 10 (October), 1177-1192.

Hatanaka, M. & Feng, L. (2006) Estimating Relative Density of Sandy Soils. *Soils and Foundations, Japanese Society of Soil Mechanics and Foundation Engineering,* 46, 3, 299-313.

Hausler, E. A. (2002) Influence of Ground Improvement on Settlement and Liquefaction: A Study Based on Field Case History Evidence and Dynamic Geotechnical Centrifuge Tests. University of California, Berkley, 364.

Heh, K. S. (1990) Dynamic Compaction of Sand. *Department of Civile Environmental Engineering.* Brooklyn, NY, Polytechnic University,

Hendy, M. S. & Muir, I. C. (1997) Experience of Dynamic Replacement on a 40 M Deep Reclamation in Hong Kong. *Third International Conference on Ground Improvement Geosystems: Ground Improvement Geosystems - Densification and Reinforcement*, London, 3-5 June 1997, 76-80.

Hertz, H. (1881) Über Die Berührung Fester Elastischer Körper. *Journal Reine U. Angew Math.,* 92, 156-171.

Hewlett, W. J. & Randolph, M. (1988) Analysis of Piled Embankments. *Ground Engineering,* 21, 3, 12-18.

Hill, R. (1950) *The Mathematical Theory of Plasticity,* Oxford, University Press

Hiller, D. M. & Hope, V. S. (1998) Ground Borne Vibration Generated by Mechanized Construction Activities. *Geotechnical Engineering,* 131, 223-232.

Hirona, T. (1948) Mathematical Theory on Shallow Earthquake. *The Geophysical Magazine,* 18, 1-4, October.

Hobbs, N. B. & Dixon, J. C. (1969) In-Situ Testing for Bridge Foundations in the Devonian Marl. *Conference on In Situ Investigations in Soils and Rocks*, London, 13-15 May, 31-38.

Holtz, R. D. (1973a) Discussion on Determination of Relative Density of Sand Below Groundwater Table. *Evaluation of Relative Density and its Role in Geotechnical Projects Involving Cohesionless Soils: ASTM STP523-EB.7744-1*, Los Angeles, 25-30 June 1972, 376-377.

Holtz, W. G. (1973b) The Relative Density Approach - Uses, Testing Requirements, Reliability, and Shortcomings. *Evaluation of Relative Density and its Role in Geotechnical Projects Involving Cohesionless Soils: ASTM STP523-EB.7744-1*, Los Angeles, 25-30 June 1972, 5-17.

Holubec, I. & D'appolonia, E. (1973) Effect of Particle Shape on the Engineering Properties of Granular Soils. *Evaluation of Relative Density and its Role in Geotechnical Projects Involving Cohesionless Soils: ASTM STP523-EB.7744-1*, Los Angeles, 25-30 June 1972, 304-318.

Hughes, J. M. & Withers, N. J. (1974) Reinforcing of Soft Cohesive Soils with Stone Columns. *Ground Engineering,* 47, 3 (May), 42-49.

Hwang, J. H. & Tu, T. Y. (2003) Ground Vibration Due to Dynamic Compaction. *13th International Offshore and Polar Engineering Conference*, Honolulu, 25-30 May 2003, 490-497.

Hwang, J. H. & Tu, T. Y. (2006) Ground Vibration Due to Dynamic Compaction. *Soil Dynamics and Earthquake Engineering*, 26, 337-346.

Iai, S., Koizumi, K. & Kurata, E. (1987) Basic Consideration for Designing the Area of the Ground as a Remedial Measure against Liquefaction (in Japanese). 590, PHRI, 2-67.

Ichese, Y., Yamakoda, A. & Takano, S. (1971) High Pressure Jet-Grouting Method. in UNITED STATES PATENT AND TRADEMARK OFFICE (Ed.). United States, 7.

Ishihara, K. (1985) Stability of Natural Deposits During Earthquakes. *11th International Conference on Soil Mechanics and Foundation Engineering,* 1, San Francisco, 321-376.

Ishihara, K. & Yamazaki, F. (1980) Cyclic Simple Shear Tests on Saturated Sand in Multi-Directional Loading. *Soils and Foundations, Japanese Society of Soil Mechanics and Foundation Engineering,* 20, 1, 49-59.

Jahangiri, G., Pak, A. & Ghassemi, A. (2011) Numerical Modelling of Dynamic Compaction in Dry Sandy Soils for Determination of Effective Print Spacing. *Journal of Structural Engineering and Geo-techniques,* 1, 1-9.

Jamiolkowski, M., Lo Presti, D. C. F. & Manassero, M. (2001) Evaluation of Relative Density and Shear Strength of Sands from CPT and Dmt. *Soil Behavior and Soft Ground Construction: Geotechnical Special Publication No. 119*, Boston, Massachusetts, 5-6 October, 201-238.

Jamiolkowski, M. & Pasqualini, E. (1992) Compaction of Granular Soils - Remarks on Quality Control. *Grouting, Soil Improvement and Geosynthetics: ASCE Geotechnical Special Publication No. 30,* 2, New Orleans, 25-28 February, 902-914.

Japanese Geotechnical Society (1998) *Remedial Measures against Soil Liquefaction, from Investigation and Design to Implementation,* Rotterdam, A A Balkema,443.

Jezequel, J. F., Lemasson, H. & Touzé, J. (1968) Le Pressiomètre Louis Ménard: Quelques Problèmes De Mise En Oeuvre Et Leur Influence Sur Les Valeurs Pressiométriques. *Bulletin de Liaison des Laboratoires des Ponts et Chaussées,* 32 (June - July), 97-120.

Jullienne, D. (2008) Ras Laffan Port Expansion - Dc Presentation. Ras Laffan,

Kelly, D. & Gil, J. (2012) Monitoring Heic Using Landpac Cir and Cis Technologies. *International Symposium on Ground Improvement (IS-GI) Brussels 2012,* 1, Brussels, 31 May - 1 June, 273-285.

Kempfert, H. G. & Gebreselassie, B. (2006) Chapter 7 Soil Stabilisation with Column Like Elements. *Excavations and Foundations in Soft Soils.* Berlin, Springer.

Kempfert, H. G., Gobel, C., Alexiew, D. & Heitz, C. (2004) German Recommendations for Reinforced Embankments on Pile Similar Elements. *EuroGeo3: 3rd European Geosynthetics Conference, Geotechnical Engineering with Geosynthetics*, Munich, 279-284.

Kopf, F. & Paulmichl, I. (2004) Deep Dynamic Compaction; Compaction Control Using Dynamic Measurements. Institute for Soil Mechanics and Geotechnical Engineering, Research Report (in German). Vienna University of Technology,

Kopf, F., Paulmichl, I. & Adam, D. (2010) Modelling and Simulation of Heavy Tamping Dynamic Response of the Ground. *14th Danube-European Conference on Geotechnical Engineering: From Research to Design in European Practice*, Bratislava, Slovak, June 2-4.

Kröber, W., Floss, E. & Wallrath, W. (2001) Dynamic Soil Stiffness as Quality Criterion for Soil Compaction. in GOMES CORREIRA, A. & BRANDL, H. (Eds.) *Geotechnics for Roads, Rail Tracks and Earth Structures.* A.A. Balkema.

Lacroix, Y. & Horns, H. M. (1973) Direct Determination and Indirect Evaluation of Relative Density and Its Use on Earthwork Construction Projects. *Evaluation of Relative Density and its Role in Geotechnical Projects Involving Cohesionless Soils: ASTM STP523-EB.7744-1*, Los Angeles, 25-30 June 1972, 251-280.

Lamb, H. (1904) On the Propagation of Tremors over the Surface of an Elastic Solid. *Philosophical Transactions of the Royal Society, London,* 203, Ser. A, 1-42.

Lambe, T. W. & Whitman, R. V. (1979) *Soil Mechanics, Si Version,* New York, Wiley

Landpac Typical Myths About Impact Compaction, Viewed 4 September 2008, htpp://www.landpac.co.za/QandA/typical_myths_about_impact_compa.htm.

Langefors, U., Kilhstrom, B. & Westerberg, H. (1958) Ground Vibrations in Blasting. *Water Power*, February, 335-338, 390-395, 421-424.

Leblanc, J. (1982) Menard Pressuremter Testing. *Symposium on the Pressuremter and its Marine Applications*, Paris, 19-20 April 1982, 23-37.

Lee, F. H. & Gu, Q. (2004) Method for Estimating Dynamic Compaction Effect on Sand. *Journal of Geotechnical and Geoenvironmental Engineering, ASCE,* 113, 2 (February), 139-152.

Lee, J. & Salgado, R. (2002) Estimation of Footing Settlement in Sand. *International Journal of Geomechanics, ASCE,* 2, 1, 1-28.

Lee, K. L. & Albeisa, A. (1974) Earthquake Induced Settlement in Saturated Sands. *Journal of Soil Mechanics and Foundations Division, ASCE,* 100, 4, 387-406.

Lee, K. M. (2001) Influence of Placement Method on the Cone Penetration Resistance of Hydraulically Placed Sand Fills. *Canadian Geotechnical Journal,* 38, 9, 592-607.

Lee, K. M., Shen, C. K., Leung, D. H. K. & Mitchell, J. K. (1999) Effects of Placement Method on Geotechnical Behavior of Hydraulic Fill Sands. *Journal of Geotechnical and Geoenvironmental Engineering, ASCE,* 125, 10, 832-846.

Lee, K. M., Shen, C. K., Leung, D. H. K. & Mitchell, J. K. (2000) Closure: Effects of Placement Method on Geotechnical Behavior of Hydraulic Fill Sands. *Journal of Geotechnical and Geoenvironmental Engineering, ASCE,* 126, 10, 943-944.

Leonards, G. A., Cutter, W. A. & Holtz, R. D. (1980) Dynamic Compaction of Granular Soils. *Journal of Geotechnical Engineering, ASCE,* 106, 1 (January), 35-44.

Li, D. (2005) Transition of Railroad Bridge Approaches. *Journal of Geotechnical and Geoenvironmental Engineering, ASCE,* 131, 11 (November), 1392-1398.

Liao, S. & Sangrey, D. A. (1978) Use of Piles as Isolation Barriers. *Journal of Geotechnical Engineering, ASCE,* 104, 9, 1139-1152.

Liu, L. & Dorby, R. (1997) Seismic Response of Shallow Foundation on Liquefiable Sand. *Journal of Geotechnical and Geoenvironmental Engineering, ASCE,* 123, 6, 557-567.

Liu, Q. B. & Lehane, B. M. (2012) The Influence of Particle Shape on the (Centrifuge) Cone Penetration Test (CPT). *Geotechnique,* 62, 11, 973-984.

Lukas, R. G. (1980) Densification of Loose Deposits by Pounding. *Journal of Geotechnical Engineering, ASCE,* 106, 4 (April), 435-446.

Lukas, R. G. (1986) Dynamic Compaction for Highway Construction, Volume 1: Design and Construction Guidelines, FHWA Report Rd-86/133. Federal Highway Administration,

Lukas, R. G. (1995) Geotechnical Engineering Circular No. 1: Dynamic Compaction, Publication No. FHWA-Sa-95-037. Federal Highway Administration,

Luongo, V. (1992) Dynamic Compaction: Predicting Depth of Improvement. *Grouting, Soil Improvement and Geosynthetics: ASCE Geotechnical Special Publication No. 30,* 2, New Orleans, 25-28 February, 927-939.

Lysmer, J. (1966) Personal Communication with F E Richart.

Madhav, M. R. & Vitkar, P. P. (1978) Strip Footings on Weak Clay Stabilized with a Granular Trench or Pile. *Canadian Geotechnical Journal,* 15, 4, 605-609.

Marcuson Iii, W. F. (1978) Determination of in Situ Density of Sands. *Dynamic Geotechnical Testing, ASTM STP 654*, Denver, 28 June 1977, 318-340.

Marcuson Iii, W. F. & Bieganousky, W. A. (1977) Laboratory Standard Penetration Tests on Fine Sands. *Journal of Geotechnical Engineering, ASCE,* 103, 6 (June), 565-589.

Marston, A. & Anderson, A. O. (1913) The Theory of Loads on Pipes in Ditches and Tests of Cement and Clay Drain Tile and Sewer Pipe. *Iowa Engineering Experiment Station Bulletin,* 31.

Massarsch, K. R. & Fellenius, B. H. (2012) Early Swedish Contributions to Geotechnical Engineering. *Full-Scale Testing and Foundation Design: Honoring Bengt H. Fellenius, ASCE Geotechnical Special Publication No. 227*, Reston, VA, USA, 25-29 March, 239-256.

Mayne, P. W. (1985) Ground Vibrations During Dynamic Compaction. *Symposium on Vibration Problems in Geotechnical Engineering: ASCE Special Publication*, Detroit, 22 October 1985, 247-265.

Mayne, P. W. (2006) The Second James K Mitchell Lecture: Undisturbed Sand Strength from Seismic Cone Tests. *Geomechanics and Geoengineering: An International Journal,* 1, 4, 239-257.

Mayne, P. W., Jones, J. S. & Dumas, J. C. (1984) Ground Response to Dynamic Compaction. *Journal of Geotechnical Engineering, ASCE,* 110, 6 (June), 757-774.

Mayne, P. W. & Kulhawy, F. H. (1982) Ko-Ocr Relationship in Soil. *Journal of Geotechnical Engineering, ASCE,* 108, 6, 851-872.

Mccamy, K., Meyer, R. P. & Smith, T. J. (1962) Generally Applicable Solutions of Zoeppritz' Amplitude Equations. *Bulletin of the Seismological Society of America,* 52, 4 (October), 923-955.

Menard, L. (1957) Msc Thesis, an Apparatus for Measuring the Strength of Soils in Place. *Civil Engineering.* Urbana, Il, USA, University of Illinois, 50.

Menard, L. (1963a) Calcul De La Force Portante Des Fondation Sur La Base Des Resultats Des Essais Pressiometriques. *Sols Soils*, 5, 9-32.

Menard, L. (1963b) Tendances Nouvelles En Mécanique Des Sols. *Bulletin de l'A.I.A.*, 1, 1-12.

Menard, L. (1965) Rules to Obtain Bearing Capacity and Foundations Settlements from Pressuremeter Results (in French). *6th International Conference on Soil Mechanics and Foundation Engineering*, Montreal.

Menard, L. (1971) A Low Cost Method of Consolidating Fills Dumped into the Sea. *Sols Soils*, 24, 9-20.

Menard, L. (1972) La Consolidation Dynamique Des Remblais Recents Et Sols Compressibles. *Travaux*, November, 56-60.

Menard, L. (1974) Fondation D'une Cale De Radoub À Brest. *6th International Harbour Conference*, Antwerp, 12-18 May.

Menard, L. (1978) La Consolidation Dynamique Comme Solution Aux Problemes De Fondation: Pour La Construction De Quais, Terminaux, Reservoirs De Stockage Et Iles Artificielles Sur Sols Compressibles. *7th International Harbour Conference*, Antwerp.

Menard, L. (1981) L'utilisation De La Consolidation Dynamique Pour La Réalisation Du Nouveau Port De Pêche De Sfax En Tunisie. *Navires, Ports et Chantiers*, April.

Menard, L., Bourdon, G. & Houy, A. (1964) Etude Expérimentale De L'encastrement D1un Rideau En Fonction Des Caractéristiques Pressiométriques Du Sol De Fondation. *Sols Soils,* 3, 9, 11-41.

Menard, L. & Broise, Y. (1975) Theoretical and Practical Aspects of Dynamic Compaction. *Geotechnique,* 25, 1, 3-18.

Menard, L. & Lambert, P. (1966) Etude Expérimentale D'un Massif De Fondation Soumis À Des Vibrations. *Sols Soils*, 17, 9-30.

Menard, L. & Rousseau, J. (1962) L'évaluation Des Tassements - Tendances Nouvelles. *Sols Soils,* 1, 1, 13-29.

Menard Soltraitement *Soil Improvement Specialists - Design, Construct ... Perform,*

Mesri, G., Feng, T. W. & Benak, J. M. (1990) Postdensification Penetration Resistance of Clean Sands. *Journal of Geotechnical Engineering, ASCE,* 116, 7, 1095-1115.

Meyerhof, G. G. (1953) The Bearing Capacity of Foundations under Eccentric and Inclined Loads. *Third International Conference on Soil Mechanics and Foundation Engineering,* 1, Zurich, 16-27 August, 440-445.

Meyerhof, G. G. (1957) Discussion on Research on Determining the Density of Sands by Spoon Penetration Testing. *4th International Conference on Soil Mechanics and Foundation Engineering,* 1, London, 110.

Meyerhof, G. G. (1959) Compaction under Impact. *Journal of Soil Mechanics and Foundations Division, ASCE,* 85, 4, 1292-1323.

Meyerhof, G. G. (1976) Bearing Capacity and Settlement of Pile Foundations. *Journal of Geotechnical Engineering, ASCE,* 102, 1, 197-259.

Michalowski, R. L. & Nadukuru, S. S. (2011a) Delayed Increase in Cone Penetration Resistance of Sand after Dynamic Compaction. *2nd International Symposium on Computational Geomechanics: Com Geo II*, Dubrovnik, Croatia, 251-261.

Michalowski, R. L. & Nadukuru, S. S. (2011b) Stress Corrosion Cracking and Delayed Increase in Penetration Resistance after Dynamic Compaction of Sand. *Geo-Frontiers 2011: Advances in Geotechnical Engineering, ASCE Geotechnical Special Publication No 211*, Dallas, 13-16 March, 519-528.

Michalowski, R. L. & Nadukuru, S. S. (2012) Static Fatigue, Time Effects, and Delayed Increase in Penetration Resistance after Dynamic Compaction of Sands. *Journal of Geotechnical and Geoenvironmental Engineering, ASCE,* 138, 5, 564-574.

Miller, G. F. & Pursey, H. (1954) The Field and Radiation Impedance of Mechanical Radiators on the Free Surface of a Semi-Infinite Isotropic Solid. *Royal Society,* 223, London, 521-541.

Miller, G. F. & Pursey, H. (1955) On the Partition of Energy between Elastic Waves in a Semi-Infinite Solid. *Royal Society,* 233, London, 55-69.

Mindlin, R. D. (1949) Compliance of Elastic Bodies in Contact. *Journal of Applied Mechanics, Transactions ASME,* 71, 259-268.

Mindlin, R. D. & Deresiewicz, H. (1953) Elastic Spheres in Contact under Varying Oblique Forces. *Journal of Applied Mechanics, Transactions ASME*, September, 327-344.

Mitchell, J. K. (1981) Soil Improvement State-of-the-Art Report. *10th International Conference on Soil Mechanics and Foundation Engineering,* 4, Stockholm, 509-565.

Mitchell, J. K., Baxter, C. & Munson, T. (1995) Performance of Improved Ground During Earthquake. *Soil Improvement for Earthquake Hazard Mitigation: ASCE Geotechnical Special Publication No. 49*, 1-36.

Mitchell, J. K. & Gardner, W. S. (1975) State of the Art: In Situ Measurement of Volume Change Characteristics. *ASCE Conference on In situ Measurements of Soil Properties,* 2, Raleigh, North Carolina, 279-345.

Mitchell, J. K. & Huber, T. R. (1985) Performance of a Stone Column Foundation. *Journal of Geotechnical Engineering, ASCE,* 111, 2 (Feb), 205-223.

Mitchell, J. K. & Solymar, Z. V. (1984) Time Dependent Strength Gain in Freshly Deposited or Densified Soil. *Journal of Geotechnical Engineering, ASCE,* 110, 11 (November), 1559-1576.

Mobil (1990) Chapter 6 - Foundation Design. *Mobil Engineering Guide: Egs 262-90.* Mobil.

Modoni, G., Croce, P. & Mongiovi, L. (2006) Theoretical Modelling of Jet Grouting. *Geotechnique,* 56, 5, 335-347.

Moretto, O. (1954) Subsoil Investigation for a Bridge over the Parana River, Argentina. *Geotechnique,* 4, 4, 137-142.

Mostafa, K. (2010) Phd Thesis, Numerical Modeling of Dynamic Compaction in Cohesive Soils. Akron, University of Akron, 182.

Müller, H. (1970) Baugrunduntersuchung Mit Dem Pressiometerverfahren Nach Menard. *Die Bautechnik,* 9, 289-295.

Murali Krishna, A. & Madhav, M. R. (2009) Engineering of Ground for Liquefaction Mitigation Using Granular Column Inclusions: Recent Developments. *American Journal of Engineering and Applied Sciences,* 2, 3, 526-536.

Murayama, S. (1962) Vibro-Compozer Method for Clayey Ground (in Japanese). *Mechanization of Construction Work,* 150, 10-15.

Na, Y. M., Choa, V., Teh, C. I. & Chang, M. F. (2005) Geotechnical Parameters of Reclaimed Sandfill from Cone Penetration Test. *Canadian Geotechnical Journal,* 42, 91-109.

Nagase, H. & Ishihara, K. (1988) Liquefaction Induced Compaction and Settlement of Sand During Earthquakes. *Soils and Foundations, Japanese Society of Soil Mechanics and Foundation Engineering,* 28, 1, 66-76.

Nashed, R. (2005) Liquefaction Mitigation of Silty Soils Using Dynamic Compaction. *Department of Civil, Structural & Environmental Engineering.* Buffalo, State University of New York, 282.

Naval Facilities Engineering Command (1997) *Soil Dynamics and Spectral Design Aspects,* Norfolk, Department of Defense

Navdocs (1962) Design Manual Dm-7, Soil Mechanics, Foundations and Earth Structures.

Nazaret, M. (1972) Influence Du Mode De Mise En Oeuvre De La Sond Pressiométrique, Rapport De Recherche Du Laboratoire Régional Des Ponts Et Chaussées D'angers, F.A.E.R 1.05.11.1.

Nicholls, H. R., Johnson, C. F. & Duvall, W. I. (1971) *USBM Bulletin 656 - Blasting Vibrations and Their Effects on Structures*, US Bureau of Mines

Office of Surface Mining Reclamation Enforcement (1983) Federal Register. in OFFICE OF SURFACE MINING RECLAMATION AND ENFORCEMENT (Ed.). Department of the Interior, 9805-9811.

Oshima, A. & Takada, N. (1994) Effect of Ram Momentum on Compaction by Heavy Tamping. *13th International Conference on Soil Mechanics and Foundation Engineering*, New Delhi, 5-10 January, 1141-1144.

Oshima, A. & Takada, N. (1997) Relation between Compacted Area and Ram Momentum by Heavy Tamping. *14th International Conference on Soil Mechanics and Foundation Engineering*, 1641-1644.

Oshima, A. & Takada, N. (1998) Evaluation of Compacted Area of Heavy Tamping by Cone Point Resistance. *Centrifuge 98*, Tokyo, 813-818.

Osterberg, J. O. & Varaksin, S. (1973) Determination of Relative Density of Sand Below Groundwater Table. *Evaluation of Relative Density and its Role in Geotechnical Projects Involving Cohesionless Soils: ASTM STP523-EB.7744-1*, Los Angeles, 25-30 June 1972, 364-378.

Parkin, A. K. (1977) The Friction Cone Penetrometer: Laboratory Calibration for the Prediction of Sand Properties. Internal Report No. 52108-5, Norwegian Geotechnical Institute,

Parkin, A. K. & Lunne, T. (1982) Boundary Effects in the Laboratory Calibration of a Cone Penetrometer for Sand. *2nd European Symposium on Penetration Testing,* 2, Amsterdam, 761-767.

Peck, R. B. & Bazaraa, A. R. (1969) Discussion of Settlement of Spread Footings on Sand. *Journal of Soil Mechanics and Foundations Division, ASCE,* 95, 3, 905-909.

Perucho, A. & Olalla, C. (2006) Dynamic Consolidation of a Saturated Plastic Clayey Fill. *Ground Improvement,* 10, 2, 55-68.

Pettijohn, F. J., Potter, P. E. & Sievin, R. (1972) *Sand and Sandstone,* New York, Springer-Verlag

Poran, C. J., Heh, K. S. & Rodriguez, J. A. (1991) Impact Response to Granular Soils. *2nd International Conference on Recent Advances in Geotechnical Earthquake Engineering and Soil Dynamics,* 2, St Louis, MO, USA, 1387-1398.

Poran, C. J. & Rodriguez, J. A. (1992) Design of Dynamic Compaction. *Canadian Geotechnical Journal,* 29, 5, 796-802.

Port and Harbour Research Institute (1997) *Handbook of Liquefaction Remediation of Reclaimed Land,* Rotterdam, A A Balkema

Power, D. V. (1966) A Study of Complaints of Seismic Related Damage to Surface Structures Following the Salmon Underground Nuclear Detonation. *Bulletin of the Seismological Society of America,* 56, 6 (December), 1413-1428.

Prandtl, L. (1920) *Uber Die Härte Plastischer Körper Nachrichten Von Der Königlichen Gesellschaft Der Wissenschaften, Gottingen, Math.- Phys. Klasse*,74-85.

Prange, B. (1977) Parameters Affecting Damping Properties. *Dynamical Methods in Soil and Rock Mechanics,* 1 Dynamic Response and Wave Propagation in Soils, Karlsruhe, 5-16 September 1977, 6-78.

Raithel, M., Kirchner, A. & Kempfert, H. G. (2008) German Recommendations for Reinforced Embankments on Pile-Similar Elements. *4th Asian Regional Conference on Geosynthetics*, Shanghai, 17-20 June, 697-702.

Rayleigh (1885) On Waves Propagated Along the Plane Surface of an Elastic Solid. *London Mathematical Society, 17*, 4-11.

Reiher, H. & Meister, F. J. (1931) The Effect of Vibration on People. *Forschung auf dem Gebeite des Ingenieurwesens,* 2, 11, 381.

Renault, J. & Tourneur, P. (1974) La Forme De Radoub No. 10 À Brest. *6th International Harbor Conference*, Antwerp, 12-18 May.

Richart, F. E. (1962) Foundation Vibrations. *Transactions, ASCE,* 127, Part 1, 863-898.

Richart, F. E., Hall, J. R. & Woods, R. D. (1970) *Vibrations of Soils and Foundations*, Prentice-Hall

Robertson, P. K. & Campanella, R. (1985) Liquefaction Potential of Sands Using the CPT. *Journal of Geotechnical Engineering, ASCE,* 111, 3, 384–403.

Robertson, P. K. & Campanella, R. G. (1989) *Guidelines for Geotechnical Design Using the Cone Penetrometer Test and CPT with Pore Pressure Measurement, 4th Ed.,* Columbia, MD, Hogentogler & Co.

Rogers, J. D. (2004) Notes for Standard Penetration Test, Viewed 23/11/2010, http://web.mst.edu/~rogersda/umrcourses/ge441/NOTES%20for%20STANDARD%20PENETRATION%20TEST.pdf.

Rollins, K. & Kim, J. (2010) Dynamic Compaction of Collapsible Soils Based on Us Case Histories. *Journal of Geotechnical and Geoenvironmental Engineering, ASCE,* 136, 9, 1178-1186.

Rollins, K. M. & Kim, J. H. (1994) Us Experience with Dynamic Compaction of Collapsible Soils. *In-Situ Deep Soil Improvement: ASCE Geotechnical Special Publication No. 45*, Atlanta, 9-13 October 1994, 26-43.

Romana Ruiz, M. & Jurado, C. (1999) Vibration Monitoring of a Dynamic Compaction on a Fill at Santa Cruz De La Palma Harbour (Canary Island). *12th European Conference on Soil Mechanics and Geotechnical Engineering: Geotechnical Engineering for Transportation Infrastructure*, 591-600.

Salencon, J. (1966) Expansion Quasi -Statique D'une Cavite a Symetric Spherique Ou Cylindrique Dans Un Milieu Elasto-Plastique. *Annales des Ponts et Chaussées,* 3, May-June, 175-187.

Sandström, A. (1994) Numerical Simulation of a Vibratory Roller on Cohesionless Soil, Internal Report. Geodynamik,

Satibi, S. (2009) *Numerical Analysis and Design Criteria of Embankments on Floating Piles,* Stuttgart, DCC Siegmar Kästl e. K., Ostfildern,166.

Scherocman, J., Rakowski, S. & Uchiyama, K. (2007) Intelligent Compaction, Does It Exist? *2007 Canadian Technical Asphalt Association (CTAA) Conference*, Victoria, BC, Canada, July.

Schmertmann, J. H. (1970) Static Cone to Compute Static Settlement over Sand. *Journal of Geotechnical Engineering, ASCE,* 96, SM3 (May) Interpretation of Cone Penetration Tests. Part I: Sand, 1101-1143.

Schmertmann, J. H. (1975) State of the Art Paper: Measure of in Situ Strength. *ASCE Conference on In situ Measurements of Soil Properties,* 2, Raleigh, North Carolina, 57-138.

Schmertmann, J. H. (1976) An Updated Correlation between Relative Density and Fugro-Type Electric Cone Bearing Qc. Contract Report, Dacw 38-76-M 6646. Waterways Experiment Station, 145.

Schmertmann, J. H. (1978) Guidelines for Cone Penetration Test, Performance and Design, Report FHWA-Ts-78-209. Federal Highway Administration, 145.

Schmertmann, J. H. (1987) Discussion on "Time Dependent Strength Gain in Freshly Deposited or Densified Soil" by Mitchell and Solymar. *Journal of Geotechnical Engineering, ASCE,* 113, 2, 173-175.

Schmertmann, J. H., Hartman, J. P. & Brown, P. R. (1978) Improved Strain Influence Factor Diagrams. *Journal of Geotechnical Engineering, ASCE,* 104, GT8 (August), 1131-1135.

Seed, H. B. & Booker, J. R. (1977) Stabilization of Potentially Liquefiable Sand Deposits Using Gravel Drains. *Journal of Geotechnical Engineering, ASCE,* 103, 7, 757- 768.

Seed, H. B. & Idriss, I. M. (1967) Analysis of Soil Liquefaction, Niigata Earthquake. *Journal of Soil Mechanics and Foundations Division, ASCE,* 93, SM 3, 83-108.

Seed, H. B. & Idriss, I. M. (1971) Simplified Procedure for Evaluating Soil Liquefaction Potential. *Journal of Soil Mechanics and Foundations Division, ASCE,* 97, SM 9, 1249-1273.

Seed, H. B., Martin, P. P. & Lysmer, T. (1976) Pore Water Pressure Changes During Soil Liquefaction. *Journal of Geotechnical Engineering, ASCE,* 102, 4, 323-346.

Selig, E. T. & Ladd, R. S. (1973) Evaluation of Relative Density Measurements and Applications. *Evaluation of Relative Density and its Role in Geotechnical Projects Involving Cohesionless Soils: ASTM STP523-EB.7744-1.*, Los Angeles, 25-30 June 1972, 487-504.

Serridge, C. J. (2002) Dynamic Compaction of Loose Sabkha Deposits for Airport Runway and Taxiways. *4th International Conference on Ground Improvement Techniques*, Kuala Lumpur, 26-28 March, 649-656.

Shibazaki, M. & Yoshida, H. (1995) Method for Controlling a Final Pile Diameter in a Cast-in-Place of Solidification of Pile by a Jet Process. in UNITED STATES PATENT AND TRADEMARK OFFICE (Ed.). United States, Chemical Grouting Company, 4.

Shrivastava, R. K. & Kameswara Rao, N. V. (2002) Response of Soil Media Due to Impulse Loads and Isolation Using Trenches. *Soil Dynamics and Earthquake Engineering,* 22, 8, 695-702.

Silver, M. L. & Seed, H. B. (1971) Deformation Characteristics of Sands under Cyclic Loading. *Journal of the Soil Mechanics and Foundations Division, ASCE,* 9, SM8, 1081-1098.

Siskind, D. E., Stagg, M. S., Kopp, J. W. & Dowding, C. H. (1980) *USBM Report of Investigations 8507 - Structure Response and Damage Produced by Ground Vibration from Surface Mine Blasting*, US Bureau of Mines

Skempton, A. W. (1986) Standard Penetration Test Procedure and the Effects in Sands of Overburden Pressure, Relative Density, Particle Size, Ageing and Overconsolidation. *Geotechnique,* 36, 3, 425-447.

Skipp, B. & Buckley, J. (1977) Ground Vibration from Impact. *9th International Conference on Soil Mechanics and Foundation Engineering,* 2, Tokyo, 397-400.

Sladen, J. A. & Hewitt, K. J. (1989) Influence of Placement Method on the in-Situ Density of Hydraulic Sand Fills. *Canadian Geotechnical Journal,* 26, 3, 453-466.

Slocombe, B. (2004) Dynamic Compaction. in MOSELEY, M. P. & KIRSCH, K. (Eds.) *Ground Improvement.* 2nd ed. New York, Spon Press.

Spaulding, C. & Zanier, L. (1997) Apron Densification at Macau International Airport Using Dynamic Consolidation and Replacement Methods. *International Conference on Ground Improvement*, Macau, 525-530.

Standards Australia (2006) Explosives - Storage and Use, Part 2: Use of Explosive. in STANDARDS AUSTRALIA (Ed.) *AS 2187.2 - 2006.* Sydney, NSW, Australia, Standards Australia,

Studer, J. & Suesstrunk, A. (1981) Swiss Standard for Vibrational Damage to Buildings. *10th International Conference on Soil Mechanics and Foundation Engineering,* 3, Stockholm, 307-312.

Tan, S. A., Tjahyono, S. & Oo, K. K. (2008) Simplified Plane-Strain Modeling of Stone-Column Reinforced Ground. *Journal of Geotechnical and Geoenvironmental Engineering, ASCE,* 134, 2 (February), 185-194.

Tatsuoka, F., Tokida, K., Yasuda, S., Hirose, M., Imai, T. & Konno, M. (1978) A Method for Estimating Undrained Cyclic Strength of Sandy Soils Using Standard Penetration Resistance. *Soils and Foundations, Japanese Society of Soil Mechanics and Foundation Engineering,* 18, 3, 43-58.

Tavenas, F. A. & La Rochelle, P. (1970) Problems Related to the Use of the Relative Density, Report S-21, Laval University.

Tavenas, F. A., Ladd, R. S. & La Rochelle, P. (1973) Accuracy of Relative Density Measurements: Results of a Comparative Test Program. *Evaluation of Relative Density and its Role in Geotechnical Projects Involving Cohesionless Soils: ASTM STP523-EB.7744-1*, Los Angeles, 25-30 June 1972, 18-60.

Terra Systems Rapid Impact Compaction Another Form of Dynamic Compaction, Viewed 7 February 2009, http://www.terrasystemsonline.com/terranotes/ric.pdf.

Terzaghi, K. (1925) *Erdbaumechanik Auf Bodenphysikalisher Grundlage,* Vienna, Deuticke

Terzaghi, K. (1943) *Theoretical Soil Mechanics,* New York, John Wiley & Sons,510.

Terzaghi, K. & Frohlich, O. K. (1936) *Theorie Der Setzung Von Tonschichten,* Leipzig, Franz Deuticke

Terzaghi, K. & Peck, R. B. (1948) *Soil Mechanics in Engineering Practice,* New York, John Wiley and Sons

Thau, S. A. & Pao, Y. (1966) Diffraction of Horizontal Shear Waves by a Parabolic Cylinder and Dynamic Stress Concentration. *Journal of Applied Mechanics, Transactions ASME*, December, 785-792.

Thevanayagam, S., Martin, G. R., Nashed, R., Shenthan, T., Kanagalingam, T. & Ecemis, N. (2006) *Liquefaction Remediation in Silty Soils Using Dynamic Compaction and Stone Columns: Technical Report Mceer-06-0009,* Buffalo, NY, MCEER,101.

Thoenen, J. R. & Windes, S. L. (1942) *USBM Bulletin 442 - Seismic Effects of Quarry Blasting*, US Bureau of Mines

Thurner, H. & Sandström, A. (1980) A New Device for Instant Compaction Control. *International Conference on Compaction*, Paris, 611-614.

Thurner, H. & Sandström, A. (2000) Continuous Compaction Control, Ccc. *Workshop on Compaction of Soils and Granular Materials, Modeling of Compacted Materials, Compaction Management and Continuous Control, ISSMGE (European Technical Committee)*, Paris, 237-246.

Tiedemann, D. A. (1973) Variability of Laboratory Relative Density Test Results. *Evaluation of Relative Density and its Role in Geotechnical Projects Involving Cohesionless Soils: ASTM STP523-EB.7744-1*, Los Angeles, 25-30 June 1972, 61-73.

Timoshenko, S. P. & Goodier, J. N. (1951) *Theory of Elasticity,* New York, McGraw Hill Book Co.

Tokimatsu, K. (1979) Generation and Dissipation of Pore Water Pressures in Sand Deposits During Earthquakes. Tokyo, Tokyo Institute of Technology,

Tokimatsu, K. & Yoshimi, Y. (1983) Empirical Correlation of Soil Liquefaction Based on SPT-N Value and Fines Content. *Soils and Foundations, Japanese Society of Soil Mechanics and Foundation Engineering,* 23, 4, 56-74.

Tokoro, T., Kashima, S. & Murata, M. (1984) Grout Injection Method and Apparatus. in UNITED STATES PATENT AND TRADEMARK OFFICE (Ed.). United Source, Nihon Soil Engineering Co., Nihon Sobo Bosui Co., Yamaguchi Kikai Kogyo Co., 12.

Tsai, P. H. & Chang, T. S. (2009) Effects of Open Trench Siding on Vibration - Screening Effectiveness Using the Two-Dimensional Boundary Element Method. *Soil Dynamics and Earthquake Engineering,* 29, 5 (May), 865-873.

Us Army Corps of Engineers (1999) *Guidelines on Ground Improvement for Structures and Facilities, Engineer Technical Letter Elt-1110-1-185,* Washington, DC, USACE,115.

Van Eekelen, S. & Bezuijen, A. (2008) Design of Piled Embankments, Considering the Basic Starting Points of the British Standard Bs8006. *EuroGeo4*, Edinburgh, September.

Van Impe, W. F. (1989) *Soil Improvement Techniques and Their Evolution,* Rotterdam, Balkema

Van Impe, W. F. & Bouazza, A. (1996) Densification of Domestic Waste Fills by Dynamic Compaction. *Canadian Geotechnical Journal,* 33, 6, 879-887.

Van Wambeke, A. (1962) Méthodes D'investigation Des Sols En Place - Etude D'une Campagne D'essais Comparatifs. *Sols Soils*, 2, September, 9-18.

Van Wieringen, J. B. M. (1982) Relating Cone Resistance and Pressuremeter Test Results. *2nd European Symposium on Penetrating Testing*, Amsterdam, 951-955.

Varaksin, S. (1970) Determination of Sand Density Below Groundwater Table. Northwestern University at Evanston, Ill,

Varaksin, S. (1981) Recent Development in Soil Improvement Techniques and Their Practical Applications. *Sols Soils*, 38-39, 7-32.

Varaksin, S. (2014) Discussions on Dynamic Compaction and Dynamic Replacement. in HAMIDI, B. (Ed.).

Varaksin, S., Hamidi, B. & D'hiver, E. (2005) Pressuremeter Techniques to Determine Self Bearing Level and Surface Strain for Granular Fills after Dynamic Compaction. *International Symposium 50 Years of Pressuremeters (ISP5- Pressio 2005)*, Paris, 22-24 August, 687-.

Varaksin, S. & Racinais, J. (2009) Etude Des Paramètres D'application De La Consolidation Dynamique Et De Ses Techniques Dérivées. *17th International Conference on Soil Mechanics and Geotechnical Engineering*, Alexandria, Egypt, 5-9 October, 2407-2410.

Vesic, A. S. (1975) Shallow Foundations. in WINTERKORN, H. F. & FANG, H. Y. (Eds.) *Foundation Engineering.* New York, Van Nostrand Company.

Villet, W. C. B. & Mitchell, J. K. (1981) Cone Resistance, Relative Density and Friction Angle. *Symposium on Cone Penetration Testing and Experience, ASCE National Convention*, St Louis, October, 178-208.

Vuola, P. & Hartikainen, J. (1999) Aspects for Dynamic Compaction of Saturated Sand. *12th European Conference on Soil Mechanics and Geotechnical Engineering: Geotechnical Engineering for Transportation Infrastructure,* 3, 1603-1606.

Waschkowski, E. (1974) Penetrometres Dynamiques, 19-21 November, Not Published. *Comptes Rendus des Journees des Laboratoire des Ponts et Chaussées*, 1-37.

Waschkowski, E. (1976) Comparisons Entre Des Resultats Des Essais Pressiometriques Et Le SPT. Rapport De Recherche Du Laboratoire Regional Des Ponts Et Chaussées De Blois, Faer 1.05.23.5. not published,

Watts, G. R. (1990) Traffic Induced Vibrations in Buildings. Transport and Road Research Laboratory Research Report 246. Transport Research Laboratory,

White, D. & Vennapusa, P. (2010) A Review of Roller-Integrated Compaction Monitoring Technologies for Earthworks, Final Report Er10-04. Earthworks Engineering Research Center (EERC), Department of Civil Construction and Environmental Engineering, Iowa State University, 36.

Windes, S. L. (1942) *Damage from Air Blast. Progress Report 1, USBM Report of Investigation 3622*, US Bureau of Mines

Windes, S. L. (1943) *Damage from Air Blast. Progress Report 2, USBM Report of Investigation 3708*, US Bureau of Mines

Wiss, J. F. (1981) Construction Vibrations: State of the Art. *Journal of Geotechnical Engineering, ASCE,* 107, 2 (February), 167-182.

Wiss, J. F. & Parmelee, R. A. (1974) Human Perception of Transient Vibrations. *Journal of the Structural Division,* 100, ST4 (April), 773-787.

Wolf, J. P. (1994) *Foundation Vibration Analysis Using Simple Physical Models,* New Jersey, Prentice Hall

Woods, R. D. (1968) Screening of Elastic Surface Waves by Trenches. *Journal of Soil Mechanics and Foundations Division, ASCE,* 94, 4 (July), 951-979.

Woods, R. D. & Jedele, L. P. (1985) Energy Attenuation Relationships from Construction Vibration. *Symposium on Vibration Problems in Geotechnical Engineering*, Detroit, MI, 229-246.

Woods, R. D. & Richart, F. E. (1967) Screening of Elastic Surface Waves by Trenches. *International Symposium on Wave Propagation and Dynamic Properties of Earth Materials*, Albuquerque, New Mexico, August 1967.

Woodward, J. (2005) *An Introduction to Geotechnical Processes*, Taylor & Francis,123.

Wu, T. H. (1957) Relative Density and Shear Strength of Sands. *Journal of the Soil Mechanics and Foundations Division, ASCE,* 83, 1 (January), 1161-1161 - 1161-1123.

Yahiro, T. & Yoshida, H. (1977) High Velocity Jet Digging Method. in UNITED STATES PATENT AND TRADEMARK OFFICE (Ed.). United States, Chemical Grout Company & Kajima Corporation, 7.

Yee, K. (1999) Upgrading of Existing Landfills by Dynamic Consolidation: A Geotechnical Aspect. *Master Builders Journal*, September.

Yoshimi, Y. & Tohno, I. (1973) Statistical Significance of the Relative Density. *Evaluation of Relative Density and its Role in Geotechnical Projects Involving Cohesionless Soils: ASTM STP523-EB.7744-1*, Los Angeles, 25-30 June 1972, 74-84.

Youd, T. L. (1973) Factors Controlling Maximum and Minimum Densities of Sands. *Evaluation of Relative Density and its Role in Geotechnical Projects Involving Cohesionless Soils: ASTM STP523-EB.7744-1*, Los Angeles, 25-30 June 1972, 98-112.

Youd, T. L., Idriss, I. M., Andrus, R. D., Arango, I., Castro, G., Christian, J. T., Dobry, R., Finn, W. D. L., Harder, L. F., Hynes, M. E., Ishihara, K., Koester, J. P., Liao, S. S. C., Marcuson Iii, W. F., Martin, G. R., Mitchell, J. A., Moriwaki, Y., Power, M. S., Robertson, P. K., Seed, R. B. & Stokoe, K. H. (2001) Liquefaction Resistance of Soils: Summary Report from the 1996 Nceer and 1998 Nceer/Nsf Workshops on Evaluation of Liquefaction Resistance of Soils. *Journal of Geotechnical and Geoenvironmental Engineering, ASCE,* 127, 10 (October), 817-833.

Zaeske, D. (2001) Zur Wirkungweise Von Unbewehrten Und Bewerhrten Mineralischen Tragschichten Über Pfahlartigen Gründungselementen, Phd Thesis. Universität Gh Kassel,

Zoeppritz, C. & Kosten, C. W. (1919) Nach D. Konigl. Gessell D. Wissen, Z. Gottingen. *math-Phys.*, 66-94.

Zou, W. L., Wang, Z. & Yao, Z. F. (2005) Effect of Dynamic Compaction on Placement of High Road Embankment. *Journal of Performance of Constructed Facilities, ASCE,* 19, 4 (November), 316-323.

Every reasonable effort has been made to acknowledge the owners of copyright material. I would be pleased to hear from any copyright owner who has been omitted or incorrectly acknowledged.

Appendix: First Page of Publications

A REVIEW ON IMPACT ORIENTED GROUND IMPROVEMENT TECHNIQUES

Babak Hamidi[1], Hamid Nikraz[2], Serge Varaksin[3]
[1] PhD Candidate, Curtin University of Technology
[2] Professor & Head of Civil Engineering Department, Curtin University of Technology
[3] Deputy General Manager of Menard and Chairman of ISSMGE TC-17

ABSTRACT

Nowadays various ground improvement techniques by impact are widely practiced as technical and economical solutions however each technique has its own use and range of application. It has come to the attention of the authors that the name of one of the techniques; i.e. Dynamic Compaction is being used generically in lieu of the proper names of the other methods. This article will review Dynamic Compaction and shall compare it with two other impact techniques; i.e. Rapid Impact Compaction and Impact Roller Compaction. As a conclusion the readers are advised to use the correct terminology to avoid misunderstanding and confusion in projects and results.

1 A REVIEW OF DYNAMIC COMPACTION

Louis Menard invented and promoted Dynamic Compaction (DC) as early as 1969 but it was not until 29 May 1970 that he officially patented his invention in France. The technique was later also patented in many other countries, including Australia in 1981.

The concept of this technique is improving the mechanical properties of the soil by transmitting high energy impacts to loose soils that initially have low bearing capacity and high compressibility potentials. The impact creates body and surface waves that propagate in the soil medium. In non-saturated soils the waves displace the soil grains and re-arrange them in a denser configuration. In saturated soils the soil is liquefied and the grains re-arranged in a more compact state. In both cases the decrease of voids and increase in inner granular contact will directly lead to improved soil properties.

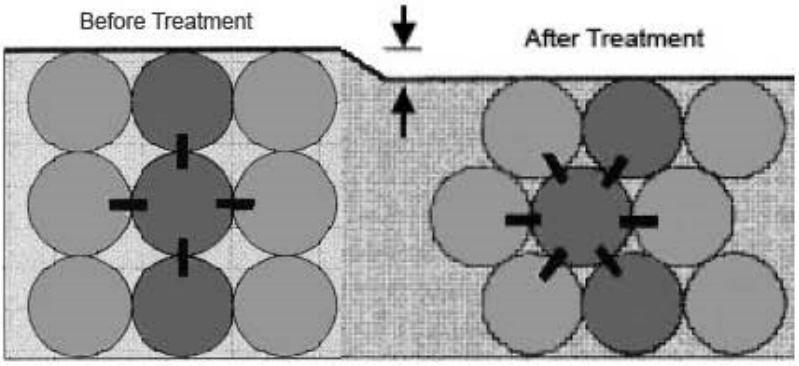

Figure 1: Displacement and rearrangement of the soil grains in a denser configuration

The impact energy is delivered by dropping a *heavy* weight or pounder from a *significant* height. The pounder weight is most often in the range of 8 to 25 tons although lighter or heavier weights are occasionally used. The current pounder weight record was set at 170 tons in 1978 with the Menard Giga machine during the ground improvement works of Nice Airport in France (Gambin, 1983). Drop heights are usually in the range of 10 to 20 m although 40 ton pounders have been dropped from 40 m by Menard's Mega machine (Mayne and Jones, 1984).

ARCHING IN GROUND IMPROVEMENT

Babak Hamidi[1], Hamid Nikraz[2] and Serge Varaksin[3]
[1] *PhD Candidate, Curtin University of Technology*
[2] *Professor & Head of Civil Engineering Department, Curtin University of Technology*
[3] *Deputy General Manager of Menard and Chairman of ISSMGE TC-17*

ABSTRACT

In some soil improvement techniques, such as dynamic replacement, stone columns, controlled modulus columns, jet grouting, compaction grouting and deep soil mixing, the ground properties are enhanced by introducing columnar inclusions to the required depths. Regardless of the technique used it is evident that the stiffness of the *in situ* soft soil and the inclusions are not the same, and the load distribution between the columns and soil must be determined as part of the process of the ground improvement solution.The distribution of load is a function of a number of parameters. This paper will discuss the mechanism of load transfer in the ground, will review a number of techniques for determining the stress and load distribution and will identify the parameters that affect the load distribution between the soil and columns.

1 INTRODUCTION

In some soil improvement techniques such as preloading with or without wick drains, vacuum consolidation, dynamic compaction and vibro compaction it can be assumed that the ground has been treated in such a way that the soil paramters are the same in any horizontal plane. Even if this assumption is a simplification of reality, the practical effect of the differences is generally negligible and will not affect the results of calculations and design.

However, the soil is not always treated in a manner where this assumption could be valid and there are a number of techniques in which columnar elements with far better properties than the soil are introduced into the ground. These columns may be constructed either by dynamically driving granular material into the soft soil, as in the case of dynamic replacement, by a vibroflot with the assistance of either a water jet or compressed air as in stone columns (vibro replacement), by specially designed augers that displace the soil and inject grout from the tip as in controlled modulus columns (CMC), by jetting a water-cement mix at very high pressure through a rotating nozzle as in jet grouting, by creating bulges by pumping grout as in compaction grouting, or by mixing the *in situ* soil with cement using specially designed paddles as in deep soil mixing. Figure 1 shows the construction of columnar inclusions using dynamic replacement, stone column, jet grouting and controlled modulus column methods.

Practically speaking, there is almost always a layer of granular fill on top of the columnar inclusions and under the level of application of the load. The fill layer may be *in situ*, may have been placed either as a working platform for safely supporting the ground improvement equipment and machines, as a filler for reaching designated elevations or as a transition layer and as part of the design.

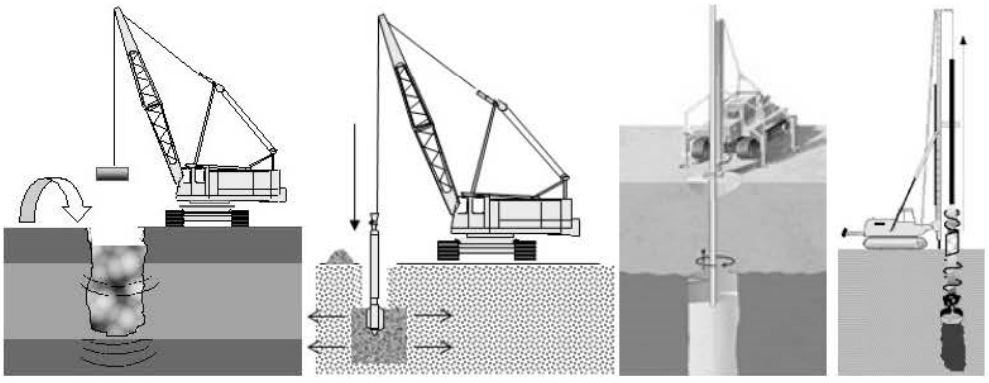

(a) (b) (c) (d)

Figure 1: (a) dynamic replacement, (b) stone column, (c) jet grouting, (d) controlled modulus columns

The transition layer plays a very important and critical role in transferring and distributing the load between the in-situ soft soil and the columnar inclusions, and it is mandatory for the geotechnical engineer to understand this phenomenon in order to be able to correctly determine the load in the columns and consequently to analyse their stability, bearing, punching, deformation and other requirements.

2 METHODS FOR DETERMINING COLUMN LOADS

Technical Note

ISSN 1996-6814 Int. J. Pavement Res. Technol. 4(2):124-130

The Treatment of a Loose Submerged Subgrade Using Dynamic Compaction

Babak Hamidi[1+], Hamid Nikraz[2], and Serge Varaksin[3]

Abstract: It is not unforeseeable to have pavements that have lost functionality and drivability due to excessive total, differential or creep settlements; liquefaction; or local shear failures of the subgrade layer. If the subgrade material does not have the necessary strength, it may be mandatory to carry out a ground treatment program to improve the ground conditions and to allow the safe construction of the subsequent layers. The causeway of Abu Dhabi to Reem Island has been constructed by reclaiming the approach road on the two sides of the bridge from the sea. The 8-m thick reclamation was performed by dumping sand into the sea. Geotechnical tests indicated that the reclaimed material did not meet the design requirements for constructing the bridge's approach roads and the foundations of the mechanically stabilized earth (MSE) walls. Dynamic Compaction was carried out to improve the ground conditions of the reclamation. Upon completion of soil improvement, pressuremeter tests were performed to verify the results. The test results demonstrated that the design and acceptance criteria were achieved.

Key words: *Dynamic Compaction; Pressuremeter; Soil improvement.*

Introduction

Reem Island, previously called Abu Shaoum, is a small island that is located about 0.4 km north of Abu Dhabi, United Arab Emirates. The island was basically vacant until 2005 when it was decided to turn it into a modern and luxurious suburb as part of the general development plan of the nation's capital city.

One of the first requirements of the new development was the construction of a causeway to link the island to the rest of the city. According to the design, the causeway was to be composed of approach roads on the two sides and a bridge structure in the center. The approaches on each side were to be approximately 150 m in length. As can be seen in Fig. 1, the reclamation was anticipated to be about 135 m long on Abu Dhabi's side and 50 m long on Reem Island's side.

The approach road was to be constructed on the coastal grounds and on reclamation. The road level was anticipated to be from +2.0 m RL (reduced level = mean sea level, MSL) to +7.00 m RL at bridge level. The maximum elevation difference between the low and high points of the approach road was 5 m, and the road slope was 3.25%.

The approach road and bridge were designed to have four lanes in each direction. The width of the approach road leading to the bridge was 28 m. An additional lane was envisaged on each side for drivers wishing to turn back without entering the bridge. In order to limit the total width of the road to 38 m, the stability of the two sides of the bridge's access road was to be provided by an MSE wall.

[1] Curtin University of Technology, 5/531Hay Street Subiaco 6008 WA Australia.
[2] Professor and Head of Civil Engineering Department, Curtin University of Technology, GPO Box U1987 Perth WA, Australia.
[3] Menard Deputy General Manager & Chairman of ISSMFE TC17, 2 rue Gutenberg, BP 28, 91620 Nozay France.
[+] Corresponding Author: E-mail babak.hamidi@postgrad.curtin.edu.au
Note: Submitted September 13, 2009; Revised February 25, 2010; Accepted March 9, 2010.

Ground Conditions and Fill Description

The longitudinal profile of the project (Abu Dhabi side) is shown in Fig. 2. The natural ground levels (NGL) in Abu Dhabi and Reem Island were respectively at about -0.5 m and +1.0 m RL but rapidly dropped to about -7.00 m RL and -5.50 m on the sides of the bridge. Groundwater level in the boreholes varied from +0.7 to -0.7 m RL.

Although NGL in the marine boreholes differed, as summarized in Table 1, the in-situ ground profile was generally the same within the project's area. The upper 0.8 to 1.5 m of soil was soft sandy, silty clay. This layer was followed by a very loose to very dense sandy layer with a variable thickness of nil to 2 m and with less than 20% fines. This latter layer overlaid bedrock. The bottom elevation of the loose sandy layer was from about -6.0 to -8.0 m RL.

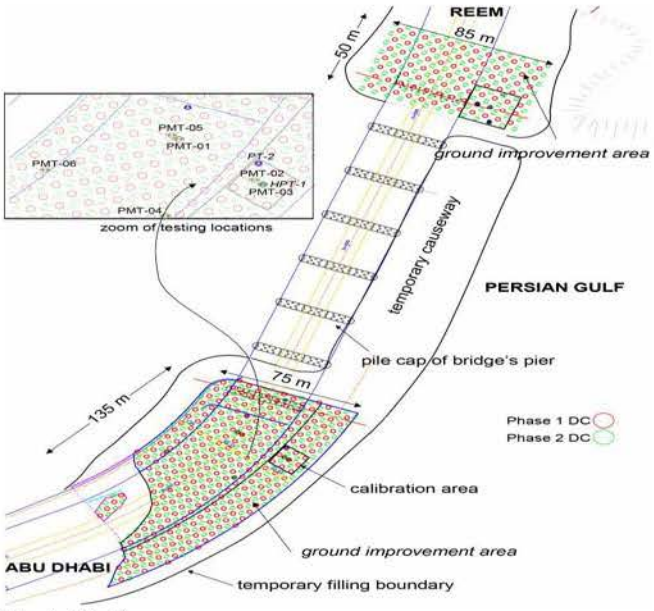

Fig. 1. Site Plan.

Ground Improvement
Volume 166 Issue GI2

Relative density concept is not a reliable criterion
Hamidi, Varaksin and Nikraz

ice | proceedings

Proceedings of the Institution of Civil Engineers
Ground Improvement 166 May 2013 Issue GI2
Pages 78–85 http://dx.doi.org/10.1680/grim.11.00014
Paper 1100014
Received 05/04/2011 Accepted 31/07/2012
Published online 22/03/2013
Keywords: foundations/geotechnical engineering/strength and testing of materials

ice Institution of Civil Engineers publishing

Relative density concept is not a reliable criterion

1 Babak Hamidi MEng(Hons), MIEAust
PhD candidate, Curtin University and member of ISSMGE Ground Improvement Technical Committee, Perth, Australia

2 Serge Varaksin MEng, CFMS
Chairman of ISSMGE Ground Improvement Technical Committee, Paris, France

3 Hamid Nikraz MEng, PhD, FIEAust, CEng, NPER
Professor and Head of Civil Engineering Department of Curtin University, Bentley, Western Australia, Australia



Many years ago, a new concept called relative density was developed with the intention of appropriately defining the looseness and denseness of sand or sand–gravel soils in a meaningful way. Soon after, relative density found its way into ground improvement as an acceptance criterion by engineers who were more familiar with the construction of engineered backfilling rather than thick mass treatment. There are considerable amounts of research and publications that are able to well demonstrate the unreliability of relative density as an acceptance criterion. Relative density has no real influence on the soil's performance, its range of application does not span across all soil types, and it is subject to large inherent errors that make its use a technical risk. Here, the reasons why the concept of relative density is unreliable and should not be used for a ground improvement acceptance criterion are presented and discussed.

Notation

$C_{\gamma d}$	error propagation factor for γ_d
$C_{\gamma d\max}$	error propagation factor for $\gamma_{d\max}$
$C_{\gamma d\min}$	error propagation factor for $\gamma_{d\min}$
D_d	relative density
D_{50}	mean particle diameter
e	the in situ or stated void ratio of a soil deposit or fill
$e_{\max}$	maximum index void ratio or the reference void ratio of a soil at the minimum index density/unit weight
$e_{\min}$	minimum index void ratio or the reference void ratio of a soil at the maximum index density/unit weight
m	number of measurements
S_{Dd}	standard deviation for D_d
$S_{\gamma d}$	standard deviation for γ_d
$S_{\gamma d\max}$	standard deviation for $\gamma_{d\max}$
$S_{\gamma d\min}$	standard deviation for $\gamma_{d\min}$
ΔD_d	deviation in relative density
$\Delta\gamma_d$	deviation in γ_d
$\Delta\gamma_{d\max}$	deviation in $\gamma_{d\max}$
$\Delta\gamma_{d\min}$	deviation in $\gamma_{d\min}$
ρ_d or γ_d	dry density/unit weight of a soil deposit or fill at the given void ratio
$\rho_{d\max}$ or $\gamma_{d\max}$	the reference dry density/unit weight of a soil in the densest state of compactness that can be attained using a standard laboratory compaction procedure that minimises particle segregation and breakdown
$\rho_{d\min}$ or $\gamma_{d\min}$	the reference dry density/unit weight of a soil in a standard state of compactness at which it can be placed using a standard laboratory procedure that prevents bulking and minimises particle segregation

1. Introduction: history

The concept of relative density (D_d) was first introduced by Terzaghi (1925) to bring the behaviour characteristics of soils together on a common basis in consistent and practically useful relations and to provide a tool for communications between engineers (Burmister, 1948). It was suggested that this parameter would be an appropriate means to define the looseness and denseness of sand or sand–gravel soils in a meaningful way because important properties were assumed to correlate quite well by this means.

Relative density is a definition rather than an inherent property of the soil. Thus, by itself, it has no significance and influence on performance and it is possible to satisfy design criteria with a higher safety factor without even complying with the relative density criterion (Hamidi *et al.*, 2010a, 2010b).

Ground Improvement
Volume 166 Issue GI4

Relative density correlations are not reliable criteria
Hamidi, Varaksin and Nikraz

ice | proceedings

Proceedings of the Institution of Civil Engineers
Ground Improvement 166 November 2013 Issue GI4
Pages 196–208 http://dx.doi.org/10.1680/grim.11.00016
Paper 1100016
Received 06/04/2011 Accepted 07/02/2013
Published online 30/05/2013
Keywords: foundations/geotechnical engineering/strength and testing of materials

ice Institution of Civil Engineers publishing

Relative density correlations are not reliable criteria

1 Babak Hamidi MEng(Hons), MIEAust
PhD candidate, Curtin University and member of ISSMGE Ground Improvement Technical Committee, Perth, Australia

2 Serge Varaksin MEng, CFMS
Chairman of ISSMGE Ground Improvement Technical Committee, Paris, France

3 Hamid Nikraz MEng, PhD, FIEAust, CEng, NPER
Professor & Head of Civil Engineering Department of Curtin University, Bentley, Western Australia, Australia



The concept of relative density was developed with the intention of appropriately defining looseness and denseness of sand or sand–gravel soils in a meaningful way; however, there are sufficient amounts of research and case studies to demonstrate the unreliability of this concept due to its large inherent errors. Nevertheless, this parameter found its way early on as a ground improvement acceptance criterion based on the same philosophy that led to its formation. As there was general agreement among engineers that, in any case, direct testing of relative density in actual deep ground improvement projects was difficult, time consuming and costly, direct methods of relative density measurement were abandoned in favour of correlation to other field tests. At first glance, this may have seemed to work out quite well as the conceptual unreliability of relative density did not come into play, but a deeper look could reveal that the proposed correlations are also as unreliable as the concept itself. This paper will discuss the reasons why relative density correlations should not be used as ground improvement acceptance criteria, and alternative reliable criteria will be proposed.

Notation

a	Skempton parameter
b	Skempton parameter
C_0, C_1 and C_2	experimental coefficients
C_{oc}	overconsolidation coefficient
C_u	coefficient of uniformity
D_R	relative density (%)
D_{50}	mean particle size
e_{max}	maximum index void ratio or the reference void ratio of a soil at the minimum index density/unit weight
e_{min}	minimum index void ratio or the reference void ratio of a soil at the maximum index density/unit weight
F_c	fines content (%)
f_{shell}	shell correlation factor
K_0	ratio of effective horizontal to vertical stress for an overconsolidated soil
K_{0NC}	ratio of effective horizontal to vertical stress for a normally consolidated soil
N	standard penetration test (SPT) blow count
N_{78}	SPT blow count corresponding to an energy rod ratio of about 78% from the theoretical free-fall energy
OCR	overconsolidation ratio
q_c	cone penetration test (CPT) cone resistance (kPa)
q_{cNC}	CPT cone resistance for normally consolidated soil (kPa)
q_{cOC}	CPT cone resistance for overconsolidated soil (kPa)
R	roundness
ΔN_F	correction term that is a function of fines content
σ'	effective vertical, horizontal or mean stress depending on the overconsolidation ratio (kPa)
σ'_v	effective overburden pressure (kPa)
ϕ'	effective internal friction angle

1. Introduction

Hamidi *et al.* (2013) have made a comprehensive review of current ASTM test methods (ASTM, 2006a, 2006b) and studies carried out by numerous researchers to demonstrate the limitations of relative density, and to show that although the objective

OFFSHORE GROUND IMPROVEMENT RECORDS

Babak Hamidi[1], Jean-Marc Debats[2], Hamid Nikraz[3], Serge Varaksin[4]
[1] Civil Engineering Department, Curtin University
[2] Vibro Services (GFWA & Menard Bachy in Australia) & immediate past Chairman of ISSMGE TC-211
[3] Professor & Head of Civil Engineering Department, Curtin University
[4] Chairman of ISSMGE TC-211

ABSTRACT

Numerous ground improvement technologies have been in use for many years on land based projects with various applications. These techniques have provided alternatives that are frequently more affordable and require shorter construction periods than deep foundations. Implementation of these methods in the sea and marine environments is more challenging as specialised equipment are usually either only appropriate for land based projects or have low efficiency and production capability at sea. However, requirement of seabed treatment and improving the characteristics of marine foundations has necessitated the introduction of soil improvement technologies to offshore projects. Some of the ground improvement techniques that have especially evolved to satisfy the requirements of offshore and seabed ground improvement are dynamic compaction, vibro compaction, dynamic replacement, and stone columns. The first two techniques are used for the treatment of granular seabed while the latter two technologies are most appropriate for improving silty and clayey marine foundations. In this paper initially marine and offshore ground improvement techniques with a focus of the mentioned above methods will be discussed. Two case studies of ground improvement for the treatment of soft clays in record water depths will also be introduced. In the first case offshore dynamic replacement was carried out in Southeast Asia at a location where seabed was approximately 30 m below sea level. In the second project stone columns were installed beneath the quay wall and breakwater of the first and second phases of Port of Patras (Greece). The sea depth was up to approximately 40 m and the columns were as long as 20 m.

1. INTRODUCTION

Ground improvement, as we know it by its modern definition, began to take the form of a branch of geotechnical engineering in the mid-20th century, and was finally realised as the 17th technical committee of ISSMGE many years ago (Varaksin and Hamidi, 2012). While it may not be immediately apparent, ground improvement methods have made considerable advances since today's commonly practiced techniques first began to develop and evolve in the first half of the 20th century; however most techniques have gone through changes, mostly due to new ideas, advances and innovations in equipment and technological capabilities and the emergence of newer technologies has provided the geotechnical engineer with additional tools for optimising foundation design and treatment of particular soils.

It can be observed that the notion of improving the ground for engineering purposes initially developed implicitly to resolve subaerial issues as foundation problems were and are most often encountered on land due to the fact that the percentage of marine foundations is much less than overland foundations. However, the 20th century was witness to a number of marine and onshore geotechnical failures such as the 1916 collapse of Gothenburg Harbour's Stigberg Quay in Sweden (Massarsch and Fellenius, 2012) and the 1979 failure of Nice Harbour in France (Dan et al, 2007). Hence, it was inevitable that sooner or later attention would be drawn towards modifying or adjusting ground improvement techniques for application to subaqueous near shore and offshore projects.

1.1. DYNAMIC COMPACTION AND DYNAMIC REPLACEMENT

Louis Menard invented and promoted Dynamic Compaction (DC) as early as 1969 but it was not until 29 May 1970 that he officially patented his invention in France. The technique was later also patented in many other countries, including Australia in 1981 (Hamidi et al., 2009a).

The concept of this technique is improving the mechanical properties of the soil by transmitting high energy impacts to loose soils that initially have low bearing capacity and high compressibility potentials. The impact creates body and surface waves that propagate in the soil medium. In non-saturated soils the waves displace the soil grains and re-arrange them in a denser configuration. In saturated ground the soil is liquefied and the grains re-arrange in a more compact state. In both cases the decrease of voids and increase in inner granular contact will directly lead to improved soil properties. Impact

TREATMENT OF THICK SATURATED LOOSE SUB-GRADES USING DYNAMIC COMPACTION

Babak Hamidi, Curtin University of Technology, Australia
Hamid Nikraz, Curtin University of Technology, Australia
Serge Varaksin, Menard, France

Abstract

Road engineers are very keen to properly compact base and sub-base layers to meet the design requirements; however these well built engineered layers are sometimes constructed on loose saturated subgrades. Consequently, the pavement may undergo undesirable deformations and settlements for a number of reasons.
Dynamic Compaction is a ground improvement technique that can and has been effectively utilized for treating the loose layers of in-situ or reclaimed granular soils. In this paper, the application of Dynamic Compaction for improving loose sub-grades will be discussed using two case studies. The case studies have been selected to demonstrate that the technique is equally applicable to hydraulic fills and truck dumped fills, very large projects such as the 900,000 m^2 Abu Dhabi Corniche (Beach Road) to relatively small projects such as the 10,000 m^2 approach roads of Reem Island Causeway. The projects can be in undeveloped locations or in urban areas.
Special attention will be designated to the development of technical specifications that can optimize or jeopardize the ground improvement programme, and recommendations will be proposed to develop optimized criteria.

Keywords: ground improvement, soil improvement, dynamic compaction, saturated fill, subgrade

1. Introduction

It is general practice in road construction to compact the pavement layers using vibratory rollers to a defined compaction that will satisfy the design. Commonly, the amount of compaction is measured by comparing the dry density of the soil with the maximum Proctor or modified Proctor dry density.

Occasionally, there are roads that are to be constructed on grounds that have been reclaimed from the sea either by hydraulically placed fill or dumping soil using tipper trucks. In any case, these fills are most often very loose to loose and frequently with a dense upper crust above groundwater level.

SOIL IMPROVEMENT OF A VERY THICK AND LARGE FILL BY DYNAMIC COMPACTION

Babak Hamidi, Curtin University of Technology, Australia
Hamid Nikraz, Curtin University of Technology, Australia
Serge Varaksin, Menard, France

Abstract

Al Quoa'a is a remote and isolated desert township in the United Arab Emirates. Desert dune sands were levelled without compaction to create a flat construction platform. The first phase of the project was constructed without implementation of specific foundations solutions. Consequently, most of the structures that were built on the fill areas suffered from very severe damages and deep cracks. The second phase of the project has also been constructed on a levelled platform with a non-engineered fill area of about 1.13 million m^2 and a maximum fill thickness of 28 metres.
Ground improvement was carried out engineered on a design and build concept. Design and acceptance criteria were specifically tailored to satisfy the project needs and Dynamic Compaction was used to treat the loose dry sands of the very thick and large fill for bearing capacity, total, differential and creep settlements within a contractual duration of 10 months using 6 specially modified rigs. The treatment was optimized by implementing a combination of different pounder weights and impact energies. For the first time ever, the innovative and patented MARS (Menard Automatic Release System) was used to efficiently drop a 35 ton pounder in free fall. Menard Pressuremeter Tests were used to verify that acceptance criteria had been fully satisfied.

Keywords: ground improvement, soil improvement, dynamic compaction, pressuremeter test

1. Introduction

Al Quoa'a is a remote and isolated Emarati desert township that is located about 100 km from Al Ain and on the border of the United Arab Emirates and Oman. The first phase of this new town was constructed by cutting and filling the dune sands and levelling the ground for creating the town's platform. Although the buildings were only two stories high, most that were built on the fill areas suffered from severe damages and substantial amounts of deep cracks, and it became evident to the developers that specific measures had to be implemented during later phases of the project to avoid more damage.

6th Australasian Congress on Applied Mechanics, ACAM 6
12-15 December 2010, Perth, Australia

Application of Dynamic Compaction in Port of Ras Laffan Expansion Project

B. Hamidi[1*], H. Nikraz[1] and S. Varaksin[2]

[1] *Department of Civil Engineering, Curtin University of Technology, Perth, Australia*
[2] *Menard, Paris, France*

[*] *Corresponding author. Email: bhamidi@menardbachy.com.au*

Abstract: Dynamic Compaction (DC) has recently been used to improve 175,000 m^2 of hydraulically reclaimed land using carbonate sand and gravel and with a variable thickness of up to 16 m as part of Port of Ras Laffan expansion in Qatar. Acceptance criterion for the project was based on a minimum relative density value with CPT verification or alternatively performance criteria with Pressuremeter Testing. Due to the required depth of treatment, the innovative MARS technology was also used to drop a 35 ton pounder in free fall. Calculations based on post improvement test results clearly suggested that implementation of acceptance criteria based on a project's specific technical requirements is able to achieve project goals at a more affordable cost and in a shorter period than using specified minimum test values. During the works pockets of fine soils were identified in the treatment area. At the end of the works in addition to the anticipated field tests, a full scale load zone test was carried out at a location within the sensitive skid beams area where it was understood that the fine soil layer was thickest. Settlement monitoring indicated that short and long term settlements of the skids will be within the project specifications.

Keywords: CPT, dynamic compaction, ground improvement, soil improvement, reclamation.

1 Introduction

Ras Laffan, located on the southern coast of the Persian Gulf and approximately 70 km north of Qatar's capital city, Doha, houses the onshore facilities of the world's largest gas field. Nakilat Ship Repair Yard, shown in Figure 1, is part of Port of Ras Laffan's expansion program, and has recently been hydraulically reclaimed.

1.1 Ground Conditions

Seabed level at the location of the project was variable from -9.1 m to -13.2 m CD (chart datum). Design (final platform) level was specified to be at +3.5 m CD. However as the engineers' past experiences suggested that hydraulic fills would generally be reclaimed in a loose state, it was conceived that ground improvement would be required. Ground subsidence due to treatment was estimated to be about 0.6 to 0.8 m; hence the working platform was reclaimed to a variable level of about +4.1 to +4.3 m CD.

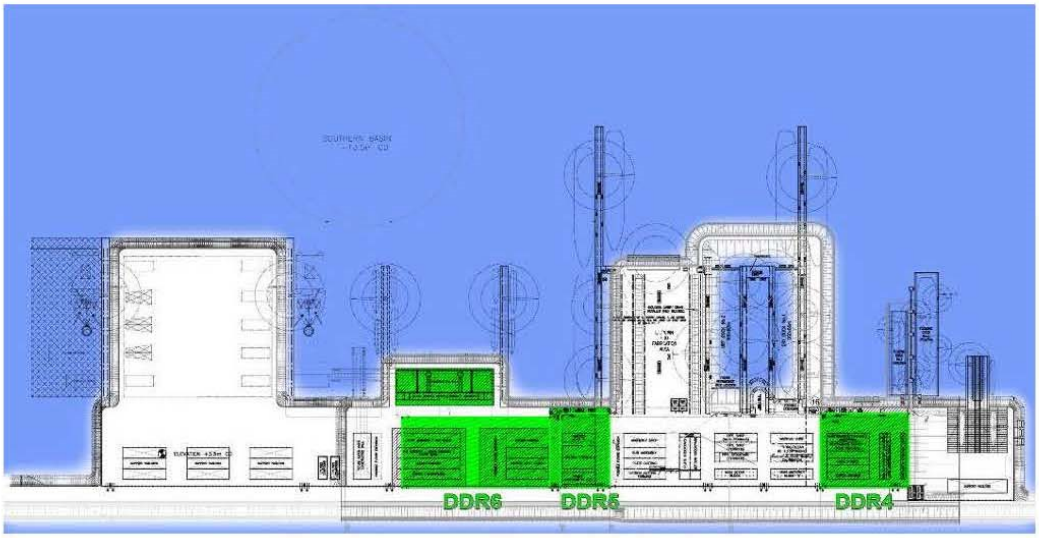

Figure 1: Nakilat Ship Repair Yard (Dynamic Compaction areas are shown in green)

DYNAMIC REPLACEMENT FOR CONSTRUCTING EMBANKMENTS AND WALLS ON SOFT SOIL

Babak Hamidi, Curtin University of Technology, Australia
Serge Varaksin, Menard, France
Hamid Nikraz, Curtin University of Technology, Australia

Abstract

The new J W Marriott Hotel in Abu Dhabi includes 90,000 m^2 of roads, manmade hills (embankments), and 100 chalets that have been built on them. The hills are up to 8 m high and retained from one side by mechanically stabilised earth (MSE) walls. The initial ground conditions of this the site was very unfavourable with loose saturated soft silty and clayey soils located at depths extending down to 5 m below ground level and exceptionally as deep as 6 m.
Dynamic Replacement (DR) and pre-excavated DR were used to improve the ground conditions and to ensure that the numerous geotechnical problems including bearing capacity, total and differential settlements, wall stability and primary consolidation period were within project specifications. Improvement phases had to be broken into sub-phases to allow the pore pressures to dissipate. Special design considerations were utilized in the wall sections by pre-excavating and backfilling the wall foundations in strips and trenches with a mixture of demolished concrete and sand.
Menard Pressuremeter Tests (PMT) were used to verify bearing capacity and to predict settlements. Actual ground settlements were measured during and after the construction of the hills by using settlement plates, and the consolidation ratio was determined using Asaoka's method.

Keywords: ground improvement, soil improvement, dynamic replacement, soft soil, pressuremeter

1. Introduction

The new J W Marriott Hotel is a luxurious resort constructed on the southern coastlands of Abu Dhabi, UAE. It is located on 210,000 m^2 of land inclusive of the previous site of the now demolished Gulf Hotel and the virgin plot of land that was situated on its southern border. An 11 storey hotel with an underground parking is located in the middle of the resort. This structure is encompassed on the north and south by two man-made hills gradually elevating to about 8 m above street level. 100 single storey chalets are spread out throughout the hills and the original ground. The hills are retained on the

TREATMENT OF A HYDRAULICALLY RECLAIMED PORT PROJECT BY DYNAMIC COMPACTION

Babak Hamidi, Curtin University of Technology, Australia
Serge Varaksin, Menard, France
Hamid Nikraz, Curtin University of Technology, Australia

Abstract

Dynamic Compaction (DC) has recently been used to improve 175,000 m^2 of hydraulically reclaimed land as part of the expansion project of Port of Ras Laffan in Qatar. The material used for reclamation was calcareous sand and gravel. The treatment thickness was variable and up to a maximum of 16 m.
Acceptance criterion for the project was originally based on minimum relative density values that had to be verified by CPT, but later alternative criteria based on performance were introduced and implemented. Pressuremeter Tests (PMT) were also carried out for verification purposes.
Due to the required depth of treatment, in this project in addition to the commonly used pounders that are typically used in heavy dynamic compaction, the innovative MARS technology was also used to drop a 35 ton pounder in free fall and to then to grab it automatically.
Post ground improvement test results and calculations have been able to demonstrate the technical, financial, construction and contractual benefits and advantages of implementing a performance based acceptance criteria instead of the relative density based criterion. Thus, this paper recommends the implementation of performance acceptance criteria that have been developed and realized by considering design criteria.

Keywords: ground improvement, soil improvement, dynamic compaction, hydraulic fill

1. Introduction

Ras Laffan is located on the southern coast of the Persian Gulf, is about 70 km north of Qatar's capital city, Doha, and houses the onshore facilities of the world's largest gas field. Nakilat Ship Repair Yard is part of Port of Ras Laffan's expansion program, and has recently been reclaimed by a hydraulic fill.

CPT'10
2nd International Symposium on Cone Penetration Testing, Huntington Beach, CA, USA, May 2010

Correlations between CPT and PMT at a Dynamic Compaction Project

B. Hamidi & H. Nikraz
Curtin University of Technology, Perth, Australia

S. Varaksin
Menard, Paris, France

ABSTRACT: In many ground improvement projects the preliminary field testing method is different from the tests that are carried out later. Hence, it may be necessary to correlate the two tests for comparative purposes.

Dynamic Compaction, using pounders weighing up to 35 tons, has been used to treat 175,000 m^2 of hydraulically reclaimed carbonate sands with a thickness of about 16 m for a port expansion project in Ras Laffan, Qatar. In this project CPT was used before and after ground improvement works. A number of Pressuremeter tests (PMT), some in the immediate vicinity of the CPT locations, were also carried out. This paper shall briefly describe the project and the ground improvement works. Previously published literature correlating CPT to PMT will be reviewed and the results of the two testing methods that have been carried out in Ras Laffan shall be correlated, and conclusions will be made based on the findings.

1 THE PROJECT: NAKILAT SHIP REPAIR YARD

Ras Laffan, located about 70 km north of Qatar's capital city, Doha, is one of the world's largest and fastest developing gas hubs. As shown in Figure 1 and as part of Port of Ras Laffan's expansion program it was decided to construct Nakilat Ship Repair Yard by hydraulically reclaiming its site from the Persian Gulf.

The land was reclaimed using the carbonate sand and gravel that was dredged for deepening the port. The material's grain size was understood to be generally less than 75 mm, but it was anticipated that stones as large as 500 mm in diameter could also be present. The maximum fines content (passing 63 μm sieve) of the fill was generally less than 10%.

The dense layer of seabed in the reclaimed area was variable from -9.1 m to -13.2 m CD (chart datum). Design (final platform) level was specified to be at +3.5 m CD.

While it was understood that other less sensitive areas of the project would require lesser treatment, three areas in the dry docks designated as DDR4, DDR5 and DDR 6 and shown in green in Figure 1 were deemed to require treatment by Dynamic Compaction (Menard, 1972-74). The surface areas of these regions were respectively 57,064 m^2, 35,643 m^2 and 82,962 m^2. Consequently, the total area was 175,669 m^2.

Implementation of Optimized Soil Improvement Techniques for a Giga Project

Babak Hamidi[1], Serge Varaksin[2] and Hamid Nikraz[3]

[1]PhD Candidate, Curtin University of Technology, 5/531Hay Street, Subiaco 6008 WA, Australia; babak.hamidi@postgrad.curtin.edu.au

[2]Deputy General Manager, Menard; Chairman, ISSMFE TC17, 2 rue Gutenberg, BP 28, 91620 Nozay France; serge.varaksin@menard-mail.com

[3]Professor and Head of Civil Engineering Department, Curtin University of Technology, GPO Box U1987 Perth WA, Australia; h.nikraz@curtin.edu.au

ABSTRACT: One of the world's largest ground improvement projects that has ever been carried out in one phase by a single specialist ground improvement contractor is the 2,600,000 m^2 King Abdulla University of Science and Technology in Jeddah. What has made this project perhaps one of the most unique ground improvement accomplishments ever is not only its size but also the ability to interpret the ground conditions based on limited geotechnical investigation and the ground's behavior during the treatment, the know-how to adapt the solution to late architectural and structural changes, and the capacity to execute the works by an optimized combination of Dynamic Compaction, Dynamic Replacement, High Energy Dynamic Replacement and Dynamic Surcharging.

INTRODUCTION

The 5.6 million m^2 King Abdulla University of Science and Technology (KAUST) is located in Rabigh on the Red Sea coast and near the city of Jeddah in Saudi Arabia. KAUST, originally anticipated to have buildings with at most two to three stories, includes the university campus and academic administration core, a desalination plant, wind turbines, residential neighborhoods, a research park, a commercial center, a waste water treatment plant and a beach club.

The concept of the project was developed in 2006. According to the schedule, master planning, architectural and structural design and construction had to be completed in less than three years and handover date was set at September 2009.

The preliminary geotechnical investigation that was carried out in a relatively wide grid indicated that the ground was very heterogeneous and composed of a

6th Australasian Congress on Applied Mechanics, ACAM 6
12-15 December 2010, Perth, Australia

Predicting Soil Parameters by Modelling Dynamic Compaction Induced Subsidence

B. Hamidi[1*], S. Varaksin[2], H. Nikraz[1]

[1] Department of Civil Engineering, Curtin University of Technology, Perth, Australia
[2] Menard, Paris, France

[*]Corresponding author. Email: bhamidi@menardbachy.com.au

Abstract: It is common practice in Dynamic Compaction to carry out a calibration programme before production and execution of actual ground improvement works to optimize the design parameters. In the calibration the ground is initially tested. Then Dynamic Compaction is carried out on a predefined grid size. One or two heave and penetration tests may be carried out during the calibration. Upon completion of Dynamic Compaction the ground will be tested again to ensure that the desired parameters were achieved. Occasionally, a number of patterns may be tried in the calibration to provide the engineer with more design options and sometimes poor test results force the repetition of the calibration with alternative patterns. Obviously testing requires time, and it can be understood that it could be beneficial to be able to predict the improvement in the ground and to take possible remedial measures if the assessment is able to demonstrate that the tests will not meet the design criteria. This may be achieved in Dynamic Compaction by developing a relation between the induced ground subsidence and the improvement of Pressuremeter Test (PMT) limit pressure. In this approach Dynamic Compaction induced ground subsidence is assumed to be the accumulation of vertical strains down to the depth of improvement according to a Rayleigh distribution. The Dynamic Compaction induced strain for each level is correlated to the increase of limit pressure with the assumption that limit pressure will double for every 3% of strain [1].

Keywords: dynamic compaction, ground improvement, pressuremeter test, soil improvement.

1 Introduction

It is common practice in Dynamic Compaction to carry out a calibration programme before production and execution of actual ground improvement works to optimize the design parameters. In the calibration the ground is initially tested to provide an understanding of the ground conditions before treatment. Then Dynamic Compaction is carried out on a predefined grid size with a number of blows that is deemed to provide the best post improvement data. One or two heave and penetration tests [2] may be carried out during the calibration to provide an understanding of the trend and amount of compaction and heave during the pounder impacts.

Upon completion of Dynamic Compaction the ground will be tested again to ensure that the desired parameters have been achieved. Occasionally, a number of patterns may be tried in the calibration to provide the engineer with more design options and sometimes poor test results force the repetition of the calibration with alternative patterns. Testing consumes time, and it would be very displeasing to realize that the results were not acceptable after the completion of the tests and interpretation of the data. Thus it is comprehensible that it could be beneficial to be able to predict the improvement in the ground, to be able to predict and judge the post treatment soil condition and to take possible remedial measures if the assessment is able to demonstrate that the tests will not meet the design criteria.

Should there be a simple method that is able to predict the design parameters based on the ground behaviour during ground improvement, this method can provide additional confidence. Such a method may be developed and will be proposed in this paper for Dynamic Compaction (DC). In this method post ground improvement Pressuremeter (PMT) limit pressure (Pl) is predicted using the induced ground settlement.

Ground Improvement in Deep Waters Using Dynamic Replacement

Babak Hamidi and Hamid Nikraz
Curtin University of Technology
Perth, Australia
Kenny Yee
Menard Geosystems
Kuala Lumpur, Malaysia
Serge Varaksin
Menard
Paris, France
Leong Toh Wong
Menard Geosystems
Singapore

ABSTRACT

Dynamic Replacement is a ground improvement technique used for treating soft compressible cohesive soils. It has been used in numerous land projects and a number of offshore works with seabed as deep as 15 m below sea level. Recently, works of similar nature was carried out in Southeast Asia with the intention of exploring the possibility of treating soils in deeper waters. In this case, the seabed was 30 m below sea level, and to the knowledge of the authors, is a world record as the deepest Offshore Dynamic Replacement or Dynamic Compaction works. The pressuremeter test was used to verify the results and to estimate the soil parameters.

KEY WORDS: dynamic; replacement; ground; soil; improvement; marine; pressuremeter

INTRODUCTION

Dynamic Replacement (DR) is a ground improvement technique developed by Louis Menard in 1975 for the treatment of soft cohesive soils. As shown in Fig. 1, in this technique a heavy pounder is systematically dropped a number of times onto specific points in order to drive granular material into soft compressible cohesive soils and to compact the driven material sufficiently to meet the project's design criteria.

Dynamic replacement is a very cost effective, efficient and rapid method of treating soft soils and has been used in numerous land projects including the 2.6 million square meter mega soil improvement project of King Abdulla University of Technology in Saudi Arabia (Chu et al., 2009).

Dynamic replacement or its counterpart ground improvement technique for granular soils, dynamic compaction, have previously been used for the treatment of soft or loose marine soils in offshore projects such as Brest Naval Port in France (Menard, 1974;Boulard, 1974; Renault and Tourneur, 1974; Gambin 1982), Pointe Noire in Gabon (Menard 1978), Uddevalla Shipyard Wharf (Techniques Louis Menard, 1975; Gambin 1982), Kuwait Naval Port (Gambin, 1982; Chu et al., 2009), Sfax Fishing Quay in Tunisia (Menard, 1981; Gambin 1982), and Lagos Dry Dock in Nigeria (Gambin, 1982; Gambin and Bolle, 1983) with seabed as deep as 15 m below seawater level.

The first offshore dynamic compaction project was carried out by Menard in 1973 as part of the construction of Brest Naval Port's dry dock. In this project a specially designed 11 ton pounder was used to compact 3 m of loose alluvium on the seabed.

In Kuwait Naval Base a 32 ton pounder was used to compact a 5 m thick layer of silty sand and a 1.5 to 2 m thick rock fill blanket at the depth of 10 m below seawater level to mitigate the risk of liquefaction of a breakwater foundation due to swell action.

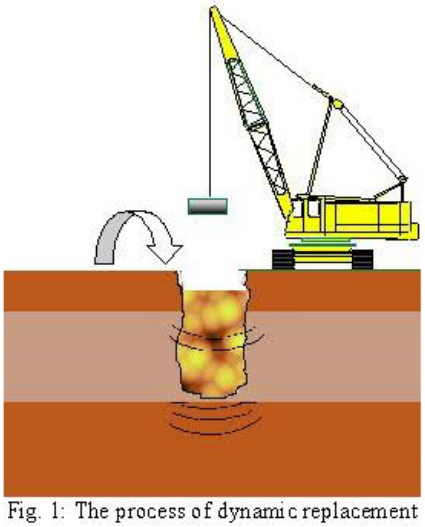

Fig. 1: The process of dynamic replacement

A case study of vibration monitoring in a dynamic compaction project

B. Hamidi & H. Nikraz
Department of Civil Engineering, Curtin University, Perth, Australia

S. Varaksin
Menard, Paris, France

ABSTRACT: Dynamic Compaction is a well established ground improvement technique in which a heavy pounder is dropped from a significant height to improve the soil's mechanical properties. The pounder impact creates waves that compact the ground; however these waves may also cause damage to neighboring structures and facilities. Peak particle velocity (PPV) has been determined as the most suitable method for assessing vibration associated risks. Previous researchers have proposed a number different equations for predicting PPV. In this paper PPV monitoring that has been carried out during Dynamic Compaction works at Fujairah Desalination Plant Phase 2 have been presented and compared to available equations. Some equations predict PPV values by a factor of up to 5 while others underestimate the measured values. Among the existing equations, the method that is able to most reliably overestimate PPV is identified. The authors also propose an alternative equation that appears to provide a better estimation of the particle velocity.

1 INTRODUCTON

1.1 *Wave propagation in Dynamic Compaction*

Dynamic Compaction is a well established ground improvement technique in which the mechanical properties of the soil is improved by dropping a heavy weight (pounder) from a significant height a number of times onto a point and in a predetermined grid (Hamidi et al., 2009). The impact creates body and surface waves that propagate in the soil medium.

The body waves, i.e. the compression and shear waves, propagate radially outwards from the pounder impact point along a hemispherical wave front as shown by the heavy black lines of Fig. 1 (Woods, 1968). Likewise, the Rayleigh or R-waves propagate radially outwards along a cylindrical wave front.

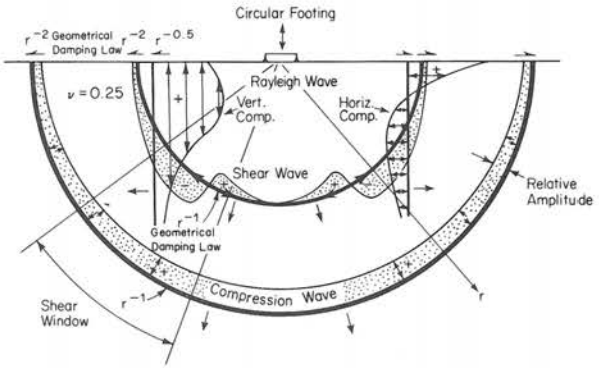

Fig. 1 Distribution of displacement waves from a circular footing on a homogeneous, isotropic, elastic half space (Woods, 1968)

The volume of material that is encompassed by each of the waves increases as the wave travels away from the source. Hence, the energy density, i.e. the energy per unit volume, in each wave front decreases with distance from the source. This decrease in energy density and consequently the decrease in displacement amplitude is called geometrical damping.

Material damping is the result of energy loss due to hysteresis damping and internal sliding of soil particles (Thevanayagam et al., 2006), and is the decrease in vibration amplitude with distance from a source due to energy losses in the soil (attenuation). Attenuation should be distinguished from geometrical damping which occurs in elastic systems because of the spreading out of the wave energy from a source.

the amplitude of the R-wave decreases proportionally with the inverse of the distance from the vibration source (Ewing et al, 1957); however in soil the wave amplitude decreases faster as soil is not an ideal elastic medium and because there is an internal or material damping. As expressed in Eq. (1), both geometrical damping and material damping can be taken into account for R-wave attenuation (Bornitz, 1931):

$$w = w_1 \sqrt{\frac{r_1}{r}} e^{-\alpha(r-r_1)} \qquad (1)$$

where r_1= distance from source to point of known amplitude; r = distance from source to point in question w= amplitude of the vertical component of the R-wave at distance r from source; and w_1=

Ground improvement acceptance criteria

B. Hamidi & H. Nikraz
Department of Civil Engineering, Curtin University, Perth, Australia

S. Varaksin
Menard, Paris, France

ABSTRACT: Once it has been established that ground improvement is required, a specification must be developed that defines the requirements of the works and the method that demonstrates that the works are acceptable. In some projects contractors are obliged to simply follow instructions and acceptance criteria are based on the quality of quantity of performed work. This method appears to be associated with the most amounts of risk and cost. Sometimes, acceptance criteria is based on minimum performance by specifying minimum acceptable test results. The ground improvement technique may or may not be specified. In this case, the associated risk and cost are less, but are still some drawbacks to this approach. Alternatively, acceptance criteria may be directly linked to design criteria. This method is associated with the least complications and will put the project at the minimal amount of risk.

1 INTRODUCTON

Ground improvement is generally taken into consideration after it has been determined by some means that the in-situ ground conditions are not able to satisfy the project requirements. It will then be necessary to develop a ground treatment specification and consequently the acceptance criteria that could have numerous forms.

It is the objective of this paper to review and to compare a number of possible and common methods of how soil improvement specifications are stipulated. It shall be seen that some specifications and acceptance criteria potentially inherit more risk and cost than others, and the outcome of a project may be determined by the quality of specifications and criteria rather than satisfying the actual project needs.

2 SPECIFICATIONS AND ACCEPTANCE CRITERIA

2.1 *Acceptance criteria based on work quality*

Sometimes, prior to the tender and the award of the contract, ground improvement specifications are developed in full detail by the party who has prepared the tender documents. In such a case, based on the geotechnical advisor's internal design which is usually not made available, a ground improvement technique is specified, the scope of work to be performed is described in detail and the construction method is outlined.

The responsibility of the contractor will usually include the procurement of the working team, equipment, material and execution of the works according to the specification's instructions.

In this type of project, acceptance criteria is generally non-technical and based on performing the works correctly as per the specified dimensions, spacing, quality and quantity of materials that have to be used.

Testing is generally specified, but obviously it will not be the contractor's responsibility to meet any specific value because other parties have developed the methodology and design of ground improvement.

Should works be performed correctly, but test results fail to meet expectations, then the contractor will be required to perform additional work using the same technology or an alternative method.

As an example, the specifications may specify stone columns. The column spacing, diameter, length and execution method will all be specified, and the contractor will have to provide the working team, vibroflot rigs and other equipment, and perform the works according to what has been described in the specifications. It will be the responsibility of the contractor to install the columns accurately in a specified grid, with the defined column diameter, to the stipulated depth. The columns' stones must be of a certain size and grading and with other specified qualities.

Even if tests carried out after the works demonstrate that the technical requirements of the project have not been satisfied, should the works have been performed correctly, the contractor will be exempted from all other responsibilities and consequences. Correction of the works to meet the project's needs will be the responsibility of others.

Dynamic Compaction Vibration Monitoring in a Saturated Site

Babak Hamidi[1], Hamid Nikraz[2] and Serge Varaksin[3]
[1]PhD Candidate, Curtin University
[2]Head of Department and Professor of Civil Engineering, Curtin University
[3]Menard and Chairman of ISSMGE TC211

Synopsis: Dynamic Compaction is a well established ground improvement technique in which a heavy pounder is dropped from a significant height to improve the soil's mechanical properties. The pounder impact creates waves that compact the soil; however these waves may also be a nuisance to and damage neighbouring structures and facilities. Peak particle velocity (PPV) has been identified as the most suitable parameter for assessing vibration associated risks. Previous researchers have proposed a number different equations for predicting PPV. Dynamic Compaction has recently been used for soil improvement in Oman's Blue City Project. Particle velocities and vibration frequencies in three directions have been monitored at several distances during the different phases of ground treatment. In all phases PPV has been recorded to be in the radial direction. It has been observed that although it appears that vibration frequency is not influenced by the deep compaction phase, does increase with the progression of work and application of later phases of Dynamic Compaction. This increase is more pronounced at farther distances, but becomes negligible when impact point is closer than a critical distance.

Keywords: Dynamic Compaction, vibration monitoring, peak particle velocity, PPV.

1. Introduction

1.1 Wave propagation in Dynamic Compaction

Dynamic Compaction is a well established ground improvement technique in which the mechanical properties of the soil is improved by dropping a heavy weight (pounder) from a significant height a number of times onto a point and in a predetermined grid [1]. The impact creates body and surface waves that propagate in the soil medium.

The body waves, the compression and shear waves, propagate radially outwards from the pounder's impact point along a hemispherical wave front. Likewise, the Rayleigh or R-waves propagate radially outwards along a cylindrical wave front.

The volume of material that is encompassed by each of the waves increases as the wave travels away from the source. Hence, the energy density, or the energy per unit volume, in each wave front decreases with distance from the source. This decrease in energy density and consequently the decrease in displacement amplitude is called geometrical damping.

Material damping is the result of energy loss due to hysteresis damping and internal sliding of soil particles [2], and is the decrease in vibration amplitude with distance from a source due to energy losses in the soil.

The amplitude of the R-wave decreases proportionally with the inverse of the distance from the vibration source [3]; however in soil the wave amplitude decreases faster as soil is not an ideal elastic medium and because there is an internal or material damping. As expressed in Eq. (1), both geometrical damping and material damping can be taken into account for R-wave attenuation [4]:

$$w = w_1 \sqrt{\frac{r_1}{r}} e^{-\alpha(r-r_1)} \qquad (1)$$

The coefficient α increases with dominant frequency, as a higher frequency wave will pass through more motion cycles than will low frequency waves when travelling the same distance [5]. For material damping, decay is a function of energy loss per cycle of deformation. This explains why in a general sense dominant frequency declines with distance for the same wave type. The lower frequency components have travelled fewer deformation cycles and have lost proportionally less energy.

The Application of Dynamic Compaction to HFO Tanks

Babak Hamidi[1], Serge Varaksin[2] and Hamid Nikraz[3]
[1]PhD Candidate, Curtin University
[2]Deputy General Manager, Menard
[3]Head of Department and Professor of Civil Engineering, Curtin University

Synopsis: Three heavy fuel oil (HFO) tanks with diameters of up to 60 m, a pump station, a pump shed station and a vent stack station have recently been constructed as part of the HFO Tank Farm in Ras Laffan, Qatar. The project was located in an area near the sea with high groundwater level. The ground was composed of 11 to 12 m of silty sand and gravel with cobbles and boulders with diameters up to 300 mm followed by limestone. The preliminary soil investigation using Standard Penetration Test (SPT) indicated that while the soil was generally dense, but a loose layer of sand was identified and soil improvement was stipulated. During later stages, a supplementary geotechnical investigation using the Menard Pressuremeter Test (PMT) indicated that the high SPT blow counts were not representative of the actual ground conditions and that due to the presence of the large cobbles the soil had erroneously been represented as dense. In fact, the soil was loose from the surface down to bedrock. Dynamic Compaction was used to improve the soil's strength and to reduce its compressibility. PMT in conjunction with finite element analysis were used to verify the ground condition after ground treatment.

Keywords: Dynamic Compaction, ground improvement, soil improvement, Menard Pressuremeter Test.

1. Introduction

The Qatari industrial city of Ras Laffan, located on the southern shores of the Persian Gulf and 80 km from Doha, is one of the world's largest oil and gas hubs. This industrial complex is continuously and rapidly being expanded to increase the production of gas from the North Field.

One of the projects that has recently been constructed is the Heavy Fuel Oil (HFO) Facility. The project involved the design and construction of an import line, the storage and process area and an export line, along with the necessary utilities and civil works. The storage and process area includes three HFO tanks, a sub-station, a pump shed and other equipment, piping, shelters and other allied facilities. The site plan can be seen in Figure 1.

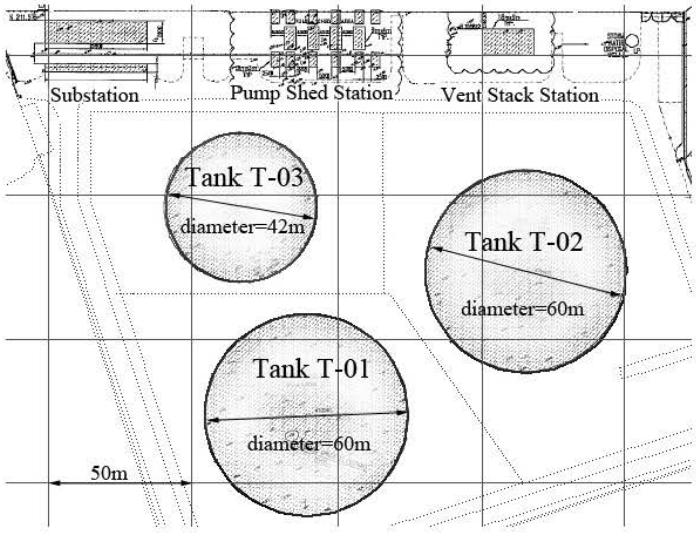

Figure 1: HFO site in Ras Laffan

Application of Dynamic Replacement in a Steel Pipe Factory

Babak Hamidi[1], Hamid Nikraz[2] and Serge Varaksin[3]
[1]PhD Candidate, Curtin University
[2]Head of Department and Professor of Civil Engineering, Curtin University
[3]Deputy General Manager, Menard

Synopsis: Prior to the construction of Al Jazira Steel Pipe Factory (AJSPF), almost all buildings in the Industrial City of Abu Dhabi were constructed on piles. This was due to the presence of compressible layers of soil, especially a superficial layer composed of one to four metres of soft sandy silts and clays. To the knowledge of the authors AJSPF is the first project in this area that has been built without the implementation of any piles and founded on shallow foundations improved by Dynamic Replacement. Variations of loading conditions and design criteria has made this pioneer project of special interest. While classical Dynamic Replacement was used for some ground slabs, pre-excavated Dynamic Replacement was applied under single footings and heavily loaded storage areas. As a cost saving method, sand from local Abu Dhabi excavations was used as granular material in lieu of the more commonly used crushed stone. Pressuremeter Tests (PMT) and finite element analysis was able to demonstrate that acceptance was achieved.

Keywords: Dynamic Replacement, ground improvement, soil improvement, Menard Pressuremter.

1. Introduction

1.1 The project's description

Al Jazirah Steel Pipe Factory (AJSPF) has recently been constructed on Plot 203ER6 of Industrial City Abu Dhabi (ICAD) Phase 1 Extension in the UAE. The plot of land is approximately a chamfered square with an area of 397,889 m^2. As can be seen in Figure 1, 6 buildings were considered for the first phase of AJSPF. These included the 31,200 m^2 main and annexed building, the 2,700 m^2 workshop, the 3,300 m^2 hot bending building, the 17,00 m^2 administration building, a mosque with associated washrooms, and the fire water tank and pump room.

Different activities including plate stacking, preparing, rolling and bending, welding, inspecting and controlling are undertaken in the main building and the maximum vertical load on a stanchion of this building was estimated to be 2,500 kN with floor loads ranging from as low as 40 kPa to as high as 200 kPa. The annexed building mainly consists of storage areas, laboratories and changing rooms, and its maximum vertical column load was estimated to be 300 kN.

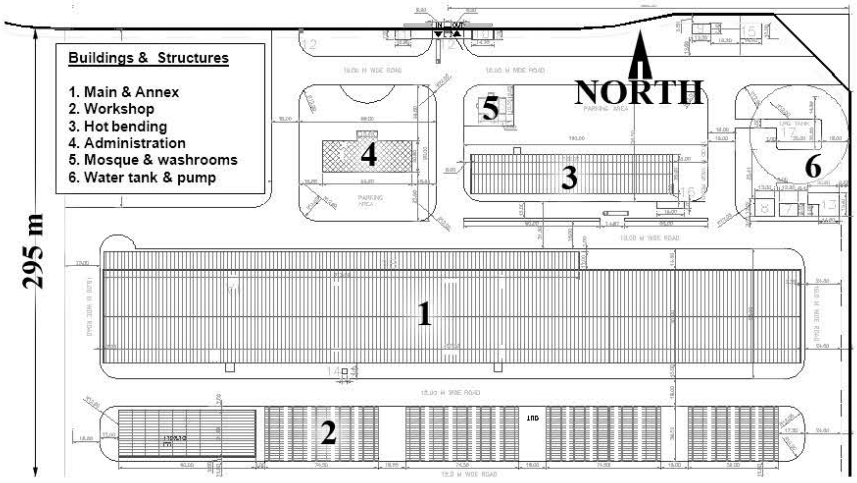

Figure 1. Layout of Al Jazira Steel Pipe Factory structures

Proceedings of Indian Geotechnical Conference
December 15-17,2011, Kochi (Paper No. H146)

ADVANCES IN DYNAMIC COMPACTION

Babak Hamidi, Curtin University, b.hamidi@gfwa.com.au
Hamid Nikraz, Curtin University, Professor & Head of Civil Engineering Department, h.nikraz@curtin.edu.au
Serge Varaksin, Menard & Chairman of ISSMGE TC211, serge.varaksin@menard-mail.com

ABSTRACT: Dynamic Compaction is a ground improvement technique that was invented more than 40 years ago with the objective of improving the strength and reducing the compressibility of thick soil layers. In this technique a heavy pounder is dropped from a significant height a number of times onto a grid pattern. Research indicates that depth of improvement is a function of the square root of the impact energy; i.e. the pounder weight and the pounder drop height. In the early days of dynamic compaction heavy duty cranes' efficient lift capacities were limited to about 150 kN; however it soon became possible to lift heavier pounders using specially designed and manufactured rigs or tripods. The introduction of commercially available special cranes equipped with appropriate lift capacity now allows the use of pounders weighing up to 250 kN. More recently an innovative and patented pounder release mechanism called MARS has been developed. This system is capable of dropping pounders weighing up to 35 tons in free fall and automatically reconnecting to the pounder. This technology has resolved many practical problems and is able to transfer energy to the ground more efficiently. MARS was first successfully used for the treatment of 1.13 million m^2 of loose desert dune sands with up to 28 m of thickness, and since then has also been used for treating saturated reclaimed sand and pre-collapsing karstic formations.

INTRODUCTION

Louis Menard invented and promoted *dynamic compaction* as early as 1969 but it was not until 29 May 1970 that he officially patented his invention in France [1].

The concept of this technique is improving the mechanical properties of the soil by transmitting high energy impacts to loose soils that initially have low bearing capacity and high compressibility potentials. The impact creates body and surface waves that propagate in the ground. In unsaturated soils the waves displace the soil grains, and re-arrange them in a denser configuration. In saturated soils the soil is liquefied and the grains are re-arranged in a more compact state. In both cases the decrease of voids and increase of inner granular contact will directly lead to improved soil properties [1].

The impact energy is delivered by dropping a heavy weight or pounder from a significant height. The pounder weight is most often in the range of 80 to 250 kN although lighter or heavier pounders are occasionally used. Drop heights are usually in the range of 10 to 20 m.

Although not well defined, the *depth of influence* or *improvement* is the depth where there is limited or practically insignificant amounts of improvement in the soil. Menard and Broise [2] developed an empirical equation in which the depth of influence was equal to the square root of the impact energy; i.e. the product of the pounder weight (in metric tons) by the drop height (in metres). Later and based on further site experiences others introduced a coefficient, less than unity, to the original equation to estimate the depth of improvement.

For example, Leonard et al. [3] proposed a coefficient of 0.5 based on results of seven sites and defining depth of influence as the depth in which SPT blow counts would increase by at least 3 to 5 blows. Without determining a criterion for the definition of depth of influence, Mayne et al. [4] studied 124 sites and observed that the coefficient can be from 0.3 to 0.8.

Although in practice this empirical equation continues to be the method of choice for estimating depth of improvement, more recently attempts have been made to estimate depth of influence using numerical models. For example, Ghassemi et al. [5] who have defined depth of influence as the depth in which relative density increases by at least 5%, have developed an equation for dry sands in terms of pounder weight, drop height and radius.

More recently, methods have also been proposed to estimate the amount of improvement in depth [6,7].

DYNAMIC COMPACTION RIGS

Once it was established that there is a direct relationship between depth of improvement and pounder weight and drop height, the notion of increasing these two parameters to obtain greater depth of improvement seemed inevitable.

Menard performed his first dynamic compaction project at Bormes-Les-Mimosas in the French [8].]. He then moved on to the marina in Mandelieu-la-Napoule, also in the Riviera, where he designed and monitored the dynamic compaction works of a 110,000 m^2 reclamation building project using an 80 kN pounder that was dropped from 10 m. Assuming a coefficient of 0.5 the treatment depth was probably less than 5 m which at that time was quite an accomplishment

Predicting Menard Modulus using Dynamic Compaction Induced Subsidence

Babak Hamidi[1], Serge Varaksin[2] and Hamid Nikraz[3]
[1]PhD Candidate, Curtin University
[2]Deputy General Manager, Menard
[3]Head of Department and Professor of Civil Engineering, Curtin University

Synopsis: Previous research by Varaksin et al. [1] suggests that it is possible to develop a relation between strain and increase in Menard Pressuremeter (PMT) limit pressure, whereas limit pressure will double every time the ground is strained strain 3%. Later, Hamidi et al. [2] proposed a new method to predict the limit pressure profile after dynamic compaction with the assumption that induced ground subsidence is the accumulation of vertical strains according to a Rayleigh distribution. Comparison of the geometric mean of predicted and post improvement measured limit pressure values suggest that this method of calculation is quite reliable. Noting that there are also established empirical relationships between the limit pressure and Menard Modulus, it would seem rational that a similar method can be used to predict the Menard modulus. This has been studied in this paper and it can be observed that for practical purposes, this method is able to provide Menard Modulus values of the correct magnitude.

Keywords: Dynamic compaction, Menard pressuremeter test, limit pressure, Menard modulus.

1. Introduction

The concept of dynamic compaction is improving the mechanical properties of the soil by transmitting high energy impacts to loose soils that initially have low bearing capacity and high compressibility potentials [3]. The impact creates body and surface waves that propagate in the soil medium. In non-saturated soils the waves displace the soil grains and re-arrange them in a denser configuration. In saturated soils the soil is liquefied and the grains re-arranged in a more compact state. In both cases the decrease of voids will cause the ground surface to subside, and the increase in granular contact will directly lead to improved soil properties.

The depth of influence is the depth where improvement in the soil is no more practically observable (or realistically speaking, more than a certain threshold value). Menard and Broise [4] developed an empirical equation in which the depth of influence was equal to the square root of the impact energy; i.e. the product of the pounder weight (in tons) by the drop height (in metres). Later and based on further site experiences others such as Mayne et al. [5] proposed the introduction of an empirical coefficient to the original equation.

The verification of dynamic compaction can be done through any suitable testing method; however as the late Louis Menard developed both dynamic compaction and the pressuremeter test (PMT) and held their patents for years, PMT is widely used in dynamic compaction projects.

PMT is a field test that measures the deformation properties of the soil in addition to a rupture or limit resistance. It consists of two main elements; i.e. a radially expandable cylindrical probe that is placed inside a borehole at the desired test elevation and a control unit which remains on the ground surface. The probe is made up of three independent cells and consequently exerts a strictly uniform pressure against the surrounding soil cylinder at the central cell level.

During each increment of loading, the ground deformation (volume of the cylinder) is measured and limit pressure (P_l) and Menard Modulus (E_M) are determined. The harmonic mean of P_l and geometric mean of E_M are respectively used to calculate ultimate bearing capacity and settlements [6].

1.1 The Relation between Dynamic Compaction Induced Subsidence and Post Dynamic Compaction Limit Pressure

Varaksin et al. [1] have developed a relation between dynamic compaction induced strain and the improvement of P_l for Al Quoa'a dune sand. In that dynamic compaction project 1.13 million m^2 of dry desert dune sand with a maximum backfill thickness of 28 m was compacted using pounders weighing up

Dynamic Compaction for Treating Millions of Square Meters of Sand

Babak Hamidi[1], Serge Varaksin[2] and Hamid Nikraz[3]
[1]PhD Candidate, Curtin University
[2]Deputy General Manager, Menard
[3]Head of Department and Professor of Civil Engineering, Curtin University

Synopsis: To the knowledge of the authors, the 4.84 million square meter ground improvement project of Al Falah Community Development in Abu Dhabi is the physically largest single contract that has ever been undertaken by a specialist ground improvement contractor. The peak ground improvement production rate of 966,000 m^2 per month also appears to be a new world record. This paper will describe the initial ground conditions of the project, the development of a foundation solution based on the utilization of ground improvement technology and the account of how mobilization, execution of Dynamic Compaction for the treatment of loose desert sands and verification testing by the Menard Pressuremeter Test were all realized within a mere period of 7 months.

Keywords: Dynamic Compaction, ground improvement, Menard Pressuremeter Test, CPT.

1. Introduction

As part of the development of Abu Dhabi, Al Falah Community Development, a mega project with an estimated value of 2.56 billion USD and an area of 12.7 million m^2, was launched in 2008 in the outskirts of the capital city of UAE. The project was anticipated to include 5,000 villas, 2,300 townhouses, 2,100 apartment houses, 14 schools, a hospital, a shopping mall, a number of hotels, restaurants, and health clubs.

The geotechnical investigation of the project indicated that the site was covered with a superficial layer of silty sand with a variable thickness of only a few centimetres to more than 18 m followed by sandstone or siltstone bedrock. the soil (white area in Figure 1) in a large portion of the site was very dense and it was possible to construct shallow foundations without any difficulty. The SPT blow counts in these areas were consistently more than 50 and CPT penetration would generally reach refusal within the first meter.

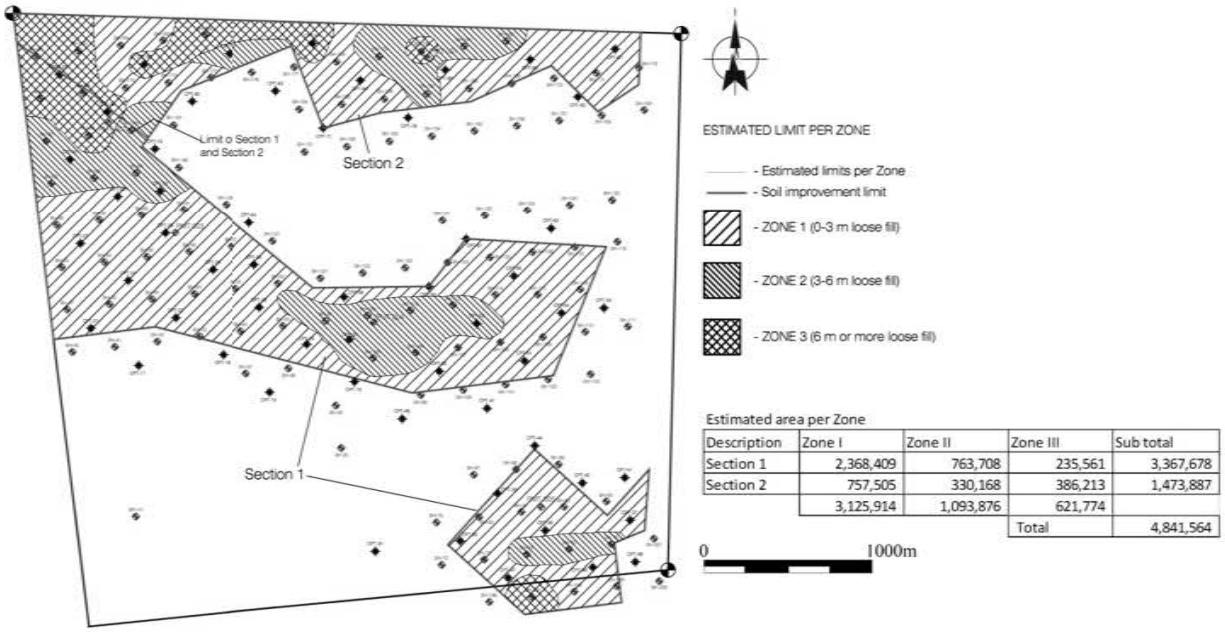

Description	Zone I	Zone II	Zone III	Sub total
Section 1	2,368,409	763,708	235,561	3,367,678
Section 2	757,505	330,168	386,213	1,473,887
	3,125,914	1,093,876	621,774	
			Total	4,841,564

Figure 1. Site plan, ground improvement zones and sections

A Case of Vibro Compaction Vibration Monitoring in a Reclaimed Site

Babak Hamidi[1], Serge Varaksin[2] and Hamid Nikraz[3]
[1]PhD Candidate, Curtin University
[2]Deputy General Manager, Menard
[3]Head of Department and Professor of Civil Engineering, Curtin University

Synopsis: Vibro Compaction is a ground improvement technique in which the soil is compacted using waves generated from an equipment called a vibroflot. As the vibration magnitude is less than some other vibratory ground improvement methods this technique is sometimes preferred when the improvement zone is relatively close to existing structures and facilities. Unfortunately, not much can be found in literature on peak particle velocity (PPV) that is generated by this method. This paper reports and interprets vibration monitoring of a Vibro Compaction project that was recently performed on about 13 m of hydraulically placed sand in Palm Jumeira, Dubai. PPV was measured at different distances from the vibroflot. The depth of the vibroflot was also varied to provide a better understanding of the critical depth that creates the largest PPV. A formula is also presented to estimate Vibro Compaction generated PPV during planning stage.

Keywords: Vibro Compaction, vibration monitoring, peak particle velocity, PPV.

1. Introduction

1.1 The concept of vibro compaction

Vibro compaction, also known as vibroflotation, is a deep ground compaction technique that was developed almost 80 years ago [1] with the invention of the first vibroprobe by W. L. Degen and S. Steuermann [2] in Germany.

This technique is best suitable for the treatment of soils with limited amounts of fines. Mitchell [1] proposes that the best desirable soils for vibro compaction are when the soil's fines content is limited to 18%. Woodward [3] suggests that best results can be achieved when fines content is less than 10%.

The vibroflot, also referred to as vibroprobe or vibrating poker is a hollow steel tube containing an eccentric weight mounted on a vertical axis in the lower part so as to give a horizontal vibration. The vibroflot itself is connected to extension tubes that are supported by a rig; usually a crane.

The vibroflot is either flushed down to the required depth in the soil using water jets or vibrated dry with air jets. When the vibroprobe reaches the required depth, material is added from the ground surface during withdrawal, and the vibroflot is moved in an up and down motion at certain intervals. The horizontal vibrations form a compacted cylinder of soil with a depression at the surface due to the reduction of void ratio in the ground. Depending on the vibroflot power, the zone of improved soil extends from 1.5 m to more than 4 m from the vibrator.

As compaction in vibro compaction is realized by the vibration of the vibroflot vibration parameters must be understood and monitored to ensure that specification limits are not exceeded.

1.2 The development of vibration parameters

Effects of vibration on structures has been under investigation for more than 80 years. From 1930 to 1942 the US Bureaus of Mines (USBM) conducted an extensive research program to study the seismic effects of quarry blasting on buildings [4]. USBM's report [5] of the tests recommended an index of damage based on the acceleration. Duvall and Fogelson [6] statistically showed that these data gave contradictory results because major damage correlated with particle velocity while minor damage correlated with acceleration. Hence, the concept of implementing particle velocity in lieu of acceleration for prediction of (major) damage was formed. Langefors, Kilhstrom and Westerberg [7] also carried out extensive studies to relate between damage and ground vibrations from nearby blasting. Statistical analyses of these data show that the degree of both major and minor damage correlates with particle velocity. Similarly, Edwards and Northwood [8] carried out a number of tests and concluded that damage was more closely related to

Application of Dynamic Surcharging for Construction of Tanks on Reclaimed Ground

Babak Hamidi[1], Serge Varaksin[2] and Hamid Nikraz[3]
[1]PhD Candidate, Curtin University
[2]Deputy General Manager, Menard
[3]Head of Department and Professor of Civil Engineering, Curtin University

Synopsis: Palm Jumeira is a reclaimed island off the coast of Dubai. While almost all heavy structures built on this island have been piled, the heaviest non-piled structures that have been constructed are two sewage treatment tanks that have used a unique and innovative Dynamic Surcharging ground improvement solution for their foundation systems. For each tank, a 4 m high surcharge was initially placed on the tank's area and left in place for several days. Then dynamic surcharging was performed by dropping the pounder at the periphery of the surcharge embankment to induce additional settlements. The surcharge was then removed, the ground level reduced, print locations additionally excavated, and dynamic compaction was carried out. Post ground improvement Menard Pressuremeter Tests (PMT) and finite element calculations demonstrated that acceptance criteria was achieved.

Keywords: Dynamic Compaction, dynamic surcharging, ground improvement, Pressuremeter Test.

1. Introduction

Palm Jumeira is a group of man-made islands that has been reclaimed off the coast of Dubai, UAE. The reclamation shape consists of a tree trunk, a crown with 17 fronds, three surrounding crescent islands that form an 11 km long breakwater and two identical smaller islands that are in the shape of the logo of project's developer on the sides of the trunk. In all, 94 million m^3 of sand and 7 million m^3 of rock has been used in this project. Calcareous sand was dredged from the Persian Gulf using trailing suction hopper dredgers [1]. When possible, the hopper was discharged by means of a big door located on the bottom of the hull, but when the water was shallow, the dredger sprayed the sand and water mixture onto the reclamation by rainbow discharge.

The variation in fill densities achievable by hydraulic placement is large and closely related to the placement method whereas hopper placed sand is denser than pipeline placed sand [2]. Sand deposited by hydraulic filling below water level generally has a low to medium relative density of about 20 to 60% due to the loose packing from self-weight sedimentation of sand particles under water ([2] and [3]). The zone with the least strength could be expected to be just beneath water level if fill is placed by subaqueous discharge through hydraulic pumping [4]. Sand placed above water table by hydraulic filling has a high relative density of 60 to 80% because of dense packing from downward seepage and reduction in void ratio as a result of sliding and rolling of the sand particles mixture [3].

Due to the low strength and high compressibility of the soil, ground improvement by vibro compaction was carried out at Palm Jumeira. Even then, heavily loaded structures were constructed on piles. The two sewerage treatment plant (STP) tanks were the only heavily loaded structures that are found on improved ground by a unique an innovative combination of techniques.

2. STP Tanks

2.1 The tanks' description and ground conditions

As shown in Figure 1, there is a sewerage treatment plant at the tip of each of the lower crescents of Palm Jumeira. The lots were designated A-A and G-G, and each plant included one reinforced concrete tank with a diameter of 35.1 m Each tank was subject to a total uniform load of 120 kPa.

The Application of Dynamic Compaction on Marjan Island

B. Hamidi[1], H. Nikraz[2] and S. Varaksin[3]

[1]Curtin University, Department of Civil Engineering, Kent Street, Bentley WA 6102, Australia; email: b.hamidi@gfwa.com.au
[2]Curtin University, Department of Civil Engineering, Kent Street, Bentley WA 6102, Australia; email: h.nikraz@curtin.edu.au
[3]Menard, 2 Rue Gutenberg, 91620 Nozay, France; email: serge.varaksin@menard-mail.com

ABSTRACT

Marjan Island is 2.7 million m^2 of development located 27 km southwest of Ras Al Khaimah in the United Arab Emirates. This project has been reclaimed from the Persian Gulf by tipping sand into the sea. Geotechnical investigations indicated that the upper 7 m of ground was composed of very loose to medium dense silty sand interbedded with layers of boulders at different depths. SPT blow counts were recorded to be as low as 4 and Menard Pressuremeter Test (PMT) limit pressure was as low as 70 kPa. Fines content was from 13 to 30%. Preliminary calculations suggested that the in-situ ground conditions could not satisfy the island's main road's settlement criteria and that ground improvement was required. Thus, 198,000 m^2 of the reclamation was treatment by Dynamic Compaction. Pounders weighing up to 20 tons were dropped from 20 m to compact the loose soil. 32 PMT were carried out after ground improvement to verify the achievements. These tests were able to demonstrate that acceptance criteria was readily achieved and that on average the soil's modulus of deformation increased by more than 400%.

Keywords: ground improvement, soil improvement, dynamic compaction

1 INTRODUCTION

Marjan Island, translating to Coral Island, is the first manmade group of islands of its kind that has ever been undertaken in the northern emirate of Ras Al Khaimah in the United Arab Emirates. This project is located approximately 27 km southwest of the city of Ras Al Khaimah and 54 km northwest of the city of Dubai.

As can be seen in the project's master plan, shown in Figure 1, the group of islands are composed of a peninsula followed by four coral shaped islands that are connected together via bridges. The project will consist of low rise villas, townhouses and high rise towers.

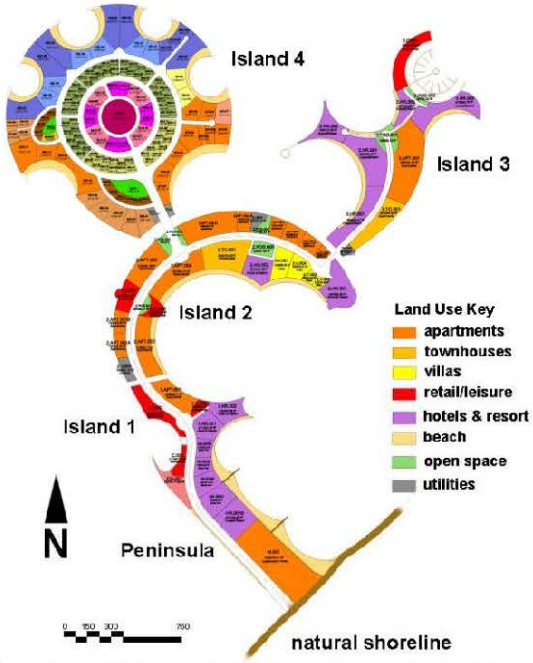

Figure 1. Master plan of Marjan Island (main road corridor shown in white)

APPLICATION OF DYNAMIC COMPACTION IN RECLAIMED ROADS

Babak Hamidi[1], Hamid Nikraz[2] and Serge Varaksin[3]
[1] *Curtin University of Technology*
[2] *Professor & Head of Civil Engineering Department, Curtin University of Technology*
[3] *Menard and Chairman of ISSMGE TC-211*

ABSTRACT

Pavement layers are systematically constructed as engineered fills with specified properties and criteria; however these well built layers may be underlain by loose saturated subgrades that, if not treated, may be subject to undesirable and damaging deformations. This may be especially true for roads that are constructed on reclaimed land.

Dynamic Compaction is a ground improvement technique that can and has been effectively utilised for treating thick loose layers of saturated *in situ* or reclaimed granular soils. In this paper, the application of Dynamic Compaction for improving loose sub-grades will be discussed using three case studies. The case studies have been specifically selected in a manner to demonstrate the applicability of this technique to hydraulic fills and truck dumped fills, to very large projects such as the 900,000 m^2 Abu Dhabi Corniche, to moderately large projects such as Marjan Island Main Road corridor and to relatively small sized projects such as the 10,000 m^2 approach roads of Reem Island Causeway. The projects can be in undeveloped locations or in urban areas.

1 RECLAIMED SUBGRADES

Inevitably, every reclamation project, regardless of its function and purpose, will have roads. The roads may have single, double, triple or more carriage ways in each direction, and will be designed to provide access to the required points in the reclaimed land.

Based on the road function and traffic expectation road pavements are designed according to engineering standards and base and sub-base layers are required to meet pre-determined minimum densities. However, the reclaimed land will not necessarily provide a subgrade that satisfies the road specifications without the implementation of certain measures.

Reclamation can either be land based and by dump trucks tipping fill into the sea or by hydraulic placement from the sea. Sladen and Hewitt (1989), Lee *et al.* (1999), Lee *et al.* (2000), Lee (2001) and Na *et al.* (2005) have studied the effects of placement methods on the geotechnical behavior of sand fills. The density of sand that is dumped by trucks and then pushed into the sea by a bulldozer is usually low, with relative density of about 20%. Exceptions can be thin layers which have been compacted by the traffic of earthmoving equipment. Hydraulic placement can be subaqueous by hoppers or bottom dump barges. When possible sand is discharged by means of a big door located on the bottom of the hull, but when the water is shallow alternative methods; i.e. pipeline discharge or subaerial rainbow discharge will be used. In pipeline discharge a low velocity water-sand slurry is pumped; however in the rainbow method the dredger sprays a high velocity water-sand mixture onto the reclamation. These processes are schematically shown in Figure 1.

The variation in fill densities achievable by hydraulic placement is large and closely related to the placement method. Hopper placed sand is denser than pipeline placed sand. Sand deposited by hydraulic filling below water level generally has a low to medium relative density of about 20% to 60% due to the loose packing from self-weight sedimentation of sand particles under water. The zone with the least strength could be expected to be just beneath water level if fill is placed by subaqueous discharge through hydraulic pumping. Sand placed above water table by hydraulic filling tends to have a higher relative density in the range of 60% to 80% because of dense packing from downward seepage and reduction in void ratio as a result of sliding and rolling of the sand particles mixture.

Hopper or bottom dumping achieves a higher density than pipeline discharging for a number of reasons. Firstly, the sand mass stored in a hopper has a higher bulk density than the sand slurry that is discharged from a pipe. Also, dumping a large quantity of sand from a hopper in a short period will result in the sand mass falling as a slug rather than as individual particles. Furthermore, the simultaneous opening of all bottom doors prohibits the entrapment of fresh water into the slug that would reduce the fall velocity and expand the slug size. The fall energy of the slug is likely to be dissipated in compaction of berm through impact and shearing. The loosest possible state would likely be achieved if the pipe discharge was placed near the water surface in such a way to allow maximum fresh water entrapment. In such a case the slurry becomes a clod with falling velocity being close to the falling velocity of individual grains. Each particle will basically come to rest in the position that it makes contact with the previously placed fill. Impact may result in some pushing around of the grains, but the impact velocities and forces can be expected to be small. Subaerial rainbow dredging can be expected to yield similar results to pipe discharging.

The Effectiveness of Vibration Reduction Trenches in a Dynamic Replacement Project

B. Hamidi[1], S. Varaksin[2] and H. Nikraz[3]

[1]Curtin University, Department of Civil Engineering, Kent Street, Bentley WA 6102, Australia; email: b.hamidi@gfwa.com.au
[2]Menard, 2 Rue Gutenberg, 91620 Nozay, France; email: serge.varaksin@menard-mail.com
[3]Curtin University, Department of Civil Engineering, Kent Street, Bentley WA 6102, Australia; email: h.nikraz@curtin.edu.au

ABSTRACT

Umm Al Quwain Marina Phase I Project is located in northern United Arab Emirates. The site is located in an area where the ground consists of 6 to 7 m of very loose heterogeneous saturated silt and silty sand. More than 86,000 m^2 of the site has been treated using dynamic replacement. Due to the presence of existing structures in the vicinity of the ground improvement works vibration monitoring and control was implemented. In this paper, initially previous studies on dynamic compaction vibration will be reviewed, then the two cases of vibration monitoring programme for UAQ Marina will be described. First, particle velocities and their associated frequencies were measured at different distances from the pounder's impact point when no specific measures were implemented. Next, a vibration reduction trench was excavated and the vibration parameters recorded again. The interpretation of the results indicates that the vibration reduction trench has been able to efficiently reduce peak particle velocities to about one half the values when the trench was not installed. This study demonstrates that simple methods such as constructing vibration reduction trenches can be an effective way for controlling vibration damage when existing structures are nearby.

Keywords: dynamic replacement, ground improvement, vibration

1 INTRODUCTION

Dynamic compaction is a ground improvement technique in which the mechanical properties of the soil is improved by dropping a heavy weight (pounder) from a significant height a number of times onto a point and in a predetermined grid (Hamidi et al., 2009). Similarly, in dynamic replacement granular material is driven in the soft soil to form a large column and compacted using a pounder that is dropped onto a number of times onto the column location. The impacts create body and surface waves that propagate in the soil medium.

1.1 Waves

The body waves, i.e. the compression and shear waves, propagate radially outwards from the pounder impact point along a hemispherical wave front as shown by the heavy black lines of Figure 1 (Woods, 1968). Likewise, the Rayleigh or R-waves propagate radially outwards along a cylindrical wave front.

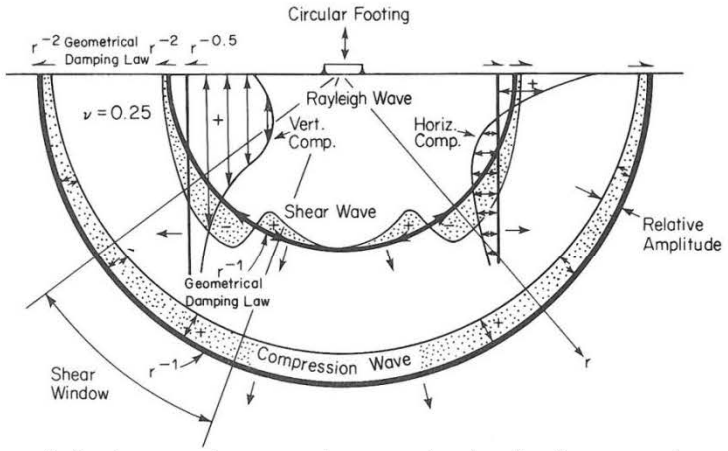

Figure 1. Distribution of displacement waves from a circular footing on a homogeneous, isotropic, elastic half space (Woods, 1968)

CONSTRUCTION OF RAW SUGAR SILOS USING DYNAMIC REPLACEMENT

Babak Hamidi[1,a], Serge Varaksin[2] and Hamid Nikraz[1,b]

[1] *Department of Civil Engineering, Curtin University, Perth, Australia.*
E-mail: [a] b.hamidi@gfwa.com.au, [b] h.nikraz@curtin.edu.au

[2] *Menard, Paris, France. E-mail: serge.varaksin@menard-mail.com*

Two raw sugar silos, each 55 m high, have been constructed on improved ground in Al Khaleej Sugar Factory located in Dubai's Jebel Ali area. The preliminary geotechnical investigation indicated that the upper 6 m of soil was composed of loose to dense silty sand followed by weak bedrock, and that it was not possible to construct the silos without implementation of special foundation measures. Ground improvement by dynamic replacement was chosen as the most affordable technical solution. Treatment was carried out by initially excavating the ground to the working platform level. For each silo, the impact points were individually excavated and backfilled with crushed rock. A rock filled shear ring trench was also realized at the periphery by excavating the silty sand to the depth of 2 m. The project faced special challenges due to the vicinity of an existing sugar silo at a minimum distance of 10 m from the works, the presence of a highly cemented and previously unidentified sand layer in parts of one of the silos, and a high groundwater table. A total of 29 Menard Pressuremter Tests (PMT) were carried out after soil improvement to verify that acceptance criteria had been satisfied.

Keywords: Ground improvement, Soil improvement, Dynamic replacement, Pressuremeter.

1. INTRODUCTION

Al Khaleej Sugar Factory is located on the coast of the Persian Gulf in Jebel Ali Free Zone, Dubai, UAE. As part of the company's development programs, it was decided to construct two additional concrete sugar silos, 3.5 m apart from one another, each 72 m high and 34 m in diameter.

1.1. *Ground Conditions*

The geotechnical investigation report indicated that ground level was variable from +4.2 to +4.8 m RL (reduced level). Mean High High Water (MHHW) and Mean Low Low Water (MLLW) were respectively at +1.7 m and +0.5 m RL, indicating a relatively high groundwater level at all times.

As part of the soil investigation 6 boreholes were drilled and SPT were carried out in them. These boreholes indicated that the first layer of soil, extending down to

Proceedings of the International Conference on Ground Improvement and Ground Control
Edited by Buddhima Indraratna, Cholachat Rujikiatkamjorn and Jayan S. Vinod

ISBN: 978-981-07-3560-9 :: doi:10.3850/978-981-07-3560-9_04-0406

APPLICATION OF DYNAMIC COMPACTION IN A PROJECT WITH SMART ACCEPTANCE CRITERIA

Babak Hamidi[1,a], Serge Varaksin[2] and Hamid Nikraz[1,b]

[1] *Department of Civil Engineering, Curtin University, Perth, Australia.*
E-mail: [a] b.hamidi@gfwa.com.au, [b] h.nikraz@curtin.edu.au

[2] *Menard, Paris, France. E-mail: serge.varaksin@menard-mail.com*

Al Madina A'Zarqa, is a multibillion dollar development project in Oman, and the first stage of this project covers an area of approximately 78,500 m^2. The preliminary geotechnical investigation showed that the top 8 m of ground was composed of very loose to dense saturated silty sand followed by 3 m of sandy silt. This study revealed that the in-situ ground conditions would not be able to safely support the structures and that ground improvement had to be carried out to ensure the safe transfer of structural loads to the foundations. While original acceptance criteria were based on minimum cone resistance values, alternative specifications were developed that stipulated quick criteria as a first check only in the form of minimum CPT test values followed by minimum value Menard Pressuremeter Tests (PMT), and ultimately bearing capacity and finite element settlement calculations for final verification and confirmation of soil improvement acceptance. Ground improvement was performed by the dynamic compaction method with pounders weighing up to 23 tons. In all 168 CPT and 43 PMT tests were used to verify that acceptance had been achieved.

Keywords: Ground improvement, Soil improvement, Dynamic compaction, Pressuremeter.

1. INTRODUCTION

Al Madina A'Zarqa, translating to Blue City, is a multibillion dollar development project in Oman (Figure 1(a)). The multiple phases of the project are to be built over a period of several years. Phase 1 of this project is located within an area that is 3 km along the coastline and measuring 2 km inland.

As shown in Figure 1(b), the first stage of Phase 1; i.e. Plots No. 1.1.2 (Amphitheatre Apartments) and 1.4.2 (City Beach Apartments), covers an area that is approximately 78,500 m^2, and will consist of a cluster of apartment buildings separated by local streets and landscaping areas. These buildings will generally consist of partially buried garage podiums overlain by a mixture of two to seven floors, and with grade level planned to be raised by approximately 2 to 3 m.

Proceedings of the International Conference on Ground Improvement and Ground Control
Edited by Buddhima Indraratna, Cholachat Rujikiatkamjorn and Jayan S. Vinod

ISBN: 978-981-07-3560-9 :: doi:10.3850/978-981-07-3560-9_04-0407

GROUND IMPROVEMENT CASE HISTORIES AND ADVANCES IN PRACTICE

Serge Varaksin[1] **and Babak Hamidi**[2]

[1] *ISSMGE TC211, Paris, France. E-mail: serge.varaksin@menard-mail.com*
[2] *GFWA, Perth, Australia. E-mail: b.hamidi@gfwa.com.au*

Ground improvement methods have made considerable advances since today's commonly practiced techniques first began to develop in the 20th century; however they continue to remain a mixture of empirical methods devised by the practitioners and analytical solutions developed by the academicians. Advances in ground improvement have been through the invention and development of new methods, influence of equipment, quality control methods and monitoring of ground improvement works, and innovations for treatment of particular soils. While analytical and empirical methods are still widely practiced and form the basis of many calculations, especially for ground improvement technologies that do not require introduction of material, commercially available geotechnical software have revolutionised the concept of design, facilitated calculations and design methods and have allowed ground improvement specialists to design concepts that were previously only attainable, if at all possible, through cumbersome and exhausting hand calculations that required excessive amounts of time. However, these advancements are highly dependent on the quality and availability of soil parameters, and results may be erroneous if proper values are not used as input data. At the same time the philosophy of quality control in ground improvement has also advanced, and the application of performance specifications based on design criteria has allowed the optimisation of ground improvement works. These advances shall be highlighted in this paper through presentation of several case studies.

Keywords: Ground improvement, Soil improvement.

1. INTRODUCTION

Ground improvement, as we would know it by its modern definition, began to take the form of a branch of geotechnical engineering in the mid 20th century, and was finally realised as the 17th technical committee of ISSMGE many years ago. Since then, this committee that has now been renamed TC211 has continuously tried to expand the domain of this knowledge by making information available to the geotechnical engineer through its numerous technical meetings, seminars, conferences, publications and the latest State of the Art Report (Chu, *et al.*, 2009).

While it may not be immediately apparent, ground improvement methods have made considerable advances since today's commonly practiced techniques first began to develop in the first half of the 20th century; however most techniques have gone through changes,

Proceedings of the International Conference on Ground Improvement and Ground Control
Edited by Buddhima Indraratna, Cholachat Rujikiatkamjorn and Jayan S. Vinod

ISBN: 978-981-07-3559-3 :: doi:10.3850/978-981-07-3559-3_103-0002

Pressuremeter for design and acceptance of challenging ground improvement works

Le pressiomètre destiné à la conception et le contrôle des grands travaux d'amélioration des sols

S. Varaksin
ISMGE TC211 Chairman

B. Hamidi
GFWA

ABSTRACT: The pressuremeter was developed more than 50 years ago by Louis Menard, and has been intertwined with ground improvement techniques such as dynamic compaction and dynamic replacement from the very time that these methods were invented. This tool has proven to be of great use throughout the life cycle of a project, commencing from the geotechnical investigation, to design, execution of ground improvement works and verification of results. In this project several challenging ground improvement case histories that have utilised the pressuremeter will be presented.

RÉSUMÉ : Le pressiomètre a été développé il y a plus de 50 ans par Louis Menard et a été étroitement lié a l'origine des techniques d'amélioration de sol tels que le compactage dynamique la substitution dynamique . Cet outil s'est avéré pour être d'une grande utilité tout au long du cycle de vie d'un projet, en commençant par l'étude géotechnique, la conception, l'exécution de travaux d'amélioration de sol et la vérification des résultats. Cet article présente ses projets innovants ou le pressiomètre s'est avéré essentiel .

KEYWORDS: Menard Pressuremeter, ground improvement, dynamic compaction, dynamic replacement, reclamation

1 INTRODUCTION

The first encounter of the first author with the Menard pressuremter dates back to approximately 40 years ago when, during his military service, he was given the task to perform two borings to the depth of 42 m and to carry out one pressuremeter test every 1.5 m. The tools used were a hand auger, a bentonite hand pump and a tripod with a mechanical winch.

After six months of hard work, he met Louis Menard who laughed about this performance, and then proposed that he join the recently created ground improvement department of Menard's organization.

1 FIRST STEPS IN GROUND IMPROVEMENT

The construction of the Mandelieu la Napoule development in the French Riviera in 1969 was one of the first opportunities for understanding dynamic compaction. There, Louis Menard proposed to the developer to compact the 110,000 m^2 reclaimed site using Menard's recently invented dynamic compaction technique, and to build his five story buildings using shallow footings rather than implementing the classical and costly piled foundations that had to additionally sustain the negative skin friction created by the fill weight. With Menard's method, the ground would have indeed become so dense that the required bearing would have become available without the risk of excessive total and differential settlements.

The first English publication of Menard and Broise (1975) proposed a relation between the behaviour of saturated fill under heavy impact and pore water pressure (see Figure 1). At that time, the concept of effective stress was only well understood in academia and still not used in the industry's common practice. However, Menard was able to implement this concept into his work and the grid definition and rest period between dynamic compaction works in phases were born.

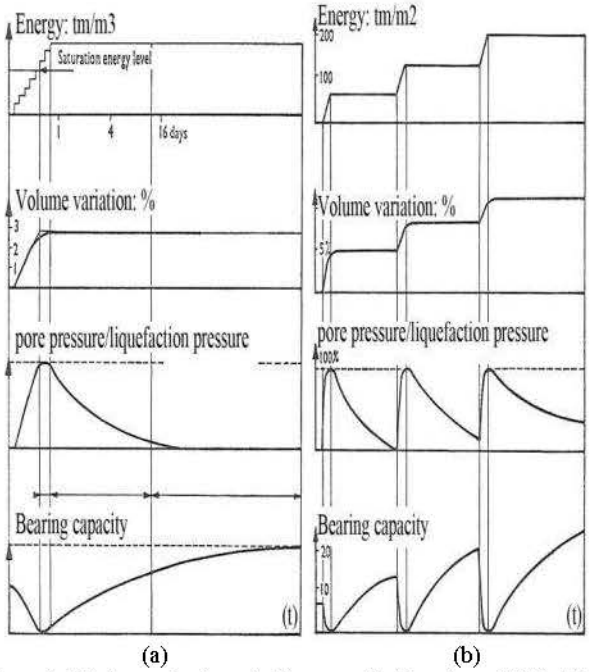

Figure 1. (a) changes in the soil after consolidation phase, (b) Variation to a soil subjected to a series of dynamic consolidation passes (Menard, 1975)

Lessons Learned from Millions of Square Metres of Ground Improvement

Babak Hamidi, GFWA and member of TC211, Australia, b.hamidi@gfwa.com.au
Serge Varaksin, Menard and Chairman of ISSMGE TC211, Menard, France, serge.varaksin@menard-mail.com

ABSTRACT

Ground improvement can be applicable to projects of any size; however there are certain delicacies that necessitates special attention when ground treatment is implemented in large size projects. It is the authors' experience from performing millions of square meters of ground improvement that soil treatment of mega and giga size projects can be optimised if specifications and testing methods have been developed properly, the ground improvement solution has been adapted according to the in-situ ground conditions and project requirements, and that allocation of equipment and working teams have been planned and managed appropriately. Unsuitable acceptance criteria can veer the ground improvement campaign into an unnecessarily costly and time consuming and sometimes impossible endeavour. This paper will review the ground improvement works of several very large size projects including Abu Dhabi Corniche (900,000 m^2), Al Quoa New Township (1,135,000 m^2), King Abdulla University of Science and Technology (2,600,000 m^2) and Al Falah New Township (4,840,000 m^2).

1. INTRODUCTION

Ground improvement includes numerous methods that are applicable to a very wide range of ground conditions, load conditions and project sizes. While a number of soil improvement solutions may all be feasible in a project, the usually the selection of the method is driven by cost or schedule.

Although it should be the intention of the engineers to develop the most economical acceptable foundation solution when dealing with any project, the sensitivity of this intent appears to be more critical in large size projects where the repetition and summation of even the smallest extras can ultimately lead to large costs and additional execution time. Thus, it may be beneficial to study the key parameters that will impact cost and programming.

2. PARAMETERS OF SIGNIFICANCE

Although all ground improvement works should be designed, performed and tested properly the chances that flaws in any of these processes in a large mega or giga size project could lead to a larger financial loss is greater, and hence it is essential that application of ground improvement in projects of considerable size be robust and flexible, well tailored to the problem, properly designed and executed and tested in accordance to the requirements.

2.1. Suitability of Technique

Regardless of the project size and all other conditions, constraints and parameters the intended ground improvement method should suit the problem.

Any one ground improvement technique is not suitable and applicable to all ground conditions. Regardless of cost, schedule and any other issues, if the wrong or inappropriate technology is used, it will not perform satisfactorily, and ultimately alternative solutions will have to be taken into consideration.

For example while particulate (permeation) grouting is less costly than other grouting techniques (Mitchell, 1981), this technology is mainly suitable for sands and gravels, and for coarse silts using chemical solutions (Semprich and Stadler, 2003, Chu et al, 2009) and cannot be used in clays. Ultra fine grout mixes can be used in medium to coarse sands, but will not permeate silts and suspensions with regular cement, at best will permeate into coarse sand. Hence, if an unsuitable grout mix is used permeation will not be realised, the project's objectives will not be met, and the project will face delays and extra costs.

In Umm Al Quwain Marina the preliminary geotechnical investigations that were based on SPT boreholes suggested that the site was composed of several layers of loose sands with fines content in the range of less than 10% to 20%. Once the ground improvement project was awarded to a specialist ground improvement contractor who had proposed dynamic compaction, further geotechnical testing revealed a

S. Varaksin (Paris, ISSMGE TC211) and B. Hamidi (Perth, Curtin University)

CONTRIBUTIONS OF THE PRESSUREMETER TO GROUND IMPROVEMENT AND PERSPECTIVES FOR THE FUTURE

Abstract

Menard not only developed the pressuremeter as an industrial tool for measuring ground characteristics, but also introduced a new approach to directly utilize the measured values to calculate bearing capacity and ground deformations without the commonly implemented classical parameters and failure criteria. The pressuremeter has also proven to be a very precious tool for verification and evaluation of ground improvement results, and has more recently contributed to providing parameters for the increasingly popular numerical analyses approaches. In this paper, the authors will review the history of the pressuremeter test and its application in ground improvement projects.

1. Introduction

Louis Ménard was born on 4 May 1931 in the Bay of Mont-Saint-Michel, France. He attended the civil engineering school of the prestigious *École des Ponts et Chaussées* in 1952. During the summer that he was employed to carry out compaction tests on a new runway in Paris, Menard realised that while strength-deformation properties were important, field tests and measurements were not able to measure them. Consequently, he developed the first prototype of the *Menard pressuremter* as his dissertation and filed for a patent for it in 1954 at the age of 23. Menard later improved his invention and carried out the first tests with the new probe while studying for a Master's degree under the supervision of Professor Peck at the University of Illinois, and filed for a second pressuremeter patent in 1959(Communication Department of Menard, 2007). Baguelin et al. (1978) and ASTM (2007) describe the device and the testing procedure in full.

This page is intentionally blank